



المؤتمر العلمي الدولي الخامس للعلوم الحرفية والتطبيقية والتكنولوجية

**V. International Scientific Congress of Pure, Applied and Technological Sciences**

**V. Uluslararası Fen, Uygulamalı ve Teknolojik Araştırmalar Kongresi**

Full Text Book

Rimar Academy

Publishing House



**Yayınevi ( دار النشر )**

أكاديمية ريمار - Rimar Academy

**Editör (المحرر)**

Prof. Dr. Ghuson H. MOHAMMED

**Yayın Koordinatörü (منسق النشر)**

Emel KAPLAN

**ISBN:**

978-605-73553-5-5

ISBN 978-605735535-5



**Baskı (تاريخ الطباعة)**

2022

**Matbaa Sertifikası No (رقم شهادة المطبعة)**

47843



## المؤتمر العلمي الدولي الخامس للعلوم الصرفة والتطبيقية والتكنولوجية (مؤتمر مينار)

رعاية



هذا الكتيب مسجل (ردمك - ISBN) في وزارة الثقافة التركية

ISBN 978-605065850-7



9 786050 658507

## الرؤساء الفخريون Honorary Committee



الأستاذ عامر كابلان  
Mr. Amir KAPLAN

مدير أكاديمية ريمار  
Manager of Rimar Academy

تركيا-توركيه  
Türkiye-Turkey



الأستاذ الدكتور نهاد أكوش  
Prof. Dr. Nihat AKKUŞ  
رئيس جامعة إسطنبول جيديك  
Rector of Istanbul Gedik University

تركيا-توركيه  
Türkiye-Turkey



الأستاذ الدكتور وعد محمود رؤوف  
Prof. Dr. Waad Mahmood  
RAOOF  
رئيس جامعة تكريت  
Rector of Tikrit University

العراق - Iraq

## رؤساء الهيئات Chairmen of committees



الأستاذة الدكتورة غصون حميد محمد  
Prof. Dr. Ghuson H. MOHAMMED

جامعة بغداد  
Baghdad University

العراق - Iraq

رئيس المؤتمر  
Chair of Congress

رئيس الهيئة الاستشارية  
Chairman of  
Consultative Committee



الأستاذ الدكتور زكريا ظلام  
Prof. Dr. Zakaria ZALLAM

جامعة غازي عنتاب  
Gaziantep University

تركيا-توركيه  
Türkiye-Turkey

الأمين العام للمؤتمر  
General Secretary

رئيس الهيئة العلمية  
Chairman of  
Scientific Committee



أ. د. عبد الكريم دهش علي  
Prof. Dr. Abdulkareem Dash ALI

عميد كلية التربية للعلوم الصرفة -  
جامعة تكريت

Dean of the College of Education Pure  
Science-Tikrit University

العراق - Iraq



أ. د. موفق شياع علوان  
Prof. Dr. Muwafaq Shyaa ALWAN

عميد كلية الهندسة / الجامعة العراقية  
Dean of Engineering Faculty / Aliraqia  
University

العراق - Iraq

## الهيئة الاستشارية

### CONSULTATIVE COMMITTEE



Prof. Dr. Nawras Abdelah Alwan  
University Of Basrah  
Iraq



Prof. Dr. Derar Eleyan  
Palestine Technical University  
Palestine



Prof. Dr. Kadhim A.Aadim  
University of Baghdad  
Iraq



Prof. Dr. Zaheda Ahmed DAKHIL  
University of Baghdad  
Iraq



Dr. Haidar Kadhim Abaas  
Basrah University  
Iraq



Assist. Prof. Dr. Sameera Ahmed  
Ebrahiem  
University of Baghdad  
Iraq



Dr. Osman TÜRK  
Harran University  
Turkey



Asst. Prof. Dr. Ahmed Hameed Kaleel  
University of Baghdad  
Iraq

## الهيئة التحضيرية

### ORGANIZING COMMITTEE



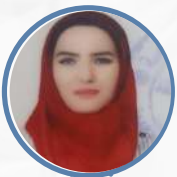
Prof. Dr. Ali A. Abdulhameed  
University of Baghdad  
Iraq



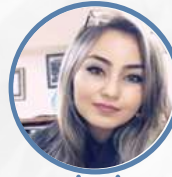
Prof. Dr. Assiya Cherif  
National School of Statistics and Applied  
Economics  
Algeria



Dr. Ameer Ibraheem Khudadad Kareem  
Ministry of Education  
Iraq



Dr. Mariam Adnan Ibrahim  
Tikrit University  
Iraq



Dr. Dinara MASHITOVNA  
Rimar Academy  
Qazakistan



Dr. Ielaf O. Abdul Majeed Dahl  
University of Mosul  
Iraq



Dr. Khalid Ahmed Hassan AHMED  
Omdurman Islamic University  
Sudan

# الهيئة العلمية

## SCIENTIFIC COMMITTEE



Prof. Dr. Thualfeqar  
Almohanna  
University of Kufa  
Iraq



Prof. Dr. Samira Negrichi  
Larbi Tebessi University  
Algeria



Lect. Dr. Sahar Mohammed  
Jawad  
University of Kufa  
Iraq



Prof. Dr. Ebtahag .Z.Sulyman  
University of Mosul  
Iraq



Prof. Dr. Fatma Mohamed  
Ahmed Yousseff  
Sue z canal university  
Egypt



Dr. Aseel M. H. H. Al Khafaji  
University of Baghdad  
Iraq



Asst. Prof. Dr. Ahmed  
Hameed Kaleel  
University of Baghdad  
Iraq



Assist. Prof. Dr. Ahmed W.  
Al Zand  
Universiti Kebangsaan  
Malaysia



Assist. Prof. Dr.  
Seyedehzahra Mirrahimi  
University of Tehran  
Iran



Assist. Prof. Dr. Hussein Hadi  
Nahi  
Al-qasim Green University  
Iraq



Dr. Muslim Muhsin Ali  
University of Missouri  
USA



Dr. Hanan Shihab Ahmad  
Northern Technical University  
A\_ Door Technical Institute  
Iraq



Lect. Dr. Batool Abd Al  
Ameer Baqer Alsafar  
Al Mustansiriyah  
University  
Iraq



Dr. Ibrahim Rahem Jassim  
Al-Aadity  
University of Sheffield  
UK



Dr. Fadhil Mahmood Oleiwi  
Ministry of Education  
Iraq



Dr. Imad N. Kashkool  
ministry of education  
Iraq



Dr. Abothur Almohana  
Jabir Ibn Hayyan  
Medical University  
Iraq



Dr. Anaam Kadhim Hadi  
Ministry of Science and  
Technology  
Iraq



Taghreed Khudhur Mohammed  
University-Institute of Medical  
Technology / Al -Mansour  
Iraq



Dr. Mustafa M. Khalifa Jabiry  
Management & Science  
University  
Malaysia



Assist. Prof. Bushra Majeed  
Issa  
Basrah University  
Iraq



Dr. Haleemah Jaber  
Mohammed  
Ministry of Science and  
Technology  
Iraq



Dr. Naela Jeries HADDAD  
Rimar Academy  
Palestine



Dr. Husam R. Abed  
Ministry of Education  
Iraq



Assist. Prof. Dr. Mohammed  
Hadi Nahi Al-Yarmouk  
Al-Yarmouk University  
Iraq



Pr Chèrif Fatima zohra  
Professor off Général  
Surgery and Oncology  
Algeria



Bushra Rashid Ibrahim  
University of Baghdad  
Iraq



Dr. Asmaa Y. Al-Baitai  
University of Baghdad  
Iraq



Dr. Ali Abdulwahab Ridha  
University of Technology  
and Applied Sciences,  
Rustaq  
Sultanate of Oman



Dr. Amel D. Hussein  
Wasit University  
Iraq



Lec. Dr. Dhuha Mahdi Jabir  
Al-Abidi  
Al-Qadisiyah University  
Iraq



Prof. Dr. Assiya CHERIF  
National School of  
Statistics and Applied  
Economics  
Algeria



Intsar Ghanim TAHA  
University of Mosul  
Iraq



Lect. Dr. Hawraa Sabah Al-  
Musawi  
University of Babylon  
Iraq



Dr. Wala Gazey Mahmood  
Dizayee  
Salahaddin University  
Iraq



Dr. Ahmed Jasim Nawfal  
University of Anbar  
Iraq

## Table of contents

EFFECTS OF ACETAMIPRID ON SOME BIOCHEMICAL PARAMETERS IN MALE ALBINO RATS AND THE AMELIORATIVE ROLE OF QUERCETIN AND HESPERIDIN <b>Arjwan. A. ALSUDANI &amp; Shaymaa Rabeea MADHKHOOR</b> .....	4
ISOLATION AND MOLECULAR IDENTIFICATION OF THE CAUSAL AGENTS OF FUSARIUM HEAD BLIGHT OF WHEAT IN AL-QAYYARAH SUB DISTRICT, NINEVAH GOVERNORATE <b>Salim I. AKRAM , Ali K. AL-TAAE &amp; Karkaz M. THALIJ</b> .....	16
STUDY THE ANTIBACTERIAL ACTIVITY OF ALCOHOLIC EXTRACT OF ALLIUM SATIVUM ON PSEUDOMONAS AERUGINOSA AND COMPARE WITH SOME ANTIBIOTICS <b>Luma Saeed MOHAMMED</b> .....	32
EVALUATE STRESSES GENERATED IN EARTHEN DAMS USING GEO-STUDIO <b>Asmaa Abdul Jabbar JAMEL</b> .....	38
SYNTHESIS AND CHARACTERISATION OF NEWCo(II), Zn(II) AND Cd(II) COMPLEXES DERIVED FROM OXADIAZOLE LIGAND AND 1,10-PHENANTHROLINE AS Co-LIGAND <b>Riyadh M. AHMED, Sarah S. ABDUL RAHMAN, Dhefaf H. BADRI, Khawla M. SULTAN, Ismaeel Y. MAJEED &amp; Ghada M. KAMIL</b> .....	50
16sr RNA SEQUENCING FOR IDENTIFICATION BACTERIA FROM FACE MASK OF STUDENTS IN MOSUL UNIVERSITY <b>Sura M.Y. AL-TAEE, Amina G.O. AL-ANI &amp; Alaa Younis MAHDY</b> .....	58
COMPUTATION OF DOUBLE DIFFERENTIAL NEUTRON CROSS SECTIONS ON DIFFERENT TARGETS AT VARIOUS PROTON ENERGIES UTILIZING PHITS CODE <b>Rabee B. ALKHAYAT, Mutaz Salih HASAN &amp; Mushtaq Abed AL-JUBBORI</b> .....	69
OPTICAL PROPERTIES OF ANTHOCYANIN EXTRACTED FROM FLOWERS <b>Fatima H. MALK, Alyaa Abdul Hasan ABDUL KAREM &amp; Dhiaa J. AGOOSH</b> .....	82
EFFECT OF METHIONINE ADDITION TO SOYBEAN MEAL INSTEAD OF PROTEIN CONCENTRATE IN THE FINISHER RATION OF BROILER <b>Rafea M.KHALEEL, Nawaf G.ALTAMI &amp; Thaer M. Abdul –BAKI</b> .....	89
NEW RESULTS OF WELL-POSEDNESS FOR HEMI-EQUILIBRIUM PROBLEMS <b>Alaa Majid JABER &amp; Bashayir Nahi ABED</b> .....	98
TOXIC KINETICS OF CIPROFLOXACIN IN MICE <b>S.M. AMIN &amp; F. K. IBRAHIM</b> .....	118



DIFFERENTIAL SUBORDINATIONS FOR MULTIVALENT FUNCTIONS ASSOCIATED WITH GENERALIZED FRACTIONAL DIFFERENTIAL OPERATOR <b>Zainab H.MAHMOOD, Aseel A.HASSAN &amp; Dunia K.MAHDI</b> .....	130
THE EFFECT OF PARTIAL AND TOTAL SUBSTITUTION OF Cd AND Mg NANOPARTICLES ON THE ELECTRICAL AND MAGNETIC PROPERTIES OF THE SUPERCONDUCTORS COMPOUND $YBa_2Cu_3O_{7-\delta}$ AT HIGH TEMPERATURES <b>Falah Mohammed ABED, Nada A. KHALIL &amp; Ismael Kalil JASIM</b> .....	144
NEW GENERALIZED OPERATOR IN TOPOLOGICAL SPACES <b>Siham I. AZIZ &amp; Nabilal . AZIZ</b> .....	152
A CROSS-SECTIONAL STUDY OF STOOL SAMPLES FOR SOME LOCAL AND INTERNATIONAL ARRIVALS TO KARBALA GOVERNORATE DURING A RELIGIOUS VISIT <b>Zainab Abed Muhsin AL-HABOOBI, Huda Dhaher AL-MARSOMY &amp; Haleema Salman SALIH</b> .....	158
LIGHTWEIGHT IMAGE COMPRESSION USING POLYNOMIAL AND TRANSFORM CODING <b>Zainab J. AHMED &amp; Loay E. GEORGE</b> .....	172
PREPARATION AND STUDY OF OXIDES AND THEIR EFFECT ON THE PROPERTIES OF $Al_2O_3/ZrO_2$ MGO , AND CAO <b>Sabah Ali KHADHIR, Omar Abdulwahhab AHMED &amp; Saif Khalel JASIM</b> .....	194
THE EFFECT OF BACKGROUND VACUUM PRESSURE ON THE LENGTH OF GAS DISCHARGE PLASMA BY USING ALUMINUM ELECTRODES <b>Mohammed R. ABDULAMEER</b> .....	208
THE CORRELATION BETWEEN COVID-19 AND DIABETES MELLITUS <b>Mouna Akeel Hamed AL-OEBADY, Hedaa .M. NAHAB &amp; Suhair. M. JABBAR</b> .....	216
EVALUATION BIOCONTROL OF TRICHODERMA SPP. AGAINST MACROPHOMINA PHASEOLINA ON SUNFLOWER <b>Zina Mohmmmed SARHAN, Waleed Khalid AHMED, Somayyeh RAZZAGHI &amp; Shimal younis ABDUL-HADI</b> .....	226
PRODUCED GENETICALLY TRANSFORMED HELIANTHUS ANNUUS L BY USING THE ISOLATE OF AGROBACTERIUM TUMEFACIENS (ATMCO1) <b>Islam Yasir ABDULLAH, Taghreed Nawaf AHMED, Aryan Mohammed HAMED &amp; Raghad Nawaf AL-ZAIDY</b> .....	236
ESTIMATION OF SOME ADIPOSE TISSUE HORMONES (VISFATIN AND ADIPONECTIN) IN PATIENTS WITH HYPOTHYROIDISM <b>Azhar Younus DHANNOON &amp; Abeer Ataallah Ayyed AL-HADIDY</b> .....	250

KNOWLEDGE OF PREGNANT WOMEN ABOUT GESTATIONAL DIABETES MELLITUS AT MOSUL CITY <b>Yamama Zuhir ABDUL KAREEM, Jwan Mohammed HASSAN &amp; Saad Hussein MURAD</b> .....	262
SPONTANEOUS HISTOPATHOLOGICAL LESIONS OF THE INTESTINES, LIVER, PANCREAS AND HEART OF THE FRESHWATER FISH MASTACEMBELUS MASTACEMBELUS (BANKS & SOLANDER 1794) <b>Fatimah Q.M. AL-HAYYALI</b> .....	274
A NEW RECORDING OF IRAQI FLORALEPIDIUM DIDYMIUM L. (BRASSICACEAE) <b>S.A.ALIWY &amp; L.G.A.AL-EZEREG</b> .....	282
COMPARATIVE STUDY FOR VAGINAL INFECTIONS IN PREGNANCY AND NON PREGNANCY WOMEN IN NINEVEH GOVERNORATE <b>Ibrahim Talal DAWOOD, Hanan Sami NOURI &amp; Najlaa Abdulla FATHI</b> .....	290
ANALYSIS OF HEAT FLOW IN DOUBLE-PIPE HEAT EXCHANGER WITH NANO-FLUID <b>Mohammed AHMED, Abdulkader Ahmed ANNAZ &amp; MohameedMhana METEAB</b> .....	304
PROTECTING THE ENVIRONMENT FROM COVID-19 MEDICAL WASTE <b>Mariam Adnan IBRAHIM</b> .....	314
TWITTER DEMOGRAPHICS FOR IRAQI GOVERNORATES <b>Azzah Hazem ZAKI &amp; Noor Ahmed QARABASH</b> .....	328
CURRENT CONTROLLED CHAOTIC SPIKING OF SEMICONDUCTOR LASER DIODE WITH OPTICAL FEEDBACK <b>Younis Th. YOUNIS, Ahmed K. AHMED &amp; Kais A. AL-NAIMEE</b> .....	340
COMPARE OF MEDIAN FILTER AND WIENER FILTER TO DETECT CONCEALED WEAPONS <b>Moumena Salah YASSEN</b> .....	354
STUDY SOME TYPE OF FISH AS INDICATORS OF POLLUTION IN AL- SANIYAH RIVER/ AL- DIWANIYAH/IRAQ <b>Lujain Ebrahim HUSSAIN</b> .....	362



**EFFECTS OF ACETAMIPRID ON SOME BIOCHEMICAL PARAMETERS IN  
MALE ALBINO RATS AND THE AMELIORATIVE ROLE OF QUERCETIN  
AND HESPERIDIN**

**ARJWAN. A. ALSUDANI  
SHAYMAA RABEEA MADHKHOOR**

## **EFFECTS OF ACETAMIPRID ON SOME BIOCHEMICAL PARAMETERS IN MALE ALBINO RATS AND THE AMELIORATIVE ROLE OF QUERCETIN AND HESPERIDIN**

**Arjwan. A. ALSUDANI<sup>1</sup>**  
**Shaymaa Rabeea MADHKHOOR<sup>2</sup>**

### **Abstract:**

Acetamiprid is one of the most wide used insecticides over the entire world. Due to the widespread use of flavonoids in the treatment of many disease, The aim of this study was to see if Quercetin and Hesperidin could help reduce the effects of Acetamiprid on biochemical parameters which include Malondialdehyde, Aspartate aminotransferase, Alanine aminotransferase, Creatinine, and Urea, as well as antioxidants like Superoxide dismutase, Glutathion-S-transferase, Catalase and expression level of MAPK8 and NFKB genes. A total of 48 male rats were used in the investigation, with each group consisting of six animals that were dosed for 30 days. The groups were divided as follows: Control group (C) given drinking water only, (T1) given orally Acetamiprid in the dose (40mg/kg/B.W),(T2) given orally Quercetin in dose (20mg/kg/B.W),(T3) given orally Hesperidin in the dose (25mg/kg/B.W), (T4) given Quercetin in the dose(20mg/kg/B.W) then Hesperidin in the dose (25mg/kg/B.W)Concurrently,(T5) given Acetamiprid e in the dose (40mg/kg/B.W) then given Quercetin in the dose(20mg/kg/B.W) Concurrently, (T6) given Acetamiprid in the dose (40mg/kg/B.W) then given Hesperidin in the dose(25mg/kg/B.W) Concurrently, and(T7) given Acetamiprid in dose (40mg/kg/B.W) then given Quercetin in the dose(20mg/kg/B.W) then given Hesperidin in the dose(25mg/kg/B.W) Concurrently. The results clarified a significant increase ( $P < 0.05$ ) in Malondialdehyde, Urea, Creatinine, liver enzymes(AST,ALT) and gene expression of MAPK8 and NFKB genes, and a significant decrease in the level of enzymatic antioxidants (SOD, GST, CAT) in (T1) compared to (C) and other groups. On the other hand, results showed that giving animals Quercetin and Hesperidin separately or both simultaneously with the pesticide Acetamiprid in treatments (T5, T6, T7)caused of a significant improvement in the studied parameters compared to (T1) that was dosed with the pesticide alone. It was sometimes close to the control group, especially in treatment (T7), which gave the best results due to the synergistic effect of Quercetin and Hesperidin in reducing the oxidative effects caused by the pesticide. Concluded of this study that administration by Quercetin and Hesperidin alone or both together and simultaneously with the pesticide has a positive effectiveness and efficiency in reducing the oxidative damage resulting from the toxicity caused by the pesticide in the biochemical parameters, antioxidants and the level of gene expression in male albino rats.

**Key words:** Acetamiprid, Quercetin, Hesperidin, MAPK8, NFKB, Flavonoids.



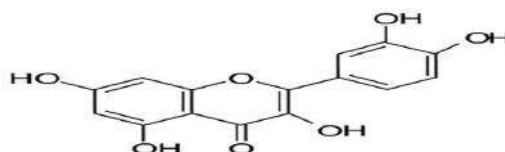
<http://dx.doi.org/10.47832/MinarCongress5-1>

<sup>1</sup>  University of Al-Qadisiyah, Iraq, [orjuwan.mahood@qu.edu.iq](mailto:orjuwan.mahood@qu.edu.iq), <https://orcid.org/0000-0002-4661-7124>

<sup>2</sup>  University of Al-Qadisiyah, Iraq, [shaymaa.rebeaa@qu.edu.iq](mailto:shaymaa.rebeaa@qu.edu.iq), <https://orcid.org/0000-0001-5461-9683>

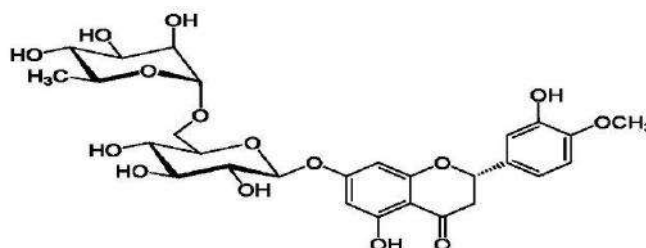
## Introduction:

Due to the ease of getting medicinal plants and their inexpensive pricing, as well as the fact that they contain numerous active compounds that play a vital part in the prevention and treatment of diseases, medicinal plants utilized in treatment of many ailments (Padmavathy& Devarajan, 2017). Plants create a wide number of chemical compounds known as "secondary plant substances" throughout their growth and development, the most significant of which include alkaloids, tannins, phenols, flavonoids, essential oils, and others (Gurnani *et al.*, 2014). The therapeutic efficacy of flavonoids is due to the fact that they have several physiological antioxidant qualities, the most significant of which are Quercetin and Hesperidin flavonoids (Zeng *et al.*, 2005). Quercetin is a yellow crystalline compound that is soluble in alcohol and aqueous solutions, and is present in many fruits, vegetables, coffee, and tea (Baghel, 2012). 2-(3,4-dihydroxy phenyl)-3,5,7-trihydroxy-4H-chromen-4-one is its chemical name, its chemical formula is (C<sub>15</sub>H<sub>10</sub>O<sub>7</sub>), and its molecular weight is 302.24 g/mol. Quercetin chemical structure is shown in (Figure1) (Winkel- Shirley, 2001).



**Figure (1): The chemical structure of Quercetin**

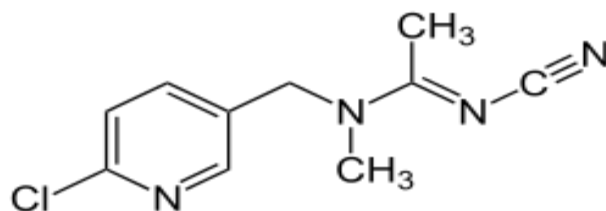
Because it contains a catechol and a hydroxyl groups with an ideal chemical arrangement necessary to resist free radicals, quercetin has a wide impact on the biological activities of the cell through its antioxidant properties and its great ability to remove free radicals, it is considered a natural antioxidant (Khoo *et al.*, 2010; Heijnen *et al.*, 2002). Hesperidin is a glycosidic flavonoids that may be found in most citrus trees and is abundant in the peels of citrus fruits including oranges, tangerines, and limes. Hesperidin has the chemical formula (C<sub>28</sub>H<sub>34</sub>O<sub>15</sub>) and 610,565 g/mol molecular weight (Figure2), which illustrates the chemical structure (Shi *et al.*, 2012).



**Figure( 2): The chemical structure of Hesperidin**

Hesperidin is a potent antioxidant that protects against a variety of ailments, including cardiovascular disorders. It also boosts vitamin C's ability to decrease cholesterol levels by scavenging free radicals produced by oxidative stress (Zhou *et al.*, 2011;Kaaya *et al.*, 2015). Pesticides have been employed all over the world in

recent years to decrease agricultural crop losses caused by insects, pests, and dangerous illnesses. Pesticides differ in terms of toxicity, environmental persistence, and bioaccumulation in the food chain. If applied incorrectly, these insecticides might cause significant infections (Johnson & Corn, 2015). Acetamiprid is a bitter neonicotinoid compound (Figure 3) that is employed against pests in various crops such as leaf hoppers, leaf beetles and white flies ( Acharya *et al.*, 2002; Singh & Kulshrestha, 2005). Pesticides' toxicity may be due to their ability to stimulate the generation and accumulation of free radicals in the body, resulting in oxidative stress (Salama *et al.*, 2013), Due to a mismatch between free radical production and the antioxidant system's capacity to scavenge them (Abdollahi *et al.*, 2004).



**Figure (3): The chemical structure of Acetamiprid**

## Materials and Methods

### 1-Experiment animals

Forty-eight male white rats were employed, all of which came from animal house in the college of Science, University of Al-Qadisiyah. The animals' weights varied from 200 to 185 grams, while their ages ranged from 12 to ten weeks. All of the animals were kept in a lab setting. Temperature (25-22°C) and illumination are similar ( 12hrs of light-12hrs of darkness ).

### 2-Preparation of the doses used in the study

1- Quercetin dosage preparation: the dose of Quercetin was created using the method of (El Mazoudy *et al.*, 2015) at a concentration of 20mg/kg of B. W. by dissolving the appropriate concentration based on the animal's average B. W..

2- Hesperdin dosage preparation: the hesperdin dose was created using the technique (Mahmoud, 2014), with a concentration 25 mg/kg of B. W., based on the average weight.

3- Acetamiprid dosage preparation: At 40 mg/kg B. W. concentration, the dose was created according to the procedure (Kenfack *et al.*, 2018).

### 3-Experimental design

For a period of 30 days, male rats were separated into eight groups, each with six animals, as follows:

- 1- Group of control (C): had simply 1 mL of standard water and a diet.
- 2- (T1) Acetamiprid was dosed at a dosage of 40 mg/kg of B. W.
- 3- (T2) Quercetin was given in a 20 mg/kg of B. W.
- 4-(T3) Hesperdin was given in a 25 mg/kg B. W.
- 5- (T4) received Quercetin at a dose of 20 mg/kg B. W., followed by 25 mg/kg B. W Hesperidin.

6- (T5) Acetamiprid was given at a dose of 40 mg/kg of B. W followed by 20 mg/kg of B. W. Quercetin.

7- (T6) Acetamiprid was administered at a dose of 40 mg/kg of B. W then, at the same time, Hesperidin was administered at a dose of 25 mg/kg of B. W..

8- (T7) Acetamiprid was administered at a dose of 40 mg/kg of B. W., followed by Quercetin at a dose of 20 mg/kg of B. W., and finally Hesperidin at a dose of 25 mg/kg of B. W.

#### 4- Sacrifice of Animals

Chloroform was used to anesthetize the animals, and blood was extracted straight from their hearts using medical needles. The blood was then placed in tubes that did not contain an anticoagulant and tilted for 30Ms, after which the tubes were centrifuged for 15 minutes at 3000 revolutions per minute to retrieve the blood serum. To evaluate the parameters under investigation, store it in labeled plastic tubes and freeze it at (-20 C) to estimate the amount of Malondialdehyde (MDA), the activity of Catalase, Superoxide dismutase, Gluathion-S-transferase (GST), Urea, Creatinine, Aspartate amino transferase (AST), Alanine aminotransferase and alanine to alanine (ALT). The animals were subsequently dissected, and a tiny sample of the liver was extracted and shocked with liquid nitrogen (C196-C), then stored in tubes containing DEPC-treated water and frozen at a temperature of (-C20) until the amount of gene expression of (MAPK8, NFkB) was determined by Real Time PCR(RT-q PCR) using SYBR Green protocol. The primers used were created using a unique gene sequence and according to the table below:

Primer	Sequence (5'-3')	
MAPK8 gene	F	GTTGCTCATAAACACAAACCTCC
	R	GGGATGGGTTATGTTTTCTAGAC
NF <sub>κ</sub> B gene	F	AGTTGAGGGGACTTTCCCAGGC
	R	GCCTGGGAAAGTCCCCTCAACT
HPRT1	F	AGGGCATATCCAACAACAACTT
	R	GTTAAGCAGTACAGCCCCAAAAG

The "Comparative Ct methodology" was then used to determine the relative gene expression (Ct method). The "Comparative Ct approach" (Ct method., Applied Biosystems) was then used to compare relative gene expression to HPRT1 (Hypoxanthine-guanine phosphoribosyl transferase 1).

## Statistical Analysis

The ANOVA test was performed to compare the groups. With a 95 percent confidence interval, the level of statistical significance was set at  $p < 0.05$ . The SPSS 21 software suite was used to conduct the statistical analysis.

## Results and Discussion

### 1-Oxidative stress indicators

The MDA level in group (T1) treated with ACP alone increased significantly ( $p < 0.05$ ) when compared with (C) and other groups, as shown in (Table 1). In comparison to the control group (T2, T3, T4, T7) did not indicate any significant changes. When comparing the results of the study groups, results revealed substantial differences across groups (T5, T6). The results (Table 1) also revealed a significant decrease ( $p < 0.05$ ) in CAT enzyme activity in the group (T1) treated with ACP alone when compared to the control group and the other groups; however, the treatment groups (T2, T3, T7) showed no significant differences when compared to the control group and each other. While the treatment group (T4) showed a large rise in comparison to the control group and other groups, the two treatment groups (T5, T6) showed a substantial reduction in comparison to the control group and other groups, with no significant differences between the two groups. When it came to GSH levels, the results showed a significant decrease in the treatment group (T1) for male rats treated with ACP when compared to the control group and other groups, with no significant differences for groups (T2, T3, T4, T7) when compared to the control group, while the two groups (T5, T6) showed a significant decrease in comparison to the control group, with significant differences between the two groups. The results also showed a significant decrease ( $p < 0.05$ ) in SOD enzyme activity in the treatment group (T1) compared to the control group and other groups, while the two treatment groups (T2, T4) showed a significant increase compared to the control group and other groups, but the two treatment groups (T3, T7) showed a significant decrease ( $p < 0.05$ ) in SOD enzyme activity compared with (C) and other groups. There were no significant differences when compared to the control group, however there were significant differences between the two groups. There were also significant differences between the two groups (T5, T6) when compared to the control group, but no significant differences between the two groups. Malondialdehyde is the end product of lipid peroxidation and is an indicator of oxidative stress for various diseases (Kamble *et al.*, 2013) These resultant are in agreement with (Guiekep *et al.*, 2019) which indicates oxidative stress and affects guinea reproductive function of male guinea pigs. On the other hand, treatment with Quercetin and Hesperidin alone or combined in the general atmosphere of treatment (T7) and this indicates the facilitative role of Quercetin and hesperidin in reducing oxidative stress and increasing antioxidants. (Cogolludo *et al.*, 2007; Abarikwu *et al.*, 2013; Zanwar *et al.*, 2014).



**Table (1): Effect of treatment with Quercetin and Hesperidin on antioxidants in male rats treated with Acetamiprid.**

SOD (U/ml)	GST (U/L)	Catalase (U/ml)	MDA (Mmol/L)	criteria	Groups
1.92±0.040 bc	2.99±0.081 a	0.83±0.011 b	1.28±0.005 d	C <sub>1</sub>	
0.88±0.041 e	1.19±0.178 d	0.35±0.006 d	3.86±0.015 a	T <sub>1</sub>	
2.15±0.006 a	3.01±0.044 a	0.84±0.012 ab	1.27±0.007 d	T <sub>2</sub>	
1.99±0.017 b	2.98±0.011 a	0.82±0.005 b	1.25±0.001 d	T <sub>3</sub>	
2.20±0.011 a	3.15±0.031 a	0.87±0.014 a	1.22±0.003 d	T <sub>4</sub>	
1.80±0.029 d	2.43±0.105 b	0.76±0.010 c	2.00±0.002 c	T <sub>5</sub>	
1.75±0.013 d	2.15±0.015 c	0.74±0.011 c	2.32±0.015 b	T <sub>6</sub>	
1.90±0.018 c	2.93±0.020 a	0.81±0.013 b	1.29±0.004 d	T <sub>7</sub>	
0.075	0.233	0.049	0.216	LSD	

. Numbers refer to mean ± standard error

Different letters between groups refer to differences at significance (P <0.05).

## 2-Plasmatic renal factors estimation

Compared with the control group(C) and the other groups, (T1) showed a significant increase, in Urea while the groups (T3,T7) were close to the control group. Significant differences also appeared in the groups(T5,T6). On the other hand, the results showed a significant increase in Creatinine in (T1) compared to the control group and other groups. While the groups (T2,T3,T4,T7) did not show any significant differences compared with the control group. The groups (T5,T6) showed significant differences with the control group

The increase in the level of Urea and Creatinine in the animals treated with the pesticide may be due to the potential nephrotoxicity of the pesticide and this was confirmed by (Arfat *et al.*, 2014) in a similar study as it was mentioned that the use of the pesticide for 15 days led to toxic effects in the kidneys.

On the other hand, Quercetin and Hesperidin protect the kidneys from the toxic effects of the pesticide by reducing oxidative stress and preventing the leakage of renal enzymes into the blood circulation (Abarikwu *et al.*, 2012; El-Ela& Abdel-Aziz, 2019).

## 3-Serum hepatic enzyme activities

The current study's findings revealed a significant rise (p0.05) in the liver enzymes AST and ALT in the pesticide-treated group (T1) compared to (C) and other groups. In comparison to (C), the groups (T2, T3.T4, T7) did not indicate any significant changes. When compared to (C) the findings revealed substantial differences between groups (T<sub>5</sub>, T<sub>6</sub>), There were no notable differences between the two groups.

Liver enzymes are among the most widely used indicators in diagnosing hepatotoxicity. Hepatocytes' transport function is altered with liver damage., leading to extravasation in the plasma membrane, and consequently an increase in the level of enzymes in the serum (Kutlu *et al.*, 2007; Bhardwaj *et al.*, 2010). Rats treated with Quercetin and Hesperidin did not show any negative effects on liver

enzymes due to their antioxidant activity and their role in mitigating the damage caused by the pesticide in hepatocytes (Amalia *et al.*, 2007).

**Table (2): Effect treatment with Quercetin and Hesperidin on the level of some liver enzymes ,Urea and Creatinine in male rats treated with Acetamidrid.**

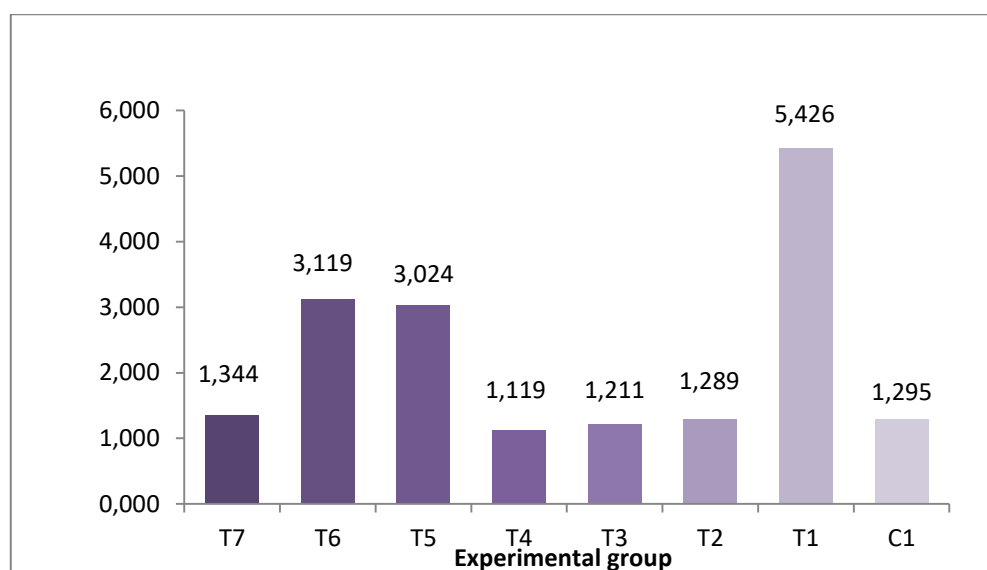
ALT (IU/L)	AST (IU/L)	Creatinin (mg/dl)	Urea (mg/dl)	criteria	Groups
1.95±1.00 c	1.33±0.15 c	0.92±0.75 c	0.9±0.15 d	C <sub>1</sub>	
3.70±1.07 a	2.99±1.07 a	3.53±0.95 a	2.9±0.09 a	T <sub>1</sub>	
1.94±0.04 c	1.40±0.77 c	1.10±0.66 c	1.2±0.01 c	T <sub>2</sub>	
1.93±0.08 c	1.59±0.52 c	0.96±0.31 c	0.9±0.05 d	T <sub>3</sub>	
1.90±0.15 c	1.31±0.61 c	0.93±0.09 c	1.0±0.13 c	T <sub>4</sub>	
3.01±0.09 b	1.84±0.03 bc	2.88±0.17 b	1.5±0.28 b	T <sub>5</sub>	
2.87±1.13 b	2.18±0.07 ab	2.80±0.06 b	1.7±0.07 b	T <sub>6</sub>	
1.97±0.02 c	1.42±0.55 c	0.98±0.92 c	0.8±0.08 d	T <sub>7</sub>	
0.30	0.55	0.34	0.27	LSD	

Numbers refer to mean ± standard error

Different letters between groups refer to differences at significance (P <0.05).

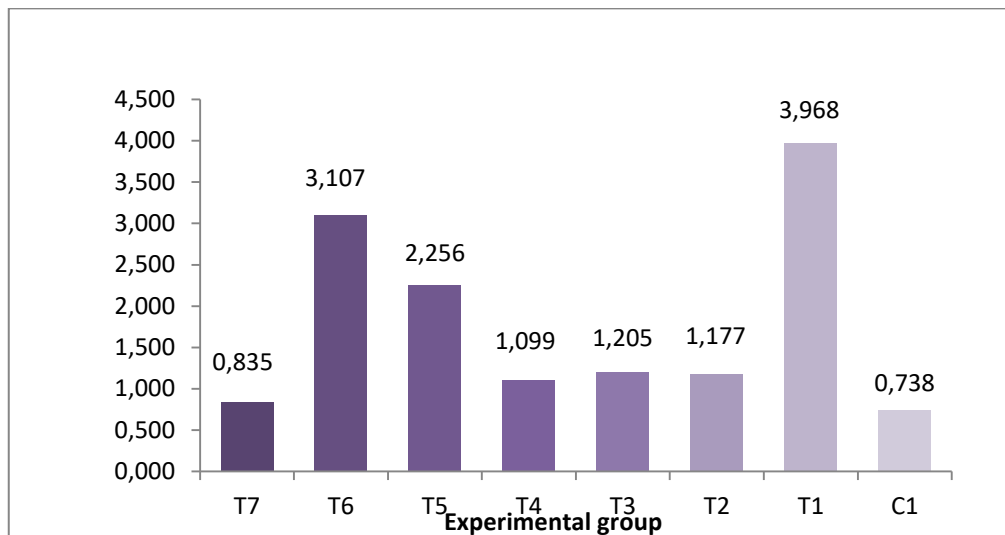
#### 4-Expression pattern of MAPK8 and NF $\kappa$ B

(Figure4) shows a substantial increase (p<0.05) in gene expression of the gene (MAPK8 gene) in (T1, T5, T6) compared to (C). The results, on the other hand, revealed an improvement in gene expression in (T2., T3, T4, T5) and they were approach to the control group.



**Figure (4): Gene expression level of the gene (MAPK8 gene) compared to the control group (HPRT1).**

In terms of NF $\kappa$ B gene expression, the results indicated in (Figure5) that the groups (T1, T5, T6) had a significant increase (p<0.05) when compared with (C) and other groups. The results also revealed that the levels of gene expression improved for the groups (T2, T3, T4, T7) and were comparable to group (C), particularly in the group (T7).



**Figure (5): Gene expression level of the gene (NFkB) in comparison with control group (HPRT1).**

This is consistent with (Raposa *et al.*, 2016), who stated that the level of gene expression was increased in rats treated with food additives. This increase could cause the activation of inflammatory pathways, mutagenicity and cancer development (Sheikh *et al.*, 2000; Zheng *et al.*, 2005). And the reason for the improvement in the level of gene expression is due to the use of quercetin and hesperidin, which act as powerful antioxidants to curb free radicals and restore antioxidant enzymes, which leads to an increase in gene expression. (AL-Awady & AL-Zamely, 2016; Tabeshpour *et al.*, 2020).

### Conclusion

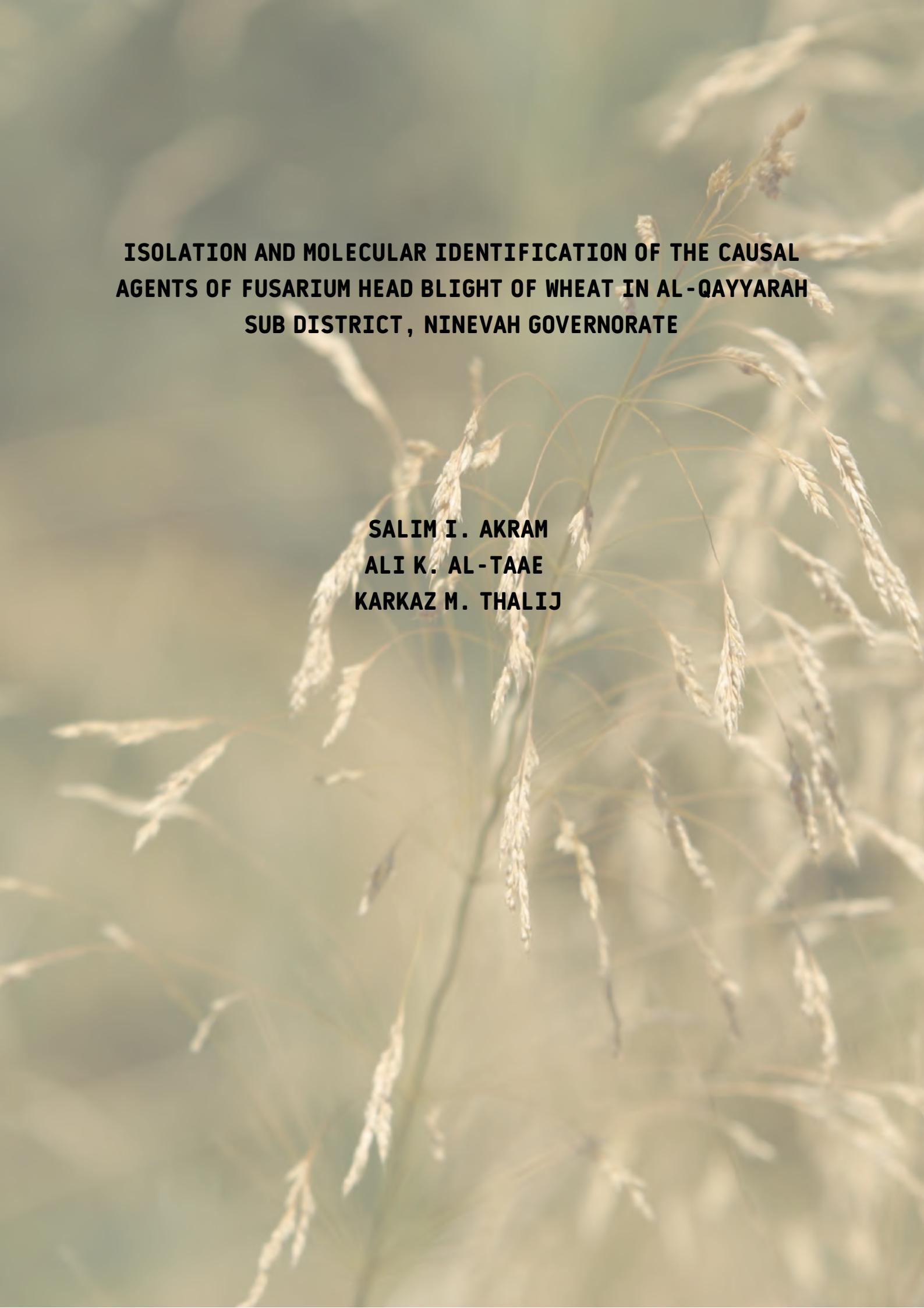
We conclude from the study that administration of Quercetin and Hesperidin alone or both together and simultaneously with the pesticide has a positive effectiveness in reducing the oxidative damage resulting from the toxicity caused by the pesticide in male albino rats.

## References

- Abarikwu ,S.O.; Pant, A.B. and Farombi, E.O.(2013). Effects of quercetin on mRNA expression of steroidogenesis genes in primary cultures of Leydig's cells treated with atrazine. *Toxicol In Vitro.*, 27(2) : 700-707.
- Abarikwu, S. O., Pant, A. B., & Farombi, E. O. (2012). Dietary antioxidant, quercetin, protects sertoli-germ cell coculture from atrazine-induced oxidative damage. *Journal of biochemical and molecular toxicology*, 26(11), 477-485.
- Abdollahi, M., Ranjbar, A., Shadnia, S., Nikfar, S., & Rezaie, A. (2004). Pesticides and oxidative stress: a review. *Med Sci Monit*, 10(6), 141-147.
- Acharya, S., Mishra, H. P., & Dash, D. (2002). Efficacy of insecticides against okra jassid, *Amrasca biguttula biguttula* Ishida. *Annals of plant protection sciences*, 10(2), 230-232.
- AL-Awady, M. A., & AL-Zamely, H. A. (2016). Effect of quercetin on gene expression of male hormone in adult Wistar rats exposure to the oxidative stress by lead acetate. *AL-Qadisiyah Journal of Veterinary Medicine Sciences*, 15(2), 47-52.
- Amália, P. M., Possa, M. N., Augusto, M. C., & Francisca, L. S. (2007). Quercetin prevents oxidative stress in cirrhotic rats. *Digestive diseases and sciences*, 52(10), 2616-2621.
- Amália, P. M., Possa, M. N., Augusto, M. C., & Francisca, L. S. (2007). Quercetin prevents oxidative stress in cirrhotic rats. *Digestive diseases and sciences*, 52(10), 2616-2621.
- Arfat, Y., Mahmood, N., Tahir, M. U., Rashid, M., Anjum, S., Zhao, F., ... & Qian, A. R. (2014). Effect of imidacloprid on hepatotoxicity and nephrotoxicity in male albino mice. *Toxicology reports*, 1, 554-561.
- Baghel, S.S.; N. Shrivastava; R.S. Baghel; P. Agrawal and S. Rajput (2012). A review of quercetin: antioxidant and anticancer properties. *World. J. Phar. Sci.*, 1(1):146–160.
- Bhardwaj, S., Srivastava, M. K., Kapoor, U., & Srivastava, L. P. (2010). A 90 days oral toxicity of imidacloprid in female rats: morphological, biochemical and histopathological evaluations. *Food and chemical toxicology*, 48(5), 1185-1190.
- Cogolludo, A., Frazziano, G., Briones, A. M., Cobeño, L., Moreno, L., Lodi, F., ... & Perez-Vizcaino, F. (2007). The dietary flavonoid quercetin activates BKCa currents in coronary arteries via production of H<sub>2</sub>O<sub>2</sub>. Role in vasodilatation. *Cardiovascular research*, 73(2), 424-431.

- El-Ela, F. I. A., & Abdel-Aziz, A. M. (2019). Investigating the potential protective effects of natural product quercetin against imidacloprid-induced biochemical toxicity and DNA damage in adults rats. *Toxicology Reports*, 6, 727-735.
- ElMazoudy, R. H., Mohamed, N. A., El-massry, A. A., & Abdelsadek, F. R.(2015). " Quercetin Impairs the Reproductive Potential of Neonatal Male Rats. *Int. J. Pharm. Sci. Rev. Res.*, 31(2): 31-39.
- Guiekep, A. J. N., Kenfack, A., Ngoula, F., Vemo, B. N., Nguemmeugne, K. S., & Tedonkeng, E. P. (2019). Attenuating effects of *Mangifera indica* leaves ethanolic extract against acetamiprid induced reproductive toxicity in male guinea pigs. In *Veterinary Research Forum* (Vol. 10, No. 3, p. 187). Faculty of Veterinary Medicine, Urmia University, Urmia, Iran.
- Gurnani, N., Mehta, D., Gupta, M., and Mehta, B. K. (2014). Natural Products: source of potential drugs. *Afr. J. Basic Appl. Sci*, 6,p: 171-186.
- Heijnen, C.G.; Haenen, G.R.; Oostveen, M.M., R.M., Stalpers, Bast, E.M.(2002). Protection of flavonoids against lipid peroxidation: the structure activity relationship revisited, *Free Radic. Res.*, 36(5) : 575–581.
- Johnson, R., & Corn, M. L. (2015). Bee health: the role of pesticides. Washington, Congressional Research Service, pp: 1-23.
- Kamble, P. R., Mishra, M., Kulkarni, S., & Bhiwgaade, D. A. (2013). Comparative Studies on Cisplatin and Etoposide Treated Liver and Kidney Protein Extract of Rat Under SDS-PAGE Gel Separation. *International. J. Pharm. Pharamceut. Sci.*, 5(30):790-792.
- Kaya, K., Ciftci, O., Cetin, A., Doğan, H., & Başak, N. (2015). Hesperidin protects testicular and spermatological damages induced by cisplatin in rats. *Andrologia.*, 47(7): 793-800.
- Kenfack, A., Guiekep, N. A. J., Ngoula, F., Vemo, B. N., Bouli, E. P., & Pamoal, E. T. (2018). Reproductive toxicity of acetamiprid in male Guinea pig (*Cavia porcellus*). *J Anim Sci Vet Med*, 3(4), 105-111.
- Khoo, N.K.H.; C.R. White; L. Pozzo-Miller; F. Zhou; C. Constance; T. Inoue; R.P. Patel and D.A. Parks (2010). Dietary flavonoid quercetin stimulates vasorelaxation in aortic vessels. *Free Radical Bio. Med.*, 49(3):339-347.
- Kutlu, S., Colakoglu, N., Halifeoglu, I., Sandal, S., Seyran, A. D., Aydin, M., & Yilmaz, B. (2007). Comparative evaluation of hepatotoxic and nephrotoxic effects of aroclors 1221 and 1254 in female rats. *Cell Biochemistry and Function: Cellular biochemistry and its modulation by active agents or disease*, 25(2), 167-172.
- Mahmoud, A. M. (2014). Hesperidin protects against cyclophosphamide-induced hepatotoxicity by upregulation of PPAR $\gamma$  and abrogation of oxidative stress and inflammation. *Canad. J. phys. pharm.*, 92(9):717-724.
- Padmavathy, J., & Devarajan, S. (2017). Natural product as a source of prodrug. *Bangladesh Journal of Pharmacology*, (2),p: 5-12.
- Roohbakhsh, A., Parhiz, H., Soltani, F., Rezaee, R., & Iranshahi, M. (2015). Molecular mechanisms behind the biological effects of hesperidin and

- hesperetin for the prevention of cancer and cardiovascular diseases. *Life sciences*, 124, 64-74.
- Salama, A. K., Omran, O. A., & Osman, K. A. (2013). Pesticides-induced oxidative damage: Possible in vitro protection by antioxidants. *Journal of Toxicology and Environmental Health Sciences*, 5(5), 79-85.
- Sheikh, M. S., Hollander, M. C., & Fornace Jr, A. J. (2000). Role of Gadd45 in apoptosis. *Biochemical pharmacology*, 59(1), 43-45.
- Shi, X., Liao, S., Mi, H., Guo, C., Qi, D., Li, F., ... & Yang, Z. (2012). Hesperidin prevents retinal and plasma abnormalities in streptozotocin-induced diabetic rats. *Molecules*, 17(11), 12868-12881.
- Singh, S. B., & Kulshrestha, G. (2005). Residues of Thiamethoxam and Acetamaprid, Two Neonicotinoid Insecticides, in/on Okra Fruits (*Abelmoschus esculentus*L). *Bulletin of environmental contamination and toxicology*, 75(5), 945-951.
- Tabeshpour, J., Hosseinzadeh, H., Hashemzaei, M., & Karimi, G. (2020). A review of the hepatoprotective effects of hesperidin, a flavanon glycoside in citrus fruits, against natural and chemical toxicities. *DARU Journal of Pharmaceutical Sciences*, 28(1), 305-317.
- Tabeshpour, J., Hosseinzadeh, H., Hashemzaei, M., & Karimi, G. (2020). A review of the hepatoprotective effects of hesperidin, a flavanon glycoside in citrus fruits, against natural and chemical toxicities. *DARU Journal of Pharmaceutical Sciences*, 28(1), 305-317.
- Winkel-Shirley, B. (2001). Flavonoid biosynthesis. A colorful model for genetics, biochemistry, cell biology, and biotechnology. *Plant. Physiol.*, 126(2):485-493.
- Zanwar, A. A., Badole, S. L., Shende, P. S., Hegde, M. V., & Bodhankar, S. L. (2014). Cardiovascular effects of hesperidin: A flavanone glycoside. In *Polyphenols in human health and disease* (pp. 989-992). Academic Press.
- Zheng, X., Zhang, Y., Chen, Y. Q., Castranova, V., Shi, X., & Chen, F. (2005). Inhibition of NF- $\kappa$ B stabilizes gadd45a mRNA. *Biochemical and biophysical research communications*, 329(1), 95-99.
- Zhou, W. Yu, Y.J. Xie, M.F .Li,X.W. Li,Y. Duan, G.L.(2011). Determination of Hesperidin from Pericarpium Citri Reticulatae Microwave Assisted Extraction by High Performance Liquid Chromatography. *Heral. Med.*, 30(5) :64-640.



**ISOLATION AND MOLECULAR IDENTIFICATION OF THE CAUSAL  
AGENTS OF FUSARIUM HEAD BLIGHT OF WHEAT IN AL-QAYYARAH  
SUB DISTRICT , NINEVAH GOVERNORATE**

**SALIM I. AKRAM  
ALI K. AL-TAAE  
KARKAZ M. THALIJ**

**ISOLATION AND MOLECULAR IDENTIFICATION OF THE CAUSAL AGENTS OF  
FUSARIUM HEAD BLIGHT OF WHEAT IN AL-QAYYARAH SUB DISTRICT,  
NINEVAH GOVERNORATE**

**Salim I. AKRAM<sup>1</sup>**

**Ali K. AL-TAAE<sup>2</sup>**

**Karkaz M. THALIJ<sup>3</sup>**

**Abstract:**

The current work was conducted on Fusarium head blight disease of wheat that was caused by Fusarium species. A survey was carried out of several wheat fields at AL-Qayyarah sub District, Ninevah Governorate during two growth stages of wheat (Booting to Heading) From the middle of April to May, and (Ripening) the second phase of the period from May to the beginning of June during the growing season 2019-2020. The highest disease incidence in both stages was 42.826% and 61.92%, respectively). The lowest disease incidence in the first period was recorded in (6.864%) and increased to (11.162%) in the second period. *F. graminearum* was isolated from spikes in high frequency 26.902%. *F. culmorum* was isolated from spikes in high frequency 26.03%, Fusarium spp. were isolated from all wheat fields in both stages. Pathogenicity of the fungus in wheat plants was also confirmed by Koch's postulates. Molecular identification of Fusarium isolates was done by amplifying the internal transcribed spacer (ITS) region of the conserved ribosomal DNA using primers ITS1 and ITS4. All the ITS sequences were compared for gaps and similarity sequences of the fungus were homologous to those of *F. graminearum* and *F. culmorum* isolates in the GenBank database with a similarity percentage of 99%, thereby confirming the identity of the causative agents of the disease. This could be the first recording of *F. graminearum* and *F. culmorum* on the wheat in AL-Qayyarah sub District, Ninevah Governorate, in Iraq. The nucleotide sequence of ITS from the Iraqi isolate has been assigned GenBank Accession No MW737663.1.and MW737664.1. respectively.

**Key words:** Fusarium head blight ,Wheat, Fusarium spp.



<http://dx.doi.org/10.47832/MinarCongress5-2>

<sup>1</sup> Ministry of Trade, Iraq

<sup>2</sup> University of Mosul, Iraq; [Prof.ali@uomosul.edu.iq](mailto:Prof.ali@uomosul.edu.iq)

<sup>3</sup> University of Tikrit, Iraq



## **Introduction:**

Fusarium head blight (FHB) is one of the main fungal diseases of grain crops such as wheat, barley and maize. The FHB species complex produces mycotoxins that cause quality and yield reductions, as well as human and animal health risks. FHB is economically one of the most important diseases of wheat throughout the world. Epidemics of FHB over the past 15 years in North America have had a devastating economic impact on agriculture (Leslie and Summerell, 2006). Many FHB outbreaks have been reported in Canada, Asia, Europe, Australia, and South America suggesting that it is a major threat to world grain production (Booth, 1971). Fusarium head blight is caused by several *Fusarium* spp. such as *F. graminearum*, *F. sporotrichioides*, *F. culmorum*, *F. cerealis*, *F. avenaceum*, *F. equiseti*, and *F. poae* (Leslie and Summerell, 2006).

Until the year 2000, members of the FGSC were considered a single cosmopolitan species as morphological approaches to species identification failed to accurately delimit species for this group. However, with the advances in DNA sequencing technology, sequence similarity at one or more diagnostic loci has become an important tool in determining the species limits with *Fusarium* spp. (Chekali et al., 2011).

The sequences most widely used to identify species of *Fusarium* are portions of DNA sequences encoding EF-1, tubulin, internally transcribed spacer (ITS) regions in the ribosomal DNA repeat region (ITS1 and ITS2), histone H3, and trichothecene biosynthesis genes, especially TRI101 (O'Donnell et al. 2004, O'Donnell et al. 2000).

Fusarium head blight (FHB) is an essential disease in crop productivity of world which is caused by many *Fusarium* species. Most problems of diseases are contamination by a different *Fusarium* mycotoxin which happens already when the crops are growing in the fields. In recent years levels of high mycotoxins, especially of the mycotoxin DON, found in Sweden (McMullen et al., 1997) This causes economic damage loss for farmer because the contaminated grain cannot be sold for feed or food. FHB leads to a decrease in return and germination; FHB is a disease occurs before harvest, but *Fusarium* types can also activate after harvest, grow fungus if wet grains are not dried quickly and efficiently (Chakraborty et al., 2006). This disease affects the return where cereals are in abnormal and unclear (O'Donnell, et., 2004). The disease reduces the nutritional value by reducing the quality of bread and the deterioration of proteins (Bailey et al., 1989), crops are vulnerable to *Fusarium* spp. Thus, the weather at this stage is one of the basic risk to the development of this disease. Wet the wet and warm weather during the facilitated *Fusarium graminearum* and Pollution DON Toxin. (Sura, 2021). The Fungal *F. graminearum* is the most common cause of FHB in USA on wheat crop but *F. culmorum* is a common in Europe (Obanor, et al., 2013). On the Durum Wheat in 2004, a survey conducted in these areas showed that 78% of them were infected, and the results of molecular and morphological diagnosis showed it where the most common on Wheat spikes *F. culmorum* by 63.5% and *F. pseudograminearum* by 26% and *F. avenaceum* by 9% and *Microdochium nivale* by 1.5% (Burgess et al., 2001).

## Materials and methods

**Field survey and sampling:** A survey was carried out on the wheat fields of AL-Qayyarah sub District, Ninevah Governorate samples were collected in two periods depended on the plant growth stage according to Zadoks scale-1 (Booting to heading, scale 40-59) in April to May 2-Ripening (Growth stage, scale 90-99) in May to June during crop season 2019-2020. Ten fields were selected randomly, field size of approximately 5-10 hectares. At each field five sampling points were made in W pattern. At each of the five points 25 plants were collected, the total number of each field was 125 plants depending on leaves yellowing and crown rot symptoms appear obviously, with browning roots and discolored sub-crown internode. Samples were removed with as much of the root system as possible and kept in cold and dry place separately from each point, with labeling name of location, wheat cultivar, date of planting, date of sampling.

**Isolation and Diagnosis:** Yellowing with lack of branching, discoloration of the internodes under the crown and leaf sheaths in dark brown symptoms were observed in AL-Qayyarah sub District, Ninevah Governorate, Iraq. Samples were taken from infected wheat seedlings. Infested root and spike, samples were sterilized by dipping in 1% NaOCl solution for 3–5 min and washed thrice with sterile water. The tissue was cut with a sterile blade to five pieces of diseased vascular tissue (*ca.*5×5 mm) and placed on the surface of potato dextrose agar (PDA, HiMedia, Mumbai) media. PDA was amended with tetracycline sulfate to minimize chances of any bacterial growth. Plates were incubated at  $28 \pm 2$  °C and observed periodically, the fungal growth was purified for the purpose of definition and use in subsequent experiments. For morphological identification, single spore isolates were grown for 10–15 days on PDA medium, Mold culture characteristics were determined from 10 to 15 day growth on PDA media. Microscopic features of conidia conidiophores and macroconidia chlamydospores were also determined based on (Waalwijk, 2003) .

**Pathogenicity tests:** The pathogenicity of fungal isolates was tested on wheat seedlings at the one-true-leaf stage. Their roots were dipped into a conidial suspension (**10<sup>7</sup> microconidia/ml**) of the test isolate for 30 min, after which seedlings they were incubated at  $28 \pm 2$  °C and observed Until the infect appears.

### Genomic DNA extraction and PCR amplification:

Pure cultures of *Fusarium* were grown in potato dextrose broth (PDB) for 12 days at 25–28°C in the dark environmental. Mycelia were harvested by filtration through filter paper (Whatman No. 1). The harvested mycelia were used immediately for DNA extraction using Fungal/Bacterial/ Yeast Quick- DNA MiniPrep™, Catalog No. D6005 according to the USA Zymo Research procedures Protocol blew:

For optimal performance, add beta-mercaptoethanol (user supplied) to the Fungal/Bacterial DNA Binding Buffer to a final dilution of 0.5%(v/v) *i.e.*, 500 µl per 100 ml. then complete the fungal DNA extraction according to the recommendation from the manufactured company. Electrophoresis has been done to determine DNA fragment after the its extraction used the agarose gel at 1.5% according to Sambrook *et al* (Sambrook, et. al.,1989).

**Preparation of sample:** Three µl of the processor loading buffer (Intron/Korea) has been mixed with 5 µl of the supposed DNA to be electrophoresis

(loading dye). An Electric current of 7 v\c2 has been exposed for 1-2 h till the tincture has reached to the other side of the gel. The gel has been tested by a UV light at 336 nm after used the 3µl of Red safe Nucleic acid staining solution and 500 ml from distilled water.

**Detection of Gene ITS Using PCR:** Detection of *ITS* gene was conducted by using primers for amplification. A fragment of *ITS* was amplified using a forward primer (*ITS1* F: 5'TCCGTAGGTGAACCTGCGG -3') and a reverse primer (*ITS4* R: 5' TCCTCCGCTTATTGATATGC-3') (Supplied by IDT, Integrated DNA Technologies company, Canada). The PCR amplification was performed in a total volume of 25µl containing 1.5µl DNA, 5 µl Taq PCR PreMix (Intron, Korea), 1µl of each primer (10 pmol) then distilled water was added into tube to a total volume of 25µl. The thermal cycling conditions were done as follows: Denaturation at 94 °C for 3 min, followed by 35 cycles of 94 °C for 45s, 52°C for 1 min and 72 °C for 1min with final incubation at 72 °C for 7 min using a thermal Cycler (Gene Amp, PCR system 9700; Applied Biosystem). The PCR products were separated by 1.5% agarose gel electrophoresis and visualized by exposure to UV light at 302 nm after staining with the red stain (Intron Korea).

**Sequencing and Sequence Alignment:** The PCR products were separated on a 2% agarose gel electrophoresis and visualized by exposure to UV light at 302 nm after staining with the red stain. Sequencing of gene was performed by national instrumentation center for environmental management (nicem) online at (<http://nicem.snu.ac.kr/main/?En-skin=index.html>), biotechnology lab, machine is DNA sequencer 3730XL, Applied Biosystem), Homology search was conducted using Basic Local Alignment Search Tool (BLAST) program which is available at the National Center Biotechnology Information (NCBI) online at (<http://www.ncbi.nlm.nih.gov>) and BioEdit program.

## **Results and Discussion**

**Field survey:** Results of the field survey were showed that in the booting to heading plant growth (first survey), the highest disease incidence and severity were at 11.475% and 0.0918, While in the ripening stage appeared the maximum disease incidence and severity reached at 17.1092% and 0.13712 respectively(Table 1). Results of field survey indicated that happen a high level of presence and distribution of disease in AL-Qayyarah sub District.

Location	Field	Records1		Records2	
		Incidence	Severity	Incidence	Severity
AL-Qayyarah sub District, Ninevah Governorate	1	42.826	0.3082	61.92	0.4696
	2	0.0	0.0	0.0	0.0
	3	32.712	0.2776	51.614	0.4066
	4	6.864	0.0534	11.162	0.0812
	5	0.0	0.0	0.0	0.0
	6	0.0	0.0	0.0	0.0
	7	32.348	0.2794	47.026	0.4138
	8	0.0	0.0	0.0	0.0
	9	0.0	0.0	0.0	0.0
	10	0.0	0.0	0.0	0.0
	Average	11.475	0.0918	17.1092	0.13712

this might be done because the semiarid conditions in this locally, which help the occurrence of the disease that causing in reduction the root density and crown rot ,Other factors associated with the prevalence of specific *Fusarium* species on wheat such as cropping history, climatic conditions especially soil moisture and temperature, host susceptibility, and fungal pathogenicity. Also plant debris and infected seeds are essential for fungi survival and represent as sources of inoculum for next cropping (Akinsanmi, et. al.,2014), especially when residue does not decompose completely or when monoculture is used because the inoculum potential of *F.graminearum* and *F.culmorum* increased in non-decomposed plant residues (Warren and Kommedahl, 1973).

**.Isolation and Diagnosis:** Species is isolated *Fusarium graminearum* and *Fusarium culmorum* from spikes in high frequency at 26.902 %and 26.03% respectively,as it appeared in the Isolation of other fungus genus(Table2).Colony characters were appeared on potato dextrose agar (PDA) media as white to pale yellow, rose, at the first incubation period and becoming brown at aged colony with dense mycelium on the surface and creamy color on the bottom (Fig. 1-A,D).The microscopic examination, of the fungal smear was investigated the conidia of the fungus and it was appeared in two types, the first was Macroconidia: that appeared slender to falcate, apical cell tapered and the basal cell foot shaped, dorsal side smooth and curved,ventral side straight, that produced from lateral phialides which may become grouped on branched conidiophores; three septate, 37–32.5×3.7µm five to seven septate 5–3.7×35–48µm, (Fig.1-B,E).And the Microconidia: was absent. Also, the Chlamydospores: that slow to form, usually formed in macroconidia but also formed in mycelium (10-12 5µm, (Fig. 1-C,F). The same or most of these characters were also shown on carnation leaf-piece agar (CLA) which is another media we used for identificationThese characteristics correspond to *Fusarium graminearum* and *Fusarium culmorum* and were in agreement to Booth, (Booth,1971) and (Leslie and Summerell ,2006) ,*F. graminearum* has been reported as a severe pathogen of many plants worldwide, as well as in Iraq. The registration of *F. graminearum* and *Fusarium culmorum* on wheat were firstly recorded in

Ninevah Governorate, in spite, they has been report in different part of Iraq (Sura,2021; Taha,2014).

No.	Fungal species	%
1	<i>Fusarium graminearum</i>	26.902
2	<i>Fusarium culmorum</i>	26.03
3	<i>Alternaria spp</i>	13.96
4	<i>Aspergillus spp</i>	8.011
5	<i>Trichoderma spp</i>	11.267
6	<i>Cladosporium spp</i>	6.904
7	<i>Stemphylium spp</i>	6.904

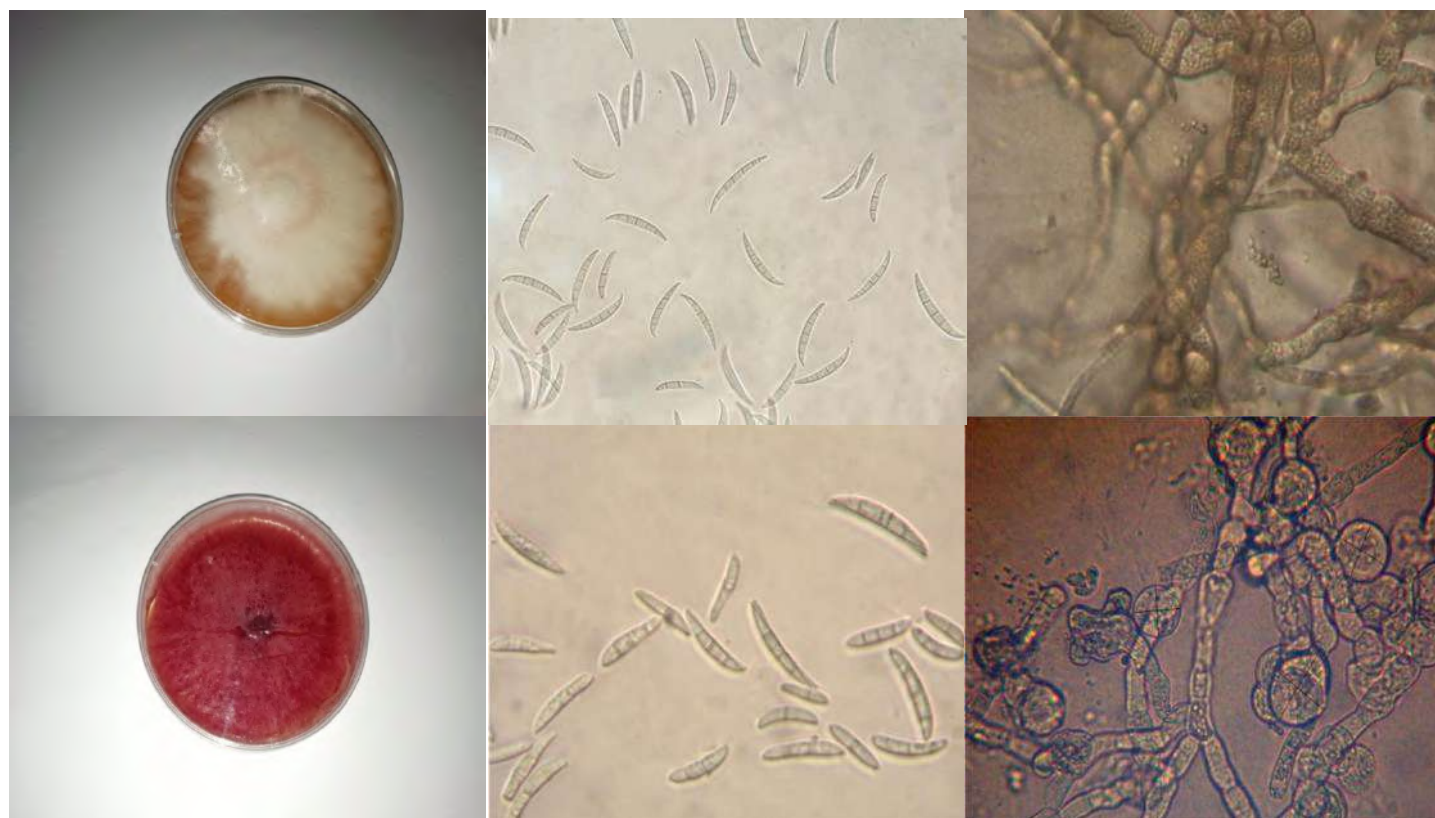


Fig 1. A, 1-week-old *F.graminearum* colony growing on agar media of potato dextrose; B, Macroconidia; C, Conidiophores and Chlamydospores; D, *F.culmorum* colony growing on agar media of potato dextrose;E, Macroconidia;F, Conidiophores and Chlamydospores.

**Fungal pathogenicity results:** The symptoms of the pathogenicity of fungal species was appeared as yellowing and wilt and wet in the leaves followed by paleness and dryness of the leaves and stems, after one month of the emergence of symptoms of infection, then begin the symptoms appeared from one side of the plant, and when cutting in the stem and roots of the infected plant were observed the brown color in wooden vessels(Fig. 1-D).. To prove that Koch's postulates were true, the final colony and conidia characteristics were analyzed to confirm that the fungal isolates was the same with what had been used for the pathogenicity test.

## Sequencing and Sequence Alignment

To confirm the morphological identification, the internal transcribed spacer (ITS) region of the *Fusarium* isolate was amplified with universal primers ITS1 and ITS4. The isolate was partially diagnosed after conformity with the copies of the gene bank at National Center Biotechnology Information (NCBI). The genes were gave 99% (diagnostic accuracy) match with isolation KY272845.1 and the Query cover of the sequence was at 99% Error Value 0.0. The results obtained showed that 2 variations: first C>A second T>G, Transversion have shown 99% compatibility as showed in table 1 and Fig.1.

**Table(1) Represent Type of Polymorphism of 16srRNA Gene from *Fusarium graminearum* Isolate**

Gene: 18S ribosomal RNA gene						
No.	Type of substitution	Location	Nucleotide	Sequence ID with compare	Source	Identities
1	Transversion; Transition	378	N(A,G,C,T)\C	ID: <a href="#">MN452715.1</a>	<i>Fusarium graminearum</i>	99%

***Fusarium graminearum* isolate W\_IASO2\_2\_16 internal transcribed spacer 1, partial sequence; 5.8S ribosomal RNA gene and internal transcribed spacer 2, complete sequence; and large subunit ribosomal RNA gene, partial sequence**

**Sequence ID: [MN452715.1](#) Length: 526 Number of Matches: 1**

Range 1: 18 to 523 [GenBankGraphics](#) [Next Match](#) [Previous Match](#)

Score	Expect	Identities	Gaps	Strand
910 bits(1008)	0.0	505/506(99%)	0/506(0%)	Plus/Plus

Query  
CTCCCAAACCCCTGTGAACATACCTTAATGTTGCCTCGGCGGATCAGCCC GCGCCCCGTA 60 1

Sbjct 18 ..... 77

Query  
AAACGGGACGGCCCGCCAGAGGACCCAAACTCTAATGTTTCTTATTGTA ACTTCTGAGTA 120 61

Sbjct 78 ..... 137

Query  
AAACAAACAAATAAATCAAACTTCAACAACGGATCTCTTGTTCTGGCATCGATGAAG 180 121

Sbjct 138 ..... 197

Query  
AACGCAGCAAATGCGATAAGTAATGTGAATTGCAGAATTCAGTGAATCATCGAATCTTT 240 181

Sbjct 198 ..... 257

Query  
GAACGCACATTGCGCCCGCTGGTATTCCGCGGGCATGCCTGTTGAGCGTCATTTC AAC 300 241

Sbjct 258 ..... 317

Query 301  
 CCTCAAGCCCCGGGTTTGGTGTGGGGATCGGCTCTGCCCTTCTGGGCGGTGCCGCCC 360  
 Sbjct 318 ..... 377

Query 361  
 CGAAATACATTGGCGGTCTCGCTGCAGCCTCCATTGCGTAGTAGCTAACACCTCGCAACT 420  
**Sbjct 378 N**..... 437

Query 421  
 GGAACGCGCGCGGCCATGCCGTA AACCCCAACTTCTGAATGTTGACCTCGGATCAGGT 480  
 Sbjct 438 ..... 497

Query 481 AGGAATACCCGCTGAACTTAAGCATA 506  
 Sbjct 498 ..... 523

**Figure (1): Sequencing of sense flanking the partial ITS gene compared with standard MN452715.1 gene, obtained from Gene Bank. Query represents of sample; Subject represent of database of National Center Biotechnology Information (NCBI).**

**Table(2) Represent Type of Polymorphism of 16srRNA Gene from *Fusarium culmorum* Isolate**

Gene: 18S ribosomal RNA gene						
No.	Type of substitution	Location	Nucleotide	Sequence ID with compare	Source	Identities
2	Transition	352	T\C	ID: <a href="#">MT032704.1</a>	Fusarium culmorum	99%

**Fusarium culmorum isolate 2268\_ITS1\_D09\_037.ab1 small subunit ribosomal RNA gene, partial sequence; internal transcribed spacer 1, 5.8S ribosomal RNA gene, and internal transcribed spacer 2, complete sequence; and large subunit ribosomal RNA gene, partial sequence**

**Sequence ID: [MT032704.1](#) Length: 562 Number of Matches: 1**

Range 1: 41 to 538 [GenBankGraphics](#) Next Match Previous Match

**Sequence ID: MT032704.1**

Score	Expect	Identities	Gaps	Strand
894 bits(991)	0.0	497/498(99%)	0/498(0%)	Plus/Plus

Query 1  
 ACTCCCAAACCCCTGTGAACATACCTTAATGTTGCCTCGGCGGATCAGCCCGCGCCCCGT 60  
 Sbjct 41 ..... 100

Query 61  
 AAAACGGGACGGCCCGCCAGAGGACCCAAACTCTAATGTTTCTTATTGTAACCTCTGAGT 120  
 Sbjct 101 ..... 160

Query 121  
 AAAACAAAACAAATAAATCAAACTTTCAACAACGGATCTCTTGGTTCTGGCATCGATGAA 180  
 Sbjct 161 ..... 220

Query 181  
 GAACGCAGCAAATGCGATAAGTAATGTGAATTGCAGAATTCAGTGAATCATCGAATCTT 240  
 Sbjct 221 ..... 280

Query 241  
 TGAACGCACATTGCGCCCGCTGGTATTCCGGCGGGCATGCCTGTTTCGAGCGTCATTCAA 300  
 Sbjct 281 ..... 340

Query 301  
 CCCTCAAGCCCCGGGTTTGGTGTGGGGATCGGCTCTGCCTTCTGGCGGTGCCGCCCC 360  
**Sbjct 341 .....T..... 400**

Query 361  
 GAAATACATTGGCGGTCTCGCTGCAGCCTCCATTGCGTAGTAGCTAACACCTCGCAACTG 420  
 Sbjct 401 ..... 460

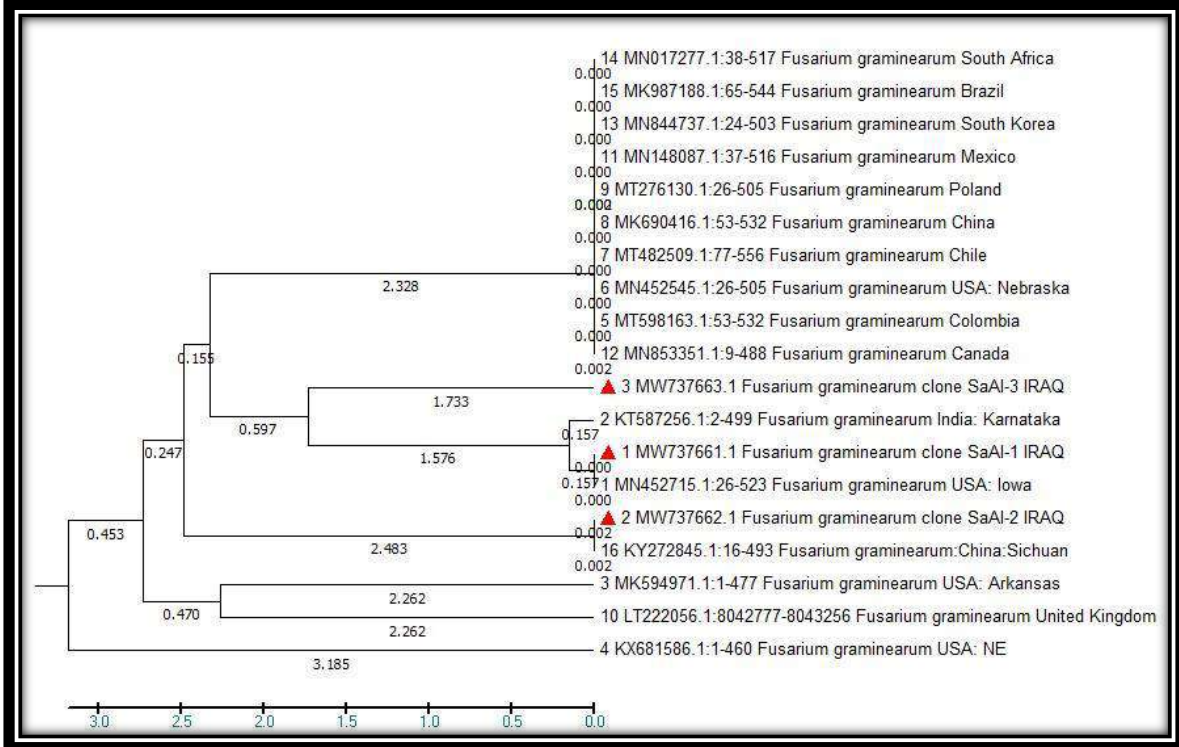
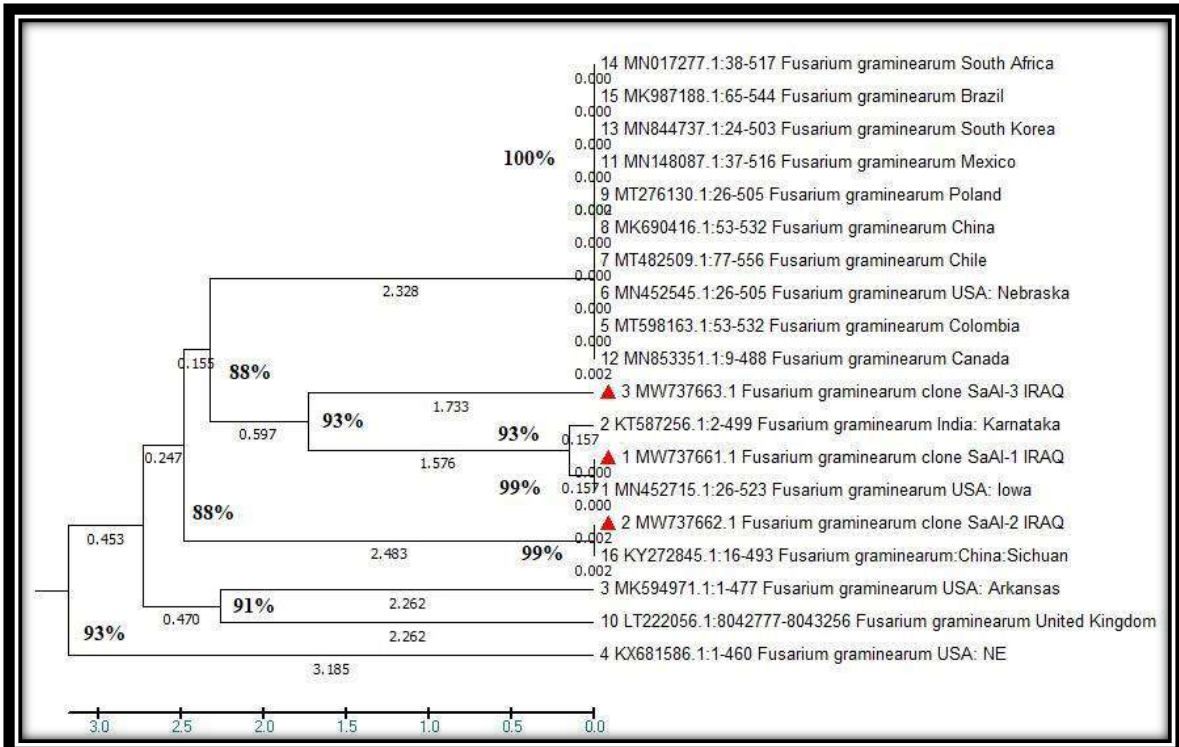
Query 421  
 GAACGCGGCGCGCCATGCCGTAACCCCAACTTCTGAATGTTGACCTCGGATCAGGTA 480  
 Sbjct 461 ..... 520

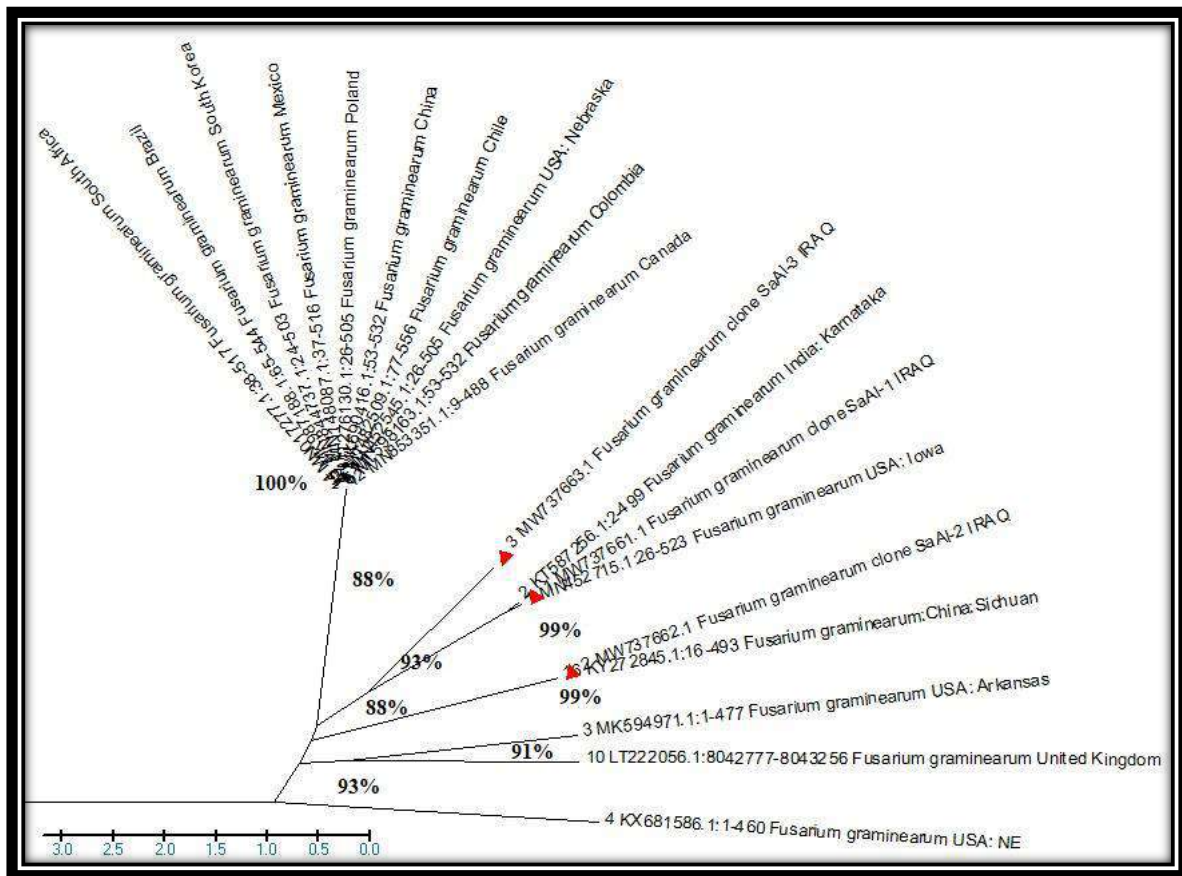
Query 481 GGAATACCCGCTGAACTT 498  
 Sbjct 521 ..... 538



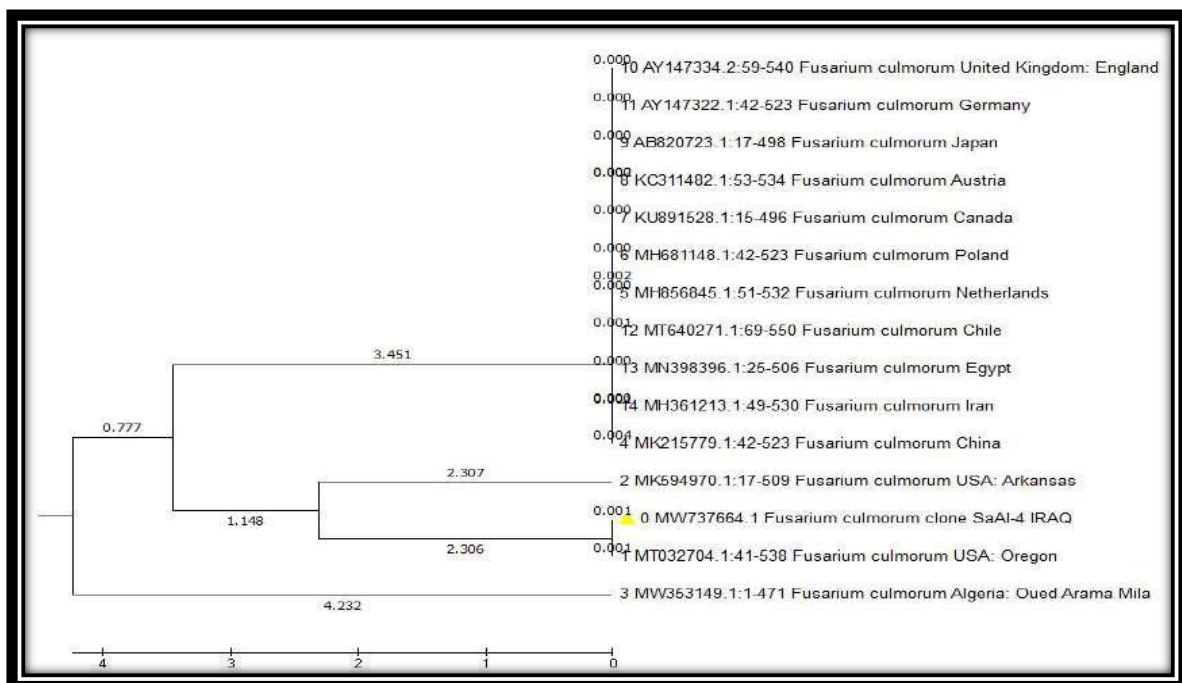
**Figure (2): Sequencing of sense flanking the partial ITS gene compared with standard MT032704.1 gene, obtained from Gene Bank. Query represents of sample; Subject represent of database of National Center Biotechnology Information (NCBI).**

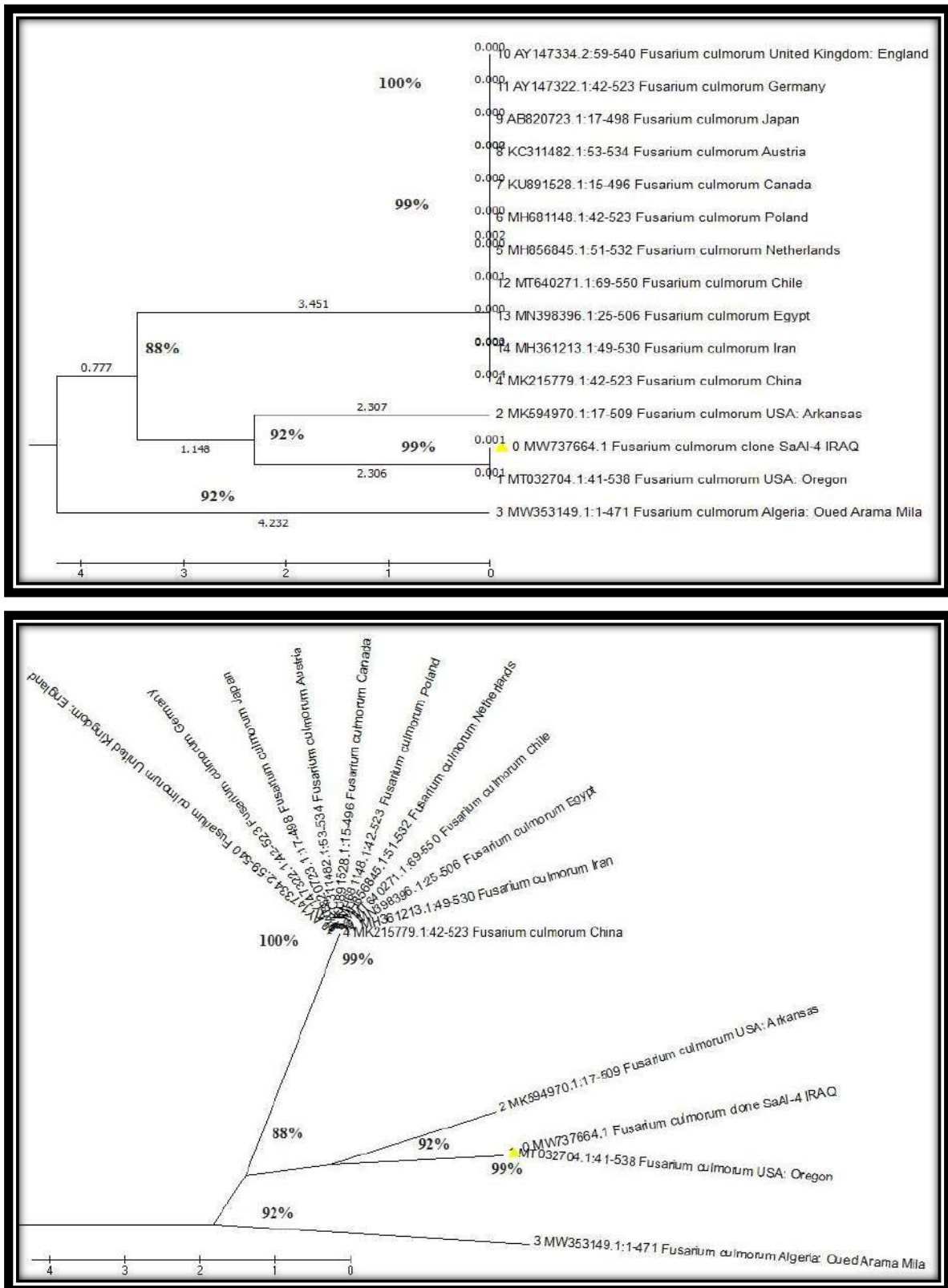
Results showed the close genetic relationship among *F. graminearum* isolated in this study (indicated with black prism) and those worldwide deposited in GenBank database. Figure (3) represents comparison between local Iraqi isolate strain of *F. graminearum* with the strain *F. graminearum* recorded in the National Center Biotechnology Information (NCBI) and isolated from different countries showed compatibility 99% with *F. graminearum* strains accession Nos **MN452715.1** from USA . The nucleotide sequence of ITS from the Iraqi isolate has been assigned GenBank Accession No MW737663.1. Thus, *F. graminearum* was identified as the causative agent of Fusarium head blight of wheat in AL-Qayyarah sub District, Ninevah Governorate, Iraq. (Fig. 4), also Results showed the close genetic relationship among *F. culmorum* isolated in this study (indicated with black prism) and those worldwide deposited in GenBank database. Figure (5) represents comparison between local Iraqi isolate strain of *F. culmorum* with the strain *F. culmorum* recorded in the National Center Biotechnology Information (NCBI) and isolated from different countries showed compatibility 99% with *F. culmorum* strains accession Nos **MT032704.1** from USA . The nucleotide sequence of ITS from the Iraqi isolate has been assigned GenBank Accession No MW737664.1. Thus, *F. culmorum* was identified as the causative agent of Fusarium head blight of wheat in AL-Qayyarah sub District, Ninevah Governorate, Iraq(Fig. 4), To the best of our knowledge, this is the first report of Fusarium head blight of wheat in AL-Qayyarah\_\_\_\_\_sub District, Ninevah Governorate, Iraq.





**Figure (3): Phylogenetic tree constructed by the neighbor-joining method showing the phylogenetic relationships of *Fusarium graminearum* compared with the reference sequences from gene bank.**






**Figure (4):**Phylogenetic tree constructed by the neighbor-joining method showing the phylogenetic relationships of *Fusarium culmorum* compared with the reference sequences from gene bank.

## References

1. **Akinsanmi, O. A., Mitter, V., Simpfendorfer, S., Backhouse, D. and Chakraborty, S. (2004).** Identity and pathogenicity of *Fusarium spp.* isolated from wheat fields in Queensland and northern New SouthWales. *Aust. J. Agric. Res.* 55: 97-107.
2. **Bailey, K. L., Harding, H. and Knott, D. R. (1989).** Disease progression in wheat lines and cultivars differing in levels of resistance to common root rot. *Canadian Journal of Plant Pathology*, 11: 273-278.
3. **Booth, C. (1971).** The Genus *Fusarium*. Commonwealth Mycological Institute, Kew, Surrey, England, 237pp.
4. **Burgess L.W., Backhouse D., Summerell B.A. and Swan L.J. (2001).** Chapter 20 in *Fusarium* - Paul E. Nelson Memorial Symposium. Edited by Summerell B.A., Leslie J.F., Backhouse D. Bryden W.L and Burgess L.W. APS Press, The American Phytopathological Society, St. Paul, Minnesota, United States of America. ISBN 0-89054-268-6. pp.271-294.
5. **Chakraborty, S., Liu, C. J., Mitter, V., Scott, J. B., Akinsanmi, O. A., Ali, S. and Simpfendorfer, S. (2006).** Pathogen population structure and epidemiology are keys to wheat crown rot and *Fusarium* head blight management. *Australasian Plant Pathology*, 35(6): 643-655.
6. **Chekali, S., Gargouri, S., Paulitz, T., Nicol, J. M., Rezgui, M. and Nasraoui, B. (2011).** Effects of *Fusarium culmorum* and water stress on durum wheat in Tunisia. *Crop Protection*, 30(6): 718-725.
7. **Leslie, J.F. and Summerell, B.A. (2006).** *The Fusarium Laboratory Manual*; Wiley-Blackwell: Ames, IA, USA,; pp. 81–96.
8. **McMullen, M.; Jones, R.; Gallenberg, D.; (1997).** America, S. Scab of Wheat and Barley: A Re-emerging Disease of Devastating Impact. *Plant Dis.*, 81.
9. **O'Donnell, K.; Ward, T.J.; Geiser, D.M.; Kistler, H.C.; Aoki, T(2004).** Genealogical concordance between the mating type locus and seven other nuclear genes supports formal recognition of nine phylogenetically distinct species within the *Fusarium graminearum* clade. *Fungal Genet. Biol.*, 41, 600–623.
10. **Obanor, F.; Neate, S.; Simpfendorfer, S.; Sabburg, R.; Wilson, P.; Chakraborty, S. (2013).** *Fusarium graminearum* and *Fusarium pseudograminearum* caused the 2010 head blight epidemics in Australia. *Plant Pathol.*, 62, 79–91.
11. **Sambrook, J., E.F. Fritsch and T. Maniatis (1989).** *Molecular Cloning: A Laboratory Manual*, 2nd ed. Cold Spring Harbor Laboratory, Cold Spring Harbor, NY.
12. **Sura ,M, AL Turaihy (2021)** Study of the common root rot disease and its control with some biological control factors in wheat growing areas in Iraq .Ph.D. thesis, College of Agriculture Engineering Sciences - University of Baghdad , Iraq.(In Arabic).
13. **Taha, Z.A. (2014).** Wheat root rot in Ninevah government and its biological control. M.Sc.

14. thesis, College of Agriculture and Forestry, University of Mosul, Iraq.(In Arabic).
15. **Waalwijk, C. ; P. Kastelein ; I. Devries ; Z. Kerenyi ; T. Vander-Lee ;T.Hesseelink ; J. Kohl and G. Kema (2003)** . Major changes in *Fusarium* spp. in wheat in the Netherlands . Plant Pathology 109 : 743 – 754 .
16. **Warren, H. L. and Kommedahl, T.(1973)**.Fertilization and wheat refuse effects on *Fusarium* species associated with wheat roots in Minnesota. Phytopathology. 63:103-108.

A petri dish containing a bacterial culture of Pseudomonas aeruginosa on a green agar medium. The culture shows numerous small, circular, yellowish-green colonies. The text is overlaid on the image.

**STUDY THE ANTIBACTERIAL ACTIVITY OF ALCOHOLIC EXTRACT OF  
ALLIUM SATIVUM ON PSEUDOMONAS AERUGINOSA AND COMPARE  
WITH SOME ANTIBIOTICS**

**LUMA SAEED MOHAMMED**

**STUDY THE ANTIBACTERIAL ACTIVITY OF ALCOHOLIC EXTRACT OF ALLIUM SATIVUM ON PSEUDOMONAS AERUGINOSA AND COMPARE WITH SOME ANTIBIOTICS**

**Luma Saeed MOHAMMED**<sup>1</sup>

**Abstract:**

Twenty isolate of *P.aeruginosa* isolated from Baghdad hospitals identified morphologically and biochemical tests then vitek system. Disk diffusion method carried out to determined the sensitivity of bacterial isolates to different antibiotics like amoxicillin, ciprofloxacin, meropenem and cefotaxim by using Muller-Hinton agar, the results showed that 100% of isolates had resistance to amoxicillin, 40% of resistance to cefotxim, 20% of resistance to ciprofloxacin and meropenem. Agar well method used to determined the minimal inhibitory concentrations for alcoholic extract of *Allium sativum* which prepared by using aqueous ethanol by soxhlet extractor ,it had inhibition effect in 50, and 25 mg/ml, the diameter of inhibition zone on agar were 15-9 mm.

**Key words:** Antibiotics Resistance, *Allium Sativum*.



<http://dx.doi.org/10.47832/MinarCongress5-3>



<sup>1</sup> University of Baghdad, Iraq, [luma.saeed@sc.uobaghdad.edu.iq](mailto:luma.saeed@sc.uobaghdad.edu.iq), <https://orcid.org/0000-0001-6410-1239>



### **Introduction:**

*Pseudomonas aeruginosa* is a Gram-negative, aerobic bacteria related to *Pseudomonadaceae* (1). It is isolated from clinical and non clinical sources (2). It is causative agent for infection in humans, its antibiotics resistance, virulence factors and adaptation to different factors of environments, it have different natural and acquired resistance mechanisms to multiple antibiotic groups such as efflux pump (3). This bacteria is an important cause of different infections as a result of its ability to form biofilms, because this bacteria found in aggregates of extracellular matrix, thus it is difficult to eliminate by antibiotics (4). It is an opportunistic pathogen and a central cause of hospital-acquired infections. There are range of antibacterial properties such as antibiofilm; antitoxin and bactericidal activity toward multidrug resistant bacteria (5).

### **Methods:**

**isolated of bact.:** one hundred samples (burns and urine) take from hospital.

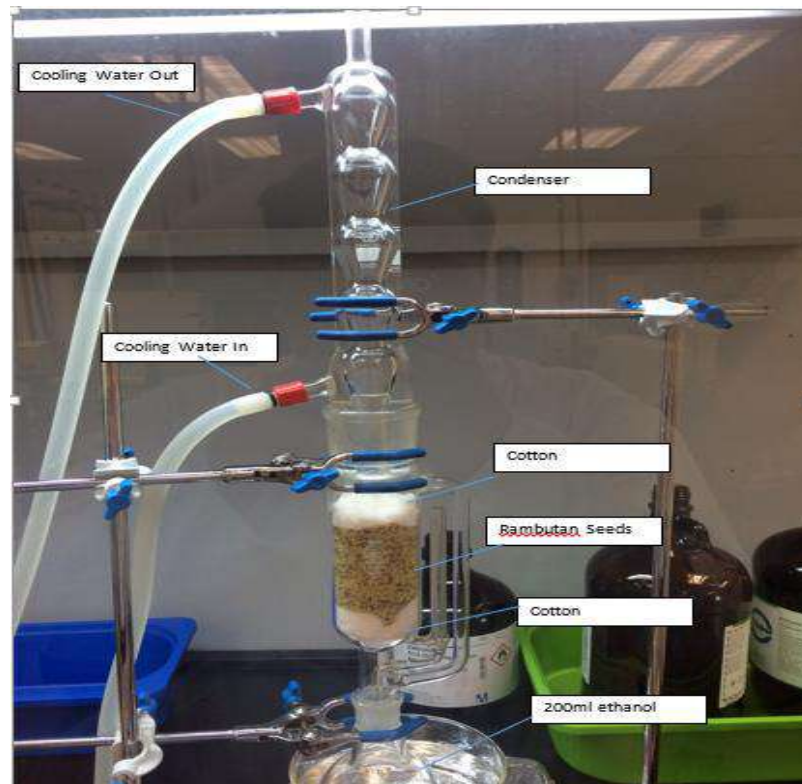
**Identification of bacteria :** bacteria identified by morphology and biochemical tests like Gram stain, oxidase, catalase, urease test, IMVIC tests, pigments, coagulase, and hemolysin (6), identification was confirmed with vitek 2 compact system.

### **Sensitivity Tests By Antibiotic:**

Kirby-Bauer method had been carried out colonies from over night culture. culture of bacteria were put in tubes contain 5 ml of saline to obtain  $1.5 \times 10^8$  CFU/ml in culture (0.5 McFarland tube). Inoculated the plates with a sterile swab, discs of antibiotics were applied on plates then Incubated for (18-24) hours. the diameter of inhibition zones were measured in millimeter (7).

### **Preparation of plant extract and Soxhlet Extraction:**

**A.sativum** dried powder was used, 25.0gram of it was extracted with 200 ml of (80%) v/v ethanol with the using of soxhlet extractor for 8 hours figure (1), extract then dried in 40 C 0 by oven. (8).



**Figure (1): alcoholic extraction of *A.sativum***

#### **Determination of MIC of plant extract:**

Macro dilution method used to determined MIC of extracts. Muller-Hinton broth tubes with plant extract, inoculated with bacteria. then incubated, then examined by turbidity. Minimum inhibitory concentration of extract was the first clear tube, negative and positive control were used for comparison.

#### **Antimicrobial activity of *A.sativum* :**

Well method was used to detrmined the antibacterial activity of ***A.sativum*** against *P.aeruginosa* Mueller-Hinton agar plates used in this experement. 8 millimeter well were made in plates after spreading of bacteria,plant extract were applied as 25 and 50 mg/ml in wells. Antibacterial activity estimat through the diameter of the zone around these wells (9).

#### **Results and Discussion:**

##### **Isolation and identification of bacteria:**

One hundred of clinical samples collected from hospitals during 2020.

##### **Identification by biochemical tests:**

The result showed that *A.sativum* isolates were Gram negative rods, positive tests to catalase, oxidase,citrate,gelatin and nitrate reduction hydrolysis and gave negative results for indole, urease,MR,VP, twenty isolate were *P.aeruginosa*.

### **Antibiotics sensitivity test:**

All isolates were resistance to amoxicillin, while 40% resistance to cefotxim,, 20% were resistance to ciprofloxacin, meropenem. Other studies recorded that there was 100% of resistance to ampicillin, tetracycline, penicillin and cloxacillin (10). In this study meropenem and ciprofloxacin had a good activity (20% of resistance), while other study reported that there was 75.3% of resistance of *P.aeruginosa* to ciprofloxacin and livofloxacin (11). Ciprofloxacin used to treat a different infections caused by the opportunistic *P. aeruginosa* ,it is related to fluoroquinolone class of antibiotics,this antibiotic inhibit DNA gyrase which is responsible for DNA relaxation and replication (12). Meropenem is a carbapenem antibiotic, meropenem is a broad-spectrum carbapenem antibiotic with excellent activity against many pathogens (13).

### **Antibacterial activity of *A.sativum*:**

*A.sativum* extract with ethanol (80%) at concentrations (50 and 25) mg/ml gave inhibition activity against bacteria under study. Other study showed that *A.sativum* had an inhibition effect on other pathogenic bacteria, *A.sativum* had biologically active substances, in its underground bulb, so that use as alternative medicine, it contains, 17 amino acids, 33 sulfur compounds, mineral salts (e.g. selenium, calcium, germanium, iron salts and phosphates ), vitamins (e.g. riboflavin, thiamine, niacin, ascorbic acid and folic acid) and enzymes (14).

### **Conclusion:**

*A.sativum* had a good antibacterial activity against *P. aeruginosa* isolated from clinical samples.

**References:**

1. Rocha,A.; Barsottini,M.; Rocha,R.; *et al.* (2019). *Pseudomonas Aeruginosa: Virulence Factors and Antibiotic Resistance Genes*. Brazilian Archives of Biology and Technology Vol.62: e19180503·
2. Gales,A.; Jones,R.; Turnidge,J.; Rennie,R. and Ramphal,R.(2001). Characterization of *Pseudomonas aeruginosa* Isolates: Occurrence Rates, Antimicrobial Susceptibility Patterns, and Molecular Typing in the Global SENTRY Antimicrobial Surveillance Program, 1997–1999. CID 2001:32 (Suppl 2).
3. **Morita,Y.; Komori, Y.; Mima,T.; Kuroda,T.; Mizushima, T.; Tsuchiya,T.** (2001). Construction of a series of mutants lacking all of the four major *mex* operons for multidrug efflux pumps or possessing each one of the operons from *Pseudomonas aeruginosa* PAO1: MexCD-OprJ is an inducible pump. *FEMS Microbiology Letters*, 202(1), :139–143.
4. Ciofu O, Tolker-Nielsen T. Tolerance and resistance of *Pseudomonas aeruginosa* biofilms to antimicrobial agents—how *P. aeruginosa* can escape antibiotics. *Front Microbiol* 2019; 10:913.
5. Magryś, A., Olender, A., & Tchórzewska, D. (2021). Antibacterial properties of *Allium sativum* L. against the most emerging multidrug-resistant bacteria and its synergy with antibiotics. *Archives of microbiology*, 203(5), 2257–2268. <https://doi.org/10.1007/s00203-021-02248-z>.
6. Collee, J. G., Miles, R. S., and Watt, B. (1996). Test for the identification of bacteria. In: Collee. J. G.; Fraser, A. G.; Marmion, B. P. and Simmons, A. (Eds). *Practical Medical Microbiology*. 14P th Edition. Churchill Livingstone, New York. pp. 131-146.
7. Kirby, W., Bauer, A., Sherhis, J. and Turck, M. (1966). Antibiotic susceptibility testing by a standardized single disc method. *Am J Clin Pathol.*, 45(4):493-6.
8. Das, K., Tiwari, R. and Shrivastava, D. (2010). Techniques for Evaluation of Medicinal Plant Products as Antimicrobial Agent. *Current Methods and Future Trends. Journal of Medicinal Plants Research*, 4(2): 104-111.
9. Mostafa, A., Al-askar, A., Almaary K., Dawoud,T. Sholkamy,E. and Bakri,M. (2018). Antimicrobial activity of some plant extracts against bacterial strains causing food poisoning diseases. *Saudi J Biol Sci*, 25(2):361-366.
10. Jombo,G., Jonah,P, and Ayeni,J.(2008). Multidrug Resistant *Pseudomonas aeruginosa* In Contemporary Medical Practice: Findings From Urinary Isolates At A Nigerian University Teaching Hospital. *Nigerian Journal of hysiological Sciences*, 23, ( 1-2), ( 105-109).
11. **Edwards,J.R.**(1995). Meropenem: a microbiological overview. *Journal of Antimicrobial Chemotherapy*, 36, Issue suppl\_A, July 1995, Pages 1–17.
12. **Bonfiglio,G.** (2001). levofloxacin as active as ciprofloxacin against *Pseudomonas aeruginosa*. *Chemotherapy*, 47(4):239-42.
13. Fish D. N. (2006). Meropenem in the treatment of complicated skin and soft tissue infections. *Therapeutics and clinical risk management*, 2(4), 401–415. <https://doi.org/10.2147/tcrm.2006.2.4.401>.
14. Tchórzewska,D.; Bocianowski,J.; Najda,A.; Dąbrowska,A.; Winiarczy,K. (2017). Effect of environment fluctuations on biomass and allicin level in *Allium sativum* (cv. Harnas, Arkus) and *Allium ampeloprasum* var. *ampeloprasum* (GHG-L). *Journal of Applied Botany and Food Quality* 90, 106 - 114 (2017), DOI:10.5073/JABFQ.2017.090.013

A large concrete dam with multiple spillways and a yellow crane on top. The dam is situated in a river valley with hills in the background. The sky is overcast.

**EVALUATE STRESSES GENERATED IN EARTHEN DAMS USING GEO-STUDIO**

**ASMAA ABDUL JABBAR JAMEL**

## EVALUATE STRESSES GENERATED IN EARTHEN DAMS USING GEO-STUDIO

Asmaa Abdul Jabbar JAMEL<sup>1</sup>

### Abstract:

Water leakage through the earth dam and the foundation is an important phenomenon that must be considered when designing earth dams, as it generates pore water pressure and causes internal erosion of the dam material that affects the stability of the dam by generating stresses and strain in it. There are a variety of technical methods available to minimize these concerns, such as using core, horizontal filter system, or by modifying the dam's geomatics specifications.

The current study observed that at steady state flow through earth dam with horizontal filter, core, and no filter. Increasing the slope of the upstream dam reduces the amount of pore water pressure inside the dam body, while the maximum increase in pore water pressure occurs in the case of no filter. Furthermore, the highest stress at the dam's base is increased by the decrease in upstream slope. Furthermore, the dam's upstream slope has a significant effect on the values of the vertical and horizontal displacements created with in dam. Since the presence of the core generates the greatest increase in the horizontal displacement of the dam and foundation section. Changing the permeability coefficient of the dam body also produces a modification in the stresses at the dam's base by about  $\pm 2\%$ .

Also, when utilizing the core, there is the lowest increase in seepage discharge, however when using the horizontal filter, there is the greatest rise in discharge (53.78 %) compared to the case without a filter. Furthermore, while using a horizontal filter, the percentage increase was (1.13%) as compared to when no filter being used.

**Key words:** Earth Dam, Stress, Displacement, PWP, Seepage.



<http://dx.doi.org/10.47832/MinarCongress5-4>



<sup>1</sup> University of Tikrit, Iraq, [ms.asmaajameel@tu.edu.iq](mailto:ms.asmaajameel@tu.edu.iq), <https://orcid.org/0000-0001-7602-3426>

## Introduction:

Earth dams will drain to some extent, and drainage has become a concern only when it affects the dam, whether by producing erosion in the downstream dam or by generating flood problems in the earth dam, weakening its strength [1].

Giglou, et al., two-dimensional finite element algorithm was used to numerically examine several homogeneous earths with different heights. A simple approach for estimating the seepage rate through a homogeneous earth dam with vertical drainage and taking into account saturated and unsaturated flow under steady-state circumstances [2]. Athani, et al., founded that analysis increasing the Young's modulus of the core and shell resulted in a reduction in the greatest top displacement. Both seepage and stability studies have shown the necessity of understanding the coupled effects on the overall stability of the earth dam [3]. Zeidan et al., under steady-state situations, the phreatic seepage surface, pore water pressure distribution, and total hydraulic head change of earth dams are collected and studied. The observed data demonstrate that failure occurs in most situations of failed dams owing to either seepage or slope instability, or a combination of seepage and slope instability [4]. Fattah et al., investigated the Al-Adhaim dam, which consists of a 3.1 km long zone embankment, and discovered that the existence of a clay core has a significant influence on lowering the exit gradient, which may rise by up to 300 % when the core was not exist [5]. Cheng et al., relying on seepage from Longtougiao homogenous earth dam. The seepage management program was designed in accordance with the criteria for earth dam design, and it used the approach of preventing on the foreside and discharging on the backside [6]. Kirra et al., studied drainage observation of the Walter F. George Dam, and a dam layout recommendation to minimize drainage [7]. Zeidan et al., investigated the top seepage line, pore water pressure distributions, and total pressure head change of Mandali dam's with in presence of coupled drainage and slope stability [8]. Salem, investigated the influence of core permeability, core thickness, core base depth, and core entry on drainage, pressure head, exit gradient, upstream and downstream slope stabilities. It is observed that increased lateral slopes cause significant decline in seepage line with rising downstream slope stability, reducing core permeability, increasing core depth, base core depth [9]. Kanchana et al., investigated the performance of top seepage line by altering the overall length of a horizontal drainage filter using various types of earth dam with a central impermeable vertical core [10]. Malekpour et al., investigated the impact of horizontally drainage length just on safety of an earth dams under constant and rapid seepage circumstances [11]. Kachare et al., used Geo-Studio technology and the finite element technique (FEM) to predict seepage loss, exit gradient, uplift pressures, top seepage line, and the quantity of seepage in order to design a suitable filtration solution [12]. Jamel A., investigated sets were carried out with three various upstream and downstream slopes of earth dam, four different upstream and downstream slopes of core, getting an analytical formula to determine the quantity of drainage flow through the homogeneous earth dam with core lying on impermeable foundation [13]. Mazaheri et al., utilized static modelling in earth dams. The data indicated that the highest stress of the dam was over the core [14]. Al-Janabi et al., Physical, theoretical, and simulation methods were used to explore seepage in dams [15]. Mostafa et al., shown according to the review study, reducing the relative permeability resulted in a considerable drop in the main seepage qualities [16].

This paper provides access to an explanation of the behavior of earthen dams via an empirical investigation of the earthen dam's materials and geometries using the Geo-Studio software. Using SIGMA/W, to estimate the stresses and strains that occur inside the dam body and on the dam's foundation, as well as the change in pore water pressure (PWP) and leakage inside the dam body using SEEP/W. And a

statement indicating the difference in behavior caused by the use of three types of filters, represented by the availability of horizontal filter, core, and the absence of any filter.

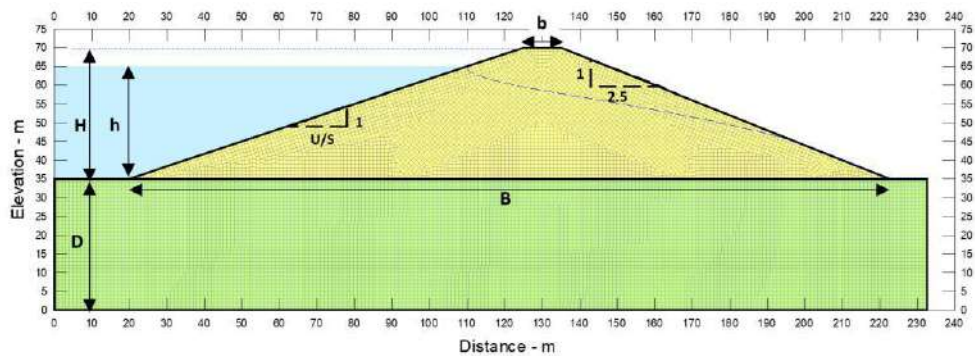
**2. PROCEDURE OF SETUP**

The current study based on models of earthen dams under the action of steady flow. Dams were represented using the Geo Studio software using three types of filters (no filter, horizontal filter, and core), three different upstream slopes (1:U/S) (1:3, 1:2.25, and 1.2.5), and three different permeability coefficient  $k_y/k_x$  values (1, 0.5, and 2). And for a set of parameters represented by  $d=35m$ ,  $x_1=20m$ ,  $x_2=10m$ ,  $L=20$ ,  $h=30m$ ,  $H=35m$ ,  $b_c=6m$ ,  $b=10m$ ,  $h_c=34$ ,  $B_c=74m$ , as shown in Figures (1-3). For each of the situations of no filter, core, and no filter, respectively.

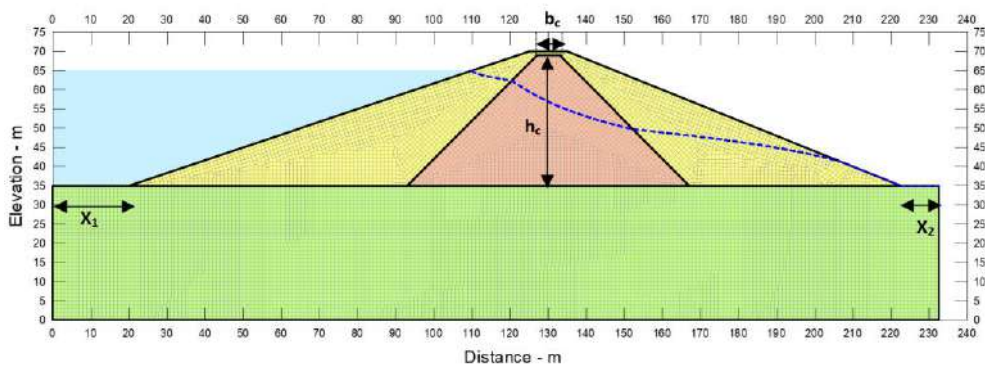
As a result, 27 experiments were represented. The outputs listed in the left-side of Equation 1 were found for each experiment.

$$\begin{bmatrix} \text{Seepage}(Q) \\ \text{Stress} \\ \text{Displacement} \\ \text{PWP} \end{bmatrix} = f\left(U/S \text{ Dam}, \frac{k_y}{k_x}, \text{Filter Type}\right) \dots \dots \dots (1)$$

In the current study, elements of the quadrant and triangle shape have been used, with the node number exceeding 12164 and the number of elements reaching 11925, while the global size distance is around 1 m. Figures (4, 5) show ways to evaluate the flow and stresses within the earth dam using the sub-programs SEEP/W and SIGMA/W to obtain output results.

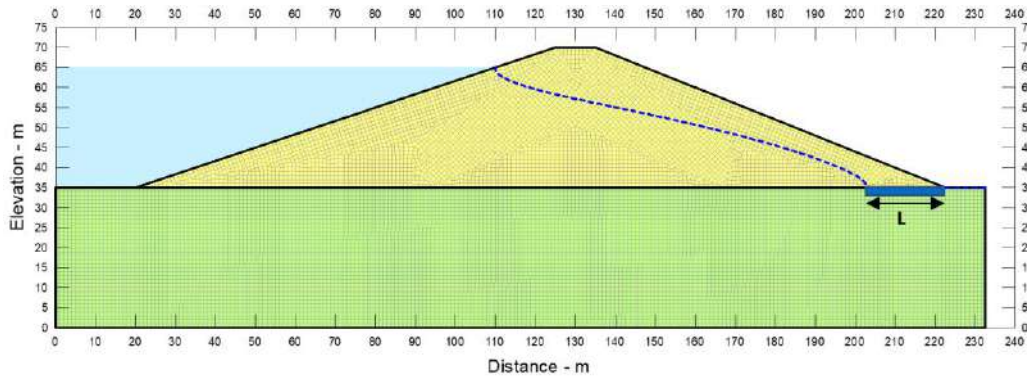


**Figure (1) The general section of homogenous earth dam without filter.**

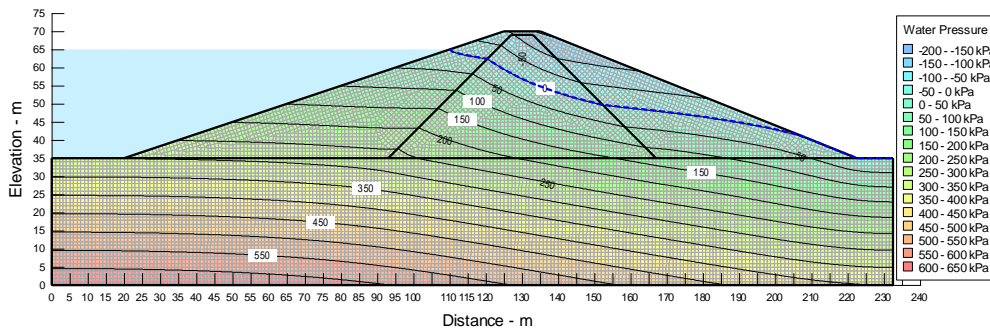


**Figure (2) The general section of homogenous earth dam with core.**

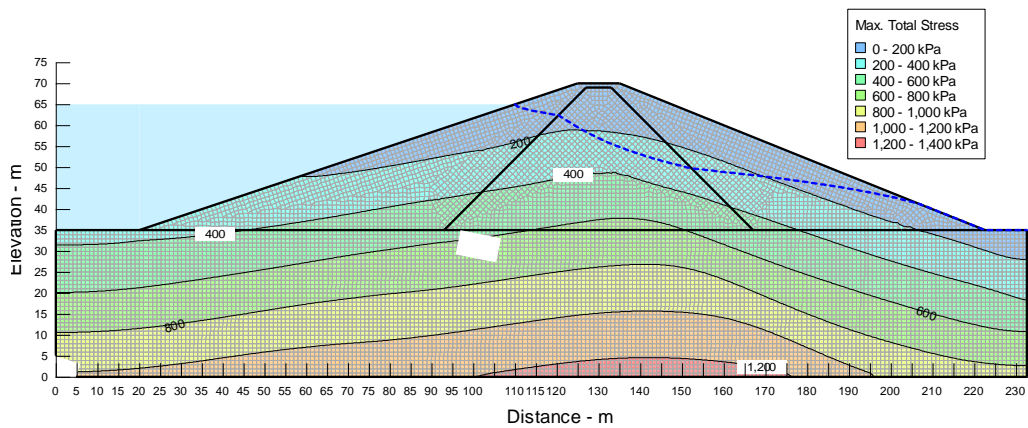




**Figure (3) The general section of homogenous earth dam with horizontal filter.**



**Figure (4) The PWP Distribution by SEEP/W.**



**Figure (5) The total stress by SIGMA/W.**

### 3. RESULTS AND DISCUSSION

The study relied on demonstrating the effect of the dam reservoir's constant level on the amount of stress generated within the dam, as well as the distribution of water pressure (Pore Water Pressure, PWP), the horizontal distance generated as a result of the greatest stress at the dam's base, and the amount of discharge (Discharge) within the dam body.

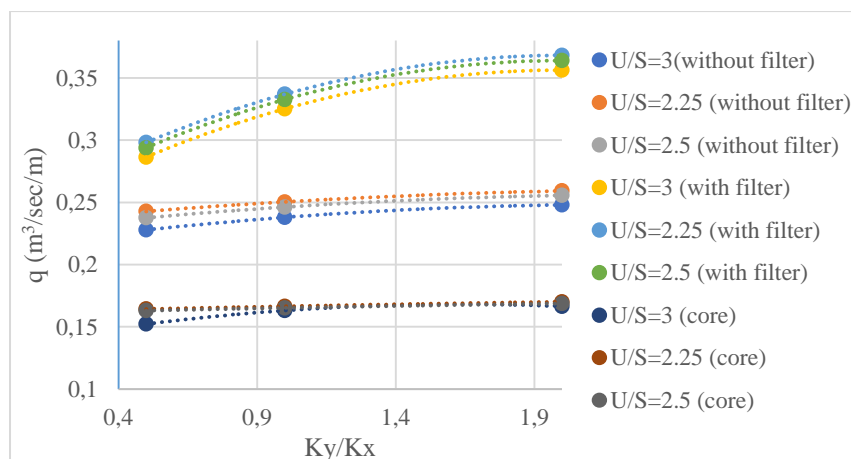
#### 3.1 Seepage Discharge behavior within the dam body

Figure (6) shows the effect of increasing the permeability coefficient ( $K_y/K_x$ ) on the quantity of discharge inside the earthen dam ( $q$ ), under various filter conditions and three different upstream slopes (1:U/S). Since increasing the permeability

coefficient increases the quantity of discharge within the dam body and for the three cases indicated by no filter, horizontal filter, and core, and the increase varies depending upon the type of the filter. Whereas, increasing the permeability coefficient from 0.5 to 1 result in an increase in discharge up to (4.23%), (11.9%), and (6.68%) for each case of no filter, horizontal filter, and core, respectively.

Thus, it is noticed that the highest increase in discharge as a result of varying the permeability occurred while employing the horizontal filter, where changing the permeability will considerably contribute to the quantity of discharge in this case. It is also noticed that the highest discharges occur when  $k_y/k_x = 2$ , that is, when the vertical permeability is greater than the horizontal permeability, and this behavior might be explained by the effect of gravity on the water pressure inside the voids.

It is also observed that decreasing the upstream slope would result an increase in the quantity of drainage, which is reasonable given that decreasing the slope will contribute to increasing the area of the dam according to Darcy's law. Furthermore, the amount of increase in drainage varies in value depending on the shape of the filter, as the lowest amount of increase in drainage would be using core for the three dam upstream slopes, and the assessment of this behavior is that the core consisting of a low-permeability material has slight infiltration and thus decreases drainage according to Darcy's law. While the highest drainage inside the dam body were when using the horizontal filter and for the three upstream slopes of dam, with an increase rate (53.78%), due to the horizontal filter providing pathways for flow within the dam body.



**Figure (6): Distribution of permeability coefficient with discharge, for  $h=30\text{m}$ , at varying upstream slopes and three conditions (no horizontal filter, horizontal filter, and core).**

### 3.2 Max. Total Stress behavior at Dam Base

Figure (7) shows the variation of Max total stress at Dam base with the permeability coefficient ( $K_y/K_x$ ) as the slope values of the upstream dam and the three states of the filters being changed. According to the form of the filter, there was a variance in the values of the maximum stress increases. Increasing the permeability coefficient from 0.5 to 1 at upstream slope (1:2.5) increases the amount of stress by (0.05%), (0.1%), and (0.03%) for each state (no horizontal filter, horizontal filter, and core) respectively.

Also, the development in the permeability coefficient was low, and the increase here is dependent on the quantity of seepage flowing through the dam's body, which affects the weight of the dam and therefore the stress value on the dam's base. The values for the maximum stress at the dam's base will be at permeability coefficient ( $K_y/K_x=1$ ), which means that the vertical permeability is equal to the horizontal

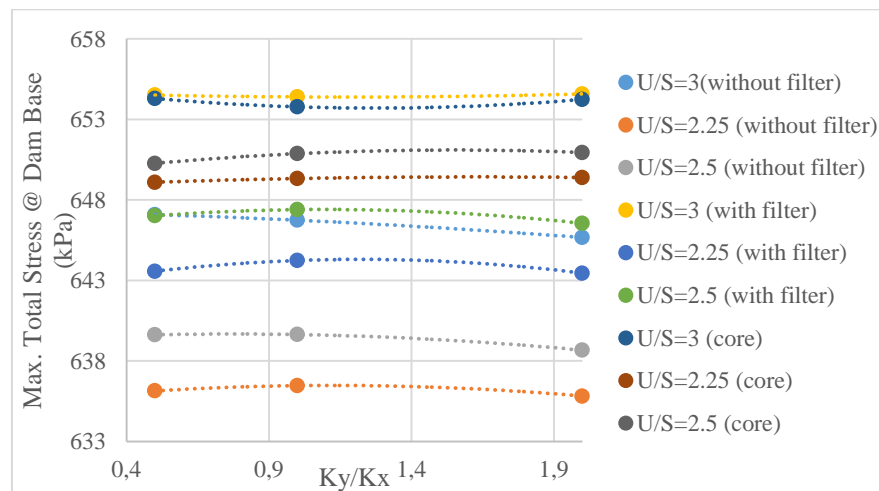
permeability value for each of the two slopes (1:2.25) and (1:2.5) and for the three cases (no filter, horizontal filter, and core).

Increasing the permeability coefficient from 0.5 to 1 at upstream slope (1:3) causes decreases in stress by (0.05%), (0.017%), and (0.079%) for each condition (no horizontal filter, horizontal filter, and core), respectively. The largest value of the Max. stress is at ( $K_y/K_x=0.5$ ), indicating that horizontal permeability is larger than vertical permeability at this slope.

Thus, in all circumstances of filters and slopes, increasing the permeability coefficient from 0.5 to 1, and from 1 to 2 results a variation in the stresses at the dam's base that can exceed  $\pm 2\%$ .

Furthermore, when the slope of the upstream decreases, the maximum stress values at the dam's base increases due to the position of the phreatic line, which is dependent on the slope of the upstream of dam. As a result, the stress increases as the slope decreases, and its maximum values occur at a slope (1:3), since the weight of the wet zone inside the dam body is larger than the weight of the dry zone.

The increased stress is also affected by the shape of the filter. In addition, increasing the slope from 2.25 to 2.5 for no horizontal filter and with a permeability coefficient ( $K_y/K_x= 0.5$ ) resulted (0.5 %) increase in stress, which is regarded very significant for the stress at the dam's base. It should be noted that the highest stress values were obtained when utilizing a horizontal filter with a upstream slope of (1:3), with a percentage increase of (1.13 %), and this increase is related to the construction of longer flow paths inside the dam in the horizontal filter case compared to the other cases. Furthermore, the lowest values of stress occur when a filter is not utilized, which is due to the fact that the discharge passing through the dam body is smaller than the filter is employed, and thus leads to its effect on reducing the stresses on the base of the dam body.

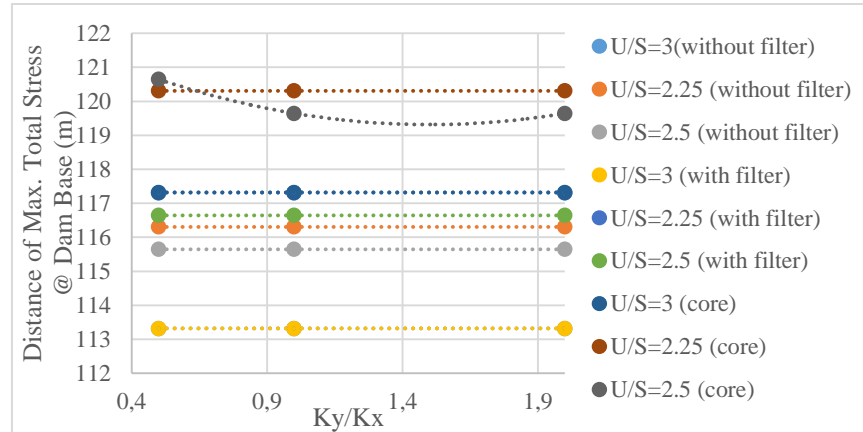


**Figure (7): Distribution of permeability coefficient with max. total stress at dam base, for  $h=30m$ , at varying upstream slopes and three conditions (no horizontal filter, horizontal filter and core).**

### 3.3 Distance of Max. Total Stress behavior at dam body

Figure (8) demonstrates the effect of increasing the permeability coefficient on the location of the stress generated at the dam's base for different filter conditions and three different upstream slope, as increasing the permeability coefficient does not cause a change in the horizontal distance, this distance is appeared at the Max. height of the top seepage line, which in turn generates the Max. stress, due to increase the weight of the wet area below the seepage line, where its value determined by a number of factors, including the geometric of the dam.

The greatest change in horizontal distance occurs in the case of a horizontal filter, where the percentage increase when increasing the slope from 0.5 to 1 equal (3.4%), and this percentage is greater if the filter is not employed and the core is available. The longest distance was equal to (120.65 m) from the dam's front upstream at case of core with upstream slope (1:2.5). For upstream slope of 1:2.5, the rate of the distance increase for no- filter compare to the presence of core was (4.14%).



**Figure (8): Distribution of permeability coefficient and distance of max. total stress at dam base for h=30m, with varying upstream slopes and three conditions (no horizontal filter, horizontal filter, and core).**

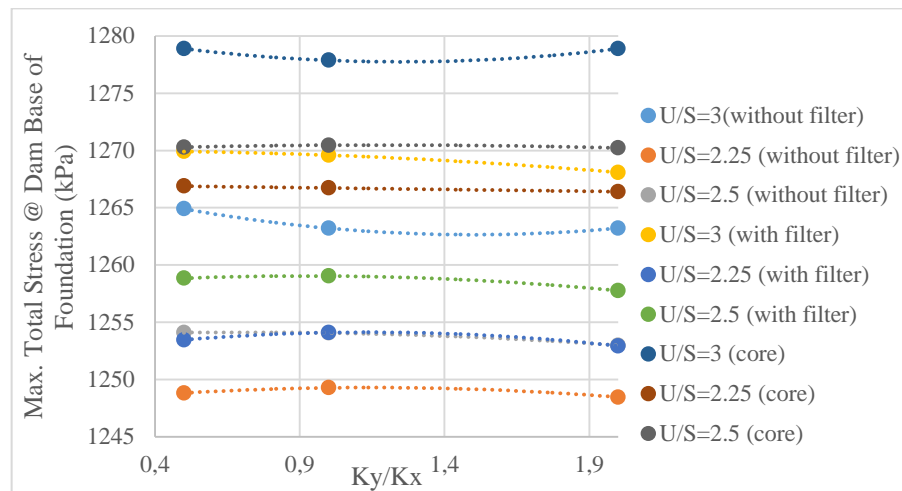
### 3.4 Max. Total Stress Behavior at Dam Base of Foundation

Figure (9) shows the affect of increasing the permeability coefficient on the amount of stress created at the dam's base, when upstream slope values of the dam are changed, and for the three filter cases. Once the permeability coefficient was changed, a minor variation in stress was detected.

Depending on the slope and geometry of the filter, an increase in the permeability coefficient causes a decrease or increase in the stress at the base of the dam foundation. Increasing the permeability coefficient from 0.5 to 1 reduces stress by (0.13 %, 0.023 %, 0.08 %) in each of the cases of no filter, using a horizontal filter, and the presence of core, respectively, at upstream slope.(1:3)

While it is obvious that the stress at the foundation's base increases when the permeability coefficient increases from (0.5) to (1) and the slope (1:2.25) by (0.04 %) when there is no horizontal filter and by (0.05 %) when there is a horizontal filter. The explanation for the overall increase and decreases in stress is the effect of increasing the slope on the discharge by increasing the permeability coefficient, as explained in Figure (6).

It is also observed that as the slope is reduced, the stress at the base of the foundation increases as a result of the increased total area of the dam. Where most stress was generated in the case of core, with an increase of 1.1 % at upstream slope 1:3, where it is possible to hold water inside the dam body in the area between the dam body and the core, known as (Shell). Core works to increase the weight of the soil and thus increase the stress generated at the base of the foundation. Thus, in general, changing the permeability coefficient from 0.5 to 2 will change the stress generated on the base of the dam by up to  $\pm 1.6\%$ .



**Figure (9): Distribution of permeability coefficient and max. total stress at dam base of foundation for h=30m, with varying upstream slopes and three conditions (no horizontal filter, horizontal filter, and core).**

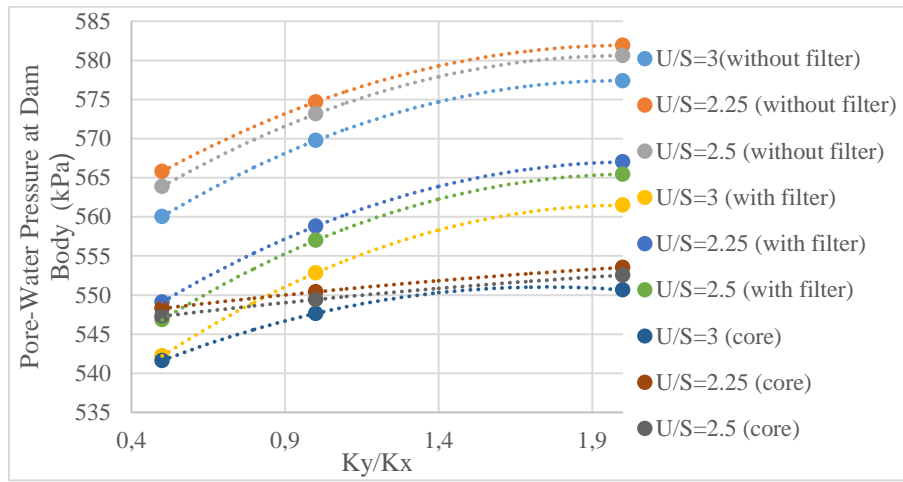
### 3.5 Pore-Water Pressure behavior at Dam Body

Figure (10) represents the effect of increasing the permeability coefficient on the pore water pressure (PWP) inside the dam body for different upstream slopes and three filter conditions (no filter, horizontal filter, and core). It is observed that increasing the permeability coefficient causes increases the amount of pore water pressure inside the dam body. When the permeability coefficient increases from (0.5) to (1), the pore water pressure rises by 1.55 %, 1.7 %, and 0.39 %, respectively, for case of no filter, horizontal filter, and core. Thus, the highest increase in pore water pressure occurs in the case of a horizontal filter (1.7 %) at a ratio of  $K_y/K_x = 2$ , since increasing the vertical permeability coefficient causes a significant increase in water flow and thus

an increase in water pressure within the earth dam body.

Furthermore, raising the slope would increase the amount of pore water pressure inside the dam body in all cases, since the wet region drops and therefore the percentage of voids decreases, so the amount of leaking water constantly increases, resulting increase in pressure inside the voids. It was also shown that increasing the permeability coefficient had no significant influence on the pore water pressure readings while employing the core at upstream slopes of 2.25 and 2.5.

The minimum pore water pressure is at a slope of 1:3, while the highest rise in pore water pressure is at a rate of 5.73 % with no filter and at a slope of 2:25. The reason for the decrease in pore water pressure when using the core is that it is characterized by having a very low permeability, so water is not allowed to pass through it, and thus the pressure inside the dam decreases as a result of restricting the flow of water, whereas when there is no filter, the water flows easily inside the dam body and by different paths, causing an increase in pore water pressure, and the percentage increase from the lowest value to the highest value is 4.88%.



**Figure (10): Distribution of permeability coefficient and maximum pore water pressure generated inside the dam body for  $h=30m$ , with varying upstream slopes and three conditions (no horizontal filter, horizontal filter, and core).**

#### 4. CONCLUSIONS

In the present study conclude the following results:

1. For the three upstream slope cases, the amount of the lowest increase in seepage discharge is when utilizing the core, whereas the largest value inside the dam body is when employing the horizontal filter.
2. Increasing the permeability coefficient from 0.5 to 1 and then from 1 to 2 results in a rate of change of the stresses at the dam's base equal to  $\pm 2\%$ . The greatest pressure exerted near the dam's base by a decrease in upstream slopes. When no filter is employed, the stress values seem to be the lowest.
3. Increasing the permeability coefficient has no effect on the horizontal distance at which the maximum stress appears within the dam body.
4. There is a slight variation in stress when the permeability coefficient is changed, as altering the permeability coefficient from 0.5 to 2 affects the stress generated at the dam's base by up to  $\pm 1.6\%$
5. Increasing the permeability coefficient raises the quantity of pore water pressure inside the dam body and under various filter conditions. The highest increase in pore water pressure will have a  $K_y/K_x = 2$ , while the greatest rise in water pressure is found at no filter and upstream slope 1:2.25, where pore water pressure increased by 5.73.%

## 5. REFERENCES

1. Stephens T., (2010), " Manual on Small Earth Dams", Food and Agriculture Organization of the United Nations, Italy.
2. Giglou A.N. et al. (2013), "Seepage through Earth Dam", Life Science Journal, Vol.10, pp.1-4.
3. Athani S. et al. (2015), "Seepage and Stability Analyses of Earth Dam Using Finite Element Method", International Conference on Water Resources, Coastal and Ocean Engineering, pp. 876 – 883.
4. Zeidan B. et al. (2017), "Combined Seepage and Slope Stability Analysis of Failed Earthen Dams" International Conference on Advances in Structural and Geotechnical Engineering, ICASGE15, Hurghada, Egypt.
5. Fattah et al. (2014), "Seepage Analysis of a Zoned Earth Dam by Finite Elements", International Journal of Civil Engineering and Technology, Vol. 5, No. 8, pp. 128-139.
6. Cheng S et al., (2009) "Study on seepage behavior and control of Longtougiao Earth Dam", International Forum on Porous Flow and Applications, Wuhan City, CHINA. 836-839.
7. Kirra et al. (2015), "Combined Seepage and Slope Stability Analysis of Reservoir Earth Dams", Msc. Thesis, Tanta University, Egypt.
8. Zeidan et al. (2018), "Seepage and Slope Stability Analysis of Earth Dams", ICOLD, Vienna.
9. Salem M., (2019), "Analysis of Seepage through Earth Dams with Internal Core", International Journal of Engineering Research & Technology, Vol. 8, No.08.
10. Kanchana H. J. and Prasanna H. S., "Adequacy of seepage analysis in core section of the earthen dam with different mix proportions", Aquatic Procedia, Vol. 4, PP. 868-875, 2015.
11. Malekpour A., Zade D. F., Dalir A. H. Z. and Sadrekarimi J., (2012), "Effect of horizontal drain size on the stability of an embankment dam in steady and transient seepage conditions", Turkish Journal of Engineering and Environmental Sciences, Vol.36, No.2, PP. 139-152.
12. Kachare J. and Jagtap S., (2017), "Seepage analysis of Gangapur, the earthen dam using geo-studio software", International Journal of Recent Advances in Engineering & Technology.
13. Jamel A., (2018), "Investigation and Estimation of Seepage Discharge Through Homogenous Earth Dam with Core by Using SEEP/W Model and Artificial Neural Network", Diyala Journal of Engineering Sciences, Vol. 11, No. 3, pp. 54-61.
14. Mazaheri et al., (2020), "Comparison of static and dynamic stress-strain analysis in earth dams (Case Study: Azadi Earth Dam)", Engineering Geology, Vol.13, No.3, pp. 83-95.
15. Al-Janabi et al., (2020), "Experimental and Numerical Analysis for Earth-Fill Dam Seepage", Sustainability, Vol.12, No.6.
16. Mostafa et al., (2021), "A Review on Analysis of Seepage in Zoned Earth Dams" 2<sup>nd</sup> International Conference on Civil Engineering: Recent Applications and Future Challenges. Hurghada, Egypt.



**SYNTHESIS AND CHARACTERISATION  
OF NEW CO(II), ZN(II) AND CD(II) COMPLEXES DERIVED FROM  
OXADIAZOLE LIGAND AND 1,10-PHENANTHROLINE AS CO-LIGAND**

**RIYADH M. AHMED  
SARAH S. ABDUL RAHMAN  
DHEFAF H. BADRI  
KHAWLA M. SULTAN  
ISMAEEL Y. MAJEED  
GHADA M. KAMIL**

**Co.**

**SYNTHESIS AND CHARACTERISATION  
OF NEW Co(II), Zn(II) AND Cd(II) COMPLEXES DERIVED FROM OXADIAZOLE  
LIGAND AND 1,10-PHENANTHROLINE AS Co-LIGAND**

**Riyadh M. AHMED<sup>1</sup>**  
**Sarah S. ABDUL RAHMAN<sup>2</sup>**  
**Dhefaf H. BADRI<sup>3</sup>**  
**Khawla M. SULTAN<sup>4</sup>**  
**Ismaeel Y. MAJEED<sup>5</sup>**  
**Ghada M. KAMIL<sup>6</sup>**

**Abstract:**

In this work, prepared new ligand namely 5-(2,4—dichloro-phenyl)-1,3,4-oxadiazole-2-(3H)-thion, which was obtained from the 2,4-dichlorobenzoyl chloride with hydrazine, after that reaction with CS<sub>2</sub>/KOH in methanol. This ligand was reaction with (Co, Zn and Cd) and 1,10-phenanthroline as co-ligand. The ligand and complexes were characterised by IR, UV-Vis, C-H-N, magnetic moment, A.A, Cl content, and m.p.. The data that collected indicate the octahedral geometry around metal ions in all complexes. In IR spectra of complexes, the small shift in  $\nu(\text{C}=\text{S})$ , indicating the exocyclic sulfur is not bonding. The ligand is present in thion form, which indicate deprotonated N-H group in complexes and is bonded to Co(II), Zn(II) and Cd(II) through the oxadiazole nitrogen.

**Key words:** *Oxadiazole, 1,10-Phenanthroline, Metal Complexes.*



<http://dx.doi.org/10.47832/MinarCongress5-5>

<sup>1</sup> University of Baghdad, Iraq, [reyadh.ahmed@yahoo.com](mailto:reyadh.ahmed@yahoo.com)

<sup>2</sup> University of Baghdad, Iraq, [sarah.s.a@ihcoedu.uobaghdad.edu](mailto:sarah.s.a@ihcoedu.uobaghdad.edu); <https://orcid.org/0000-0002-2316-0774>

<sup>3</sup> University of Baghdad, Iraq, [dhefafhashim1990@gmail.com](mailto:dhefafhashim1990@gmail.com), <https://orcid.org/0000-0003-3490-6049>

<sup>4</sup> University of Baghdad, Iraq, [khaola.m.s@ihcoedu.uobaghdad.edu.iq](mailto:khaola.m.s@ihcoedu.uobaghdad.edu.iq); <https://orcid.org/0000-0003-3576-6615>

<sup>5</sup> University of Baghdad, Iraq, [ismaeel.y.m@ihcoedu.uobaghdad.edu.iq](mailto:ismaeel.y.m@ihcoedu.uobaghdad.edu.iq)

<sup>6</sup> University of Technology, Iraq, [ghada.m.kamil@uotechnology.edu.iq](mailto:ghada.m.kamil@uotechnology.edu.iq)

## Introduction:

The coordination mode of oxygen and nitrogen in hetero-cyclic ligands has a significant application, such as in the creation of supramolecular structures, polydentate aromatic nitrogen heterocyclic ligands such as polyazoles, imidazoles, and triazoles Azole rings (five-membered rings) have been widely employed [1- 5]. The shape and behaviors of metal ion in complexes are influenced by the metal and the atoms that acts as donor in ligands, the structure of ligand and ligand/metal-interactions[6]. The salts of N-aryol dithiocarbazates could be transformed to physiologically significant 1,3,4-oxadiazole derivatives [7, 8]. The shape of the metal base on both of characteristics of the ligands and counter ion, all play a role in the complexes' formation. Because of their strong coordination ability and various coordination modes, ligands based on azole heterocycles are attracting a lot of attention [9]. Their chemistry and applications have been noted in numerous papers [10, 11]. These ligands are a tautomeric molecule containing both thiol and thion forms, known as thiophene ligands, which are employed to protect metals against corrosion [12, 13]. Because the major pharmacological properties, such as analgesics, antiviral, antibacterial, depressive, and antifungal effects, these types of complexes are gaining greater attention [14-18]. It is vital to characterize the bonding mode of complexes in oxadiazole since 1,3,4-oxadiazole-2-thion has both type of bonding thion and thiol forms [19-21].

## 2. Experimental

**2.1 Materials and methods:** All of the reagents were purchased from Aldrich.- and utilized with-out purification. Prior to use, the solvents utilized in the preparation were purification from the suitable drying agent.

**2.2 Instrumental Used:** (C.,H.,and N.) were performed on a Heraeus Instrument (Vario- EL). The spectra of I.R. used as K-Br discs from 4000 to 400  $\text{cm}^{-1}$  using a Shimadzu- 8400.S F.T.I.R. spectrophotometer. Ultra-violet spectra in range 200 to 1100 nm for 0.001 M solutions of complexes in  $(\text{CH}_3)_2\text{SO}$  at temperature 25°C were analyzed using a Shimadzu -1800. Spectra were acquired in  $\text{DMSO}-d_6$  solution using a Jeol 300-MHz spectrometer using tetra-methylsilan(TMS) as an internal standard for  $^1\text{H-N.M.R.}$  and mass spectroscopy. Electro-thermal Stuart melting point SMP/40 capillary melting point equipment was used to produce uncorrected melting points. The determination of metals was achieved by a Shimadzu -(A.A.) 680-G. The determination of  $\text{Cl}^-$  in complexes was obtained by the potentiometer titration method using a 686-Titrip processor-665Dosimat-.Metrohim Swiss .A PW 9526 digital conductivity meter was used to evaluate  $\text{DMSO}$  solutions' conductivity, and a magnetic susceptibility balance was used to quantify room temperature magnetic moments.

## 3. Synthesis

### 3.1 Synthesis of 5-(2, 4-dichlorophenyl)-1,3,4-oxadiazole-2-(3H)-thion[8]

Carbon disulphid (1 g, 13.1 mmol) was added dropwise to a solution of 2,4-dichlorobenzohydrazide (2.63 g, 13.1 mmol) and KOH (0.730 g, 13.1 mmol) in  $\text{CH}_3\text{OH}$ (40 ml) during stirring, after that the solution of reaction was refluxed for 5 hours. The residue was then dissolved in water after concentration to a small

volume. The solution of reaction was adding to ice containing HCl produced a precipitate. The solid compounds was filtered-out and dried, then washed with a 10% (v/v) EtOH–ether combination and dried in vacuo[22]., . Yield: (1.34 g, 50.9%; Mp 171 °C. I.R. (K-Br, cm<sup>-1</sup>):  $\nu$ (N-H) 3157,  $\nu$  (C=N) 1627,  $\nu$  (C-O-C) 1354,  $\nu$  (N-N) 1104,  $\nu$  (C=S) 1155. <sup>1</sup>H-N.M.R. (300-MHz, DMSO.-d<sub>6</sub>):  $\delta$  = 7.693, 7.702 (C<sub>2</sub>, d, 1H), 7.184, 7.192 (C<sub>1</sub>, d, 1H), 7.884 (C<sub>4</sub>, s, 1H), 11.672 (s, 1H, N-H)).

### 3.2 Synthesis of complexes

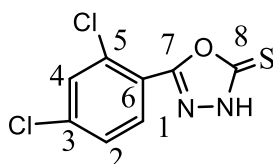
The complexes were made by dissolving L (2 mmol) in H<sub>2</sub>O (30 ml), and adding MClx.nH<sub>2</sub>O (1 mmol) that dissolve in H<sub>2</sub>O (15 ml) containing [M=Co, Zn, and Cd], for 30 minutes. The mixture was mixed, and the substance that separated as brown was filtered-out, washed with mixed of CH<sub>3</sub>OH/H<sub>2</sub>O. After shaking for a few minutes, a solution of 1,10-phenanthroline (2 mmol) in methanol (10 ml) was added to a CH<sub>3</sub>OH suspension of the aforementioned compound, and the resulting was filtered to yield the product. The elemental analytical data, colours, and yields of the complexes are listed in (Table-1).

## 4. Results and discussion

### 4.1. Chemistry

The heterocyclic ligand (L) were achieved by the reaction of CS<sub>2</sub> and potassium hydroxide (KOH) with 2,4-dichlorobenzohydrazide to obtained 5-(2,4-dichlorophenyl)-1,3,4-oxadiazole-2-(3H)-thion L in mole ratio of 1:1:1, respectively (Scheme 1). The ligand that have more than one atom can be coordinate to metal ions as mono-dentate or bi-dentate ligand. Elemental analysis (Table:1), I.R. (Table:2), U.V.–Vis. (Table:3), and <sup>1</sup>H., <sup>13</sup>C - N.M.R. were used to characterize the ligand. Using water and methanol, monomeric complexes of L with Co, Zn, and Cd(II.) were created by stirring (2, 1, 2 mmol) of ligand, metal chloride and 1,10-phenanthroline, respectively. The generic formula [M (L) 2(phen)<sub>2</sub>] neutral complexes [23]. H<sub>2</sub>O was obtained (where M = Cobalt, Zinc, and Cademium (Scheme- 2).

The product complexes are solids stable in air and soluble only in DMF and DMSO. Other organic solvents do not dissolve them. The shape of prepared complexes were obtained according to the measurments. The analytical results (Table-1) are in conformity with the proposed equations. This section contains the I.R. bands for both ligands and their complexes, as well as their nomenclature. (Table-2).



**Scheme-1. The structure of ligand**

**Table1. The data of Colour, Yield, Micro-analysis and M.P. of compounds.**

Compound	Colour	Yield (%)	m.p.	Found. (Calc.) (%)					$\Lambda_M(\text{cm}^2\Omega^{-1}\text{mol}^{-1})$
				M.	C.	H.	N.	Cl	
L	Pal-yellow	50.9	171	-	38.49 (38.89)	1.57 (1.63)	11.48 (11.34)	-	-
[Co <sup>II</sup> (L <sup>1</sup> ) <sub>2</sub> (phen) <sub>2</sub> ]	Pale brown	40	282*	10.51 (10.69)	34.68 (34.87)	1.04 (1.10)	10.27 (10.17)	Nil	11.48
[Zn <sup>II</sup> (L <sup>1</sup> ) <sub>2</sub> (phen) <sub>2</sub> ]	Pale green	43	267	6.89 (7.12)	52.09 (52.34)	2.36 (2.42)	12.16 (12.21)	Nil	13.61
[Cd <sup>II</sup> (L <sup>1</sup> ) <sub>2</sub> (phen) <sub>2</sub> ]	Pale Yellow	47	286*	11.37 (11.65)	49.64 (49.79)	2.18 (2.30)	11.35 (11.61)	Nil	10.12

**(Calculated) , Decomposed**

**4.2 I.R. and N.M.R. Spectrum:** (Table- 2) presented infrared bands for both L and complexes. The absorption ascribed to the  $\nu(\text{NH})$  at  $3157\text{ cm}^{-1}$  is seen in the I.R. spectra of free-ligand [24]. Bands at  $1627$  and  $1604\text{ cm}^{-1}$  are due to the  $\nu(\text{C}=\text{N})$  and  $\nu(\text{C}=\text{C})$  [25], respectively. The band at  $1354\text{ cm}^{-1}$  can be assigned to  $\nu(\text{C}-\text{O}-\text{C})$ , the absorption at  $1155\text{ cm}^{-1}$  assigned to  $\nu(\text{C}=\text{S})$ [26], Due to  $\nu(\text{N}-\text{N})$ , the bands are at  $1107\text{ cm}^{-1}$ , due to complex formation. The I.R. of complexes showed bands of ligand with some shifts and M-N frequencies (Table-2). The  $\nu_{\text{as}}(\text{NH})$  vibration at  $3157\text{ cm}^{-1}$  in the free ligands is disappeared which indicate the coordination between nitrogen with metal ion. The spectra of complexes show bands at  $1587-1602$  due to  $\nu(\text{C}=\text{N})$ . The shifted to a lower frequency can be attributed to complexation when compared to the free ligand,. This is due to the delocalization of metal electron density ( $t_{2g}$ ) to the ligand's  $\pi$ -system[27, 28]. The small shift in  $\nu(\text{C}=\text{S})$ , indicating the exocyclic sulfur is not bonding. The ligands are present in thion form, which indicate deprotonated N-H group in complexes and is bonded to Co(II), Zn(II) and Cd(II) through the oxadiazole nitrogen[29]. The bands at  $466-523\text{ cm}^{-1}$  that attributed to  $\nu(\text{M}-\text{N})$  for the complexes [30].

<sup>1</sup>H-NMR spectrum of L show the expected signals (see Experimental). <sup>1</sup>H-N.M.R. of the ligand L 7.184, 7.192 (s, 1H, C<sub>2</sub>). The chemical shift at 7.693, 7.702 (d, 1H, C<sub>1</sub>). While the resonance at 7.884 ppm, assigned to proton in carbon C<sub>4</sub> (s, 1H, C<sub>4</sub>). This signal appeared in downfield due to neighboring with two chloro atoms (electron withdrawing group) which lead to deshielding the electron density. The final signal at 11.672ppm attributed to the proton of N-H in triazole.

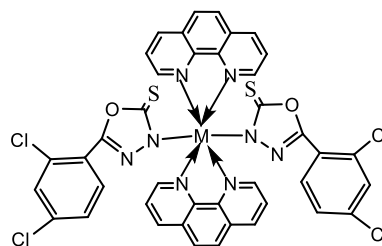
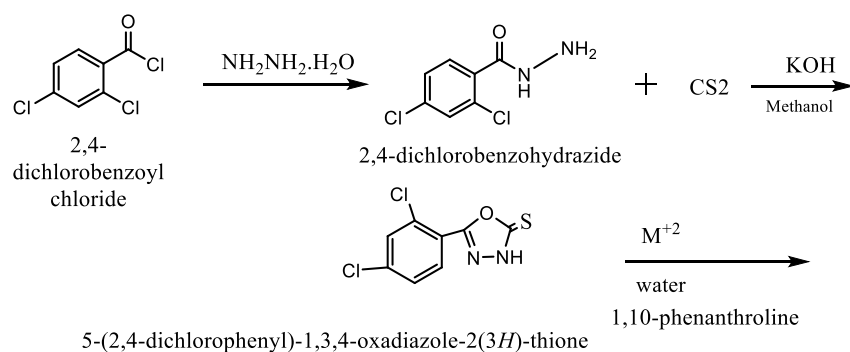
**Table-2. I.R. frequencies (cm<sup>-1</sup>) of the compounds.**

Compound.	$\nu_{as}, \nu_{as}(\text{NH}_2)$	$\nu_{as}(\text{C}=\text{N})$	$\nu(\text{N}-\text{H})$	$\nu(\text{C}-\text{O}-\text{C})$	$\nu(\text{C}=\text{S})$	$\nu(\text{N}=\text{N})$	$\nu(\text{M}-\text{N})$
L <sup>I</sup>	3157	1627	1574	1354	1155	1107	-
[Co <sup>II</sup> (L <sup>I</sup> ) <sub>2</sub> (phen) <sub>2</sub> ]	-	1587	-	1311	1131	1095	474,523
[Zn <sup>II</sup> (L <sup>I</sup> ) <sub>2</sub> (phen) <sub>2</sub> ]	-	1593	-	1359	1143	1106	466,516
[Cd <sup>II</sup> (L <sup>I</sup> ) <sub>2</sub> (phen) <sub>2</sub> ]	-	1602	-	1307	1156	1167	503,515

### 4.3 U.V.-Vis., magnetic moments and conductivity measurements.

U.V.-Vis. spectra shows a high absorption peak at 255nm, which is attributed to over-lap of the  $\pi \rightarrow \pi^*$  and  $n \rightarrow \pi^*$  transitions. In Co, Zn, and Cd complexes, the U.V.-Vis. of complexes, showed varied degrees of hypsochromic shift of the bands due to the intra-ligand  $\pi \rightarrow \pi^*$  transition (Table 3). In the Zn spectra of the complexes, bands linked to the (CT) transition were identified (Table:3). The d-d bands in the spectrum of the Co(II) complex could be attributed to a spin prohibited transition in an octahedral-geometry[31, 32]. This compound has a magnetic moment indicate octahedral structure with high-spin. The octahedral assignment of Co(II) complexes is consistent [25,33]. The Zn(II) and Cd(II) complexes favor octahedral coordination in most cases. The non-electrolyte nature of the Co.(II)., Zn.(II)., and Cd.(II) complexes is indicated by their molar conductivities. [23] (Table:1).

Compound	$\mu_{\text{eff.}}$ (BM) (per atom)	Band position ( $\lambda$ nm)	Extinction coefficient $\epsilon_{\text{max}}$ (dm <sup>3</sup> mol <sup>-1</sup> cm <sup>-1</sup> )	Assignments
[Co(L <sup>I</sup> ) <sub>2</sub> (phen) <sub>2</sub> ]	3.21	274 445 667	1145 85 72	$\pi \rightarrow \pi^*$ ${}^4\text{T}1\text{g}^{(\text{F})} \rightarrow {}^4\text{T}1\text{g}^{(\text{P})}$ ${}^4\text{T}1\text{g}^{(\text{F})} \rightarrow {}^4\text{A}_2\text{g}^{(\text{F})}$
[Zn(L <sup>I</sup> ) <sub>2</sub> (phen) <sub>2</sub> ]	diamagnetic	266 397	1752 1093	$\pi \rightarrow \pi^*$ C.T
[Cd(L <sup>I</sup> ) <sub>2</sub> (phen) <sub>2</sub> ]	diamagnetic	267 405	1227 76	$\pi \rightarrow \pi^*$ CT



Where M= Co<sup>II</sup>, Zn<sup>II</sup> and Cd<sup>II</sup>

**Scheme 2: Synthesis route of ligand and the proposed complexes.**

## 5. Conclusion

The synthesis of the metal-complexes generated from the interaction of the oxadiazole ligand, 1,10-phenanthroline as co-ligand with some metal-ions were investigated in this work. Physico-chemical and spectroscopic approaches such as IR, UV-Vis, C.H.N., magnetic moment, A.A, Cl content, and m.p. were used to determine the mode of coordination and the shape of the complexes. The data that collected indicate the octahedral geometry around metal ions in all complexes. This type of complexes that contain heterocyclic atom can be used to study the bacterial activity.

## References

1. B. J. Cormick, R. Bereman, D. M. Baird, *Coord. Chem. Rev.* 54, 99, 1984.
2. Y. T. Wang, G. M. Tang, W. Y. Ma, W. Z. Wan, *Polyhedron* 26, 782, 2007.
3. A. Mavrova, D. Wesselinova, Y. Tsenov, P. Denkova, *Eur. J. Med. Chem.* 44, 63, 2009.
4. R. Bronisz, *Inorg. Chem.* 46, 6733, 2007.
5. R. Bronisz, *Inorg. Chem.* 44, 4463, 2005.
6. N. A. Negm, M. F. Zaki, *Colloids Surf., B*, 64, 179, 2008.
7. A. Hetzheim, K. Mockel, *Adv. Heterocycl. Chem.* 7, 183, 1966.
8. B.L. Sharma, S. K. Tandon, *Pharmazic*, 39, (H-12), 858, 1984.
9. Y. T. Wang, G. M. Tang, W. Y. Ma, W. Z. Wan, *Polyhedron* 26, 782, 2007.
10. A. Hetzheim, K. Mockel, *Adv. Heterocycl. Chem.*, 7, 183, 1966.
11. M. Du, X. J. Zhao, *J. Mol. Struct.* 694, 235, 2004.
12. F. Zucchi, *ACH – Models in Chemistry*, 132, 579, 1995.
13. L. Ying, F. Haitao, Z. Yifan and W. Wuji, *J. Mater. Sci.*, 38, 407, 2003.
14. B. Tozkoparan, E. Kupeli, E. Yesilada, M. Ertan, *Bioorg. Med. Chem.*, 15, 1808, 2007.
15. M. T. Abdel-Aal, W.A. El-Sayed, S. M. El-Kosy, E. S. El-Ashry, *Arch. Pharm.*
16. *Chem. Life Sci.*, 341, 307, 2008.
17. [16] C. Jay, F. Groliere, O. Kahn, J. Krober, *Mol. Cryst. Liq. Cryst.* 234, 255, 1993.
18. L. Antolini, A. Fabretti, D. Gatteschi, A. Giusti, R. Sessoli, *Inorg. Chem.* 30, 4858, 1991.
19. Y. T. Wang, G. M. Tang, Z. W. Qiang, *Polyhedron* 26, 4542, 2007.
20. K. Obi, A. Kojima, H. Fukuda, K. Hirai, *Bioorg. Med. Chem. Lett.* 5, 2777, 1995.
21. S. P. Suman, S. C. Bahel, *J. Indian Chem. Soc.* 56, 712, 1979.
22. D. A. Charistos, G. V. Vagenas, L. C. Tzavellas, C. A. Tsoleridis, N. A. Rodios, *J. Heterocyclic Chem.*, 31, 1593, 1994.
24. Y. T. Wang, G. M. Tang, Z. W. Qiang, *Polyhedron* 26, 4542–4550, 2007.
25. W. J. Geary, *Coord. Chem. Rev.*, vol. 7, no.1, pp. 81-122, 1971.
26. Mohamed A. Al-Omar, *Molecules*, 15, 502-514, 2010.
27. N. K. Singh a, M. K. Bharty, R. Dulare a, R. J. Butcher b, *Polyhedron* 28, 2443–2449, 2009.
28. A. Bharti, M. K. Bharty, S. Kashyap, U. P. Singh, R. J. Butcher, N. K. Singh, *Polyhedron*, 50, 582–591, 2013.
29. M. Al-Jeboori, A. Al-Dujaili, and A. Al-Janabi, *Trans. Met. Chem.*, vol.34, pp. 109-113, 2009.
30. S. E. Livingston, J. H. Mayfield, D. S. Moore, *Aust. J. Chem.*, vol. 28, no.11, pp. 2531-2533, 1975.
31. G.S. Patricia, G.T. Javier, A.M. Miguel, J.A. Francisco, R. Teofilo, *Inorg. Chem.* 41, 1345, 2002.
32. A. Z. El-Sonbati, A. Z., El-bindary A. A., Al-Sarawy, *Spectrochim Acta Part A*, vol.58, no. 12, pp. 2771-2778, 2002.
33. R. M. Silverstein, *“Spectrometric Identification of Organic Compounds”*, Wiley; 7<sup>th</sup> Edition, 2005
34. K. Nakamoto, *Infrared Spectra of Inorganic and Coordination Compounds*, (1996) 4<sup>th</sup> ed., J. Wiley and Sons, New York.
35. C. K. Modi, *Spectrochim Acta Part A*, 71, 1741, 2009. doi:10.1016/j.saa.2008.06.024



A 3D molecular model of a 16S ribosomal subunit, showing a complex structure of yellow and orange subunits with a purple stalk and red/pink structures. The model is set against a dark blue background.

**16S RRNA SEQUENCING FOR IDENTIFICATION BACTERIA FROM FACE MASK OF  
STUDENTS IN MOSUL UNIVERSITY**

**SURA M.Y. AL-TAEE  
AMINA G.O. AL-ANI  
ALAA YOUNIS MAHDY**

## 16s rRNA SEQUENCING FOR IDENTIFICATION BACTERIA FROM FACE MASK OF STUDENTS IN MOSUL UNIVERSITY

Sura M.Y. AL-TAEE <sup>1</sup>

Amina G.O. AL-ANI <sup>2</sup>

Alaa Younis MAHDY<sup>3</sup>

### Abstract:

The use of masks has increased recently under the conditions of the Covid-19 pandemic as a prevention from the Covid-19, the research dealt with the study of bacterial contamination of masks from the surrounding environment, where in addition to the ability of masks to prevent the spread of viruses and bacteria, they are likely to be a source of bacterial contamination from the face, hands and air. 45 samples of face masks were collected from students of Mosul University in Iraq and the face mask was printed directly on Nutrient agar for 5 sec. Sixty isolates were obtained purely, Gram-positive bacteria were predominated after smearing the pure isolates and staining them with Gram stain.

Gram-positive isolates were grown on mannitol salt agar, which showed that they were not capable of fermenting mannitol sugar, oxidase and catalase assay was also performed, which gave a positive result for catalase and negative for oxidase. Three isolates were selected for molecular diagnosis by 16S rRNA. According to the 16S rRNA gene sequencing, three isolates were designated as:- *Staphylococcus equorum* and two isolates for *Staphylococcus saprophyticus*. The isolates showed sensitivity to Amikacin, Vancomycin, Chloramphenicol and Erythromycin antibiotics except for the antibiotic ofloxacin, *Staphylococcus equorum* and one isolate for *Staphylococcus saprophyticus* were intermediate to it.

**Key words:** Face Mask, 16s rRNA Sequencing, *Staphylococcus Equorum*, *Staphylococcus Saprophyticus*.



<http://dx.doi.org/10.47832/MinarCongress5-6>

<sup>1</sup>  University of Mosul, Iraq, [suramahmoud@uomosul.edu.iq](mailto:suramahmoud@uomosul.edu.iq), <https://orcid.org/0000-0001-6023-6355>

<sup>2</sup>  University of Mosul, Iraq, [amesbio115@uomosul.edu.iq](mailto:amesbio115@uomosul.edu.iq); <https://orcid.org/0000-0002-5524-0867>

<sup>3</sup>  Northern Technical University Mosul, Iraq, [Alaa.mahdy156@ntu.iq](mailto:Alaa.mahdy156@ntu.iq), <https://orcid.org/0000-0003-2276-0484>

## **Introduction:**

Using the face masks is increased now and this followed the recommendation of World Health Organization (WHO) during the COVID-19 outbreak. This study looked at the bacterial bioburden of disposable masks to see if there was a risk of bacterial cross-contamination (1,2). Masks are most commonly used to minimize transfer of respiratory droplets and to reduce respiratory virus transfer from infected to uninfected people. (2,3)

*Staphylococcus aureus*, *Candida albicans*, *Pseudomonas aeruginosa*, *Klebsiella pneumoniae*, *Veillonella spp.* and *Neisseria*, *Prevotella* are found in human saliva which can cause health risks when wearing masks for an extended period of time. (4,5).

Microbes thrive in cotton masks as it holds moisture therefore serving as an ideal substrate for microbial growth. Furthermore, when compared to surgical masks, the transmission of microbes is increased due to retention of moisture, reusing cotton masks in addition to insufficient filtration. (6)

Use of face masks incorrectly can increase the harm of infection and transmission of bacterial and viral infections. Because people touch their faces an average of 23 times per hour (7), with 44 percent of those touches including contact with a mucous membrane, self-inoculation of mucous membranes of the nose, eyes, and mouth is a popular route for viruses to spread (8). In addition to not taking other important precautions, such as social isolation and hand hygiene, may also be disregarded (9). Finally, wearing a face mask has been associated to irritation, acne, headaches, and respiratory problems.

The aim of the research: isolation of bacteria contaminating the face mask of students of the University of Mosul and then molecular diagnosis by 16s rRNA technology.

## **Material and methods:**

### **1-1- Isolation of Bacteria**

45 samples of face masks from students in Mosul University were taken after five hours from wearing it. Face masks directly imprinted for 5 seconds on Nutrient Agar (N.A) after assistance person using sterile gloves removed the face masks without contacting the surface as shown in Figure (1). Then incubation the plates at 37°C for 24-48 hours, after that the isolates were constantly purified until pure colonies were obtained. (10)

Swabs were made and stained with Gram stain in order to distinguish the shape and type of cells whether they were Gram positive or negative.



**Figure (1): Face masks directly imprinted for 5 second on Nutrient Agar**

### **1-2- Growing on the Mannitol Salt Agar**

The isolates with gram positive stain were grown on Mannitol Salt Agar to test their ability for fermenting mannitol sugar and Then incubation the plates at 37°C for 24-48 hours.(11)

### **1-3- Catalase and Oxidase tests .**

Two tests were conducted to distinguish between the isolates under study and the results were recorded(12).

### **1-4-16S rRNA sequencing**

Total DNA of three isolates were extracted using the G-spin DNA extraction kit according to the instructions from the manufacturer (intron biotechnology). Agarose electrophoresis was used to detect DNA. Table 1 shows the PCR reaction conditions in a 25 Ml final volume and table 2 shows the 16S rRNA sequencing reaction conditions. The National Center for Biotechnology Information (NCBI) program was used to find homologies.

**Table 1: The PCR reaction**

Material	Volume
Tag PCR Pre Mix	5 $\mu$ l
Forward primer (5'-AGAGTTTGATCCTGGCTCAG-3')	1 $\mu$ l
Reverse primer (5'-GGTACCTTGTACGACTT-3')	1 $\mu$ l
Total DNA	1.5 $\mu$ l
Distill water	16.5 $\mu$ l

**Table 2: The optimum condition of 16S rRNA sequencing reaction**

Stage	Cycles	Temperature	Time
Initial denaturation	1	95°C	5 min
Second denaturation	35	95 °C	45 sec
Annealing	35	58°C	45 sec
Initial extension	35	72°C	45 sec
Final extension	1	72°C	7min

**1-5- Phylogenetic Treeanalysis:**

The UPGMA method was used to infer the evolution. The best tree is displayed, with a branch length sum of =0.19035088. The branch lengths (next to the branches) are in the same units as the evolutionary distances used to estimate the phylogenetic tree and the tree is shown to scale. The evolutionary distances were calculated using the greatest composite likelihood approach. Three nucleotide sequences were analyzed and MEGA7 was used in evolutionary analyses .

**1-6- Antibiotic sensitivity**

On Mueller–Hinton agar, three isolates were tested for antimicrobial susceptibility using the disk diffusion (Kirby Bauer's) technique. standard antibiotics were used: Amikacin (AK 10 mcg) , Vancomycin (VA 30 mcg) , Chloramphenicol ( C 10mcg), Erythromycin ( E 10 mcg), Ofloxacin (OFX 5 mcg). 0.1mL from suspension for three isolates were dispersed onto Muller-Hinton agar with the concentration adjusted to around  $1 \times 10^8$  CFU/mL using the 0.5 McFarland standard. The agar was loaded with antibiotic discs. The diameter of each antibiotic's inhibitory zone was evaluated after a 24-hour incubation period at 37°C. (13).

**Result and Discussion****2-1- Isolation of Bacteria:**

The results of the initial isolation which was taken from face mask and imprinted on Nutrient Agar , showed that face masks were contaminated by a wide range of bacterial communities after the end of the incubation period . 60 pure isolates obtained from face masks samples were dyed with gram stain.

The prevailed bacteria in the samples were gram positive 82% while gram negative bacteria 18 . %

This is consistent with what were indicated (14) in the predominance of positive bacteria over negative bacteria of microbial contamination of the outer surface of face masks, where the dominant bacteria were *staphylococcus* spp. The face mask provide a suitable environment for microbial growth through the moisture and nutrient due to water vapor and exhaled air availability (15) .

The research of (10) showed the dominant bacteria were gram positive and this related the immunity of the person , in which the skin and mouth bacteria such as *Staphylococcus epidermidis* and *Bacillus* which represent the flora of nature but is more harmful to people who suffer from immunodeficiency.

## 2-2- Growing on the Mannitol Salt Agar

In this reasearch ,the isolates with gram positive showed their inability to ferment ate mannitol sugar on mannitol salt agar medium as a result of not forming a yellow color as shown in Figure (2).



**Figure 2: Bacteria nonfermentationmannitol sugar onMannitol Salt Agar**

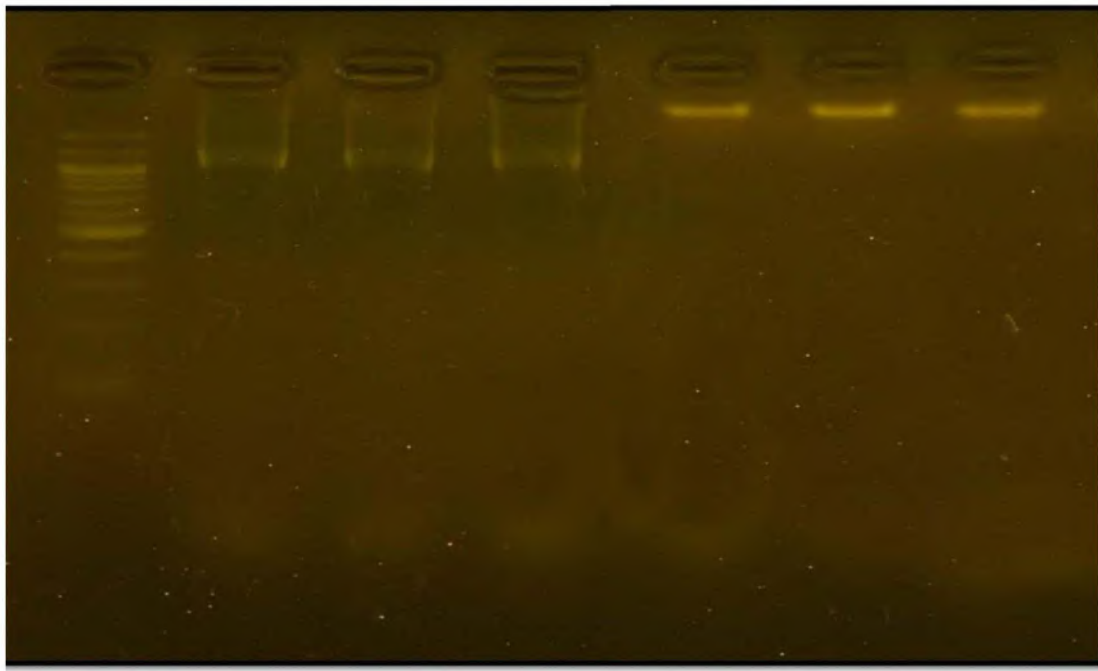
## 2-3-Catalase and Oxidase tests .

The unfermented isolates of mannitol sugar gave a positive result for the catalase test due to the formation of air bubbles, while the oxidase test gave a negative result due to the absence of violet color.

The oxidase and catalase tests showed that the isolates convert hydrogen peroxide into water and oxygenbecause of containing the enzyme catalase. Negative for the oxidase test because it does not contain the enzyme cytochrome oxidase.All *Staphylococci* species are catalase-positive and oxidase-negative, and certain species are unable to ferment mannitol sugar, which is compatible with what was mentioned by (16).

## 2-4- 16S rRNA sequencing

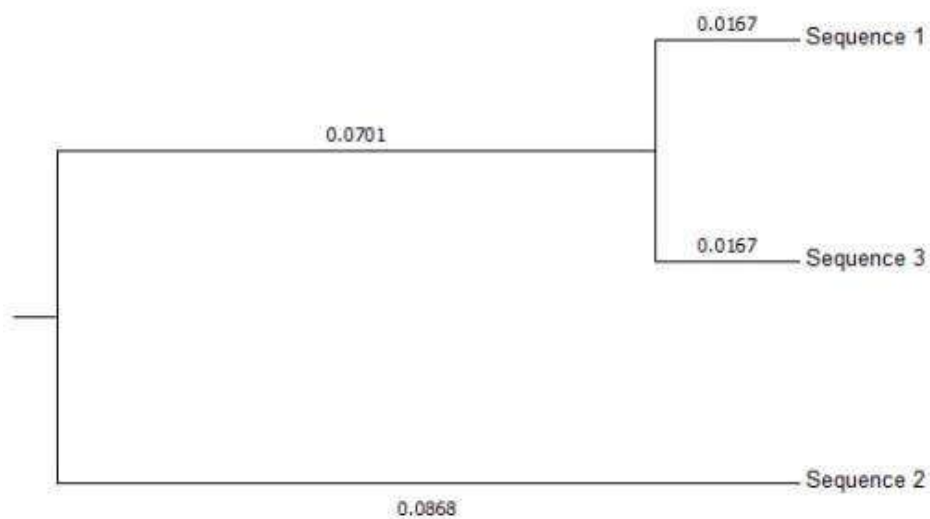
Universal primers of 16S rRNA sequencing was used for analysis and identification of one isolate for *Staphylococcus equorum* and two isolates for *Staphylococussaprophyticus* ,Figure (3) shows the bands on a garose gel .The partial 16S rRNA sequence was compared to NCBI data.



**Figure (3) Electrophoresis gel of 16S rRNA gene amplified from two isolates for *Staphylococcusaprophyticus* and one isolate for *Staphylococcus equorum***

### **2-5-Phylogenetic Treeanalysis**

The results show that Sequence 1 was closely related to the Sequence 3 as 98% while the cluster of the sequence 1 and 3 are less related to the Sequence 2 as 92 % Figure (4).



**Figure (4): phylogenetic tree using MEGA7 , that of *Staphylococcusaprophyticus* Sequence 1 and Sequence 3 while *Staphylococcus equorue* Sequence 2.**

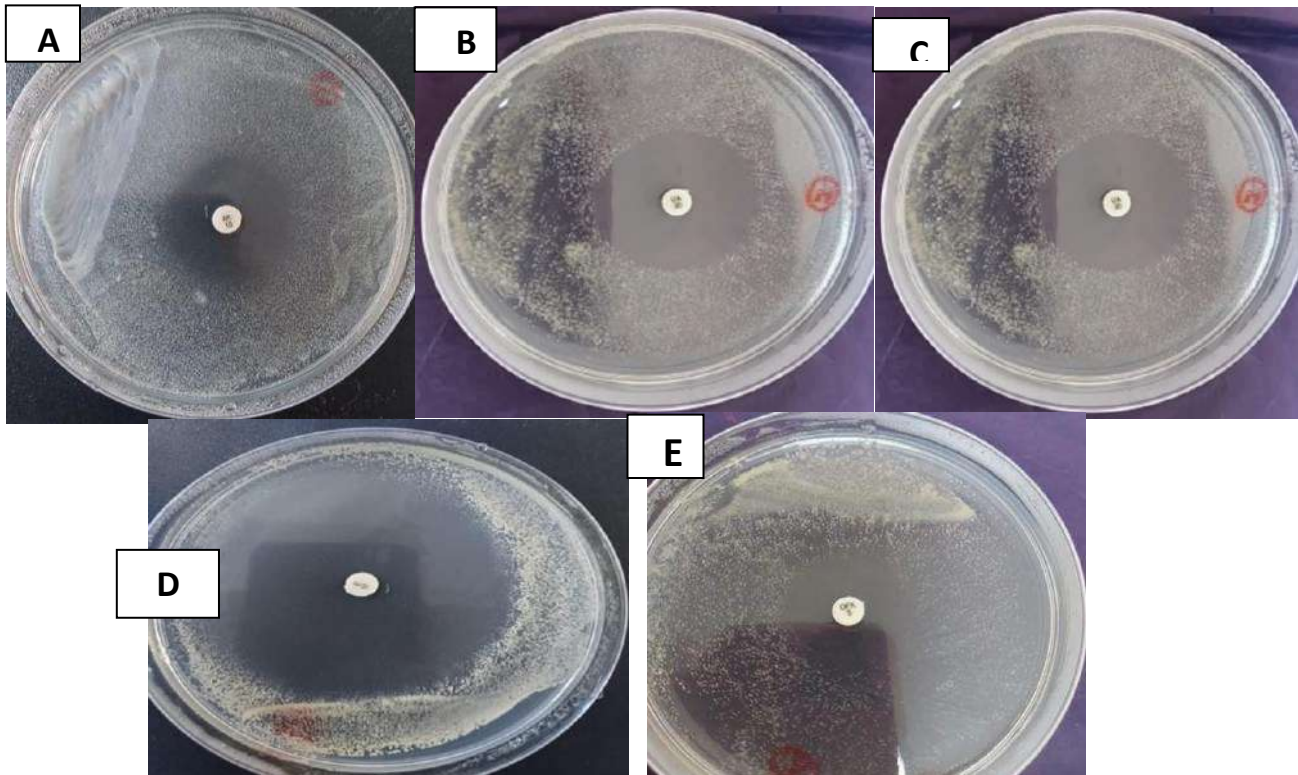
## 2-6- Antibiotic sensitivity

The results of Table (3 ) showed that three isolates have sensitivity to Amikacin, Vancomycin, Chloramphenicol and Erythromycin antibiotics except for the antibiotic Ofloxacin, *Staphylococcus equorum* and one isolate for *Staphylococcus saprophyticus* were intermediate to Ofloxacin.

**Table :(3): Sensitivity to Amikacin (AK 10 mcg) , Vancomycin( VA 30 mcg), Chloramphenicol (C 10 mcg) , Erythromycin (E10 mcg) , Ofloxacin ( OFX 5 mcg).**

Isolates	AK 10	VA 30	C 10	E 10	OFX 5
<i>Staphylococcus equorum</i>	s	s	s	s	intermediate
<i>Staphylococcus saprophyticus</i>	s	s	s	s	intermediate
<i>Staphylococcus saprophyticus</i>	s	s	s	s	s





**Figure (5): Antibiotic susceptibility for *Staphylococcus saprophyticus***

**A:AK 10 / B:VA 30/ C: C 10/ D:E 10 / E:OFX 5)**

Amikacin, chloramphenicol and erythromycin inhibit the protein synthesis process in the bacterial cell (17,19), While vancomycin inhibits the building of the cell wall in bacteria(18) and Ofloxacin effect on bacterial cell by binding to DNA gyrase and this result to inhibition of DNA replication(20).

**Conclusion:**

Despite the importance of face masks in reducing viral and bacterial infections, they may be a source of bacterial contamination from the hands, face and the surrounding environment. Therefore, the face mask must be changed from time to time, frequent hand washing and destroying the used face mask under health conditions.

## References

1. Liang, M., Gao, L., Cheng, C., Zhou, Q., Uy, J. P., Heiner, K., & Sun, C. (2020). Efficacy of face mask in preventing respiratory virus transmission: A systematic review and meta-analysis. *Travel medicine and infectious disease*, 36, 101751
2. Cowling, B. J., & Leung, G. M. (2020). Epidemiological research priorities for public health control of the ongoing global novel coronavirus (2019-nCoV) outbreak. *Eurosurveillance*, 25(6), 2000110
3. Leung, N. H., Chu, D. K., Shiu, E. Y., Chan, K. H., McDevitt, J. J., Hau, B. J., ... & Cowling, B. J. (2020). Respiratory virus shedding in exhaled breath and efficacy of face masks. *Nature medicine*, 26(5), 676-680
4. Hasan, N. A., Young, B. A., Minard-Smith, A. T., Saeed, K., Li, H., Heizer, E. M., ... & Colwell, R. R. (2014). Microbial community profiling of human saliva using shotgun metagenomic sequencing. *PLoS One*, 9(5), e97699
5. Rôças, I. N., & Siqueira Jr, J. F. (2006). Culture-independent detection of *Eikenellacorrodens* and *Veillonellaparvula* in primary endodontic infections. *Journal of endodontics*, 32(6), 509-512
6. Szostak-Kotowa, J. (2004). Biodeterioration of textiles. *International Biodeterioration & Biodegradation*, 53(3), 165-170
7. Akram, M. Z. (2020). Inanimate surfaces as potential source of 2019-nCoV spread and their disinfection with biocidal agents. *Virusdisease*, 31(2), 94-96
8. Kwok, Y. L. A., Gralton, J., & McLaws, M. L. (2015). Face touching: a frequent habit that has implications for hand hygiene. *American journal of infection control*, 43(2), 112-114
9. Feng, S., Shen, C., Xia, N., Song, W., Fan, M., & Cowling, B. J. (2020). Rational use of face masks in the COVID-19 pandemic. *The Lancet Respiratory Medicine*, 8(5), 434-436
10. Gund, M., Isack, J., Hannig, M., Thieme-Ruffing, S., Gärtner, B., Boros, G., & Rupf, S. (2021). Contamination of surgical mask during aerosol-producing dental treatments. *Clinical Oral Investigations*, 25(5), 3173-3180.
11. Budiarmo, T. Y., Prihatmo, G., Restiani, R., Pakpahan, S., & Sari, L. (2019, December). Detection *Staphylococcus aureus* Producing Enterotoxin A on the Skewers Meatballs Product in Yogyakarta City Indonesia. In *Journal of Physics: Conference Series* (Vol. 1397, No. 1, p. 012044). IOP Publishing.
12. Baron, E. J. (2001). Rapid identification of bacteria and yeast: summary of a National Committee for Clinical Laboratory Standards proposed guideline. *Clinical infectious diseases*, 33(2), 220-225
13. Zulkhairi Amin, F. A., Sabri, S., Ismail, M., Chan, K. W., Ismail, N., MohdEsa, N., & Zawawi, N. (2020). Probiotic properties of *Bacillus* strains isolated from stingless bee (*Heterotrigona itama*) honey collected across Malaysia. *International journal of environmental research and public health*, 17(1), 278.
14. Luksamijarulkul, P., Aiempradit, N., & Vatanasomboon, P. (2014). Microbial contamination on used surgical masks among hospital personnel and microbial air quality in their working wards: A hospital in Bangkok. *Oman Medical Journal*, 29(5), 346

15. Delanghe, L., Cauwenberghs, E., Spacova, I., De Boeck, I., Van Beeck, W., Pepermans, K., ... & Lebeer, S. (2021). Cotton and surgical face masks in community settings: bacterial contamination and face mask hygiene. *Frontiers in Medicine*, 1477.
16. Thakur, P., Nayyar, C., Tak, V., & Saigal, K. (2017). Mannitol-fermenting and tube coagulase-negative staphylococcal isolates: unraveling the diagnostic dilemma. *Journal of laboratory physicians*, 9(01), 065-066.
17. Gumustas, M., Sengel-Turk, C. T., Gumustas, A., Ozkan, S. A., & Uslu, B. (2017). Effect of polymer-based nanoparticles on the assay of antimicrobial drug delivery systems. In *Multifunctional systems for combined delivery, biosensing and diagnostics* (pp. 67-108). Elsevier.
18. Srinivasan, A., Dick, J. D., & Perl, T. M. (2002). Vancomycin resistance in staphylococci. *Clinical microbiology reviews*, 15(3), 430-438.
19. Fikai, A., & Grumezescu, A. M. (Eds.). (2017). *Nanostructures for antimicrobial therapy*. Elsevier.
20. Millanao, A. R., Mora, A. Y., Villagra, N. A., Bucarey, S. A., & Hidalgo, A. A. (2021). Biological Effects of Quinolones: A Family of Broad-Spectrum Antimicrobial Agents. *Molecules*, 26(23), 7153.



**COMPUTATION OF DOUBLE DIFFERENTIAL NEUTRON CROSS SECTIONS  
ON DIFFERENT TARGETS AT VARIOUS PROTON ENERGIES UTILIZING  
PHITS CODE**

**RABEE B. ALKHAYAT  
MUTAZ SALIH HASAN  
MUSHTAQ ABED AL - JUBBORI**

## COMPUTATION OF DOUBLE DIFFERENTIAL NEUTRON CROSS SECTIONS ON DIFFERENT TARGETS AT VARIOUS PROTON ENERGIES UTILIZING PHITS CODE

Rabee B. ALKHAYAT <sup>1</sup>  
Mutaz Salih HASAN<sup>2</sup>  
Mushtaq Abed AL-JUBBORI<sup>3</sup>

### Abstract:

In this paper, the PHITS program was used to measure the neutron production cross sections of <sup>12</sup>C, <sup>27</sup>Al, <sup>56</sup>Fe, <sup>91</sup>Zr, <sup>184</sup>W, <sup>207</sup>Pb, and <sup>232</sup>Th at 256, 800, 1200, and 1600 MeV proton energies at different scattering angles. A comparison of available experimental data to PHITS computations revealed some discrepancies, particularly with low incidence proton energy and light nuclei targets. PHITS estimates the production neutron cross section at low and intermediate energies for light nuclei significantly higher due to neutron evaporation happening in this range (10 - 30 MeV). The PHITS code's ability to determine the double differential cross section DDXs for a wide range of incident protons is accurate, notably above 800 MeV incident particles for all angles to precisely calculate neutron angular distributions. Moreover, the cross section of neutron generation reduces in forward angles while increases in backward angles as the target thickness increases due to proton energy loss, which increases scattering events.

**Key words:** PHITS; INCL Code; High Energy; Cross-Section; Angular Distribution.



<http://dx.doi.org/10.47832/MinarCongress5-7>



<sup>1</sup> University of Mosul, Iraq, [khayatrabee@uomosul.edu.iq](mailto:khayatrabee@uomosul.edu.iq), <https://orcid.org/0000-0002-0449-5923>



<sup>2</sup> University of Mosul, Iraq, [mutazsalih2017@gmail.com](mailto:mutazsalih2017@gmail.com), <https://orcid.org/0000-0001-7193-5266>



<sup>3</sup> University of Mosul, Iraq, [mushtaq\\_phy@yahoo.com](mailto:mushtaq_phy@yahoo.com), <https://orcid.org/0000-0002-8299-340X>

## Introduction:

Researchers have been impressed by the interaction of high-energy proton with atomic nuclei for several years, especially to understanding the elastic and inelastic scattering process [1]. However, in latest days, scientists have developed a greater involvement in more forceful forms of physics. Several laboratories have been working hard in recent years to collect spallation information on neutron angular distributions, and charged particles (heavy and light) to be able to build a basis for testing and validating spallation models [2]–[10]. Neutrons can be produced through reactions of protons with a heavy nuclei target. Recent studies have focused on the spallation reaction for applications such as spallation neutron sources and accelerator-driven transmutation systems. Nuclear data in the energy range of a few GeV is required for these purposes. Nuclear data packages like ENDF/B-VI [11] and JENDL-3.1 [12] were tested to a maximum energy of 20 MeV, while those in the higher energy range have yet to be fully established. For engineering applications of the spallation reaction, computer codes such as the High Energy Transport Code (HETC), which used the elastic scattering cross section of free nucleon-nucleon interactions [13], and the Nucleon Meson Transport Code (NMTC) [14], which considers the in medium impact in nucleus, have been used. The nuclear computation procedures in these codes are based on Bertini's intranuclear cascade evaporation (INCE) model [15]. Several groups altered the original codes to create HETC-3STEP [16], LAHET [17], and NUCLEUS [18] versions. These codes were used to design spallation neutron applications facilities as well as to estimate nuclear data in the middle energy region.

Normally, common spallation targets are made from solid materials (such as W and Pb) or liquids (such as Hg and eutectic). Target materials require a good optimization and performance to produce neutrons and to assessment the accelerator problems that may occur in system such as radioactivity, damaging in target, structural materials, and shielding requirements during a penetration process of a high neutron. The accelerator driven system which used spallation neutron to drive subcritical reaction is useful to extract the nuclear waste as an example [19]. In a thick target, secondary particles play a major role in the propagation of the intranuclear cascade, so it's critical to improve the target geometry. Even the scattering events occur with thin target as well [20]. All those variations can be handled by simulation codes such as PHITS and MCNP [21], [22]. The prevalent computation used in these models are intranuclear cascades followed by fission. Some modifications to the target nucleus are possible. It can probably disintegrate into many parts if the excitation energy is relatively high.

The interaction process between proton and nucleus target can be broken down into two steps. In the first step, the proton enders a few incoherent scattering with target's nucleons, depositing some of its energy in this way. The second step, which presumably begins after the proton has left the target, is transformation and evaporation of the nucleus gained energy [23]. The energy is released by the nucleons that collide in the first step, leaving the nucleus unaffected. the residual nucleus may release some of the energy attained from its deformation [24].

The discrepancies between the experimental results and different model calculations were obvious examined in a high proton energy. It further came to the fact that the models needed to be improved, although there was a scarcity of

experimental results to make an excellent verification, practically above 0.8 GeV [25], [26]. The energy of spallation nucleons and their angular distributions become crucial in simulation models because the highly energetic region of the spectrum allows for the detection of intranuclear cascades. Whereas the low-energy region of the spectrum is sensitive to excitation energy at the conclusion of the intranuclear cascades and evaporation model. In addition, energy and angular distribution results important to enhance the target geometry as mentioned.

In this work, the results of the measurements of neutron production DDXs using the Particle and Heavy Ion Transport Code System (PHITS) were evaluated by using the theoretical model of the Liège Intranuclear Cascade (INCL) of  $^{12}\text{C}$ ,  $^{27}\text{Al}$ ,  $^{56}\text{Fe}$ ,  $^{91}\text{Zr}$ ,  $^{184}\text{W}$ ,  $^{207}\text{Pb}$  and  $^{232}\text{Th}$  at proton energies of 256, 800, 1200 and 1600 MeV at different scattering angles. The PHITS code was then validated by comparing the results to previously collected experimental data.

## 2. Heavy Ion Transport Code System (PHITS) simulation

Monte Carlo particle transport simulation codes are useful in a variety of fields, including radiation shielding, radiological safety, and medical physics. It is capable of transporting a variety of particle types with energies of up to 1 TeV by utilizing various nuclear reaction models and database libraries. On the basis of a comparison study of more than 50 irradiation situations, the code was thoroughly validated and verified for various applications [27]. The Monte Carlo simulation codes were accomplished in PHITS version 3.24 on an appropriate computer operating on Windows system using the theoretical model Liège intranuclear cascade (INCL) [28]. PHITS simulation can be used to calculate various quantities such as heat deposition, track length, and production yields using the implemented "tally" measurement functions. A simulation's geometrical configuration must be set with general geometry in the same way that MCNP requires (GG). In PHITS, the proton induced reaction is utilized as a standard model in the INCL calculations. It really is a time-like intranuclear cascade template which depicts the kinetic procedure of a nuclear chain process by describing successive binary interactions between protons and neutrons inside a nucleus under the influence of a nucleus average field. Following the dynamic procedure operation, PHITS changes the interaction model from INCL to the Generalized Evaporation Model (GEM) [29], which uses the Weisskopf-Ewing theory to treat the evaporation and fission process in equilibrium [30].

In the simulation model, the dimensions of targets and energy of bombarded proton were used as described in the experimental data publications as displayed in Table 1 [20], [31]. Moreover, the neutrons emitted were detected through a detector that was located along the proton axis at the same solid angle as the experimental described. The additional geometry was occupied with ideal vacuum to complete the simulation structure as well as speed up the simulation process. Also, as a way to reduce variance, the forced collision method was employed using the "istdev" parameter. The statistical error of the current simulation was below 7% throughout most of energy bins. For both protons and neutrons, the lower energy threshold for stopping transport was set at 0.7 MeV.



Table 1. Characterization of target and proton beams.

Target	Density (g/cm <sup>3</sup> )	Mean excitation energy (eV)	Thickness (cm); Beam energy loss (MeV)			
			256 MeV MeV	800 MeV	1200 MeV	1600
<sup>12</sup> C	1.75	78	<u>10</u> ; 60	<u>10</u> ; 37	-----	-----
<sup>27</sup> Al	2.69	166	<u>10</u> ; 82	<u>4</u> ; 20	<u>3</u> ; 14	-----
<sup>56</sup> Fe	7.87	286	<u>10</u> ; 214	<u>3</u> ; 40	<u>3</u> ; 36	<u>3</u> ; 35
<sup>91</sup> Zr	6.51	393	-----	-----	<u>3</u> ; 27	-----
<sup>184</sup> W	19.35	727	-----	-----	<u>1</u> ; 23	-----
<sup>207</sup> Pb	11.34	823	<u>10</u> ; 226	<u>2</u> ; 28	<u>2</u> ; 26	<u>2</u> ; 26
<sup>232</sup> Th	11.72	847	-----	-----	<u>2</u> ; 26	-----

### 3. Results and Discussion

Double differential neutron production cross sections for <sup>12</sup>C, <sup>27</sup>Al, <sup>56</sup>Fe, and <sup>207</sup>Pb at energy 256 MeV are shown in Fig.1. The black solid circles and blue lines denote the experimental data [32] and PHITS results respectively. The neutron peaks in forward direction distinguish the spectrum at forward angles. The quasielastic peak observed at energies tight to those of the incident charged particle. This happens when the projectile collides with a neutron in the nucleus target directly. Likewise, the pion emission caused by excitation of the 1232 MeV resonance in inelastic nucleon–nucleon colliding is linked to the widening peak a little below the quasielastic peak [33]. Results of 30° and 60°, PHITS calculations are in good agreement with the experiment data, especially for nuclei larger than <sup>56</sup>Fe. The PHITS results at 7.5° provide a good estimate except for <sup>12</sup>C. Above 50 MeV, the computed cross section underestimates the experimental data, possibly because the pre-equilibrium process dominates in this energy and angle regime. Finally at 150°, the PHITS calculations are slightly less than the experimental results, and the differences become more prominent above 30 MeV by factor of 1. In comparison to HETC calculations, which give a difference with 256 MeV proton data up to a factor of 7 for backward angles [32], PHITS gives a difference up to a factor of 1. In overall, the PHITS results exceed the results of the experiment at neutron energies greater than 2 MeV. This is due to uncorrected time walk impacts. Besides that, there might be some variation in carbon cross sections [34]. Furthermore, a study of a surface coalescence model included in the INCL4.6 model found that Clusters are formed in the cascade stage at the expense of neutron and proton production. As a result, there is a miscalculation in energy range of 30 to 80 MeV [28].

At 800 MeV, Fig 2 displays the computed neutron spectra compared to

experimental data [31], [34] for the  $^{12}\text{C}$ ,  $^{27}\text{Al}$ ,  $^{56}\text{Fe}$ , and  $^{207}\text{Pb}$  targets. The PHITS calculation replicates the data very well for  $^{56}\text{Fe}$  and  $^{207}\text{Pb}$ , excluding neutron production at quite forward angles and high energies for light nuclei such as  $^{12}\text{C}$ , where the apex associated with resonance excitation seems to be somewhat lower. Moreover, as the target becomes lighter, PHITS slightly overestimates the yield of neutrons with intermediate and low energy as seen in  $^{12}\text{C}$  and  $^{27}\text{Al}$  targets. In general, PHITS accurately predicts the spectral low energy region. High energy neutrons above  $40^\circ$  are quite well recognized by the PHITS code, particularly for heavy targets. However, there is an underestimation of the cross section at backward angles in the intermediate energy region about 10 - 30 MeV for  $^{56}\text{Pb}$ . PHITS calculations typically yield slightly higher cross sections for the 0.8-MeV proton than the experiment data for 1 to 10 MeV because the neutron evaporation region dominates at this energy, and the disagreement being more pronounced for the  $^{12}\text{C}$  target. Generally, the enhanced agreement obtained by PHITS can be attributed to use of nucleon-nucleon scattering cross sections.

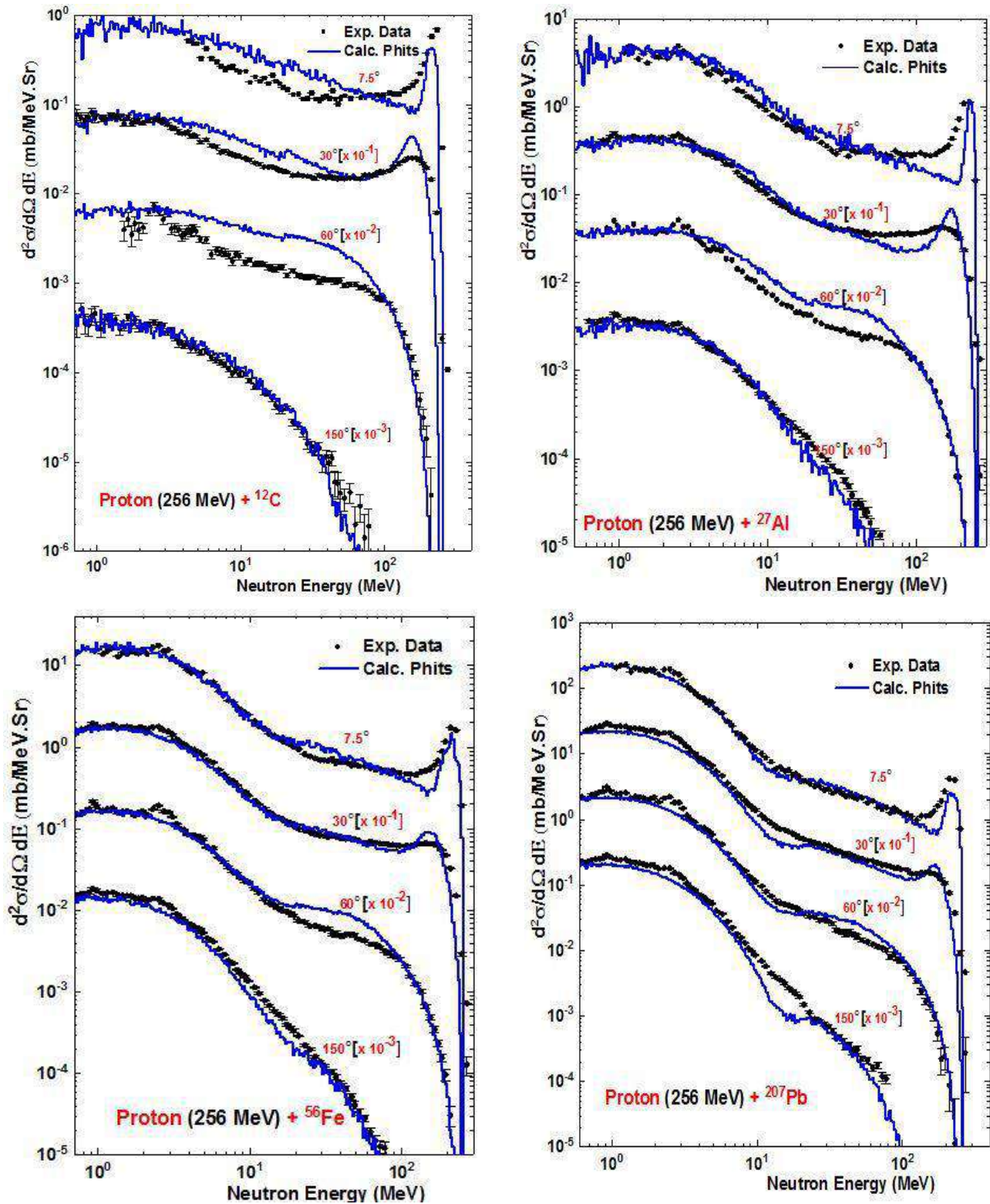
PHITS provides an appropriate agreement with the experimental data [31] for 1200 MeV regardless of the target type, revealing that PHITS has a proper mass dependence. High energy neutron production is predicted to be underestimated only for targets with lower atomic weight at extreme reverse angles. PHITS code calculations estimate a slightly lower neutron cross section at intermediate energy (10 -40 MeV) for  $^{184}\text{W}$ ,  $^{207}\text{Pb}$ , and  $^{232}\text{Th}$  targets.

The results for the  $^{56}\text{Fe}$  and  $^{207}\text{Pb}$  targets at 1600 MeV are shown in Fig. 4. PHITS agrees well with the experimental data [31] used for both targets, indicating a high dependence of the pre-equilibrium emission on incident energy. The high energy part of the spectra, on the other hand, is always rather reproduced, particularly at the peak for forward angles. At incident proton energies greater than 1 GeV, the fragmentation reaction, capable of emitting nuclei such as Na and Mg, is thought to occur frequently after the cascade process. The excitation energy of the residuals decreases as a result of fragment emission [35]. The experiment data for neutrons with energies greater than 100 MeV were primarily calculated at forward and intermediate angles. The calculations, in general, reproduce the experimental data. At the highest neutron energies, for instance,  $60^\circ$  and  $90^\circ$  data, there are discrepancies between the calculated and experimental results. This is due to the fact that the flight path length in some cases was as small as 1 m, and the time walk correction was insufficient as mentioned before. At neutron energies ranging from 10 to 30 MeV, the PHITS results become less than the experimental data as incident proton energy decreases, and the underestimation is more pronounced in lighter targets.

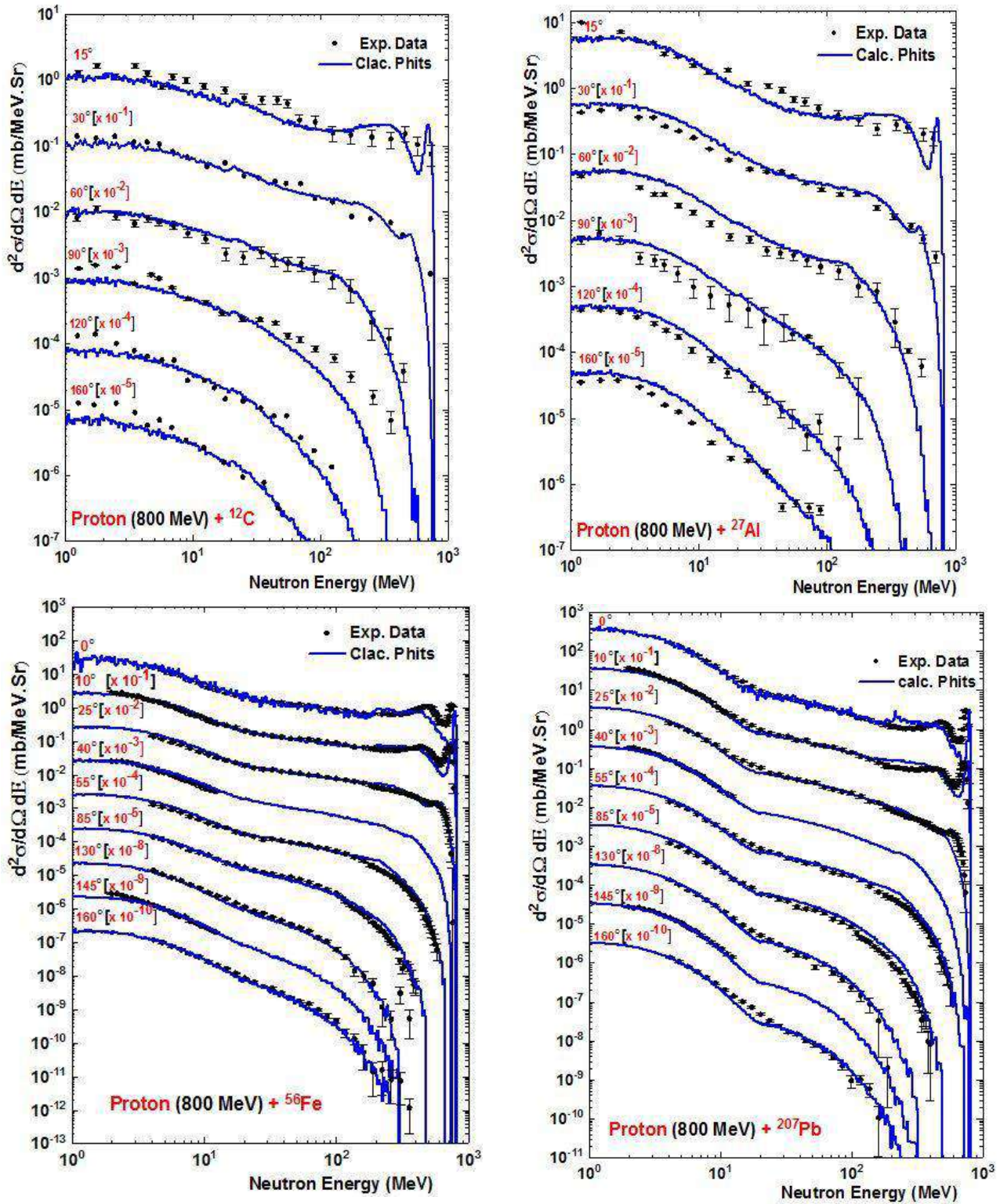
## Conclusion

PHITS simulation was used to determine neutron double differential cross sections for the targets  $^{12}\text{C}$ ,  $^{27}\text{Al}$ ,  $^{56}\text{Fe}$ ,  $^{91}\text{Zr}$ ,  $^{184}\text{W}$ ,  $^{207}\text{Pb}$  and  $^{232}\text{Th}$  at proton beams with energies of 256, 800, 1200, and 1600 MeV. PHITS is capable of globally reproducing the major portion of experimental results, with few minor differences in neutron angular distributions. PHITS calculations better reproduce experimental data at incident proton energies greater than or equal to 800 MeV. However, as the energy is reduced below 800 MeV and the target's atomic weight significantly reduces,

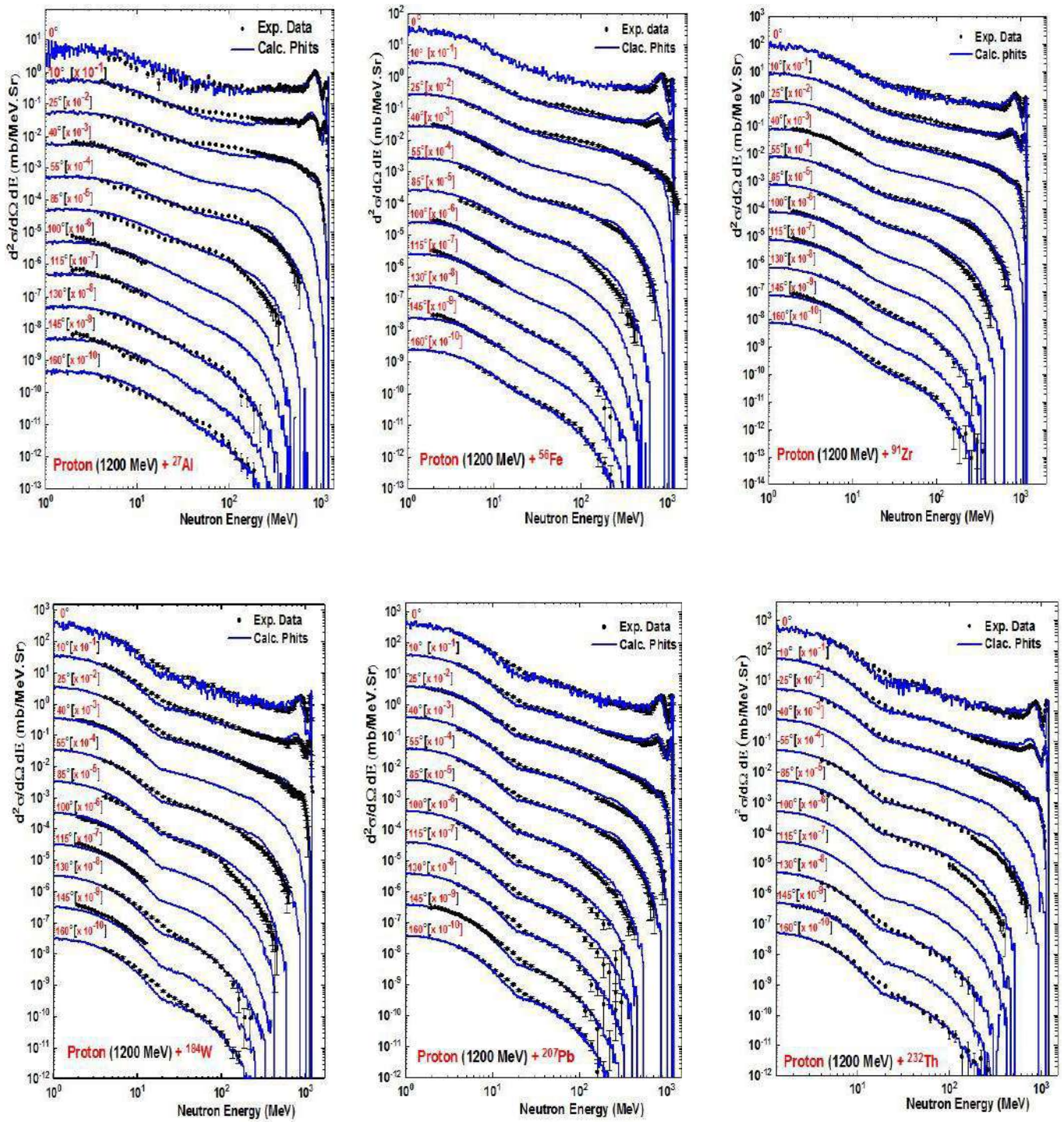
discrepancies begin to appear and grow larger. Furthermore, the measured cross section increases as the projectile particle energy increases for all target nuclei. At neutron energies ranging from 10 to 30 MeV, the PHITS results deviate from the experimental data as incident proton energy decreases, with the underestimation being more pronounced in lighter targets. Finally, this paper provides a good estimate of the PHITS code's potential to determine the double differential cross section for a wide range of incident protons.



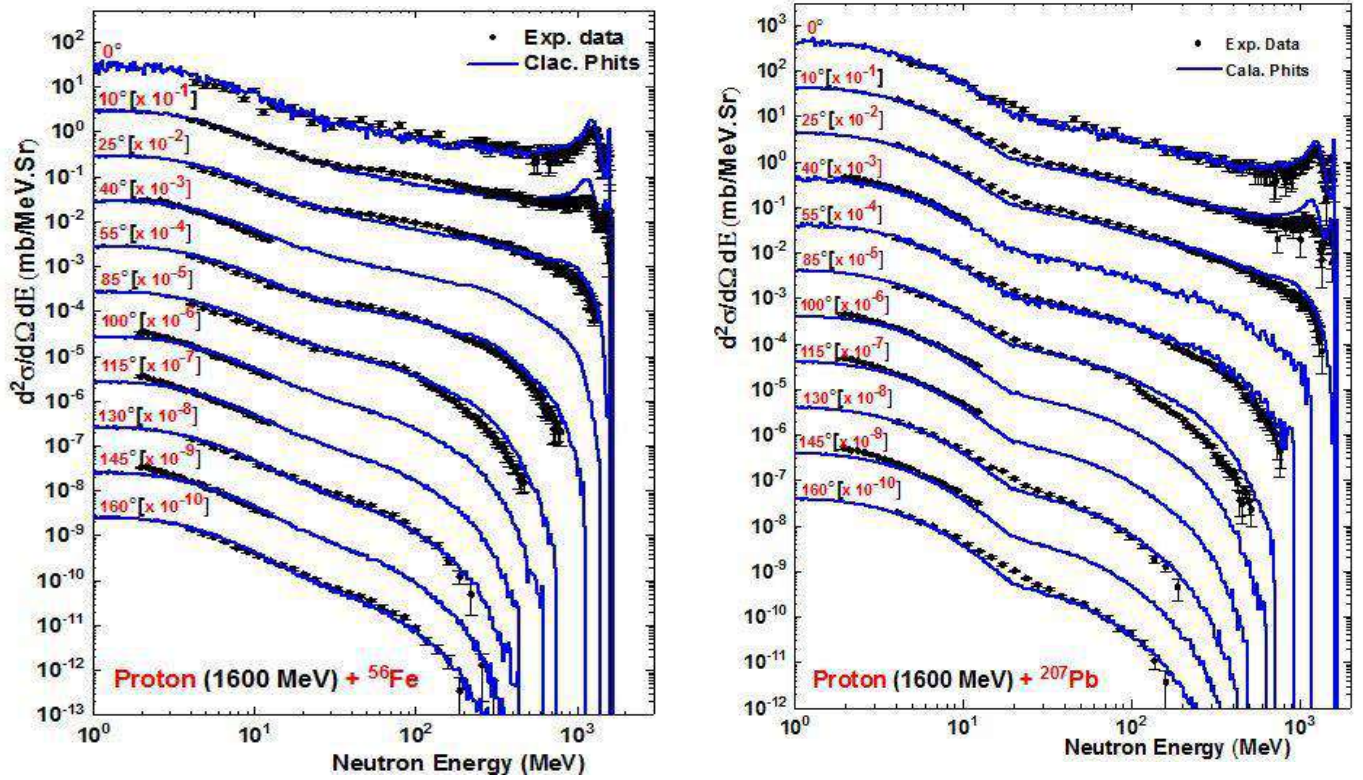
**Fig. 1. Neutron DDXs for 256 MeV proton beams incident on  $^{12}\text{C}$ ,  $^{27}\text{Al}$ ,  $^{56}\text{Fe}$ , and  $^{207}\text{Pb}$  at various scattering angles. Every consecutive curve is multiplied by a factor of  $10^{-1}$  except the first angle.**



**Fig. 2. Neutron DDXs for 800 MeV proton beams incident on  $^{12}\text{C}$ ,  $^{27}\text{Al}$ ,  $^{56}\text{Fe}$ , and  $^{207}\text{Pb}$  at various scattering angles.**



**Fig. 3. Neutron DDXs for 1200 MeV proton beams incident on  $^{27}\text{Al}$ ,  $^{56}\text{Fe}$ ,  $^{91}\text{Zr}$ ,  $^{184}\text{W}$ ,  $^{207}\text{Pb}$ , and  $^{232}\text{Th}$  at various scattering angles.**



**Fig. 4. Neutron DDXs for 1600 MeV proton beams incident on <sup>56</sup>Fe and <sup>207</sup>Pb at various distribution angles.**

## References

1. G. W. Hoffmann *et al.*, “ $A_y(\theta)$  for  $p \rightarrow +$  Pb208 elastic scattering at 0.8 GeV and a test of multiple scattering theory,” *Phys. Rev. C*, vol. 24, no. 2, pp. 541–551, 1981.
2. L. Pienkowski, F. Goldenbaum, D. Hilscher, U. Jahnke, H. Berlin, and D.- Berlin, “Neutron multiplicity distributions for 1.94 to 5 GeV/c proton-, antiproton-, pion-, kaon-, and deuteron-induced spallation reactions on thin and thick targets,” *Phys. Rev. C*, vol. 56, no. 4, pp. 1909–1917, 1997.
3. X. Ledoux *et al.*, “Formation and decay of hot nuclei in 475 MeV, 2 GeV proton- and 2 GeV 3He-induced reactions on Ag, Bi, Au, and U,” *Phys. Rev. C - Nucl. Phys.*, vol. 57, no. 5, pp. 2375–2392, 1998.
4. B. Lott *et al.*, “Neutron multiplicity distributions for 200 MeV proton-, deuteron- and 4He-induced spallation reactions in thick Pb targets,” *Nucl. Instruments Methods Phys. Res. Sect. A Accel. Spectrometers, Detect. Assoc. Equip.*, vol. 414, no. 1, pp. 117–124, Sep. 1998.
5. D. Hilscher, U. Jahnke, F. Goldenbaum, L. Pienkowski, J. Galin, and B. Lott, “Neutron production by hadron-induced spallation reactions in thin and thick Pb and U targets from 1 to 5 GeV,” *Nucl. Instruments Methods Phys. Res. Sect. A Accel. Spectrometers, Detect. Assoc. Equip.*, vol. 414, no. 1, pp. 100–116, Sep. 1998.
6. M. Enke *et al.*, “Evolution of a spallation reaction: experiment and Monte Carlo simulation,” *Nucl. Phys. A*, vol. 657, no. 3, pp. 317–339, Sep. 1999.
7. R. Michel *et al.*, “Cross sections for the production of residual nuclides by low- and medium-energy protons from the target elements C, N, O, Mg, Al, Si, Ca, Ti, V, Mn, Fe, Co, Ni, Cu, Sr, Y, Zr, Nb, Ba and Au,” *Nucl. Instruments Methods Phys. Res. Sect. B Beam Interact. with Mater. Atoms*, vol. 129, no. 2, pp. 153–193, Jul. 1997.
8. F. Rejmund *et al.*, “Measurement of isotopic cross sections of spallation residues in 800 A MeV 197Au+p collisions,” *Nucl. Phys. A*, vol. 683, no. 1–4, pp. 540–565, Feb. 2001.
9. [9] T. Enqvist *et al.*, “Isotopic yields and kinetic energies of primary residues in 1 A GeV 208Pb+p reactions,” *Nucl. Phys. A*, vol. 686, no. 1–4, pp. 481–524, Apr. 2001.
10. Y. Y. Kassim and R. B. Alkhayat, “Influence of UV irradiation on the diameters and depths of alpha-particle tracks in CR-39 detectors,” *Nucl. Instruments Methods Phys. Res. Sect. B Beam Interact. with Mater. Atoms*, vol. 503, pp. 6–10, Sep. 2021.
11. F. Rose, R., “BNL-NCS-17541,” 1991.
12. et al. Shibata, Keiichi, “Japanese Evaluated Nuclear Data Library, Version-3: JENDL-3,” 1990.
13. K. C. Armstrong, T. W. and Chandler, “HETC Monte-Carlo Nucleon-Meson Transport Code,” *Nucl. Sci. Eng*, vol. 49, p. 110, 1972.
14. E. Suetomi, N. Kishida, and H. Kadotani, “An analysis of the intranuclear cascade evaporation model with in-medium nucleon-nucleon cross sections,” *Phys. Lett. B*, vol. 333, no. 1–2, pp. 22–26, Jul. 1994.
15. H. W. Bertini, “Results from low-energy, intranuclear-cascade calculation,” *Nucl. Phys.*, vol. 87, no. 2, pp. 138–140, 1966.
16. N. Yoshizawa, K. Ishibashi, and H. Takada, “Development of high energy transport code HETC-3STEP applicable to the nuclear reaction with incident energies above 20 MeV,” *J. Nucl. Sci. Technol.*, vol. 32, no. 7, pp. 601–607, 1995.
17. R. E. Prael and H. Lichtenstein., “LANL Report LA-UR-89-3014, Los Alamos,” 1989.
18. H. Takada, “Nuclear medium effects in the intranuclear cascade calculation,” *J. Nucl. Sci. Technol.*, vol. 33, no. 4, pp. 275–282, 1996.
19. C. D. Bowman *et al.*, “Nuclear energy generation and waste transmutation using an accelerator-driven intense thermal neutron source,” *Nucl. Instruments Methods Phys. Res. Sect. A Accel. Spectrometers, Detect. Assoc. Equip.*, vol. 320, no. 1–2, pp. 336–367, Aug. 1992.
20. D. Satoh, Y. Iwamoto, and T. Ogawa, “Measurement of neutron-production double-



- differential cross sections of natC, 27Al, natFe, and natPb by 20, 34, 48, 63, and 78 MeV protons in the most-forward direction,” *Nucl. Instruments Methods Phys. Res. Sect. A Accel. Spectrometers, Detect. Assoc. Equip.*, vol. 920, no. September 2018, pp. 22–36, 2019.
21. T. Sato *et al.*, “Features of Particle and Heavy Ion Transport code System (PHITS) version 3.02,” *J. Nucl. Sci. Technol.*, vol. 55, no. 6, pp. 684–690, 2018.
  22. C. J. Werner *et al.*, “MCNP6.2 Release Notes,” *Rep. LA-UR-18-20808*, pp. 1–39, 2018.
  23. J. Cugnon, “Proton-nucleus interaction at high energy,” *Nucl. Phys. A*, vol. 462, no. 4, pp. 751–780, Feb. 1987.
  24. G. Rudstam, “Systematics of Spallation Yields,” *Zeitschrift fur Naturforsch. - Sect. A J. Phys. Sci.*, vol. 21, no. 7, pp. 1027–1041, 1966.
  25. R. D. Filges, D. Nagel, P., & Neef, “OECD thick target benchmark for lead and tungsten,” *Rep. NSC/DOC*, vol. 95, no. 2, 1995.
  26. Y. T. Al-Khalil, M. Fromm, E. M. Awad, R. B. Alkhatat, A. T. Zakar, and M. A. Al-Jubbori, “On the question of track etch rate amplitude variation in the Bragg-peak vicinity: Experimental verification for low-energy  $1\ \mu\text{m}^{1/4}$ -particle tracks in CR-39,” *Nucl. Inst. Methods Phys. Res.*, vol. 1031, p. 166516, 2022.
  27. Y. Iwamoto *et al.*, “Benchmark study of the recent version of the PHITS code,” *J. Nucl. Sci. Technol.*, vol. 54, no. 5, pp. 617–635, 2017.
  28. A. Boudard, J. Cugnon, J. C. David, S. Leray, and D. Mancusi, “New potentialities of the Liège intranuclear cascade model for reactions induced by nucleons and light charged particles,” *Phys. Rev. C - Nucl. Phys.*, vol. 87, no. 1, 2013.
  29. S. Furihata, “Statistical analysis of light fragment production from medium energy proton-induced reactions,” *Nucl. Instruments Methods Phys. Res. Sect. B Beam Interact. with Mater. Atoms*, vol. 171, no. 3, pp. 251–258, Nov. 2000.
  30. J. Halpern, I. Estermann, O. C. Simpson, O. Stern, and V. Weisskopf, “STATISTICS AND NUCLEAR REACTIONS 295 section, thus permitting a check of the consistency of the whole theory. Note added in proof: Recently published experiments by Statistics and Nuclear Reactions,” vol. 344, 1937.
  31. S. Leray *et al.*, “Spallation neutron production by 0.8, 1.2, and 1.6 GeV protons on various targets,” *Phys. Rev. C - Nucl. Phys.*, vol. 65, no. 4, pp. 446211–4462117, 2002.
  32. M. M. Meier, W. B. Amian, C. A. Goulding, G. L. Morgan, and C. E. Moss, “Differential neutron production cross sections for 256-MeV protons,” *Nucl. Sci. Eng.*, vol. 110, no. 3, pp. 289–298, 1992.
  33. X. Ledoux *et al.*, “Spallation neutron production by 0.8, 1.2, and 1.6 GeV protons on pb targets,” *Phys. Rev. Lett.*, vol. 82, no. 22, pp. 4412–4415, 1999.
  34. K. Ishibashi *et al.*, “Measurement of neutron-production double-differential cross sections for nuclear spallation reaction induced by 0.8, 1.5 and 3.0 GeV protons,” *J. Nucl. Sci. Technol.*, vol. 34, no. 6, pp. 529–537, 1997.
  35. Lynch W. G, “Nuclear fragmentation in proton and heavy ion induced reactions,” *Ann. Rev. Nucl. Part. Sci.*, vol. 37, pp. 493–535, 1987.

The image features two glass vials with cork stoppers, each containing a pink liquid. In the foreground, a single pink flower with five petals is in focus. The background is a soft, out-of-focus green and white. The text is centered over the image.

**OPTICAL PROPERTIES OF ANTHOCYANIN EXTRACTED FROM FLOWERS**

**FATIMA H. MALK**

**ALYAA ABDUL HASAN ABDUL KAREM**

**DHIAA J. AGOOSH**

## OPTICAL PROPERTIES OF ANTHOCYANIN EXTRACTED FROM FLOWERS

**Fatima H. MALK<sup>1</sup>**

**Alyaa Abdul Hasan ABDUL KAREM<sup>2</sup>**

**Dhiaa J. AGOOSH<sup>3</sup>**


### **Abstract:**

Extract of the dye contained in the flower known locally as the morning rose, which has the scientific name (*Portulaca grandiflora*), was used in this study. UV-VIS spectroscopy, which is represented by optical qualities such as absorbance (A), which was within the boundaries of the visible spectrum at wavelengths (490-740nm), and optical constants such as absorption coefficient ( $\alpha$ ), is effective due to the bonding that create the dye. Which has a value more than  $10^4$ , and the electrical transmission is direct, as well as the refractive index (n) equal (1.6), Decay coefficient (k) between (0.001-0.005), and optical energy gap  $E_g$ , which is equivalent to 3.5eV.


**Key words:** *Portulaca Grandiflora*, Optical Properties, Absorption Coefficient.

---

 <http://dx.doi.org/10.47832/MinarCongress5-8>

<sup>1</sup>  Materials Science Department -University of Basrah, Iraq, [Fatima.hameed16@yahoo.com](mailto:Fatima.hameed16@yahoo.com), <https://orcid.org/0000-0003-1446-3359>

<sup>2</sup>  Chemistry and Polymer Technology- University of Basrah, Iraq, [aliaa\\_raed@gmail.com](mailto:aliaa_raed@gmail.com), <https://orcid.org/0000-0001-7129-8332>

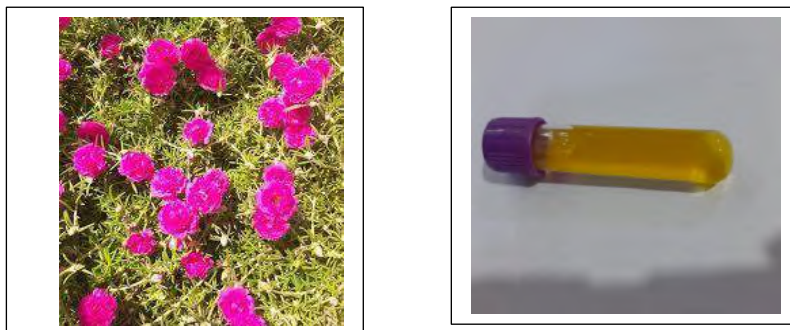
<sup>3</sup>  Dhi Qar Education- Ministry of Education, Iraq, [dhiaajapear@gmail.com](mailto:dhiaajapear@gmail.com), <https://orcid.org/0000-0003-1086-1130>

### **Introduction:**

Natural dyes have been used extensively for many applications, due to the ease of obtaining them and their cheapness, including the dyes found in many flowers, such as the dye found in the locally known *Portulaca grandiflora*, which bears the scientific, It has been used in oriental traditional medicine to relieve sore throats, rashes, and remove toxins. No research has been published linking these actions to the active substances of the plant. For this reason, the chemical composition of the species grown in Romania was studied, in order to determine its therapeutic potential. Species were identified by comparing their morphological characteristics with those described for treatment. The chemical composition was evaluated by specific chemical reactions and thin layer chromatography (TLC)(1,2,3). The total phenols, carboxyl polyphenols and flavonoids were quantitatively determined by spectrophotometric methods (4), Qualitative phytochemical examination revealed the presence of alkaloids, carbohydrates, saponins, steroids, triterpenoids. Conclusions: The results of the study can be useful in defining quality standards to determine the method and field of uses of dye(5). In our research, the optical properties and the possibility of using the dye in electronic fields were studied.

### **Material and method**

Distilled water, flower petals, glass beaker, water bath. The flower petals were collected and placed in a glass container and left to dry for 24 hours at room temperature, after which the petals were carefully washed with distilled water from the dust and dirt stuck in it as a result of exposure to the atmosphere. Then I took 1 g of dry petals and took 50 ml of solvent (distilled water). The petals were placed completely immersed in water in a glass beaker, that is, the ratio between the dye and the solvent was 1:50. An aluminum cap was placed on the nozzle of the beaker to prevent the volatilization of fumes. Then it was placed in a water bath at a temperature of 45 °C for 60 minutes, after which the dye was extracted(6), Figure (1).



**Figure(1): Extraction of dye by *Portulaca grandiflora***

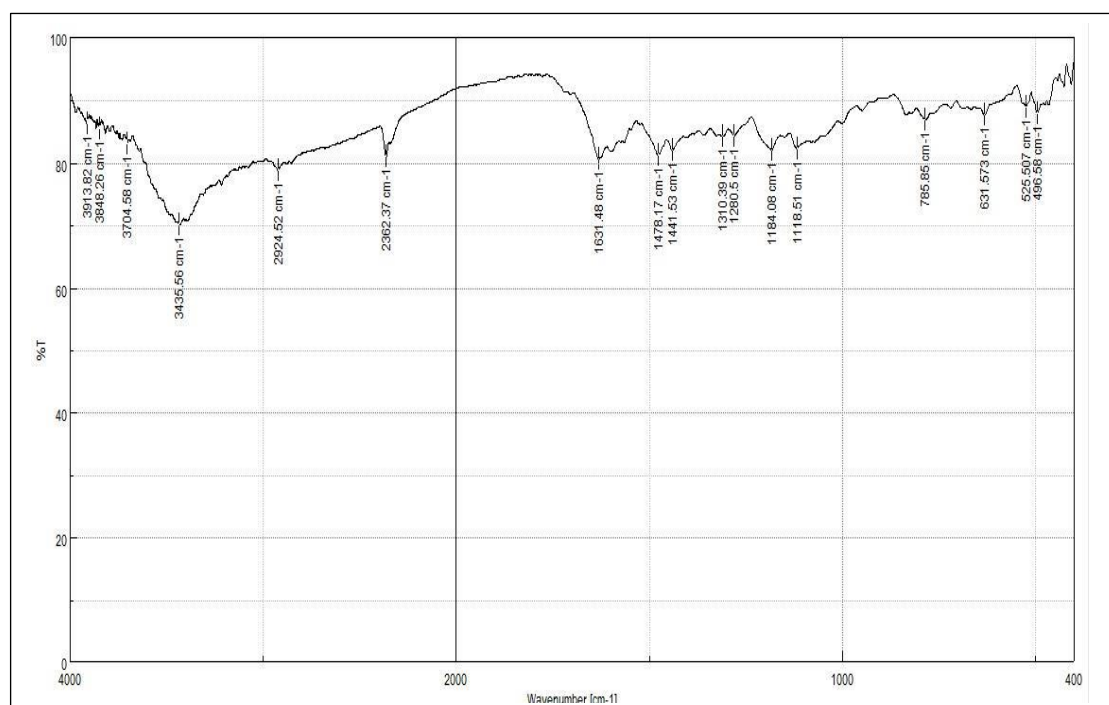
## Results and discussion

### FT-IR spectrum analysis.

Spectroscopy was used to identify the extracted dye, which exhibited effective bands. Figure (3) depicts the dye bands that are inside the limitations of 400-4000 $\text{cm}^{-1}$

The following bands were found:

3435 $\text{cm}^{-1}$  corresponds to the N-H amplitude vibration, 2924.52 $\text{cm}^{-1}$  to the CH<sub>3</sub> vibration, and 2362.37 $\text{cm}^{-1}$  to the C = O vibration, showing the presence of these groups in the dye. The N-O stretch peaks at 1478.17 -1441.63-1280.5  $\text{cm}^{-1}$  indicate the existence of azo-like groups in the dye. Peak 1164.06-1118.51  $\text{cm}^{-1}$  - first for S = O expansion (2,7).

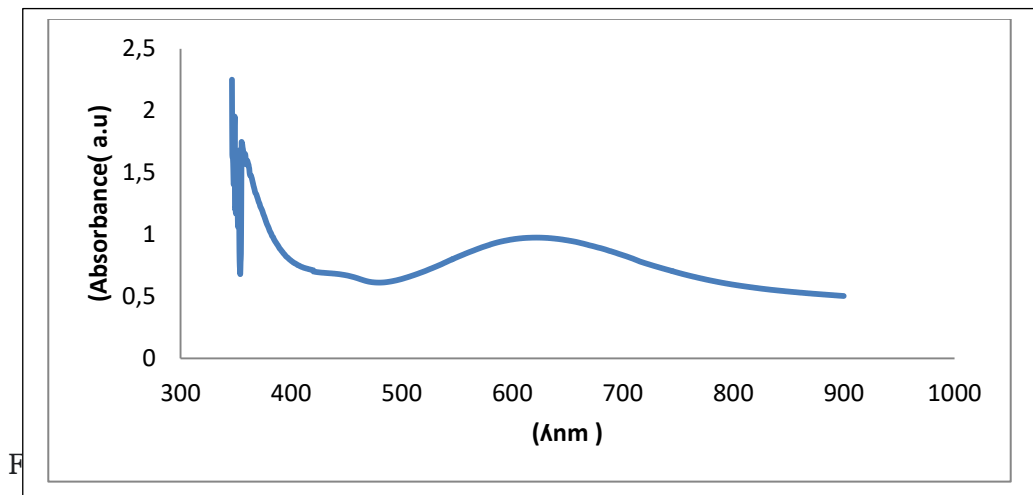


Figure(2):FT-IR of dye extraction of flowers

### UV-VIS Spectrophotometry

#### Absorbance Spectrum.

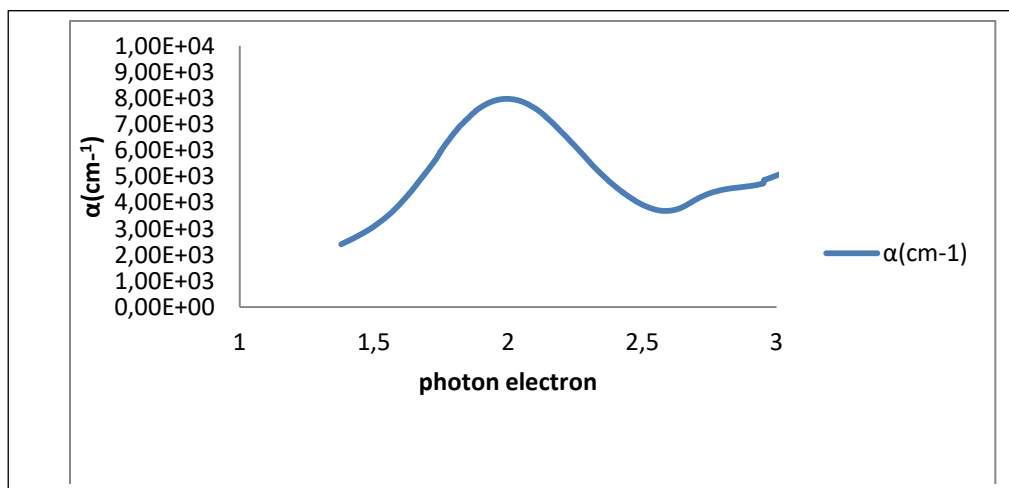
The absorbance spectrum was measured within the range (300-900nm) for the obtained dye. Figure (3) shows the absorption spectrum of morning rose dye with the wavelength, as from the existing curve it shows that the absorption spectrum has two peaks, the first at wavelength 345nm and the edge is narrow The absorbance is wide and the absorption edge is wide at wavelengths (490-740nm), i.e. within the visible spectrum. This is due to the double bond  $\text{-N=N-}$  in the composition of the dye used and the lower energy transitions from type  $n - \pi^*$  [7].



**Absorption Coefficient (α).**

Figure (4) represents the curve of linear absorption coefficient (α) with photon energy (hv). The absorption coefficient is a property of the material, absorption from beam to beam leads to the generation of a pair (electron-gap), meaning that electrons from valence beam to beam conduction, leaving gaps of equal number in the valence band. It is possible to distinguish two basic types of electronic transitions, they are direct transmission and indirect transmission, and that is from knowing the values of absorption coefficients.  $10^4$ . The absorption coefficient can be calculated from relationship ( 8 )

$$\alpha = 2.303 * \left( \frac{A}{d} \right) \dots \dots \dots :$$



**Figure (4) Absorption coefficient (α) with photon energy (hv).**

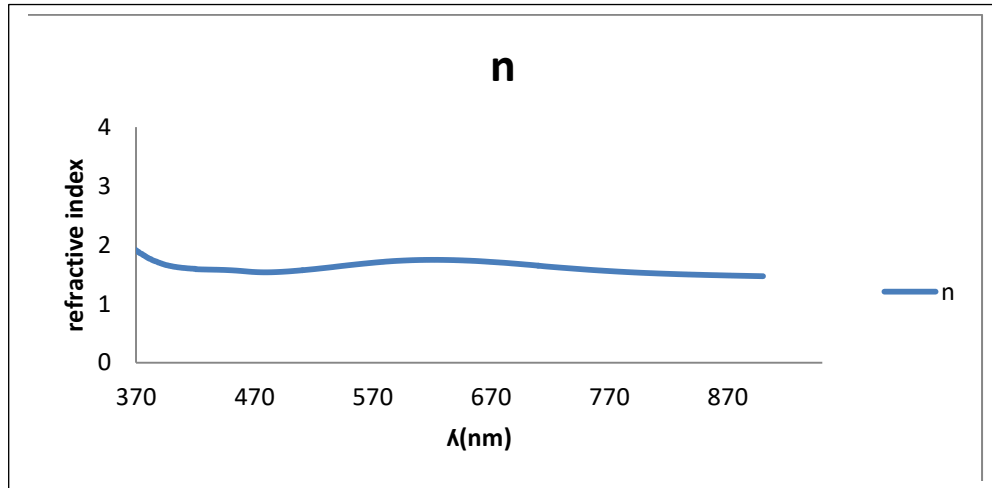
**Refractive index (n)**

The refractive index (n) is of scientific and technological importance, as it gives information about the optical energy gap and measurements of the thickness of the thin film. It is possible to calculate the refractive index from the following relationship( 8 ):

$$n = \frac{1 + R}{1 - R} + \sqrt{\frac{4R}{(1 - R)^2} - K^2} \dots \dots$$

Since: R: represents the optical reflectivity,  
K represents the decay coefficient.

Figure (5) represents the relationship between linear refractive index and wavelength. It shows from the curve that the value of the refractive index is 1.6



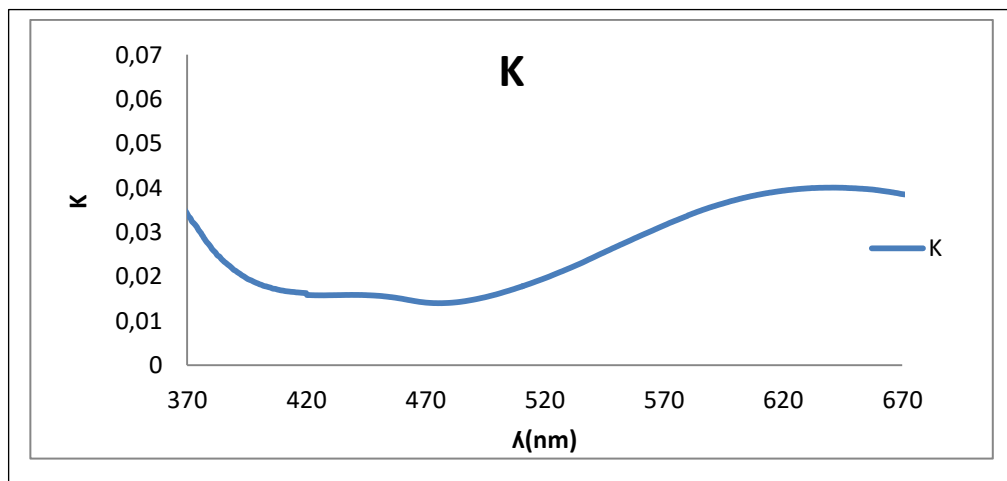
**Figure (5) Refractive index and wavelength**

**Decay Coefficient (K):**

It is possible to determine the values of the energy lost when light enters the material when determining the absorption coefficient at a wavelength corresponding to the absorption coefficient according to the following relationship(9):

$$k = (\alpha \lambda / 4\pi) \dots \dots \dots^{***}$$

From Figure (6) it is noted that the lost energy is small and is within the range (0.1-0.5). This explains the direct transfers of the electron between the valence band and the conduction band.



**Figure (6) functions decay Coefficient and wavelength**

### Optical energy gap Eg

It is necessary to know the optical energy gap in order to know the method or place of investing the material. As the relationship between  $\alpha h\nu$  (2) was drawn against the energy of photons ( $h\nu$ )(10,11), and then a straight line was drawn along the region in which a rapid increase in the amount of  $(\alpha h\nu)^2$  occurs so that it cuts off the amount of energy of the photons and the intersection point represents the value of the energy gap. Figure (7) illustrates the relationship Above, he found the value of the energy gap 3.5eV.

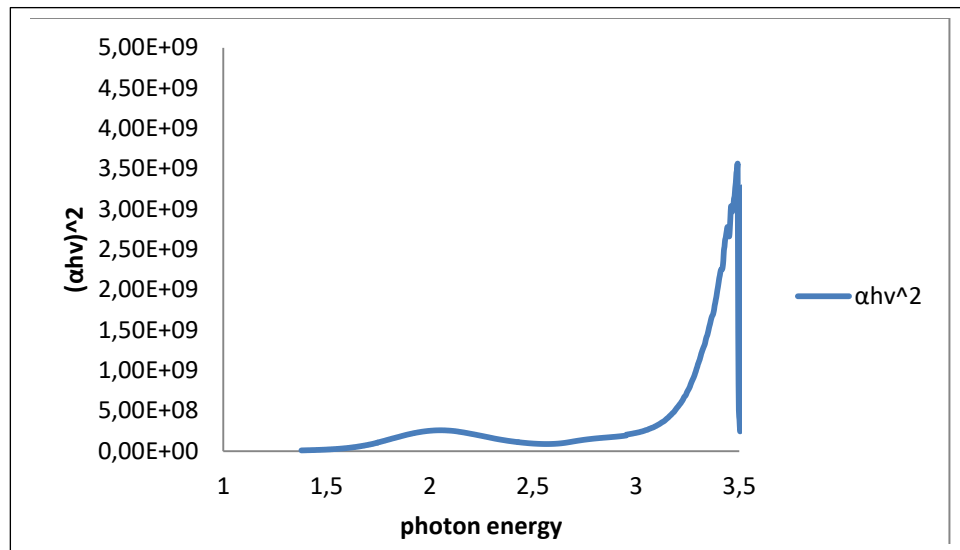


Figure (7): function of photon energy and  $h\nu$

### Conclusions

Aim of this research is to employ natural dyes that are widely available and reasonably price. This dye was extracted in this type of flower so that the physical properties and effective groups can be learned and used in applications in this area of the spectrum, such as a layer of solar cells or a photo sensor .



## References

1. R. W. SABNIS "Handbook of biological dyes and stains and industrial application" ,John Wiley & Sons, Inc. New Jersey,(2010).
2. Ra. V. K.e,A. D. W,A.l Nand ets.....,Development of a low-cost, phyto-tunnel system using *Portulaca grandiflora* and its application for the treatment of dye-containing wastewaters, *B iotechnol Lett* (2014) 36:47–55 DOI 10.1007/s10529-013-1324-1.
3. V. K. a , A. N. Kabra a , M. B. K.e a , Sanjay P. Short Communication Phytoremediation potential of *Portulaca grandiflora* Hook. (Moss-Rose) in degrading a sulfonated diazo reactive dye Navy Blue HE2R (Reactive Blue 172) Rahul Govindwar, / *Bioresource Technology* 102 (2011) 6774–6777.
4. An, O. T. O., FL. G., Preliminary Research on *porulaca grand flora hook*. Species (PORTULACACEAE) for therapeutic use *Adriana iuliana* .Mihael diui , 2013, Vol. 61.
5. Si. N, As. Pr, M, Pr.a R, Na. Tej., Sum. Sha. Md, Nan. Ku. S. Comparative Pharmacognostic Studies on Three Species of *Portulaca*, [International Journal of Pharmacognosy and Phytochemical Research](#), 2014 ,6(4):704-714.
6. E. H. and. Has. Alb. , Thesis of M.Sc Chemical Study of The Essential Oil Extracted from *Pistacia Atlantica* (Fruits and Flowers) Distributed in The Syrian Coast 2018.
7. .A. AlZumahi· N. Aro.H.Ta. Humay unKabir ,Ru. M.S.Bashar F.A.Md AbulH. M. Ma.R. Extraction, optical properties, and aging studies of natural pigments of various flower plants, Volume 6, Issue 9, September 2020, e05104.
8. H.F. Hussein, G. M. Shabeeb, S.Sh. Hashim . Preparation ZnO Thin Film by using Sol-gel-processed and determination of thickness and study optical properties. *J. Mater. Environ. Sci.* 2 (4) (2011) 423-426.
9. R. V. K.,A. N. K, A. V. ORIGINAL PAPER Synergistic degradation of diazo dye Direct Red 5B by *Portulaca grandi flora* and *Pseudomonas putida* Awate in *Int. J. Environ. Sci. Technol.* (2013) 10:1039–1050 DOI 10.1007/s13762-013-0244-x
10. S. M. M. ,G. H. MOHAMME, OPTICAL PROPERTIES OF V2O5:TIO2 THIN FILM PREPARED BY PLD TECHNIQUE, *Minar Journal*, 2019, Volume 1, Issue 1,P48-52.
11. N.F. Abd JABBAR1, N.K.HASSAN, Raid A.ISMAIL, Enhancement In2s3 nanostructures Optical And Electrical Characteristics Using Spray Pyrolysis Growth As Promising Material For Optoelectronic Applications, *Minar Journal*, 2021, Volume 3, Issue 2,



**EFFECT OF METHIONINE ADDITION TO SOYBEAN MEAL INSTEAD OF PROTEIN  
CONCENTRATE IN THE FINISHER RATION OF BROILER**

**RAFEA M.KHALEEL  
NAWAF G.ALTAMI  
THAER M. ABDUL -BAKI**

## **EFFECT OF METHIONINE ADDITION TO SOYBEAN MEAL INSTEAD OF PROTEIN CONCENTRATE IN THE FINISHER RATION OF BROILER**

**Rafea M.KHALEEL<sup>1</sup>**  
**Nawaf G.ALTAMI<sup>2</sup>**  
**Thaer M. Abdul -BAKI<sup>3</sup>**

### **Abstract:**

This study was conducted in the College of Agriculture and Forestry , University of Mosul During the period from 23 Sep. to 4 Nov. 2021 .The aim of study to know effect of replacing protein concentrate with soybean meal as a source of protein with the addition of synthetic methionine. 120 chicks Day-Old Broiler chicks raised during the first three weeks collectively on a starter ration, the birds were distributed into three treatments with 4 replicates(10 birds each replicate), the first treatment was a control that contains protein concentrate, the second and third treatments without protein concentrate and it was replaced with soybean meal with 0.1 and 0.2% of synthetic methionine, respectively. The results showed that there were no significant differences in the final body weight at 6 weeks of age, in the total and daily weight gain, total and daily feed intake, feed conversion, total and daily protein intake, protein conversion, during the period (3- 6) weeks and the total period (0-6) weeks of age (  $P \leq 0.05$  ), and the dressing percentage, and treatment 3 (0.2% methionine) showed the best economic efficiency.

**Key words:** Soybean Meal, Broiler, Methionine, Replacing, Protein Concentrate.



<http://dx.doi.org/10.47832/MinarCongress5-9>



<sup>1</sup> University of Mosul, Iraq, [rafkhulel@uomosul.edu.iq](mailto:rafkhulel@uomosul.edu.iq)



<sup>2</sup> University of Mosul, Iraq, [nawaf.gazi@uomosul.edu.iq](mailto:nawaf.gazi@uomosul.edu.iq), <https://orcid.org/0000-0001-5986-4565>



<sup>3</sup> University of Mosul, Iraq, [thaer.alhashimy@uomosul.edu.iq](mailto:thaer.alhashimy@uomosul.edu.iq), <https://orcid.org/0000-0002-2848-2852>

## Introduction:

Chicken meat is an essential source of animal protein for human when compared with other sources of animal protein. It also contributes to environmental preservation by minimizing gas emissions (Selle et al, 2020). Protein concentrates, which are utilized as an alternative to animal protein sources because of it supply essential amino acids to birds, are among the most expensive components of chicken feed. However, because of its substantial and well-balanced protein content, soybean meal (SBM) is an excellent protein source for animal diets (Marsman et al, 1997). It's utilized as the essential ingredient in poultry diets all over the world, although it's lacking in the limiting amino acid methionine (Kalbandi et al 2009). The use of fish meal as an animal protein source in developing nations is limited, according to Frempong et al (2019), due to its expensive cost price. Bunchasak (2009) lists the advantages of adding methionine to chicken diets as lowering production costs, providing an appropriate balance of essential amino acids that increasing growth, increasing meat consumable, decreasing content of carcass fat, and balancing bird nutrition intake. Millemcam et al (2021) investigated the effect of adding 0.05 or 0.1 % of methionine to corn-soybean meal diets on broiler performance, finding that adding 0.05 or 0.1 % methionine to basal diets increased body weight significantly ( $P \leq 0.05$ ) at the end of the starter phase (10 days), while increasing the added methionine to 0.15, 0.25, 0.35, 0.45 % had no significant effect on body weight and weight gain, and the same results were found in the grower period from (11-23 days), whereas in the finisher period, there was a significant improvement in body weight in 0.15, 0.30, 0.40 % addition treatments only, and did not differ significantly in 0.05, 0.1, 0.2 % addition treatments. Based on feed conversion, Dozier and Mercier (2013) found that the optimal Total Sulfure Amino Acids (TSAA) to lysine ratio was 0.74, and did not detect a significant effect of different digestible TSAA to digestible lysine ratios. By adding 0.04 on body weight, weight gain, feed intake, feed conversion, and mortality %, lysine ranged from 0.56 to 0.84. Frempong et al. (2019) investigated the effect of replacing fishmeal with soybean meal on Cobb broiler performance, finding a significant increase ( $P \leq 0.05$ ) in body weight at 42 days of age and daily feed intake during (0–42) days, but no significant differences in feed conversion ratio, and a reduction in feed cost per kilogram of weight gain when fish meal was replaced with soybean meal. Jariyahatthakij et al. (2018) investigated the effect of methionine addition to a low protein broiler diet on Ross performance, finding that there were a significant decrease in body weight and feed intake compared to the control diet, while the feed conversion ratio did not differ significantly. Methionine addition significantly decreased protein intake and improved protein conversion ratio ( $P \leq 0.05$ ). According to Chattopadhyay et al. (2006), adding 1 gm of DL-Methionine/Kg to broiler feeds enhanced body weight, weight gain, feed conversion, and reduced feed consumption, as well as abdominal fat considerably ( $P \leq 0.05$ ), but had no effect on Dressing percentage. Mohammed (2012) investigated the effect of adding lysine and TSAA to broiler rations in a ratio of (10, 20, 30, 40) % more than the NRC recommendation, finding that this did not significant effect on body weight gain, and that the 30, 40 % treatments showed a significant decreasing in feed conversion compared to the 10% treatment, a significant decrease in abdominal fat, and a significant increase in liver and heart weight. Kalbande et al. (2009) compared the effects of employing herbal methionine with synthetic methionine in broiler feeds, finding that the herbal methionine had a better performance.

Mikulec et al. (2004) investigated the effect of replacing fish meal with sunflower meal or soybean meal in broiler rations, finding no significant difference in live body weight, weight gain, feed efficiency, dressing percentage, or carcass cuts % in the soybean meal treatment, but significantly less body weight, weight gain, and feed conversion in the sunflower meal treatment. Saki et al (2011) found no

significant effects on body weight, feed intake, feed conversion, small intestine sections length cm (duodenum, Jejunum, Ileum), villi height, width, or surface area when 25 or 35 % soybean meal was replaced with fishmeal in broiler rations. When (25, 50, 75, and 100) % of fishmeal was replaced with soybean meal, Aziz et al (2001) found no significant influence on body weight, feed consumption, or body composition.

The aim of this study is to know supplementing protein concentrate in broiler finisher rations with soybean meal and 0.1 or 0.2 % synthetic methionine affects some productive performance of broilers.

### **Materials and Methods**

From September 23<sup>th</sup> to November 4<sup>th</sup>, 2021, this study was conducted in the poultry house of the Animal Production Department, College of Agriculture and Forestry, University of Mosul. A local hatchery in Nineveh Governorate provided 120 Ross broiler female chicks. Cleaning, sanitizing, and separating the raising house into pens with 1.25 × 1.25 m<sup>2</sup> dimensions. Plastic feeders and drinkers, sawdust litter, and electrical heaters were all included in the pens. One day old chicks weighed an average of 41.5 grams, the chicks were weighed at 3 weeks of age and divided into three groups of four replicates with 10 birds of each: T1 control, T2, T3 finisher diets without protein concentrate, with additional methionine 0.1 and 0.2 %, respectively table (1). During the raising period, chicks were vaccinated against Newcastle and IB at the hatchery and then with Newcastle and Gumboro on a veterinarian schedule. Weekly weight and feed consumption were recorded on a digital scale with a sensitivity of 1 gram. Feed and water were provided freely, lighting was continuous for 24 hours a day. The studied traits were live body weight, weight gain, feed consumption, feed conversion, protein consumption, protein conversion, dressing percentage, Economic efficiency. Data were analyzed statistically using SPSS 10 software and the test of significance between means was done by Duncan's multiple range test. The economic efficiency calculated by (Ibrahim, 1987) equation as Economic efficiency = Feed conversion × Feed cost ID/Kg = Cost of feed used to produce 1 kg of live body weight.

Table (1) Feed ingredients Chemical composition of experimental rations \*

Ingredients	Starter	Finisher		
		Control 0% Meth.	T2 0.1% Meth.	T3 0.2% Meth.
Corn	59.41	66.96	66.20	66.0
Soybean meal	32.89	25.38	29.64	29.7
*Protein concentrate	5	5	0	0
Veg.oil	0	0.35	0.7	0.77
Lime	2.40	1.95	1.51	1.54
Di-cal.phosphate	0.05	0.11	1.5	1.44
Salt	0.25	0.25	0.25	0.25
Minvit premix	0	0	0.1	0.1
Methionine	0	0	0.1	0.2
The chemical composition				
Me	2900	3000	3000	3000
CP	23	20	20	20
Lysine	1.35	1.15	1.05	1.05
Meth+Cys.	0.88	0.8	0.75	0.85
Ca	1.18	1	1	1
Av. P	0.4	0.4	0.4	0.4
CF	2.71	2.58	2.61	2.61
EE	2.84	3.40	3.5	3.57
Cost ID/Kg	823.9	807	761	762

\*Chemical composition of protein concentrate ( Wafi b.v ) was ( ME 2149.14 ,CP 40% , crude fat 5%crude fibre 2.41%, crude ash 21.54 , Ca 3.08 ,Av . P 5.41% , Na2.50 % , Cl 3.91, Lysine 4.4% ,Methionine 3.70 ,Tryptophan 0.43 % , Threonine 1.80%, Isoleucine 1.48 % , Valine 1.73% , Arginine 2.58% .

## Result and Discussion

Table (2) shows the results of the statistical analysis to the effect of the experimental treatments on the productive traits, where showed no significant differences ( $P \leq 0.05$ ) in the final live body weight at the age of 6 weeks. This result is consistent with what we found in a previous study using soybean meal supplemented with synthetic methionine at 0.1 and 0.2% in the starting ration instead of the protein concentrate, where we found an insignificant difference ( $P \leq 0.05$ ) in the final body weight (Taher and Abdul-Baki 2011). Bodyweight of 6 weeks of age in our study was similar to the bodyweight of Ross weight found by (Udeh *et al*,2015). Drew *et al* ( 2004) found that protein source ( fish meal or soybean protein) affects body weight at 28 days of age when protein level were 23, 31.5 % significantly (  $P \leq 0.05$ ) but not significant ( $P \leq 0.05$ ) effect when was 40% during the period 14-28 days of age. These unusual weights may be due to the sex of most of the birds being females. Islam *et al* (1997) found that substituting a fish meal with soybean meal at different levels decreased body weight gain, total feed consumption, feed conversion ratio. This result agreed with Mikulec *et al* ( 2004) who found that replacing fishmeal with soybean meal did not affect weight gain in the starter and finisher period of broiler.

Table( 2) Effect of treatments on productive traits of broiler

Traits	Control	0.1% Methionine	0.2 % Methionine
Bodyweight(Week)			
0	41.5		
3	571.83±5.01	575.00±1.32	578.50±1.00
6	1212.33±92.5	1255.33±51.40	1122.67±86.56
Total weight gain(Week)			
0-3	530.33±5.00	533.50±1.32	537.00±1.00
3-6	640.50±93.30	680.33±51.43	544.17±83.23
0-6	1170.83±92.31	1213.83±51.42	1081.17±43.27
Daily weight gain(Week)			
0-3	33.33±1.13	34.03±0.85	35.36±2.00
3-6	30.50±4.44	32.40±2.45	25.91±2.08
0-6	27.87±2.20	28.90±1.22	25.74±2.05
Total feed intake(Week)			
0-3	739.09	739.09	739.09
3-6	1606.01±35.41	1662.57±31.95	1314.25±33.34
0-6	2345.10±35.42	2401.65±31.43	2053.34±33.35
Daily feed intake(Week)			
0-3	35.19	35.19	35.19
3-6	76.48±3.37	79.17±7.32	62.58±1.58
0-6	55.84±1.68	57.18±7.24	48.89±0.79
Feed conversion(Week)			
0-3	1.39±0.01	1.39±0.01	1.38±0.01
3-6	2.64±0.36	2.40±0.26	2.46±0.19
0-6	2.04±0.16	1.96±0.17	1.91±0.14
Total protein intake(Week)			
0-3	169.99	169.99	169.99
3-6	321.20±7.08	332.51±30.16	262.85±6.67
0-6	491.19±7.10	502.50±30.15	432.84±6.66
Daily protein intake(Week)			
0-3	8.09	8.09	8.09
3-6	15.29±0.33	15.83±0.37	12.52±0.16
0-6	11.69±0.16	11.96±0.45	10.30±0.15
Dressing percentage%	70.92±0.23	72.38±1.82	73.32±1.06
Economic efficiency	1905	1874.2	1610.4

There were an insignificant difference in daily and total feed intake between treatments, which agrees with the finding of (Taher and Abdul-Baki,2011) in the starter period, and with (Saki *et al*,2011) when replaced 25 or 35% of soybean meal with fish meal, but disagreed with (Frempong *et al*,2019) who found a significant increase in feed intake when replaced fish meal with soybean meal in broiler ration. Table (2) explains that feed conversion didn't differ significantly between treatments( $P \leq 0.05$ ), these results agree with the finding of (Frempong *et al*,2019) who did not find a significant difference in feed conversion when substituting fish meal with either soybean meal or poultry byproduct in broiler rations during 42 days of age. Also (Mikulec *et al*, 2004) found that replacing fishmeal with soybean meal or sunflower meal in starter and finisher broiler rations did not affect feed conversion significantly.

There was an insignificant difference between treatments in protein intake due to experimental rations where iso-nitrogenous, and feed intake was closed between treatments. The dressing percentage %age did not differ significantly ( $P \leq 0.05$ ) although there was a mathematical difference, and 0.2% methionine treatment showed the best result of about 3% best than control. Islam *et al* (1997) found that substituting a fish meal with a soybean meal at different levels did not affect on dressing percentage significantly.

The control treatment was the highest cost, while treatment 3 (0.2% methionine) had the lowest and best economic efficiency.

**Conclusion:**

Under the circumstance of our study we found that substituting protein concentrate with soybean meal supplemented with 0.1 or 0.2% synthetic Methionine did not affect significantly, final body weight, weight gain, feed intake, feed conversion ratio, protein intake, protein conversion ratio, dressing percentage %age, while improving economic efficiency by 1.62, 15.5 %.



## References

1. Aziz, M. A., Khandaker, Z. H., & Islam, M. M. (2001). Effect of replacing protein from fish meal with soybean on the performance of broiler chicken. *Indian Journal of Animal Nutrition*, 18(1), 23-28.
2. Bunchasak, C. (2009). Role of dietary methionine in poultry production. *The Journal of Poultry Science*, 46(3), 169-179.
3. Dozier III, W. A., & Mercier, Y. (2013). Ratio of digestible total sulfur amino acids to lysine of broiler chicks from 1 to 15 days of age. *Journal of Applied Poultry Research*, 22(4), 862-871.
4. Drew, M. D., Syed, N. A., Goldade, B. G., Laarveld, B., & Van Kessel, A. G. (2004). Effects of dietary protein source and level on intestinal populations of *Clostridium perfringens* in broiler chickens. *Poultry Science*, 83(3), 414-420.
5. Frempong, N. S., Nortey, T. N., Paulk, C., & Stark, C. R. (2019). Evaluating the Effect of replacing fish meal in broiler diets with either Soybean meal or poultry by-product Meal on Broiler Performance and total feed cost per kilogram of gain. *Journal of Applied Poultry Research*, 28(4), 912-918.
6. Ibrahim. I.KH. (1987), *Poultry nutrition*, 1st Ed, Dar al-kotob press. Mosul University.
7. Islam, K. M. S., Shahjalal, M., Tareque, A. M. M., and Howlider, M. A. R. (1997). Complete replacement of dietary fish meal by duckweed and soybean meal on the performance of broilers. *Asian-Australasian Journal of Animal Sciences*, 10(6), 629-634.
8. Jariyahatthakij, P., Chomtee, B., Poeikhampha, T., Loongyai, W., & Bunchasak, C. (2018). Effects of adding methionine in low-protein diet and subsequently fed low-energy diet on productive performance, blood chemical profile, and lipid metabolism-related gene expression of broiler chickens. *Poultry science*, 97(6), 2021-2033.
9. Kalbande, V. H., Ravikanth, K., Maini, S., & Rekhe, D. S. (2009). Methionine supplementation options in poultry. *Int. J. Poult. Sci*, 8(6), 588-591.
10. Marsman, G. J., Gruppen, H., Van der Poel, A. F., Kwakkkel, R. P., Verstegen, M. W., & Voragen, A. G. (1997). The effect of thermal processing and enzyme treatments of soybean meal on growth performance, ileal nutrient digestibilities, and chyme characteristics in broiler chicks. *Poultry Science*, 76(6), 864-872.
11. Mikulec, Ž., Mas, N., Mašek, T., & Strmotić, A. (2004). Soybean meal and sunflower meal as a substitute for fish meal in broiler diet. *Veterinarski arhiv*, 74(4), 271-279.
12. Millecam, J., Khan, D. R., Dedeurwaerder, A., & Saremi, B. (2021). Optimal methionine plus cystine requirements in diets supplemented with L-methionine in starter, grower, and finisher broilers. *Poultry Science*, 100(2), 910-917.
13. Mohammed Taher, R. and T.M.Abdul-Baki (2011). effect of added methionine to soybean meal as a substitute for protein concentrate in broiler starter diet on some productive traits. *Mesopotamia Journal of Agriculture*, 39(1), 69-75.
14. Mohammed, D. (2012). Effect of excess lysine and methionine on immune system and performance of broilers. *Annals of Biological Research*, 3(7), 3218-3224.
15. Saki, A. A., Abbasinezhad, M., Ghazi, S., Tabatabai, M. M., Ahmadi, A., & Zaboli, K. (2012). Intestinal characteristics, alkaline phosphatase, and broilers performance in response to extracted and mechanical soybean meal replaced by fish meal. *J. Agr. Sci. Tech.* 14: 105-114

16. Selle, P. H., de Paula Dorigam, J. C., Lemme, A., Chrystal, P. V., & Liu, S. Y. (2020). Synthetic and crystalline amino acids: alternatives to soybean meal in chicken-meat production. *Animals*, 10(4), 729.
17. SPSS Inc, SPSS for windows 10.0 Base system user's guide, release 10.0 SPSS Inc. USA, 2001.

# NEW RESULTS OF WELL-POSEDNESS FOR HEMI-EQUILIBRIUM PROBLEMS

ALAA MAJID JABER  
BASHAYIR NAHI ABED

## NEW RESULTS OF WELL-POSEDNESS FOR HEMI-EQUILIBRIUM PROBLEMS

Alaa Majid JABER <sup>1</sup>  
Bashayir Nahi ABED <sup>2</sup>

### Abstract:

Well-posedness is worth noting that plays important role in the field of optimization and nonlinear operator problems. The goal of present work is to study concepts of well-posedness for hemi- equilibrium problems ( $HE_p$ ) for short and to optimization with equilibrium constraint involving monotone bifunction. Some metric characterizations and sufficient conditions for these kinds of well-posedness are obtain. Finally, we prove that the well-posedness of hemi-equilibrium problems (OPPHEC) is equivalent to the existence and uniqueness of its solution. In order to achieve the a above goal, the work is divide in to the following section. In section 2, we recall needful definition and motioned some results. In section 3, we introduction new concepts of well-posedness for optimization problems with constraints described by parametric hemi-equilibrium problems. Additionally, under appropriate conditions, we prove that the well-posedness of generalized equilibrium problems is equivalent to the existence and uniqueness of its solution.

**Key words:** Hemi-Equilibrium Problem; Optimization Problems; Well-Posedness; Metric Characterizations; Monotone Bifunction.



<http://dx.doi.org/10.47832/MinarCongress5-10>



<sup>1</sup> General Directorate of Education in Thi-Qar, Iraq, [alaamajid@utq.edu.iq](mailto:alaamajid@utq.edu.iq), <https://orcid.org/0000-0003-2485-8565>



<sup>2</sup> General Directorate of Education in Thi-Qar, Iraq, [bashayirnahi@gmail.com](mailto:bashayirnahi@gmail.com), <https://orcid.org/0000-0002-6885-7444>

## Introduction:

Nowadays, idea well-posedness plays a significant turn in numerical methods for optimization and nonlinear operator problems. The classical notion of well-posedness for minimization problem is a classical notion which first was a lesson by Tykhonov [26] in 1966 and Levitin-Polyak [17] that essential the existence and uniqueness of a solution to the global minimization problem and convergence of every minimizing sequence to the unique solution. We noticed there are many papers in the literature that treated Tykhonov well-posedness concept with optimization and optimal control problem [9,13,15, 23, ]. Since then, many authors examined the well-posedness and generalizations for optimization problems, equilibrium problems, best approximation problems, variational inequality problems, fixed point problems and Nash equilibrium problems [2,5,7,18,19,21,29]. The well-posedness of equilibrium problems is introduced by Fang et.al [9]. Furthermore, the parametric well-posedness for vector equilibrium problems is investigated by Kimura et.al [8]. Whereas two types of well-posedness for equilibrium problems were introduced by Bianchi et.al [3]. Wang and Huang in 2012 established the essential and adequate provisos for the Levitin-Polyak well-posedness of generalized quasi-variational inclusion and disclusion problems and for optimization problems with constraints [25]. Later, the Hadamard well-posedness of parametric vector equilibrium problems is analyzed by Salomon in 2010 [22]. As Peng et.al examined numerous types of Levitin-Polyak well-posedness of generalized vector equilibrium problems in [4]. We would like to point out that the notion of well-posedness problems by perturbation of parameters in the vector problems is regarded in most of these papers. In this work, we investigate the concept and extend the notion of well-posedness by using parameters for a class of hemi-equilibrium problems and furthermore for minimization problems with perturbations. The idea of well-posedness for generalized hemi-equilibrium problems has the equivalent notion to prove the existence and uniqueness of the solution. In order to ascertain the above goal, the study is divided into the following sections. In section two, we introduce essential definitions and reference some results. In section three, we present generalized notions of well-posedness for hemi-equilibrium problems ( $HE_p$ ). In section four, we introduce new notions of well-posedness for optimization problems with constraints described by parametric hemi-equilibrium problems, under appropriate conditions, we prove that the well-posedness of generalized equilibrium problems is equivalent to the existence and uniqueness of its solution.

## 2. Preliminaries

In this work, we continue our study in the idea of well-posedness which has an important role in the field of optimization. Assume that two Banach spaces  $P$  and  $S$  and  $K$  is a nonempty closed convex subset of a Banach space  $P$ . Let  $P^*$  be a topological dual space and its norm is denoted by  $\|\cdot\|$ . For the convenience of the reader, we recall some significant definitions and auxiliary results that need to be imposed in order to prove our main results. Here, we recall that a function  $Q: S \rightarrow R$  is said to be local Lipschitz if for every  $u \in S$  there exists a neighborhood  $U$  of  $u$  and a constant  $\Gamma_u$  is a positive such that

$$|Q(a) - Q(b)| \leq \Gamma_u \|a - b\|_S \text{ for each } a, b \in U.$$

Definition 2.1 Assume that  $Q: P \rightarrow R$  is a locally Lipschitz function. The generalized derivative of  $Q$  at  $u \in P$ , in the direction of  $v \in X$ , denoted by

$$Q^\circ(u, v) = \limsup_{\substack{w \rightarrow u \\ \alpha \downarrow 0}} \frac{Q(w + \alpha v) - Q(w)}{\alpha}$$

Lemma 2.2. Assume that  $Q: p \rightarrow R$  be locally Lipschitz of rank  $I_u$  near the point  $u \in P$ . Then

(1) The function  $v \rightarrow Q^\circ(u, v)$  is finite, positively, homogeneous, sub additive and satisfies that

$$|Q^\circ(u, v)| \leq I_u \|v\|_P;$$

(2)  $Q^\circ(u, v)$  is upper semicontinuous as a function of  $(u, v)$ ;

$$(3) Q^\circ(u, -v) = (-Q)^\circ(u, v).$$

One can be found the proof in [4]

Definition 2.3. Assume that  $\beta$  areal-valued function defined on convex subset  $K$  of  $P$ . Then  $\beta$  is said to be hemi continuous, if

$$\lim_{t \rightarrow 0^+} \beta(ax + (1 - a)y) = \beta(y); \text{ for every } x, y \in K.$$

Here, we consider in this article the hemi-equilibrium problem (shortly  $HE_p$ ):

Find  $u \in K$  such that

$$\vartheta(u, v) + Q^\circ(u; \delta(u, v)) \geq 0, \quad \forall v \in K, \quad (2.1)$$

where  $\vartheta$  bi-function from  $K \times K$  in to  $R$ , in which  $\vartheta(u, u) = 0$  for every  $u \in K$ .

$\delta: P \times P \rightarrow R$  singl-valued function and  $Q: P \rightarrow R$  locally Lipschitze function.

Remark 2.4 From the convexity of  $Q^\circ(u, v)$  and linearity of  $\delta(u, \cdot) \forall u \in S$ . One can get that  $v \rightarrow Q^\circ(u, \delta(u, v))$  is convex function.

Remark 2.5. It is clear that  $u_n$  converges strongly to some  $u \in K$ . Hence,  $\delta(u_n, v)$  converges strongly to  $\delta(u, v)$  in which  $v \in K$ . From this fact, together with Lemma 2.2 (2), we obtain

$$\lim_n \sup Q^\circ(u_n; \delta(u_n, v)) \leq Q^\circ(u; \delta(u, v)). \quad (2.2)$$

In the sequel, we assumption the formulation of optimization problem with hemi-equilibrium constraint. Let  $H: T \times K \rightarrow R$  and  $\vartheta: T \times K \times K \rightarrow R$  be two functions, such that  $T \subset S$  is a nonempty set. The optimization problem with hemi-equilibrium problem constraint which is denoted shortly by (OPPHEC) is formulalted as follows:

$$\min H(t, u) \text{ s.t. } (t, u) \in T \times K \text{ and } u \in \psi(t),$$

where  $\Psi(t)$  is the solution set of the parametric hemi-equilibrium problem ( $HE_p(t)$ ) defined by,  $u \in \Psi(t)$  if and only if

$$\vartheta(t, u, v) + Q^\circ(u; \delta(u, v)) \geq 0, \quad \forall u \in K. \tag{2.3}$$

Henceforth, we shall write  $\{HE_p(t), t \in T\}$  for family of hemi-equilibrium problem i.e., the parametric problem, we simple write  $(HE_p)$  in the article. The hemi-equilibrium problem contain many problems as special state been studied intensively. In the following, we recall some special state of the problem  $(HE_p)$ .

(1) If  $Q = 0$ , then problem  $(HE_p)$  is reduce to the parametric equilibrium problem (for shortly, EP(t)). In fact, finding  $u \in K$  in which  $\vartheta(t, u, v) \geq 0, \forall v \in K$  [1].

(2) If  $Q = 0$ , and  $\vartheta(t, u, v) = -\tau(t, u, u - v) \forall v \in K$ , then  $(HE_p)$  is reduces to the parametric quasivariational inequality (for short QVI(t)) [30].

(3) If  $\delta(u, v) = u - v, \vartheta(t, u, v) = \langle Z_u - l, v - u \rangle$ , then  $(HE_p)$  is reduces to the parametric hemivariation inequality [28].

In recent years, some of authors have proposed many essential generalizations of monotonicity which it plays an essential role in the study of well-posedness and hemi-equilibrium problems[10, 14,20,27].

We shall use a type of generalized monotonicity so said to be  $\psi$ -monotone bi-function [20].

Definition 2.6. Assume that  $\zeta, \psi : K \times K \rightarrow \mathbb{R}$  are two bifuncations. Then  $\zeta$  is said to be  $\psi$ -monotone if

$$\zeta(x, y) + \zeta(y, x) \leq \psi(x, y) + \psi(y, x) \quad \forall x, y \in K$$

Example 2.7. Assume that  $X = \{x = \{x_n\} \subseteq \mathbb{R} : \|x\| = (\sum_{n \geq 1} |x_n|^r)^{\frac{1}{r}}\}$ .

Define a set  $K = \{x \in \ell^r : \|x\| \leq 1\}$  which is nonempty closed and convex subset of  $\ell^r$ . let  $X = \ell^r$  be a reflexive Banach space, where  $1 < r < \infty$

$\zeta : K \times K \rightarrow \mathbb{R}$  such that  $\zeta(x; y) = \|y - x\|^2$  then,

$\zeta(x; y) + \zeta(y; x) = 2 \|y - x\|^2 > 0$ , for  $x \neq y$ , in which  $\zeta$  is not monotone bifunction. But one can choose

$\psi : K \times K \rightarrow \mathbb{R}$  such that  $\psi(x; y) = 2 \|y - x\|^2$ . Then,  $\zeta$  is  $\psi$ -monotone bifunction.

Remark 2.8. Throughout this work, in addition to investigate some characterization of well-posedness for  $(HE_p)$  we consider for every  $\mu \in (0,1)$

$$\lim_{\mu \rightarrow 0} \frac{\psi(x, x_\mu)}{\mu} + \psi(x, y) = 0. \tag{2.4}$$

In order to solution hemi-equilibrium problem (2.3), we suppose the following assumptions:

$R_1$ : The mapping  $\delta(\cdot, \cdot); P \times P \rightarrow P$  satisfies the following hypotheses

- (1)  $\delta(u; u) = 0$  for all  $u \in P$ ;
- (2)  $\delta(u; \cdot)$  is linear operator for all  $u \in P$ ;
- (3)  $\delta(u^m; v) \rightarrow \delta(u; v)$ , whenever  $u^m \rightarrow u$  for any  $v \in P$ .

$R_2$ :  $\vartheta : T \times K \times K \rightarrow \mathbb{R}$  is a function, satisfies the following hypotheses

- (1)  $\vartheta(t, u, u) = 0$  for all  $t \in T, u \in K$ ;
- (2)  $\vartheta(t, \cdot, \cdot)$  is  $\psi$ -monotone bi-function ;
- (3)  $\vartheta(t, \cdot, v)$  is hemicontinuous for all  $t \in T$  ;
- (4)  $\vartheta(t, u, \cdot)$  is convex for all  $t \in T, u \in K$ ;
- (5)  $\vartheta(\cdot, u, \cdot)$  is lower semicontinuous for shortly (*l.s.c*) for all  $u \in K$ .

$R_3$ :  $\psi : K \times K \rightarrow \mathbb{R}$  is a function, satisfies the following hypotheses

- (1)  $\psi(\cdot, v)$  is hemicontinuous for all  $t \in T$ ;
- (2)  $\psi(u, \cdot)$  is convex for all  $t \in T, u \in K$ ;
- (3)  $\psi(\cdot, \cdot)$  is upper semicontinuous for shortly (u.s.c).

$R_4$ :  $Q: T \times K \rightarrow \mathbb{R}$  is a function, satisfies the following hypotheses

- (1)  $Q(\cdot, \cdot)$  is convex;
- (2)  $Q(\cdot, \cdot)$  is l.s.c.

The following let us recall that the concepts of non-compactness and Hausdorff metric.

Definition 2.9. Suppose that  $I, G$  are two nonempty subsets of  $P$ . The Hausdorff metric  $H(\cdot, \cdot)$  between  $I, G$  defined by  $H(I, G) = \max\{e(I, G), e(G, I)\}$  where

$$e(I, G) = \sup_{a \in I} d(a, G) \text{ with } d(a, G) = \inf_{b \in G} \|a - b\|.$$

Note that  $\{I_n\}$  of nonempty is a sequence subset of  $P$ . The sequence  $I_n$  is convergent to  $I$  by Hausdorff metric if  $H(I_n, I)$  converges to zero. It is easy to see that  $e(I_n, I) \rightarrow 0$ , if and only if  $d(a_n, I) \rightarrow 0, \forall a_n \in I$ .

Definition 2.10. Assume that  $C$  is a nonempty subset of  $P$ . The measure of non-compactness of the set  $C$

$$\text{is defined by } \mathcal{U}(C) = \inf \{ \epsilon > 0 : C \subseteq \bigcup_{j=1}^n C_j, \text{diam}(C_j) < \epsilon, j = \bar{n} \},$$



where  $\text{diam } C_j$  means the diameter of a set  $C_j$ .

### 3. Well-Posedness of Hemi-Equilibrium Problem (HE<sub>p</sub>)

In this section, we introduce ideas of well-posedness for generalized hemi-equilibrium problems involving of  $\psi$ -monotone bi-function. We will start the analysis of our results by present some sate under which the hemi-equilibrium problem are generally well-posedness.

**Definition 3.1** A sequence  $\{(t_n, u_n)\} \subseteq T \times K$  is called an approximating sequence for hemi-equilibrium problem (HE<sub>p</sub>) if there exists  $\{\epsilon_n\}$  is a nonnegative sequence which  $\{\epsilon_n\} \rightarrow 0$  as  $n \downarrow \infty$  such that

$$\vartheta(t, u_n, v) + Q^0(u_n; \delta(u_n, v)) \geq -\epsilon_n \|v - u_n\|, \forall n \in \mathbb{N}, v \in K \quad (3.1)$$

**Definition 3.2.** The hemiequilibrium problem (HE<sub>p</sub>) is said to be strongly (respectively, weakly) well-posedness if (HE<sub>p</sub>) has a unique solution  $u$ , and for every approximating sequence for (HE<sub>p</sub>) convergent strongly (resp., weakly) to a unique solution  $u$ .

**Definition 3.3** The hemi-equilibrium problem (HE<sub>p</sub>) is said to be strongly (respectively, weakly) well-posedness in the generalized sense if the solution set  $\Psi(t)$  for (HE<sub>p</sub>) is a nonempty set and every approximating solution sequence has a subsequence which strongly (respectively, weakly) convergent to some point  $\Psi(t)$ .

In the sequel, let us some characterizations, of well-posedness the hemi-equilibrium problem (HE<sub>p</sub>) are recalled. For any  $\epsilon > 0$ , we define two sets.  $D(\epsilon) = \{(t, u) \in T \times K : \vartheta(t, u, v) + Q^0(u; \delta(u, v)) \geq -\epsilon \|v - u\|, v \in K\}$ , and

$$E(\epsilon) = \{(t, u) \in T \times K : \vartheta(t, v, u) - \psi(u, v) \leq \epsilon \|v - u\| + Q^0(u; \delta(u, v)) + \psi(v, u), \forall v \in K\}.$$

**Lemma 3.4.** let  $P$  be a Banch space, and  $K$  is a nonempty convex, closed subset  $P$ , if conditions  $R_1, R_2(1-5)$  and  $R_3(1-2)$  be satisfied. Then  $D(\epsilon) = E(\epsilon)$ .

**Proof.** Assume that  $(t, u) \in D(\epsilon)$ , and there exists  $(t, u) \in T \times K$ , such that

$$\vartheta(t, u, v) + Q^0(u; \delta(u, v)) \geq -\epsilon \|v - u\|, \forall v \in K. \quad (3.2)$$

Now, from (3.2) and according to  $R_2(2)$  for  $\vartheta(t, \cdot, \cdot)$ , we have

$$\begin{aligned} \vartheta(t, v, u) - \psi(u, v) - \psi(v, u) &\leq -\vartheta(t, u, v) \\ &\leq \epsilon \|v - u\| + Q^0(u; \delta(u, v)). \end{aligned} \quad (3.3)$$

Therefore,  $(t, u) \in E(\epsilon)$ , then  $D(\epsilon) \subseteq E(\epsilon)$ .

Conversely, assume that  $(t, u) \in E(\epsilon)$  and  $v \in K$  is fixed.

Let  $u_\mu = u - \mu(u - v)$ ,  $\mu \in (0, 1)$ , and since  $K$  is convex. Then  $u_\mu \in K$ .

$$\leq \mu[\epsilon \|v - u\| + Q^0(u; \delta(u, v))] + \psi(u, u_\mu) + 2\psi(u_\mu, u)$$

Now, from Remark 2.4, we obtain

$$\begin{aligned} \vartheta(t, u_\mu, u) &\leq \epsilon \|u_\mu - u\| + Q^0(u; \delta(u, u_\mu)) + \psi(u, u_\mu) + \psi(u_\mu, u) \\ &= \mu[\epsilon \|v - u\| + Q^0(u; \delta(u, v))] + \psi(u, u_\mu) + \psi(u_\mu, u). \end{aligned} \quad (3.4)$$

By convexity of  $\vartheta(t, u, \cdot)$ , we get

$$0 = \vartheta(t, u_\mu, u_\mu) \leq \vartheta(t, u_\mu, u) - \mu[\vartheta(t, u_\mu, u) - \vartheta(t, u_\mu, v)].$$

Then,

$$\mu[\vartheta(t, u_\mu, u) - \vartheta(t, u_\mu, v)] \leq \vartheta(t, u_\mu, u) \quad (3.5)$$

At similarity from convexity of  $\psi(u, \cdot)$  all  $u \in K$ , we get

$$\mu[\psi(u_\mu, u) - \psi(u_\mu, v)] \leq \psi(u_\mu, u). \quad (3.6)$$

from the estimation (3.4), (3.5) and (3.6) we obtain

$$\mu[\vartheta(t, u_\mu, u) - \vartheta(t, u_\mu, v) + \psi(u_\mu, u) - \psi(u_\mu, v)] \leq \vartheta(t, u_\mu, u) + \psi(u_\mu, u)$$

Since the hemicontinuously of  $\vartheta(t, \cdot, v)$  and  $\psi(\cdot, v)$ , we obtain

$$\begin{aligned} &\mu[-\vartheta(t, u, v) - \psi(u, v) - \epsilon \|v - u\| - Q^0(u; \delta(u, v))] \leq \psi(u, u_\mu) \\ &\vartheta(t, u, v) + Q^0(u; \delta(u, v)) + \epsilon \|v - u\| \geq -\frac{\psi(u, u_\mu)}{\mu} - \psi(u, v). \end{aligned} \quad (3.7)$$

from the estimations (2.4) and (3.7), we obtain

$$\vartheta(t, u, v) + Q^0(u; \delta(u, v)) \geq -\epsilon \|v - u\|, \forall v \in K.$$

Therefore,  $(t, x) \in D(\epsilon)$  and  $D(\epsilon) = E(\epsilon) \forall \epsilon > 0$ . This completes the proof.

Lemma 3.5. let  $P$  be a Banach space, and  $K$  is a nonempty convex, closed subset of  $P$ , if conditions  $R_1, R_2(5)$  and  $R_3(3)$ . Then,  $E(\epsilon)$  is closed in  $T \times K$  for any  $\epsilon > 0$ .

Proof. Assume that  $\{(t_n, u_n)\} \subseteq E(\epsilon)$  is a sequence such that  $(t_n, u_n) \rightarrow (t, u)$  in  $T \times K$ . Then,

$$\vartheta(t_n, v, u_n) - \psi(u_n, v) \leq \epsilon \|v - u_n\| + Q^0(u_n; \delta(u_n, v)) + \psi(v, u_n) \quad \forall v \in K$$

By Remark 2.5 and conditions  $R_2(5)$  and  $R_3(3)$  we get

$$\begin{aligned} & \vartheta(t, v, u) \\ & \leq \liminf_n [\vartheta(t_n, v, u_n)] \\ & \leq \limsup_n [\epsilon \|v - u_n\| + Q^0(u_n; \delta(u_n, v)) + \psi(v, u_n) + \psi(u_n, v)] \\ & \leq \epsilon \|v - u\| + Q^0(u; \delta(u, v)) + \psi(v, u) + \psi(u, v). \end{aligned}$$

Thus,  $E(\epsilon)$  is closed in  $T \times K$  for  $\epsilon > 0$ . This completes the proof.

Forthcoming, the result is a consequence of Lemmas (3.4) and (3.5).

Theorem 3.6. let  $P$  be a Banach space, and  $K$  is a nonempty convex, closed subset of  $P$ . If conditions  $(R_1 - R_3)$  satisfy. Then,  $D(\epsilon)$  is closed in  $T \times K \forall \epsilon > 0$ . Moreover, the  $(HE_p)$  is equivalent to following problem.

Find a  $x \in K$  such that,

$$\vartheta(y, x) - \psi(x, y) \leq Q^0(x; \delta(x, y)) + \psi(y, x) \quad (\forall y \in K). \quad (3.8)$$

Here, the essential result in this article is given.

Theorem 3.7. let  $P$  a Banach space, and  $K$  is a nonempty convex, closed subset of  $P$ . If the hemi-equilibrium problem  $(HE_p)$  is strongly well-posedness, then

$$\forall \epsilon > 0, \lim_{\epsilon \rightarrow 0} \text{diam } D(\epsilon) = 0, \text{ where } D(\epsilon) \neq \emptyset. \quad (3.9)$$

While, if conditions  $(R_1 - R_3)$  satisfy. Then the opposite is true.

Proof. Let the hemi-equilibrium problem  $(HE_p)$  be strongly well-posedness, then the problem  $(EHP)$  admit a unique solution  $(t, u) \in T \times K$ , which

$$\vartheta(t, u, v) + Q^0(u; \delta(u, v)) \geq 0, \forall v \in K.$$

Evidently,  $D(\epsilon) \neq \emptyset$  for any given  $\epsilon > 0$ . Implementing the contradiction, assume that

$$0 < \rho < \lim_{\epsilon \rightarrow 0} \text{diam } D(\epsilon).$$

Now, we estimate two sequences  $\{(t_n, u_n)\}$  and  $\{(t_n, v_n)\}$  to hold  $(t_n, u_n) \in D(\epsilon), (t_n, v_n) \in D(\epsilon)$  and

$$\|(t_n, u_n) - (t_n, v_n)\| > \rho, \forall n \in \mathbb{N} \quad (3.10)$$

Since the sequence  $\{(t_n, u_n)\}$  and  $\{(t_n, v_n)\}$  are approximating sequence for the problem  $(HE_p)$ , and

the well-posedness of the problem  $(HE_p)$ , they are strongly convergent to a unique solution, so we could a contradiction of problem (3.10).

Conversely, suppose that the estimation (3.9) satisfy. Assume that  $\{(t_n, u_n)\}$  is approximating sequence for the problem  $(HE_p)$  so, the sequence  $\{\epsilon_n\}$  is positive with  $\{\epsilon_n\} \downarrow 0$  as  $n \uparrow \infty$  such that

$$\begin{aligned} \vartheta(t_n, u_n, v) + Q^0(u_n; \delta(u_n, v)) &\geq -\epsilon_n \|v - u_n\| \quad \forall n \in \mathbb{N}, v \\ &\in K. \end{aligned} \quad (3.11)$$

Thus,  $\{(t_n, u_n)\} \in D(\epsilon_n)$ . It follows from estimation( 3.9) that  $\{(t_n, u_n)\}$  is Cauchy sequence and so it converges strongly to point  $(t, u) \in T \times K$ . Taking into account that conditions  $R_1, R_2(2-5)$  and  $R_3(3)$  in addition (2.2) and (3.11), we get

$$\begin{aligned} 0 &= \liminf_n \epsilon_n \|v - u_n\| \\ &\geq \liminf_n [-\vartheta(t_n, u_n, v) - Q^0(u_n; \delta(u_n, v))] \\ &\geq \liminf_n [\vartheta(t_n, v, u_n) - \psi(u_n, v) - \psi(v, u_n) - Q^0(u; \delta(u_n, v))] \\ &\geq \vartheta(t, v, u) - \psi(u, v) - \psi(v, u) - Q^0(u; \delta(u, v)). \end{aligned}$$

The fact together with Theorem (2.6),  $(t, u)$  solution  $(HE_p)$ . To complete the proof, it is adequate to show that  $(HE_p)$  has a unique solution for  $(EHP)$ , let us suppose that  $(u_1, v_1), (u_2, v_2) \in D(\epsilon_n), \forall \epsilon > 0$ . It is follows that

$$0 < \| (u_1, v_1) - (u_2, v_2) \| \leq \text{diam } D(\epsilon) \rightarrow 0.$$

We get  $(u_1, v_1) = (u_2, v_2)$  and so the problem  $(HE_p)$  has a unique solution. This completes the proof.

Theorem 3.8. Let  $S$  and  $P$  be real Banach spaces. A suppose that  $T \subseteq S, K \subseteq P$  are nonempty close convex subset, If the problem  $(HE_p)$  is strongly well-posedness in the generalized sense, then

$$\forall \epsilon > 0, \lim_{\epsilon \rightarrow 0} \cup D(\epsilon) = \emptyset, \quad \text{where} \quad D(\epsilon) \neq \emptyset. \quad (3.12)$$

Moreover, if the conditions  $(R_1 - R_3)$  satisfy. Then the opposite case satisfy.

Proof. Assume that the problem  $(HE_p)$  is strongly well-posedness in the generalized sense. Then the solution sets of the problem  $(HE_p)$  is a nonempty, it means that  $D(\epsilon) \neq \emptyset$  for any  $\epsilon > 0$ , since  $\psi \subset D(\epsilon)$ . Our claim that the set of solution  $\psi$  for the problem  $(HE_p)$  is compact. In fact any sequence  $\{(t_n, u_n)$  sub set of  $\psi$ , the sequence  $\{(t_n, u_n)\}$  is an approximating sequence for the problem  $(HE_p)$ .

Therefore, we obtain from that a subsequence which converges to some point of  $\psi$ . Then the solution set  $\psi$  of  $(HE_p)$  is compact.

Now, we have that  $\lim_{\epsilon \rightarrow 0} \cup D(\epsilon) \rightarrow \emptyset$ . From  $\psi \subseteq D(\epsilon) \forall \epsilon > 0$  we get,

$$H(D(\epsilon), \psi) = \max\{e(D(\epsilon), \psi), e(\psi, D(\epsilon))\} \quad (3.13)$$

Taking into account the compactness of solution set  $\psi$ , we obtain by (3.13)

$U(D(\epsilon)) \leq 2H(D(\epsilon), \psi) + U(\psi) = 2e(D(\epsilon), \psi)$ , where  $U(\psi) = 0$ , since  $\psi$  is compact. To show that  $\lim_{\epsilon \rightarrow 0} U(D(\epsilon)) = 0$  is equivalent to prove that

$e(D(\epsilon), \psi) \rightarrow 0$  as  $\epsilon \rightarrow 0$ . If not,  $\exists \alpha > 0$  and  $\{\epsilon_n\} \rightarrow 0$ , and  $\{(t_n, u_n)\}$  is a sequence in  $D(\epsilon_n)$  such that

$$(t_n, u_n) \notin \pi + B_{\alpha/2}(0), \forall n \in \mathbb{N}, \quad \text{where } B_{\alpha/2}(0) \quad (3.14)$$

is an open ball with center 0 and radius  $\frac{\alpha}{2}$ . But the sequence  $\{(t_n, u_n)\}$  is an approximating sequence in  $D(\epsilon_n)$  for the problem  $(HE_p)$  then there exists convergent subsequence to some point in  $\psi$ . This is contradiction (3.14).

conversely, assume that (3.12) satisfy. By Lemmas (3.4) and (3.5), we get  $D(\epsilon)$  is a nonempty and closed for all  $\epsilon > 0$ . From the Kuratowsky theorem [20], we obtain  $\lim_{\epsilon \rightarrow 0} U(D(\epsilon)) = 0$ , in which

$\psi = \bigcap_{\epsilon > 0} D(\epsilon)$  is a nonempty and compact set. Assume that  $\{(t_n, x_n)\} \subseteq K$  an approximate sequence for the problem  $(HE_p)$ , then there exists appositve sequence  $\{\epsilon_n\}$  with  $\{\epsilon_n\} \downarrow 0$  as  $n \uparrow \infty$  in which,

$$\vartheta(t_n, u_n, v) + Q^0(u_n; \delta(u_n, v)) \geq -\epsilon_n \|v - u_n\| \quad \forall n \in \mathbb{N}, v \in K.$$

Then we get that the estimate  $(t_n, u_n) \in D(\epsilon_n)$ . Moreover this result with the estimation (3.12) point out that

$$d((t_n, u_n), \psi) \leq e(D(\epsilon), \psi) \rightarrow 0.$$

Since  $\psi$  is compact set, it follows that there exists  $(\bar{t}_n, \bar{u}_n) \in \pi$ , in which

$$\|(t_n, u_n) - (\bar{t}_n, \bar{u}_n)\| = d((t_n, u_n), \psi) \rightarrow 0.$$

Again, since the set of solutions  $\psi$  is compact, then the sequence  $\{(\bar{t}_n, \bar{u}_n)\}$

has a subsequence  $\{(\bar{t}_{nk}, \bar{u}_{nk})\}$  converging strongly to  $\{(\bar{t}_n, \bar{u}_n)\} \in \psi$ . Thus, the corresponding  $\{(t_{nk}, u_{nk})\}$  subsequence of  $\{(t_n, u_n)\}$  which is strongly converges in  $\psi$ , then  $(HE_p)$  is well-posedness strongly in generalized sense. This completes the proof.

#### 4. WELL-POSEDNESS FOR OPTIMIZATION PROBLEMS WITH PARAMETRIC HEMI-EQUILIBRIUM CONSTRAINT (OPPHEC)

The goal of this section is to introduce some criteria and characterizations of the well-posedness for optimization problems with hemi-equilibrium constraint.

Additionally, we will introduce the following ideas of measures of noncompactness.

Definition 4.1. A sequence  $\{(t_n, u_n)\} \subseteq T \times K$  is called an approximating sequence for the problem (OPPHEC) if there exists a nonnegative sequence  $\{\epsilon_n\}$  with  $\{\epsilon_n\} \rightarrow 0$  as  $n \downarrow \infty$  in which

$$\begin{cases} \vartheta(t_n, u_n, v) + Q^0(u_n; \delta(u_n, v)) \geq -\epsilon_n \|v - u_n\| \quad \forall n \in \mathbb{N}, v \in K \quad \text{and} \\ \limsup_n \Lambda(t_n, u_n) \leq \inf_{r \in T, v \in \Psi(r)} \Lambda(r, v) \end{cases}$$

Definition 4.2. assume that the problem (OPPHEC) is strongly well-posedness, if it has a unique solution and for every an approximating sequence for the problem (OPPHEC) converges strongly to the unique solution.

Definition 4.3. let The problem (OPPHEC) is said to be strongly well-posedness in the generalized sense if it has a nonempty solution set  $\Psi$ , and every approximating sequence of solutions has subsequence which strongly converges to some point in  $\Psi$ .

To obtain metric characterizations of well-posedness of the problem (OPPHEC), we consider the set of approximating solutions for the problem (OPPHEC) which is denoted by  $\Gamma(\epsilon, \sigma)$  and defined as:

$$\Gamma(\epsilon, \sigma) = \left\{ (t, u) \in T \times K : \Lambda(t, u) = \inf_{r \in T, v \in \Psi(r)} \Lambda(r, v) + \sigma \quad \text{and} \right. \\ \left. \vartheta(t, u, v) + Q^0(u; \delta(u, v)) \geq -\epsilon_n \|v - u\|, \forall v \in K. \right.$$

Theorem 4.4. let  $S$  be a Banach space and  $K \subseteq S$  be a nonempty convex, closed subset of  $S$ . If the problem (OPPHEC) is strongly well-posedness, then

$$\Gamma(\epsilon, \sigma) \neq \emptyset \quad \forall \epsilon, \sigma > 0, \quad \text{diam } \Gamma(\epsilon, \sigma) \rightarrow 0 \quad \text{as} \quad (\epsilon, \sigma) \rightarrow (0, 0). \quad (4.1)$$

Moreover, if conditions  $(R_1 - R_3)$  and  $R_4(2)$  satisfies. Then the converse is true.

Proof. Let the problem (OPPHEC) be strongly well-posedness, then the problem (OPPHEC) has a unique solution for all  $(t, x) \subseteq T \times K$  such that

$$\begin{cases} \Lambda(t, x) = \inf_{r \in T, y \in \Psi(r)} \Lambda(r, y) & \text{and} \\ \vartheta(t, x, y) + Q^0(x; \delta(x, y)) \geq 0 & \forall y \in K. \end{cases}$$

$\Gamma(\epsilon, \sigma) \neq \emptyset \quad \forall \epsilon, \sigma > 0$ , since  $(t, x) \in \Gamma(\epsilon, \sigma)$  for any  $\epsilon, \sigma > 0$ . If  $\text{diam } \Gamma(\epsilon, \sigma) \rightarrow 0$  as, then  $\exists \mathcal{F} > 0$  and  $\{\epsilon_n\}, \{\sigma_n\}$  are nonnegative sequences with  $\epsilon_n \rightarrow 0, \sigma_n \rightarrow 0$  as  $n \downarrow \infty$  and  $(t_n, x_n), (t_n, y_n) \in \Gamma(\epsilon_n, \sigma_n)$  such that

$$\mathcal{F} < \|(t_n, x_n) - (t_n, y_n)\| \quad \forall n \in \mathbb{N}. \tag{4.2}$$

Since  $(t_n, x_n), (t_n, y_n) \in \Gamma(\epsilon_n, \sigma_n) \quad \forall n \in \mathbb{N}$ , therefore both  $(t_n, x_n)$  and  $(t_n, y_n)$  are approximating sequences for the problem (OPPHEC). By the well-posedness of the problem (OPPHEC), they have converged strongly to the unique solution of the problem (OPPHEC) a contradiction to (4.2).

On the contrary, suppose that estimation (4.1) holds and  $\{(t_n, x_n)\}$  is an approximating sequence for the problem (OPPHEC). Then we obtain a nonnegative sequence  $\{\epsilon_n\}$  with  $\{\epsilon_n\} \rightarrow 0$  as  $n \rightarrow \infty$  in which

$$\begin{cases} \vartheta(t_n, x_n, y) + Q^0(x_n; \delta(x_n, y)) \geq -\epsilon_n \|y - x_n\| \quad \forall n \in \mathbb{N}, y \in K \text{ and} \\ \limsup_n \Lambda(t_n, x_n) \leq \inf_{r \in T, y \in \Psi(r)} \Lambda(r, y) \end{cases} \tag{4.3}$$

This yields that  $(t_n, x_n) \in \Gamma(\epsilon_n, \sigma_n)$ . Then from estimation (4.1), we get  $\{(t_n, x_n)\}$  is a Cauchy sequence, and it converges strongly to a point  $(t, x) \in T \times K$ . It follows from the estimation (4.3) and (2.2) and conditions  $R_1, R_2(2-5)$  and  $R_3(3)$  we obtain

$$\begin{aligned} 0 &= \liminf_n \epsilon_n \|y - x_n\| \\ &\geq \liminf_n \{-\vartheta(t_n, x_n, y) - Q^0(x_n; \delta(x_n, y))\} \\ &\geq \liminf_n \vartheta(t_n, y, x_n) - \psi(x_n, y) - \psi(y, x_n) - Q^0(x_n; \delta(x_n, y)) \\ &\geq \vartheta(t, y, x) - \psi(x, y) - \psi(y, x) - Q^0(x; \delta(x, y)). \end{aligned}$$

Furthermore, we can obtain from the estimation (4.3) and hypotheses  $R_4(2)$

$$\begin{aligned} \inf_{r \in T, v \in \Psi(r)} \Lambda(r, v) &\geq \limsup_n \Lambda(t_n, x_n) \\ &\geq \liminf_n \Lambda(t_n, x_n) && \geq \Lambda(t, x). \end{aligned}$$

Therefore, from Theorem 3.6, we obtain  $(t^*, x^*)$  is solution of the problem (OPPHEC). Also, the unique solution follows immediately from the estimation (4.1). This completes the proof.

Theorem 4.5. Let  $S$  and  $P$  be real Banach and  $T \subseteq S, K \subseteq P$  be nonempty, closed and convex. If the problem (OPPHEC) is strongly well-posedness in the generalized sense, the

$$\Gamma(\epsilon, \sigma) \neq \emptyset, \forall \epsilon, \sigma > 0 \text{ and } \lim_{(\epsilon, \sigma) \rightarrow (0,0)} \cup(D(\epsilon, \sigma)) = 0 \tag{4.4}$$

Moreover, if conditions  $(R_1 - R_3)$  and  $R_4(2)$  holds. Then the opposite satisfy.

In the way as the prove of Theorem (3.8), we can prove above theorem for the well-posedness of (OPPHEC).

Following to attain the uniqueness of solution to the problem (OPPHEC), we show that under favourable conditions the well-posedness of the problem (OPPHEC) is equivalent to the existence and uniqueness of solutions.

Theorem 4.6. Let  $S$  and  $K$  be finite dimensional Banach space and  $T \subseteq S, K \subseteq P$  be a nonempty, closed and convex. Consider conditions  $(R_1 - R_4)$  holds, then the problem (OPPHEC) is strongly well-posedness if and only if it has a unique solution.

Proof. "Obligation " suppose that the problem (OPPHEC) has unique solution  $(t^*, x^*)$ , then

$$\begin{cases} \Lambda(t^*, x^*) = \inf_{(r,y) \in T \times K, y \in \Psi(t)} \Lambda(r, y) \\ \vartheta(t^*, x^*, y) + Q^0(x^*; \delta(x^*, y)) \geq 0, \forall y \in K. \end{cases} \tag{4.5}$$

Assume that  $\{(t_n, x_n)\} \subseteq T \times K$  be an approximating sequence for the problem (OPPHEC), there exists, nonnegative sequence  $\{\epsilon_n\}$  with  $\epsilon_n \rightarrow 0$  in which

$$\begin{cases} \lim_n \sup \Lambda(t_n, x_n) \leq \inf_{r \in T, y \in \Psi(r)} \Lambda(r, y) \\ \vartheta(t_n, x_n, y) + Q^0(x_n; \delta(x_n, y)) \geq -\epsilon_n \|y - x_n\| \quad \forall y \in K, \forall n \in \mathbb{N}. \end{cases} \tag{4.6}$$

We claim  $\{(t_n, x_n)\}$  is bounded .If not without loss of generality, one can suppose  $\|(t_n, x_n)\| \rightarrow +\infty$  . Let us that  $f_n = \frac{1}{\|(t_n, x_n) - (t^*, x^*)\|}$  and

$$(k_n, m_n) = f_n(t_n, x_n) + (1-f_n)(t^*, x^*) = (f_n t_n + (1-f_n)t^*, f_n x_n + (1-f_n)x^*).$$

Suppose that  $f_n \in (0,1)$  and  $(k_n, m_n) \rightarrow (k, m)$  in which  $(k, m) \neq (t^*, x^*)$ . Now, since  $E \times S$  is finite dimensional, one can take into calculating the closeness and



convexity of  $T$  and  $K$ , one has  $(k_n, m_n) \in T \times K$ . From the estimates (4.5), (4.6) and condition  $R_4(1)$ , for any  $(k, m) \in T \times K$ , we get

$$\begin{aligned}
 \Lambda(t^*, x^*) &= \lim_n \sup f_n \Lambda(t_n, x_n) + \lim \sup (1 - f_n) \Lambda(t^*, x^*) \\
 &\geq \lim_n \sup [f_n \Lambda(t_n, x_n) + (1 - f_n) \Lambda(t^*, x^*)] \\
 &\geq \lim_n \sup \Lambda(k_n, m_n) \\
 &\geq \lim_n \inf \Lambda(k_n, m_n) \\
 &\geq \Lambda(k, m).
 \end{aligned} \tag{4.7}$$

Furthermore, it follows from conditions  $R_2(1,4$  and  $5)$ , and the estimates (4.5), (4.6) and

Remark (2.5) we obtain

$$\begin{aligned}
 0 &= \lim_n \inf f_n \epsilon_n \|y - m_n\| \\
 &\geq \lim_n \inf (-f_n [\vartheta(t_n, x_n, y) + Q^0(x_n; \delta(x_n, y))] - (1 - f_n) [\vartheta(t^*, x^*, y) + Q^0(x^*; \delta(x^*, y))]) \\
 &\geq \lim_n \inf - [f_n \vartheta(t_n, x_n, y) + (1 - f_n) \vartheta(t^*, x^*, y) - [f_n Q^0(x_n; \delta(x_n, y)) + (1 - f_n) Q^0(x^*; \delta(x^*, y))]] \\
 &\geq \lim_n \inf - [\vartheta(k_n, m_n, y) + Q^0(m_n; \delta(m_n, y))] \\
 &\geq \lim_n \inf [\vartheta(k_n, y, m_n) - Q^0(x_n; \delta(m_n, y)) - \psi(m_n, y) - \psi(y, m_n)] \\
 &\geq \vartheta(k, y, m) - Q^0(m; \delta(m, y)) - \psi(m, y) - \psi(y, m).
 \end{aligned} \tag{4.8}$$

By Theorem(3.6) we get that

$$\vartheta(k, m, y) + Q^0(m; \delta(m, y)) \geq 0 \quad \forall y \in K$$

So, from the estimate (4.7) and (4.8),  $(k, m)$  solutions for the problem (OPPEC), that is a contradiction. Therefore  $\{(t_n, x_n)\}$  is bounded.

Assume that  $\{(t_{ni}, x_{ni})\}$  is any subsequence of  $\{(t_n, x_n)\}$  in which

$(t_{ni}, x_{ni}) \rightarrow (t_0, x_0)$  as  $i \rightarrow \infty$ . It follows that

$$0 = \lim_i \inf \epsilon_{ni} \|y - x_{ni}\|$$

$$\begin{aligned}
 &\geq \lim_i \inf [ - \vartheta((t_{ni}, x_{ni}, y) - Q^0(x_{ni}; \delta(x_{ni}, y))) ] \\
 &\geq \lim_i \inf [\vartheta(t_{ni}, y, x_{ni}) - Q^0(x_{ni}; \delta(x_{ni}, y)) - \psi(x_{ni}, y) - \psi(y, x_{ni})] \quad (4.9) \\
 &\geq \vartheta(t_0, y, x_0) - Q^0(x_0; \delta(x_0, y)) - \psi(x_0, y) - \psi(y, x_0), \quad \forall y \in K
 \end{aligned}$$

By applying Theorem 3.6, we have that

$$\vartheta(t_0, x_0, y) + Q^0(x_0; \delta(x_0, y)) \geq 0, y \in K \quad (4.10)$$

From the estimate (4.6) and  $R_4(2)$ , we have

$$\begin{aligned}
 \inf_{r \in T, v \in \pi(r)} \Lambda(r, v) &\geq \limsup_i \Lambda(t_{ni}, u_{ni}) \\
 &\geq \liminf \Lambda(t_{ni}, u_{ni}) \quad (4.11) \\
 &\geq Q(t_0, u_0)
 \end{aligned}$$

Now, from the estimate (4.10) and (4.11),  $(t_0, u_0)$  solutions the problem (OPPHEC). Taking into account the uniqueness of the solution, we obtain

$(t_0, u_0) = (t^*, u^*)$ . Therefore,  $(t_n, u_n)$  converges to  $(t^*, u^*)$ . Hence, the problem (OPPHEC) is strongly well-posedness, this completes the proof.

**Theorem 4.7.** Let  $S$  and  $P$  be two finite dimension Banach spaces and  $T \subseteq S$  and  $K \subseteq P$  be a nonempty closed convex . If there exists some  $\sigma > 0$  in which  $\Gamma(\sigma, \sigma)$  is a nonempty and bounded and suppose that conditions  $(R_1 - R_4)$  satisfy, then the problem(OPPHEC) is strongly well-posedness in the generalized sense.

*Proof.* Assume that  $\{(t_n, x_n)\} \subseteq T \times K$  is an approximating sequence for the problem (OPPHEC). Then there exists nonnegative sequence  $\{\epsilon_n\}$  with  $\epsilon_n \rightarrow 0$  as  $n \rightarrow \infty$  in which

$$\begin{cases}
 \vartheta(t_n, x_n, y) + Q^0(x_n; \delta(x_n, y)) \geq \epsilon_n \|y - x_n\| \quad \forall y \in K, \forall n \in \mathbb{N} \text{ and} \\
 \limsup_n \Lambda(t_n, x_n) \leq \inf_{(r,y) \in T \times K, y \in \psi(r)} \Lambda(r, y)
 \end{cases}$$

Since  $\Gamma(\sigma, \sigma)$  is a nonempty and bounded . That there exists  $n_0$  in which  $(t_n, x_n) \in \Gamma(\sigma, \sigma)$  for all  $n \geq n_0$ . Taking into account the boundedness of  $\Gamma(\sigma, \sigma)$  there exists some subsequence  $\{(t_{ni}, x_{ni})\}$  of  $\{(t_n, x_n)\}$  such that

$(t_{ni}, x_{ni}) \rightarrow (t_0, x_0)$  as  $i \rightarrow \infty$  consequently, as proved in Theorem 4.6,  $(t_0, x_0)$  solution (OPPHEC), then the problem (OPPHEC) is strongly well-posedness in the generalized sense. This completes the proof.

## 5. Conclusions

In this work, we present the well-posedness for the problem  $(HE_p)$ . Under relatively weak conditions for the data  $\vartheta$  and  $\delta$  involving  $\psi$ -monotonicity [see Theorems 3.7 and 3.8].

Ditto, we investigate some metric characterizations of well-posedness of the problem  $(OPPHEC)$  are given. Our results generalize and improve many known results and can be applicatively to many other problems [see [6,12]].

## References

1. L. Q. Anh, P. Q. Khanh, and D. T. M. Van, Well-posedness under relaxed semicontinuity for bilevel equilibrium and optimization problems with equilibrium constraint, *Journal of Optimization Theory and Application*, 153, 42-59, (2012).
2. B. Brogliato and A. Tanwani. Dynamical systems coupled with monotone set-valued operators. *Formalisms. Applications, Well-posedness, and Stability*, 62, 3-129, (2020).
3. M. Binachi, G. Kassay, and R. Pini. Well-posedness for vector equilibrium problems. *Math, Methods Oper. Res*, 70, 171-182, (2009).
4. F. H. Clarke, *Optimization and Nonsmooth Analysis*, John Wiley (1983).
5. B. Choudhury, N. Metiy and S. Kundu, Existence, well-posedness of coupled fixed points and application to nonlinear integral equations, *CUBO, A mathematical Journal*, 23, 171-190, (2021)
6. Caijing Jiang. Well-posedness for a class of generalized variational-hemivariational inequalities involving set-valued operators. *Journal of Inequalities and Applications*, 1, 187, (2018).
7. D. Fajman, Local well-posedness for the Einstein-Vlasov System, *Journal on Mathematical Analysis* 48, 3270-3321, (2016).
8. Y. P. Fang, N. J. Huang and J. Y. Yao : Well-posedness of mixed variational inequalities, inclusion problems and fixed point problems, *J. Glob. Optim.* 41, 117-133, (2008).
9. X. X. Huang, Extended and strongly extended well-posedness of set-valued optimization problems, *Math. Methods. Oper. Res.* 53, 101-116. (2001)
10. [10] A. E. Hashoosh, Well-posedness for class of hemi-equilibrium problems with perturbations in Banach spaces, *Journal of Dynamical and Control Systems*, 10, 478-487, (2019).
11. Hashoosh, M. Alimohammady and A. Almusawi, Well-posedness Techniques in the Qualitative Analysis for a class of Equilibrium problems, *Journal of Zankoy Sulaimani*, 19, 211-220, (2017).
12. Huzem, A. A. Alwan, W. K. Ghafil and A. E. Hashoosh, Existence and Uniqueness of solutions to Hemi equilibrium problems with application, *Journal of Adv Research in Dynamical and Control Systems*, 11, 1754 -1758, (2019).
13. E. Hashoosh, and M. Alimohammady, On well-posedness of generalized equilibrium problems involving  $\alpha$ - monotone bifunction, *Journal of Hyperstructures*, 5, 151-168, (2016).

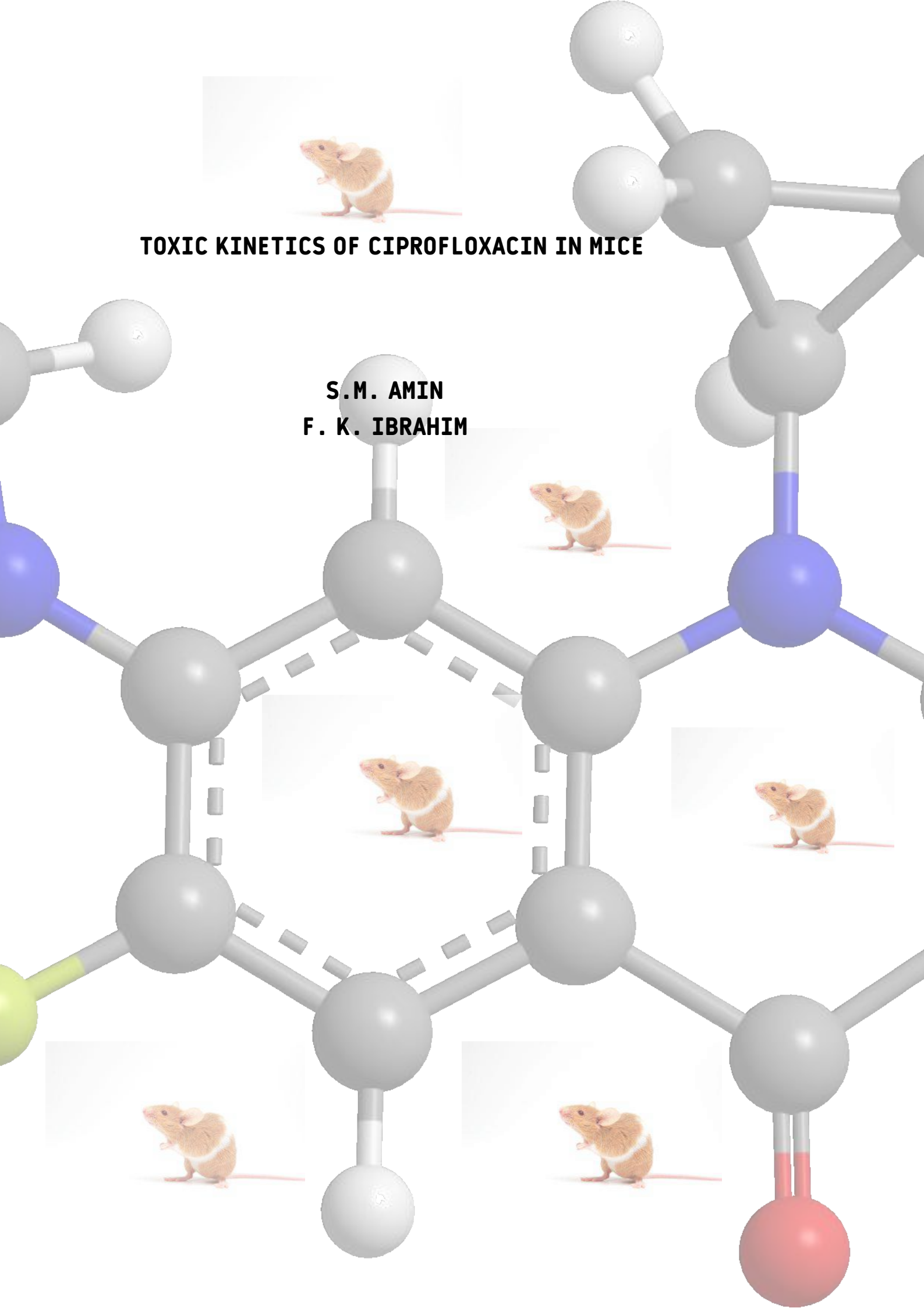
14. A. E. Hashoosh and A. M. Jaber, Improvement of Well-posedness For Hemiequilibrium Problems, *Mathematics in Engineering and Science Aerospace*, acceptance (2020).
15. K. Kimura, Y. C. Liou, S. Y. Wu and J. C. Yao, Well-posedness for parametric vector equilibrium with applications, *J. Ind, Manag. Optim.* 4, 313–327, (2008).
16. K. Kuratowski, *Topology*, vols, Academic Press, New York, NY, 1–2, (1989).
17. E. S. Levitin and B. T. Polyak, Convergence of minimizing sequences in conditional extremum problem, *Soviet Mathematics Doklady*.7, 764–767, (1966).
18. M. B. Lignola and J. Morgan, Well-posedness for optimization problems with constraints defined by variational inequalities having a unique solution, *J. Global Optim.* 16, 57-67, (2000).
19. H. A. Naser A. A. Alwan and A. E. Hashoosh. He solutions of mixed hemiequilibrium problem with application in sobolev space. *Material Science and Engineering*, 571, 1-9, (2019).
20. W. Oettli and H. Riahi, On maximal  $\psi$ -monotonicity of sum of operator, *Communication on Applied Nonlinear Analysis* 1-15, (1998).
21. F. Patrone M. Margiocco and L. P. Chicco. A new approach to Tikhonov well-posedness for nash equilibrium. *J. Optimization*, 4, 385-400, (1997).
22. J. Peng, Y. Wang and S. Wu, Levitin-Polyak well-posedness of generalized vector equilibrium problems, *J. Math. Taiwan*, 15, 2311-2340, (2011).
23. J. P. Revalski. Hadamard and strong well-posedness for convex programs. *Journal on Optimization.*, 7, 519-526, (1997)
24. S. Reich and A. J. Zaslavski, A note on well-posedness null and fixed point problems. *Fixed Point Theory Appl.*, 207-211, (2005).
25. J. Salamon. Closedness and Hadamard well-posedness of the solution map for parametric vector equilibrium problems. *J. Glob, Optim.* 47, 173–183, (2010).
26. S. Treanta and S. Jha, ON WELL-POSEDNESS ASSOCIATED WITH A CLASS OF CONTROLLED VARIATIONAL INEQUALITIES, *Mathematical Modelling of Natural Phenomena*, 15, 1-16, (2021).
27. R. U. Verma. On generalized variational inequalities involving relaxed lipschitz and relaxed monotone operator. *Jour of Mathematical Analysis and Applications*, 387-392, (2006).
28. [28] Y. Xiao, N. Huang and M. Wong, well-posedness of hemivariation inequalities and inclusion problems, *taiwanese journal of mathematics*, 3, 1261-1276, (2011).

29. Y. Zhanga and T. Chen, "A note on well-posedness of Nash-type games problems with set payoff", *J. Nonlinear Sci, Appl*, 9, 486–492, (2016).
30. K. Zhang, Z. Quan HE and D. Peng GAO, "Extended well- posedness for quasivariational inequality", 10, 1-10. (2009).



## **TOXIC KINETICS OF CIPROFLOXACIN IN MICE**

**S.M. AMIN  
F. K. IBRAHIM**



## TOXIC KINETICS OF CIPROFLOXACIN IN MICE

S.M. AMIN <sup>1</sup>

F. K. IBRAHIM <sup>2</sup>

### Abstract:

Ciprofloxacin belongs to a class of drugs called quinolone antibiotics. It is widely used in humans and animals. Excessive use of it increases the risk of poisoning, which occurs due to medical errors or due to the use of high doses to overcome antibiotic resistance. Due to the lack of research on its toxic kinetics. Therefore, the goal of our research was to measure its toxic kinetics in mice. First, the median lethal dose (LD50) was accounted for by the Dixon method. It was 1280,5 mg/kg body weight. Then mice were injected intraperitoneally at a dose of 800 mg/kg body weight. Blood samples were collected from mice (five/each time interval) after zero, 0.15, 0.30, 0.45, 1, 2, and 4 hours after drug administration. Its concentration in plasma was accounted for by the HPLC method. Its highest plasma concentration was 0.88 $\mu$  g/ml in 15 minutes of injection, and the second rise was 0.76 in 45 minutes of injection. Its toxic kinetic parameters were calculated by non-compartmental analysis. The  $t_{1/2}$  was 1.52 h with a  $V_{ss}$  of 2551.18 (mg)/( $\mu$ g/ml) and a CL of 1162,26 (mg)/( $\mu$ g/ml)/h. The MRT for the drug was 1,31 hours and the AUC (0- $\infty$ ) was 0,69 $\mu$  g/ml\*h. In conclusion, the acute toxicity of ciprofloxacin in the peritoneum is low and the data show the toxic kinetic profile of a single peritoneal dose of ciprofloxacin in mice.

**Key words:** Ciprofloxacin, Toxic Kinetics, LD50, Mice.



<http://dx.doi.org/10.47832/MinarCongress5-11>



<sup>1</sup> University of Mosul, Iraq, [sawsanmohammad2018@gmail.com](mailto:sawsanmohammad2018@gmail.com), <https://orcid.org/0000-0001-8409-0637>



<sup>2</sup> State Company for Drug Industries and Medical Appliances, Iraq, [dr.fawaz1970@yahoo.com](mailto:dr.fawaz1970@yahoo.com), <https://orcid.org/0000-0001-6410-1239>



## **Introduction:**

Ciprofloxacin is 1-cyclopropyl-6-fluoro-1,4-dihydro-4-oxo-7- (1-piperazinyl)-3-quinolinecarboxylic acid. It belongs to a class of drugs called quinolone antibiotics (1). It is widely used in humans and animals (2, 3). It can be taken orally, in the form of eye drops, in the form of ear drops, or intravenously (4). It is effective in the therapy of infections in the urinary tract, respiratory system, digestive system, skin, bones, joints, and soft tissues that occur due to gram-positive and negative bacteria. (5). The main mechanism of its action is the inhibition of both type II DNA gyrase and type IV topoisomerase. Both are required for bacterial DNA replication (6). Its kinetic profile shows that it is quickly absorbed next oral administration and has a high oral bioavailability (7). Its binding to plasma protein is low. The amount of its distribution is large and has good penetration into various liquids and tissues. It is mainly metabolized by CYP1A2 and eliminated by the liver and kidneys (8,9,10). It has adverse reactions, which have been categorized into common, uncommon, and rare adverse reactions. Common adverse reactions include vomiting, transient increase in transaminases, and rash. While uncommon adverse reactions include thrombocytopenia, thrombocythaemia, confusion, and disorientation. Hallucinations, Part and dysaesthesia, Seizures, Vertigo, Visual disturbances, Hearing loss, Tachycardia, Vasodilatation, Hypotension, Transient hepatic impairment, Jaundice, Renal failure, Oedema. While rare adverse reactions include Pancytopenia, Bone marrow depression, Anaphylactic shock, Psychotic reactions, Migraine, Smell disorders, Hearing impairment, Vasculitis, Pancreatitis, Liver necrosis, Petechiae, Tendon rupture (11,12). Frequent and inappropriate use of Ciprofloxacin and other antibiotics can cause a change in the bacteria so that the antibiotic does not work, and this is called antibiotic resistance. These resistant bacteria may require higher doses of antibiotics, which increases the risk of adverse effects (13).

## **Material and methods**

### **Laboratory animals**

40 mature male mice were used, whose weight ranged between 20-30 grams. They were acquired from the animal house of the Faculty of Veterinary Medicine.

### **Medicines used**

Ciprofloxacin was obtained from Samarra Pharmaceuticals and Medical Supplies Laboratory. Distilled water was used to prepare the required doses. The size of the dose used was 10 ml/kg of body weight.

### **Experiments**

Calculation of the mean lethal dose of ciprofloxacin by intraperitoneal injection in mice

In this experiment, five mice were used. An initial dose of ciprofloxacin (1000 mg/kg body weight, intraperitoneally) was administered, and this dose was reached based on preliminary trials. After 24 hours, the final result was read (the survival of the animal is denoted by the letter O or death by the letter X), as well as the signs of poisoning and the time of its onset. The amount of increase or decrease in

ciprofloxacin dose in case of animal survival or subsequent animal death was a constant amount of 250 mg/kg body weight, and this method was repeated by increasing and decreasing the dose for three mice after the change (death to life or vice versa) (14). The dose of ciprofloxacin ranged between 1000-1500 mg/kg of body weight, and the survival or death of the used mice was determined by the above codes and compared with the table of lethal dose measurements mentioned by Dixon in order to obtain a tabular k value( appendix 1). The lethal dose can be calculated using the following law:

$$LD50 = XF + KD$$

Whereas:

LD50 = median lethal dose

XF = the last dose used in the experiment

K = represents the tabular value

D = the amount of increase and decrease in the given dose

Account of ciprofloxacin concentration in mice's blood

In this experiment, 35 mature male mice were used, they were randomly split into seven groups, each group of five animals. The first group was injected with a carrier of ciprofloxacin (distilled water) and the other groups were injected with ciprofloxacin at a dose of 800 mg/kg body weight (The dose was selected based on the first experiment, which causes signs of poisoning. Without animal death). Blood samples were collected of the maxillary vein (15) after 0.15, 0.30, 0.45, 1, 2, 4 hours after the injection, then the samples were transferred to a centrifuge to separate the serum, which was kept in freezing at -20 until the analyzed. The serum concentration of ciprofloxacin was determined by an HPLC.

### Calculation

The concentration of ciprofloxacin in plasma was calculated by the linear regression equation of the standard curve of the peak area versus the concentrations of the standard solution of ciprofloxacin. The concentrations of the standard solution ranged from 1 to 25 parts per million, while the linear equation was as follows

$$y = a + bx \text{ (linear regression equation of the standard curve)}$$

$$y = \text{area of ciprofloxacin in the serum samples at 276 nm}$$

a = intercept

b = slope

x = the concentration of ciprofloxacin in the serum

The mean and standard error of the concentrations of ciprofloxacin in the serum was found using MICROSOFT EXCEL 2010 program, next The means of serum concentrations at each sampling time (0.15-4 h) were used to calculate the toxic kinetic parameters by a non-compartmental analysis using pharmacokinetic add-in package for Microsoft excel 201631 applying non-compartmental analysis (17)

## Results

The median LD<sub>50</sub> of ciprofloxacin in male mice by intraperitoneal injection was 1280,5 mg/kg body weight (Table 1). Observed signs of poisoning were lack of movement, piloerection, Straub tail, shivering, ataxia in walking, lacrimination, respiratory disturbance and flat body appearance and death.

Ciprofloxacin appeared in plasma at mean concentrations of 0.88, 0.15, 0.76, 0.11, 0.06, 0.03 µg/ml post-injection 0.15, 0.30, 0.45, 1, 2, and 4 hours later, respectively (Table 2).

The log plasma concentrations vs. time of ciprofloxacin are shown in figure 2 and the related pharmacokinetic variables of the drug are shown in table 3. The t<sub>1/2</sub> of ciprofloxacin was 1.52 h with a V<sub>ss</sub> 2551.18(mg)/(µg/ml) and CL of 11162.26( mg)/(µg/ml)/h. The MRT of the drug was 1.31 h and its AUC (0-∞) was 0.69 µg/ml\*h (Table 3). Other related pharmacokinetic parameters are also shown in table 3.

Table 1: acute LD<sub>50</sub> value of ciprofloxacin in mice by injection i.p .

Parameters	Result
Acute LD <sub>50</sub> value	1280,5 mg/kg
The dose range	1000-1500 mg/kg
Intimal dose	1000 mg /mg
Last dose	1500 mg/kg
Increase and decrease at dose	250 mg
Number of mice	5(oxoox)
k tabular value	- 0.878
Start of acute toxicity	7- 11 min
Poisoning signs	lack of movement, piloerection , straub tail , shivering, ataxia in walking, lacrimination ,respiratory disturbance , flat body appearance and death.

X= death

O = survival

Table 2: Ciprofloxacin concentration (mean + SE.) in mice serum after administration of a dose of 800 mg/kg body weight in the intraperitoneal.

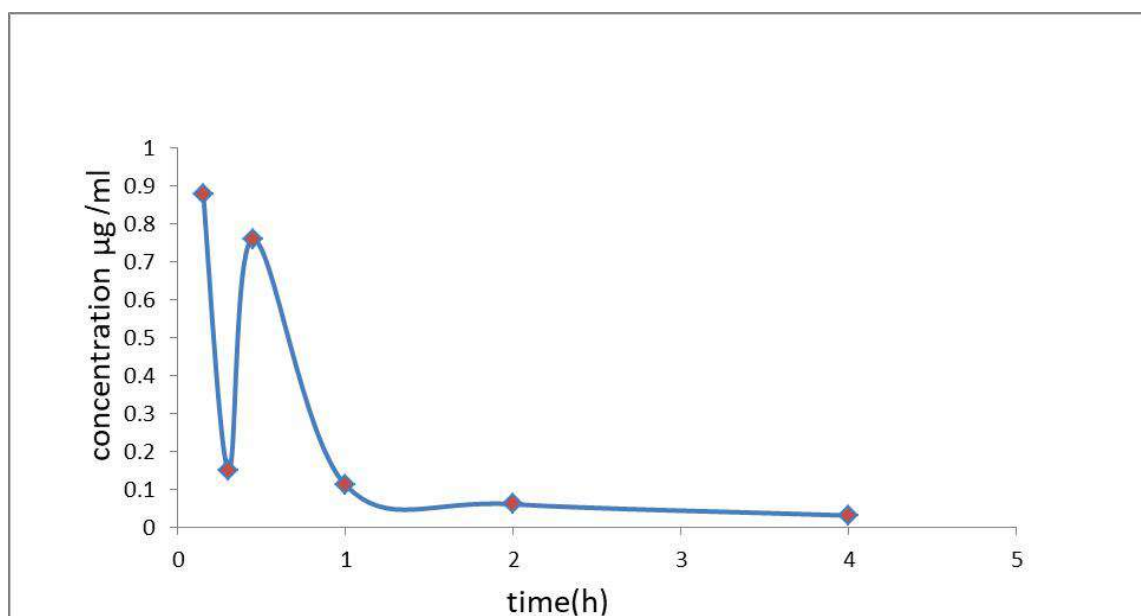
Time ( h)	Serum (µg/ml)
0.15	0.88±0.02
0.30	0.15±0.03
0.45	0.76±0.01
1	0.11±0.01
2	0.06±0.01
4	0.03±0.00

N=5 mice / each time

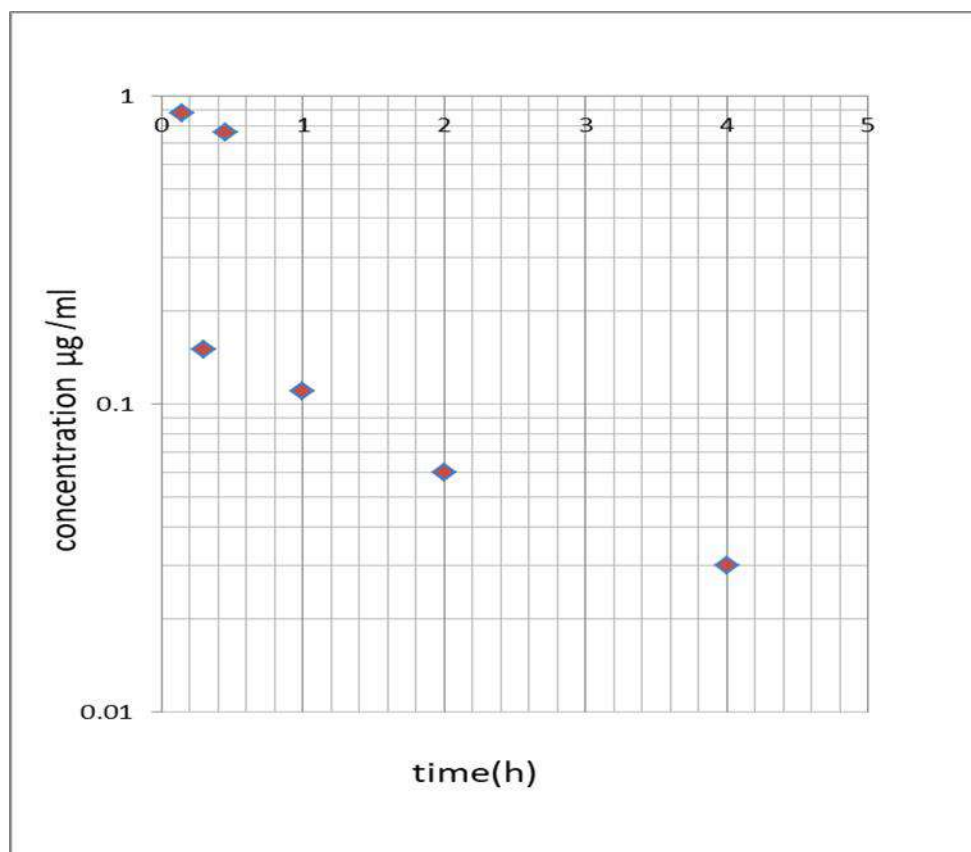
Table 3 :Toxic kinetics of ciprofloxacin in mice after administration of a dose of 800 mg/kg body weight in the intraperitoneal

Parameter	Abbreviation	Unit	Value
Elimination rate constant	kel	1/h	0.45
Elimination half-life	t <sub>1/2</sub>	h	1.52
Time maximum	T <sub>max</sub>	h	0.15
Concentration maximum	C <sub>max</sub>	g/ml $\mu$	0.88
Steady state volume of distribution	V <sub>ss</sub>	(mg)/( $\mu$ g/ml)	2551.18
Total clearance	CL	(mg)/( $\mu$ g/ml)/h)	1162.26
Mean residence time	MRT	H	1.31
Area under the plasma concentration–time curve to infinity	(AUC <sub>0-<math>\infty</math></sub> )	g/ml* $h\mu$	0.69

\*The means of serum concentrations of ciprofloxacin at all sampling time (0.15-4 h) were utilized to account the toxic kinetics parameters by a non-compartmental analysis using pharmacokinetic add-in package for Microsoft excel 201631 applying non-compartmental analysis.



**Figure 1: The concentration of ciprofloxacin in the serum of mice treated at a dose of 800 mg / kg body weight in the intraperitoneal..**



**Figure 2: The log plasma concentrations vs. time of ciprofloxacin in mice following a single intraperitoneal administration with ciprofloxacin by a dose of 800 mg/kg body weight.**

### Discussion

Ciprofloxacin is an antibacterial drug widely used in veterinary medicine. Extensive use increases the risk of poisoning due to medical errors (such as an excessive increase in the dose of a particular drug or the frequency of the drug over a short period (18). Some research recommends the use of high doses of up to 1200 mg per day in order to overcome antibiotic resistance.( 19). Many studies have indicated its pharmacokinetics in humans and many types of animals(20,21,22,23).

But research on its toxic kinetic is few. Therefore, the goal of the research was to measure the toxic kinetics of ciprofloxacin.

The results of the research showed that the median lethal dose  $DL_{50}$  when injected into the intraperitoneal after it was measured by up-and-down method.it was 1280,5 mg/kg of body weight, It is close to the dose set by Mahammad 2003 (24).

The treated mice showed lack of movement, piloerection, Straub tail, shivering, ataxia in walking, lacramination ,respiratory disturbance and flat body appearance , These are neurological signs as a result of ciprofloxacin crossing the blood-brain barrier due to its low partial weight, solubility in fats, and its low binding to plasma proteins (8, 25).The appearance of these symptoms is due to a decrease in the activity of AchE, whose activity also decreases in the case of using

other antibiotics such as metronidazole. AchE has a role in neurotransmission (26,27). Other causes of these symptoms are the inhibition of the neurotransmitter GABA and the decrease of K + Atpase + Na that regulates sodium and potassium ions across the cell membrane, moreover, the oxidative stress that occurs due to ciprofloxacin even at low doses (200 and 150 mg/kg). It has an effect on neurons and their antioxidant system (26,28,29,30). The highest concentration of ciprofloxacin in plasma was 0.88  $\mu\text{g}/\text{ml}$  within 15 minutes of injection. Then the concentration decreases to 0.15  $\mu\text{g}/\text{ml}$  within 30 minutes of injection. Due to the diffusion of ciprofloxacin in peripheral tissues. (31) After 45 minutes of injection, the concentration of ciprofloxacin in the plasma increased to 0.76  $\mu\text{g}/\text{ml}$ ., [MF1] This may be due to the oxidative stress caused by ciprofloxacin and its imbalance with the antioxidant system leads to severe tissue damage and the change in the permeability of cell membranes will cause a portion of ciprofloxacin to be released into the blood again (28).

The steady-state volume of distribution for ciprofloxacin in high-dose rats was 2551.18(  $\text{mg}/(\mu\text{g}/\text{mL})$ ), which is widely distributed and rapidly excreted, with an elimination half-life of 1.52 hours. The area under plasma concentration time was 0.69  $\mu\text{g}/\text{mL}^*\text{h}$ , while the total clearance was very high 1162.26(  $\text{mg}/(\mu\text{g}/\text{mL}) /\text{h}$ ). In addition, the average residence time was 1.31 hours. These parameters are useful in selecting dose levels for short- and long-term toxicological and carcinogenic studies (32).

## References

1. Sharma, D., Patel, R. P., Zaidi, S. T. R., Sarker, M., Rahman, M., Lean, Q. Y., & Ming, L. C. (2017). Interplay of the quality of ciprofloxacin and antibiotic resistance in developing countries. *Frontiers in pharmacology*, 8, 546.
2. Papich, M. G. (2020). *Papich Handbook of Veterinary Drugs-E-Book*. Elsevier Health Sciences.2-
3. Thai, T., Salisbury, B. H., & Zito, P. M. (2020). Ciprofloxacin. In *StatPearls [Internet]*. StatPearls Publishing.
4. Singh, A., Kurkure, S., & Anardi, S. (2020). FORMULATION AND EVALUATION OF IN-SITU GELLING SYSTEM FOR SUSTAINED RELEASE OPHTHALMIC DRUG DELIVERY OF CIPROFLOXACIN.
5. Dey, B., Katakam, P., Assaleh, F. H., Chandu, B. R., Adiki, S. K., & Mitra, A. (2015). In vitro–in vivo studies of the quantitative effect of calcium, multivitamins and milk on single dose ciprofloxacin bioavailability. *Journal of pharmaceutical analysis*, 5(6), 389-395.
6. Rosenthal, L., & Burchum, J. (2020). *Lehne's Pharmacotherapeutics for Advanced Practice Nurses and Physician Assistants-E-Book*. Elsevier Health Sciences.
7. Sharma, D., Patel, R. P., Zaidi, S. T. R., Sarker, M., Rahman, M., Lean, Q. Y., & Ming, L. C. (2017). Interplay of the quality of ciprofloxacin and antibiotic resistance in developing countries. *Frontiers in pharmacology*, 8, 546.
8. Ibrahim, O. M. S., & Shakir, A. F. (2017). Pharmacokinetic Interactions Between Intravenous Ciprofloxacin and Oral Ferrous Sulfate. *Adv. Anim. Vet. Sci*, 5(2), 70-77.
9. Alabdaly, Y. Z. (2021). Effect of diclofenac on the pharmacokinetics of ciprofloxacin in quail. *Iraqi Journal of Veterinary Sciences*, 35(4), 777-781.
- 10.10- Schlender, J. F., Teutonico, D., Coboeken, K., Schnizler, K., Eissing, T., Willmann, S., ... & Stass, H. (2018). A physiologically-based pharmacokinetic model to describe ciprofloxacin pharmacokinetics over the entire span of life. *Clinical pharmacokinetics*, 57(12), 1613-1634.
- 11.Thai, T., Salisbury, B. H., & Zito, P. M. (2020). Ciprofloxacin. In *StatPearls [Internet]*. StatPearls Publishing.
- 12.Rossi, G., & Mazoki, K. (2018). Acute psychosis after treatment of epididymitis with ciprofloxacin. *Cureus*, 10(5).
- 13.Day, T., & Read, A. F. (2016). Does high-dose antimicrobial chemotherapy prevent the evolution of resistance?. *PLoS computational biology*, 12(1), e1004689.
- 14.Dixon ,W . J.( 1980) Efficient analysis of experimental observations .Ann Rev Pharmacol. Toxicol., 20, 441-462..
- 15.Joslin, J. O. (2009). Blood collection techniques in exotic small mammals. *Journal of Exotic Pet Medicine*, 18(2), 117-139.
- 16.Alswayeh, R., Hussein, R. F., Alvi, S. N., & Hammami, M. M. (2016). Rapid determination of ciprofloxacin concentration in human plasma by high performance liquid chromatography. *WJPPS*, 5(3), 1765-1774.
- 17.Zhang, Y., Huo, M., Zhou, J., & Xie, S. (2010). PKSolver: An add-in program for pharmacokinetic and pharmacodynamic data analysis in Microsoft Excel. *Computer methods and programs in biomedicine*, 99(3), 306-314.

18. Siroka, Z., & Svobodova, Z. (2013). The toxicity and adverse effects of selected drugs in animals—overview. *Polish Journal of Veterinary Sciences*.
19. van Zanten, A. R., Polderman, K. H., van Geijlswijk, I. M., van der Meer, G. Y., Schouten, M. A., & Girbes, A. R. (2008). Ciprofloxacin pharmacokinetics in critically ill patients: a prospective cohort study. *Journal of critical care*, 23(3), 422-430.
20. Šíma, M., Michaličková, D., Ryšánek, P., Cihlářová, P., Kuchař, M., Lžičařová, D., ... & Slanař, O. (2021). No Time Dependence of Ciprofloxacin Pharmacokinetics in Critically Ill Adults: Comparison of Individual and Population Analyses. *Pharmaceutics*, 13(8), 1156.
21. Nouws, J. F. M., Mevius, D. J., Vree, T. B., Baars, A. M., & Laurensen, J. (1988). Pharmacokinetics, renal clearance and metabolism of ciprofloxacin following intravenous and oral administration to calves and pigs. *Veterinary Quarterly*, 10(3), 156-163.
22. Islam, M. S., Sikder, M. M. H., Awal, M. A., Mostofa, M., & Trisha, A. A. (2008). Plasma pharmacokinetics of ciprofloxacin in sheep. *Bangladesh Journal of Veterinary Medicine*, 6(1), 93-97.
23. Papich, M. G. (2017). Ciprofloxacin pharmacokinetics in clinical canine patients. *Journal of veterinary internal medicine*, 31(5), 1508-1513.
24. Mohammad, F .K. , Abachi , F. T., & AL-Baggou, B. Kh .(2003). Toxicity and neurobehavioral effect of ciprofloxacin in mice. *Iraqi Journal of Pharmacy* ,3,1-5.
25. Rageh, A. H., Atia, N. N., & Abdel-Rahman, H. M. (2018). Application of salting-out thin layer chromatography in computational prediction of minimum inhibitory concentration and blood-brain barrier penetration of some selected fluoroquinolones. *Journal of Pharmaceutical and Biomedical Analysis*, 159, 363-373.
26. Abdullah, A. T., & Ahmed, M. A. (2021). Ameliorative role of Arabic gum against nephrotoxicity induced by ciprofloxacin in rats. *Iraqi Journal of Veterinary Sciences*, 35(4), 789-798.
27. Alsanjary, D. H., & Amin, S. M. (2021). Acute toxicity of metronidazole and its interaction with chlorpyrifos in chicks. *Iraqi Journal of Veterinary Sciences*, 35, 13-18.
28. Nazef, C., & Arif, A. (2019). Ciprofloxacin-Induced Acute Psychosis: A Case Report. *American Journal of Medical Case Reports*, 7(7), 143-144.
29. Dogan, Z., Elbe, H., Taslidere, E. L. İ. F., Soysal, H., Cetin, A. Y. M. E. L. E. K., & Demirtas, S. (2017). Effects of ciprofloxacin on fetal rat liver during pregnancy and protective effects of quercetin. *Biotechnic & Histochemistry*, 92(7), 481-486.
30. Dawood, K. F. (2020). In vivo effects of different doses of ciprofloxacin on glutathione reductase activity in some rat tissues. *EurAsian Journal of BioSciences*, 14(2), 3019-3023.



31. Igbayilola, Y. D., Saka, W. A., Aina, S. O., Mofolorunso, A. M., Oyabambi, A. O., & Morakinyo, A. O. (2020). Adverse effect of graded Ciprofloxacin oral intake in male Sprague-Dawley rats. *Journal of African Association of Physiological Sciences*, 8(1), 62-70.
32. Fadeel, B., Pietroiusti, A. and Shvedova, A. (2017). Adverse effect of engineered nanomaterial exposure, toxicology, and impact on human health. Academic Press

**( 1 ) Appendix**( Dixon, 1980) median lethal dose table (LD<sub>50</sub>)

The second part of the series	K represents the series of tests that begin as follows					Standard error (LD50)
	O	OO	OOO	OOOO		
XOOO	157 -,0	154 -,0	154 -,0	154 -,0	OXXX	σ 0.61
XOOX	878 -,0	861 -,0	860-,0	860 -,0	OXXO	
XOXO	701,0	737,0	741,0	741,0	OXOX	
XOXX	084,0	169,0	181,0	182,0	OXOO	
XXOO	305,0	372,0	380,0	381,0	OOXX	
XXOX	305 -,0	169 -,0	144 -,0	142 -,0	OOXO	
XXXO	288,1	500,1	544,1	549,1	OOOX	
XXXX	555,0	897,0	985,0	000,1	OOOO	
	X	XX	XXX	XXXX		
	K - represents the series of tests that begin as follows					

$$LD_{50} = Xf + Kd$$

Whereas:

LD<sub>50</sub>: median lethal dose (LD 50)

Xf: the last dose used in the experiment

K: table value

D: the amount of constant increase and decrease in the given dose and that:

X: The animal dies within 24 hours of administration

O: Animal survival 24 hours after administration

**DIFFERENTIAL SUBORDINATIONS FOR MULTIVALENT FUNCTIONS  
ASSOCIATED WITH GENERALIZED FRACTIONAL DIFFERENTIAL OPERATOR**

**ZAINAB H. MAHMOOD**

**ASEEL A. HASSAN**

**DUNIA K. MAHDI**

**DIFFERENTIAL SUBORDINATIONS FOR MULTIVALENT FUNCTIONS  
ASSOCIATED WITH GENERALIZED FRACTIONAL DIFFERENTIAL OPERATOR**

**Zainab H.MAHMOOD<sup>1</sup>**

**Aseel A.HASSAN<sup>2</sup>**

**Dunia K.MAHDI<sup>3</sup>**

**Abstract:**

In this paper, we derive some subordination results for certain subclasses of  $p$ -valent analytic functions defined by generalized fractional differintegral operator using the principle of differential subordination, producing the best dominant univalent solutions. We have also derived inclusion relations and solved majorization problem.

**Key words:** Analytic Function, Univalent Function, Multivalent Function, Differential Subordination, Linear Operator.



<http://dx.doi.org/10.47832/MinarCongress5-12>

<sup>1</sup>  University of Baghdad, Iraq, [zainab\\_hd@yahoo.com](mailto:zainab_hd@yahoo.com), <https://orcid.org/0000-0001-9731-6340>

<sup>2</sup>  University of Baghdad, Iraq, [aselamer16@gmail.com](mailto:aselamer16@gmail.com), <https://orcid.org/0000-0002-9550-162X>

<sup>3</sup>  University of Baghdad, Iraq, [duniaphysics95@yahoo.com](mailto:duniaphysics95@yahoo.com), <https://orcid.org/0000-0002-2705-3327>

**Introduction:**

Let  $\Delta = \{z \in \mathbb{C} : z < 1\}$  be the open unit disk in the complex plane  $\mathbb{C}$  and let  $\mu = \mu(\Delta)$  denote the class of analytic functions defined in  $\Delta$ , for  $n$  positive integer and  $a \in \mathbb{C}$ . Let  $\mu[a, n] = \{f \in \mu : f(\omega) = a + a_n \omega^n + a_{n+1} \omega^{n+1} + \dots\}$ , with  $\mu_0 = \mu[0, 1]$ ,  $\mu = \mu[1, 1]$ .

Let  $f$  and  $g$  be members of  $\mu$ . The function  $f$  is said to be subordinate to  $g$ , written  $f < g$  or  $f(\omega) < g(\omega)$ , if there exists a Schwarz function  $w(\omega)$  analytic in  $\Delta$ , with  $w(0) = 0$  and  $|w(\omega)| < 1$  such that  $f(\omega) = g(w(\omega))$ ,  $(\omega \in \Delta)$ . In particular, if the function  $g$  is univalent in  $\Delta$ , then  $f < g$  if and only if  $f(0) = g(0)$  and  $f(\Delta) \subset g(\Delta)$ .

Let  $\psi : \mathbb{C}^3 \times \Delta \rightarrow \mathbb{C}$  and let  $h$  be univalent in  $\Delta$ . If  $f$  is analytic in  $\Delta$  and satisfies the (second-order) differential subordination

$$\psi(f(\omega), \omega f'(\omega), \omega^2 f''(\omega); \omega) < h(\omega), \tag{1.1}$$

then  $f$  is called a solution of the differential subordination. The univalent function  $q$  is called a dominant of the solutions of the differential subordination, or more simply dominant if  $f < q$  for all  $f$  satisfying (1.1). A dominant  $\hat{q}$  that satisfies  $\hat{q} < q$  for all dominants  $q$  of (1.1) is said to be the best dominant of (1.1).

Let  $\mathcal{D}_p$  denote the classes of function of the form :

$$f(\omega) = \omega^p + \sum_{n=1}^{\infty} a_{n+p} \omega^{n+p} \quad (\omega \in \Delta, p \in \mathbb{N} = \{1, 2, 3, \dots\}), \tag{1.2}$$

which are analytic and  $p$ -valent in  $\Delta$ .

**Definition 1.1:** The fractional integral of order  $\lambda (\lambda > 0)$  is defined, for a function  $f(\omega)$ , analytic in a simply-connected region of the complex plane containing the origin by

$$\mathcal{D}_\omega^{-\lambda} f(\omega) = \frac{1}{\Gamma(\lambda)} \int_0^\omega \frac{f(\zeta)}{(\omega - \zeta)^{1-\lambda}} d\zeta, \tag{1.3}$$

where the multiplicity of  $(\omega - \zeta)^{1-\lambda}$  is removed by requiring  $\log(\omega - \zeta)$  to be real when  $\omega - \zeta > 0$ .

**Definition 1.2 :** Under the hypothesis of Definition 1.1 the fractional derivative of  $f(\omega)$  of order  $\lambda (\lambda \geq 0)$  is defined by

$$\mathcal{D}_\omega^\lambda f(\omega) = \left\{ \begin{array}{l} \frac{1}{\Gamma(1-\lambda)} \frac{d}{d\omega} \int_0^\omega \frac{f(\zeta)}{(\omega - \zeta)^{1-\lambda}} d\zeta \quad (0 \leq \lambda < 1), \\ \frac{d^n}{d\omega^n} \mathcal{D}_\omega^{\lambda-n} f(\omega) \quad (n \leq \lambda < n+1; n \in \mathbb{N}_0 = \mathbb{N} \cup \{0\}). \end{array} \right\} \tag{1.4}$$

where the multiplicity of  $(\omega - \zeta)^{-\lambda}$  is removed as in Definition 1.1.

**Definition 1.3.** [2] The generalized Bernardi-Libera-Livingston integral operator  $\mathcal{F}_{\beta,p} : \mathcal{D}_p \rightarrow \mathcal{D}_p$  is defined by

$$\mathcal{F}_{\beta,p}(f)(\omega) = \frac{\beta + p}{\omega^\beta} \int_0^\omega t^{\beta-1} f(t) dt$$

$$\begin{aligned}
 &= \left( \omega^p + \sum_{\kappa=1}^{\infty} \frac{\beta+p}{\beta+p+\kappa} \omega^{p+\kappa} \right) * f(\omega) \\
 &= \omega^p {}_2F_1(1, \beta+p; \beta+p+1; \omega) \quad (\beta > -p; \omega \in \Delta). \tag{1.5}
 \end{aligned}$$

Now we define the extended fractional differintegral operator [4].

**Definition 1.4** . The extended fractional differintegral operator  $\Omega_{\omega}^{(\lambda,p)} : \mathcal{D}_p \rightarrow \mathcal{D}_p$  for a function  $f(\omega)$  of the form (1.2) and for a real number  $\lambda$  ( $-\infty < \lambda < p+1$ ) is given by

$$\Omega_{\omega}^{(\lambda,p)} f(\omega) = \frac{\Gamma(p+1-\lambda)}{\Gamma(p+1)} \omega^{\lambda} \mathcal{D}_{\omega}^{\lambda} f(\omega) \quad (-\infty < \lambda < p+1; z \in \Delta), \tag{1.6}$$

Where  $\mathcal{D}_{\omega}^{\lambda} f(\omega)$  is , respectively, the fractional integral of  $f(\omega)$  of order  $-\lambda$  when  $-\infty < \lambda < 0$  and the fractional derivative of  $f(\omega)$  of order  $\lambda$  when  $0 \leq \lambda < p+1$ .

We note that

$$\begin{aligned}
 \Omega_{\omega}^{(\lambda,p)} f(\omega) &= \omega^p + \sum_{n=1}^{\infty} \frac{\Gamma(n+p+1)\Gamma(p+1-\lambda)}{\Gamma(p+1)\Gamma(n+p+1-\lambda)} \alpha_{p+n} z^{p+n} \\
 &= \omega^p {}_2F_2(1, p+1; p+1-\lambda; \omega) * f(\omega) \quad (-\infty < \lambda < p+1; \omega \in \Delta). \tag{1.7}
 \end{aligned}$$

In particular ,

$$\Omega_{\omega}^{(0,p)} f(\omega) = f(\omega), \quad \Omega_{\omega}^{(1,p)} f(\omega) = \frac{\omega f'(\omega)}{p}, \quad \Omega_{\omega}^{(-1,p)} f(\omega) = \frac{p+1}{\omega} \int_0^{\omega} f(\zeta) d\zeta.$$

For integral values of  $\lambda$  , (1.6) further simplifies to

$$\Omega_{\omega}^{(\kappa,p)} f(\omega) = \frac{(p-\kappa)! \omega^{\kappa} f^{(\kappa)}(\omega)}{p!} \omega^{\lambda} \mathcal{D}_{\omega}^{\lambda} f(\omega) \quad (\kappa \in \mathbb{N}; \kappa < p+1)$$

and

$$\Omega_{\omega}^{(-m,p)} f(\omega) = \frac{p+m}{\omega^m} \int_0^{\omega} t^{m-1} \Omega_{\omega}^{(-m+1,p)} f(\omega) d\omega \quad (m \in \mathbb{N})$$

$$\begin{aligned}
 &\mathcal{F}_{1,p} \circ \mathcal{F}_{2,p} \circ \dots \circ \mathcal{F}_{m,p}(f)(\omega) \\
 &= \mathcal{F}_{1,p} \left( \frac{\omega^p}{1-z} \right) * \mathcal{F}_{2,p} \left( \frac{\omega^p}{1-z} \right) * \dots * \mathcal{F}_{m,p} \left( \frac{\omega^p}{1-z} \right) * f(\omega),
 \end{aligned}$$

where  $\mathcal{F}_{m,p}$  is the familiar integral operator defined by (1.5) and  $\circ$  stands for the usual composition of functions.

**Definition 1.5.**[2] For real numbers  $\lambda > 0, \mu$  and  $\eta$ , Saigo hypergeometric fractional integral operator  $I_{0,z}^{\lambda,\mu,\eta}$  is defined by

$$I_{0,\omega}^{\lambda,\mu,\eta} f(\omega) = \frac{\omega^{-\lambda-\mu}}{\Gamma(\lambda)} \int_0^{\omega} (\omega-t)^{\lambda-1} {}_2F_1 \left( \lambda+\mu-\eta; \lambda; 1-\frac{t}{\omega} \right) f(t) dt,$$

where the function  $f(\omega)$  is analytic in a simply-connected region of the complex  $\omega -$  plane containing the origin, with the order

$$f(\omega) = O(|\omega|^{\varepsilon}) \quad (\omega \rightarrow 0; \varepsilon > \max\{0, \mu-\eta\} - 1),$$

and the multiplicity of  $(\omega - t)^{\lambda-1}$  is removed by requiring  $\log(\omega - t)$  to be real when  $(\omega - t) > 0$ .

**Definition 1.6.** Under the hypotheses of Definition 1.5, the Saigo hypergeometric fractional derivative operator  $\mathfrak{S}_{0,\omega}^{\lambda,\mu,\eta}$  is defined by

$$\mathfrak{S}_{0,\omega}^{\lambda,\mu,\eta} f(\omega) = \begin{cases} \frac{1}{\Gamma(1-\lambda)} \frac{d}{d\omega} \left\{ \omega^{\lambda-\mu} \int_0^\omega (\omega-t)^{-\lambda} {}_2F_1\left(\mu-\lambda, 1-\eta; 1-\lambda; 1-\frac{t}{\omega}\right) f(t) dt \right\} & (0 \leq \lambda < 1); \\ \frac{d^n}{d\omega^n} \mathfrak{S}_{0,\omega}^{\lambda,\mu,\eta} f(\omega) & (n \leq \lambda < n+1; n \in \mathbb{N}) \end{cases}$$

where the multiplicity of  $(\omega - t)^{-\lambda}$  is removed as in Definition 1.5. It may be remarked that

$$I_{0,\omega}^{\lambda-\lambda,\eta} f(\omega) = \mathcal{D}_\omega^{-\lambda} f(\omega) \quad (\lambda > 0) \text{ and } \mathfrak{S}_{0,\omega}^{\lambda,\lambda,\eta} f(\omega) = \mathcal{D}_\omega^\lambda f(\omega) \quad (0 \leq \lambda < 1);$$

where  $\mathcal{D}_\omega^{-\lambda}$  denotes fractional integral operator and  $\mathcal{D}_\omega^\lambda$  denotes fractional derivative operator considered by Owa [6].

Recently Goyal and Prajapat [9] introduced a family of generalized fractional differintegral operators  $\mathcal{S}_{0,\omega}^{\lambda,\mu,\eta}: \mathcal{D}\rho \rightarrow \mathcal{D}\rho$ , by

$$\mathcal{S}_{0,\omega}^{\lambda,\mu,\eta} f(\omega) = \begin{cases} \frac{\Gamma(1+p-\mu)\Gamma(1+p+\eta-\lambda)}{\Gamma(1+p)\Gamma(1+p+\eta-\mu)} \omega^\mu \mathfrak{S}_{0,\omega}^{\lambda,\mu,\eta} f(\omega) & (0 \leq \lambda < \eta + p + 1, \omega \in \Delta); \\ \frac{\Gamma(1+p-\mu)\Gamma(1+p+\eta-\lambda)}{\Gamma(1+p)\Gamma(1+p+\eta-\mu)} \omega^\mu I_{0,\omega}^{-\lambda,\mu,\eta} f(\omega) & (-\infty \leq \lambda < 0, \omega \in \Delta). \end{cases}; (1.8)$$

It is easily seen from (1.8) that for a function  $f(\omega) \in \mathcal{D}\rho$  given by (1.2), we have

$$\begin{aligned} \mathcal{S}_{0,\omega}^{\lambda,\mu,\eta} f(\omega) &= \omega^p + \sum_{n=1}^{\infty} \frac{(1+p)_n (1+p+\eta-\mu)_n}{(1+p-\mu)_n (1+p+\eta-\lambda)_n} a_{p+n} \omega^{p+n} \\ &= \omega^p {}_3F_2(1, 1+p, 1+p+\eta-\mu; 1+p-\mu, 1+p+\eta-\lambda; \omega) * f(\omega) \\ & \quad (\omega \in \Delta; p \in \mathbb{R}; \mu, \eta \in \mathbb{R}; \mu < p+1; -\infty < \lambda < \eta+p+1). \end{aligned} \tag{1.9}$$

Note that

$$\mathcal{S}_{0,\omega}^{0,0,\eta} f(\omega) = f(\omega),$$

$$\mathcal{S}_{0,\omega}^{1,1,1} f(\omega) = \mathcal{S}_{0,\omega}^{1,0,0} f(\omega) = \frac{\omega f'(\omega)}{p}$$

and

$$\mathcal{S}_{0,\omega}^{2,1,1} f(\omega) = \frac{\omega f'(\omega) + \omega^2 f''(\omega)}{p} \tag{1.10}$$

We also note that

$$\mathcal{S}_{0,\omega}^{\lambda,\lambda,\eta} f(\omega) = \mathcal{S}_{0,\omega}^{\lambda,\mu,0} f(\omega) = \Omega_\omega^{(\lambda,p)} f(\omega), \tag{1.11}$$

where  $\Omega_{\omega}^{(\lambda, p)}$  is an extended fractional differintegral operator studied very recently in

[4]. On the one hand, if we set

$$\lambda = -\alpha, \mu = 0, \eta = \beta - 1,$$

in (1.8) and using

$$I_{0, \omega}^{\alpha, 0, \beta-1} f(\omega) = \frac{1}{\omega^{\beta} \Gamma(\alpha)} \int_0^{\omega} t^{\beta-1} \left(1 - \frac{t}{\omega}\right)^{\alpha-1} f(t) dt,$$

we obtain following  $p$ -valent generalization of multiplier transformation operator

[3, 10, 5].

$$\begin{aligned} \mathcal{Q}_{\beta, p}^{\alpha} f(\omega) &= \binom{p + \alpha + \beta - 1}{p + \beta - 1} \frac{\alpha}{\omega^{\beta}} \int_0^{\omega} t^{\beta-1} \left(1 - \frac{t}{\omega}\right)^{\alpha-1} f(t) dt, \\ &= \omega^p + \sum_{n=1}^{\infty} \frac{\Gamma(p + \beta + n) \Gamma(p + \alpha + \beta)}{\Gamma(p + \alpha + \beta + n) \Gamma(p + \beta)} a_{p+n} \omega^{p+n} \\ &(\beta > -p; \alpha + \beta > -p). \end{aligned} \tag{1.12}$$

On the other hand, if we set

$$\lambda = -1, \mu = 0, \text{ and } \eta = \beta - 1 \tag{1.13}$$

in (1.8), we obtain the generalized Bernardi-Libera-Livingston integral operator  $\mathcal{F}_{\beta, p}$

defined by

$$\begin{aligned} \mathcal{F}_{\beta, p}(f)(\omega) &= \frac{\beta + p}{\omega^m} \int_0^{\omega} t^{\beta-1} f(t) dt \\ &= \left( \omega^p + \sum_{\kappa=1}^{\infty} \frac{(p + \beta)}{(p + \beta + \kappa)} \omega^{p+\kappa} \right) * f(\omega) \\ &= \omega^p {}_3F_1(1, \beta + p, \beta + p + 1; \omega) \quad (\beta > -p; \omega \in \Delta). \end{aligned} \tag{1.14}$$

For the choice  $p = 1$ , where  $\beta \in \mathbb{N}$ , the operator  $\mathcal{F}_{\beta, p}$  reduces to the well-known Bernardi integral operator [8].

It is easily seen from (1.8) that

$$\omega \left( \mathcal{S}_{0, \omega}^{\lambda, \mu, \eta} f(\omega) \right)' = (p + \eta - \lambda) (\mathcal{S}_{0, \omega}^{\lambda+1, \mu, \eta} f(\omega) - (\eta - \lambda) (\mathcal{S}_{0, \omega}^{\lambda, \mu, \eta} f(\omega))) \tag{1.15}$$

In order to prove our results, we need the following definitions and theorem.



**Definition 1.7.** [7] Denote by  $Q$  the set of all function  $q$  that are analytic and injective on  $\bar{\Delta} \setminus E(q)$ , where

$$E(q) = \{\xi \in \partial \Delta : \lim_{\omega \rightarrow \xi} q(\omega) = \infty\}, \tag{1.16}$$

are such that  $q'(\xi) \neq 0$  for  $\xi \in \partial \Delta \setminus E(q)$ . Further let the subclass for which  $q(0) = a$  be denoted by  $Q(a)$ ,  $Q(0) \equiv Q_0$  and  $Q(1) = Q_1$ .

**Definition 1.8.** [7] Let  $\Omega$  be a set in  $\mathbb{C}$ ;  $q \in Q$  and  $n$  be appositive integer. The class of admissible functions  $\psi[\Omega, q]$  consists of those functions  $\psi: \mathbb{C}^3 \times \Delta \rightarrow \mathbb{C}$  that satisfies the admissibility condition:

$$\psi(r, s, v; \omega, \xi) \in \Omega,$$

Whenever

$$r = q(\xi), s = k\xi q'(\xi), \text{ and}$$

$$\Re \left\{ \frac{t}{s} + 1 \right\} \geq k \Re \left\{ \frac{\xi q''(\xi)}{q'(\xi)} + 1 \right\}, \tag{1.17}$$

where  $\omega \in \Delta, \xi \in \partial \Delta \setminus E(q)$  and  $k \geq n$ . We write  $\psi_1[\Omega, q] = \psi[\Omega, q]$ .

when  $\omega \in \Delta, \xi \in \partial \Delta$  and  $b \geq n \geq 1$ . In particular, we write  $\psi_1'[\Omega, q] = \psi'[\Omega, q]$ .

**Theorem 1.1.** [7] Let  $\Psi \in \psi_n[\Omega, q]$ , with  $q(0) = a$ . if the analytic function  $F \in \mu[a, n]$  satisfies  $\Psi(g(\omega), \omega g'(\omega), \omega^2 g''(\omega); \omega) \in \Omega$ , then  $F(\omega) < q(\omega)$ .

**2.Main Results**

**Definition 2.1:** Let  $\Omega$  be a set in  $\mathbb{C}$  and  $q \in Q_0 \cap \mu[0, p]$  and  $\sigma > -p$ . The class of admissible functions  $\Phi_k[\Omega, q]$  consists of those functions  $\Phi: \mathbb{C}^3 \times \Delta \times \bar{\Delta} \rightarrow \mathbb{C}$  that satisfy the admissibility condition:

$$\Phi(u, v, w; \omega, \xi) \in \Omega, \tag{2.1}$$

whenever

$$u = q(\xi), v = \frac{k\xi q'(\xi) + (\eta - \lambda)q(\xi)}{(\eta - \lambda + p)}, (\sigma > -p),$$

and

$$\Re \left\{ \frac{(p + \eta - \lambda - 1)(p + \eta - \lambda)w + (p + \eta - \lambda)(\lambda - \eta + 1)v + (\lambda - \eta)^2 u}{(p + \eta - \lambda)v - (\eta - \lambda)u} \right\} \geq k \Re \left\{ \frac{\xi q''(\xi)}{q'(\xi)} + 1 \right\}, \tag{2.2}$$

$\omega \in \Delta, \zeta \in \partial \Delta \setminus E(q), \xi \in \bar{\Delta}$  and  $k \geq p$ .

**Theorem 2.1:** Let  $\Phi \in \Phi_k[\Omega, q]$ . If  $f \in \mathcal{D}_p$  satisfies

$$\left\{ \Phi(S_{0,\omega}^{\lambda,\mu,\eta} f(\omega), S_{0,\omega}^{\lambda+1,\mu,\eta} f(\omega), S_{0,\omega}^{\lambda+2,\mu,\eta} f(\omega); \omega \in \Delta, \xi \in \bar{\Delta}) \right\} \subset \Omega, \tag{2.3}$$

Then

$$S_{0,\omega}^{\lambda,\mu,\eta} f(\omega) < q(\omega).$$

**Proof:** We note from (1.15) that , we have

$$\omega \left( \mathcal{S}_{0,\omega}^{\lambda,\mu,\eta} f(\omega) \right)' = (p + \eta - \lambda) (\mathcal{S}_{0,\omega}^{\lambda+1,\mu,\eta} f(\omega) - (\eta - \lambda) (\mathcal{S}_{0,\omega}^{\lambda,\mu,\eta} f(\omega)))$$

Is equivalent

$$\mathcal{S}_{0,\omega}^{\lambda+1,\mu,\eta} f(\omega) = \frac{\omega (\mathcal{S}_{0,\omega}^{\lambda,\mu,\eta} f(\omega))' + (\eta - \lambda) \mathcal{S}_{0,\omega}^{\lambda,\mu,\eta} f(\omega)}{(p + \eta - \lambda)}. \quad (2.4)$$

Assume that  $F(\omega) = \mathcal{S}_{0,\omega}^{\lambda,\mu,\eta} f(\omega)$ . Then

$$\mathcal{S}_{0,\omega}^{\lambda+1,\mu,\eta} f(\omega) = \frac{\omega F'(\omega) + (\eta - \lambda) F(\omega)}{(p + \eta - \lambda)}.$$

Therefore,

$$\mathcal{S}_{0,\omega}^{\lambda+2,\mu,\eta} f(\omega) = \frac{\omega (\mathcal{S}_{0,\omega}^{\lambda+1,\mu,\eta} f(\omega))' + (\eta - \lambda - 1) \mathcal{S}_{0,\omega}^{\lambda+1,\mu,\eta} f(\omega)}{(p + \eta - \lambda - 1)} \quad (2.5)$$

then we have by ( 2.4),

$$\left( \mathcal{S}_{0,\omega}^{\lambda+1,\mu,\eta} f(\omega) \right)' = \frac{\omega F''(\omega) + (\eta - \lambda + 1) F'(\omega)}{(p + \eta - \lambda)}. \quad (2.6)$$

So,

$$\begin{aligned} \mathcal{S}_{0,\omega}^{\lambda+2,\mu,\eta} f(\omega) &= \frac{1}{(p + \eta - \lambda - 1)} \left[ \omega \left( \frac{\omega F''(\omega) + (1 + \eta - \lambda) F'(\omega)}{(p + \eta - \lambda)} \right) \right. \\ &\quad \left. + (\eta - \lambda - 1) \left( \frac{\omega F'(\omega) + (\eta - \lambda) F(\omega)}{(p + \eta - \lambda)} \right) \right] \\ &= \frac{1}{(p + \eta - \lambda - 1)} \left[ \frac{\omega^2 F''(\omega) + (1 + \eta - \lambda) \omega F'(\omega)}{(p + \eta - \lambda)} \right. \\ &\quad \left. + \frac{(\eta - \lambda - 1) \omega F'(\omega) + (\eta - \lambda - 1)(\eta - \lambda) F(\omega)}{(p + \eta - \lambda)} \right] \\ &= \frac{1}{(p + \eta - \lambda - 1)} \left[ \frac{\omega^2 F''(\omega) + 2(\eta - \lambda) \omega F'(\omega) + (\eta - \lambda)(\eta - \lambda - 1) F(\omega)}{(p + \eta - \lambda)} \right] \\ &= \frac{1}{(p + \eta - \lambda - 1)(p + \eta - \lambda)} (\omega^2 F''(\omega) + 2(\eta - \lambda) \omega F'(\omega) + (\eta - \lambda)(\eta - \lambda - 1) F(\omega)) \end{aligned} \quad (2.7)$$

$$\text{Let } u = r, v = \frac{\mathcal{S} + (\eta - \lambda)r}{(p + \eta - \lambda)}, w = \frac{t + 2(\eta - \lambda)\mathcal{S} + (\eta - \lambda)(\eta - \lambda - 1)r}{(p + \eta - \lambda - 1)(p + \eta - \lambda)}.$$

Assume that

$$\begin{aligned} \psi(r, \mathcal{S}, t; \omega, \xi) &= \mathcal{O}(u, v, w; \omega, \xi) \\ &= \mathcal{O} \left( r, \frac{\mathcal{S} + (\eta - \lambda)r}{(p + \eta - \lambda)}, \frac{t + 2(\eta - \lambda)\mathcal{S} + (\eta - \lambda)(\eta - \lambda - 1)r}{(p + \eta - \lambda - 1)(p + \eta - \lambda)}; \omega, \xi \right). \end{aligned} \quad (2.8)$$

By using (2.4 ) and (2.5) , we obtain

$$\begin{aligned} \psi(F(\omega), \omega F'(\omega), \omega^2 F''(\omega); \omega, \xi) \\ = \mathcal{O}(\mathcal{S}_{0,\omega}^{\lambda,\mu,\eta} f(\omega), \mathcal{S}_{0,\omega}^{\lambda+1,\mu,\eta} f(\omega) \mathcal{S}_{0,\omega}^{\lambda+2,\mu,\eta} f(\omega); \omega, \xi). \end{aligned} \quad (2.9)$$

Therefore, by making use of (2.3), we get

$$\Psi(F(\omega), \omega F'(\omega), \omega^2 F''(\omega); \omega, \xi) \in \Omega. \tag{2.10}$$

Also, by using

$$w = \frac{t + 2(\eta - \lambda)s + (\eta - \lambda)(\eta - \lambda - 1)r}{(p + \eta - \lambda - 1)(p + \eta - \lambda)},$$

and by simple calculations, we get

$$\frac{(p + \eta - \lambda - 1)(p + \eta - \lambda)w - (p + \eta - \lambda)(\lambda - \eta + 1)v + (\lambda - \eta)^2 u}{(p + \eta - \lambda)v - (\eta - \lambda)u} = \frac{t}{s} + 1. \tag{2.11}$$

and the admissibility condition for  $\varnothing \in \Phi_k[\Omega, q]$  is equivalent to the admissibility condition for  $\psi$  then,  $F(\omega) < q(\omega)$ . Hence, we get.

**Example 2.1.** Let the class of admissible function  $\Phi_{k\nu}[\Omega, q]$  consists of those functions  $\varnothing: \mathbb{C}^3 \times \Delta \rightarrow \mathbb{C}$  that satisfies the admissibility condition :

$$v = \frac{k\xi q'(\xi) + (\eta - \lambda)q(\xi)}{(\eta - \lambda + p)} \notin \Omega$$

$\omega \in \Delta, \zeta \in \partial\Delta \setminus E(q)$ , and  $m \geq p$ . If  $f \in \mathcal{D}_p$  satisfies  $S_{0,\omega}^{\lambda,\mu,\eta} f(\omega) \subset \Omega$ , then

$$S_{0,\omega}^{\lambda,\mu,\eta} f(\omega) < q(\omega)$$

We consider the special situation when  $\Omega \neq \mathbb{C}$  is a simply connected domain.

If we assume that  $\Omega \neq \mathbb{C}$  is a simply connected domain. So,  $\Omega = h(\Delta)$ , for some conformal mapping  $h$  of  $\Delta$  onto  $\Omega$ . Assume the class is written as  $\Phi_k[h, q]$ . Therefore, we conclude immediately the following Theorem.

**Theorem 2.2 :** Let  $\varnothing \in \Phi_k[h, q]$ . If  $f \in \mathcal{D}_p$  satisfies

$$\varnothing(S_{0,\omega}^{\lambda,\mu,\eta} f(\omega), S_{0,\omega}^{\lambda+1,\mu,\eta} f(\omega), S_{0,\omega}^{\lambda+2,\mu,\eta} f(\omega); \omega \in \Delta) \ll h(\omega), \tag{2.12}$$

Then

$$S_{0,\omega}^{\lambda,\mu,\eta} f(\omega) < q(\omega).$$

The next result is an extension of Theorem (2.1) to the case where the behavior of  $q$  on  $\Delta$  is not known.

**Corollary 2.1.** Let  $\Omega \subset \mathbb{C}$ ,  $q$  be univalent in  $\Delta$  and  $q(0)=0$ . Let  $\varnothing \in \Phi_k[\Omega, q_\rho]$  for some  $\rho \in (0,1)$ , where  $q_\rho(\omega) = q(\rho\omega)$ . If  $f \in \mathcal{D}_p$  satisfies

$$\varnothing(S_{0,\omega}^{\lambda,\mu,\eta} f(\omega), S_{0,\omega}^{\lambda+1,\mu,\eta} f(\omega), S_{0,\omega}^{\lambda+2,\mu,\eta} f(\omega); \omega \in \Delta) \in \Omega, \tag{2.13}$$

Then

$$S_{0,\omega}^{\lambda,\mu,\eta} f(\omega) < q(\omega).$$

**Proof.** From Theorem 2.1, we have  $S_{0,\omega}^{\lambda,\mu,\eta} f(\omega) < q_\rho(\omega)$  and the proof is complete.

**Theorem 2.1.** Let  $h$  and  $q$  be univalent in  $\Delta$ , with  $q(0)=0$  and set  $q_\rho(\omega) = q(\rho\omega)$  and  $h_\rho(\omega) = h(\rho\omega)$ . Let  $\emptyset: \mathbb{C}^3 \times \Delta \times \bar{\Delta} \rightarrow \mathbb{C}$  satisfy one of the following conditions:

- (1)  $\emptyset \in \Phi_k[\Omega, q_\rho]$  for some  $\rho \in (0,1)$  or
- (2) there exists  $\rho_0 \in (0,1)$  such that  $\emptyset \in \Phi_k[h_\rho, q_\rho]$  for all  $\rho \in (\rho_0, 1)$ .

If  $f \in \mathcal{D}_\rho$  satisfies (2.12), then

$$S_{0,\omega}^{\lambda,\mu,\eta} f(\omega) < q(\omega).$$

**Proof:Case (1):** By using Theorem (2.1), we get  $S_{0,\omega}^{\lambda,\mu,\eta} f(\omega) < q_\rho(\omega)$ . Since  $q_\rho(\omega) < q(\omega)$ , we deduce

$$S_{0,\omega}^{\lambda,\mu,\eta} f(\omega) < q(\omega).$$

**Case (2):** Assume that  $F(\omega) = S_{0,\omega}^{\lambda,\mu,\eta} f(\omega)$  and  $F_\rho(\omega) = F(\rho\omega)$ . So,

$$\emptyset(F_\rho(\omega), \omega F'_\rho(\omega), \omega^2 F''_\rho(\omega); \rho\omega) = \emptyset(F(\rho\omega), \rho\omega F'(\rho\omega), \rho^2 \omega^2 F''(\rho\omega); \rho\omega) \in h_\rho(\Delta).$$

By using Theorem 2.1 with associated

$$\emptyset(F(\omega), \omega F'(\omega), \omega^2 F''(\omega); w(\omega)) \in \Omega, \text{ where } w \text{ is any function mapping from}$$

$\Delta$  onto  $\Delta$ , with  $w(\omega) = \rho\omega$ , we obtain  $F_\rho(\omega) < q_\rho(\omega)$  for  $\rho \in (\rho_0, 1)$ . By letting  $\rho \rightarrow 1^-$ , we get  $F(\omega) < q(\omega)$ .

Therefore

$$S_{0,\omega}^{\lambda,\mu,\eta} f(\omega) < q(\omega)$$

The next theorem gives the best dominant of the differential subordination (2.12).

**Theorem 2.4.** Let  $h$  be univalent in  $\Delta$  and let  $\emptyset: \mathbb{C}^3 \times \Delta \times \bar{\Delta} \rightarrow \mathbb{C}$ . Suppose that the differential equation

$$\emptyset \left( q(\omega), \frac{\omega q'(\omega) + (\eta - \lambda)q(\omega)}{(p + \eta - \lambda)}, \frac{\omega^2 q''(\omega) + 2(\eta - \lambda)\omega q'(\omega) + (\eta - \lambda)(\eta - \lambda - 1)q(\omega)}{(p + \eta - \lambda)(p + \eta - \lambda - 1)}; \omega, \zeta \right) = h(\omega), \quad (2.14)$$

has a solution  $q$  with  $q(0)=0$  and satisfies one of the following conditions:

- (1)  $q \in Q_0$  and  $\emptyset \in \Phi_k[h, q]$ .
- (2)  $q$  is univalent in  $\Delta$  and  $\emptyset \in \Phi_k[h, q_\rho]$  for some  $\rho \in (0,1)$ , or
- (3)  $q$  is univalent in  $\Delta$  and there exists  $\rho_0 \in (0,1)$  such that  $\emptyset \in \Phi_k[h_\rho, q_\rho]$ ,

for all  $\rho_0 \in (0,1)$ . If  $f \in \mathcal{D}_\rho$  satisfies (2.12), then  $S_{0,\omega}^{\lambda,\mu,\eta} f(\omega) < q(\omega)$  and  $q$  is the best dominant.

**Proof.** By using Theorem 2.2 and Theorem 2.3, we get that  $q$  is a dominant of (2.12). Since  $q$  satisfies (2.14), it is also a solution of (2.12) and therefore  $q$  will be dominant by all dominants of (2.12). Hence  $q$  is the best dominant of (2.12).

**Definition 2.2.** Let  $\Omega$  be a set in  $\mathbb{C}$  and  $M > 0$ . The class of admissible functions  $\Phi_k[\Omega, q]$  consists of those functions  $\emptyset: \mathbb{C}^3 \times \Delta \times \bar{\Delta} \rightarrow \mathbb{C}$  such that

$$\emptyset \left( Me^{i\theta}, \frac{(k + \eta - \lambda)Me^{i\theta}}{(p + \eta - \lambda)}, \frac{L + [2(\eta - \lambda)k + (\eta - \lambda)(\eta - \lambda - 1)]Me^{i\theta}}{(p + \eta - \lambda - 1)(p + \eta - \lambda)}; \omega \right) \notin \Omega, \quad (2.15)$$

Where  $\lambda > 0, \theta \in R, R(Le^{i\theta}) \geq k(k - 1)M$  for all real  $\theta, k \geq 1, \omega \in \Delta$ .

**Corollary 2.2:** Let  $\emptyset \in \Phi_k[\Omega, M]$ . If  $f \in \mathcal{D}_p$  satisfies that

$$\emptyset(S_{0,\omega}^{\lambda,\mu,\eta} f(\omega), S_{0,\omega}^{\lambda+1,\mu,\eta} f(\omega), S_{0,\omega}^{\lambda+2,\mu,\eta} f(\omega); \omega, \zeta) \in \Omega, \text{ then } S_{0,\omega}^{\lambda,\mu,\eta} f(\omega) < M\omega.$$

**Corollary 2.3:** Let  $\emptyset \in \Phi_k[\Omega, M]$ . If  $f \in \mathcal{D}_p$  satisfies that

$$|\emptyset(S_{0,\omega}^{\lambda,\mu,\eta} f(\omega), S_{0,\omega}^{\lambda+1,\mu,\eta} f(\omega), S_{0,\omega}^{\lambda+2,\mu,\eta} f(\omega); \omega, \zeta)| < M, \text{ then } |S_{0,\omega}^{\lambda,\mu,\eta} f(\omega)| < M$$

**Corollary 2.4:** Let  $M > 0$ , and Let  $C(\xi)$  be an analytic function in  $\bar{\Delta}$  with  $\Re\{C(\xi)\} \geq 0$  for  $\xi \in \partial \Delta$ . If  $f \in \mathcal{D}_p$  satisfies

$$(p + \eta - \lambda - 1)(p + \eta - \lambda)S_{0,\omega}^{\lambda+2,\mu,\eta} f(\omega) - (p + \eta - \lambda)S_{0,\omega}^{\lambda+1,\mu,\eta} f(\omega) - \lambda^2 S_{0,\omega}^{\lambda,\mu,\eta} f(\omega) + C(\xi) < \lambda M,$$

$$\text{then } |S_{0,\omega}^{\lambda+1,\mu,\eta} f(\omega)| < M.$$

**Proof:** From Corollary (2.2) by taking  $\emptyset(u, v, w, \omega, \xi) = (p + \eta - \lambda - 1)(p + \eta - \lambda)w - (p + \eta - \lambda)v - \lambda^2 u + C(\xi)$  and  $\Omega = h(\Delta)$ , where  $h(\omega) = \lambda M \omega$ . By using Corollary (2.2), we need to show that

$\emptyset \in \Phi_k[\Omega, M]$ , that is, the admissible condition (2.15) is satisfied. We get

$$\begin{aligned} & \left| \emptyset \left( Me^{i\theta}, \frac{(k + \eta - \lambda)Me^{i\theta}}{(p + \eta - \lambda)}, \frac{L + [2(\eta - \lambda)k + (\eta - \lambda)(\eta - \lambda - 1)]Me^{i\theta}}{(p + \eta - \lambda - 1)(p + \eta - \lambda)}; \omega, \xi \right) \right| \\ &= |L + [2(\eta - \lambda)k + (\eta - \lambda)(\eta - \lambda - 1)]Me^{i\theta} - (k + \eta - \lambda)Me^{i\theta} - \lambda^2 Me^{i\theta} + C(\xi)| \\ &= |L + (2\eta - 2\lambda - 1)kMe^{i\theta} + \eta(\eta - 2) - \lambda(2\eta + 1) + C(\xi)| \\ &\geq (2\eta - 2\lambda - 1)kM + \Re \{ Le^{-i\theta} + \Re \{ C(\xi)e^{-i\theta} \} \} \\ &\geq \lambda M. \text{ Hence by Corollary (2.3), we get the result.} \end{aligned}$$

**Definition 9:** Let  $\Omega$  be a set in  $\mathbb{C}$  and  $q \in \mu[0, p]$  with  $q'(\omega) \neq 0$ . The class of admissible functions  $\Phi'_k[\Omega, q]$  consists of those functions  $\emptyset: \mathbb{C}^3 \times \bar{\Delta} \times \Delta \rightarrow \mathbb{C}$  that satisfies the admissibility condition:

$$\emptyset(u, v, w, \omega, \xi) \in \Omega, \quad (2.16)$$

whenever

$$u = q(\omega), v = \frac{1}{m} \omega q'(\omega) + (\eta - \lambda)q(\omega), (\sigma > -p),$$

and

$$\Re \left\{ \frac{(p + \eta - \lambda - 1)(p + \eta - \lambda)w - (p + \eta - \lambda)(\lambda - \eta + 1)v + (\lambda - \eta)^2 u}{(p + \eta - \lambda)v - (\eta - \lambda)u} \right\} \geq \frac{1}{m} \Re \left\{ \frac{\omega q''(\omega)}{q'(\omega)} + 1 \right\}, \tag{2.17}$$

$\omega \in \Delta, \zeta \in \partial \Delta \setminus E(q), \xi \in \bar{\Delta}$  and  $m \geq p$ .

**Theorem 2.5.** Let  $\emptyset \in \Phi'_k[h, q]$ . If  $f \in \mathcal{D}_p, \mathcal{S}_{0,\omega}^{\lambda,\mu,\eta} f(\omega) \in Q_0$  and

$$\emptyset(\mathcal{S}_{0,\omega}^{\lambda,\mu,\eta} f(\omega), \mathcal{S}_{0,\omega}^{\lambda+1,\mu,\eta} f(\omega), \mathcal{S}_{0,\omega}^{\lambda+2,\mu,\eta} f(\omega); \omega, \xi)$$

is univalent in  $\Delta$ , then

$\Omega \subset \{\emptyset(\mathcal{S}_{0,\omega}^{\lambda,\mu,\eta} f(\omega), \mathcal{S}_{0,\omega}^{\lambda+1,\mu,\eta} f(\omega), \mathcal{S}_{0,\omega}^{\lambda+2,\mu,\eta} f(\omega); \omega \in \Delta, \xi \in \bar{\Delta})\}$ , implies that

$$q(z) < \mathcal{S}_{0,\omega}^{\lambda,\mu,\eta} f(\omega).$$

**Proof:** By (11) and  $\Omega \subset \{\emptyset(\mathcal{S}_{0,\omega}^{\lambda,\mu,\eta} f(\omega), \mathcal{S}_{0,\omega}^{\lambda+1,\mu,\eta} f(\omega), \mathcal{S}_{0,\omega}^{\lambda+2,\mu,\eta} f(\omega); \omega \in \Delta, \xi \in \bar{\Delta})\}$ ,

we have  $\Omega \subset \{\psi(F(\omega), \omega F'(\omega), \omega^2 F''(\omega); \omega, \xi); \omega \in \Delta, \xi \in \bar{\Delta})\}$ .

from

$$u = r, v = \frac{S + (\eta - \lambda)r}{(p + \eta - \lambda)}, w = \frac{t + 2(\eta - \lambda)S + (\eta - \lambda)(\eta - \lambda - 1)r}{(p + \eta - \lambda - 1)(p + \eta - \lambda)}$$

we see that the admissibility for  $\emptyset \in \Phi'_k[\Omega, q]$  is equivalent to admissibility condition for  $\psi$ . Hence,  $\psi \in \Psi'[\Omega, q]$  and so we have  $q(z) < \mathcal{S}_{0,\omega}^{\lambda,\mu,\eta} f(\omega)$ .

The following Theorem is an immediate consequence of Theorem(2.5).

**Theorem 2.6.** Let  $q \in \mu[0, p], h$  be analytic in  $\Delta$  and  $\emptyset \in \Phi'_k[h, q]$ . If  $f(\omega) \in \mathcal{D}_p,$

$$\mathcal{S}_{0,\omega}^{\lambda,\mu,\eta} f(\omega) \in Q_0$$

and

$$\{\emptyset(\mathcal{S}_{0,\omega}^{\lambda+2,\mu,\eta} f(\omega), \mathcal{S}_{0,\omega}^{\lambda+1,\mu,\eta} f(\omega), \mathcal{S}_{0,\omega}^{\lambda,\mu,\eta} f(\omega); \omega, \xi)\}$$

is univalent in  $\Delta$ , then

$$h(\omega) < \{\emptyset(\mathcal{S}_{0,\omega}^{\lambda+2,\mu,\eta} f(\omega), \mathcal{S}_{0,\omega}^{\lambda+1,\mu,\eta} f(\omega), \mathcal{S}_{0,\omega}^{\lambda,\mu,\eta} f(\omega); \omega, \xi)\}, \tag{2.18}$$

implies that  $q(\omega) < \mathcal{S}_{0,\omega}^{\lambda,\mu,\eta} f(\omega)$ .

**Theorem 2.7.** Let  $h$  be analytic in  $\Delta$  and  $\emptyset: \mathbb{C}^3 \times \Delta \times \bar{\Delta} \rightarrow \mathbb{C}$ . Suppose that the differential equation

$$\emptyset \left( q(\omega), \frac{\omega q'(\omega) + (\eta - \lambda)q(\omega)}{(p + \eta - \lambda)}, \frac{\omega^2 q''(\omega) + 2(\eta - \lambda)\omega q'(\omega) + (\eta - \lambda)(\eta - \lambda - 1)q(\omega)}{(p + \eta - \lambda - 1)(p + \eta - \lambda)}; \omega, \xi \right) = h(\omega),$$

has a solution  $q \in Q_0$  . If  $\emptyset \in \Phi'_k[h, q]$  ,  $f \in \mathcal{D}_\rho$  ,  $\mathcal{S}_{0,\omega}^{\lambda,\mu,\eta} f(\omega) \in Q_0$  and  $\{\emptyset(\mathcal{S}_{0,\omega}^{\lambda+2,\mu,\eta} f(\omega), \mathcal{S}_{0,\omega}^{\lambda+1,\mu,\eta} f(\omega), \mathcal{S}_{0,\omega}^{\lambda,\mu,\eta} f(\omega); \omega, \xi)\}$  is univalent in  $U$  , then

$$h(z) \ll \emptyset(\mathcal{S}_{0,\omega}^{\lambda+2,\mu,\eta} f(\omega), \mathcal{S}_{0,\omega}^{\lambda+1,\mu,\eta} f(\omega), \mathcal{S}_{0,\omega}^{\lambda,\mu,\eta} f(\omega); \omega, \xi), \quad (2.19)$$

implies that  $q(z) < \mathcal{S}_{0,\omega}^{\lambda,\mu,\eta} f(\omega)$ , and  $q$  is the best dominant.

**Proof:**The proof of this Theorem is the same of proof Theorem (2.4).

Theorem (2.2) and Theorem (2.6), we obtained the following Theorem.

**Theorem 2.8** Let  $h_1$  and  $q_1$  be analytic functions in  $\Delta$ ,  $h_2$  be a univalent function in  $\Delta$ ,  $q_2 \in Q_0$  with  $q_1(0) = q_2(0) = 0$  and  $\emptyset \in \Phi_k[h_2, q_2] \cap \Phi'_k[h_1, q_1]$ .

If  $f \in \mathcal{D}_\rho$  ,  $\mathcal{S}_{0,\omega}^{\lambda,\mu,\eta} f(\omega) \in \mu[0, p] \cap Q_0$  and

$$\{\emptyset(\mathcal{S}_{0,\omega}^{\lambda+2,\mu,\eta} f(\omega), \mathcal{S}_{0,\omega}^{\lambda+1,\mu,\eta} f(\omega), \mathcal{S}_{0,\omega}^{\lambda,\mu,\eta} f(\omega); \omega, \xi)\}$$

is univalent in  $\Delta$ , then

$$h_1(\omega) \ll \emptyset(\mathcal{S}_{0,\omega}^{\lambda+2,\mu,\eta} f(\omega), \mathcal{S}_{0,\omega}^{\lambda+1,\mu,\eta} f(\omega), \mathcal{S}_{0,\omega}^{\lambda,\mu,\eta} f(\omega); \omega, \xi) \ll h_2, \quad (2.20)$$

implies that  $q_1(\omega) < \mathcal{S}_{0,\omega}^{\lambda,\mu,\eta} f(\omega) < q_2(\omega)$

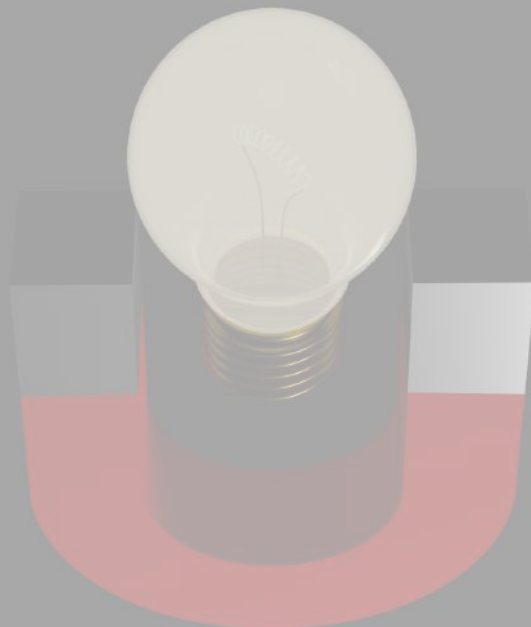
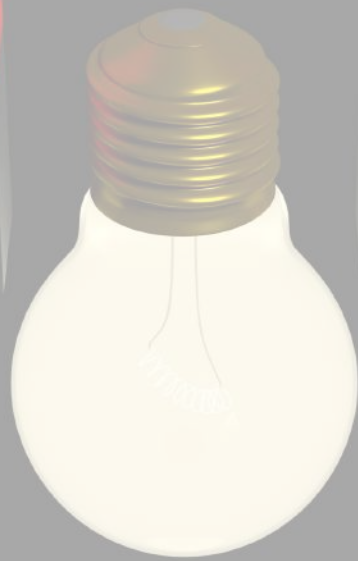
**Reference**

1. A.W. Goodman, On the Schwarz-Christoffel transformation and  $p$ -valent functions, *Trans. Amer. Math. Soc.*, 68 (1950), 204 – 223.
2. H.M. Srivastava and S. Owa (Eds.), *Current Topics in Analytic function Theory*, World Scientific, Singapore, 1992.
3. I.B. Jung, Y.C. Kim and H.M. Srivastava, The Hardy space of analytic functions associated with certain one-parameter families of integral operators, *J. Math. Anal. Appl.*, 176(1993), 138 – 147.
4. J. Patel and A.K. Mishra, On certain subclasses of multivalent functions associated with an extended differintegral operator, *J. Math. Anal. Appl.*, 332 (2007), 109 – 122.
5. J.-L. Liu and S. Owa, Properties of certain integral operators, *Int. J. Math. Sci.*, 3 (2004), 69 – 75.
6. S. Owa, On the distortion theorems I, *Kyungpook Math. J.*, 18 (1), (1978), 53 – 59.
7. S. S. Miller and P. T. Mocanu, Differential subordinations and univalent functions , *Michigan Math. J.* , 28(1981) , 157-171.
8. S.D. Bernardi, Convex and starlike univalent functions, *Trans. Amer. Math. Soc.*, 135 (1969), 429 – 446.
9. S.P. Goyal and J.K. Prajapat, A new class of analytic  $p$ -valent functions with negative coefficients and fractional calculus operators, *Tamsui Oxf. J Math. Sci.*, 20 (2004), 175 – 186.
10. Y.C. Kim and F. Rønning, Integral transforms of certain subclasses of analytic functions, *J. Math. Anal. Appl.*, 258 (2001), 466 – 489.



**THE EFFECT OF PARTIAL AND TOTAL SUBSTITUTION OF CD AND MG NANOPARTICLES  
ON THE ELECTRICAL AND MAGNETIC PROPERTIES OF THE SUPERCONDUCTORS  
COMPOUND  $\text{YBa}_2\text{Cu}_3\text{O}_{7-\delta}$  AT HIGH TEMPERATURES**

**FALAH MOHAMMED ABED  
NADA A. KHALIL  
ISMAEL KALIL JASIM**



درجات الحرارة تأثير التعويض الجزئي والكلبي لعنصري Cd,Mg النانوية على الخواص الكهربائية والمغناطيسية للمركب الفائق التوصيل الكهربائي  $YBa_2Cu_3O_{7-\delta}$  عند درجات الحرارة العالية  
<http://dx.doi.org/10.47832/MinarCongress5-13>

فلاح محمد عبد 1

عبد الكريم دهش علي 2

اسماعيل خليل جاسم 3

الملخص:

تم تحضير نموذجين لهذا البحث بطريقة تفاعل الحالة الصلبة وباستخدام طريقة التلدين وتحت ضغط  $8 \text{ tan/cm}^2$  ودرجة حرارة  $800^\circ\text{C}$  في النموذج الأول تم التعويض الجزئي للعنصر Cd بالعنصر Y بنسبة  $x=0.4$  ليصبح المركب  $Y_{1-x}Cd_xBa_2Cu_3O_{7+\delta}$  وفي النموذج الثاني تم استبدال كلبي للعنصر Y وتعويضة بعنصري Cd,Mg النانوية  $X=1$  ليصبح المركب  $Y_{1-x}Cd_xMg_xBa_2Cu_3O_{7+\delta}$  أظهرت الفحوصات الكهربائية للنموذج الأول زيادة كبيرة في قيمة درجة الحرارة الحرجة حيث وصلت درجة الحرارة الحرجة  $T_c$  إلى قيمة  $148.5$  وفي النموذج الثاني استمرت بصعود حيث وصلت درجة الحرارة الحرجة  $T_c$  إلى  $150 \text{ k}$  أظهرت فحوصات النموذجيين في جهاز SEM النموذج الأول بقوة تكبير  $100.00 \times$  وجد تشكيل الحجم الحبيبي يتراوح من  $29 \text{ nm}$  إلى  $170 \text{ nm}$  وبقوة تكبير  $500 \times$  وجد تشكيل حجم حبيبي يتراوح من  $440 \text{ nm}$  إلى  $3.6 \mu\text{m}$  وبصور واضحة و متجانسة اما النموذج الثاني بقوة تكبير  $100.00 \times$  وجد تشكيل الحجم الحبيبي يتراوح من  $29 \text{ nm}$  إلى  $391 \text{ nm}$  وبقوة تكبير  $500 \times$  وجد تشكيل حجم حبيبي يتراوح من  $332 \text{ nm}$  إلى  $2.8 \mu\text{m}$  وبصور واضحة و متجانسة و متراصة وأظهرت الفحوصات المغناطيسية ومن خلال منحى الهسترة للنموذجيين الأول والثاني والعلاقة بين مغناطيسية التشبع  $M_s$  والمغناطيسية المتبقية  $M_r$  والقوة المرغمة  $H_c$  ان حلقات الهسترة المتكونة في النموذجيين تكون ضيقة جدا وان هناك علاقة عكسية تماما بين ضيق الحلقات وتحسن درجة الحرارة الحرجة  $T_c$  وهذا ينطبق على النموذجيين حيث أن ضيق حلقات الهسترة في النموذج الثاني أكبر من ضيق حلقات الهسترة في النموذج الأول.

الكلمات المفتاحية:  $YBa_2Cu_3O_{7-\delta}$ , Cd,Mg، الخواص الكهربائية والمغناطيسية.

المقدمة:

تعتبر الموصلية الفائقة تقنية واعدة لمنع فقدان الطاقة الناتج عن المقاومة الكهربائية. تجذب هذه التقنية اهتمامًا كبيرًا إلى الأبحاث نظراً لسببين رئيسيين: يمكن إجراء الكهرباء عند مقاومة صفرية ويمكن طرد التدفق المغناطيسي تماماً من جسم مادة فائقة التوصيل. منذ اكتشافها في عام 1911 [1] تم العثور على الموصلية الفائقة فقط في العناصر والسبائك حيث تكون درجة الحرارة الحرجة (TC) لهذه المواد منخفضة جداً [2]. في عام 1986، تم العثور على اللانثانم كبريتات ليكون أول مادة مركبة تظهر الموصلية الفائقة (مولر وبدنورز، 1986) [3]. تبع هذا الاختراق اكتشاف مركب فائق التوصيل من أكسيد الإيتريوم الباريوم والنحاس ( $YBa_2Cu_3O_7$ ) في عام 1987 والذي جلب إثارة كبيرة داخل المجتمع العلمي لأن هذه المادة يمكنها توصيل الكهرباء دون وجود مقاومة عند درجات حرارة أعلى من  $77$  كلفن. تسهيل النيتروجين، وبالتالي فإن  $YBa_2Cu_3O_7$ -غيرت منظور تطبيقات الموصلية الفائقة وفتحت إمكانية حدوث تطورات عديدة في التقنيات [4]. تم إجراء بحوث كبيرة عن الخواص التركيبية والكهربائية والمغناطيسية على خصائص مركبات التوصيل الفائقة عند درجات الحرارة العالية حيث قام M. Zargar Shoushtari وآخرون عام 2008 بدراسة تأثير استبدال الكاديوميوم Cd في المركب  $Bi_{1.6}PbxCd_zSr_2Ca_2Cu_3O_{10}$  وتم الحصول على أقصى تيار حرج  $J_c$  ودرجة حرارة حرجة  $T_c$  عند  $Z=0.04$  [5]. كما درس Nasri وآخرون عام 2011 تأثير إضافة جسيمات  $MgO$  النانوية على مركبات الفائقة  $Bi_2Sr_2Ca_2Cu_3O_8$  التوصيل فوجدوا بان عند إضافة 5% من جسيمات  $MgO$  تعطي أفضل خواص ميكانيكية وكهربائية [6]. وقام الباحث Mohd Shahadan 2013 بدراسة إضافة جسيمات  $Al_2O_3$  على المركب  $YBa_2Cu_3O_{7-\delta}$  بطريقة تفاعل الاحتراق الذاتي العينات التي تم انتاجها كانت فائقة التوصيل الكهربائي اعلى من  $85 \text{ k}$  [7]. و الباحث Jabbar Abdul عام 2015 درس تأثير إضافة حبيبات Au النانوية على مركبات  $Bi_2223$  فائق التوصيل فلاحظ بأنها احتفظت بتركيبها الرباعي القائم كلما ازداد التعويض مع زيادة بقيم  $T_c$  [8] قاما Jannah Abdshukor & عام 2017 بدراسة الخصائص التركيبية عند إضافة جسيمات  $Co_3O_4$  النانوية إلى مركب  $Bi_{1.6}Pb_0.4Sr_2Ca_2Cu_3O_{10}$  فائق التوصيل فوجدوا انه عند إضافة  $0.1$  من هذه الجسيمات تعطي أفضل خواص تركيبية تؤدي إلى زيادة قيم  $T_c$  إلى  $102 \text{ k}$  [9].

<sup>1</sup> جامعة التقنية الشمالية، العراق، [abdulkaremdahashali2290@gmail.com](mailto:abdulkaremdahashali2290@gmail.com)

<sup>2</sup> جامعة تكريت، العراق، [prof.I.K.Jassim@gmail.com](mailto:prof.I.K.Jassim@gmail.com)

<sup>3</sup> جامعة تكريت، العراق، [falah.ma@ntu.edu.iq](mailto:falah.ma@ntu.edu.iq)

بحث Alyaa واخرون عام 2019 تأثير تعويض Ag<sub>2</sub>O النانوي على المركبات Ti<sub>1.6</sub>Hg<sub>0.4</sub>AgxBa<sub>2</sub>Ca<sub>2</sub>Cu<sub>3</sub>O<sub>10</sub> الفائق التوصيل عند X=0، 0.05، 0.1، 0.2 فأزادت قيمة Tc من 120k إلى 130k [10]

درس Foud و Hussain 2020 تأثير إضافة Al<sub>2</sub>O<sub>3</sub> النانوي على الخواص التركيبية والكهربائية للمركب Bi<sub>2</sub>Ba<sub>2</sub>Ca<sub>2</sub>Cu<sub>3</sub>O<sub>10</sub> أظهرت الإضافة بان قيمة Tc تزداد من 126k إلى 139k مع زيادة قيمة التعويض من X=0 إلى X=0.5 [11].

يهدف هذا البحث إلى التوصل إلى أفضل نسبة استبدال كلي وجزيئي لعنصري Mg، Cd النانوية من عنصر Y للمركب YBa<sub>2</sub>Cu<sub>3</sub>O<sub>7-δ</sub> الفائق التوصيل الكهربائي لتحسين الخواص الكهربائية ومنها درجة الحرارة الحرجة Tc وكذلك الحصول على خواص مغناطيسية جديدة.

### 1. تحضير العينات :

تم تحضير نموذجيين من العينات وذلك باستخدام الايتروم اكسيد Y<sub>2</sub>O<sub>3</sub> وأكسيد الباريوم BaO، واكسيد النحاس CuO و اوكسيد الكاديوم CdO النانوي واكسيد المنغيسيوم MgO النانوي بعد وزنها بميزان حساس واعتمادا على وزنها الذرية مع مراعاة إضافة أكسيد الكاديوم Cd النانوي وبنسبة x=0.4 من قيم العنصر Y لنموذج الأول للمركب فائق التوصيل الكهربائي ليصبح المركب بهذه الصيغة Y<sub>1-x</sub>CdxBa<sub>2</sub>Cu<sub>3</sub>O<sub>7+δ</sub> ، وللنموذج الثاني وذلك بإضافة كل من اوكسيد الكاديوم CdO النانوي اكسيد المنغيسيوم MgO النانوي بنسبة x=1 من قيم عنصر Y ليصبح المركب بهذه الصيغة Y<sub>1-x</sub>CdxMgxBa<sub>2</sub>Cu<sub>3</sub>O<sub>7+δ</sub> يتم مزج هذه المساحيق وذلك بعد وضعها في هاون من العقيق Agate mortar ويستمر الطحن ويتم إضافة كحول ايزوبروبانول propanol لتسهيل عملية الطحن إلى ان نحصل على مسحوق متجانس، ولتخلص من الكحول الموجودة في المركب توضع داخل فرن كهربائي لمدة ساعة واحدة ودرجة، 100°C ثم يتم وزن العينات بعد التسخين تكبس العينات على هيئة اقراص بقطر 15 mm، وسمك 2 mm وذلك باستخدام مكبس هيدروليكي وبضغط 8 tan/cm<sup>2</sup>. ثم توضع الاقراص في فرن كهربائي ويتم اختيار درجة 800°C مراعاة لدرجة انصهار المواد المكونة للمركب. ويستمر التسخين من درجة حرارة الغرفة وبمعدل C°/ hr إلى 120°C ان تصل إلى درجة 600°C لتسمى هذه العملية بعملية التلييد sintering ، بعدها يتم ضخ الأوكسجين في الفرن ويتم رفع درجة الحرارة من 600°C إلى 800°C وبمعدل 20 C°/ hr لتسمى هذه العملية بالتلدين Annealin تبقى العينات بهذه الدرجة داخل الفرن لمدة 24 hr مع الاستمرار بضغط الأوكسجين بعدها يبرد وبمعدل 5 C°/hr إلى ان تصل لدرجة حرارة الغرفة. ان عمليتي التلييد والتلدين لها دور كبير للتخلص من العيوب التركيبية والتصنيعية للمركبات وكذلك تقوم هذه المركبات بأخذ قالبها التركيبية. [12]

### 2. القياسات الكهربائية للعينات:

تستخدم هذه القياسات لحساب درجة حرارة التحول Tc وذلك بعد قياس مقاومة العينات. وباستخدام الأجهزة التالية:

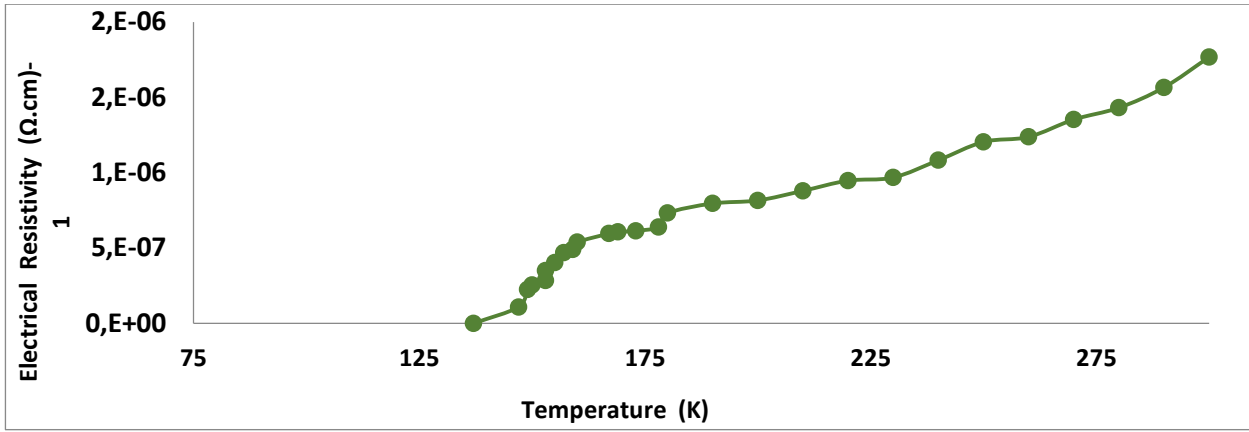
- 1 - منظومة تبريد (Cryostat System) تعمل بالنتروجين السائل،
- 2 - مجهز قدرة مستمر (D.C power supply)
- 3 - فولتميتر رقمي نانوي (Digital Nano voltmeter) ،
- 4 - اميتر (Ammeter)،
- 5 - جهاز قياس درجات الحرارة Digital Nano voltmeter
- 6 - مضخة مفرغة (Rotary Pump).

حيث يتم دراسة تغير المقاومة مع درجة الحرارة وباستخدام المنظومة والتي تعمل بالنتروجين السائل وبذلك يتم حساب Tc على أساس انها منتصف المسافة بين بداية هبوط المقاومة ونهاية هبوط المقاومة اي أن :-

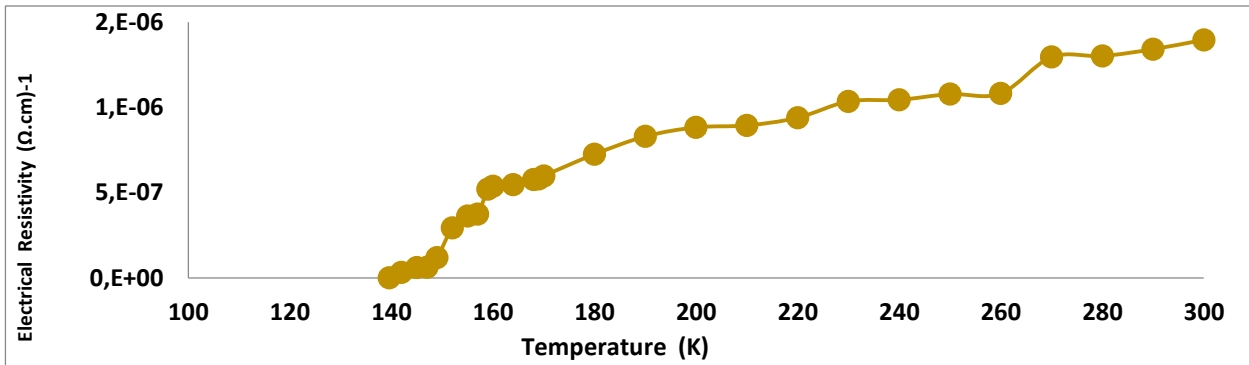
$$Tc(\text{Mid}) = Tc(\text{Onset}) + Tc(\text{Offset})/2$$

### 3. النتائج والمناقشة:

أظهرت دراسة الخصائص الكهربائية للنموذج الأول للمركب Y<sub>1-x</sub>CdxBa<sub>2</sub>Cu<sub>3</sub>O<sub>7+δ</sub> عند تعويض الكاديوم Cd بنسبة x=0.4 من قيمة Y زيادة كبيرة في قيمة درجة الحرارة الحرجة Tc حيث وصلت 148.5k وفي النموذج الثاني للمركب Y<sub>1-x</sub>CdxMgxBa<sub>2</sub>Cu<sub>3</sub>O<sub>7+δ</sub> عند تعويض الكاديوم Cd والمنغيسيوم Mg النانوية بشكل كامل بنسبة x=1 استمرار الزيادة الكبيرة في قيمة درجة الحرارة الحرجة Tc حيث وصلت 150k وكما في الشكل رقم 1 والشكل رقم 2

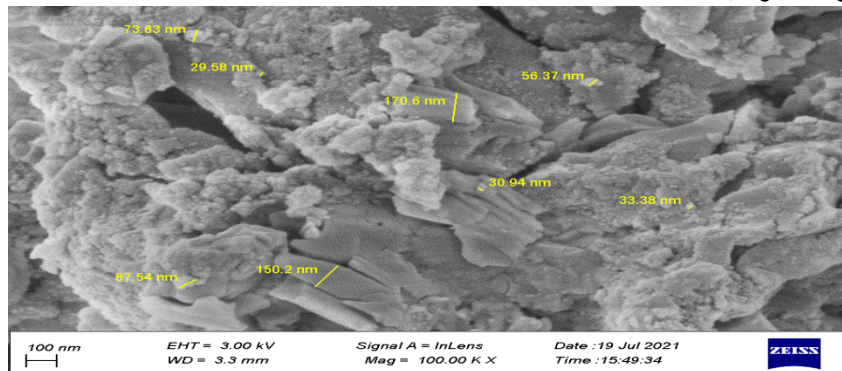


شكل 1: يبين تغير المقاومة مع درجة الحرارة للمركب  $Y_{1-x}Cd_xBa_2Cu_3O_{7+\delta}$  لقيم  $x=0.4$

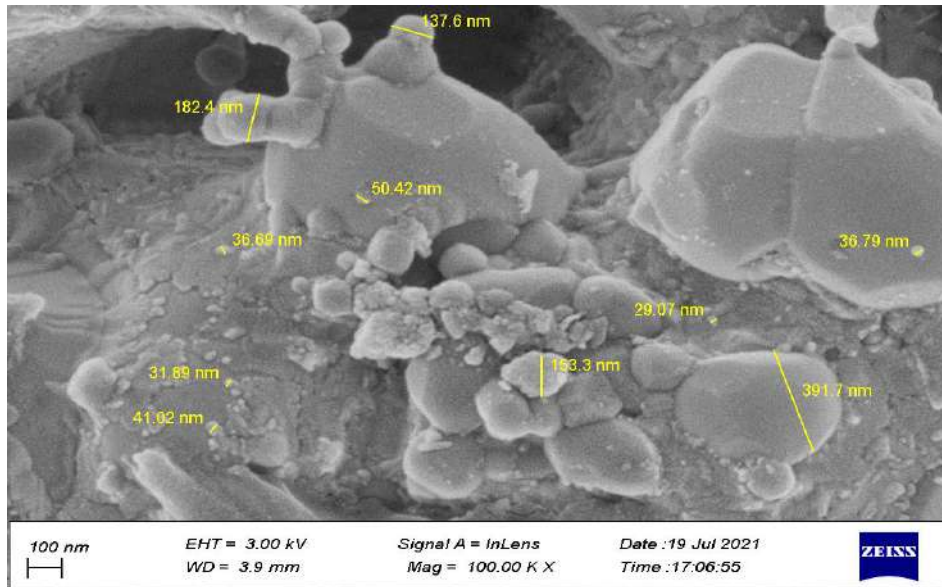


شكل 2 يبين تغير المقاومة مع درجة الحرارة للمركب  $Y_{1-x}Cd_xMg_xBa_2Cu_3O_{7+\delta}$  لقيم  $x=1$

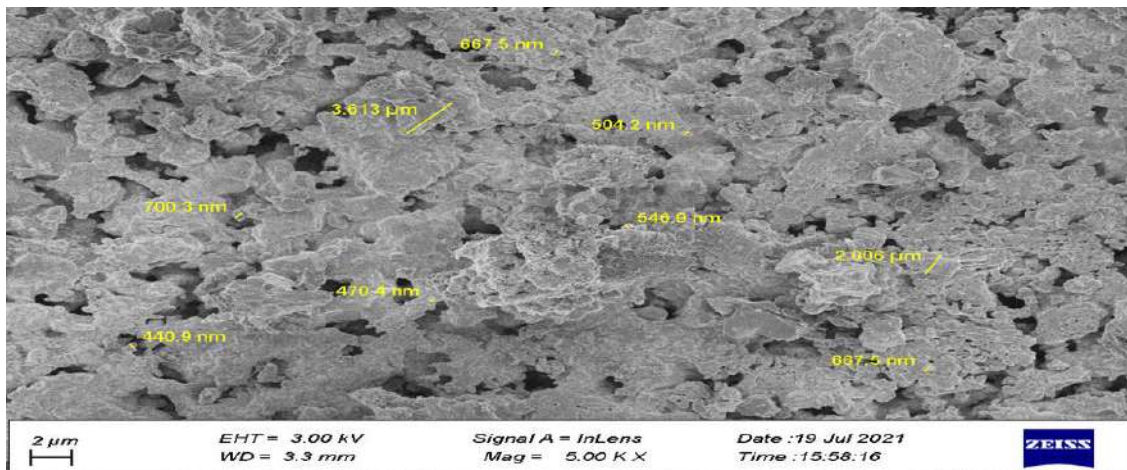
أوضحت الفحوصات بجهاز EDX للنموذجيين في النموذج الأول والذي اخذ صيغة المركب  $Y_{1-x}Cd_xBa_2Cu_3O_{7+\delta}$  عند قوة تكبير  $100.00kx$  نلاحظ من الصور تشكل حجم حبيبي يتراوح من  $29nm$  إلى  $170nm$  وتكون الصور عبارة عن كتل متجانسة فاتحة اللون وبقوة تكبير  $500kx$  نلاحظ من الصور تشكل حجم حبيبي يتراوح من  $3.6\mu m$  إلى  $440nm$  وشكل الصور تكون متراصة فيها تكون المناطق فاتحة اللون بشكل عام كما في الشكل 3 والشكل 4 اما النموذج الثاني والذي اخذ صيغة المركب  $Y_{1-x}Cd_xMg_xBa_2Cu_3O_{7+\delta}$  عند قوة تكبير  $100.00 kx$  وجد تشكيل الحجم الحبيبي يتراوح من  $29 nm$  إلى  $391 nm$  وبقوة تكبير  $500kx$  وجد تشكيل حجم حبيبي يتراوح من  $332nm$  إلى  $2.8 \mu m$  وبصور واضحة ومتجانسة.



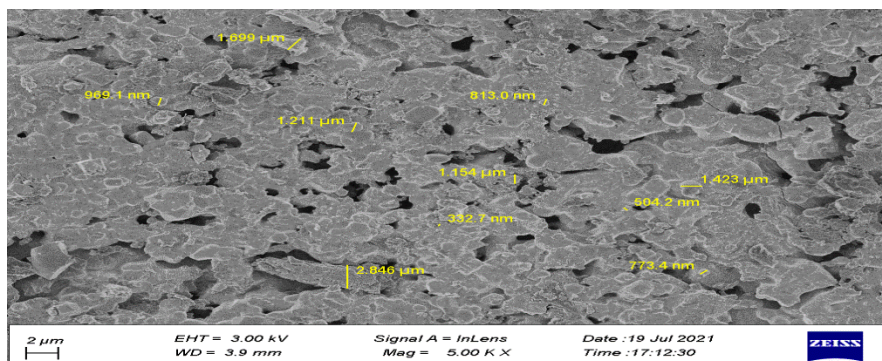
شكل 3 صور فوتوغرافية للمركب  $Y_{1-x}Cd_xBa_2Cu_3O_{7+\delta}$  لقيم  $x=0.4$  بقوة تكبير  $10000kx$



شكل 4 صور فوتوغرافية للمركب  $Y_{1-x}Cd_xBa_2Cu_3O_{7+\delta}$  لقيم  $x=0.4$  بقوة تكبير 500kx

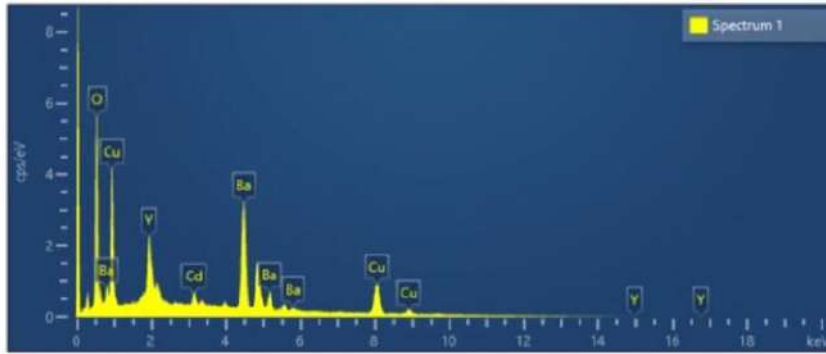


شكل 5 صور فوتوغرافية للمركب  $Y_{1-x}Cd_xMg_xBa_2Cu_3O_{7+\delta}$  لقيم  $X=1$  بقوة تكبير 10000kx



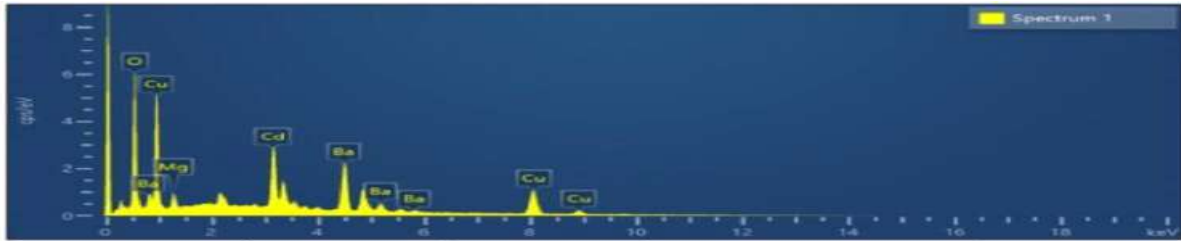
شكل 6 صور فوتوغرافية للمركب  $Y_{1-x}Cd_xMg_xBa_2Cu_3O_{7+\delta}$  لقيم  $X=1$  بقوة تكبير 500kx

تم استخدام تقنية EDX لتحليل العناصر المستخدمة في العينات ان هذه التقنية تستخدم لقياس تراكيز المواد المكونة النماذج ويظهر فيها مكونات النماذج بشكل واضح ومدى التطابق بينها وبين المواد المكونة لها



Spectrum 1				
Element	Line Type	Weight %	Weight % Sigma	Atomic %
O	K series	23.01	0.29	63.84
Cu	L series	25.37	0.34	17.73
Y	L series	8.93	0.26	4.46
Ba	L series	40.12	0.35	12.97
Cd	L series	2.56	0.16	1.01
Total		100.00		100.00

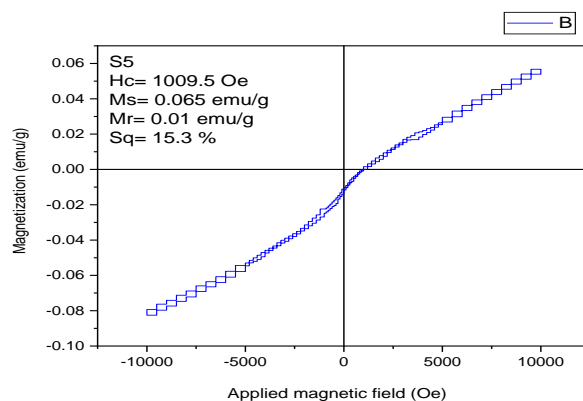
شكل 7 يمثل العلاقة بين الطاقة والشدة وجدول نسب العناصر للمركب  $Y_{1-x}Cd_xBa_2Cu_3O_{7+\delta}$  لقيم  $x=0.4$



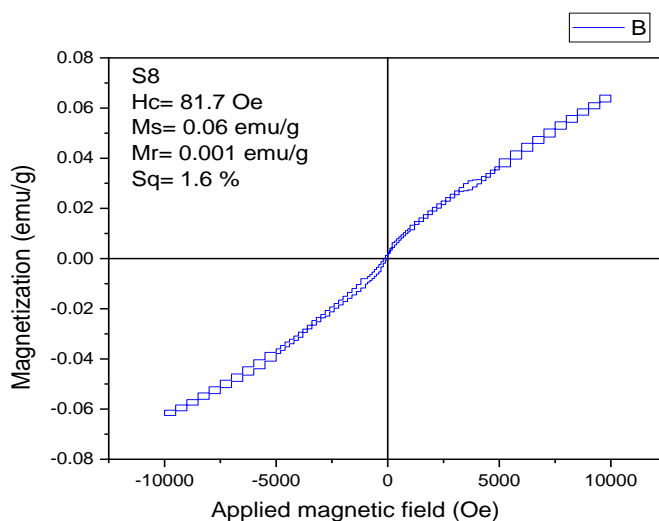
Spectrum 1				
Element	Line Type	Weight %	Weight % Sigma	Atomic %
O	K series	25.92	0.31	65.31
Cu	L series	28.96	0.32	18.37
Cd	L series	17.36	0.23	6.23
Ba	L series	26.34	0.29	7.73
Mg	K series	1.43	0.08	2.36
Total		100.00		100.00

شكل 8 يمثل العلاقة بين الطاقة والشدة وجدول نسب العناصر للمركب  $Y_{1-x}Cd_xMg_xBa_2Cu_3O_{7+\delta}$  لقيم  $x=1$

وتم فحص النموذجين والمرفقة في الاشكال ادناه والمرقم (9 - 10) بجهاز VSM والذي يختص بقياس الخواص المغناطيسية للمواد المستخدمة في الابحاث العلمية لتحديد وتطوير جودتها للقابلية المغناطيسية ومن منحى الهسترة والعلاقة Sq والتي تمثل نسبة المغناطيسية المتبقية Remanance Magnetization Mr مقسومة على مغناطيسية التشبع Saturation Magnetization Ms في النسبة المؤية نلاحظ الفرق الواضح بين النموذج الأول والنموذج الثاني وضيق حلقات الهسترة في النموذج الثاني اكثر من النموذج الأول وربط ضيق حلقات الهسترة بعلاقة عكسية مع درجة الحرارة الحرجة Tc وأفضل نتيجة هي في النموذج الثاني عندما  $X=1$  حيث قيمة  $Sq=1.6\%$  والنموذج الأول حيث  $X=0.4$  حيث اصبحت قيمة  $Sq=15.3\%$  هذا يتطابق تماما مع الابحاث ان مواد التوصيل الفائق هي مواد دابا مغناطيسية [13]



شكل 9 يمثل العلاقة بين المجال المطبق والمغنطة وشكل حلقات الهستيرة للمركب  $Y_{1-x}Cd_xBa_2Cu_3O_{7+\delta}$  لقيم  $x=0.4$



شكل 10 يمثل العلاقة بين المجال المطبق والمغنطة وشكل حلقات الهستيرة للمركب  $Y_{1-x}Cd_xMg_xBa_2Cu_3O_{7+\delta}$  لقيم  $x=1$

#### 4. الاستنتاجات:

عند تحضير النموذجين في النموذج الأول تم تعويض Cd النانوي بنسبة  $x=0.4$  من قيمة عنصر Y للمركب حصلت زيادة كبيرة في درجة الحرارة الحرجة Tc وفي النموذج الثاني تم استبدال كلي لعنصر Y وتعويضه بعنصري Cd، Mg؛ النانوية استمرت الزيادة في درجة الحرارة الحرجة Tc اي الزيادة الكبيرة هي بالدرجة الكبيرة لعنصر Cd. الفحص بجهاز EDX أظهرت ومن خلال الصور للنموذجين تشكيل حجم حبيبي بابعاد مختلفة متجانسة وشبه منتظمة فاتحة اللون تعود للناصر الخفيفة المكونة للمركب كما أظهر تحليل العناصر تطابق كلي للعناصر المكونة للمركب. وتم فحص الخواص المغناطيسية بجهاز VSM للنموذجين الأول والثاني ومن منحى الهستيرة ان العلاقة بين مغناطيسية التشبع (Ms) و Saturation Magnetization (Ms) والمغناطيسية المتبقية (Mr) Remanance Magnetization والقوة المرغمة Coercivity Hc وجود علاقة عكسية بين ضيق حلقات الهستيرة ودرجة الحرارة الحرجة Tc.

## References

1. Meissner W., & Ochsenfeld R. (1933). Ein neuer Effekt bei Eintritt der Supraleitfähigkeit. *Naturwissenschaften*, 21 (44), 787–788.
2. [2] Bardeen J., Cooper L. N., & Schrieffer J. R.. (1957). Microscopic theory of superconductivity. *Physical Review*, 106, 162–164.
3. Mueller K. A. & Bednorz J.G. (1986). Possible high  $T_C$  superconductivity in the Ba-La-Cu-O system. *Zeitschrift für Physik B*, 189–193.
4. Wu L, & Chu P. (1987). Superconductivity at 93 K in a new mixed-phase Y-Ba-Cu-O compound system at ambient pressure. *Physical Review Letters*, 908–910
5. M. Zargar Shoushtari, S.E. Mousavi Ghahfarokhi and M. Farbod, 2008. The Effect of Cd Doping on Bi-Based Superconductor. *Journal of Applied Sciences*, 8: 2613-2618
6. Nasri A. Hamid, Mohd Y, Abd Rahman and Noor F. Shamsudin, "Mechanical and Superconducting proprieties of Nano size MgO added dip-coated Bi<sub>2</sub> Sr<sub>2</sub> Ca Cu<sub>2</sub>O<sub>8</sub> Superconducting Tape", *Natural Science*, 3(6), 484 (2011).
7. Mohd Shahadan Mohd Suan, Mohd Rafie Johan (2013). Synthesis of Al<sub>2</sub>O<sub>3</sub> nanoparticles highly distributed in YBa<sub>2</sub>Cu<sub>3</sub>O<sub>7</sub> superconductor by citrate–nitrate auto-combustion reaction, *Physica C* 492, 49–54 .
8. Abdul Jabbar, Irfan Q., Khalid M. Khan, Zulqurnain A., Nadeem K., Mumtaz M., "Synthesis and superconducting properties of (Au)<sub>x</sub>/ CuTi-1223 Composites ", *Journal of Alloys and Compound*, 618, 110 (2015).
9. Abd shukor R. and Jannah A, "Advances in Superconductivity and CO<sub>3</sub>O<sub>4</sub>Nano Particles as flex pinning center in (Bi-Pb) 2223/Ag superconductor Tapes", *Alp conference proceeding*, AIP Publishing LLC, USA, 1877(1), 020003 (2017)
10. Alyaa H., Abdu Kareem A. and Kareem J, " Influence of Simultaneous doping of Ag on the wircal Temperature and Laitice conslout of Ti<sub>1.6</sub> Hg<sub>0.4-x</sub> Ag<sub>x</sub>Ba<sub>2</sub>Ca<sub>2</sub>Cu<sub>3</sub>O<sub>10</sub> Superconductors", *Alp Conference Proceedings*, AIP Puplishing LLC, USA, 2123, 020079 (2019).
11. Fouad K.and Hussein A. "The Effect of Addition of (Al<sub>2</sub>O<sub>3</sub>) Nano Particles on Structural and Electrical Properties of Bi<sub>2</sub>Ba<sub>2</sub>Ca<sub>2</sub>Cu<sub>3</sub>O<sub>10</sub> + $\delta$  Superconductors at High Temperature "Kirkuk University Journal /Scientific Studies (KUJSS) Volume 15, Issue 4,December 2020
12. Abbas M. and Razzaq A., "The effect of Nd Nano particles on (Bi, Pb)2223 Superconductivity", *Journal of chemical and pharmaceutical science*, 10, 10111(2017).
13. Chang Yen ,conventional superconductivity NTU-222D5220,(2007).





**NEW GENERALIZED OPERATOR IN TOPOLOGICAL SPACES**

**SIHAM I. AZIZ  
NABILA I. AZIZ**

## NEW GENERALIZED OPERATOR IN TOPOLOGICAL SPACES

**Siham I. AZIZ**<sup>1</sup>

**Nabila I . AZIZ**<sup>2</sup>

### **Abstract:**

The aim of this paper is to introduce a new class of operators namely ( $V$ -regular generalized\*,  $V$ -regular generalized\*\*,  $V$ -generalized\*\* regular) (briefly,  $V$ -rg\*,  $V$ -rg\*\*,  $V$ -g\*\*r, respectively) in topological space and provided several key examples and theorems.

**Key words:**  $V$ - Regular Generalized\*\*,  $V$ -Generalized\*\* Regular.



<http://dx.doi.org/10.47832/MinarCongress5-14>



<sup>1</sup> Ministry of Education General Directorate of Kirkuk Province Education, Iraq, [suham\\_70100@yahoo.com](mailto:suham_70100@yahoo.com), <https://orcid.org/0000-0002-6828-6418>



<sup>2</sup> Tikrit University, Iraq, [nabila.be@tu.edu.iq](mailto:nabila.be@tu.edu.iq)

## Introduction:

Crossley and Hildebrand [7] defined semi-closure in 1971, Dunham [9] studied concept of closure operator with some properties, Savita R., Ridam G. and Kusum D.[8], introduced soft  $\omega$ -interior and soft  $\omega$ -closure. in soft topological spaces. [5] Caldas, Georgiou and Jafari introduced some weak separation axioms by utilizing the notions of pre-Open sets and the pre-closure operator. Some researchers have proved some theorems of this nature theorem : Let  $(X,T)$  be a T.S.(topological spaces) and  $A$  subset of  $X$ , is the intersection of all closed (resp. semi-closed, pre-closed, semi-pre-closed, b-closed) sets of  $X$  containing  $A$  is called the closure of  $A$  [3](resp. semi-closure [7], pre-closure [1], semi-pre-closure [4], b-closure [3]) of  $A$ .

The goal of this study is to provide a new class of regular generalized closed set operators (regular generalized, regular generalized, generalized regular) (briefly  $V$ ,  $V - rg^*$ ,  $V - rg^{**}$ ,  $V - g^{**}r$ , respectively) in topological space and give some important examples and some theorems.

## 2. Preliminaries

This section of the paper includes some of the required definitions and theorems.

**Definition 2.1[2]:** Let  $(x, \tau)$  be a topological space we define operator as

$$V-(A)=\cup\{G:G \subseteq A, G \text{ is closed } \subseteq X\}$$

**Definition 2.2 [6]:** A subset  $A$  of a space  $X$  is called regular generalized [resp. regular generalized] closed set (briefly,  $rg^*$ ,  $rg^{**}$ )closed set if  $U \subseteq Cl(A)$ ,  $A \subseteq U$ ,  $U$  is regular [resp. pre regular] open  $\subseteq X$ .

**Definition 2.3[6]:** A subset  $W$  of a space  $H$  is called generalized regular closed set (briefly  $g^{**}r$ ) closed if  $U \subseteq Rcl(W)$ ,  $W \subseteq U$ ,  $U$  is pre regular open  $\subseteq H$ .

**Definition 2.4[2]:** Let  $(x, \tau)$  be a topological space we define operator as  $V_{GR}(A)=\cup\{G:G \subseteq A, G \text{ is generalized regular closed } \subseteq X\}$

## 3 .New generalized Operator in Topological Spaces

**Definition 3.1:** Let's define some new operators, as shown in the paper below.. Let  $\mu \in [rg^*, rg^{**}]$ closed set.

$$V_{\mu}(A)=\cup\{U:U \subseteq A, U \text{ is } \mu \in (rg^*, rg^{**}) \text{ closed } \subseteq X\}$$

**Example 3.2:**  $X=\{a, b, c, d, e\}$ ,  $\tau =\{\emptyset, X, \{a, c, e\}, \{a, b, c, e\}, \{a, b\}$

$Ro(x)=\{\emptyset, X\}$ ,  $PRO(X)=\{\emptyset, X, \{a\}, \{b\}, \{c\}, \{d\}, \{e\}, \{a, b\}, \{a, c\}, \{a, d\}, \{a, e\}, \{b, d\}, \{b, e\}, \{c, e\}, \{c, d\}, \{a, b, c\}, \{a, b, d\}, \{a, b, e\}, \{a, c, e\}, \{a, c, d\}, \{b, c, d\}, \{b, c, e\}, \{c, d, e\}, \{b, d, e\}, \{a, d, e\}, \{a, b, c, d\}, \{a, b, c, e\}, \{a, c, d, e\}, \{b, c, d, e\}, \{a, b, d, e\}\}$ ,  $A=\{a, b, c\}$ ,  $\forall \mu (A)=\{a, b, c\}$ ,  $\mu \in [rg^*, rg^{**}]$ closed-set= $\{\emptyset, X, \{a\}, \{a, b\}, \{a, e\}, \{b, c\}, \{b, e\}, \{a, b, c\}, \{a, c, e\}, \{a, b, d\}, \{a, b, e\}, \{a, b, c, d\}, \{a, b, c, e\}, \{b, c, d, e\}\}$

**Lemma 3.3:** Let  $(x, \tau)$  be a topological space  $V_{\mu}: P(x) \rightarrow P(x)$  be an operator which satisfies the following properties.

1.  $V_{\mu}(\emptyset)=\emptyset$ ,  $V_{\mu}(x)=x$
2.  $V_{\mu}(A) \subseteq A$
3.  $V_{\mu}V_{\mu}(A)=V_{\mu}(A)$

4. If  $B \supseteq A$ ,  $v_\mu(B) \supseteq v_\mu(A)$ .
5.  $v_\mu(A \cap B) \subseteq v_\mu(A) \cap v_\mu(B)$ .
6.  $v_\mu(A \cup B) \supseteq v_\mu(A) \cup v_\mu(B)$ .

Proof: 2-  $v_\mu(A) \subseteq A$ , Since  $U \subseteq A$ ,  $U$  is  $\mu \in [rg^*, rg^{**}]$  closed  $\subseteq X$ , by definition we get  $v_\mu(A) \subseteq (A) \rightarrow v_\mu(A) \subseteq A$ .

$$3- v_\mu v_\mu(A) = v_\mu(A), v_\mu(A) = \cup \{U : U \subseteq A, U \text{ is } \mu \in (rg^*, rg^{**}) \text{ closed } \subseteq X\}$$

$$v_\mu(A) = \cup \{U : U \subseteq A, U \text{ is } \mu \in (rg^*, rg^{**}) \text{ closed } \subseteq X\}$$

$$v_\mu[v_\mu(A)] = \cup [\cup \{U : U \subseteq A, U \text{ is } \mu \in (rg^*, rg^{**}) \text{ closed } \subseteq X\}]$$

$$= \cup \{U : U \subseteq A, U \text{ is } \mu \in (rg^*, rg^{**}) \text{ closed } \subseteq X\} = v_\mu(A).$$

4- If  $B \supseteq A$ ,  $v_\mu(B) \supseteq v_\mu(A)$ ,  $v_\mu(A) = \cup \{U : U \subseteq A, U \text{ is } \mu \in (rg^*, rg^{**}) \text{ closed } \subseteq X\}$ , since  $A \subseteq B$ , then  $\cup \{U : U \subseteq A, U \text{ is } \mu \in (rg^*, rg^{**}) \text{ closed } \subseteq X\}$

$$\subseteq v_\mu(B) = \cup \{U : U \subseteq B, U \text{ is } \mu \in (rg^*, rg^{**}) \text{ closed } \subseteq X\}$$

$$\Rightarrow v_\mu(B) \supseteq v_\mu(A).$$

5-  $v_\mu(A \cap B) \subseteq v_\mu(A) \cap v_\mu(B)$ , since  $A \cap B \subseteq A$ ,  $A \cap B \subseteq B$ , then  $v_\mu(A \cap B) \subseteq v_\mu(A)$ ,  $v_\mu(A \cap B) \subseteq v_\mu(B)$ . Hence  $v_\mu(A \cap B) \subseteq v_\mu(A) \cap v_\mu(B)$

$$6. -v_\mu(A \cup B) \supseteq v_\mu(A) \cup v_\mu(B).$$

Since  $A \subseteq A \cup B$ ,  $B \subseteq A \cup B$ , then  $v_\mu(A \cup B) \supseteq v_\mu(A)$ ,  $v_\mu(A \cup B) \supseteq v_\mu(B)$ .

Hence  $v_\mu(A \cup B) \supseteq v_\mu(A) \cup v_\mu(B)$ .

**Remark 3.5:** The converse part [5-6] of lemma [ 3.3 ] is false, as the following example demonstrates.

**Example 3.6:**  $X = \{a, b, c, d, e\}$ ,  $\tau = \{\emptyset, X, \{e\}, \{a, b\}, \{d, e\}, \{a, b, e\}, \{c, d, e\}, \{a, b, c, d\}, \{a, b, d, e\}\}$ ,  $Rox = \{\emptyset, X, \{e\}, \{a, b\}, \{c, d, e\}, \{a, b, c, d\}$ ,  $PRox = \{\emptyset, X, p(x)\}$ ,  $U = X$

$[rg^*, rg^{**}] \text{cloed} = \{\emptyset, X, \{a, e\}, \{b, e\}, \{a, b, e\}, \{a, c, e\}, \{a, d, e\}, \{b, c, e\}, \{b, d, e\}, \{a, b, d, e\}, \{a, c, d, e\}, \{b, c, d, e\}\}$ .  $A = \{b, e\}$ ,  $B = \{a, e\}$ ,  $v_\mu(A) = \{b, e\}$ ,  $v_\mu(B) = \{a, e\}$ ,  $v_\mu(A \cap B) = v_\mu(\{e\}) = \emptyset$ , then  $v_\mu(A \cap B) \neq v_\mu(A) \cap v_\mu(B)$ .

$A = \{a, b\}$ ,  $B = \{c, d, e\}$ ,  $v_\mu(A) = \emptyset$ ,  $v_\mu(B) = \emptyset$ ,  $v_\mu(A \cup B) = X$ , then  $v_\mu(A \cup B) \neq v_\mu(A) \cup v_\mu(B)$

**Lemma 3.7:** Let  $(x, \tau)$  be a topological space  $v_{g^{**r}}: P(x) \rightarrow P(x)$  be an operator which satisfies the following properties.

- 1-  $v_{g^{**r}}(\emptyset) = \emptyset$ ,  $v_{g^{**r}}(x) = x$
- 2-  $v_{g^{**r}}(A) \subseteq A$
- 3-  $v_{g^{**r}} v_{g^{**r}}(A) = v_{g^{**r}}(A)$
- 4- If  $B \supseteq A$ ,  $v_{g^{**r}}(B) \supseteq v_{g^{**r}}(A)$ .
- 5-  $v_{g^{**r}}(A \cap B) \subseteq v_{g^{**r}}(A) \cap v_{g^{**r}}(B)$ .
- 6-  $v_{g^{**r}}(A \cup B) \supseteq v_{g^{**r}}(A) \cup v_{g^{**r}}(B)$ .

Proof: [ 2- 3-4-5-6] The steps are the same as in the last lemma proof. [3-3] .

**Remark 3.8:** The converse part [5-6] of lemma [3.7] is false, as the following example demonstrates.

**Example 3.9:**

Let  $X = \{a, b, c, d, e\}$ ,  $\tau = \{\emptyset, X, \{d\}, \{c, d\}, \{c, d, e\}, \{a, b, c, e\}\}$ ,  $Rox = \{\emptyset, X, \{d\}, \{a, b, c, e\}\}$ ,  $PROx = \{\emptyset, X, \{a\}, \{b\}, \{c\}, \{d\}, \{e\}, \{a, b\}, \{a, c\}, \{a, d\}, \{a, e\}, \{b, c\}, \{b, d\}, \{b, e\}, \{c, d\}, \{c, e\}, \{d, e\}, \{a, b, c\}, \{a, b, d\}, \{a, b, e\}, \{a, c, d\}, \{a, c, e\}, \{a, d, e\}, \{b, c, d\}, \{b, c, e\}, \{b, d, e\}, \{c, d, e\}, \{a, b, c, d\}, \{a, b, c, e\}, \{a, b, d, e\}, \{a, c, d, e\}, \{b, c, d, e\}\}$

$g^{**}rClosedset = \{\emptyset, X, \{a, d\}, \{b, d\}, \{c, d\}, \{d, e\}, \{a, b, d\}, \{a, d, e\}, \{a, c, d\}, \{b, d, e\}, \{c, d, e\}, \{b, c, d\}, \{a, c, d, e\}, \{a, b, d, e\}, \{b, c, d, e\}, \{a, b, c, d\}\}$ .

$$1-A = \{a, d\}, B = \{b, d\}, \vee_{g^{**}r} (A) = \{a, d\}, \vee_{g^{**}r} (B) = \{b, d\}, \vee_{g^{**}r} (A \cap B) = \vee_{g^{**}r} (\{d\}) = \emptyset.$$

$$\vee_{g^{**}r}(A) \cap \vee_{g^{**}r}(B) = \{d\}. \text{ then } \vee_{g^{**}r} (A \cap B) \neq \vee_{g^{**}r} (A) \cap \vee_{g^{**}r} (B).$$

$$2- W = \{a, c, e\}, H = \{b, e\}, \vee_{g^{**}r}(W) = \emptyset, \vee_{g^{**}r}(H) = \emptyset$$

$$\vee_{g^{**}r} (W \cup H) = \vee_{g^{**}r} (\{a, b, c, e\}) = X \neq \emptyset$$

$$\text{then } \vee_{g^{**}r} (A \cup B) \neq \vee_{g^{**}r} (A) \cup \vee_{g^{**}r} (B).$$

**Theorem 3.10:** (1)  $\vee_{\mu} (A) = A \leftrightarrow A$  is a regular generalized  $[rg^*, rg^{**}]$  closed set.

Proof: Let  $A$  be a regular generalized  $(rg^*)$  [resp.  $rg^{**}$ ] closed set. Since  $\vee_{\mu} (A) \subseteq A$  and  $U \subseteq Cl(A)$ ,  $U$  is regular open [resp. pre regular open] set then  $A \subseteq \vee_{\mu} (A)$  thus  $\vee_{\mu} (A) = A$ .

Conversely: if  $\vee_{\mu} (A) = A$

To prove  $A$  be a regular generalized  $[rg^*, rg^{**}]$  closed set.

Since arbitrary union of regular generalized  $[rg^*, rg^{**}]$  closed set is regular generalized  $[rg^*, rg^{**}]$  closed set. , then  $A$  is a regular generalized  $[rg^*, rg^{**}]$  closed set.

**Theorem 3.11:** (1)  $\vee_{\mu} (A) = A \leftrightarrow A$  is a generalized $^{**}$  regular closed set.

Proof: Let  $A$  be a generalized $^{**}$  regular closed set. Since  $\vee_{\mu} (A) \subseteq A$  and  $U \subseteq R Cl(A)$ ,  $U$  is. pre regular open set then  $A \subseteq \vee_{\mu} (A)$  thus  $\vee_{\mu} (A) = A$ .

Conversely: if  $\vee_{\mu} (A) = A$

To prove  $A$  be a generalized $^{**}$  regular closed set.

Since arbitrary union of generalized $^{**}$  regular closed set is generalized $^{**}$  regular closed set, then  $A$  is a generalized $^{**}$  regular closed set.

**4. Conclusion**

In this paper We introduced operators on regular generalized closed sets ( $\vee$  –regular generalized,  $\vee$  –regular generalized,  $\vee$  –generalized regular) closed set (briefly ,  $\vee$  – $rg^*$ ,  $\vee$  –  $rg^{**}$ ,  $\vee$  –  $g^{**}r$ , respectively) in topological space and gave some important examples and some theorems.

We will be able to investigate generalized to the graph, space and micro topological space in the future. The definition of operator  $\vee$  can also be generalized on  $(\alpha, \beta)$  with all of these properties and theorems.

## References

- A. S. Mashhour, I. A. Hasanein and S. N. El-Deeb., (1983), " $\alpha$ -continuous and open mappings", *Acta Math. Hungar.*, 41, 213–218.
- Bhattacharya, S. (2011) "On Generalized Regular Closed Sets" , *Contemp. Math. Sciences*, 6 : (3) 145-152.
- D. Andrijević, (1996), "On b-open sets", *Mat. Vesnik*, 48 ,59–64.
- D. Andrijević.,(1986),"Semi-preopen sets",*Mat. Vesnik*, 38 ,24–32.
- M. Caldas, T. Fukutake, S. Jafari and T. Noiri.(2005)," Some applications of  $\alpha$ -preopen sets in topological spaces) *bulletin of the institute of mathematics academia sinica* volume 33, number 3, september .
- Nabila I. Aziz (2021) " On some Generalized rare regular Closed sets in topologicalSpaces" *Journal of Physics: Conference Series ICMAICT 2020*, IOP Publishing,1804 012065 , doi:10.1088/1742-6596/1804/1/012065.
- S. G. Crossley and S. K. Hildebrand(1971), "Semi-closure", *Texas J. Sci.*, 22 ,99–112.
- Savita Rathee, Ridam Girdhar and Kusum Dhingra, ,(2020), On soft  $\omega$ -interior and soft  $\omega$ -closure in soft topological spaces, *Journal of Interdisciplinary Mathematics*, Vol.23,Issue6,<https://doi.org/10.1080/09720502.2020.1815399>.
- W. Dunham, (1982), "A new closure operator for non-T1topologies", *Kyungpook, Math.J.*. 22 ,55-602009.



**A CROSS-SECTIONAL STUDY OF STOOL SAMPLES FOR SOME LOCAL AND  
INTERNATIONAL ARRIVALS TO KARBALA GOVERNORATE DURING A  
RELIGIOUS VISIT**

**ZAINAB ABED MUHSIN AL-HABOOBI  
HUDA DHAHER AL-MARSOMY  
HALEEMA SALMAN SALIH**

## **A CROSS-SECTIONAL STUDY OF STOOL SAMPLES FOR SOME LOCAL AND INTERNATIONAL ARRIVALS TO KARBALA GOVERNORATE DURING A RELIGIOUS VISIT**

**Zainab Abed Muhsin AL-HABOOBI**<sup>1</sup>

**Huda Dhafer AL-MARSOMY**<sup>2</sup>

**Haleema Salman SALIH**<sup>3</sup>

### **Abstract:**

Background: Every year in Karbala/ Iraq, millions of visitors (pilgrims) from different nationalities were meet, which give the possibility for the parasitic diseases to spread between them. Objective: The study of the pilgrims(Iraqi and non-Iraqi)-associated infections in Karbala during the period of invist. Subjects And Methods :A wet amount of smear were done for 567 patients severing from intestinal symptoms. Results: A high number of visitors were male in the age group below thirty .most patients were in the mild stage of the disease. Monilia was the comments infectious agent in both patients group( Iraqi and non -Iraqi ),Entameaba histolytica /E. dispar and Giardia lamblia was the common protozoal infection in Iraqi patients.In non-Iraqi Giardia lamblia had the high per centage than Iraqi type ,The mean age of the patients was 26.56 ±5.573 years and the age below thirty was the majority percentage (46%). A total of 198 males and 119 females were enrolled. . According to the governorate, results showed the highest numbers were from Babylon (17.4%)and the lower from Mathnaa governorate (3.5%) Conclusion: Through the results, it was found that the parasite Giardia lamblia appears in all cases is resistant to all climatic conditions, indifferent in time or place and that it is necessary to develop an effective measure to prevent the parasite transmission between the visitors. It appeared the presence of Diphylobothrium latum which does not live in our local atmosphere, and the intermediate host and carrier need a cold atmosphere. This is why its appearance in some arrivals from the Hilla area indicates a change in the presence of the host.

**Key words:** Protozoa, Helminth, Karbala, Iraq, Diphylobothrium latum, Giardia lamblia.



<http://dx.doi.org/10.47832/MinarCongress5-15>

<sup>1</sup> AL-Furat AL-Awsat Technical University, Iraq, [drzainababed2017@gmail.com](mailto:drzainababed2017@gmail.com), <https://orcid.org/0000-0002-3648-4524>

<sup>2</sup> Al-Nahrain University, Iraq, [Hudaalmarsome@yahoo.com](mailto:Hudaalmarsome@yahoo.com)

<sup>3</sup> Al-Nahrain University, Iraq, [ahlamlab@yahoo.com](mailto:ahlamlab@yahoo.com)



## **Introduction:**

One of the important medical problems in most developing countries is infection with intestinal parasites, as socio-economic conditions and malnutrition contribute to exacerbating this problem, despite the great development that has occurred in the quality of medical services in terms of diagnosing, treating, and controlling parasitic diseases, which led to a clear reduction in The spread of these diseases in many countries of the world, the various parasitic diseases are still a great challenge to health authorities in many developing and poor countries, The effect of geographical difference, population growth, and economic and health level of the countries of the world has a great impact on the spread of parasitic diseases to form part of the medical problems that have not yet been solved. Whereas, it's widespread not related to vector factors has a role in the ease of spreading these diseases under the influence of various climatic and environmental conditions such as temperature, humidity, and poor economic and social conditions such as poverty, lack of clean water supply, and low level of health services, attributed to the spread of these intestinal parasites and reduced the chances of combating or eliminating them(Al Saqur *et al*, 2017; Lansing & John, 2005)

Although there are many types of parasites that are very harmless, there are other types that cause serious damage and diseases, and the effects resulting from infection with intestinal parasites (acute and chronic diarrhea, anemia, colic, wasting, vomiting, poor growth, lethargy, some of the Parasites cause itching ,Parasites compete with their hosts for food, and this leads to a loss of appetite for the host, accompanied by a lack of food intake or an increase in the speed of the passage of food in the gut and this leads to a decrease in the rate of the host's use of food, withdrawal of fluids and consumption of the host's tissues, or the destruction of this tissue due to mechanical action due to Migration of parasites or their larval stages through the tissues or feeding of the parasite. This may be in the form of breaking down cells, blocking the transmission of food through the cell membrane, and blocking vessels and ducts such as the digestive channels. Into the bloodstream, causing changes in the blood, enzymes, and vitamins, Parasites may cause intestinal obstruction, as is the case in infection with *Ascaris* worms. The presence of large numbers of these worms is sufficient to close the intestine and kill the host or be less harmful as is the case in the tapeworm that feeds on digested food without causing tissue damage.( Despommier *et al* ,2017; Haghighi *et al*, 2009 ). Where there are many ways for the parasite to be transmitted between visitors, including the use of the same utensils for eating and the lack of tools to prevent the presence of the infected phase among contaminated hands after leaving health facilities, especially in the weak presence of water, sterilizers and lotion in some cases, the visitor's neglect of some hygiene conditions, as well as transmission through The use of shared bedding and the difficulty of changing sheets and tools, as well as drinking water sometimes that is not sterile

Karbala is the capital of Karbala Governorate in Central Iraq. Far from Baghdad about 100Km south east(Houghton, 2019).it is best Known as the location of shrines of Imam Husseyn and Abbas(holy please to Shi-ite Muslum).About 8 million pilgrims visited the city from the tenth day of Muharrum till the 10th of safar (the [Arba'in](#) )( Malise, 2006).

These visitors come from different nationality exposed them to new cultural and microbiological exposures and challenge and also, they may carried pathogens to areas of the world where these pathogens were rare or had been eliminated like malaria in Greece(Seif, 2015)

### **Methods:**

The study was conducted in the holy areas of Karbala on Yahasin Road, where random stool samples were taken from arrivals of all nationalities(foreigners and Iraqi) for both genders and ages for the year 2018.

**Study design:** A general stool examination was performed after taking stool samples in cups designated On the tube, the patient's name, age and gender are shown for collection, and the examination was done within a half-hour or one hour.

**Sample size :**246 samples were taken from foreign arrivals and 321 samples from Iraqi arrivals from different governorates of Iraq.

**Parasite methods:** All stool samples were collected between 9 and 10 am every morning and then transferred to the Parasite laboratory at AL-Furat AL-Awsat Technical University/ Karbala Technical Institute.

Samples were processed and microscopic examination by direct wet method as described by the World Health Organization (1991). All slides were examined by experienced laboratory technicians within 30-60 minutes of preparation.

**Data analysis:** Data were coded, entered, cleaned, and analyzed using SPSS to identify the parasites that appeared in the stool samples . Information about the gender, age and country of the arrival were recorded. ( Jejaw,2014)

### **General Stool Examination(GSE)**

Before preparing the fecal samples for direct examination, the consistency and shape of the stool were observed, and then determine whether the semi-solid consistency is in the form of watery or bloody diarrhea.

An appropriate amount of semi-solid stool or 2 drops of liquid stool were mixed with a drop of Lugol's iodine solution on the tip of a clean slide, and another portion of the same sample was mixed with normal saline on the second end of the slide, Samples examined under the strength 10x and 40X to check for the presence of intestinal parasites or some microscopic causes that can be diagnosed by microscopic examination Direct. ( Singh, 2009 )

### **Statistical analysis**

Statistical analysis of data was performed using SAS (Statistical Analysis System - version 9.1 The percentages were assessed using Chi-square test.  $P < 0.05$  is considered statistically significant.

## Results

In this study, the wet amount smear was dependent for diagnosis because it is easy, fast, not costly and it method depended on the routine work in Iraqi hospitals.

Results for Iraqi patients:

The mean age of the patients was  $26.56 \pm 5.573$  years and the age below thirty was the majority percentage (46%). A total of 198 males and 119 females were enrolled. . According to the governorate, results showed the highest numbers were from Babylon (17.4%) and the lower from Mathnaa governorate (3.5%)(Table1,2).

In stools examination the appearance of Red Blood cells and Pus cells are parameters detection for infection stage (acute or chronic), the result of this study appeared 36.3% of the patients had a mild stage of infection, 34.1% had Pus cell and 10.4% had a normal with a low present of pus cells (Table 3) while Table 4 which appears 1.5% of samples were infection with helminth and 35.5% infected with the protozoa parasite.

General Stool sample result demonstrates the presence of Monellia (51.7%), Food drops (6.6%), and bacteria (2.5%), also, parasitic infection were detected, (Table 5). The highest number of Protozoal infections was *Entameoba histolotica/E.dispar* (16.7%) and *Giardia lamblia* (15.1%), both in trophozoite, Helminthic infection was *Ascaris lumbricoid* and *Diphylobothirum latum*, both parasites in the eggs stage (Tables 5).

According to Iraqi governorates, demonstrate the high number of Amebiasis and Giardiasis were in Najafe followed by Karbala which appeared in (Table 6). the examination of stool in the study sample detected Ascariasis, one from Karbala and the other from Babylon.

Table 1: Age groups and sex Distributions in Iraqi visitors.

		No	Percentages
<b>Age groups</b>	<b>=&lt;25</b>	133	41.9%
	<b>26-30</b>	146	46%
	<b>31-35</b>	16	5%
	<b>&gt;35</b>	22	6.9%
	<b>P-value</b>		<0.0001
<b>Gender</b>	<b>Male</b>	198	62.4%
	<b>Female</b>	119	37.6%
	<b>Total</b>		<0.0001

Table 2: Iraqi visitors frequency according to the governorate.

Governorate	Frequency	Percent	
Baghdad	55	17.4%	
Basra	29	9.1%	
Diwaniya	15	4.7%	
Najaf	59	18.6%	
Babylon	65	20.5%	
Mathnaa	11	3.5%	
Karbla	59	18.6%	
Thi-Qar	24	7.6%	
P-value		<0.0001	

Table 3: Red Blood Cell and Pus Cell Frequency in Iraqi Patients.

	Red Blood Cell		Pus Cell	
	N=317	Percent	No	Percent
Normal	33	10.4	18	5.7%
Mailed	115	36.3	108	34.1%
Moderate	59	18.6	86	27.1%
Sever	110	34.7	105	33.1%
P-value		<0.0001		<0.0001

Table 4: Frequency of Parasite infection among the Iraqi patients

	No	Percentage
Helminth	5	1.5%
Protozoa	114	35.9%
Other	198	62.6%
P-value		<0.0001

Table 5: Frequency of Parasite according to the types infection among the Iraqi patients.

	Parasite	No	Percent
Helminth	<i>Ascaris lumbricoides</i>	2	0.6
	<i>Strongyloid stercoralis</i>	1	.3
	<i>Diphylobotharium latum</i>	2	.6
Protozoa	<i>Giardia lamblia</i> ,cyst	2	.6
	<i>Giardia lamblia</i> , Trophozoite	48	15.1
	<i>Entamoeba histolytica</i> , cyst	5	1.6
	<i>Entamoeba histolytica</i> , Trophozoite	53	16.7
	<i>Trichomonas hominas</i>	6	1.9
	Porozonan	5	1.6
	Food droops	21	6.6
	Bacteria	8	2.5
	Monellia	164	51.7

Table 6: Parasite distribution according to the Iraqi governorate.

Parasite												
	<i>A. lumbricoide s</i>	<i>S.stercoralis</i>	<i>D. latum</i>	<i>G.lambli a, cyst</i>	<i>G.lambli a. Trophozoite</i>	<i>E..cyst</i>	<i>E.histolytica, Trophozoite</i>	<i>T.homin as</i>	Porozon an	Food droops	Bacter ia	Moneli a
	Count	Count	Count	Count	Count	Count	Count	Count	Count	Count	Count	Count
Baghdad	0	1	0	0	8	1	6	2	2	6	0	29
Basrah	0	0	0	0	4	0	5	1	1	3	1	14
Diwaniya	0	0	0	0	5	0	2	0	0	0	0	8
Najaf	0	0	0	1	9	3	14	0	0	2	4	26
Babylon	1	0	1	1	10	1	13	0	0	4	2	32
Mathnaa	0	0	0	0	0	0	2	0	1	0	0	8
Karbla	1	0	0	0	8	0	8	1	1	4	1	34
Thi-Qar	0	0	0	0	4	0	3	2	0	2	0	13

**Results of Non-Iraqi Patients** The mean age was  $24.31 \pm 0.473$  years, the lower age was 12 years and the maximum was 45 years. The ratio of Male to female was 3:1,(145 and 46 respectively) which appeared in (Table 7) and Age below thirty had the highest percentage (52.4% ) and the .lower age group above 40 years and in percentage (1.6%).

One hundred -thirty of the patients were from Iran (68.1%), while 34 in percentage (17.8%) from Lebanon. Others were from India (11.5%), Afghanistan (1.6%) , Pakistan(1%) (Table 8) . The frequency of RBC in the stool samples of the patients was normal in 126 (66%) , 35(18.3%) severe ,29 (15.2%) mild case, and only one had moderate frequency (Table 9). Table 9, showing the frequency of pus cell,113(59.2%) had severe range and only 2 had normal range.

Most of the patients had Diarrhea and abdominal cramps by examining their feces, 92(48.2%) was Monilia,44(23%) Fat drop, Only 13 (6.8%) had Parasitic infection with *G. lamblia*(Both Trophozoite and cyst were percent), and 41(21.5%) had infectious agents . (Table 10) .

Sixty-two of Manila patients had normal RBC, in only 7 patients infected with Giardiasis no RBC in stool examination , other range between mailed and severe. Also, a severe count of pus cells observed on patients with Monilia, In Giardiasis only 9 had severe counts (Table11).

According to age groups, under thirty had a high number of monilia, parasitic infections 47,6 %.In comparison with women, men had a high number of infections with monilia, fat drops, giardiasis, and non-infection patients.

in Iranian, a high number of Giardiasis were patients(8/13), Lebanon(3/13), and two from India. In Monilia infection and Fat drops, the seem disruption was recorded. Afghans had only 3 patients with monilia. which appears in (Table 12).

Results revealed that there is a significant ( $P < 0.0001$ ) relationship between the type of parasite and age category as the age group 21-30 years showed the highest infection by monilia (51%). Concerning the relationship between the type of parasite

and sex results also illustrated the significant ( $P=0.4$ ) relationship between them as men showed the highest percentages (Table 12).

Table 7: Age ,sex and other variables Frequency in Non-Iraqi visitors

Group		No	Percent
Age/year	=<20	65	34.0%
	21-30	100	52.4%
	31-40	23	12.0%
	>40	3	1.6%
P-value			<0.0001
		Frequency	Percent
Gender	Man	145	75.9
	Women	46	24.1
P-value			<0.0001

Table 8 :Non- Iraqi patients frequency according to their country.

Country	No	Percent
Afghanistan	3	1.6%
India	22	11.5%
Iran	130	68.1%
Pakistan	2	1.0%
Lebanon	34	17.8%
P-value		<0.0001

Table 9: Red Blood Cell and Pus Cell Frequency in Non- Iraqi Patients.

RBC			Pus cells	
	No	Percent	No	Percent
Normal	126	66.0	2	1.0%
maild	29	15.2	40	20.9%
moderat	1	0.5	36	18.8%
sever	35	18.3	113	59.2%
P-value		<0.0001		<0.0001

Table 10: Frequency of Parasite infection among the Non-Iraqi patient .

Parasite		No	Percent
Valid	Nil	41	21.5%
	<i>G.Lambli</i> a	13	6.8%
	Monila	92	48.2%
	Fat drop	44	23.0%
	Vab	1	0.5%
P-value			<0.0001

Table 11: Frequency of RBC and Pus Cell with infectious agents in Non-Iraqi patients

Infectious agents	RBC				Pus cells			
	Normal	Maild	moderat	sever	Normal	maild	moderat	sever
	Count	Count	Count	Count	Count	Count	Count	Count
Nil	26	10	1	4	1	7	6	27
<i>G.Lambli</i> a	7	3	0	3	0	3	1	9
Monilai	62	7	0	23	1	22	20	49
Fatdrop	30	9	0	5	0	8	9	27
Vab	1	0	0	0	0	0	0	1

Table 12: The No. of Parasitic infection according to the age ,gender and country.

		Nil	G.Lambli a	Monilai	Fatdrop	Vab	
		Count	Count	Count	Count	Count	<0.000 1
		Age groups	=<20	8(12.3%)	3(8.4%)	34(52.3%)	20(30.7%)
	21-30	28(28%)	6(6%)	47(47%)	19(19%)	0(0%)	
	31-40	4(17.3%)	3(13%)	11(47.8%)	5(21.7%)	0(0%)	
	>40	1(33.3%)	1(33.3%)	0(0%)	0(0%)	1(33.3%)	
Gender	Man	25(17%)	9(6.2%)	71(49%)	39(26.8%)	1(0.6%)	0.04
	Wome n	16(34.7%)	4(8.6%)	21(45.6%)	5(10%)	0(0%)	
Country	Afghan istan	0(0%)	0(0%)	3(100%)	0(0%)	0(0%)	<0.000 1
	India	2(9%)	2(9%)	12(54.5%)	6(27.2%)	0(9%)	
	Irian	31(23%)	8(6%)	58(44.6%)	32(24.6%)	1(0.7%)	
	Pakista n	0(0%)	0(0%)	1(50%)	1(50%)	0(0%)	
	Leban on	8(23.5%)	3(8.8%)	18(52.9%)	5(14.7%)	0(0%)	



### **Discussion:-**

Every year there are several religious occasions in Karbala city /Iraq, especially the forty visits of the martyrdom of Imam Hussein (Grandson of the Muslim Prophet Muhammad), peace be upon him. People from all parts of the world are coming to Iraq to meet so that people of all religions and genders mix together. To the best of our knowledge, this is one of the few studies conducted in Iraqi and non-Iraqi visitors to determine the common pathogens causing Abdominal symptoms.

The difference in numbers between sex and age groups is due to the difficulty in obtaining samples from the arrivals, as well as that walking on foot requires effort, so we find the percentage of females is less than males. The study also clarified that the age group of all arrivals From all countries of the world and Iraq, were among the youth (under the age of thirty) and this agreed with what AL-Khikani1 *et al.*(2019) and Al-Zubaidi *et al.*(2020).

The study also showed that most of the arrivals are from neighboring countries, where the infection rate was distributed among countries (Iran, Lebanon, India, Afghanistan, and Pakistan) respectively, as stool samples showed that most of the infections were Monilia, intestinal fungi in diarrhea in humans, especially when Traveling and eating food from different environments and water from different sources, the study found some cases coincided with infection with the Giardia lamblia parasite, which is one of the endemic parasites in all parts of the world, as it was in all stages in that in the acute and chronic phase, Since this parasite has the ability to adapt in all regions with climatic conditions, the statistics of many researchers that agreed with our research in these countries confirmed the Endemicity of this parasite in these countries, including in Iran Rafiei *et al* (2020). As for India, the researcher confirmed India Ira Praharaj *et al* (2017), Lebanon Araj *et al*, (2011), and researcher Youssef and his group (2018) from Pakistan. The age group most at risk is less than 30 years old, as it has been associated with an increase in the number of red blood cells associated with it in conjunction with the presence of fungi may, this because of the low awareness of personal hygiene.

As giardiasis causes diarrhea and malabsorption, and symptoms can appear in the absence of any major morphological injury to the intestinal mucosa. It affects the permeability of the epithelium in vivo. Some research has confirmed Giardia spp. Alter gut permeability in vivo. These T cell-dependent abnormalities (Scott *et al*, 2002; Lass *et al*, 2017).

In the study, some single infections appeared in one of the arrivals from Babil governorate, with a parasite that does not live in our areas due to the loss of the secondary host, which is the most popular aquatic crustaceans to be an adult worm and with the potential for climate change, it made the Fusarium species appear in the region, so it needs an in-depth study.

### **Conclusion:**

A high number of visitors were male in the age group below thirty .most patients were in the mild stage of the disease. Monilia was the comments infectious agent in both patients groups ( Iraqi and non -Iraqi ). *Entameaba histolytica* /*E. dispar* and *Giardia lamblia* was the common protozoal infection in Iraqi patients,

while in non-Iraqi *Giardia lamblia* had the high percent .and The research also showed the emergence of a case of infection with the parasite *Diphylobotharium latum*, which is one of the tapeworms transmitted by the second intermediate host through marine fish among the examinees from Babylon Governorate, and this is a dangerous indicator.

The presence of an infection resulting either from imported meat or an adaptation and the appearance of the carrier host in the region in the local waters, and this needs research and study.

## References:

- Al Saqur I M, Al-Warid HS, and Albahadely HS.(2017) The prevalence of some gastrointestinal nematodes and cestodes in Iraqis, *Asian Biomedicine*10 (1),61-66,DOI: <https://doi.org/10.5372/1905-7415.1001.466>
- AL-Khikani F H O, Almosawey HAS, Hameed RM; Abid alhussain BAA, Ayit AS, Mirdan MK, Al-Ibraheemi, Alsalami MMAY(2019) Prevalence of Entamoeba histolytica and Giardia lamblia Associated with Infectious Diarrhea in Al-Shomally Population, Babil, Iraq , *BBRJ* 3(4),245-248.
- Al-Zubaidi Hanan Abbas Majeed ; Zainab Abed Muhsin AL-Haboob I ; Shaima Abd Muhsin AL-Haboobi(2020) Epidemiological study on some endemic parasitic diseases to know the efficiency of the health system in the holy province of Karbala, *Int. J. Res. Pharm. Sci* 11(3), 4195-4200 .
- Araj ,Georg F; Umayya M Musharrafi; Ayat Haydar, Amal Ghawi; Raja Itani; Ramez Saliba(2011) Trends and prevalence of intestinal parasites at a tertiary care center in Lebanon over a decade,*J Med Liban* Jul-Sep 59(3),143-8.
- Despommier,Dickson D.; Daniel O. Griffin; Robert W. Gwadz; Peter J. Hotez ; Charles A. Knirsch(2017) Parasitic Disease (6<sup>th</sup> edition) Parasites . Springer-Verlag, New York, Inc. Parasites Without Borders, Inc. NY Printing by Sentinel Printing, 250 North Highway 10, St. Cloud, MN 65302. DOI: 10.4103/ijmr.IJMR\_1236\_14.
- Haghighi A, Khorashad AS, Nazemalhosseini Mojarad E, *et al.*(2009) Frequency of enteric protozoan parasites among patients with gastrointestinal complaints in medical centers of Zahedan, *Iran Trans R Soc Trop Med Hyg.* May;103(5),452- 4. DOI: 10.1016/j.trstmh.2008.11.004.
- Houghton Mifflin Harcourt (2019) "Karbala". The American Heritage Dictionary of the English Language (5th ed.). Boston:. Retrieved 30 July 2019.
- Ira Praharaj; Rajiv Sarkar; Sitara Swarna Rao Ajjampur; Sheela Roy; Gagandeep Kang(2017)Temporal trends of intestinal parasites in patients attending a tertiary care hospital in south India: A seven-year retrospective analysis, *Indian J Med Res.* 146(1),111-120.
- Jejaw A, Zeynudin A, Zemene E, Belay T. (2014) Status of intestinal parasitic infections among residents of Jimma Town, Ethiopia. *BMC Res Notes* 7:502. doi:10.1186/1756-0500-7-502.
- Lansing, M. P.; John, P. H. (2005). Text book of Microbiology. (human diseases caused by Fungial protozoa). 6th ed. 12: 926-930.
- Lass ,Anna ; Panagiotis Karanis ; Krzysztof Korzeniewski (2017) First detection and genotyping of Giardia intestinalis in stool samples collected from children in Ghazni Province, eastern Afghanistan and evaluation of the PCR assay in formalin-fixed specimens, *Parasitol Res* ,2017 Aug;116(8),2255-2264.
- Malise Ruthven (2006) Islam in the World. Oxford University Press. p. 180. ISBN 9780195305036.
- Rafiei,Abdollah; Raheleh Baghlaninezhad; Pamela C. Koester<sup>3</sup> , Begoña Bailo; Marta Hernández de Mingo; David CarmenaID ; Esmat Panabad; Molouk BeirromvandID (2020)Multilocus genotyping of *Giardia duodenalis* in

- Southwestern Iran. A community survey, *PLOS ONE* | <https://doi.org/10.1371/journal.pone.0228317> February 6, 2020.
- SAS.2010.SAS/STAT Users Guide for Personal Computer. Release 9.1..SAS Institute, Inc., Cary, N.C., USA.
- Scott ,Kevin G-E ; Jonathon B Meddings, David R Kirk, Susan P Lees-Miller, André G Buret(2002) Intestinal infection with *Giardia spp.* reduces epithelial barrier function in a myosin light chain kinase-dependent fashion PMID: 12360480 *Gastroenterology* 123(4):1179-90
- Seif S. Al-Abri , Doaa M. Abdel-Hady , Salem S. Al Mahrooqi , Hanan S. Al-Kindi , Amina K. Al-Jardani , Idris S. Al-Abaidani (2015) Epidemiology of travel-associated infections in Oman 1999-2013: A retrospective analysis. *Travel Medicine and Infectious Disease* 13, 388-393.
- Singh, A. ; Ericctouft, B.H and Willim, A.C.(2009) Rapid diagnosis of intestinal parasitic protozoa. *J. infect. Dis.*,61 (3),280-286 .
- Yousaf ,Muhammad; Sadullah Jan; Muhammad Shafee; Abdul Samad1, Muhammad Barkhurdar; Farah Sabeen Bugti; Tabeel Tariq; Saima; Roomeela; Sundus Saifullah; Waseem Akhtar; Shafiq Ahmed(2018) Prevalence of *Giardia lamblia* in stool samples of diarrhea patients in Quetta, Pakistan , *International Journal of Biosciences | IJB* | 12( 3), 106-111 .

# **LIGHTWEIGHT IMAGE COMPRESSION USING POLYNOMIAL AND TRANSFORM CODING**

**ZAINAB J. AHMED  
LOAY E. GEORGE**

## LIGHTWEIGHT IMAGE COMPRESSION USING POLYNOMIAL AND TRANSFORM CODING

Zainab J. AHMED <sup>1</sup>

Loay E. GEORGE <sup>2</sup>

### Abstract:

This article implies a proposal for a lossy compression system using polynomial coding with color and gray images. The proposed system contains two main parts: coding and decoding. In the coding, each block of the image is represented as a two-dimensional quadratic polynomial to prune the main low variation component to get better compression gain. The size of each image block is variable depending on quadtree partitioning. Then, the signal residue of the polynomial representation (i.e., the residue is the component produced due to subtraction of polynomial from the original image); then the polynomial coefficients and the residue are encoded, separately in different manners. The transformation coding (i.e., Discrete Cosine transform or bi-Orthogonal Wavelet transform) is used to compress the residual component of each band. The applied transform on the residue band can map the values more compactly. Also, uniform quantization is applied to the residue to effectively reduce the number of consumed bits required to represent the residue. Various encoding operations are performed to encode the polynomial coefficients. Finally, the all-out output is compressed using an LZW encoder. The results of the conducted test indicated that the introduced structure is lightweight and its implementation is straightforward. Besides that, it can lead to high compression ratios with an acceptable fidelity tolerance. The results are comparable to those of the current study and it has made progress.

**Key words:** Image Compression, Polynomial Representation, Transform Coding, Uniform Quantization, LZW.



<http://dx.doi.org/10.47832/MinarCongress5-16>



<sup>1</sup> University of Baghdad, Iraq, [zainabjahmed83@gmail.com](mailto:zainabjahmed83@gmail.com); <https://orcid.org/0000-0001-7403-2134>



<sup>2</sup> University of Information Technology and Communications, Iraq, [loayedwar57@uoitc.edu.iq](mailto:loayedwar57@uoitc.edu.iq), <https://orcid.org/0000-0001-9028-0816>

**Introduction:**

In the past recent years, the topic of digital image processing and the applications of these images has become the focus of modern and important research due to the increasing need for this type of application [1]. Image compression is essential for the effective transmission and storage of image data. As a result of the surge in the number of images and multimedia data, network bandwidth and storage of storage devices have become inadequate. Therefore, the image data should be compressed with little or no loss of quality. The compression techniques used work to reduce the number of bits needed to represent images. These time-frequency-based compression techniques have the characteristics of multi-scale description, thus resulting in high-quality image reconstruction [2]. Currently, Joint Photographic Experts Group (JPEG) and JPEG 2000 are the main compression algorithms for still images. JPEG is the first commonly accepted compression standard for black and white and color images [3]. The core algorithm of JPEG is the conversion coding of the Discrete Cosine Transform (DCT). In the JPEG algorithm, the image is first divided into non-overlapping blocks, and then each block is processed by a 2D DCT. The transformed coefficients are uncorrelated and the energy of the coefficient matrix is concentrated in the low-frequency range [4]. The well-known JPEG 2000 compression algorithm uses a discrete waveform transformation that splits the image into a small number of tiles. Then these Wavelet transformations are performed on each tile separately to improve the quality of the reconstructed image. However, the problem that restricts the work of this technique is that increasing the number of tiles will have an aliasing effect [5].

Some compression algorithms use wavelets and DCT. A hybrid method using discrete cosine transform (DCT) and discrete wave transform (DWT) is presented. This project presented assessment and comparison results of DCT, DWT, and Hybrid (i.e.; DWT DCT) compression technologies. The results of the work showed that DWT using a two-threshold method called "improved DWT" gives excellent image quality compared to DCT and DWT and using a single threshold method. Lastly, it has been shown that when combining the two technologies (i.e.; DWT DCT), has been shown to outperform DCT in terms of image quality [6]. This study showed DCT, DWT, and hybrid applications as a fusion of both previous transformations in the process of digital image data compression. From the experimental results, it can be seen that the compression ratio increases when DWT is used. This means that using the DWT method results in less compression. Better images got by using the DCT method [7]. The Daubechies wavelet filter is used to segment the image into low and high-frequency sub-bands, and then a 1st-degree quantization is applied to these sub-bands. Low-frequency sub-bands are compressed by using fractional Fourier resampling with perfect fractional transform, and high-frequency sub-bands are compressed by removing zeros and keeping non-zero blocks with their positions only. The compressed wavelet coefficients are compressed by a degree 2 quantization and stored as a reduced array. This array is encoded by the use of a mathematical encoder observed by the run-length encoder. The results of this work with different sets of test images compared to several current image compression algorithms. The results showed that the proposed work led to obtaining high quality in image reconstruction [5].

The main objective of the work was to test image compression systems that rely on polynomial and transformation techniques to transfer and store data with high efficiency while providing the right and appropriate compromise between compression ratio and signal-to-noise ratio with maintaining the visual quality of the reconstructed image as close as possible. This project focuses on (1) the introduction of a compressed image scheme based on linear polynomial approximation with variables partitioning using a quadtree. A polynomial is applied to each band to decrease the number of data elements in the image block to some coefficients. Then the output is subtracted and the residue components are retrieved; (2) decompose the residual components of the image signal using the biorthogonal wavelet transform or the discrete cosine transform (DCT). The reason for using transformation coding is the required low computational power to implement it. (3) Introducing LZW for processing residue and coefficients. LZW is used because of its simplicity; it allows for quick execution and can compress the input stream with a single pass. (4) Comparing the results of compression system of DCT and wavelet and explain the effect of using polynomials on work.

### Image Compression System

The essential attention of the suggested work system is:

- Demonstrates the effectiveness of the extended approximate second-order polynomial model in image compression compared to the first-order polynomial model.
- Fully utilize spatial redundancy (i.e.; correlation) with 6 coefficients ( $a_0, a_1, a_2, a_3, a_4, a_5$ ) for 2<sup>nd</sup> order polynomial compared to the linear model, that's using 3 coefficients ( $a_0, a_1, a_2$ ).

As with all common image coding methods, the deployed framework be composed of two different entities: (i) image compressor utilized to compress true color still images with little self-distortion, and (ii) image decompressor (reconstruct image) utilized to recover the original image. The next section explains the design phase of each unit. As illustrated in Figure 1, the first entity is the encoding unit that consists of the following phases:

**A. Loading image information:** First, the input original image is loaded in bitmap form and the image information is obtained. The data of the loaded image is decomposed into basic components (RGB). While for gray images, the data of the loaded image is saved into a gray 2D array.

**B. Color Transform:** For color images, it reduces redundancy between color components (R, G, B) by converting them to less correlated color space components (such as YUV).

**C. Quadtree Partitioning:** A quadtree is a data structure such as a tree, each node in this tree finish with a leaf of practical information or sometimes branch into four dependent quadtrees [2]. Quadtrees are hierarchical divisions and can be seen as the first step in overcoming the weaknesses of fixed-size divisions. This means that there are areas in the image that are difficult to cover well this way [8]. Each image band is partitioned using a quadtree partitioning scheme with starting depth blocks (Blk) such as (16x16) or (14x14) etc., and in case the image dimensions are not multiples of the start depth of



quadtree then the remaining blocks are handled using padding extension with the starting depth blocks that reduced by half ( $8 \times 8$ ) or ( $7 \times 7$ ).

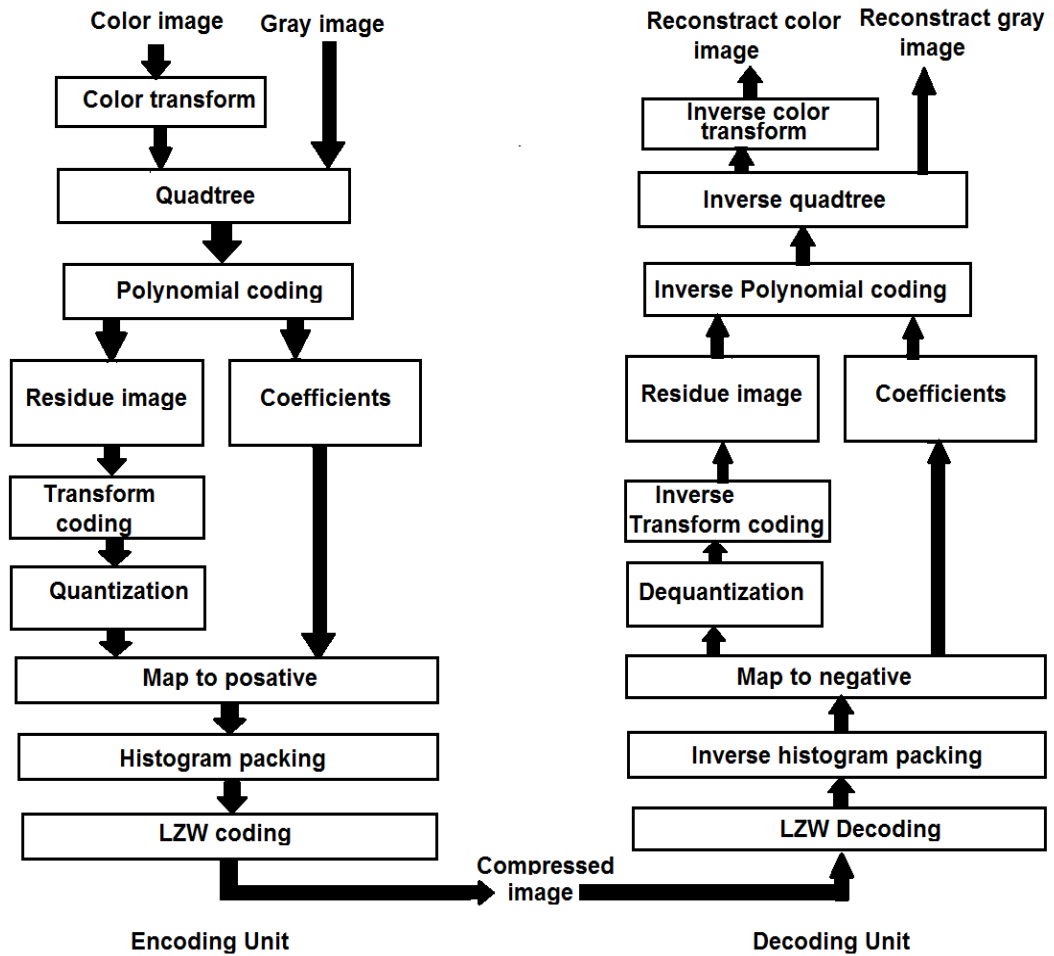


Figure (1) System layout

**D. Polynomial Coding:** Polynomial approximation is used to reduce the spatially slow variation component assigned to the image data [9]. The polynomial signal represents the smooth part of the original signal, the residue represents the fluctuations and spikes present in the original signal. High compression ratios can be achieved by using polynomials to describe the smooth parts of the signal. Calculate the second-order polynomial coefficients for each block according to equations [10, 11].

$$a_0 = \frac{1}{S} [TS_g + U(S_{gx} + S_{gy})] \quad (1)$$

$$a_1 = \frac{1}{p} \sum_{y=0}^{L-1} \sum_{x=0}^{L-1} B(x, y)(x - c) \quad (2)$$

$$a_2 = \frac{1}{p} \sum_{y=0}^{L-1} \sum_{x=0}^{L-1} B(x, y)(y - c) \quad (3)$$

$$a_3 = \frac{1}{S} [US_g + VS_{gx} + ZS_{gy}] \quad (4)$$

$$a_4 = \frac{1}{S} [US_g + ZS_{gx} + VS_{gy}] \quad (5)$$

$$a_5 = \frac{1}{R} \sum_{y=0}^{L-1} \sum_{x=0}^{L-1} B(x, y)(x - c)(y - c) \quad (6)$$

Where,

$$c = \frac{L - 1}{2} \quad (7)$$

$$S = L^2(Q^2 + R^2) + 2P^2(R - Q) \quad (8)$$

$$P = \sum_{y=0}^{L-1} \sum_{x=0}^{L-1} (x - c)^2 \quad (9)$$

$$P = \sum_{y=0}^{L-1} \sum_{x=0}^{L-1} (x - c)^4 \quad (10)$$

$$T = Q^2 + R^2 \quad (11)$$

$$U = P(R - T) \quad (12)$$

$$V = L^2Q + P^2 \quad (13)$$

$$Z = P^2 - L^2R \quad (14)$$

$$S_g = \sum_{y=0}^{L-1} \sum_{x=0}^{L-1} B(x, y) \quad (15)$$

$$S_{gx} = \sum_{y=0}^{L-1} \sum_{x=0}^{L-1} B(x, y)(x - c)^2 \quad (16)$$

$$S_{gy} = \sum_{y=0}^{L-1} \sum_{x=0}^{L-1} B(x, y)(y - c)^2 \quad (17)$$

Where:  $B(x, y)$  array is the original input value of each block;  $L$  is the width block and height block.

Uniform scalar quantization is used to quantize the specified polynomial coefficients to obtain the compression gain.

$$b_k = \text{round} \left( \frac{a_k}{q_k} \right) \rightarrow \widetilde{a}_k = b_k \times q_k \quad (18)$$

Where  $k=0, 1, \dots, 5$

$a_k$  is the polynomial coefficient ( $k^{\text{th}}$ ),  $q_k$  is the specified quantization step ( $k^{\text{th}}$ ),  $b_k$  is the specified  $k^{\text{th}}$  quantization step-index, and  $\widetilde{a}_k$  is the dequantized quantity of the specified  $k^{\text{th}}$  polynomial coefficient. Use the unquantized polynomial coefficients represented by each coding block to create a predicted image  $\widetilde{G}$ :

$$\widetilde{G} = \widetilde{a}_0 + \widetilde{a}_1 \widetilde{x} + \widetilde{a}_2 \widetilde{y} + \widetilde{a}_3 \widetilde{x}^2 + \widetilde{a}_4 \widetilde{y}^2 + \widetilde{a}_5 \widetilde{x} \widetilde{y} \quad (19)$$

$$\widetilde{x} = (x - c) \quad (20)$$

$$\widetilde{y} = (y - c) \quad (21)$$

To maintain image quality, errors are formed as a result of polynomial approximation, and these errors will not be neglected. This is called residue (Res) and is specified using the difference between the original image band and the predicted band generated in the previous step and determined using the following equation:

$$\text{Res}(x, y) = G(x, y) - \widetilde{G}(x, y) \quad (22)$$

Where, Res ( $x, y$ ) is the residual value at ( $x, y$ ); and  $G(x, y)$  is the input image.

The residue goes through several stages before the process of compressing the data, and these stages are:

**1. Transform coding:** Use the transform coding (DCT or Biorthogonal wavelet transform) to decompose the residue component.

- **DCT (Discrete Cosine Transform):** Use the well-known DCT transform [12] for all block entries to determine the importance of the block (i.e., high, low & middle-frequency components) divided into parts. Where the size of these parts depends on the size used in the quadtree mechanism. In this step, the DCT is applied on residual parts only.

- **Bio-orthogonal tap 9/7 wavelet transform:** The wavelet transform is widely accepted, especially in the study of image compression. Wavelets have also been selected as a basic feature of JPEG 2000 and one of the most important processing elements of image compression is the wavelet transforms [13]. The bio-orthogonal tap 9/7 wavelet filters are implemented only on residual parts in unrelated methods. Each residue color band data will decompose to the four subbands by using this transform (LL, LH, HL, and HH).

**2. Quantization:** To do this, divide each element in the frequency domain by the fixed of this element and then round to the close integer. This is the most important lossy process in the compression system. As a result, many of the high-frequency components are usually rounded to zero, and many of the

remaining components are small numbers [14]. Scalar quantization is applied to the transform coding (DCT subband or wavelet subband) generator.

As a result of the distinguished significance of the DCT coefficients, uniformed scalar quantization had been calculated by applying the equation [15]:

$$C(u) = \alpha(u) \sum_{i=0}^{N-1} s(i) \cos\left(\frac{u\pi(2i+1)}{2N}\right) \quad (23)$$

$$\alpha(u) = \begin{cases} \sqrt{1/N} & \text{if } u = 0 \\ \sqrt{2/N} & \text{if } u \neq 0 \end{cases} \quad (24)$$

Where  $u=0.., N-1$ .  $C(u)$  is the  $u^{\text{th}}$  coefficient of the DCT and  $s(i)$  is the amount of the input data signal in the time domain.

Hierarchical uniform quantization is utilized to quantize all the coefficients of wavelet subband and the quantization step was calculated by applying the equation [16]:

$$Q_{stp}(n) = \begin{cases} Q_0 & \text{for LL in } n^{\text{th}} \\ Q_1 \alpha^{n-1} & \text{for LH, HL in } n^{\text{th}} \\ Q_1 \beta \alpha^{n-1} & \text{for HH in } n^{\text{th}} \end{cases} \quad (25)$$

**E. Differential Pulse Code Modulation (DPCM):** The principle of DPCM coding is to make numerical predictions of the signal to be coded. The difference between each sample and its respective estimate is encoded. Predictive coding theory consists of predicting the value of a sample signal and coding the prediction error [17]. This process is only performed to reduce the value of  $A_0$  by executing the following equation [18]:

$$\text{DPCM}(A_0) = \text{DCM}(a_0 + 1) - \text{DCM}(a_0) \quad (26)$$

**F. Mapping:** The mapping process is needed to avoid the coding complexity of converting negative values to positive numbers, removing negative signs, and storing these numbers. This is done simply by mapping all negative values to positive odds and positive values to even. The numbers shown are generated by applying the following equations to the residuals and coefficients [19].

$$\text{Map}(x, y) = \begin{cases} 2P & \text{if } P \geq 0 \\ 2|P| - 1 & \text{if } P < 0 \end{cases} \quad (27)$$

**H. Histogram Packing:** Because the histogram of mapped elements values. This long tail is very unlikely to occur but is caused by the presence of large element values. These long tails cause a significant decrease in compression gain when entropy coding is applied. Therefore, to address this issue, packing (that is, reduction) is applied to the histogram of residual and polynomial coefficients.

**I. LZW (Lempel-Ziv-Welch):** The lossless image compression technology is Lempel Ziv Welch (LZW). This is a dictionary-based compression algorithm. Search the entire file for strings that appear multiple times. These sequences are stored in the created dictionary. References are stored where the repeated

data occurs. LZW compression replaces strings with individual codes. The length of the code output by the LZW algorithm is arbitrary, but it must contain more than one bit.

- Step 1: The dictionary will start to make the length of all input strings as one.
- Step 2: Use the dictionary to identify the longest string of the current input symbol.
- Step 3: Dictionary index. This string will be deleted from the input sequence and will be released for output.
- Step 4: The same thing does for all input symbols until reaching the end [20].

This compression method is used to compress the residue with the coefficients together.

The second entity in the deployed framework is the image decompressor (reconstruct image) utilized to recover the original image, beginning with the LZW decoding process, then, stratifying the same stages applied in the image compressor in reverse order. Figure (1) indicates the steps for reconstructing the image.

## Results



Two types of images were used to test the results; grayscale and color image. These images are in "bitmap" format, where all pixels are stored in 24-bit true color, except for Lena Gray 8-bit. The test image characteristics have shown in table (1). Table (2) shows the control parameters to be considered, including the name of these parameters with their ranges. The effects of the following control parameters were investigated. The test was run using the following devices: the operating system is Windows 10, Dell laptop computer (processor: Intel (R) Core (TM) i74600U, CPU=2.10 GHz, RAM=4GB). C # programming language was used to implement the proposed scheme. The test results are scored using the fidelity criteria (PSNR) and compression performance (CR).

Table (3) shows the best results in terms of compression ratio and accuracy of all samples using the two transformations. Comparing the results in this table it is noted, the compression results are good and the DCT shows better compression results than the wavelet transform. The table also shows the images reconstructed after the compression and decompression process. This table shows that the image was returned while maintaining accuracy. Also, in the same table, there is a comparison of time (in seconds) for compression and decompression between wavelet and DCT transformation. The results presented in this table show that the use of wavelet transform takes less time in encoding and decoding because it has less complexity than DCT transform. Figure (2) shows the influence of the control parameters described in Table (2), performance measures: CR and PSNR have been studied at various values using Lena-image. The results proved that increasing these parameters ( $Q_{stp}$ ,  $Q_0$ ,  $Q_1$ , Alpha, Beta,  $N_{pass}$ , and Blk) tends to increase the CR and decrease the PSNR of the acquired images.

A comparison was made between a polynomial of the first order and the second-order; as depicted in Figure 3. It indicates that the use of second-order outperformed the first order and produced better results. Also in Figure 4, there is a

comparison between using a polynomial and not using it, and as it appears from the figure that the polynomial has a significant impact on improving the results in both types of transformation. In Figure 5 a comparison was made between the RGB and YUV color space and seeing which color space provides the best results, and from this figure, YUV color space showed progress in results and gave better values in terms of CR and PSNR on the recovered image. This scheme compared with the results of using the standard JPEG methods in Table (4). Compared to the JPEG compression method, it is noted that the compression result of the method used is very good.

**Table 1. The characteristics of the tested standard images**

Image Sample	Bit depth	Dimensions	Size (KB)	Original image
Lena	24	256×256	192	
Pepper	24	256×256	192	
Girl	24	256×256	192	
Child	24	256×256	192	
Barbara	24	256×256	192	
House	24	256×256	192	
Lena-Gray	8	256×256	66	

**Table 2. Control parameter ranges**


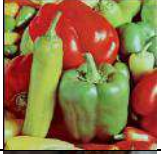





Notation	Description	Range	Scope of Effects
$Q_{stp}$	Quantization step for polynomial coefficients	{1,1.5,2,2.5,3}	DCT and Wavelet
$Q_0$	The quantization step for DC coefficients	The size depends on the block size (Blk) used in the quadtree mechanism	DCT Wavelet
$Q_1$	The quantization step for AC coefficients	{2,3,...,20}	DCT
		{15, 16,...,30}	Wavelet
Alpha	The scaling factor for AC coefficients	{0.1, 0.2,..., 1.1}	DCT
		{1,2,3,4}	Wavelet
Beta	Multiplication parameter	{1,1.1,1.2,1.3}	Wavelet
$N_{pass}$	The number of wavelet passes	{3,4,5}	Wavelet
Blk	Block depth in quadtree mechanism	{8×8, 10×10, 12×12, 14×14, 16×16, 18×18, 20×20}	DCT and Wavelet

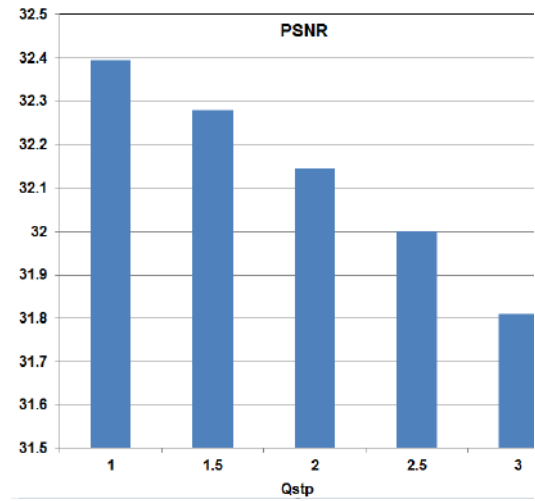
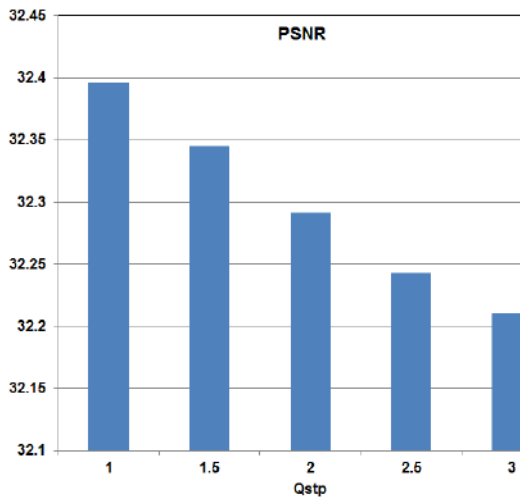
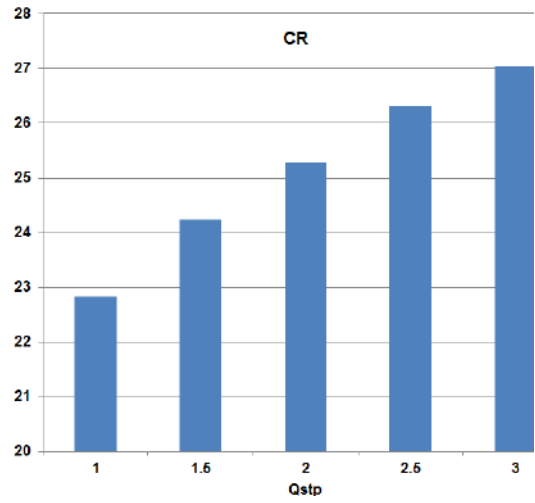
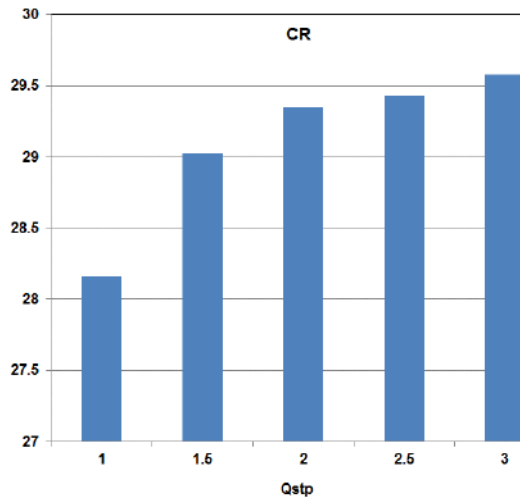
**Table 3. Optimal PSNR and CR for the default values of the control parameters****A. DCT**

Names	$Q_{stp}$	$Q_1$	Alpha	CR	PSNR	ET	DT	Retrieved image
Lena	2	12	0.5	29.3488	32.29111	0.221	0.130	
Pepper	2.5	3	0.6	14.9238	32.1265	0.237	0.186	
Girl	1	2	0.9	19.6514	32.91323	0.247	0.140	
Child	1	5	0.9	19.9829	32.99132	0.230	0.186	
Barbara	1.5	5	0.5	14.8931	32.04662	0.218	0.144	
House	1	5	0.5	15.4105	32.00407	0.206	0.126	
Lena(Gray)	3	19	1.1	22.00856	32.0161	0.234	0.125	



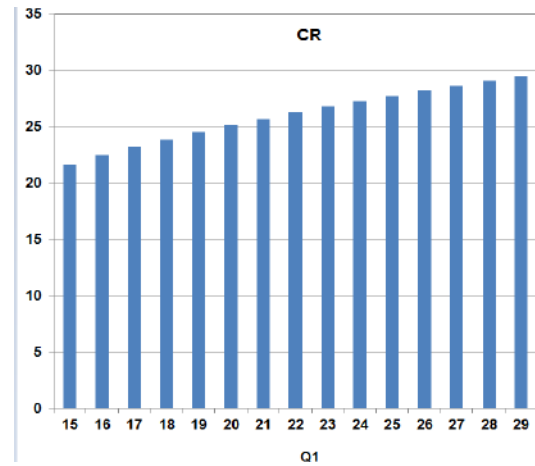
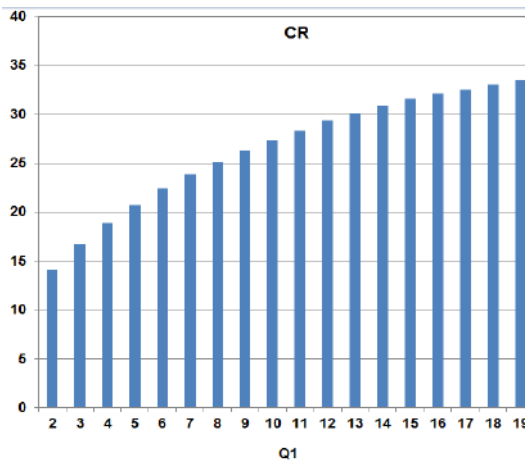
**B. Wavelet**

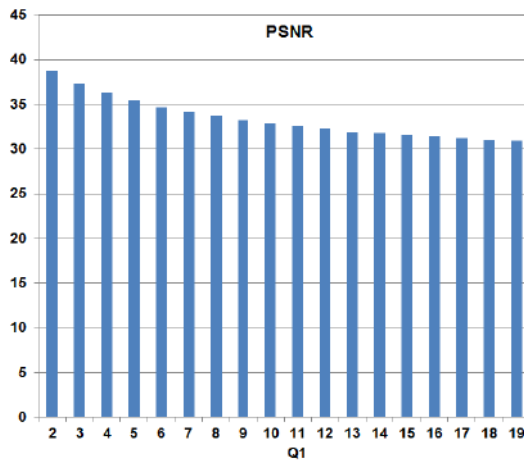
Names	$Q_{stp}$	$N_{pass}$	$Q_1$	Alpha	Beta	CR	PSNR	ET	DT	Retrieved image
Lena	2.5	5	22	1	1.2	26.31263	32.00006	0.200	0.121	
Pepper	2.5	5	12	1	1.1	13.35347	32.23068	0.216	0.159	
Girl	2	5	15	1	1.2	18.72457	32.01398	0.222	0.123	
Child	3	5	19	1	1	18.36643	32.04858	0.215	0.164	
Barbara	2.5	5	17	1	1.1	13.72673	32.01758	0.189	0.125	
House	3	5	15	1	1.1	14.82033	32.0065	0.173	0.105	
Lena(Gray)	3	5	40	1	1.3	20.96984	32.23349	0.217	0.104	



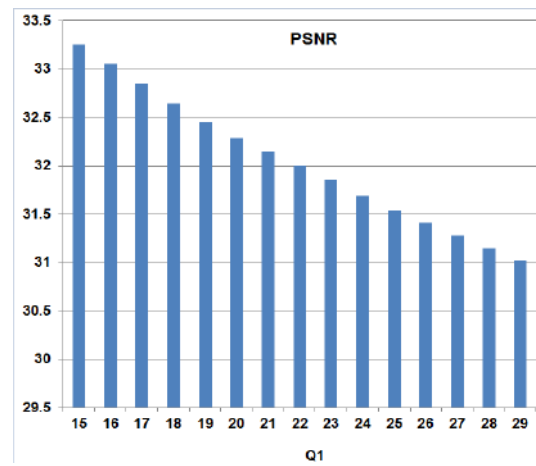
**DCT**

**Wavelet**

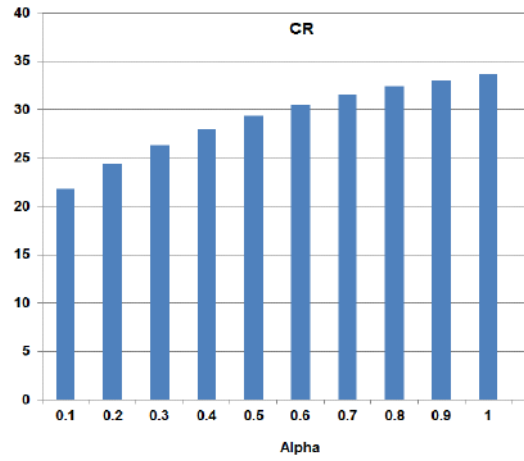




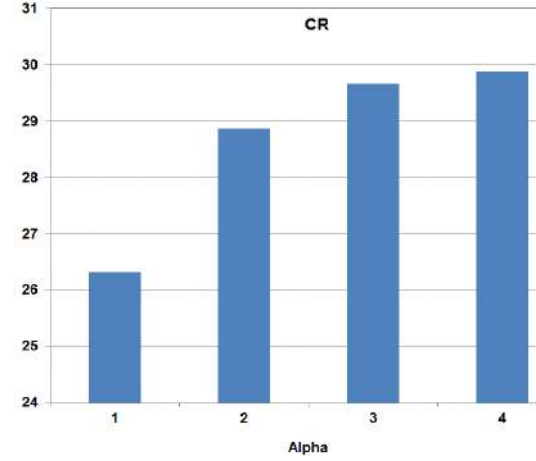
**DCT**



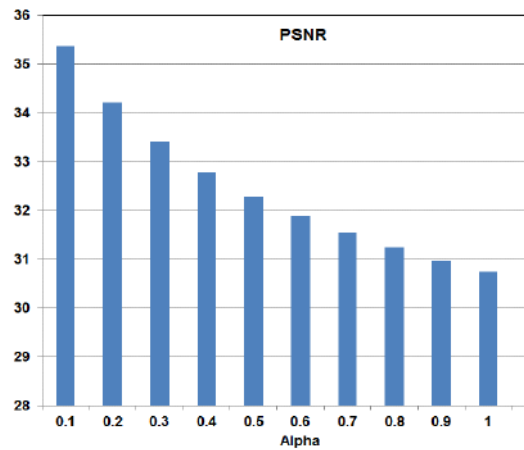
**Wavelet**



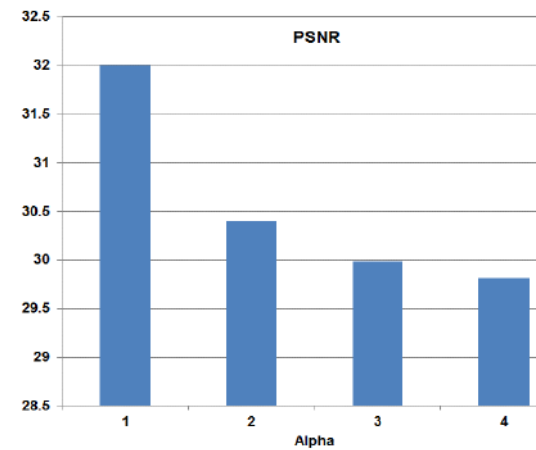
**DCT**



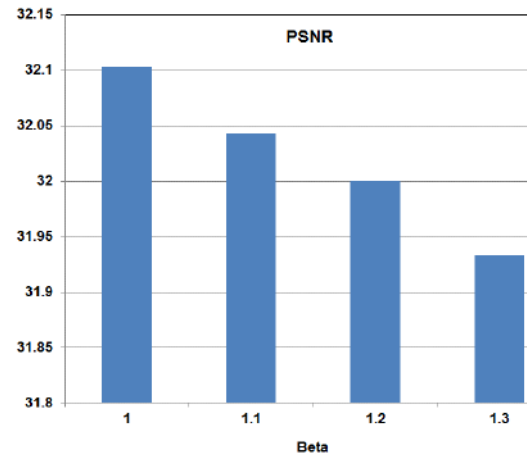
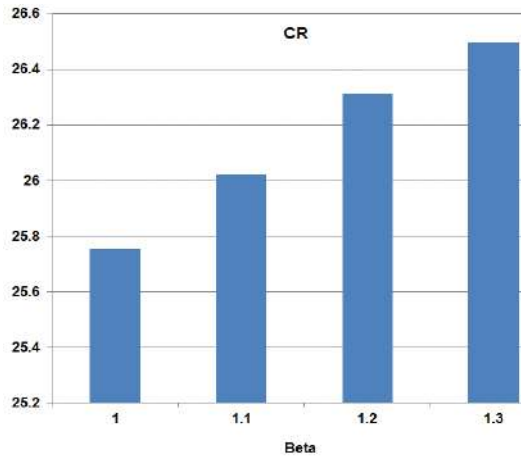
**Wavelet**



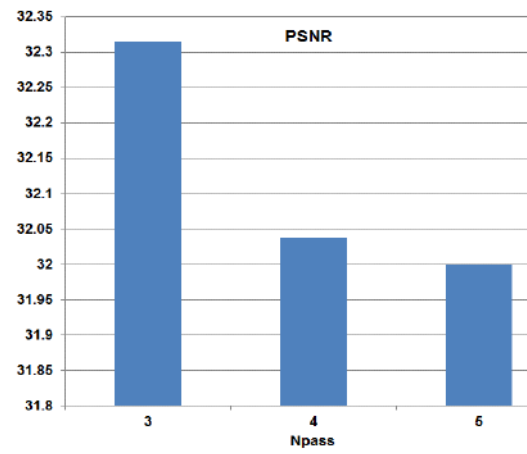
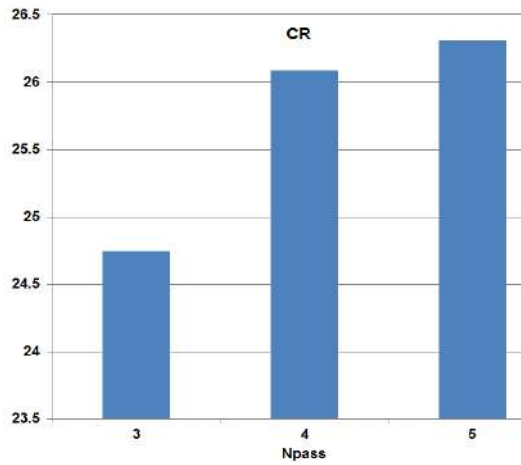
**DCT**



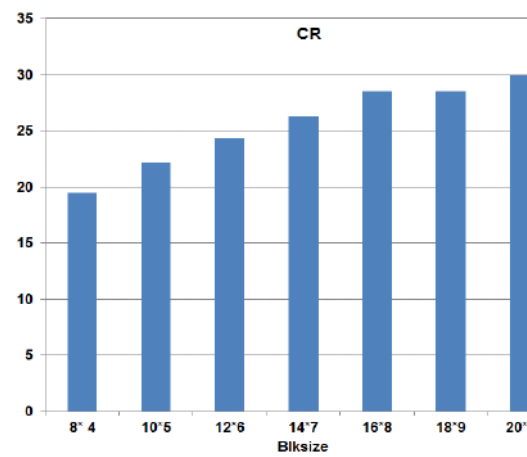
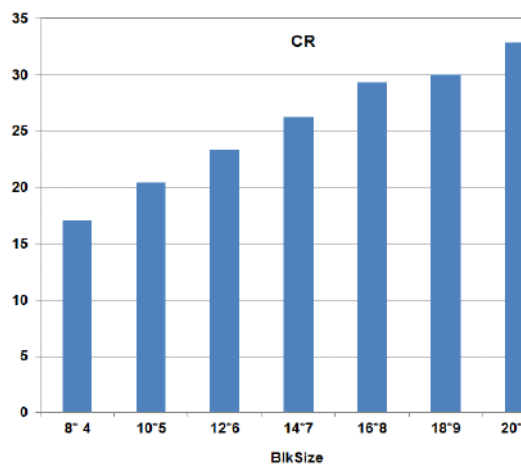
**Wavelet**

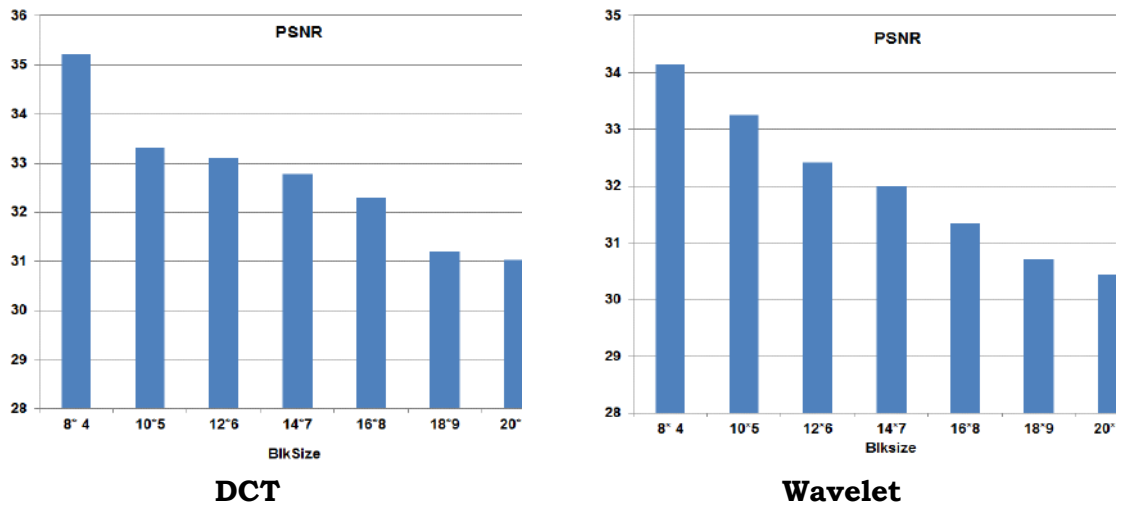


**Wavelet**

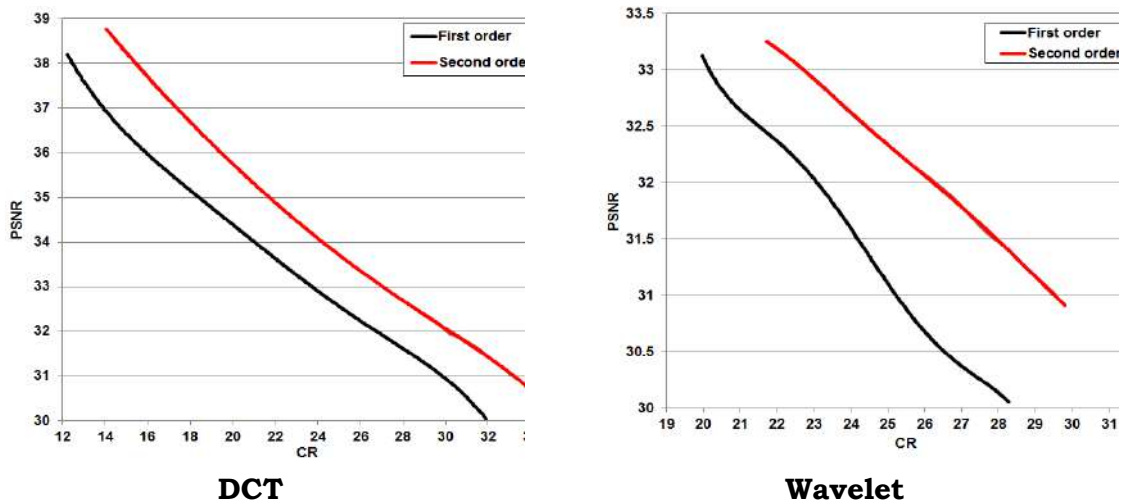


**Wavelet**

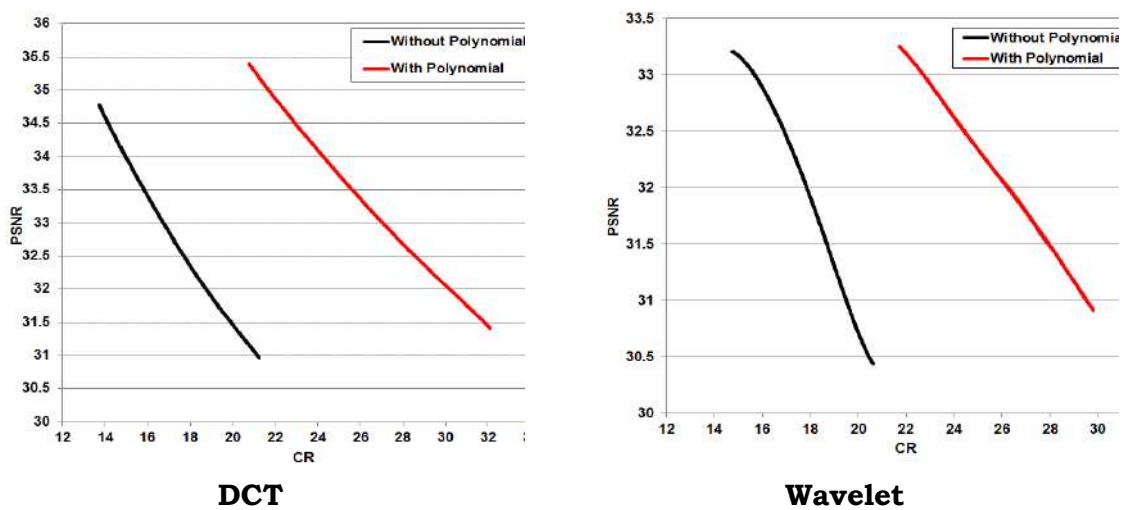




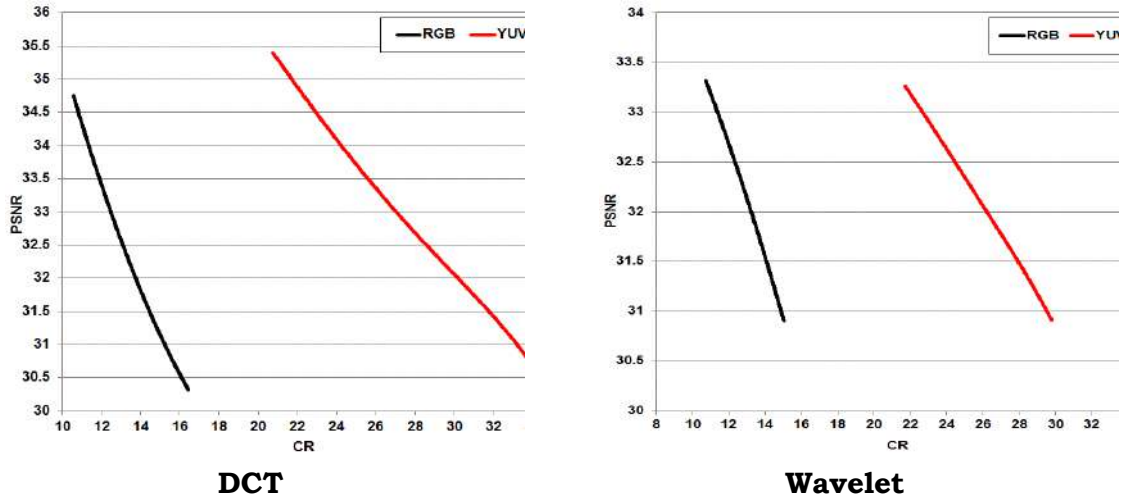
**DCT** **Wavelet**  
**Figure (2) The effect of control parameters on the system**



**DCT** **Wavelet**  
**Figure (3) Compression performance for first-order and second-order polynomial coding**



**DCT** **Wavelet**  
**Figure (4) Comparison polynomial coding and without using it**



**Figure (5) Comparison between RGB and YUV color space**

**Table 4. Comparison of JPEG with the compression system proposed for Lena test images**

The name of the method used	Quality	CR	PSNR
JPEG standard	20%	23.4	30.77
	40%	21.6	31.60
	80%	10.3	34.56
The proposed system using DCT transform		29.349	32.291 1
The proposed system using bi-orthogonal wavelet transform		26.313	32.000 1

A comparative assessment was included in this work to demonstrate the robustness of the proposed approach. In this evaluation, five different approaches were compared and obtained five evaluation points. Table 5 shows a comparison of the simulation results of the presented mechanism with other related prior works. The compression system used showed excellent results with the compression method in the previous works.

**Table 5. Comparing the results with previous work**

Articles	CR	PSNR
[21]	20.49	36.468
[15]	20.18	32.02
[22]	24.523	31.302
[23]	21.33	29.14
[24]	6.9977	31.0126
Proposed method	29.349	32.2911

### Conclusion

A new lossy image compression coding technique that uses polynomial coding to represent the low variation that locally exists within adjacent pixels, where the residue of the polynomial (of 1<sup>st</sup> or 2<sup>nd</sup> order) was processed by the transformation and quantization system. Each of the coefficients and the residue part are processed separately to obtain a good compression ratio then compressed with an LZW algorithm.

The evaluation results are summarized in the following remarks: “the implemented system is characterized by ease and speed for compressing images, and it has been tested on a group of well-known images. For the compression phase based on DCT for Lena grayscale images reached 22.00856 and for color, Lena images reached 29.34886 with acceptable error. While For the compression phase that based on wavelet transform for Lena grayscale images reached 20.96984. For the color Lena image, the compression reached 26.31263with acceptable error. The obtained PSNR is well beyond 32 dB for two types of images. If different control parameters are used, the resulting DWT and DCT compression ratios are subject to change. Increasing the values of the control parameters leads to an increase in the compression ratio and, accordingly, a decrease in the value of the image quality. The work achieved very suitable results in terms of compression and decompression time, noting that the wavelet transformation outperformed the DCT transformation in terms of time because the latter is more complex. The use of polynomial in compression systems achieved excellent results in terms of compression. When comparing the results of a second-order polynomial with a first-order polynomial, the second-order polynomial progressed over the first-order in terms of compression and the quality of the resulting image. Converting the test image to the YUV color space provides the best outputs than the RGB color space does and progresses the CR and PSNR for the rebuilt images. The work has been compared with the well-known compression method jpeg and the system used has achieved advanced results. Finally, the work has been compared with several previous works and has achieved agreed results. In the future, the work can be developed using another technique instead of the polynomial to improve the compression ratio.

## References

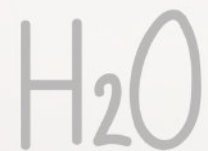
1. Shaimaa Othman, Amr Mohamed, Abdelatif Abouali, Zaki Nossair, Lossy Compression using Adaptive Polynomial Image Encoding, *Advances in Electrical and Computer Engineering*, 21(1), pp:91-98, 2021.
2. Alvaro CASSINELLI, Makoto Naruse, Masatoshi Ishikawa, Quad-tree Image Compression using reconfigurable free-space optical interconnections and pipelined parallel processors, *International Topical Meeting on Optics in Computing (OC'2002)*, Taiwan, pp:23-25, April 2002.
3. Graham Hudson, Alain Léger, Birger Niss, István Sebestyén, Jørgen Vaaben, JPEG-1 standard 25 years: past, present, and future reasons for a success, *Journal of Electronic Imaging*, 27(4), pp: 040901- 040901-19, August 2018.
4. Weidong Xiao, Nianbin Wan, Alan Hong, Xiaoyan Chen, A Fast JPEG Image Compression Algorithm Based on DCT, 2020 IEEE International Conference on Smart Cloud (SmartCloud), USA, pp:106-110, November 2020.
5. R. Naveen Kumar, B. N. Jagadale, J. S. Bhat, A lossless image compression algorithm using wavelets and fractional Fourier transform, *SN Applied Sciences* (2019) 1:266, Springer, pp:1-8, February 2019.
6. Salam Benchikh and Michael Corinthios, A Hybrid Image Compression Technique Based on DWT and DCT Transforms, International Conference on Advanced Infocom Technology 2011 (ICAIT 2011), China, pp: 1-8, July 2011.
7. Andri Kurniawan, Tito Waluyo Purboyo, Anggunmeka Luhur Prasasti Implementation of Image Compression Using Discrete Cosine Transform (DCT) and Discrete Wavelet Transform (DWT), *International Journal of Applied Engineering Research*, 12(23) pp: 13951-13958, 2017.
8. Z. F. Muhsin, A. Rehman, A. Altameem, T. Saba, M. Uddin, Improved quadtree image segmentation approach to region information, *The Imaging Science Journal*, 62(1), pp:56-62, July 2014.
9. Tai-hoon Kim, Hojjat Adeli, Carlos Ramos, Byeong-Ho Kang, Signal Processing, Image Processing and Pattern Recognition: International, International Conferences, SIP 2011, Held as Part of the Future Generation Information Technology Conference, FGIT 2011, in Conjunction with GDC 2011, Jeju Island, Korea, December 2011.
10. Loay E. Goerge and Bushra A. Sultan, The Use of Biorthogonal Wavelet, 2D Polynomial and Quadtree to Compress Color Images, International Conference on Signal Processing, Image Processing, and Pattern Recognition SIP 2011: Signal Processing, Image Processing and Pattern Recognition Part of the Communications in Computer and Information Science book series (CCIS, volume 260), pp: 379–390, December 2011.



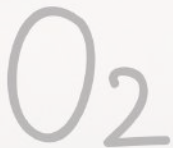
11. Dr. Loay E. George and Dr. Ghadah Al-Khafaji, Image Compression based on Non-Linear Polynomial Prediction Model, *International Journal of Computer Science and Mobile Computing*, 4(8), pp:91 – 97, August 2015.
12. David Salomon, Giovanni Motta, *Handbook of Data Compression*, Springer, 5th Edition, 2010.
13. Shaymaa D. Ahmed, Loay E. George, Ban N. Dhannoon, The Use of Cubic Bezier Interpolation, Biorthogonal Wavelet and Quadtree Coding to Compress Color Images, *British Journal of Applied Science & Technology*, 11(4), pp: 1-11, September 2015.
14. Maneesha Gupta, Dr.Amit Kumar Garg, Analysis Of Image Compression Algorithm Using DCT, *International Journal of Engineering Research and Applications (IJERA)*, 2(1), pp: 515-521, February 2012.
15. Zainab J. Ahmed, Loay E. George, A Comparative Study Using LZW with Wavelet or DCT for Compressing Color Images, *Third International Conference on Advanced Science and Engineering (ICOASE2020)*, Iraq, pp: 53-58, 2020.
16. Dr. Ashwaq T. Hashim, Dr. Suhad A. Ali, Color Image Compression Using DPCM with DCT, DWT and Quadtree Coding Scheme, *Engineering and Technology Journal*, 34 (4), pp: 585-597, 2016.
17. Welba Colince, Ntsama Eloundou Pascal, Pierre Ele, Exploitation of Differential Pulse Code Modulation for Compression of EMG Signals by a Combination of DWT and DCT, *American Journal of Biomedical Engineering*, 4(2), pp: 25-32, 2014.
18. Enas Kh. Hassan, Loay E. George, Faisal G. Mohammed, Color Image Compression Based on DCT, Differential Pulse Coding Modulation, And Adaptive Shift Coding, *Journal of Theoretical and Applied Information Technology*, 96(11), pp: 3160- 3171, June 2018.
19. Abdallah A. Ibrahim, Loay E. George, Enas Kh. Hassan, Color Image Compression System by using Block Categorization Based on Spatial Details and DCT Followed by Improved Entropy Encoder, *Iraqi Journal of Science*, vol. 61, no. 11, pp. 3127-3140, 2020.
20. S. Boopathiraja, P. Kalavathi, and S. Chokkalingam, A Hybrid Lossless Encoding Method for Compressing Multispectral Images using LZW and Arithmetic Coding, *International Journal of Computer Sciences and Engineering*, 6(4), pp:313-318, May 2018.
21. Abdullah A. Hussain, Ghadah K. AL-Khafaji and Mohammed M. Siddeq, Developed JPEG Algorithm Applied in Image Compression, *2nd International Scientific Conference of Al-Ayen University (ISCAU-2020)* IOP Publishing, pp:1-17, 2020.
22. Ghadah Al-Khafaji, Marwa Bassim, Polynomial Color Image Compression, *International Journal of Engineering Trends and Technology*, 61(3), 161-165, July 2018.

23. Loay E. George, Enas Kh. Hassan, Sajaa G. Mohammed, Faisel G. Mohammed, Selective Image Encryption Based on DCT, Hybrid Shift Coding and Randomly Generated Secret Key, Iraqi Journal of Science, 61(4), pp: 920-935, 2020.
24. Shaimaa Othman, Amr Mohamed, Abdelatif Abouali, Zaki Nossair, Lossy Compression using Adaptive Polynomial Image Encoding, Advances in Electrical and Computer Engineering, 21(1), pp:91-98, February 2021.

**PREPARATION AND STUDY OF OXIDES AND THEIR EFFECT ON THE  
PROPERTIES OF  $Al_2O_3$  \  $ZrO_2$   $MgO$  , AND  $CaO$**



**SABAH ALI KHADHIR  
OMAR ABDULWAHHAB AHMED  
SAIF KHALEL JASIM**



## PREPARATION AND STUDY OF OXIDES AND THEIR EFFECT ON THE PROPERTIES OF $Al_2O_3/ZrO_2$ MgO , AND CaO

Sabah Ali KHADHIR <sup>1</sup>

Omar Abdulwahhab AHMED <sup>2</sup>

Saif Khalel JASIM<sup>3</sup>

### Abstract:


Samples in this research were prepared by combined chemical precipitation of raw materials with a ratio of (0.7)  $Al_2O_3$  and a ratio of (0.3) for each of the ( $ZrO_2$ , MgO, CaO) and mixed at a temperature of 60 °C for a certain period, then dried for two days at room temperature and burned at a temperature of 600 °C as primary burning in order to get rid of the non reactive materials they are then ground and sintered at a temperature of 1300 °C . After completing the preparation of the samples designated for the study, some tests are carried out, including XRD structural tests , and the FE-SEM field scan electron microscope is examined . Whereas, X-ray diffraction (XRD) tests showed the appearance of four different phases, where the alumina-alpha phase appears in all samples (A1, A2, A3). Sample A1 shows the ( $AlO-ZrO$ ) phase of zirconium, which is symbolized by ( $t-ZrO_2$ ), while sample A2 shows the ( $MgAl_2O_3$ ) phase of magnesium, and sample A3 shows the phase ( $Al_{12}CaO_{19}$  ) of calcium , and all the prepared samples are of crystal sizes Nano scale, and as for the FE-SEM assay, the shape of the formed particles is the capillary dendrites in the first sample A1 and it is of nano scale size, and in the second sample A2 the shape of the granules formed is spiny cilia distributed on spherical granules and it has nano-granular sizes , And the third sample A3 has the shape of the granules or granules overlapping with each other, different in size and the size of the product being nanoparticles, and the practical benefit of the research is that the characteristics of the samples change with the change of the materials used and the multiplicity of their applications and uses in many areas of life.

**Key words:** Zirconia, Alumina, XRD, FE-SEM, chemical precipitation method.



<http://dx.doi.org/10.47832/MinarCongress5-17>

<sup>1</sup>  Diyala Education Directorate, Iraq, [Sabah3807@gmail.com](mailto:Sabah3807@gmail.com), <https://orcid.org/0000-0002-6828-6418>

<sup>2</sup>  Diyala Education Directorate, Iraq

<sup>3</sup>  Bilad Alrafidain University College, Iraq

### **Introduction:**

Alumina is one of the ceramic materials that possesses high abrasion and resistance to corrosion reactions and the disadvantage is that its mechanical properties are poor and is widely used in engineering applications (1). Alumina ceramics are used as high-purity high-temperature ceramics due to their excellent mechanical properties such as high strength, hardness and corrosion resistance (2) (3). Zirconia-alumina is becoming increasingly important for biomedical implants and as hip and joint prostheses (4) . And also Zirconia-alumina has its effectiveness in orthopedic applications. Recently, the first composite femoral heads in this system with high strength and rigidity were developed and marketed. Quadrangular zirconia exerts effective strengthening thanks to its controlled transformation to monoclinic phase from  $t\text{-ZrO}_2 \rightarrow \text{monoclinic-ZrO}_2$  to binary (5) . (6). Alumina compounds such as reinforced ceramics have many advantages and have wide uses and applications in electronic fields that can be processed at lower cost and with certain desired properties which include increasing the surface area and generally strengthening the mechanical properties. It is also used in the manufacture of tools (7). Many dyes are also made, and they are catalysts for magnetic materials (8). And that these materials are used to improve the physical and optical properties (9). It is used in the packaging of portable devices because of its good mechanical properties (10). As for the magnesium compound, it is the best material for crystallization due to its multiple properties and possesses a high degree of resistance against corrosion and its applications are very wide (11). Its industrial uses are extensive and is included in electronic devices (12). and also as electrical resistors in electronic devices (13).

and since calcium-alumina as a compound possesses many good mechanical properties and good physical properties it is used in refractory ceramics furnace linings pipe linings industry building materials and furnace linings which make their melting points very high (14) .

## 2. Experimental

We have prepared samples from the following raw materials:-

**Table (1) The raw materials used to prepare the composites.**

Materials	Chemical formula	Molar Mass g/mol	purity	Country product	The company
Aluminum nitric-9-hydro	$\text{Al}(\text{NO}_3)_3 \cdot 9\text{H}_2\text{O}$	375.13	95.0%	German	RIEDEL-DEHAENA
Zirconia nitric-technical	$\text{ZrO}(\text{NO}_3)_2 \cdot \text{H}_2\text{O}$	231.23	99.9%	England	BDH Brchesh-dary-hoase
Ammonium hydroxide solution	$\text{NH}_4\text{OH}$	35.04	99%	Germany	Sigma Aldrich
Magnesium nitric-6-hydro	$\text{Mg}(\text{NO}_3)_2 \cdot 6\text{H}_2\text{O}$	256.41	90.0%	England	BDH Brchesh-dary-hoase
Calcium nitric-4-hydro	$\text{Ca}(\text{NO}_3)_2 \cdot 4\text{H}_2\text{O}$	236.15	98%	Analyse	

Samples were taken from the raw materials of their molecular weights and multiplied by the required ratio, the quantity is extracted in grams and the calculation is done as  $(\text{molecular weight} \times \text{ratio})$  and the condition is to dissolve the materials in 100 ml of distilled water and after complete dissolution they mix together for a certain period and then dilute ammonia with an acidic function  $\text{pH} = 12$  with continuous mixing at  $60^\circ\text{C}$  temperature for a certain period and filtered. It is washed several times then dried for two days and at room temperature then burned at  $600^\circ\text{C}$  as a preliminary burning for four hours to get rid of unwanted substances then grinded to its homogeneity and sieved with a sieve then sintered at  $1300^\circ\text{C}$  for a period of four hours after which it is examined with the required tests as well as other samples are worked in the same way. The purpose of burning at  $600^\circ\text{C}$  and sintering at  $1300^\circ\text{C}$  is to get rid of the non-reactive materials and get the required phase.

And Table (2) represents the weight ratios of the prepared samples and taken from the original reactants 0.9 from alumina, and from zirconia 0.3 will be according to the molar fraction base and calculated from the molecular weight of the reactants and multiplied by the percentage taken for each substance and mixed together.

**Table (2) represents the symbols of the prepared models for the complexes and weight ratios .**

Code	Composites	weight ratio Mg(NO <sub>3</sub> ) <sub>2</sub> .6H <sub>2</sub> O	weight ratio ZrO(NO <sub>3</sub> ) <sub>2</sub> .H <sub>2</sub> O	weight ratio (Al(NO <sub>3</sub> ) <sub>3</sub> .9H <sub>2</sub> O)
A1	(ZrO <sub>2</sub> ) <sub>0.3</sub> (Al <sub>2</sub> O <sub>3</sub> ) <sub>0.7</sub>	0	0.6936	5.2518
A2	(MgO) <sub>0.3</sub> (Al <sub>2</sub> O <sub>3</sub> ) <sub>0.7</sub>	0.7692	0	5.2518
A3	(CaO) <sub>0.3</sub> (Al <sub>2</sub> O <sub>3</sub> ) <sub>0.7</sub>	0.7084	0	5.2518

### 3. Results and discussion

#### 1-X-Ray Diffraction

**A** - The results of the X-ray diffraction patterns for sample (A1) of the (ZrO<sub>2</sub>)<sub>0.3</sub>-(Al<sub>2</sub>O<sub>3</sub>)<sub>0.7</sub> compound prepared in the form of powder at sintering point 1300°C showed of two crystal phases according to the percentage of alumina (0.7wt) and zirconia (0.3wt):

The first phase \ It was note the appearance of the alumina - alpha phase ( $\alpha$  -Al<sub>2</sub>O<sub>3</sub>) in sample A1 and the peaks appear at the following angles and according to the order  $2\theta=$  (25.58, 37.78, 41.68, 43.36, and 57.51) corresponding to the levels and according to the standard card (ICDD) and numbered (00-010-00 0173) and these results are identical to the results obtained by (Yesica) et al (7) .

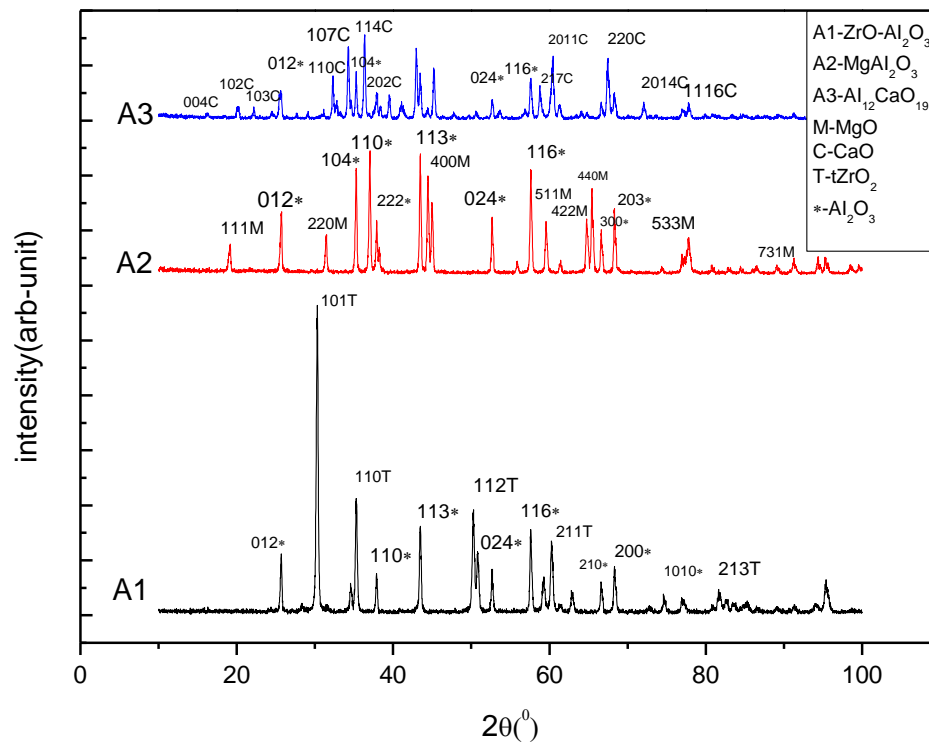
The second phase \ It was note the appearance of the zirconia - alumina phase (AlO-ZrO) (t-ZrO<sub>2</sub>) in sample (A1) . The peaks appear at the following angles  $2\theta=$  (30.20, 35.27, 42.92, 50.17, 60.20, 68.60, and 95.20) corresponding to the levels and according to the standard card ( ICDD) and numbered (00-053-0294) belonging to zirconia – alumina as in Figure (1) which shows the diffraction patterns of Miller's coefficients and this appearance is consistent with (Pingan Chen) and others (8) .

**B** - The results of the X-ray diffraction patterns of sample A2 for the compound (MgO)<sub>0.3</sub>-(Al<sub>2</sub>O<sub>3</sub>)<sub>0.7</sub> prepared in the form of a powder at a sintering point of 1300 ° C showed the appearance of two crystal phases according to the percentage of alumina (0.7wt) and magnesium (0.3wt):

The first phase \ note the appearance of the alumina – alpha phase ( $\alpha$  - Al<sub>2</sub>O<sub>3</sub>) in sample A1 and the peaks appear at the following angles according to the order  $2\theta=$  (25.58, 37.78, 41.68, 43.36, and 57.51) corresponding to the levels and according to the standard card (ICDD) and numbered (00-010- 0173), and these results are identical to the results obtained by (Yesica) et al (7) .

The second phase \ which was inferred by X-ray diffraction patterns is the cubic phase of the compound magnesium - alumina (Al<sub>2</sub>MgO<sub>4</sub>) with the appearance of a group of peaks at angles  $2\theta=$ (19.02, 36.85, 44.83, 65.24, 74.13, 82.64) and when it was compare the locations of the apparent peaks with the standard card (ICDD) numbered (00-021-1152) we find that they are identical to a large extent and

this agrees with the results obtained by (Harloff) (14) . shows the diffraction patterns of the and Miller's indices for the prepared composites .



**Fig (1) x-ray diffraction patterns and Miller's coefficients for the prepared composites.**

**C** - The results of the X-ray diffraction patterns of sample A3 for the complex  $(\text{CaO})_{0.3}-(\text{Al}_2\text{O}_3)_{0.7}$  prepared in the form of a powder at a sintering point of  $1300\text{ }^\circ\text{C}$  showed the appearance of two crystal phases according to the ratio of alumina (0.7wt) and magnesium (0.3wt):

The first phase \ note the appearance of the alumina - alpha phase ( $\alpha$  -  $\text{Al}_2\text{O}_3$ ) in sample A1 and the peaks appear at the following angles and in the order  $2\theta=(25.58, 37.78, 41.68, 43.36, \text{ and } 57.51)$  corresponding to the levels and according to the standard card (ICDD) and numbered (00-010-00 0173) and these results are identical to the results obtained by (Yesica) et al (7) .

The second phase \ shows through the X-ray diffraction patterns that the formed phase is the calcium - alumina phase which is symbolized by the symbol  $(\text{Al}_{12}\text{CaO}_{19})$  through the appearance of a group of peaks at the following angles  $2\theta=(20.13, 34.15, 37.32, \text{ and } 68.47)$  which is identical to a certain extent Large with the standard card (ICDD) and numbered (00-038-470) and these results are close to the results obtained by (Dominka and Jacek) (13) . Also Table (3) shows the locations of the peaks at the corners and their comparison with the standard cards for the prepared composite powders .



**Table (3) The locations of the vertices at the corners and their comparison with the locations on the standard cards composite powders.**

2 $\theta$ (deg) of A1	2 $\theta$ (deg) of A2	2 $\theta$ (deg) of A3	Card( 00-010-0173) - Al <sub>2</sub> O <sub>3</sub>	Card( 00-053-0294) - t-ZrO <sub>2</sub>	Card(00-021-1152) Al <sub>2</sub> MgO <sub>4</sub>	Card(00-038-0470) Al <sub>12</sub> CaO <sub>19</sub>
	19.14				19.02	
		16.34				16.14
	25.71	20.19				20.13
		22.23				22.08
25.70	35.28	25.66	25.58			
30.31		30.89		30.20	36.85	30.70
	37.03	34.28				34.15
35.30	43.71	35.29	35.13	35.27		
	44.46	36.05			44.83	36.22
37.90		37.90	37.78			37.32
43.42	52.67	43.48	43.36			
50.25	57.62	50.60		50.17		50.28
52.66		52.68	52.55			
57.60	65.44	57.60	57.51		65.24	57.38
	66.63	59.10				
60.27	68.31	60.04		60.20	68.69	60.03
	74.38				74.13	62.35
68.32	76.96		68.19	68.60		68.47
74.65	82.85		74.26	74.61	82.64	74.19

**a-Crystal size**

The crystal size was calculated from the Scherer's formula :-

$$D = K\lambda / \beta \cos\theta$$

Whereas :-

K: - the form factor, which depends on the shape of the material and its value within the range (0.9-1) .

$\beta$ : - the width of the curve at the half (FWHM), measured in radial units.

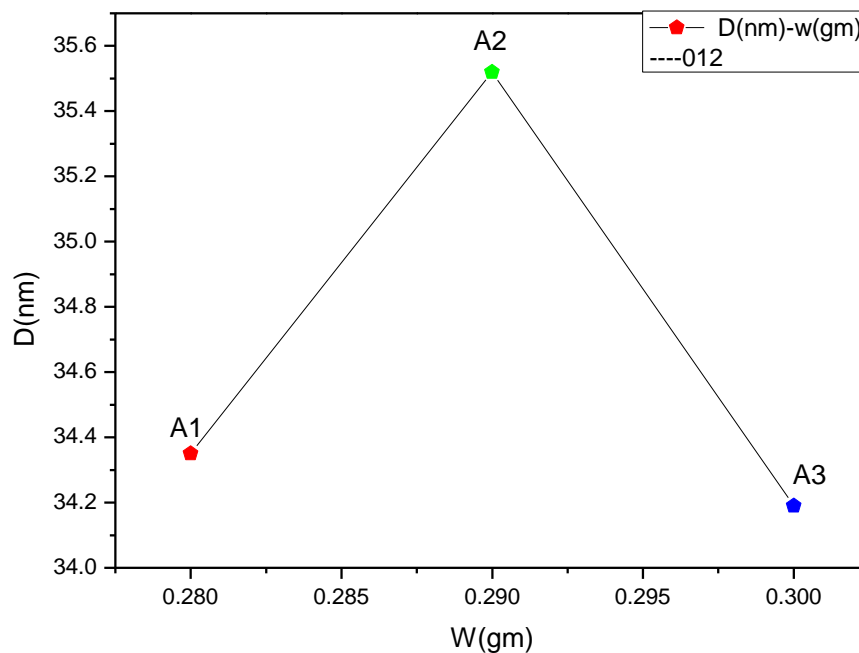
$\theta$ : - Brack diffraction angle .

$\lambda$ : - The wavelength of the X-rays falling on the target is (1.54056) .

From the values of the compositional information for all the compound powders prepared at the weight ratios (A1,A2, and A3) in both directions (116) , (012) take the two samples to find the difference between the angles . Table (4) values of the composition information at the directions (116) and (012) for the prepared composite powders. Figure (2) shows the change in the crystal volume with a change in the weight ratios used in the process of preparing the prepared compounds at the level (012) . conclude that the volume increases and decreases due to the different ionic diameter of the samples . The size increases and decreases in the crystal level (012) Iqbal Others showed that they are identical (19) .

**Table (4) values of composition information in directions (116) and (012) for the prepared composite powders .**

Sample	A1	A2	A3
Hkl	116	116	116
2 $\theta$ (deg)	57.60	37.92	57.60
$d_{hkl}(A^{\circ})$	1.59	2.37	1.59
FWHM(deg)	0.223	0.18	0.241
D(nm)	40.63	37.92	37.11
Sample	A1	A2	A3
hkl	012	012	012
2 $\theta$ (deg)	25.70	25.51	25.53
$d_{hkl}(A^{\circ})$	3.46	3.46	3.48
FWHM(deg)	0.234	0.22	0.235
D(nm)	34.35	35.52	34.19



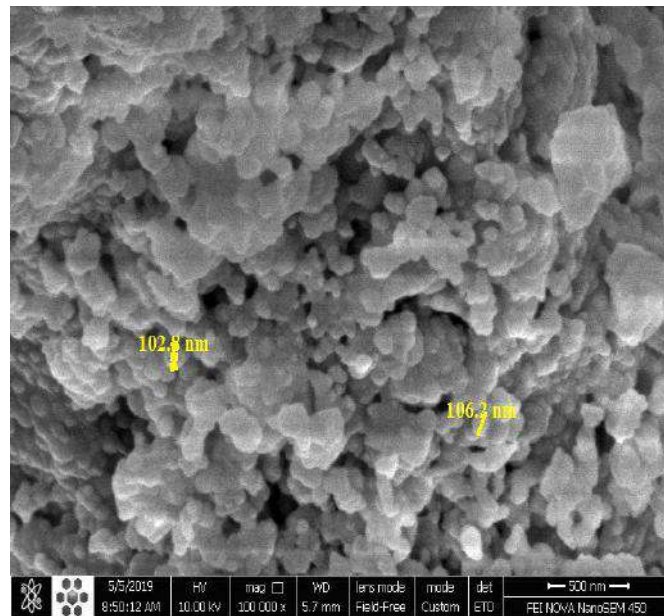
**Fig (2) The change in the crystal size with a change in the weight ratios used in the process of preparing the prepared composites at the level (012) .**

## 2- Field emitter scan Electron microscope (FE-SEM)

This technique is used to study the shapes of the granular surfaces formed by the powders of the prepared composites which provides us with a clear three-dimensional image in addition to the granular size of those particles with a size of (500) nm .

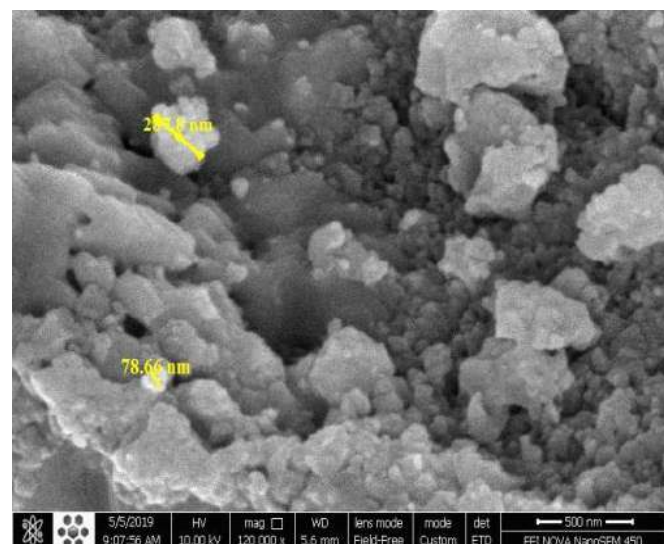
The results of field emitting electron microscopy (FESEM) for sample A1 showed that the shape of the formed particles is the dentin of capillaries (Tandens kapillärer) or the resulting shape is spherical granules

whose average granular size is between (75nm-120nm) and means that the particle size is sandwiched between these two numbers as the results are in agreement with the results obtained by (Rajum) (1) . which showed that its shape is like the teeth of filaments or its shape may be in the form of small and overlapping granules and these particles are of different size and this results are consistent with the results obtained by (Hussein) (18) . The size is taken directly from the image because it is ready without any change and Which shows that the resulting shape is granules as in the figure ( 3) .



**Fig(3) is an image (FESEM) of sample A1 with a size of 500nm .**

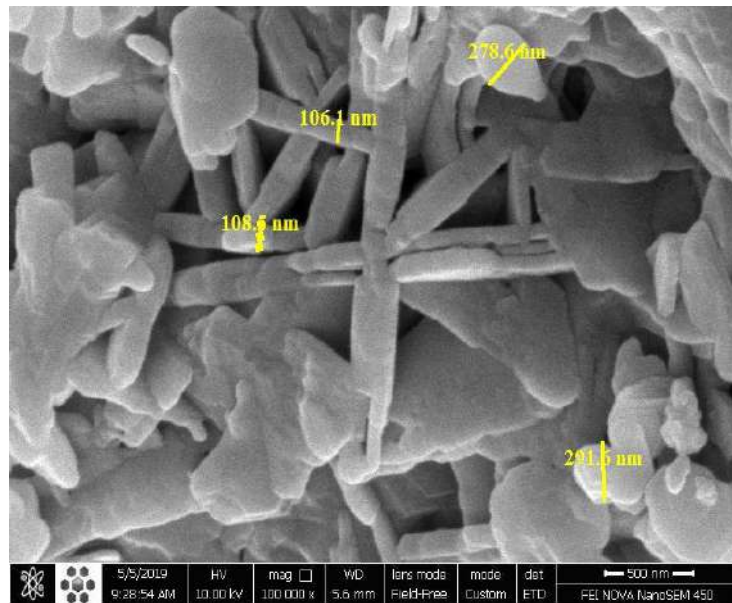
The results of the examination by field emitting electron microscope (FESEM) of sample A2 showed that the formed granules are spiny cilia distributed over spherical granules or the resulting shape is the wedge of capillaries and have Nano - granular sizes confined between (69nm-250nm) and means that the particle size is sandwiched between these two numbers belonging to the spiny cilia of magnesium, which are distributed on the spherical granules that belong to the Also these results are in agreement with the results obtained by (Jacek) (15) . Who showed that the shape of the formation is spherical grains as shown in Figure (4) .



**Fig(4) is an image (FESEM) of sample A2 with a size of 500nm.**

The results of the field emitting electron microscope (FESEM) examination of the sample showed that the resulting form is fine granules

or the resulting granular sizes are Nano scale and confined between (104nm-300nm) and means that the particle size is sandwiched between these two numbers the granular shape formed is overlapping granules with different sizes and these results we obtained are consistent with the results obtained by (Magdalena) (16) and also the results we obtained agree with the results obtained by (Leqa'a) (17) The results are close to the last sample A3 and Figure Shows the resulting figure (5) .



**Fig (5) is an image (FESEM) of sample A3 with a size of 500nm.**

#### 4. Conclusion

We can conclude from the preparation of the composites the following:-

1- In the X-ray diffraction test, four different phases appear, and the required alpha alumina phase appears in all samples (A1, A2, A3) due to the high sintering heat in it. Sample A1 shows a phase ( $t\text{-ZrO}_2$ ) of zirconium, while sample A2 shows a phase ( $\text{MgAl}_2\text{O}_3$ ) of magnesium and sample A3 showing the phase ( $\text{Al}_{12}\text{CaO}_{19}$ ) of calcium and all samples have nanocrystal sizes.

2- In FE-SEM the particle shape is spherical in sample A1. For sample A2, the shape of the granules formed is spiny cilia distributed over spherical granules or capillary wedge and has granular sizes. For the A3 sample, the shape of the grains, inter-interstrap granules, or needle grains are different, and all samples are of nano sizes.

## References

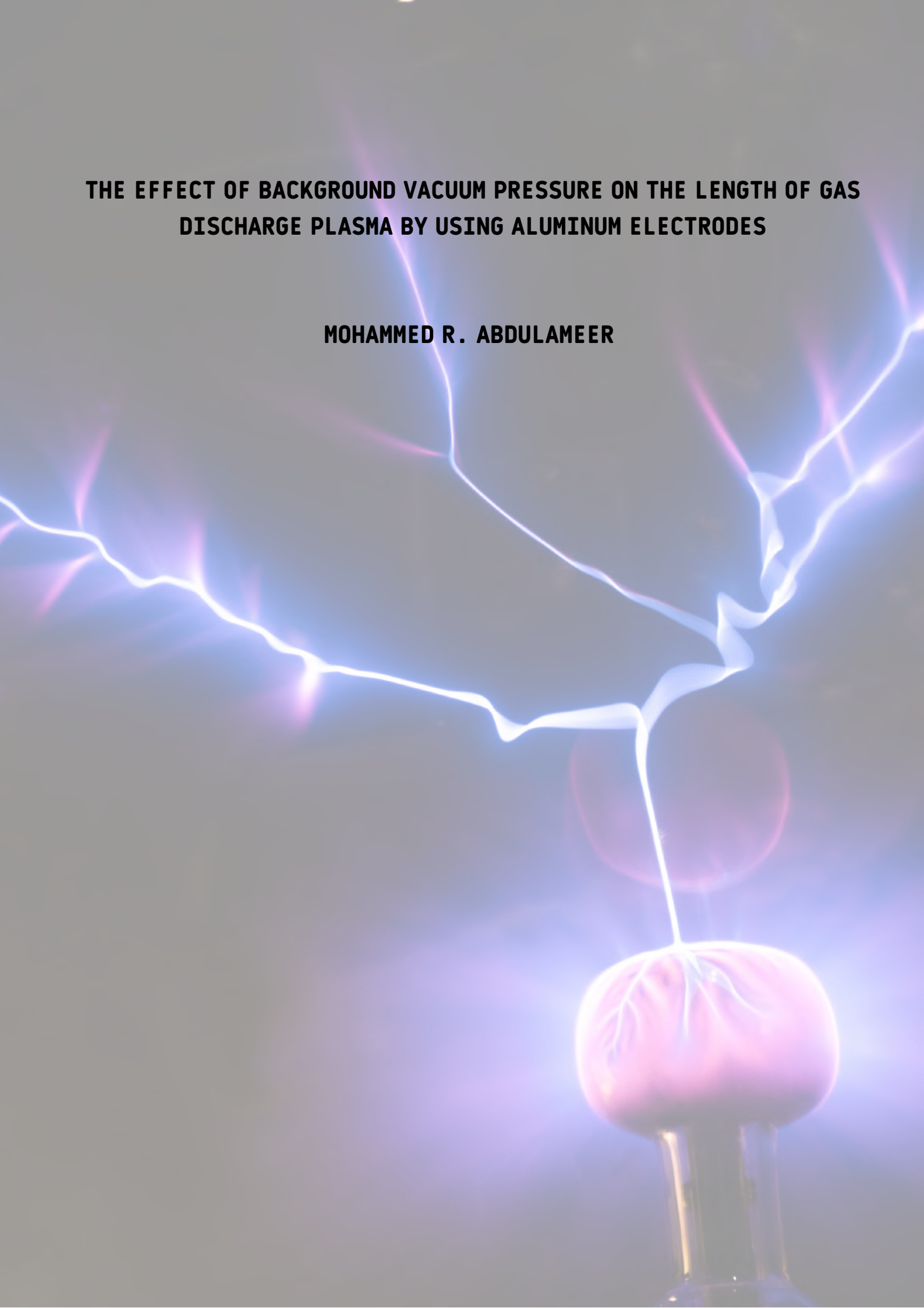
- 1- Rajum. Belekhar, p.s.sawadh & R. K. mahdulesysynthis and structural properties of Al<sub>2</sub>O<sub>3</sub>-ZrO<sub>2</sub>" nano composite" Research in Engineering & Technology ISSN(E): 2321- 8843; ISSN(P): 2347-4599 Vol. 2, Issue 3, Mar, 145-152(2014).
2. Wang, J.; Stevens, R. Review: Zirconia-toughened alumina (ZTA) ceramics. J. Mater. Sci. 1989, 34, 3421–3440 .
3. Bartolomé, J.F.; Pecharrómán Moya, J.S.; Martín, A.; Pastor, J.Y.; Llorca, J. Percolative mechanism of sliding wear in alumina/zirconia composites. J. Eur. Ceram. Soc. 2006, 26, 2619–2625 .
4. Roualdes, O.; Duclos, M.E.; Gutknecht, D.; Frappart, L.; Chevalier, J.; Hartmann, D.J. In vitro and in vivo evaluation of an alumina-zirconia composite for arthroplasty applications. Biomaterials 2010, 31, 2043–2054 .
5. Lange, F.F. Transformation toughening Part 4: Fabrication, fracture toughness and strength of Al<sub>2</sub>O<sub>3</sub>-ZrO<sub>2</sub> composites. J. Mater. Sci. 1982, 17, 247–254 .
6. Evans, A.G. Toughening of brittle solids by martensitic transformations. Acta Metall. 1986, 34, 761–800 .
- 7-Yesica L. Brunia,b , Liliana B. Garridoa , Esteban F. Aglietti "International Congress of Science and Technology of Metallurgy and Materials, SAM -Conamet Properties of CaO-ZrO<sub>2</sub> Based Composites Procedia Materials Science 8 203 – 210 ( 2015) .
- 8-Pingan Chen , Yulong Wang , Xiangcheng Li , Boquan Zhu "Effect of submicron spinel powders on the micro structure volution and properties of alumina-based refractory cas tables" Accepted: 10 April (2017).
- 9-O. Sahina,A. Hasdea, H. Göcmezb, M. Tuncerb, H. Ali Cetinkaraa, H. Salih Güdera.E. Sahina and A. Rza Tuncdemirc"Hardness Behavior of AluminaZirconia Nanocomposites Synthesized by Gel Process "Vol. 123 (2013).
- 10-Papaspyridakos ,Panos; Kunal Lal .5 (2008). "Complete arch implantrehabilitation using subtractive rapidprototyping and porcelain fused tozirconia prosthesis: A clinical report". TheJournal of Prosthetic Dentistry. 100 (3)-165–172. PMID 18762028. doi: 10.1016/S0022-3913(08)00110-8. Cite uses deprecated parameterمساعدة ) = |coauthorApple seeks patent on radio-" .6transparent zirconia CE casings". Appleالمحتوى متاح وفق CC BY-SA 3.0. إن لم يرد خلاف ذلك. Insider. 30 November 2006.
- 11- T. Kameda, A.Kodama and T.Yoshioka, "Simultaneous removal of SO<sub>2</sub> and NO<sub>2</sub> using a Mg–Al oxide slurry treatment", Chemosphere, Vol. 93, PP. (2889-2893), (2013).
- 12-M. Akter<sup>1</sup>, M. J. Abden<sup>2</sup>, M. K. Newaz<sup>3</sup> and M. M. Haque<sup>4</sup>"Microstructures and Mechanical Properties of Al<sub>2</sub>O<sub>3</sub>-30wt%ZrO<sub>2</sub> Doped with MgO and TiO<sub>2</sub>" Vol. 24. No. 1&2. 2015.
- 12-D.Zhang, B.Li, Y.Hu, J.Li, and Y.Guo, "synthesis and characterization of (MgAl<sub>2</sub>O<sub>4</sub>) micro - rods by a molten salt method", ceramics international, Vol.41, PP(5881-5887), (2015) .

- 13-Dominika madej and Jacek szczerba "prepara of  $\text{Al}_2\text{O}_3\text{-CaAl}_{12}\text{O}_{19}\text{-ZrO}_2$  composite ceramic" material by the hydration and sintering of  $\text{Ca}_7\text{ZrAl}_6\text{O}_{18}$  reactive alumina mixture *Ceramics-Silikáty* 60 (2), 27-33 (2016).
- 14- Jan Harloff "In-situ quantitative measurement of electric fields in zinc oxide thin films using electrostatic force microscopy" ,A Master theses of Science , University of Pennsylvania , PP. (14-18) (1995) .
- 15-Jacek Szczerba and Dominika Madej” Potencjalne sk\_ady fazed dla tworzyw ogniotrwa\_ych wuk\_adzie  $\text{MgO-CaO-Al}_2\text{O}_3\text{-ZrO}_2$ ” *Material* £Y *Ceramics /Ceramic Materials*, 63, 2342-349, (2011).
- 16-Magdalena Dudek , Grzegorz Róg , Władysław Bogusz ,Mirosław Bućko, Anna Kozłowska Róg” Composite solid electrolytes in the  $\text{CaO-ZrO}_2\text{-Al}_2\text{O}_3$  system properties, and application to the solid galvanic cells” Faculty of Physics, Warsaw University of Technology (1988).
- 17- Leqa’a Hamid Majid , Mahdi Hatem Dewan "Study of the Structural properties of Nickel Calisum Alumena Composites Prepared by Co-precipitation Method "Dayala University , College of Science , Department of Physics(2019).
- 18-M. M .Hussein, I. A. Disher, and S .J .I dress, "Synthesis of Stoichiometric phase pure  $\text{NiAl}_2\text{O}_4$  using Molten Salt Method", *International Journal of Applied Engineering Research*, Vol. 12, No. 24, pp. (14818-14827) (2017) .
- 19-M. J. Iqbal and B .Ismail, "Correlation between structural and electrical properties of  $\text{Mg}_{1-2x}\text{Ni}_x\text{Zn}_x\text{Al}_2\text{O}_4$  (x= 0.0, 0.5) ceramic Nano materials synthesized by a urea assisted microwave combustion method", *Journal of alloys and compounds*, Vol.504, PP(440-445) ( 2010).



**THE EFFECT OF BACKGROUND VACUUM PRESSURE ON THE LENGTH OF GAS  
DISCHARGE PLASMA BY USING ALUMINUM ELECTRODES**

**MOHAMMED R. ABDULAMEER**



## **THE EFFECT OF BACKGROUND VACUUM PRESSURE ON THE LENGTH OF GAS DISCHARGE PLASMA BY USING ALUMINUM ELECTRODES**

**Mohammed R. ABDULAMEER<sup>1</sup>**

### **Abstract:**

Length of plasma generated by dc gas discharge under different vacuum pressures was studied experimentally. The cylindrical discharge tube of length 2m was evacuated under vacuum pressure range (0.1-0.5) mbar at constant external working dc voltage 1500V. It was found that the plasma length (L) increased exponentially with increasing of background vacuum air pressure. Empirical equation has been obtained between plasma length and gas pressure by using Logistic model of curve fitting. As vacuum pressure increases the plasma length increases due to collisions, ionizations, and diffusions of electrons and ions.

**Key words:** Gas Discharge Plasma, Plasma Length, Ionization, Ion And Electron Diffusion.



<http://dx.doi.org/10.47832/MinarCongress5-18>



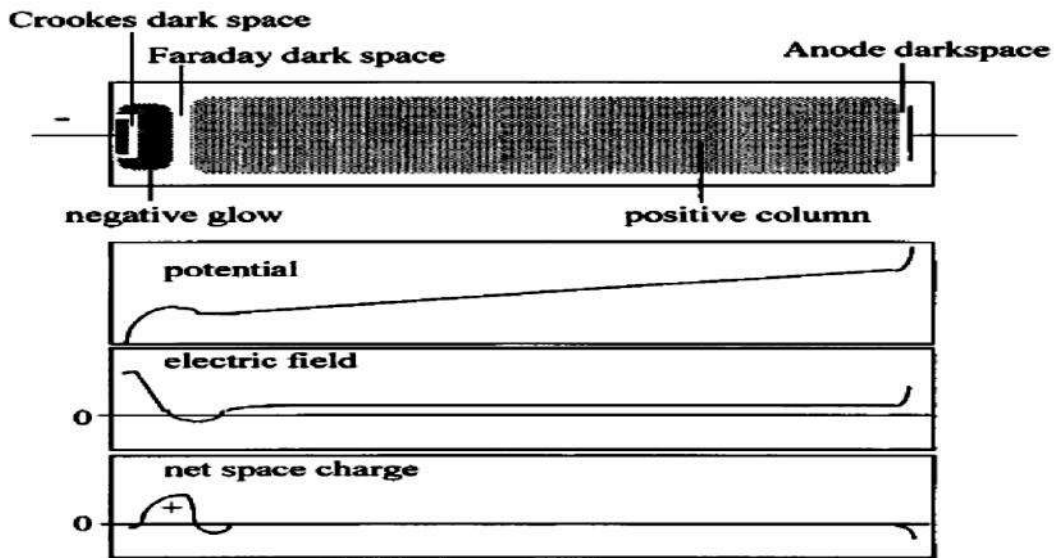
<sup>1</sup> University of Baghdad, Iraq, [mohammed\\_plasma@sc.uobaghdad.edu.iq](mailto:mohammed_plasma@sc.uobaghdad.edu.iq), <https://orcid.org/0000-0002-7395-9840>

**Introduction:**

A gas discharge is the passage of an electric current through a gas as a result of an external electric field [1]. Glow and arc discharges in a cylindrical tube subjected to a fixed electric field are the most prevalent types of gas discharges. In recent years, atmospheric-pressure glow discharge (APGD) has advanced to overcome the challenges posed by low-pressure glow discharges, which necessitate the use of a costly and specialized vacuum apparatus [2]. Atmospheric pressure plasma has attracted a lot of attention for a wide range of applications in industry [3], electrical equipment, and textile materials [4]. The breakdown voltage that transforms the gas from insulator to conductor follows Paschen's law: A gas discharge is defined as the passage of an electric current through a gas as a result of an external electric field [1]. Glow and arc discharges in a cylindrical tube subjected to a fixed electric field are the most prevalent types of gas discharges. In recent years, atmospheric-pressure glow discharge (APGD) has advanced to overcome the challenges posed by low-pressure glow discharges, which necessitate the use of a costly and specialized vacuum apparatus [2]. Atmospheric pressure plasma has attracted a lot of attention for a wide range of applications in industry [3], electrical equipment, and textile materials [4]. The breakdown voltage that transforms the gas from insulator to conductor follows Paschen's law: A gas discharge is defined as the passage of an electric current through a gas as a result of an external electric field [1]. Glow and arc discharges in a cylindrical tube subjected to a fixed electric field are the most prevalent types of gas discharges. In recent years, atmospheric-pressure glow discharge (APGD) has advanced to overcome the challenges posed by low-pressure glow discharges, which necessitate the use of a costly and specialized vacuum apparatus [2]. Atmospheric pressure plasma has attracted a lot of attention for a wide range of applications in industry [3], electrical equipment, and textile materials [4]. Paschen's law governs the breakdown voltage that turns an insulator to a conductor: [5]

$$V_b = \frac{Bpd}{\ln(Apd) - \ln[\ln(1 + \gamma^{-1})]} \dots\dots\dots(1)$$

Where  $V_b$ : breakdown voltage,  $p$ : background gas pressure,  $d$ : distance between the two electrodes,  $\gamma$ : the rate of secondary electron emission from the negative electrode,  $A$  and  $B$  are constants related to the gas used in the discharge. The schematic structure of a d.c. discharge is shown in figure (1).



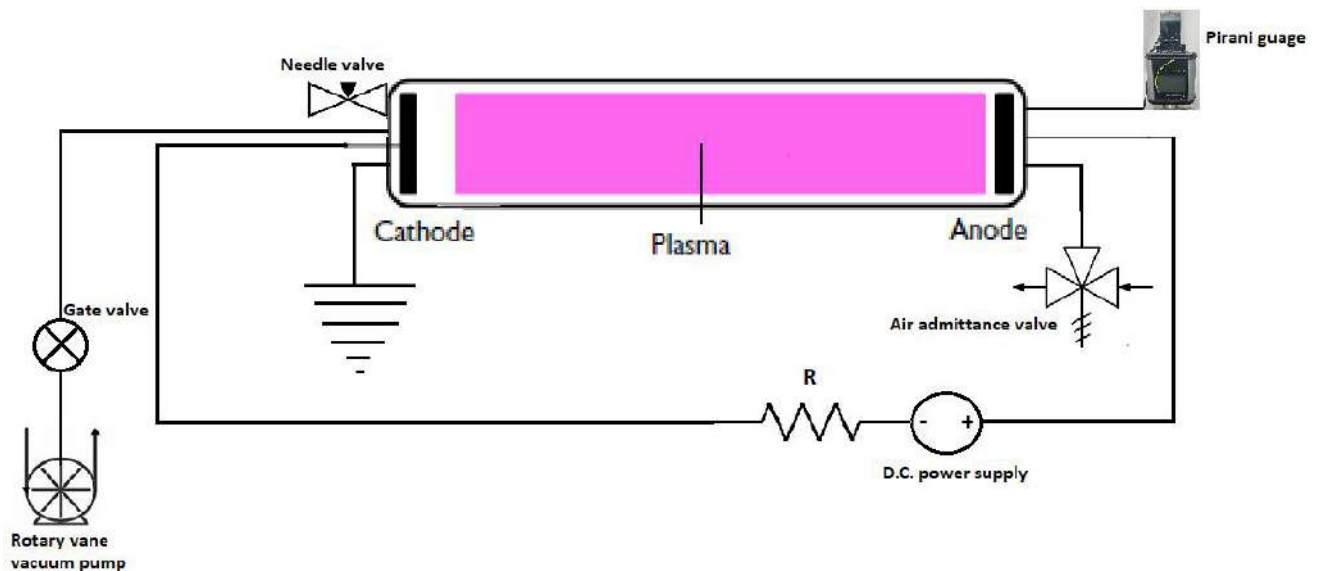
**Figure (1):-** Schematic structure of a dc discharge [5].

In gas discharge plasma, various plasma-chemical processes occur that are significantly influenced by electron energy [6]. R. Castell and et.al [7] investigated these processes experimentally, focusing on ionization, excitation, and molecular dissociation. Eric Wagenaars [8] is interested in two types of discharges: a pulsed discharge between parabolic metal electrodes and a parallel-plate, low-pressure dielectric barrier discharge. Modeling has been used to examine plasma constriction in the positive column [9]. DC glow discharges can occur when the anode and cathode electrodes are of various shapes, sizes, and relative positions, such as two simple parallel plane electrodes, a plane anode-cylindrical hollow cathode, a hollow cathode with holes, and a hollow anode [10,11]. The length of the plasma positive column was measured and the effect of background pressure on the length of plasma region (positive column region) in a DC glow discharge of the air was studied in this present work.

**1. Experimental setup**

Fig.(2) shows the experimental setup of gas discharge plasma system.

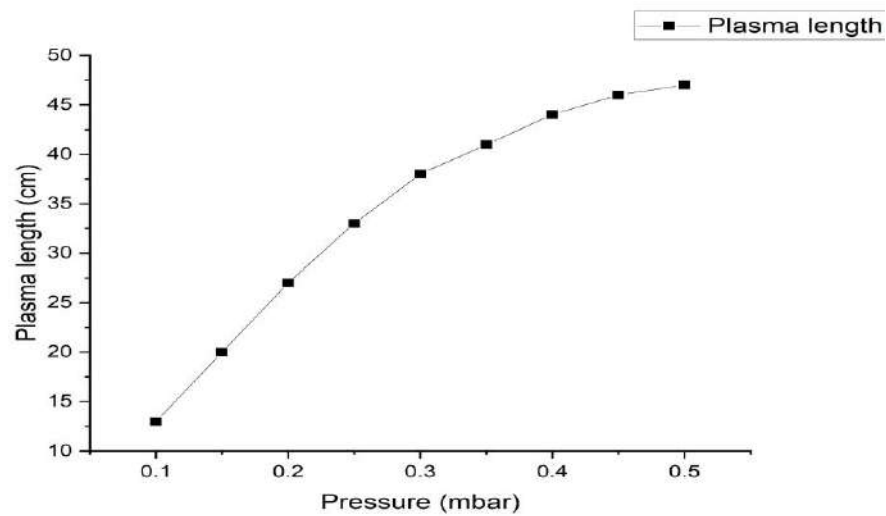
**Figure (2):-** Experimental setup of gas discharge plasma.



The material of the two electrodes is aluminum element with radius 3 cm and thickness 5mm. The two electrodes (cathode and anode) are connected to external high voltage power supply (D.C. voltage maximum 5 kV). The cylindrical tube was evacuated at different vacuum air pressure (0.1-0.5) mbar by using rotary vane vacuum pump (Varian DS602). The control of the pressure was done by using needle valve connected to the tube. The body of the cylinder tube was grounded to ensure leakage of additional charges from the system to the ground. The background gas pressure was measured by reading of Pirani gauge scale data (THYR CONT). A thermal resistance was put between the DC power supply and the cathode electrode to control the current output from the power supply. The applied voltage from the power supply was fixed to 1500 volt in order to study the effect of changing background vacuum pressure from 0.5 to 0.1 mbar on the length of the plasma in a DC gas discharge. The distance between the electrodes is kept constant 70 cm a part.

### 1. Results and Discussion

Figure (3) represents the plasma length  $L$ (cm) as a function of vacuum pressure  $P$ (mbar).



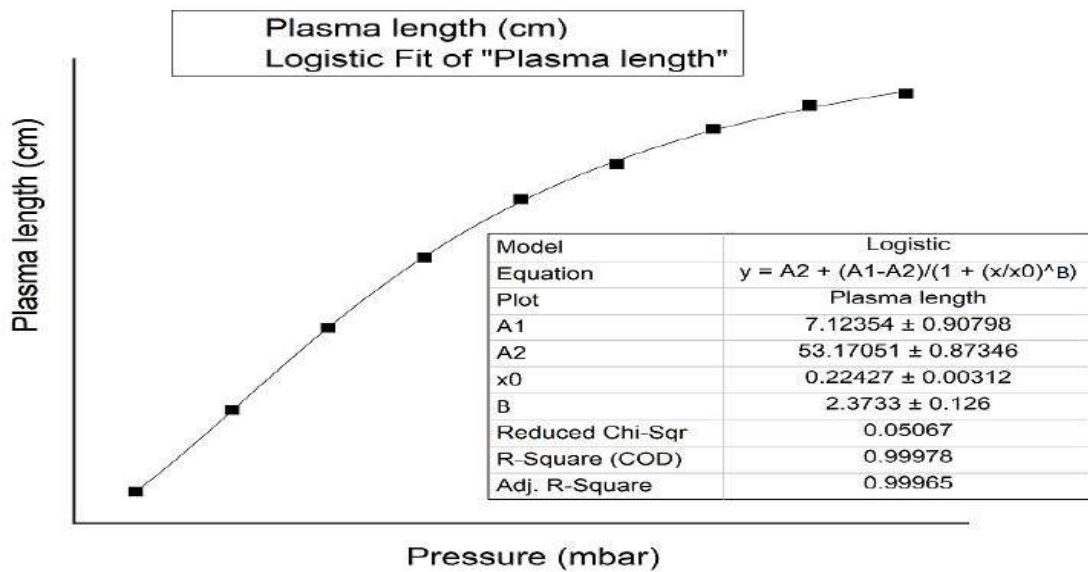
**Figure(3):- Plasma length as a functions of vacuum pressure in gas discharge plasma.**

It is clear from this figure that the plasma length was increases with increasing the air pressure. Figure (4) schematic the image of the normal glow discharge region that generated by DC glow discharge.



**Figure(4):- Image of the gas discharge system and positive column region**

The curve fitting has been done and shown in figure (5) of the data between P and L to simulate the relationship.



**Figure(5):- Curve fitting (logistic fit) of the relation between L and P.**

It is found that the growth fitting is the best suitable fit with R<sup>2</sup> value (the scale of curve fitting goodness) of 0.99978, the model of the fitting is logistic taken from origin 2019b software, and the curve fitting logistic relation which govern the relationship between P and L is found to be:

$$L = A_2 + \frac{A_1 - A_2}{\left(1 + \frac{P}{P_0}\right)^B} \dots \dots \dots (2)$$

L: plasma length, P: vacuum pressure,  $A_1$ ,  $A_2$ , B,  $P_0$  and d: fitting constants parameters 7.12 cm, 53.17 cm., 2.37, 0.224 mbar respectively. In figure (5) for the logistic fitting equation y replaced by L, x replaced by P and  $x_0$  by  $P_0$ . The exponent relation between L and P is due to increasing of ionization of atoms and molecules of air components  $N_2$ ,  $O_2$ , Ar because of increasing vacuum pressure which leads to more collision between the species of air in cylindrical discharge tube, this collision will transfer additional energy to electrons to escape from the outmost orbit of the molecules. So, the free electrons and ions will have more and more energy to move away freely and randomly so the diffusion of these charged particle will increase in both vertical and in horizontal range. As vacuum air pressure increases, the temperature increases too. So, the electron temperature will increase as a result of that and the ionization will become more. Finally, the diffusion of these free electrons will increase due to the famous equation of diffusion[1]:

$$D = \frac{\sqrt{T}}{N\sigma(\sqrt{m})} \dots\dots\dots (3)$$

Where T: temperature of species, N: number density of species in sample,  $\sigma$  : typical cross section for elastic collisions, m: mass of the species. From eq, (3) electrons acquire more energy and temperature due to increasing the vacuum pressure, this will lead to increase diffusion coefficient, electrons diffuses more than ions because of its lighter mass compared to the ion. As a result of this diffusion, the electrons and ions diffuse in the vertical and horizontal (axial) directions, and this lead to an increase in the length of plasma produced from the gas discharge with an increase in the vacuum pressure with an observed in the figure (5). On the other hand , when the gas pressure increases , the plasma density and ionization rate increases, at higher pressure , the regions of gas discharge will shrink and this behavior leads to expand positive column (plasma column) due to the increasing in electron diffusion and ionization , also with the increasing of the gas pressure , the density of the neutral atoms becomes larger than ones at lower gas pressure, so the ionization rate increases and finally plasma density increases. The increasing of gas pressure leads to increase ion current density on the grounded electrode and this cause the particle to grow more at the electrode and the second electron emission from cathode also grow rapidly, and the electron density increases, The width of the sheath region becomes less. The width of the bulk plasma (positive column) increases as the gas pressure increases because of the changes of the electron and ion densities.

## 2. Conclusions

The relationship between plasma length L in a gas discharge plasma and vacuum pressure P was investigated experimentally in this study. The gas discharge experiment was carried out under vacuum with varying vacuum pressures and a constant external voltage. The plasma length increases with exponent as vacuum pressure increases at constant applied voltage due to ionization of atoms and molecules, decreasing sheath width and, as a result, expansion of positive column region (plasma bulk region), and diffusion of ions and electrons in all directions due to the additional temperature and energy they acquire from the increasing vacuum pressure.

## References

1. Boris M. Smirnov, "Physics of ionized gases", book, Wiley-interscience publications, 2001.
2. Jin-Pyo Lim , Han S. Uhm," Atmospheric-pressure argon/oxygen plasma-discharge source with a stepped electrode", Applied physics letters, 90, 051504 ,2007.
3. José Asenjo-Castillo1, Iván Vargas-Blanco , "Emission spectroscopy of an atmospheric pressure plasma" , Tecnología en Marcha, 29, Número Especial Estudiantes 3, 47-58.2016.
4. E.V. Endiarova, G.S. Eritsyán , "Treatment of textile in a low-temperature gas-discharge plasma", Materials Today: Proceedings, 1-4,2020.
5. N. St. J. Braithwaite , "Introduction to gas discharges", Plasma Sources Sci. Technol., 9, 517–527,2000.
6. V. A. Godyak, "Electron energy distribution function control in gas discharge plasmas", Physics of plasmas, 20, , 101611,2013.
7. R. Castell, E. J. Iglesias, J. Ruiz-Camacho," Glow Discharge Plasma Properties of Gases of Environmental Interest", Brazilian Journal of Physics, 34, 4B, 1734-1737,2004.
8. Erik Wagenaars, "Plasma Breakdown of Low-Pressure Gas Discharges", Phd thesis, Technische Universiteit Eindhoven, 2006.
9. Mykhaylo Gnybida, "Theoretical studies of the constriction of rare-gas glow discharge plasmas", Phd thesis, Ernst-Moritz-Arndt university, 2010.
10. A. Chalkha, C. Despenes, A. Janulyte, Y. Zerega, J Andre, B. Brkic ,S. Taylor, "A dc glow discharge as a source of electrons for a portable mass spectrometer: characterization of the electron current intensity and electron kinetic energy distribution", Plasma Sources Sci. Technol., 24, 015001, 1-8,2015.
11. Mohammed R. Abdulameer, Ali A-K. Hussain, Kadhim A. Aadim," Electron density spectroscopic measurement in Al laser induced plasma", MINAR International Journal of Applied Sciences and Technology, 2, 41-47,2020.



The background is a light blue surface. In the upper right, a portion of a silver stethoscope is visible. In the center, a clear plastic test tube with a red cap lies horizontally, with 'COVID-19' handwritten in black marker on its side. Below the test tube, several blue and white capsules are scattered across the surface, some in sharp focus and others blurred in the foreground and background.

**THE CORRELATION BETWEEN COVID-19 AND DIABETES MELLITUS**

**MOUNA AKEEL HAMED AL - OEBADY**

**HEDAA . M . NAHAB**

**SUHAIR . M . JABBAR**

## THE CORRELATION BETWEEN COVID-19 AND DIABETES MELLITUS

**Mouna Akeel Hamed AL-OEBADY<sup>1</sup>**

**Hedaa.M.NAHAB<sup>2</sup>**

**Suhair.M.JABBAR<sup>3</sup>**

### **Abstract:**

COVID-19 and diabetes mellitus have a complicated relationship. Diabetes was first of the most significant risk factors for severe COVID-19 therapy. The link between COVID-19 and diabetes was investigated in this study utilizing data from the Martyr Yousuf Hospital in the Al-Muthanaa region. The data was divided into three groups: T1D (n = 641), T2D (n = 477), and normal (non-diabetic cases, n = 1745) males and females of different ages. The findings show a strong positive association coefficient of 0.8165 between infection with COVID-19 and age in 641 patients with diabetes mellitus type I, with a P-Value of 0.00001 at p 0.05, but a poor relationship between infection with covid-19 and gender.

**Key words:** COVID-19, Diabetes Mellitus.



<http://dx.doi.org/10.47832/MinarCongress5-19>



<sup>1</sup> Al Muthanna University, Iraq, [mouna@mu.edu.iq](mailto:mouna@mu.edu.iq), <https://orcid.org/0000-0001-7274-5536>



<sup>2</sup> Al Muthanna University, Iraq



<sup>3</sup> Sawa University, Iraq

## **Introduction:**

At the end of 2019, a novel RNA beta corona virus has emerged in Wuhan, China, causing corona virus disease 2019 (Covid-19). The disease has rapidly spread in several countries (114 with more than 120 000 confirmed cases when this article was written) and by March 11, 2020, the Director-General of the World Health Organization, Tedros Adhanom Ghebreyesus, has declared Covid-19 a pandemic disease. The case fatality ratio of Covid-19 has been initially described in China to be about 1%-2% (1).

Corona virus is a zoonotic virus, which were first isolated in 1937 and designated corona viruses, they have a crown-like appearance under microscopy . RNA virus in the family Coronaviridae of the order Nidovirales , It is cause respiratory infections (2).

The types of corona virus known to date are as follows: the alpha corona viruses HCoV-229E and HCoV-NL63; the beta corona viruses HCoV-OC43 and HCoV-HKU1; SARS-CoV, which causes severe acute respiratory syndrome (SARS); MERS-CoV, which causes Middle East respiratory syndrome (MERS); and SARS-CoV-2, a new corona virus described in late 2019 after cases were reported in China(2), which causes the disease known as corona virus disease 2019 (COVID-19).

The clinical spectrum of corona virus infection is broad, can range in severity from a simple cold to severe pneumonia. Clinically, The initial sign of COVID-19 is a flu-like syndrome. Individuals with COVID-19 usually develop signs and symptoms, such as mild respiratory disorder and the fever persists for 5–6 days after infection (range, 1–14 days), in contrast contrast with the progressive decline observed incases of influenza(1).

Fever may not be present in some cases, such as those occurring in patients with immunocompromised, very young, or elderly.

Diabetes mellitus is a complicated chronic disease characterized by glucose dysregulation due to an absolute or relative insulin deficiency. It contains various different types, with type 1 diabetes mellitus (T1D) and type 2 diabetes mellitus (T2D) as the most widespread subtypes. Diabetes is due to either the pancreas does not produce enough insulin, or the cells of the body do not responding to the insulin produced. Type 1 diabetes is caused by autoimmune damage to insulin-producing pancreatic b-cells result in the body's failure to produce enough insulin (3).

This form was previously referred to as "insulin-dependent diabetes mellitus" (IDDM) or "juvenile diabetes". while Type 2 DM result[s] from a combination of b-cell secretory defect and insulin resistance. Type 2 DM begins with insulin resistance, a condition in which cells fail to respond to insulin properly. As the disease progresses a lack of insulin may also develop. This form was previously referred to as "non insulin-dependent diabetes mellitus" (NIDDM) or "adult-onset diabetes"(4). It is often accompanied by various complications, including hypertension, obesity, a proinflammatory, vasculopathy, and cardiovascular disease (5,6).

The presence of diabetes mellitus and the individual degree of hyperglycaemia seem to be independently associated with COVID-19 severity and increased mortality(7,8,9,10). Numerous factors that are often present in diabetes mellitus are

likely to participate to this risk, such as hyperglycemia, older age, a proinflammatory, and underlying comorbidities (cardiovascular disease, hypertension, obesity and chronic kidney disease) that COVID-19 mortality (7,11).

The aim of this research is explain the relationship between covid 19 and diabetes mellitus.

### **Materials and Methods**

Clinical, laboratory, radiologic, treatments, complications, and clinical outcomes data were extracted from medical records of martyr Yousuf Hospital at Al-muthanaa province, data was classified into three groups including T1D (n= 641) T2D (n= 477) and Normal (non-diabetic cases n = 1745) male and female, in different age group.

Routine analysis were applied to determine the risk factors for the prognosis of COVID-19, blood sugar, blood urea, serum creatinine, T.Serum Bilirubin, serum glutamic-oxaloacetic transaminase, Serum glutamic pyruvic transaminase (S.GPT), alkaline phosphatase test and S. Uric were tested.

### **Statistical Analysis**

Microsoft Excel 2010 and Minitab 19 Statistical Software, were used to analysis the data.

### **Results and Calculation**

The infection with covid-19 and age correlation in patient with diabetes mellitus type I. Coefficient of correlation = 0.8165.

The P-Value is <0.00001. The result is significant at  $p < 0.05$ .

#### *X Values*

$$\sum = 641$$

$$\text{Mean} = 80.125$$

$$\sum(X - M_x)^2 = SS_x = 3914.875$$

#### *Y Values*

$$\sum = 323.5$$

$$\text{Mean} = 40.438$$

$$\sum(Y - M_y)^2 = SS_y = 4235.219$$

#### *X and Y Combined*

$$N = 8$$

$$\sum(X - M_x)(Y - M_y) = 3679.562$$

#### *R Calculation*

$$r = \frac{\sum((X - M_x)(Y - M_y))}{\sqrt{(SS_x)(SS_y)}}$$

$$r = \frac{3679.562}{\sqrt{(3914.875)(4235.219)}} = 0.9036$$

*Meta Numerics (cross-check)*

$$r = 0.9036$$

The value of R is 0.9036.

This is a strong positive correlation, which means that high X variable scores go with high Y variable scores (and vice versa).

The infection with covid-19 and gender correlation in patient with diabetes mellitus type I. Coefficient of correlation = 0.027.

The P-Value is 0.000029. The result is significant at  $p < 0.05$

*X Values*

$$\sum = 288$$

$$\text{Mean} = 36$$

$$\sum(X - M_x)^2 = SS_x = 1452$$

*Y Values*

$$\sum = 353$$

$$\text{Mean} = 44.125$$

$$\sum(Y - M_y)^2 = SS_y = 1914.875$$

*X and Y Combined*

$$N = 8$$

$$\sum(X - M_x)(Y - M_y) = 274$$

*R Calculation*

$$r = \frac{\sum(X - M_x)(Y - M_y)}{\sqrt{(SS_x)(SS_y)}}$$

$$r = 274 / \sqrt{(1452)(1914.875)} = 0.1643$$

*Meta Numerics (cross-check)*

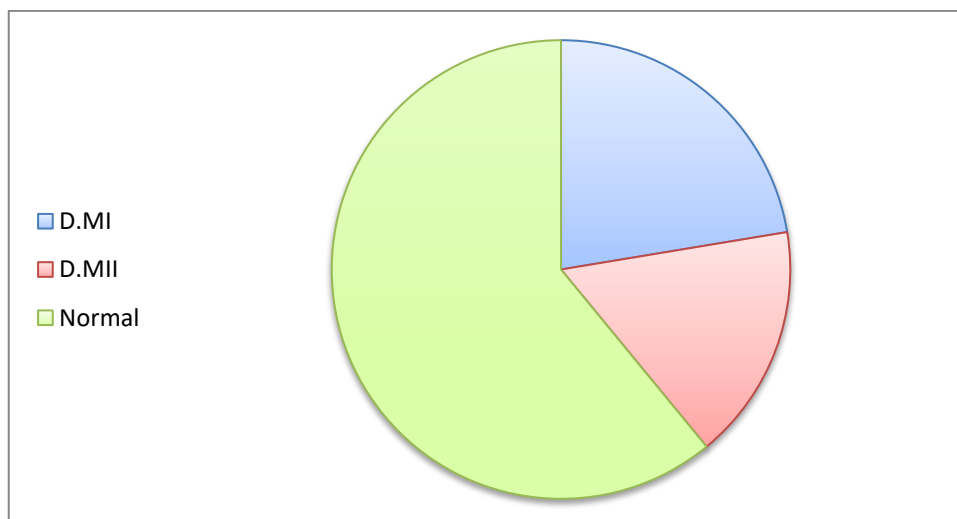
$$r = 0.1643$$

The value of R is 0.1643.

Although technically a positive correlation, the relationship between your variables is weak (the nearer the value is to zero, the weaker the relationship).

## Results and discussion

Clinic characteristics were collected from a total of 2863 confirmed cases of COVID-19, including 641 subjects with T1D (n = 353 male, n=288 female), 477 subjects with T2D and 1745 non-diabetic cases (Figure 1).



**Figure 1: Total of 2863 confirmed cases of COVID-19, including 641 subjects with T1D 477 subjects with T2D and 1745 non-diabetic cases(normal).**

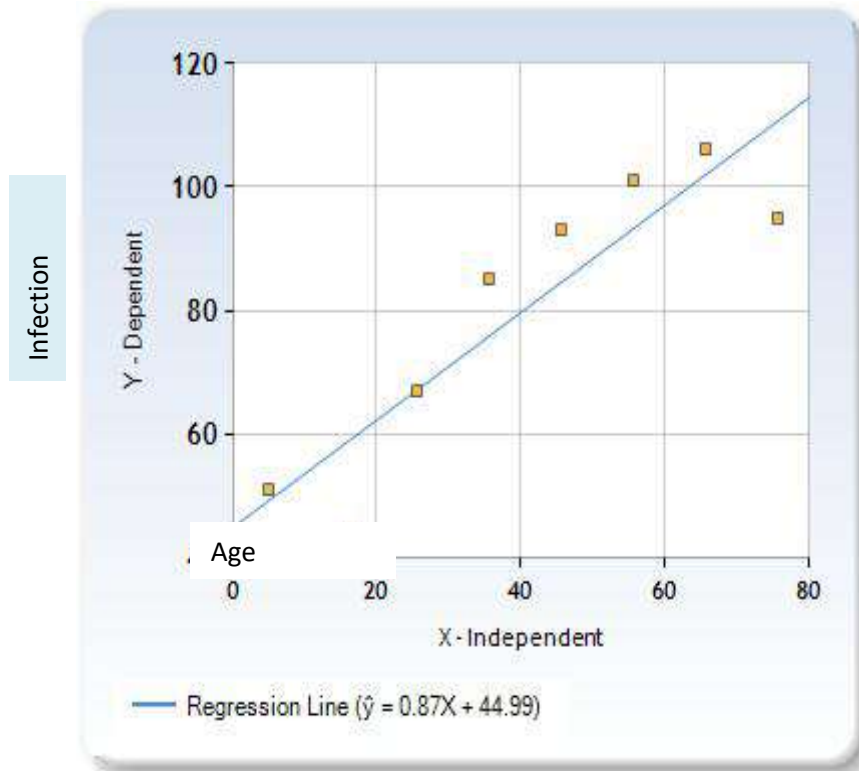
**(DMI : diabetes mellitus 1 , DMII :diabetes mellitus 2)**

The results show a significant positive correlation coefficient between two disease this indicate that if the prevalence of Diabetes Mellitus increases, the prevalence of COVID-19 cases may also increase.

It has been well established that patients with diabetes are more susceptible to infections in general and exhibit worse prognosis once infected compared to the non-diabetic population (12,13). Such a higher susceptibility has also been previously observed for other coronaviral epidemics. For example, in patients with severe acute respiratory syndrome (SARS), pre-existing T2D was independently associated with poor outcomes. The percentage of known T2D history was significantly higher among patients who succumbed to SARS than who survived (14, 15). Further, epidemiological studies also indicate that T2D was the primary comorbidity associated with severe or lethal MERS-CoV infections (16). And with regard to the current COVID-19 pandemic, several recent studies, though with limited participants, have already suggested that T2D is a common comorbidity and constitutes a higher proportion of patients with severe and ICU-admitted cases of COVID-19 than patients with mild symptoms (17, 18, 19). These associations between diabetes and worse outcome in viral infections are not unexpected as hyperglycemia is detrimental to the control of viremia and inflammation, aggravating morbidity and mortality in a variety of patients (20). However, an overly rigid glucose control may increase the risk of severe hypoglycemia, which can also lead to an increased mortality (21).

**The infection with covid-19 and age correlation in patient with diabetes mellitus type I.**

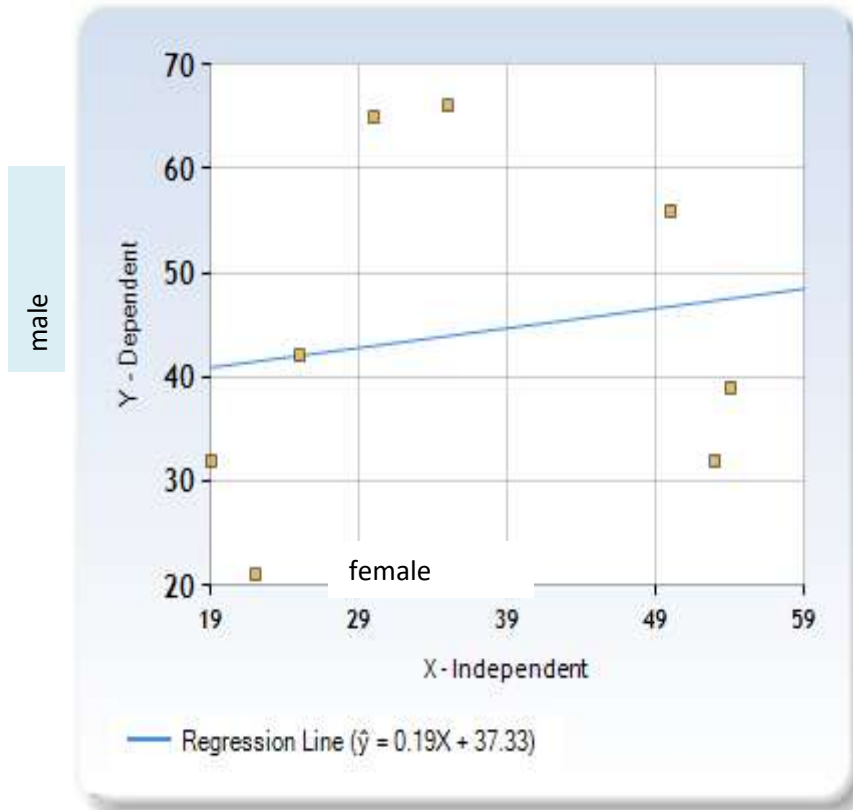
The correlation of coefficient between infection with covid-19 and age in 641 patient with diabetes mellitus type I equals to 0.8165 with P-Value <0.00001 at  $p < 0.05$  which indicates that there is a strong positive correlation between two variable (figure 2).



**Figure 2: Scatterplot for infection with covid-19 and age in 641 patient with diabetes mellitus type I .**

**The infection with covid-19 and gender correlation in patient with diabetes mellitus type I.**

The correlation of coefficient between infection with covid-19 and gender in 641 patient with diabetes mellitus type I equals to 0.027. with P-Value = 0.000029. at  $p < 0.05$  which indicates that the relationship between your variables is weak. Figure 3.



**Figure 3: Scatterplot for infection with covid-19 and gender in 641 patient with diabetes mellitus type I.**

**Conclusions**

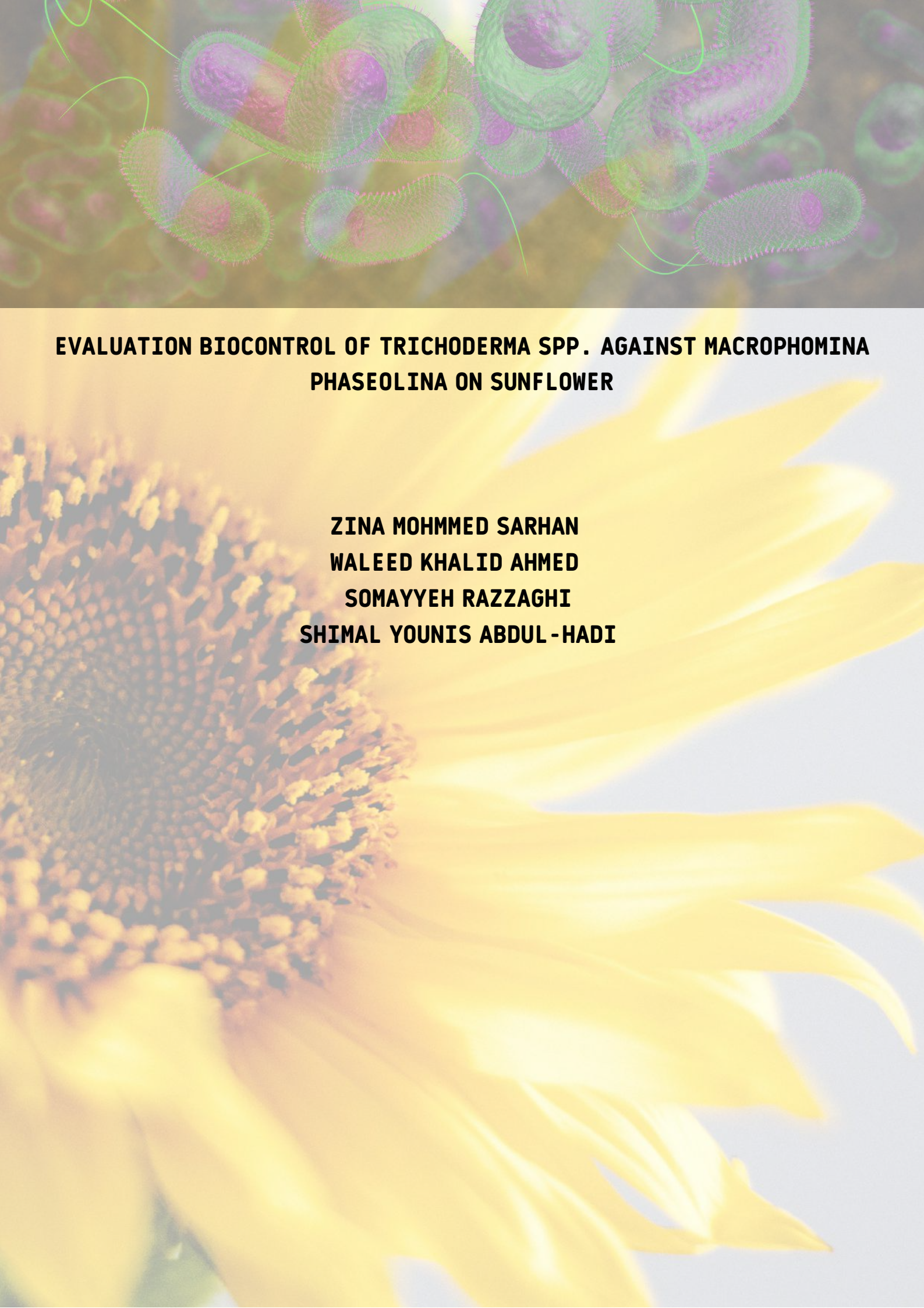
During the COVID-19 pandemic, patients with diabetes mellitus should be aware that COVID-19 can increase blood levels of glucose and, as such, they should follow clinical guidelines for the management of diabetes mellitus .



## References

1. Guan W, Ni Z, Hu Y, et al. Clinical characteristics of coronavirus disease 2019 in China. *N Eng J Med.* 2020. (Epub ahead of print) <https://doi.org/10.1056/NEJMoa2002032>.
2. Remuzzi A, Remuzzi G. COVID-19 and Italy: what next? *Lancet.* 2020. [https://doi.org/10.1016/S0140-6736\(20\)30627-9](https://doi.org/10.1016/S0140-6736(20)30627-9).
3. World Health Organization. (2020). Report of the WHO-China joint mission on coronavirus disease 2019 (COVID-19).
4. Cefalu, W. T., Berg, E. G., Saraco, M., Petersen, M. P., Uelman, S., & Robinson, S. (2019). Classification and diagnosis of diabetes: standards of medical care in diabetes-2019. *Diabetes Care*, 42, S13-S28.
5. FazeliFarsani, S., Souverein, P. C., van der Vorst, M. M., Knibbe, C. A., de Boer, A., & Mantel-Teeuwisse, A. K. (2014). Population-based cohort study of anti-infective medication use before and after the onset of type 1 diabetes in children and adolescents. *Antimicrobial Agents and Chemotherapy*, 58(8), 4666-4674.
6. Harding, J. L., Pavkov, M. E., Magliano, D. J., Shaw, J. E., & Gregg, E. W. (2019). Global trends in diabetes complications: a review of current evidence. *Diabetologia*, 62(1), 3-16.
7. Holman, N., Knighton, P., Kar, P., O'Keefe, J., Curley, M., Weaver, A., ... &Valabhji, J. (2020). Risk factors for COVID-19-related mortality in people with type 1 and type 2 diabetes in England: a population-based cohort study. *The lancet Diabetes & endocrinology*, 8(10), 823-833.
8. Grasselli, G., Zangrillo, A., Zanella, A., Antonelli, M., Cabrini, L., Castelli, A., ... &Zoia, E. (2020). Baseline characteristics and outcomes of 1591 patients infected with SARS-CoV-2 admitted to ICUs of the Lombardy Region, Italy. *Jama*, 323(16), 1574-1581.
9. Yang, J. et al. Prevalence of comorbidities and itseffects in patients infected with SARS- CoV-2:a systematic review and meta- analysis. *Int. J. Infect.Dis.* **94**, 91–95 (2020).
10. Zhu, L. et al. Association of blood glucose controland outcomes in patients with COVID-19 and preexistingtype 2 diabetes. *Cell Metab.* **31**, 1068–1077(2020).
11. Barron, E. et al. Associations of type 1 and type 2diabetes with COVID-19-related mortality in England:a whole- population study. *Lancet Diabetes Endocrinol.***8**, 813–822 (2020).
- 12- Kumar Nathella, P., &Babu, S. (2017). Influence of diabetes mellitus on immunity to human tuberculosis. *Immunology*, 152(1), 13-24.
- 13- Xu, M., Liu, P. P., & Li, H. (2019). Innate immune signaling and its role in metabolic and cardiovascular diseases. *Physiological reviews*, 99(1), 893-948.
- 14- Booth, C. M., Matukas, L. M., Tomlinson, G. A., Rachlis, A. R., Rose, D. B., Dwosh, H. A., ... &Detsky, A. S. (2003). Clinical features and short-term outcomes of 144 patients with SARS in the greater Toronto area. *Jama*, 289(21), 2801-2809.
- 15- Yang, J. K., Feng, Y., Yuan, M. Y., Yuan, S. Y., Fu, H. J., Wu, B. Y., ... & Chan, J. C. N. (2006). Plasma glucose levels and diabetes are independent predictors for mortality and morbidity in patients with SARS. *Diabetic medicine*, 23(6), 623-628.

- 16- Alqahtani, F. Y., Aleanizy, F. S., Mohamed, R. A. E. H., Alanazi, M. S., Mohamed, N., Alrasheed, M. M., ... & Alhawassi, T. (2019). Prevalence of comorbidities in cases of Middle East respiratory syndrome coronavirus: a retrospective study. *Epidemiology & Infection*, 147.
- 17-Deng, S. Q., & Peng, H. J. (2020). Characteristics of and public health responses to the coronavirus disease 2019 outbreak in China. *Journal of clinical medicine*, 9(2), 575.
- 18-Park, S. Y., Kim, J. H., Kim, H. J., Seo, B., Kwon, O. Y., Chang, H. S., ... & Cho, Y. S. (2018). High prevalence of asthma in elderly women: findings from a Korean national health database and adult asthma cohort. *Allergy, asthma & immunology research*, 10(4), 387-396.
- 19-Zhou, F., Yu, T., Du, R., Fan, G., Liu, Y., Liu, Z., ... & Cao, B. (2020). Clinical course and risk factors for mortality of adult inpatients with COVID-19 in Wuhan, China: a retrospective cohort study. *The lancet*, 395(10229), 1054-1062.
- 20-Forbes, A., Murrells, T., Mulnier, H., & Sinclair, A. J. (2018). Mean HbA1c, HbA1c variability, and mortality in people with diabetes aged 70 years and older: a retrospective cohort study. *The lancet Diabetes & endocrinology*, 6(6), 476-486.



**EVALUATION BIOCONTROL OF TRICHODERMA SPP. AGAINST MACROPHOMINA  
PHASEOLINA ON SUNFLOWER**

**ZINA MOHMED SARHAN  
WALEED KHALID AHMED  
SOMAYYEH RAZZAGHI  
SHIMAL YOUNIS ABDUL -HADI**

## EVALUATION BIOCONTROL OF TRICHODERMA SPP. AGAINST MACROPHOMINA PHASEOLINA ON SUNFLOWER

Zina Mohmmmed SARHAN <sup>1</sup>

Waleed Khalid AHMED <sup>2</sup>

Somayyeh RAZZAGHI<sup>3</sup>

Shimal younis ABDUL-HADI<sup>4</sup>

### Abstract:

Sunflower disease *Macrophomina phaseolina* reduces yields by 35 percent in Iraq. The effectiveness of two species of *Trichoderma* against the disease was evaluated because there are no long-term control strategies and it is also difficult to eradicate it chemically. Using universal primer pairs, namely ITS, the *Trichoderma* species *T. asperellum* and *T. longibrachitum* molecular identities were verified. The results showed the highest reduction in the infection percentage and disease severity resulting in 21.07% and 0.18 compared to 74.65% and 0.74, in the presence of pathogen alone, respectively. and lead to an increase in seeds germination percentage, root and shoot dry weight were 93.55%, 33.86, and 200.85 g, respectively, compared to 60.3%, 10.5 and 125.52 g, respectively, in the presence of pathogen alone, also increase in shoot and root heights were 127.3 and 14.8 cm respectively, compared to control 56.67 and 8.36cm, respectively.

**Key words:** *Macrophomina*, Molecular diagnosis, *Trichoderma* spp.



<http://dx.doi.org/10.47832/MinarCongress5-20>

<sup>1</sup> University of Baghdad, Iraq, [zzina6677@gmail.com](mailto:zzina6677@gmail.com), <https://orcid.org/0000-0003-1478-3651>

<sup>2</sup> AL-Hadba University College, Iraq

<sup>3</sup> University of Çukurova, Turkey

<sup>4</sup> University of Mosul, Iraq

## **Introduction:**

*Macrophomina phaseolina*, The pathogen responsible for charcoal rot is a polyphagous pathogen that can be found in soil and seeds. Initially, a virulent isolate of *M. phaseolina* in combination with low moisture and high temperature is required for the development of the charcoal rot disease in sunflowers to succeed. The severity of infection varies depending on the relative humidity, temperature, type of isolation, climate region, and host organism cultivar (Ahmad, 1996). The fungus infects the plants, causing necrotic lesions on various parts of the plant, including the branches, peduncles, and stems. The development of disease is aided by high temperatures and low moisture levels (Aegerter, Gordon, & Davis, 2000). Soybean, sunflower, corn, sorghum, and cowpea are just a few of the economically important hosts that are infected by this pathogen (Csöndes et al., 2012). Non-crop species, such as grasses and weeds, can also be infected by the disease. The ailment in humans many clinical studies have shown that *M. phaseolina* is an intermittent human pathogen that can cause a variety of fungal infections as well as cutaneous infections in addition to its role as a plant pathogen (Srinivasan et al., 2009; D. H. Tan et al., 2008). Prophylactic antifungal treatment for patients with compromised immune systems may result in *M. phaseolina* neutralizing their plant, animal, and human immune systems, according to recent research (Arora, Dilbaghi, & Chaudhury, 2012). Among the world's sunflower crops, *M. phaseolina* (Tassi) Goid. a fungus that causes rot in sunflowers, causes a significant economic loss. The weight and diameter of the head, as well as the height and weight of the stem, have been found to be reduced by the charcoal rot (Khan 2007). Color rot, damping off, charcoal rot, stem rot, root rot, and seedling blight are among the diseases caused by *M. phaseolina*, which affect a wide range of crops important to the economy (Babu, Saxena, Srivastava, & Arora, 2007). Public health and environmental concerns about the use of chemical fungicides have increased as there has been an increase in fungicide-resistant fungal isolates and the availability of fungicides. Several biocontrol organisms, such as AM fungi and Bacillus, Pseudomonas, and *Trichoderma* species, have been isolated, characterized and commercialized over the past few decades. Bacillus, Pseudomonas, and *Trichoderma* species are included in this group. Thus, biocontrol of plant diseases has received more consideration in disease management strategies (Shali et al. 2010).

Previously identified *M. phaseolina* by plating infected plant material or soil on culture media and observing the pathogen's distinct fungal characteristics, which included its black microsclerotia, on the culture media. The enumeration of soil borne inoculum densities has been accomplished through the development of several techniques (Mihail and Alcorn 1982), though these procedures can be time-consuming to complete. Over the last few years, some species-specific molecular diagnostic tools have been developed to help identify the pathogen in a more comprehensive manner. It was first reported by Babu et al. that conventional polymerase chain reaction (PCR) markers could be generated from the internal transcribed spacer (ITS) region of ribosomal DNA (rDNA) (Ijaz et al. 2013). As part of this effort, researchers developed an isothermal loop-mediated isothermal amplification assay for the detection of *M. phaseolina* in soybean plants (Lu et al. 2015). The study aims to control charcoal rot disease biologically. The essential task in this work is to examine the effect of different concentrations of biological

resistance (*Trichoderma*) on the *M. Phaseolina* fungi disease. Also, inspect the effect of this biological resistance on the root height and root dry weight.

### Materials and Method

An intensive survey was conducted on the incidence of charcoal rot in the sunflower growing districts of Salah AL-Din Province (Table 1). Sunflower plants showing typical symptoms on stems bearing and characteristic symptoms of charcoal rot were collected from fields at different locations of Salah AL-Din. In each field, samples of 3–5 plants were collected and taken to the lab. The genus and species names of *M. phaseolina* were used to name the isolates. i.e. M.P

Table 1: Salah al-Din *M. phaseolina* isolates collected from various locations.

S. No.	Name of Region	Isolates
1	AL Alam	M.P1
2	Tikrit	M.P2
3	AL Dour	M.P3
4	Samarra	M.P4

Running water was used to remove soil from the infected plants. After sanitizing the surface of the infected specimen with 1% sodium hypochlorite for 2 minutes, it is rinsed twice with distilled water to remove the disinfectant. Antibiotics were added to Potato Dextrose Agar (PDA) medium to prevent bacterial contamination of the pieces. For 2-3 days, the inoculated petri dishes were kept in the dark at 25 °C. A small portion of the fastest-growing colony of *M. phaseolina* was collected from the perimeter of a 1 cm diameter petri dish and refrigerated at 4°C. The isolated culture (0.5 cm disc) grown on PDA was transferred to a petri dish and incubated for molecular identification.

### Isolation of *Trichoderma spp*

To make 100 ml of distilled water, 5g of the samples were weighed and added. 1000 microliters of diluted samples were then added to potato dextrose medium (PDA). 4-6 days of incubation at 28°C followed the inoculation of PDA plates. Every day, the plates were checked. New PDA plates were incubated at 28°C for 5 days with visible fungal colonies.

### DNA extraction

DNA was extracted using the Chelex®100 rapid extraction method from cultures containing only pure, young, and actively growing hyphae (Dong and Zhao 2006). It was necessary to place the mycelia in a 0.6 mL tube, add 50 L of Chelex®100 solution, and heat for 10 minutes at 95°C to activate them. For 5 minutes, a centrifuge at 12,000 g separated the crude DNA suspension from the cellular fragments. The DNA-containing aqueous layer was carefully removed from the samples and resuspended in 0.2 mL test tubes.

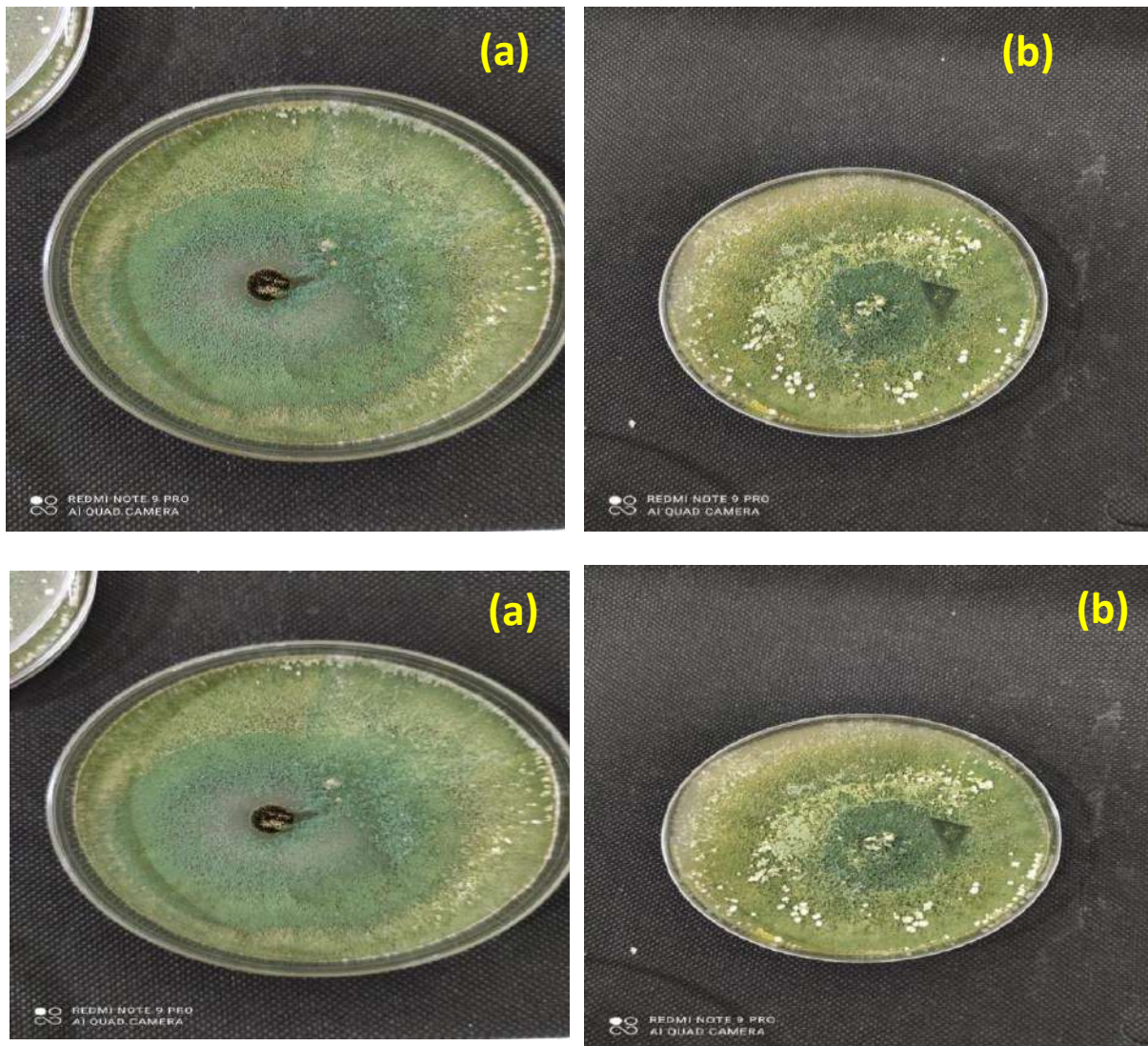
Amplification of DNA using PCR

Use the primers 5'-TCC TCC TAT TAT TGA TAT GC and ITS4 (Integrated DNA Technologies Company, USA) for amplification of the ITS gene. (White et al., 1990)

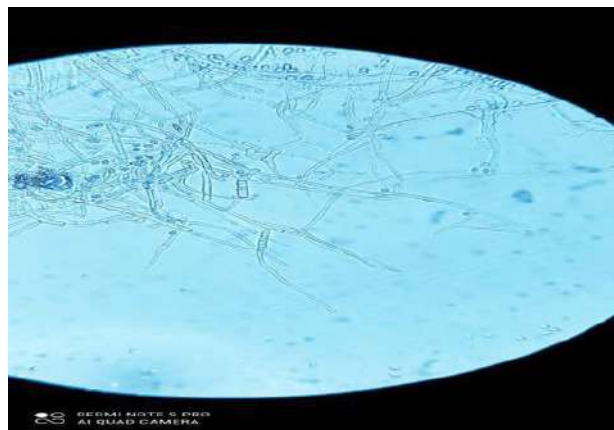
All of the components were mixed in a total volume of 25 milliliters: 5 ml master mix, 1 ml forward primer and the reverse primer, 16ml double-distilled H<sub>2</sub>O, 2 ml of genomic DNA, and 2 ml of double-distilled H<sub>2</sub>O. The reaction was performed in an applied biosystem thermal cycler, which denaturated the mixture at 95°C for 3 minutes, followed by 35 cycles of 94–58°C for 1 minute and 72–72–72°C for 1 minute. The final extension was performed for 7 minutes. Ethidium bromide-coated 1.5 percent agarose gels were used to separate and visualize PCR products.

### **Results and Discussion**

Two types of fungi *Trichoderma* have been isolated in the PDA medium as shown in figure 1. *Trichoderma longibrachiatum* is revealed in figure 1a, this figure depicts the green surface of grown *T. longibrachiatum* with unwanted impurities in the center of the layer (black color). While the *Trichoderma asperellum* is demonstrated in figure 1b, it shows a perfect culture of resistant fungi with a green color over the layer. It should be mentioned that the ability of the *Trichoderma asperellum* to kill the unwanted fungi is connected to the fact that this type of *Trichoderma* is able to produce organic compounds which have agglomerated molecular shapes called Siderfore, as revealed in figure 2 (taken by microscope). These compounds act as preservation of essential elements which are important for the root of the plant and hence it will be easy to absorb the elements from the root.



**Figure 1: Isolate of *Trichoderma* in PDA medium for (a) *Trichoderma longibrachitum*, (b) *Trichoderma asperellum*.**

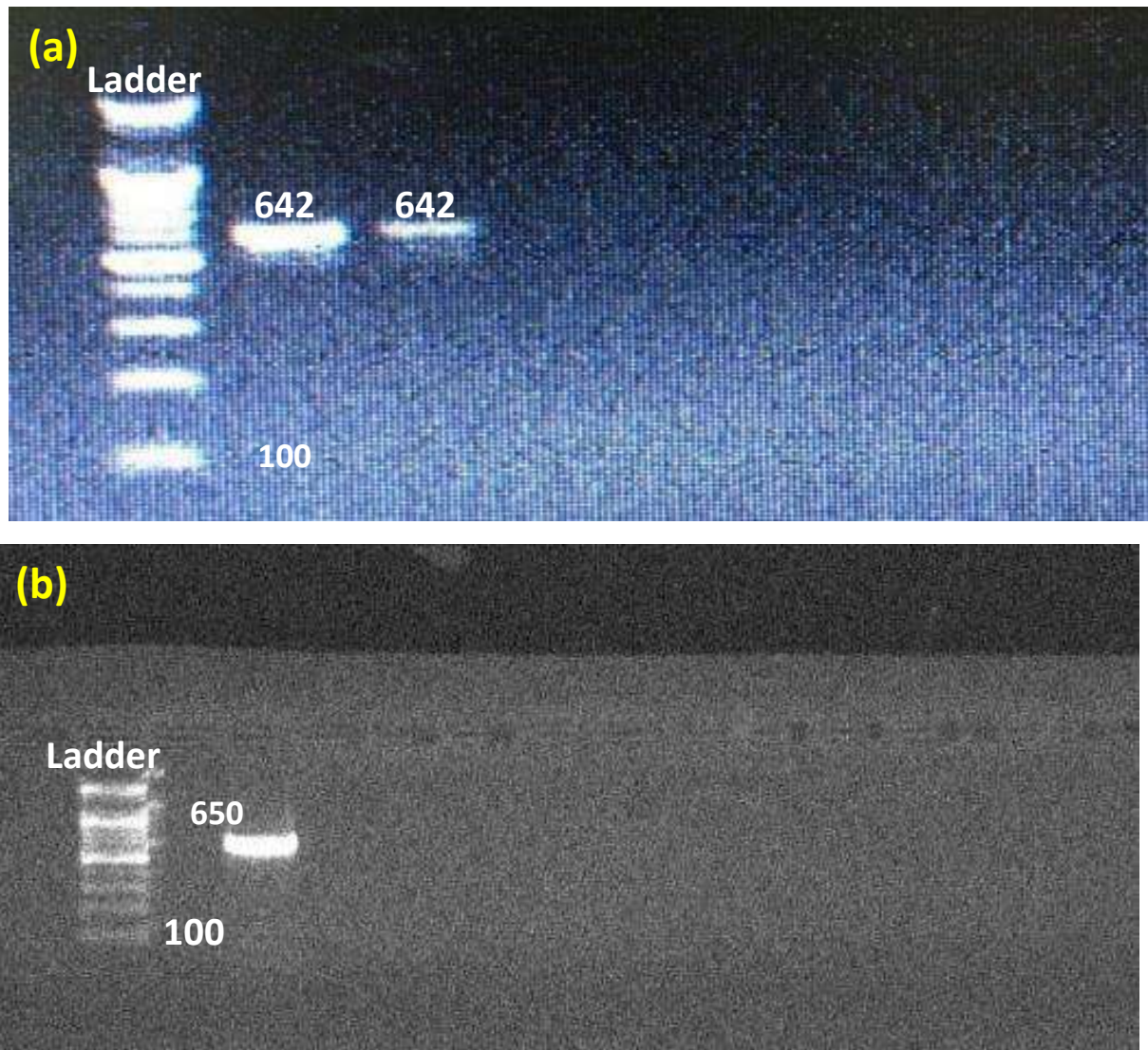


**Figure 2: Microscopic image of *Trichoderma*.**



### Molecular diagnosis

The results of electrophoresis of DNA extracted from isolates of the fungus *Trichoderma spp* and after multiplication with the polymerase chain device using the universal primers ITS4, ITS1 showed the formation of bands with a molecular amount of approximately 642 base pairs, Figure 3a. Molecular 650 base pairs (Figure 3b) of the Tc isolate of *T. longbrachaitum*, and the nucleotide sequences of Derice were determined for the tested isolates. It was compared with global isolates in GenBank under accession numbers MW559031, MW559030. It was also found that the Tc isolates belonging to the fungus *T. longbrachaitum* are 98% identical to the global isolates, and the application of nucleotides for the isolate was deposited in the gene bank under accession number MW559032. Which, based on their nucleotide sequences, lined the Iraqi *T. asperellum* isolates into one group with global *T. asperellum* isolates from Oman and India. While the Iraqi isolates of *T.longbrachaitum* lined up in a second group with global isolates of *T.longbrachaitum* from China, which were separated from *T.harzianum* and *Fusarium sp*.



**Figure 3: Electrophoresis of the genetic material of (a) *Trichoderma asperellum*, (b) *Trichoderma longibrachiatum***

Data in Table (2) indicates that, All studied control treatments superior in decreasing infection percentage and severity of disease of *M.phaseolina* compared with the pathogens alone, the highest value was in *T. longibrachiatum* + *T asperellum* treatment which reached 21.07% and 0.18 respectively, compared to the control (pathogens alone) 74.65% and 0.74.

Table 2: Effect of *T. longibrachiatum* + *T asperellum* in decreasing Infection percentage and severity of charcoal rot disease on sunflower

Treatments	Infection percentage%	Disease severity
<i>M.phaseolina</i>	74.65	0.74
<i>T. l+ M.phaseolina</i>	52.4	0.48
<i>T a+ M.phaseolina</i>	44.7	0,42
<i>T. l+ T a + M.phaseolina</i>	21.07	0.18
Control	0.00	0.00
L.S.D P<0.05	2.45	0.04

**T.l** *T. longibrachiatum* .**T.a** *T asperellum*

Table 3, it can be noted that there is a significant influence from the bio-resistant fungi on the shoot height and root height. The shoot height increases up to (127.6 cm) and root height to (14.8 cm) when the sunflower plant is treated with *Trichoderma* fungi. These results are related to the fact that the threads of the resistant fungi have wrapped around the threads of the *M. Phaseoline*. Thus, the growth of *M. Phaseoline* will be reduced with the increase of resistant biological fungi concentration

Table 3: Effect of *T. longibrachiatum* + *T asperellum* against charcoal rot disease on sunflower plant.

Treatments	Shoothight (cm)	root height (cm)	shoot dry weight (gm)	root dry weight (gm)
<i>M.phaseolina</i>	56.67	8.36	125.52	10.5
<i>T. l + M.phaseolina</i>	100.0	11.4	134.01	15.01
<i>T.a+ M.phaseolina</i>	107.0	12.1	152.40	18.40
<i>T.l+T.a+ M.phaseolina</i>	127.6	14.8	200.85	33.86
Control	150.0	20.00	230.7	37.55
L.S.D P<0.05	1.05	0.94	1.81	0.67

## References

1. Aegerter, B., Gordon, T., & Davis, R., 2000. Occurrence and pathogenicity of fungi associated with melon root rot and vine decline in California. *Plant Disease*, 84(3), 224-230.
2. Ahmad, Y. 1996. Biology and control of corn stalk rot. Ph. D. Thesis, Department of Biological Science, Quaid-i-Azam University, Islamabad, Pakistan,
3. Arora, P., Dilbaghi, N., & Chaudhury, A., 2012. Opportunistic invasive fungal pathogen *Macrophomina phaseolina* prognosis from immunocompromised humans to potential mitogenic RBL with an exceptional and novel antitumor and cytotoxic effect. *European journal of clinical microbiology & infectious diseases*, 31(2), 101-107.
4. Babu, B. K., Saxena, A. K., Srivastava, A. K., & Arora, D. K., 2007. Identification and detection of *Macrophomina phaseolina* by using species-specific oligonucleotide primers and probe. *Mycologia*, 99(6), 797-803.
5. Csöndes, I., Cseh, A., Taller, J., & Poczai, P., 2012. Genetic diversity and effect of temperature and pH on the growth of *Macrophomina phaseolina* isolates from sunflower fields in Hungary. *Molecular biology reports*, 39(3), 3259- 3269.
6. Ijaz, S., Sadaqat, H. A., & Khan, M. N. 2013. A review of the impact of charcoal rot (*Macrophomina phaseolina*) on sunflower. *Journal of Agricultural Science*, 151(2), 222-227
7. Khan, S. N. 2007. *Macrophomina phaseolina* as causal agent for charcoal rot of sunflower. *Mycopath*, 5(2), 111-118.
8. Lu, C., Song, B., Zhang, H., Wang, Y., & Zheng, X. 2015. Rapid diagnosis of soybean seedling blight caused by *Rhizoctonia solani* and soybean charcoal rot caused by *Macrophomina phaseolina* using LAMP assays. *Phytopathology*, 105(12), 1612-1617.
9. Mihail, J., & Alcorn, S. 1984. Effects of soil solarization on *Macrophomina phaseolina* and *Sclerotium rolfsii*. *Plant disease*, 68(2), 156-159.
10. Shali A., Ghasemi S., Ahmadian G., Ranjbar G., Dehestani A., Khalesi N., Motallebi E., Vahed M. 2010. *Bacillus pumilus* SG2 chitinases induced and regulated by chitin, show inhibitory activity against *Fusarium graminearum* and *Bipolaris sorokiniana*. *Phytoparasitica* 38 (2): 141–147.

11. Srinivasan, A., Wickes, B. L., Romanelli, A. M., Debelenko, L., Rubnitz, J. E., Sutton, D. A., . . . Hayden, R. T. 2009. Cutaneous infection caused by *Macrophomina phaseolina* in a child with acute myeloid leukemia. *Journal of clinical microbiology*, 47(6), 1969-1972
12. Tan, D. H., Sigler, L., Gibas, C. F., & Fong, I. W. 2008. Disseminated fungal infection in a renal transplant recipient involving *Macrophomina phaseolina* and *Scytalidium dimidiatum*: case report and review of taxonomic changes among medically important members of the Botryosphaeriaceae. *Medical Mycology*, 46(3), 285-292



**PRODUCED GENETICALLY TRANSFORMED HELIANTHUS ANNUUS L BY  
USING THE ISOLATE OF AGROBACTERIUM TUMEFACIENS (ATMC01)**

**ISLAM YASIR ABDULLAH  
TAGHREED NAWAF AHMED  
ARYAN MOHAMMED HAMED  
RAGHAD NAWAF AL-ZAIDY**

**PRODUCED GENETICALLY TRANSFORMED HELIANTHUS ANNUUS L BY USING THE ISOLATE OF AGROBACTERIUM TUMEFACIENS (ATMCO1)**

**Islam Yasir ABDULLAH<sup>1</sup>**  
**Taghreed Nawaf AHMED<sup>2</sup>**  
**Aryan Mohammed HAMED<sup>3</sup>**  
**Raghad Nawaf AL-ZAIDY<sup>4</sup>**

**Abstract:**

The study was conducted at The Research Unit of the Department of Biology/College of Education for Pure Sciences/University of Mosul. The current study succeeded in finding an efficient protocol to produce genetically transformed vegetative branches of *Helianthus annuus* by direct injection with different densities of the bacterial inoculum of *Agrobacterium tumefaciens*, and this was represented in inducing crown gall to cut the hypocotyls within (13-19) days of injection. The tumors formed on them were characterized by their rapid formation and expansion of their appearance to other unvaccinated sites that exceeded the crown gall in only thirteen days of infection. The genetic transformation callus derived from crown gall is its ability to grow and reproduce on the selective media containing Rifampicin and Gentamycin at a concentration of 40,100 mg / L, in addition to the ability of the vegetative branches resulting from crown gall to grow on the MSO medium Supported by the two antibiotics .The isolated DNA of genetically tissue was amplified by PCR. With specialized primers for the *rol A* gene, as the results of the electrophoresis on the agarose gel showed the separation of one band from each sample to represent the amplified segment of the *rol A* gene and matched the 308 bp molecular weight of the standard used prefixes. The results of the detection of (Octopine) in the tissues of crown gall arising and its callus showed a positive detection indicative of the separation of open spots at sites corresponding to the sites of the standard opines stains mentioned above.

**Key words:** *Helianthus Annuus*, *Tumefaciens*, PCR.



<http://dx.doi.org/10.47832/MinarCongress5-21>



<sup>1</sup> Mosul University, Iraq, [ahellah@uomosul.edu.iq](mailto:ahellah@uomosul.edu.iq), <https://orcid.org/0000-0002-9575-3966>



<sup>2</sup> Mosul University, Iraq, [taghreed.nawaf.ahmed@gmail.com](mailto:taghreed.nawaf.ahmed@gmail.com), <https://orcid.org/0000-0003-3436-9829>



<sup>3</sup> University of Al-Hamdaniya, Iraq, [aryanmohmed@uohamdaniya.edu.iq](mailto:aryanmohmed@uohamdaniya.edu.iq), <https://orcid.org/0000-0003-0772-4864>



<sup>4</sup> Mosul University, Iraq, [raghadnawaf@uomosul.edu.iq](mailto:raghadnawaf@uomosul.edu.iq), <https://orcid.org/0000-0002-6808-8913>

## **Introduction:**

The compound family includes more than a species of economic plants (Silva *et al.*, 2005), including food and oil, many of which are decorative plants (Cronquist, 1977), and the distinctive species of this family is sunflower plants (Heiser, 1976) and lettuce (Ryder, 1986). The compound family plants have received the attention of researchers in the field of plant tissue culture one of the most important biotechnology, which was used in raising and improving the breeding of sunflower (Sarraf et al., 2000). Returns the genus of *Agrobacterium* (Collins, 2001; Furuya *et al.*, 2004) to the Family Rhizabiaceae this genus includes two species the first type *Agrobacterium tumefaciens* that cause crown gall (Young *et al.*, 2001) and *Agrobacterium rhizogens* which causes hairy root disease (Gelvin, 1990). These bacteria enter the plant from modern wounds with vaccination and various agricultural processes, parasitic nematodes and others, and the pathogenic ability of bacteria is due to possess a large extrachromosome plasmid called Ti-plasmid (tumor-stimulating plasmid) which owns the T-piece. DNA is transmitted to the host cell (Zaenen *et al.*, 1974) a specialized inoculative controlled by the onco-gene, which includes t-DNA and interferes with the genetic material of the host plant (Nester *et al.*, 1984) which, when reproduced, causes the formation of crown gall on the infected plant (Deng and Nester, 1998) Note that the T-DNA contains two types of genes, namely the Oncogenic genes that encode the enzymes of the manufacture of oxins and cytocaines responsible for the formation of tumors, and the genes responsible for the manufacture of opines compounds, which express their formation after the interference of bacteria genes with the plant's genetic material (Hooykass and Shilperoort, 1992; Zupan and Zambrysky, 1995). The use of *Agrobacterium tumefaciens* has been highlighted in the genetic transformation of many plants such as Tobacco (Block *et al.*, 1984), Soy (Zhang *et al.*, 1999) and lentils (Samac et al., 2004; Dogan et al., 2005) and Bird's Slipper (Nikolic *et al.*, 2007).

## **2. Materials and Methods**

The study was conducted at the laboratories of the Research Unit in the Department of Biology / College of Education for Pure Sciences / University of Mosul.

### **2.1. Formation of crown gall cultures**

We obtained the seeds of *H. annuus* plants, which were sourced from the local markets and sterilized, then planted the medium of MS, which was used in the development of seedlings used as a source for obtaining the cut hypocotyls for the purpose of inoculating with *A. tumefaciens* and creating the hypocotyls and their crown gall and reconstructing the plants from them, and using the medium above the container (BA 1.0 mg / L + NAA 0.5 mg / L) for the development and differentiation of subocular the calluses of hypocotyl (Al-Aqidi, 2004).

### **2.2. Source of bacteria and preparation of the bacterial suspension**

In this study, *A. tumefaciens* strain (AtMcO1) with a known genotype (rif R), which is isolated from crown galls formed on stems of *Myrtus communis* (Al-Zaidy *et al.*, 2013), prepared a suspension of *A. tumefaciens* (AtMcO1) in YEB medium. The liquid was mixed with a lube campaign of bacteria with 10 ml of liquid medium, and

it was incubated in a vibrating incubator under conditions of  $(28 \pm 2)^\circ\text{C}$  (24) hours in dark conditions.

### **2.3. Inoculation hypocotyl of sunflower seedlings**

The 3-week-old intact sunflower seedlings were prepared in solid MS medium and using a hypocotyls cut of 3 cm long and injected directly with a sterile micro-needle dipped end in the bacterial suspension of *A. tumefaciens* (AtMcO1) and implanted in an upright position in the solid WP medium. At half its synthetic strength, the samples were incubated in the growth room in conditions of complete darkness (24) hours to ensure the growth of bacteria, then the samples were incubated in the growth room under conditions of temperature  $(25 \pm 2)^\circ\text{C}$  (16) hours lighting 1000 lux.

### **2.4. The introduction of crown gall on hypocotyl and the formation of their cultures free of bacteria**

Crown gall formed at the inoculation sites were excised on hypocotyl and transferred to glass flasks with a capacity of 250 ml containing 20 ml of OMS medium supported with progressive gradient concentrations of 100, 250, 500 and 1000 mg / l Chloramphenicol, which was added to the medium after sterilization and reaching a degree  $(45)^\circ\text{C}$  and the period between shift and another was (5-7) days for the purpose of getting rid of bacteria and maintaining them periodically in this medium.

### **2.5. Development of callus cultures from genetically modified crown gall**

The pieces of the crown gall devoid of bacteria were transferred to the solid medium (MS, 1/2 MS) containing the antibiotics mentioned in paragraph (4) (free or supported by some combined interference from the growth regulators of BA), (0.0, 0.250, 0.5 and 0.1). Mg / L and NAA (0.0, 0.250, 0.5, and .01) mg / L and the samples were kept in the culture room under the previously mentioned conditions.

### **2.6. 2.6 Formation of vegetative branches from a crown gall callus**

Transfer 1 gm of crown gall -derived callus on medium (1 / 2MS + 1.0 mgL-1 NAA) into (100) mL flasks each containing 30 mL of 1/2 MSO medium supported with specific additives of BA growth regulators.( 0.0, 0.250, 0.5, .01 and 1.5 (mg / l) and NAA (0.0, 0.250, 0.5, 0.1, and 1.5). mg / l. The samples were kept in the culture room under the previously mentioned conditions

### **2.7. Tolerance test for differentiated vegetative branches of the crown gall callus of rifampicin and gentamicin**

Vegetative branches of 1.5 cm long from the callus of transgenic crown gall were separated using a sterile sharp scalpel, and individually infused into 100 mL flasks containing 30 mL 1 / 2MS medium solid fortified with 1.5 mg / L NAA supplement with 100 mg / L Rifampicin addition And 40 mg / L Gentamycin derived from crown gall callus. The bottles were kept in the culture room, and results were observed within 30 days.

### **2.8.Using the downward paper chromatography technique to detect Napoline in the tissues and callus of crown gall**

The physiological method (Szegedi *et al.*, 1988) was used to detect opins in crown gall cultures and compare them with intact subcellular stalk cultures (not inoculated), and the downstream paper chromatography was performed using



Whatman No.3 filter papers and the spots of transgenic samples were compared with the standard nopalene spots.

### **2.9. Polymerase Chain reaction**

For molecular analysis, DNA was extracted from the crown galls and their callus and the hypocotyls of the differentiated vegetative branches of the crown galls callus using the Genomic DNA Mini Kit Plant from Geneaid.

PCR analysis was performed using a programmed DNA thermal cycler (Gradients PCR). The *rol A* gene (Bushra *et al.*, 2012) forward 5'AGAATGGAATTAGCCGGACTA-3' and reverse primer 5'-GTATTAATCCCGTAGG TTTGTT-3', was used for PCR analysis. The PCR reaction was carried out in 25 µl final reaction volume containing 50 ng DNA template with the following thermal cycling conditions: 35 cycle, three cycle each, [35 cycles of 3 minutes at 94°C, 30 second at 51°C and 30 second at 72°C]. Agarose gel (1.5% w/v) electrophoresis was carried out to analyze PCR product.

## **3. Results and Discussion**

### **3.1. Induction of crown gall on hypocotyl removed from the sunflower *H. annuus* by direct injection with *A. tumefaciens***

The subcellular hypocotyls excised from the sunflower *H. annuus* expressed its response to direct inoculation with *A. tumefaciens* from the formation of the crown gall at the injection sites, and the optical density of the vaccine was superior to OD (0.25) and OD (0.1) in the formation of crown gall on the hypothalamic injected with the vaccine *A. tumefaciens* (AtMcO1) with rates (43.6 and 36.3)%, respectively, Table (1), At high densities (1.0 and 1.5) OD which the cutting of the hypocotyls did not show any response to the formation of tumors as a result of the death of the inoculated pieces and implanted in the middle 10 days after fertilization and the time required for the emergence of these tumors ranged on the pieces after (13-19) days after the injection. In the form of rough swellings (shape) that developed in a number of cases to a large crown with a brown color at the top of the legs or at the crown area. And its positive in induction of

crown gall on the injection areas of the hypocotyls under the injected sites (McCullen and Binns, 2006). The reason for this is attributed to the transmission of the piece of T-DNA that contains the genes responsible for the formation of crown gall and their interference with the genome of the cells of sunflower plants, and its creation of crown gall which are the first signs of a genetic transformation in plants (Islam *et al.*, 1994).

**Table (1) Response of hypocotyl excised from *H. annuus* to direct inoculation with varying densities of *A. tumefaciens* (AtMcO1).2.1Tissue culture**

Optical density for the vaccine(OD)	Num of ber luxury pieces	Resp onse ratio(%)	Duration of tumor formation
0.1	5	36.3	13
0.25	7	43.6	11
0.5	4	26.6	15
0.75	1	6.6	19
1.0	0.0	0.0	0.0
1.5	0.0	0.0	0.0
control	0.0	0.0	0.0

**The numbers represent 15 repeats / comparison**

### 3.2 Formation crown gall cultures.

The results showed that transferring crown gall cultures 3-4 consecutive transfusions on solid MSO medium containing 500 mg / liter of the antibiotic chloramphenicol led to their neutralization of the bacteria as a sign of the absence of bacterial growth in the medium (YEB). The effectiveness of this antibiotic from its expected role in changing the osmosis of bacterial cellular membranes and its effect on the pathways for the manufacture of proteins and enzymes, the multiplication of nucleic acids and the processes of cell division that lead to the death of bacteria and eliminate their effects in plant tissues (Shishido and Piepper., 1990; Yassin *et al.*, 2005) .

### 3.3. Induction of a genetically modified crown gall callus in media free and supported by growth regulators

Culturing of crown gall pieces on MSO and MSO1 / 2 medium, supplemented with different additions of growth regulators, showed their ability to generate callus from them with different proportions Table (2).

Crown gall developing on the MSO and MSO1 / 2 comparison media were characterized by swelling and then developed into lumps of callus 14-17 days after implantation on these two media. The newly introduced callus was characterized by its cream color and semi-coherent structure (figure), and the data in the passing table show that the mean NAA 1.0 + MS 1/2 was superior to its encouragement of callus development in terms of its percentage of 65.2%, which is higher than the rate of creation (45.7%) that we obtained when Culturing of crown gall on 2/1 MS medium supplemented with two overlapping concentrations of BA (1.0) and NAA (2.0).

The ability of crown gall to generate callus in environments devoid of growth regulators or in the absence of cytokinin is explained by their ability to produce growth regulators in quantities that exceed their physiological needs and enhance the occurrence of a state of changes in the hormonal balance, representing a state of selection for genetically transformed callus as in the case of *Vicia faba* crown

gall. (Jelenic *et al.*, 2000) induced on MS0 medium, and selection of *Medicago sativa* plant resistant Neomycin and Kanamycin transgenic (Mckersie *et al.*, 1993).

**Table (2) Generation of crown gall callus of *H. annuus* plants growing on solid 1/2 MS medium with different concentrations of growth regulators.**

Generation medium (mg/l)	Number of tumor/ generation	Generation callus (%)	Duration of callus formation(day)
MSO 1/2	9/32	26.6	14
NAA 1.0+MS 1/2	30/45	65.2	12
NAA 1.0+ BA1.0 +MS 1/2	17/36	45.7	15
MSO (control)	8/36	25.7	17

### 3.4. Maintenance of transgenic crown gall and soft weight estimation

The results of separating the small isolation of the resulting callus from crown gall on the medium of their development and placing them on the appropriate media showed their good growth and the establishment of callus culture, which was distinguished by its semi-cohesive structure and cream color. Based on the results of table (2), the mean medium NAA 1.0 + MS 1/2 was adopted as the best medium for the maintenance of crown gall callus, in which the callus was superior in giving the highest soft weight to the tumor callus was 3.0 g compared with other interventions for 1 / 2 MS medium and the comparison treatment free of growth regulators( table 3)

**Table (3) Estimation of soft weights of callus derived from crown gall of *H. annuus***

Medium (mg/l)	Callus Source	Wet weight (gm)
MS+1.0 BA+0.5NAA	Hypocotyl callus (control)	2.3
1/2 MS+1.0NAA	crown gall callus	3.0
1/2 MS+1.0BA+2.0NAA	crown gall callus	2.0
1/2 MSO	crown gall callus	1.9

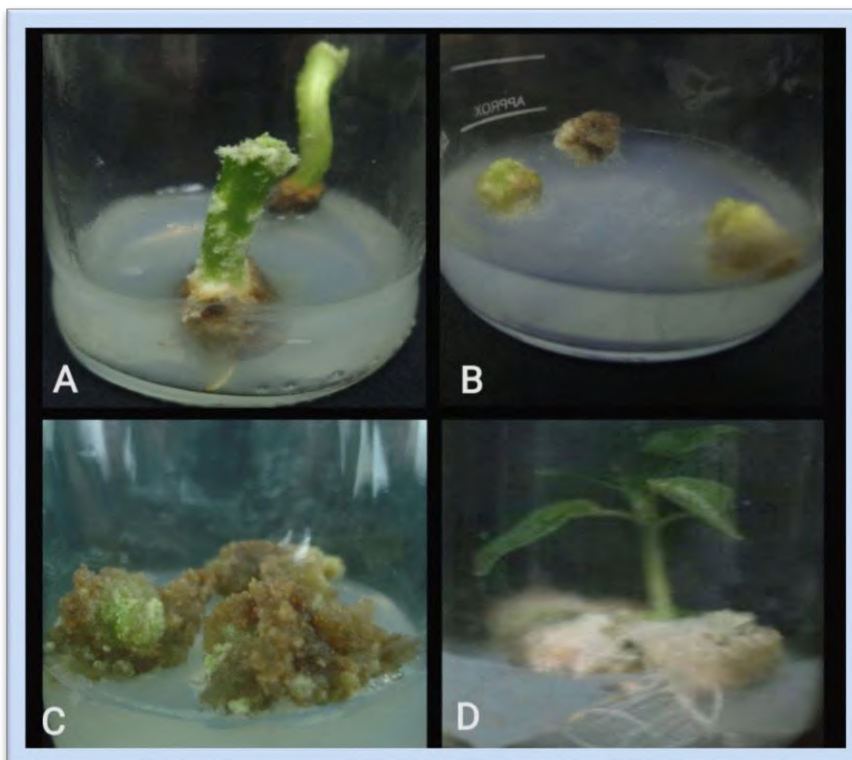
### 3.5. Differentiation of genetically modified crown gall to form vegetative branches

The results of the crown gall callus subjecting to some of growth regulator compntion table (4) showed that some of these compntion encouraged the growth of callus, but did not stimulated its differentiation, as experiments showed the difficulty of callus differentiation derived from genetically transformed crown gall , in comparison with differentiation from hypocotyl callus in one step regenrtion , And due to the need to differentiate this callus and to increase the support of the results of this study in this field, a compntion of 1/2 MS media supported by additions of growth regulators were tested. One of these interactions, which was the medium 1/2 MS + 1.5 mg / L NAA, encouraged the formation of a number of green structures. Green leaves emerged from this callus Piece in 9 days, they developed into vegetative-shaped branches figure (1), And the percentage of its formation was 37% compared to the comparison sample represented by hypocotyl callus

The distinct branches were characterized by their different appearance from the branches arising from the callus of the hypocotyl, where they were characterized by the stunting of their vegetative and the shortening of their leaves, similarly to the genetically modified *Colletotrichum graminicola* plants, which were also characterized by their short lengths and the size of their leaves, the shortening of phalanges and the reduction of the number of leaves. (Flowers & Vaillancourt, 2005).

**Table (4) Composition of the vegetative branches of *H. annuus* from *A. tumefaciens*(AtMcO1) crown gall callus cultures**

Source of vegetative branches (%)	Medium mg/l)(	Number of callus cultures / differentiated	The total number for vegetative branches	Average number of branches / piece	Formation start time	Differentiated %
hypocotyl stem callus (control)	BA+MS + 1.0 NAA 0.5	8/40	20	3	23	25
Transgenic crown gall	1/2MS +1.5 NAA	14/40	24	2	21	37



**Figure (1) Induction and differentiation of (induced) genetically modified crown gall by *A. tumefaciens* on the hypocotyl stem of *H. annuus* plants.**

**A. Development of a crown gall on the hypocotyl stems injected with bacteria.****B. Resection of the crown gall from (A).****C. Callus of crown gall from (B) at the age of 45 days on the medium of induction.****D. The vegetative branches of the crown gall callus are formed in (C).****3.6. Variation of the phenotypic and genetical characteristics of transgenic crown gall callus**

The data presented in table (5) showed that there are several of phenotypic and genetic differences for crown gall callus counterpart the hypocotyl callus. The first was distinguished by its resistance to rifampicin and gentamicin, as well as the containment of a number of green cellular aggregations and who distinguished with creamy-brown color and its semi-coherent nature, in contrast to the callus of the hypocotyl, which was distinguished by its loss of these characteristics of antibiotic resistance and the formation of cellular aggregations and was distinguished by its cream color and fragile nature. The emergence of these phenotypic changes expected to occur in transgenic cultures depends on the type of bacterial strain used and the type of plant (Porter, 1991).

**Table (5) Difference in phenotypic traits between the normal callus of *H. annuus* and the crown gall callus.**

Phenotypic traits	hypocotyl stem callus	transgenic crown gall callus
The color	Light yellow	Dark yellow / brown
Callus resistance to rifampicin and gentamicin	-	+
Formation of a green colored cell pool on the callus	-	+
The nature of callus	crisp	Semi-cohesive

(-): losing the adjective (+): possession of the adjective

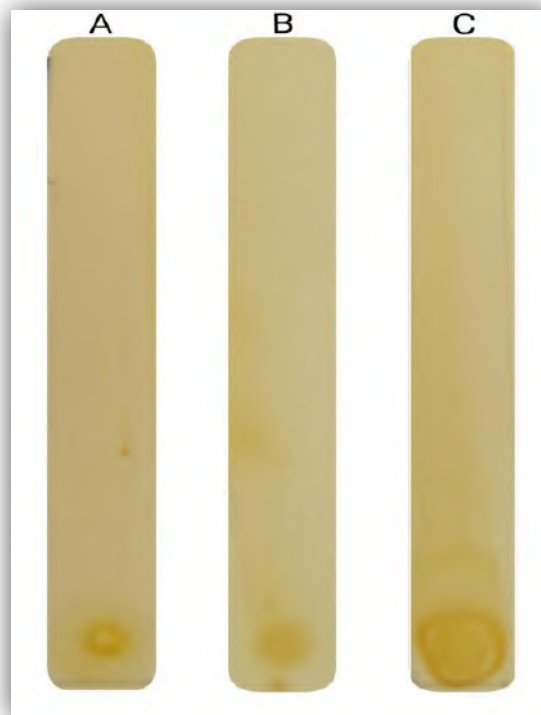
**3.7 The ability of differentiated vegetative branches of crown gall and their transgenic callus to grow in concentrations containing rifampicin and gentamicin.**

The differentiated vegetative branches of *A. tumefaciens* (AtMcO1) induced crown gall showed their ability to grow in the differentiation medium containing (40,100) mg / L of rifampicin and gentamicin respectively and these branches did not show signs of wilting and yellowing, unlike the branches. Differentiated vegetatively from the callus of the hypocotyl (comparison samples) as on the branches treated with these antibiotic with a phenomenon of wilting, yellowing and death appeared. These results show the success of the gene expression of the T-DNA genes in the Ti plasmid of *A. tumefaciens*, and as it happened in the tissues of chickpea plant resistant to Kanamycin at a concentration of (100-150) mg / L

(Sanyal *et al.*, 2002) and the resistance of *M. sativa* to Kanamycin and Streptomycin (Palumbo *et al.*, 1998).

### 3.8 Detection of Octopine in crown gall tissue and callus derived from it

The results of the migration of the extracts of crown gall originating on the hypocotyl injected with the bacteria *A. tumefaciens* (AtMcO1) and there callus on the detachment of the opines stains corresponding to the stains of the standard Octopine, with absence of their appearance from the hypocotyls extracts from the usual hypocotyls and its callus form Figure(2)and explains the response of the hypocotyls of the sunflower in their formation of crown gall, To the overlap between the sunflower plant and the bacterial strain under study and the genome overlap of plant and bacterial cells which resulted in the formation of genetically transformed crown gall according to the evidence for building the Octopine in these tumors which is formed by the genes responsible for coding for the manufacture of opins transferred on the T-DNA segment into a genome of transgenic plant cells and their expression in the manufacture of these unusual amino acids (Fraley *et al.*, 1983).



**Figure( 2):Chromatography of Octopine from crown gall tissue extracts of *H. annuus* induced by *A. tumefaciens* and callus derived from it**

**A-Standard Octopine Spot.**

**B- Octopine blot separated from *A. tumefaciens* induced genetically modified crown gall tissue .**

**C- Octopine stain separation from *A. tumefaciens* induced crown gall callus**

### 3.9. Detection of the genotype of sunflower plants at the molecular level

#### 3.9.1 Concentration and purity of DNA isolated from lant tissues of *H. annuus* transgenic plants

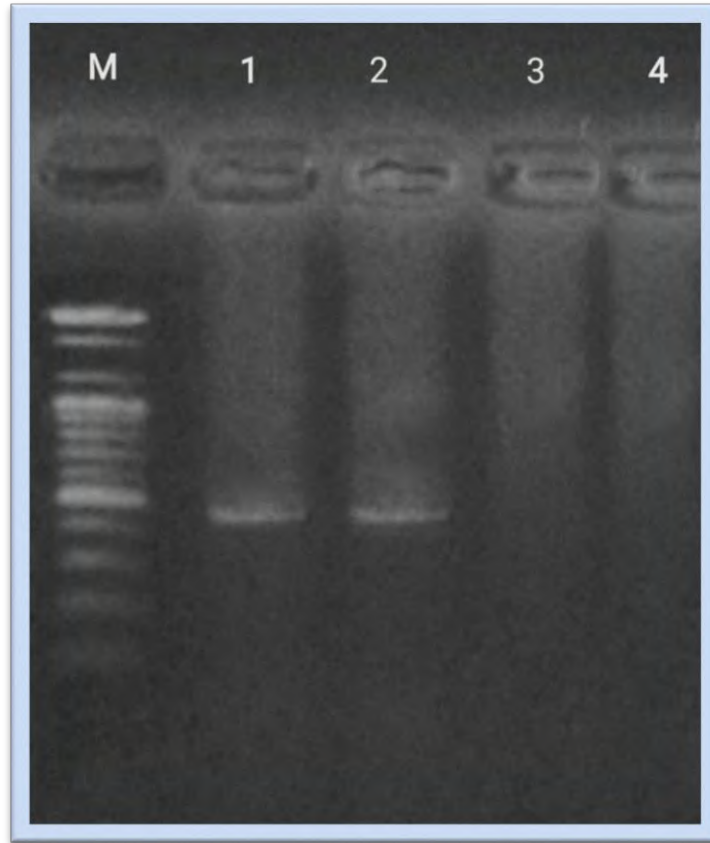
The data on the DNA concentrations of table (6) DNA isolated from the tissues of the crown gall, their callus, and the branches that result from them showed that its concentration in the callus of crown gall formed on the hypocotyls subaploid than that of the callus of hypocotyls under the epithelium, as well as The results of its concentration showed the distinct vegetative branches of Callus of crown gall compared to its concentration from the differential branches of the sub-epithelial callus, and the results showed the purity of the DNA isolated from hypocotyls and their callus, of crown gall and their genetically modified callus by *A. tumefaciens* and the resulting branches at a purity rate ranging between 1.64-1.8.

**Table (6) Concentration and purity of DNA isolated from sub-annular stalk callus tissues of *H. annuus*, *A. tumefaciens*, and the resulting plants.**

Source of DNA		Concentration of DNA (ng/ $\mu\text{g}^{-1}$ )	Purity
Explant	hypocotyl stem piece	980	1.64
	crown gall	1091	1.72
Callus tissues	hypocotyl stem callus	1675	1.7
	crown gall callus	1794	1.68
Regeneration plants	Regeneration from hypocotyl stem callus	1532	1.66
	Regeneration from crown gall	1927	1.8
	Regeneration from crown gall callus	1854	1.7

#### 3.9.2 Molecular analysis

For molecular analysis of transformed regeneration / crown galls and their callus, PCR was performed for *rol A*, gene and the amplified products (308 bp) was observed to confirm transformation. Same size amplified product was also obtained from the plasmid DNA of *Agrobacterium* strains. *rol A* gene was detected in all transformed lines (1, 2) but not in callus and our regeneration Fig (3) The results confirmed the integration of the *Agrobacterium* T-DNA in the genome of *H. annuus* transgenic lines and This is the important result of successful transformation of *H. annuus*; There are some studies in the world within this field, and the outputs of their results are consistent with the results of this study, as the *rol A* gene was diagnosed in *Artemisia dubia* plants (Bushra *et al.*, 2012) Likewise, the researcher's findings (Kiani *et al.*, 2012) revealed that the T-DNA of *A. tumefaciens* strain (LBA 4404) interfered with the tissues of *Artemisia dubia* transgenic plants by diagnosing the ABC *rol* genes and fixing their gene expression in them.



**Figure (3) Presence of the *rol A* gene in DNA amplified samples extracted from the tissues of *H. annuus* transgenic plants with *A. tumefaciens* using 1.5% electrophoresis in agarose.**

**Path (M): A DNA marker of 100 base pairs**

**Path (1): Amplified DNA isolated from a transgenic crown gall callus**

**Path(2): The amplified DNA isolated from the vegetative branches arising from the genetically modified crown gall callus.**

**Pathway (3): The amplified DNA isolated from the callus of the hypocotyl stem**

**Pathway (4): The amplified DNA isolated from the regeneration of hypocotyl stem callus**



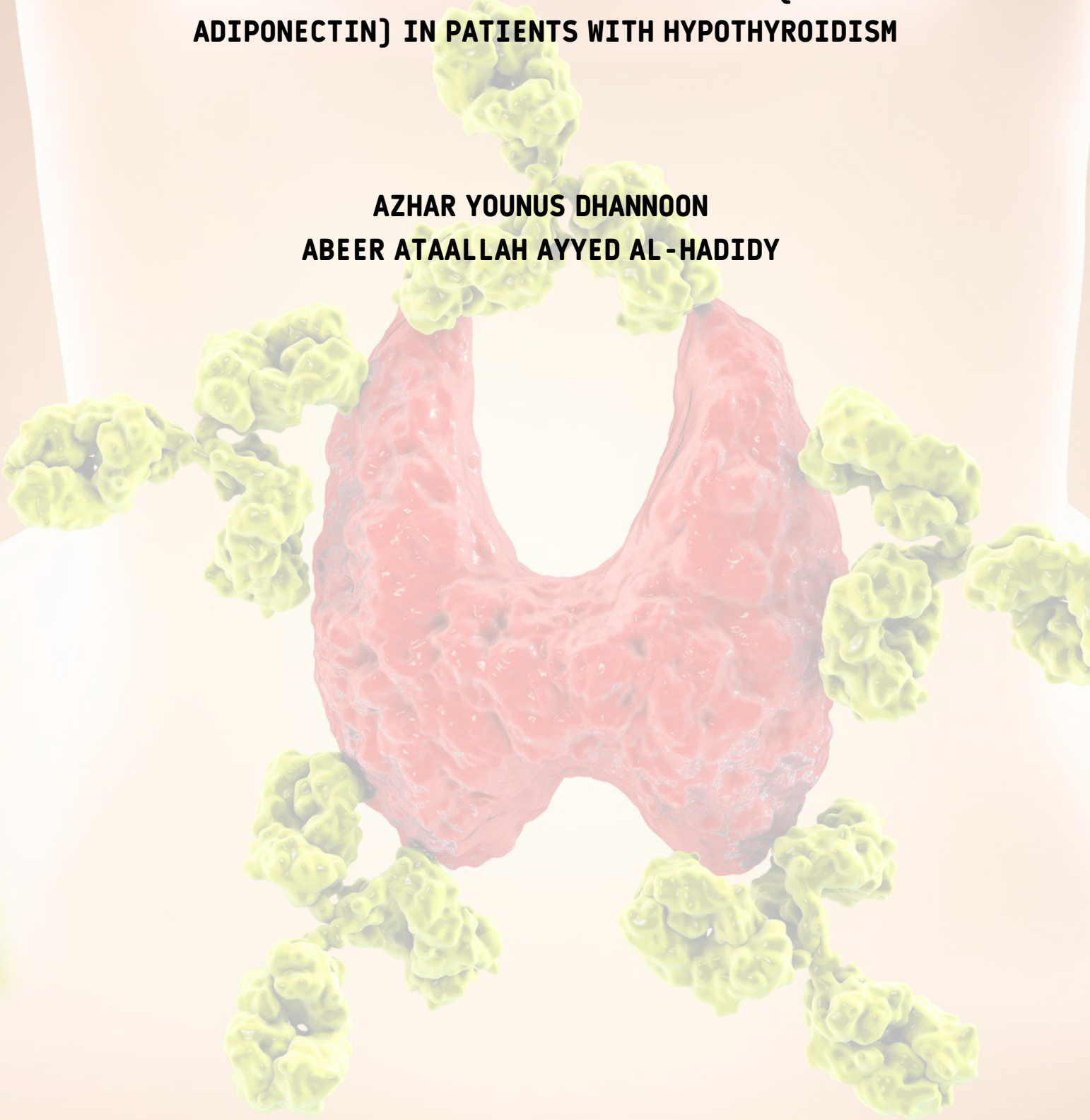
## References

1. Al-Aqidi, Taghreed Nawaf Ahmad (2004). The effect of gamma rays in inducing variations in protein, oil and fatty acid content in the callus of the sunflower plant *Helianthus annuus* L and its differentiation. Master Thesis . College of. Education . University of Al Mosul.
2. Al-Zaidy R. N ., Abdullah N .And Najwa I .(2013) Isolation and identification of *Agrobacterium tumefaciens* from the Crown gall of Myrtus communis plants. The Second International Sixth Annual Scientific Conference of the College of Basic Education - University of Mosul/Iraq.
3. Block, E.D; Herrera-Estrella, M.L; Van Montagu,M;Schell and Zambryski,P. (1984) Expression of foreign genes in regenerated plants and in their progeny. J.EMBO., 3:1681-1689.
4. Bushra Hafeez Kiani<sup>1</sup>, Naila Safdar<sup>1</sup>, Abdul Mannan and Bushra Mirza (2012).Comparative Artemisinin analysis in Artemisia dubia transformed with two different Agrobacteria harbouring rol ABC genes. Pant Omics Journal . 5(4):386-391.
5. Collins, A.( 2001).*Agrobacterium tumefaciens* <http://www.cals.ncsu.edu/course/PP728/Agrobacterium/Alyssa-collins/profile.Htm>.
6. Cronquist , A.(1977) , The Compositae Revisited . Brittonia .29:137-153 .
7. Deng,W.and Nester,E.W.(1998) .Determinants of Host Specificity of *Agrobacterium* and Their Function. In the Rhizobiaceae. Kluwer Academic Publishers, P. 321-338.
8. Dogan, D.; Khawar, K, M and Sebattin, O. (2005).*Agrobacterium* mediated tumor and hairy root for motion from different explant of lentils derived from yong seedlings.Int. J. of Agriculturs and Bio.,6:1019-1025.
9. Flowers,W and Vaillancourt, L. (2005). *Agrobacterium tumefaciens* mediated transformation of Colletotrichum graminicola and Colletotrichum sublineolum .Current Genetics., 48:380-388.
10. Fraley, R.T.; Rogers, R.B.; Horch. P. R .; Sanders, S.P.; Flick, S.P.; Adams, M.L.; Brttner, L. A.; Brand, C. L.; Fink, J.S.; Fry, G. R.; Galvppi, S.P.; Goldbery,N.L. and Hoffmann , S .(1983).
11. Expression of bacterial genes in plant cells.Proc. Natl.Acad.Sci., USA., 80:4803-4807.
12. Furuya, N.; Shimokusuzono, y.; Nakamura, K. N.M.; Takeshita, N. M. and Takanami, K.M.Y.(2004). Crown gall of tobacco caused by *Agrobacterium tumefaciens* Biovar I in tobacco fields. J. Gen. Plant Pathol., 70:39-44.
13. Gelvin, S.B. (1990).Crown gall disease and hairy root disease. Plant Physiol., 92:281-285.
14. Heiser,C.B.(1976). Sunflower In: Evolution of Crop Plants .Ed.N.W. Simonds.Pp 36-38 .
15. Hooykass, P.J.J. and Shilperoot, R.A.( 1992).*Agrobacterium* and plant genetic engineering. plant Molecular Biology, 19:15-38.
16. Islam,R.;Malik,T;Husnian,T.;and Riazudding,S.(1994). Strain and cultivar specificity in the *Agrobacterium* Chickpea ineteraction .Plant Cell Reports., 13:561-563.
17. Jelenic, S.; Peter, T.; Mitrikeski, D. P. and Jelaska, A. (2000). *Agrobacterium* mediated transformation of bread bean *Vicia faba* L. Food Technol and Biotechnol., 38: 167-172.
18. Kiani,B.H.; Nailasafdar., A. M. and Mirza, B. (2012.) Comparative artemisinin analysis in Artemisia dubai transformed with different Agrobacterium harbouringrol ABC genes. J.Omics, 5: 386-391.
19. Mccullen, C.A.and Binns, A.N. (2006) .*Agrobacterium tumefaciens* and plant cell interactions and activities required for interkingdom macromolecular transfer. Annual review of Cell and Developmental Biology, 22:101-127.
20. Mckersie ,B. D.;Yurong, C.; Mitchel, B.; Stephen ,R.B.;Chris,D .;Kathleen, D.; Halluin ,D. and Johan ,B.(1993). Superoxide dismutase enhances tolerance of freezing stress in transgenic Alfalfa (*Medicago sativa* L). Plant Physiol.,103:1155-1167.
21. Nester, E.W.; Gordon, P. M; Amasino, R and Yanofsky, M. (1984). Crown gall: amdecular and physiological analysis .Ann. Rev. Plant Pathology, 35:387-413.

22. Nikolic ,R.;Nevena, N.;Slavtca, N. and Mirjana, N. (2007) .Efficient genetic transformation of *Lotus corriculatus* L using a direct shot regeneration protocols,stepwise Hygromycin B-selection ,and A super-binary *Agrobacterium tumefaciens* vector. Arch. Biol. Sci.,59 (4):311-317.
23. Palumbo, D. J. ; Donald A.P.and Clavence I Kade .(1998). Characterization of A new *Agrobacterium tumefaciens* strain from Alfalfa (*Medicago sativa* L). Arch Microbiol.169:381-386.
24. Porter,J.R.(1991). Host range and implications of plant infection by *Agrobacterium rhizogenes*. Crit.Rev.Plant.Sci.,10:387-421.
25. Ryder ,E.J.(1986) . Lattuca Breeding . InBreeding Vegetable Crops . AUI Pub .West port, Ct.pp 433-474 .
26. Samac, D.A.; Mesfin ,T.;Melinda, D.; Purev, S.and Stephen J.T.(2004) A comparison of constitutive promoters for expression of transgenic in alfalfa.Trangenic Research.13:349-361.
27. Sanyal,L.; Singh,A.K and Amla,D.V.(2002). *Agrobacterium tumefaciens* mediated transformation of Chickpen (*Cicer arietinum* L) using mature embryogenic axes and cotyledonary nodes. Ind. J.Biot., 2(4): 533-538.
28. Sarrafi , A.; Kayyal , H.; Al-Chaarani , R.G.;Cantin , F., Cheline ,A.S.and Durielle ;E.(2000). Inheritance of organogenesis parameters in cotyledons of sunflower *Helianthus annuus* L.J.Genet.& Breed . 54: 227-231 .
29. Shishido, M. and Pepper,I.L. (1990). Identification of dominant indigenous *Rhizobium meliloti* by plasmid profiles and intrinsic antibiotic resistance. Soil Bio. Bioch., 22: 11-16.
30. Silva ,N.C.B.; Macedo , A.F.;Lage ,C.L.S.;Esquibel , M.A.and Sato ,A.(2005) .Brazilian Archives of Biology and Technology . An International Journal .48(5) : 779-786.
31. Szegedi ,E.; Czako, M.; Otten, L.; Koncz, C. (1988). Opines in crown gall tumors induced by biotype 3 isolates of *Agrobacterium tumefaciens*. Physiol. Mol. Plant Pathol.,32:237-24.
32. Yassin,A.; Fredrick,K. and Mankin, A. S. (2005). Deleterious mutation in small subunit ribosomal RNA identify functional sites and potential targets for antibiotics. Proc. Nat.Acad.Sci.,102: 16620-16625.
33. Young, J.M.; Kuyken, L.D.;Martinez ,R. E.; Kerr A.;Sawada, H. .(2001).A revision of *Rhizobium* 1889 with an emended description of the genus, and the inclusion of all species of *Agrobacterium* and *Allorhizobium undicola*. As new combinations: *Rhizobium radiobacter*, *R.rhizogenes*, *R.rubi*, *R. undicola* and *R.vitis*. International Journal of systematic and Evolutionary Microbiology ,51: 89-103.
34. Zaenen, I.; Van, L. N.; Van, M. M. and Schell ,J. (1974). Supercoiled circular DNA in crown-gall inducing *Agrobacterium* strains. Journal of Molecular Biology, 86: 109-127.
35. Zhang,Z.;Aliqinxing,P.; Staswick and Thomas,E.E. (1999). The use of glufosinate as a selective agent in *Agrobacterium* mediated transformation of Soybean.Plant Cell,Tissue and Organ Culture, 56: 37-46.
36. Zupan, J. R. and Zambryski, P.C. (1995). Transfer of T-DNA from *Agrobacterium* to the plant cell. Plant Physiology, 107:1041-1047.

**ESTIMATION OF SOME ADIPOSE TISSUE HORMONES (VISFATIN AND ADIPONECTIN) IN PATIENTS WITH HYPOTHYROIDISM**

**AZHAR YOUNUS DHANNOON  
ABEER ATAALLAH AYYED AL-HADIDY**



## **ESTIMATION OF SOME ADIPOSE TISSUE HORMONES (VISFATIN AND ADIPONECTIN) IN PATIENTS WITH HYPOTHYROIDISM**

**Azhar Younus DHANNOON<sup>1</sup>**

**Abeer Ataallah Ayyed AL-HADIDY<sup>2</sup>**

### **Abstract:**

Hypothyroidism is a medical state referring to the lack of secretion of thyroid hormones (THs) in the body. It occurs when the thyroid gland starts to produce and secrete a small amount of thyroid hormones Thyroxine (T4) and Triiodothyronin (T3), this will affect body cells, resulting in a slowing of the body's metabolic rate, weight gain, and tachycardia. Visfatin and adiponectin are two hormones from type adipokine produced from fat tissue. Those hormones have an important function in protein, lipid and glucose metabolism, as well their role in energy expenditure. Eighty cases of both sexes (male and female) have been collected from the hospitals and private laboratories of Iraq. They are divided into two groups. Group1 (control group) includes (40) healthy individuals and the group2 includes (40) hypothyroid patients, All patients and controls underwent history taking, determination of levels of visfatin, adiponectin, Thyroid-stimulating hormone (TSH), T4, T3 and lipid profile. The results showed that Visfatin levels in group 2 were significantly higher than in group1, on the other hand, Adiponectin levels decreased in group2 compared with the control group at probability ( $P \leq 0.01$ ), and concerning the lipid profile, there was a significant increase in the levels of lipid parameters total cholesterol (TC), triglycerides (TG), low density lipoprotein (LDL-c) and very low density lipoprotein (VLDL) while high density lipoprotein (HDL) was decreased in group2 compared to control group.

**Key words:** Adipokine Hormones, Hypothyroidism, Lipid Levels.



<http://dx.doi.org/10.47832/MinarCongress5-22>



<sup>1</sup> University of Mosul, Iraq, [Zezobss82@gmail.com](mailto:Zezobss82@gmail.com), <https://orcid.org/0000-0003-4917-7731>



<sup>2</sup> University of Mosul, Iraq, [abesbio53@uomosul.edu.iq](mailto:abesbio53@uomosul.edu.iq), <https://orcid.org/0000-0001-8981-1229>

## **Introduction:**

Hypothyroidism is a medical term referring to lack of production and secretion of  $T_3$  and  $T_4$  from the thyroid gland. These hormones are necessary for body growth and development of the brain, so deficiency of THs in infancy and childhood leads to a serious delay in neurological development resulting in mental retardation (Mohammadi *et al.*, 2019).

Initially, Adipose Tissue (AT) was thought to be a site for fat storage. Recently, it is considered as an endocrine gland that secretes a variety of hormones, adipokines, cytokines and growth factors (Ahima and Lazar, 2008). It is participated in some disorders such as heart diseases like hypertension by initiating fat cell inflammation or in diseases related to metabolism including obesity, diabetes type 2 (Gulcelik *et al.*, 2009).

Thyroid dysfunction may affect fat tissue action that involves to disorders related to metabolism. Changes of lipolysis occur in patients with thyroid dysfunction (Chen *et al.*, 2016). Several types of adipose tissue, including white, brown, and beige, have been identified so far, and they are found in various anatomical locations throughout the body. According to location, it can be classified as visceral and subcutaneous (Chait and den Hartigh, 2020). The adipokine which called visfatin is produced by different types of tissues, this hormone regulate the metabolism of glucose and involved in resistance mechanism of insulin as well as in inflammation mechanism (Qiu *et al.*, 2019). This hormone secreted by visceral adipose tissue (VAT) having a similar effect of Insulin, this useful role was confirmed by experimental studies (Hajianfar *et al.*, 2012). It known first as Nicotinamide Phosphoribosyl Transferase (NAMPT) because of its functional and biochemical homology with NAD biosynthesized from nicotinamid. Visfatin hormone has the ability to bind to insulin receptors and is in a distinct position from insulin, thus allowing it to exert its effect on blood sugar level by preventing the liver from secreting glucose from its cells and increasing the ability of peripheral tissues to use glucose. In addition, studies show the ability of visfatin to cross into the cell cytoplasm and nucleus, where it enhances various biological behaviors development such as the metabolism of energy, inflammation and the longevity of the cell. Visfatin had a positive correlation with obesity, since weight gain is one of the hypothyroidism symptoms leading to obesity, so visfatin levels were be higher in hypothyroid subjects (Yang *et al.*, 2016).

Adiponectin (ADP) is another adipokine secreted from the AT. This glycoprotein (30-kDa) consist of an N-terminal signal sequence, hypervariable region, a collagenous domain, and a C-terminal globular domain (Fang and Judd, 2018). ADP had a negative correlation with adiposity, it has been demonstrated that it is down-regulated in metabolic syndrome. (Yildiz *et al.*, 2013). ADP had a role in lipid and carbohydrate metabolism via its receptors (AdipoR<sub>1</sub> and AdipoR<sub>2</sub>), in mouse liver disturbances of these receptors causes an increase in content of triglyceride tissue, oxidative stress and inflammation that leads to insulin resistance and characterized glucose in tolerance (Tsuchida *et al.*, 2005). Additionally, it has been showed to be associated with the metabolism of lipoprotein parameters, most notably the HDL and TG metabolism (Christou and Kiortsis, 2013). Adiponectin reduced serum TG through activation of the breakdown of lipoproteins which is riches with triglyceride by increasing skeletal muscle lipoprotein lipase LPL and

VLDL receptors expression and consequently VLDL-TG catabolism (Qiao *et al.*, 2008).

**Aims:** The current study aims to determine visfatin and adiponectin levels in hypothyroid patients as well as to a better understanding of the relation between visfatin, adiponectin with related hormones T<sub>3</sub>, T<sub>4</sub> with lipids level.

### Materials and Methods

Samples were collected for eighty patients of both gender from Iraqi public hospitals, health centers and private laboratories in the governorates of Nineveh and Erbil for a period of 7 months. High TSH and low T<sub>3</sub> and T<sub>4</sub> were adopted as the basis for diagnosing cases of hypothyroidism, and they were divided into:

Group<sub>1</sub>: Control group, involve forty patients with normal thyroid function test and without chronic disease.

Group<sub>2</sub>: the hypothyroidism group, involve forty patients with high TSH and low T<sub>3</sub> and T<sub>4</sub> level.

The patients were subjected to a set of questions that included personal information, what are the symptoms of the disease and what are the other comorbidities, then blood samples were collected for the purpose of measuring the hormones required in the research by 5 ml of venous blood and after separating the serum by centrifuge, the serum was frozen at (- 20) °C until the collection of samples is completed for the purpose of measuring the level of hormones and lipid levels.

### Hormonal and Biochemical Analysis

The level of TSH, T<sub>3</sub> and T<sub>4</sub> was estimated using the French Biomerieux analysis kit and its method is based on the enzyme immunoassay competition method with final Fluorescent detection (ELIFA).

Adiponectin was estimated using the Sunlong company analysis kit and Visfatin was estimated using the by American Mybiosource company analysis kit, each of them depend on the enzyme-linked immunosorbent assay (ELISA).

French company Biolabo SAS analysis kit used to estimated TC, TG and HDL-c. Serum level of LDL-c was calculated by Friedewald equation (Friedewald *et al.*, 1972).

$$\text{VLDL-C}=\text{TG}/5 \quad \text{Therefore: } \text{LDL-c} = \text{TC} - [\text{HDL-c} + \text{TG} / 5]$$

### Statistical Analysis

Complete random design and the one way analytic of variance (ANOVA) and Duncan multi-range test were used to analyzed the data according to the simple experiments system, different alphabetic letters indicates that there are significant different parameters (SAS, 2004).

In addition, Pearson's correlations were used in this study to determine the relationship between the hormones visfatin and adiponectin with thyroid function tests (TSH, T<sub>4</sub> and T<sub>3</sub>) and lipid profile (Steel *et al.*, 1997).

## Results

According to table 1 and table 2, the results observed a significant decrease at ( $P \leq 0.01$ ) in  $T_4$ ,  $T_3$  and the hormone adiponectin in group<sub>2</sub> (the hypothyroidism group) which involve forty patients with high TSH and low  $T_3$  and  $T_4$  level, .when compared with group<sub>1</sub> (control group) which involve forty patients with normal thyroid function test and without chronic disease. On the other hand observed a significant increase at ( $P \leq 0.01$ ) in visfatin, TSH and all parameters of lipid in hypothyroidism group except in HDL parameter had a significant decrease compared with control group. In addition we found that visfatin has a positive correlation with TSH ( $r = 0.776$ ) and a negative correlation with  $T_4$  ( $r = 0.809$ ) and  $T_3$  ( $r = 0.781$ ) at ( $P \leq 0.01$ ) as shown in table (3), and we found that ADP has a positive correlation between  $T_4$  ( $r = 0.627$ ) and  $T_3$  ( $r = 0.608$ ) in addition to a negative correlation with TSH ( $r = 0.797$ ) at ( $P \leq 0.01$ ) as shown in table (3).

**Table 1: Hormonal levels in the two studied groups**

Groups Parameters	Group <sub>1</sub> means $\pm$ standard deviation	Group <sub>2</sub> means $\pm$ standard deviation
TSH $\mu$ IU/ml	1.78 $\pm$ 0.70 b	15.39 $\pm$ 3.62a
$T_4$ pmol/l	11.29 $\pm$ 2.29 a	2.81 $\pm$ 1.55 b
$T_3$ pmol/l	4.20 $\pm$ 0.71 a	1.54 $\pm$ 0.72 b
ADP (ng/ml)	5.13 $\pm$ 0.94 a	2.09 $\pm$ 0.83 b
Visfatin (ng/ml)	9.29 $\pm$ 1.90 b	14.12 $\pm$ 2.38 a

\*Group<sub>1</sub>: (control group): involve forty patients with normal thyroid function test and without chronic disease.

\*Group<sub>2</sub>: (the hypothyroidism group): involve forty patients with high TSH and low  $T_3$  and  $T_4$  level.

\*The results of the control group were within normal limits

**Table 2: Lipid profile levels in the two studied groups**

Groups Parameters	Group <sub>1</sub> means $\pm$ standard deviation	Group <sub>2</sub> means $\pm$ standard deviation
TC (mg/dl)	152.5 $\pm$ 10.34 b	221.36 $\pm$ 42.11 a
TG (mg/dl)	117.20 $\pm$ 14.82 b	225.24 $\pm$ 46.17 a
HDL (mg/dl)	33.01 $\pm$ 8.41 a	25.51 $\pm$ 5.19 b
LDL (mg/dl)	96.2 $\pm$ 12.33 b	151.13 $\pm$ 43.83 a
VLDL (mg/dl)	23.29 $\pm$ 2.98 b	45.04 $\pm$ 9.23 a

\*Group<sub>1</sub>: (control group): involve forty patients with normal thyroid function test and without chronic disease.

\*Group<sub>2</sub>: (the hypothyroidism group): involve forty patients with high TSH and low T<sub>3</sub> and T<sub>4</sub> level.

\*The results of the control group were within normal limits

**Table 3: Correlation between visfatin and adiponectin with others parameters in group 2.**

Parameters		ADP ng/dl	Visfatin ng/dl
TSH $\mu$ IU/ml	Pearson Correlation	-.797	.776
T4 pmol/l	Pearson Correlation	.627	-.809
T3 pmol/l	Pearson Correlation	.608	-.781
TC mg/dl	Pearson Correlation	-.682	.715
TG mg/dl	Pearson Correlation	-.730	.780
HDL mg/dl	Pearson Correlation	.639	-.541
LDL mg/dl	Pearson Correlation	-.531	.571
VLDL mg/dl	Pearson Correlation	-.722	.781

## Discussion

The results showed that Visfatin levels in group 2 were significantly higher than in group<sub>1</sub>, on the other hand, Adiponectin levels decreased in group<sub>2</sub> compared with the control group at probability ( $P \leq 0.01$ ), and concerning the lipid profile, there was a significant increase in the levels of lipid parameters total TC, TG, LDL-c and VLDL while HDL was decreased in group<sub>2</sub> compared to control group.

According to the results, there is a significant increase of visfatin concentrations in hypothyroid group compared to the control group. This is agree with the study of Cinar and Gurlek, they reported that visfatin levels were higher in hypothyroidism patients (Cinar and Gurlek, 2013).

Several studies have investigated the correlation between visfatin and thyroid hormones, controversial findings have been reported. The cytokine IL-6 considered as pro-inflammatory cytokine, which can stimulate visfatin expression in vitro, and this cytokine is higher in patients with thyroid disorders. As a result, pro-inflammatory cytokines linked to thyroid dysfunction are likely to have an directly or indirectly effects on visfatin secrete from fat tissue (Mishra *et al.*, 2018).

Abdelsalam and Edrees, (2015) in their experiment on rats, they discovered irregular levels of adipokines, which they induced experimentally by administering propylthiouracil (0.05% in drinking water) and L-thyroxine (subcutaneous) for 3 weeks, as well as they found that hyperthyroid rats had a lower concentration of visfatin compared to controls. While in rats with hypothyroidism, it caused a significant increase in visfatin levels. They also discovered relationship, but in reverse between visfatin and T<sub>3</sub> and T<sub>4</sub>, also a positive link between visfatin and



TSH (Abdelsalam and Edrees, 2015). Depending on some experimental results,  $T_3$  has an important role by increasing the level of visfatin, thus accelerating the differentiation of fat cells (Tanaka *et al.*, 2007). Whilst, MacLaren *et al.*, (2007) observed that the expression of visfatin mRNA is reduced by  $T_3$  in fat cells type 3T3-L<sub>1</sub> (MacLaren *et al.*, 2007).

Some studies have reported a positive correlation between visfatin and adiposity. The excess visfatin could be due to the activation of macrophages in AT because visfatin plays a role in the differentiation of adipocytes (Fukuhara *et al.*, 2005). Gaining weight is elevated in hypothyroidism, leading to obesity (Yildiz *et al.*, 2013). The expression of the visfatin gene in visceral fat is higher in obese people, and the plasma concentration of visfatin is closely connected to visceral fat more than subcutaneous fat (Fukuhara *et al.*, 2005).

Our findings are consistent with Ozkaya *et al.* (2009) who noticing a strong positive correlation between levels of visfatin with TSH, as well as a negative association between levels of visfatin with values of  $T_3$  and  $T_4$  (Ozkaya *et al.*, 2009). These correlations might be explained throughout the downregulation of visfatin with  $T_3$  (MacLaren *et al.*, 2007). Moreover, a strong positive correlation between levels of visfatin with TSH had better understand by the receptors of TSH, which distributed and expressed in fat cells so stimulation of this receptors may causing visfatin secretion (Alshaikh *et al.*, 2019; Briet *et al.*, 2018).

Our results observed a significant decrease of adiponectin concentrations in group<sub>2</sub> compared to the control group. Available research in vivo has indicated a biologically interaction between thyroid hormones and that adiponectin hormone. Thyroid hormones' action on expression of adiponectin gene in thyroid disorder, on the other hand, are unknown (Seifi *et al.*, 2011).

Thyroid hormones may directly induce ADP production. Peroxisome proliferator activated receptor gamma (PPAR $\gamma$ ) agonists have been proven to elevate the plasma level of ADP by transcriptional stimulation in fat tissues because there is a functional response component in ADP promoter in human. Thyroid hormones can stimulate the expression of PPAR in liver cells. Therefore, there may be a cross talk between the peroxisome proliferator signaling pathways and the thyroid hormones in the setting of peroxisome proliferator responsive genes (Yilmaz *et al.*, 2004). It is likely that THs increase directly the transcriptional stimulation of ADP by PPAR or sterol regulatory element binding protein (SREBP) stimulation. Obese people showed to have lower value of ADP than lean people and the losing of weight increases plasma ADP values significantly. These factors can be linked to the regions promoter of various lipogenic genes including ADP and regulates the expression of ADP gene in differentiated adipocytes (Mishra *et al.*, 2018).

Reduced ADP levels in hypothyroidism may indicate that thyroid hormones are the regulators of adiponectin in the living organism, as plasma  $T_4$  levels were found to be associated with higher levels of adiponectin. Moreover, TSH and adiponectin have an inverse relationship (Aragão *et al.*, 2007).

According to the findings of the Seifi *et al* (2011) study, adiponectin mRNA values in rats with hypothyroidism were lower after methimazol treatment for six weeks compared to control rats, but increased after two weeks of treatment discontinuation. This is most likely may related to thyroid hormones direct effect on

adiponectin regulation or to thyroid hormone-induced weight variations. This drop in adiponectin gene expression coincided with a drop in concentrations of  $T_3$ ,  $T_4$ ,  $FT_3$  and  $FT_4$ . In contrast to hypothyroid rats, adiponectin gene expression was elevated in hyperthyroid rats through the six weeks of treatment in tandem with an elevated in concentrations of THs (Seifi *et al.*, 2011).

Results show a significant decrease in levels of  $T_4$  and  $T_3$  in the hypothyroid group at ( $P \leq 0.01$ ) compared to the control group, while results show a significant increase in levels of TSH in hypothyroid group compared to the control group.

The Anterior pituitary gland produces TSH after it is induced by TRH from the hypothalamus. This production depends on Thyroid hormone levels in circulation. Because of the inverse correlation between TSH and THs levels or the negative regulatory relationship between THs and the pituitary gland, this hormone is considered a sensitive indicator for Thyroid function in clinical diagnosis because it influence by small alteration in  $T_4$  concentration. A low TSH usually indicates hyperthyroidism disease, whereas the high levels of TSH usually means hypothyroidism (Mortimer, 2011). In addition, there is a positive regulation between TRH and TSH. Other study mice lacking the TRH gene have hypothyroidism, which is accompanied by low circulating TSH levels and a decrease in the number of TSH immune-positive cells in their anterior pituitary glands (Yamada *et al.*, 1997).

In our study, results show significant increase in parameters of lipid profile (TC, TG, LDL and VLDL) in group<sub>2</sub> except HDL levels, which was low compared to the group<sub>1</sub>.

Thyroid hormones have an impact on every major metabolic signaling including lipid metabolism. These hormones effect on the composition, metabolism and disintegration of lipid but the disintegration is affected more than composition. Through a variety of mechanisms, TH regulates the synthesis of cholesterol in the liver, which is consider the main organ for cholesterol production. THs stimulate the rate-limiting enzyme 3-Hydroxy-3-Methyl-Glutaryl Coenzyme A Reductase (HMGCR or HMG-Co A), which is responsible for biosynthesis of cholesterol (Pucci *et al.*, 2000).

They also lower cholesterol levels via improving the cholesterol removal pathway and regulating the enzyme cholesterol 7-hydroxylase (CYP7A1), which converts cholesterol to bile acids, which are necessary for maintaining cholesterol balance throughout the body (Lammel Lindemann *et al.*, 2014).

$T_3$  binds to SREBP, which increases the synthesis of LDL-c receptors as well as the regulatory enzymes of cholesterol synthesis. The absence of THs would increase LDL-c levels in the circulation. Therefore, hypothyroidism causes hypercholesterolemia due to decreased expression of LDL receptors (LDLr) (Habib and Habib, 2020), leading to an imbalance in cholesterol uptake, resulting in a significant increase in Apo lipoprotein B (Apo B), TC and LDL-c levels and decreased clearance of LDL-c and TC in the blood (Duntas and Wartofsky, 2007). In addition, a reduction in clearance of TG levels in circulation as well as aggregation of IDL is due to decreased lipoprotein lipase activity (LPL). Excessive levels of THs increase the activity of these enzymes and reduce serum TC and TG levels due to increased removal via reverse cholesterol transport (RCT) signaling, and increasing  $\beta$ -oxidation in the liver due to lipolysis in the AT (Alsamghan *et al.*, 2020).

THs control the LPL, which is responsible for removing TG present in VLDL-c and chylomicrons molecules. It activates the TG breakdown into non-esterified fatty acids and transports it to the AT and storage as TG after re-esterification (Jin and Teng, 2014). cholesterol ester transfer protein (CETP) exchange and transfer cholesterol ester from HDL<sub>2</sub> to the lipoproteins (VLDL-c, intermediate LDL-c (IDL) and remnants) and transfer TG from them to HDL<sub>2</sub> resulting in decrease HDL levels. Hepatic lipase (HL) hydrolyzes the TG in HDL<sub>2</sub> molecules and convert it into HDL<sub>3</sub>. Moreover, it is convert IDL into LDL-c and eventually into small density LDL. The lack of THs in blood stream would inhabit these enzymes in hypothyroid patient, whereas in patients with hyperthyroid they were increased (Sabharwal *et al.*, 2017; Tan *et al.*, 1998).

The study of Ahmed, (2017) showed a significant reduction in the levels of HDL-c in the hypothyroid patients compared to the control, and this is compatible with our results. Hypothyroidism patients had a higher ratio of LDL-c to HDL-c due to the increase in LDL-c and a slight decrease in the levels of HDL-c, leading to an increase in the risk of cardiovascular disease. However, in hyperthyroidism, as previously stated, THs affect the expression of LDL receptors and LPL activity (Ahmed, 2017). In addition, they influence the HDL-c metabolism by increasing the activity of CEPT, which converts HDL-c to VLDL-c (Chen *et al.* 2016). This could explain the decrease in HDL-c levels in our study. Pérez-Echarri *et al.*, (2005) found that reduce in the expression of adiponectin gene in fat tissue of rats with hypothyroidism was correlated with elevated cholesterol, LDL-c, TG with decreased serum HDL concentration (Pérez-Echarri *et al.*, 2005).

## References

1. **Abdelsalam, M. H. and Edrees, H. M.** (2015). Effect of Different Conditions of Thyroid Function on Serum Adiponectin, Visfatin and Vaspin Levels in Rats. *Basic Sciences of Medicine*, 4(1): 12- 19.
2. **Ahima, R.S. and Lazar, M.A.** (2008). Adipokines and the peripheral and neural control of energy balance. *Mol Endocrinol*, 22(5):1023-1031.
3. **Ahmed, H. S.** (2017). A Comparative Estimation of Metabolic and Hormonal Parameters among Iraqi Hypothyroid Patients. *The Iraqi Postgraduate Medical*, 16 (2): 204-210.
4. **Alsamghan, A. S.; Alsaleem, S. A.; Alzahrani, M. A. S.; Patel, A.; Mallick, A. K. and Sheweita, S. A.** (2020). Effect of Hypovitaminosis D on Lipid Profile in Hypothyroid Patients in Saudi Arabia. *Oxidative Medicine and Cellular Longevity*, 2020(4): 1- 8.
5. **Alshaikh, E. M.; Omar, U. M.; Alsufiani, H. M.; Mansouri, R. A.; Tarbiah, N. I.; Alshaikh, A. A.; Rahimulddin, S. A. and Al Doghaither, H. A.** (2019). The Potential Influence of Hyperthyroidism on Circulating Adipokines Chemerin, Visfatin, and Omentin. *International journal of health sciences*, 13(2): 44- 47.
6. **Aragão, C. N.; Souza, L. L.; Cabanelas, A.; Oliveira, K. J. and Pazos-Moura, C. C.** (2007). Effect of Experimental Hypo- and Hyperthyroidism on Serum Adiponectin. *Metabolism: Clinical and Experimental*, 56(1): 6- 11.
7. **Briet, D. C.; Suteau-Courant, V.; Munier, M. and Rodien, P.** (2018). Thyrotropin Receptor, Still much to be Learned from the Patients. *Best Practice and Research: Clinical Endocrinology and Metabolism*, 32(2): 155- 164.
8. **Chait, A. and den Hartigh, L.J.** (2020). Adipose Tissue Distribution, Inflammation and Its Metabolic Consequences, Including Diabetes and Cardiovascular Disease. *Front Cardiovasc Med*, 7(22):1-41.
9. **Chen, Y.; Wu, X.; Wu, R.; Sun, X.; yang, B.; Wang, Y. and Xu, Y.**(2016). Changes in profile of lipids and adipokines in patients with newly diagnosed hypothyroidism and hyperthyroidism. *Sci Rep*;6(1):1-7.
10. **Christou, G. A. and Kiortsis, D. N.** (2013). Adiponectin and lipoprotein metabolism. *Obesity Reviews*, 14(12): 939–949.
11. **Cinar, N. and Gurlek, A.** (2013). Association between novel adipocytokines adiponectin, vaspin, Visfatin, and thyroid: An experimental and clinical update. *Endocr Connect* ,2(4): 30-38.
12. **Duntas, L. H. and Wartofsky, L.** (2007). Cardiovascular Risk and Subclinical Hypothyroidism: Focus on Lipids and New Emerging Risk Factors. What is the Evidence?. *Thyroid*, 17(11): 1075- 1084.
13. **Fang, H, and Judd, R.J.** (2018). Adiponectin Regulation and Function. *Compr Physiol*, 8(1): 103- 163.
14. **Friedwald, W.; Levy, R.I. and Fredrickson, D.S.** (1972) Estimation of the concentration of low-density lipoprotein cholesterol in plasma, without use of preparative ultracentrifuge. *Clin. Chem.*, 18(6): 499-502.
15. **Fukuhara, A.; Matsuda, M.; Nishizawa, M. et al.,** (2005). Visfatin: a protein secreted by visceral fat that mimics the effects of insulin. *Science*, 307:426-430.
16. **Gulcelik, N.; Usman, A. and Gürlek, A.** (2009). Role of adipocytokines in predicting the development of diabetes and its late complications. *Endocrine*, 36(3): 397-403.

17. **Habib, A. and Habib, A.** (2020). Association of Subclinical Hypothyroidism and Dyslipidemia in Children and Adolescents. *BMC Pediatrics*, 20(1): 1- 14.
18. **Hajianfar, H.; Bahonar, A.; Entezari, M.H.; Askari, G. and Yazdani, M.** (2012). Lipid profiles and serum Visfatin concentrations in patients with type II diabetes in comparison with healthy controls. *Int J Prev Med*, 3(5):326-331.
19. **Lammel Lindemann, J. A.; Angajala, A.; Engler, D. A. Webb, P. and Ayers, S. D.** (2014). Thyroid hormone Induction of Human Cholesterol 7 Alpha-Hydroxylase (Cyp7a1) in Vitro. *Molecular and Cellular Endocrinology*, 388(1): 32-40.
20. **Jin, T. and Teng, X.** (2014). Update on Lipid Metabolism and Thyroid Disorders. *Journal of Endocrinology, Diabetes & Obesity Review*, 2(3):1043.
21. **MacLaren, R.; Cui, W. and Cianflone, K.** (2007). Visfatin Expression is Hormonally Regulated by Metabolic and Sex Hormones in 3T3-L1 pre-Adipocytes and Adipocytes. *Diabetes, Obesity and Metabolism*, 9(4): 490- 497.
22. **Mishra, M.; Panta, R.; Miyares, M. and Solanki, R.** (2018). Association of Diabetes Mellitus and Thyroid Disorders: An Adipocytokines Prospective. *Journal of Endocrinology and Thyroid Research*, 3(3): 555-612.
23. **Mohammadi, M. M.; Saeb, M. and Nazifi, S.** (2019). Experimental Hypothyroidism in Adult Male Rats: the Effects of Artemisia Dracunculus Aqueous Extract on Serum Thyroid Hormones, Lipid Profile, Leptin, Adiponectin, and Antioxidant Factors. *Journal of Endocrinology and Thyroid Research*, 29(2): 485- 494.
24. **Mortimer, R. M.** (2011). Abnormal laboratory results: Thyroid Function Tests. *Australian Prescriber*, 34(1): 12-15.
25. **Ozkaya, M.; Sahin, M.; Cakal, E.; Yuzbasioglu, F.; Sezer, K.; Kilinc, M. and Imrek, S.** (2009). Visfatin Plasma Concentrations in Patients with Hyperthyroidism and Hypothyroidism before and after Control of Thyroid Function. *Journal of Endocrinological Investigation*, 32(5): 435- 439.
26. **Pérez-Echarri, N.; Pérez-Matute, P.; Martínez, J. A.; Marti, A. and Moreno-Aliaga, M. J.** (2005). Serum and gene expression levels of leptin and adiponectin in rats susceptible or resistant to diet-induced obesity. *Journal of Physiology and Biochemistry*, 61(2): 333–342.
27. **Pucci, E.; Chiovato, L. and Pinchera, A.** (2000). Thyroid and Lipid Metabolism. *International Journal of Obesity*, 24(2): 109- 112.
28. **Qiao, L.; Zou, C.; Van Der Westhuyzen, D. R. and Shao, J.** (2008). Adiponectin reduces plasma triglyceride by increasing VLDL triglyceride catabolism. *Diabetes*, 57(7): 1824–1833.
29. **Qiu, Y.; Wang, S.F.; Yu, C.; Chen, Q.; Jiang, R.; Pei, L.; Huang, L.; Pang, N.Z.; Zhang, Z.; Ling, W. and Yang, L.** (2019). Association of circulating adiponectin, Visfatin, and adiponectin with nonalcoholic fatty liver disease in adults: A case-control study. *Ann Nutr Metab*, 74(1):44-52.
30. **Sabharwal, R.; Mahajan, P. and Bhatia, A.S.** (2017). Association of Subclinical Hypothyroidism with Dyslipidemia. *JK Science*, 19(2): 81- 84.
31. **SAS Institute.** SAS User's Guide: Statistics. Cary (NC): SAS Institute Inc. 2004.
32. **Seifi, S.; Tabandeh, M.R.; Nazifi, S.; Saeb, M.; Shirian, S. and Sarkoohi, P.** (2011). Regulation of Adiponectin Gene Expression in Adipose Tissue by Thyroid Hormones. *Journal of Physiology and Biochemistry*, 68(2): 193-203.

33. **Steel, R. D.; Torrie, J. H. and Dicky, D. A.** (1997). Principles and Procedures of Statistics, A Biometrical Approach. 3rd Edition, McGraw Hill, Inc. Book Co., New York, 352-358.
34. **Tan, K. C. B.; Shiu, S. W. M. and Kung, A. W. C.** (1998). Plasma Cholesteryl Ester Transfer Protein Activity in Hyper- and Hypothyroidism. *Journal of Clinical Endocrinology and Metabolism*, 83(1): 140- 143.
35. **Tanaka, M.; Nozaki, M.; Fukuhara, A.; Segawa, K.; Aoki, N.; Matsuda, M.; Komuro, R. and Shimomura, I.** (2007). Visfatin is Released from 3T3-L1 Adipocytes via a Non-classical Pathway. *Biochemical and Biophysical Research Communications*, 359(2): 194- 201.
36. **Tsuchida, A.; Yamauchi, T.; Takekawa, S.; Hada, Y.; Ito, Y.; Maki, T.; and Kadowaki, T.** (2005). Peroxisome proliferator-activated receptor (PPAR) $\alpha$  activation increases adiponectin receptors and reduces obesity-related inflammation in adipose tissue: Comparison of activation of PPAR $\alpha$ , PPAR $\gamma$ , and their combination. *Diabetes*, 54(12): 3358–3370.
37. **Yamada, M.; Saga, Y. and Shibusawa, N.** (1997). Tertiary Hypothyroidism and Hyperglycemia in Mice with Targeted Disruption of the Thyrotropin- Releasing Hormone Gene. *Proceedings of the National Academy of Sciences of the United States of America*, 94(20): 10862- 10867.
38. **Yang, J.; Zhang, K.; Song, H.; Wu, M.; Li, J.; Yong, Z.; Jiang, S.; Kuang, X. and Zhang, T.** (2016). Visfatin is involved in promotion of colorectal carcinoma malignancy through an inducing EMT mechanism. *Oncotarget* , 7(22):32306-32317.
39. **Yildiz, B.; Aksoy, D.; Harmanci, A.; Unluturk, U.; Cinar, N.; Isildak , M.; Usman, A. and Bayraktar, M.** (2013). Effects of L-thyroxine therapy on circulating leptin and adiponectin levels in subclinical hypothyroidism: a prospective study. *Arch Med Res*, 44(4):317-20.
40. **Yilmaz, M.I.; Sonmez, A.; Caglar, K.; Gok, D. E.; Eyiletten, T.; Yenicesu, M.; Acikel, C.; Bingol, N.; Kilic, N.; Oguz, Y. and Vural, A.** (2004). Peroxisome Proliferator-activated Receptor  $\gamma$  (PPAR- $\gamma$ ) agonist Increases Plasma Adiponectin Levels in Type 2 Diabetic Patients with Proteinuria. *Endocrine*, 25(3): 207-214.

**KNOWLEDGE OF PREGNANT WOMEN ABOUT GESTATIONAL DIABETES  
MELLITUS AT MOSUL CITY**

**YAMAMA ZUHIR ABDUL KAREEM  
JWAN MOHAMMED HASSAN  
SAAD HUSSEIN MURAD**



## **KNOWLEDGE OF PREGNANT WOMEN ABOUT GESTATIONAL DIABETES MELLITUS AT MOSUL CITY**

**Yamama Zuhir ABDUL KAREEM<sup>1</sup>**

**Jwan Mohammed HASSAN<sup>2</sup>**

**Saad Hussein MURAD<sup>3</sup>**

### **Abstract:**

Background: Gestational diabetes mellitus (GDM) , also called transient diabetes or glucose intolerance with first onset and recognition in pregnancy and usually resolves not long after delivery. The study aims to assess the knowledge of pregnant women regarding gestational diabetes mellitus (GDM) at Mosul city. Methodology: A cross-sectional study was conducted among (60) pregnant women at two maternity teaching hospitals at Mosul city, Al-Batool and AL Khansa teaching hospital in antenatal care unit. A purposive sampling technique was adopted in the study. A detailed questionnaire and interview face to face was used to obtain basic data regarding to Socio-Demographic data of the study sample, and general knowledge about GDM. SPSS, version 25 was used to analyze the data in this study. Results: The results of the study showed majority (51.7%) of the sample were age group between (15-25) years and the high percentage (51.7%) of the sample were primary school education. A majority (25%) of participating stated the family history (Type 2 diabetes) had been a significant risk factor for GDM. Fifty percent of participating didn't aware about GDM for long-term complications for infants born mothers with GDM, only (23.3%) of the participants answered that postpartum testing should be done between 6-12 weeks after childbirth. The study found, there are statistically significant between overall knowledge and socio-demographic characteristic at p-value < 0.05. Conclusions and Recommendation: The study concluded majority of the pregnant women had poor knowledgeable concerning gestational diabetes (GDM). This study recommended to provision of medical staff at antenatal care from the physicians and nurses are specialists to setting educational program or workshop on GDM; and interventions such as mass media promotions to educate the community as a whole.

**Key words:** Knowledge, Pregnant Women, Gestational Diabetes Mellitus, Mosul.



<http://dx.doi.org/10.47832/MinarCongress5-23>

<sup>1</sup> University of Mosul, Iraq, [yamama.zyhair@uomosul.edu.iq](mailto:yamama.zyhair@uomosul.edu.iq), <https://orcid.org/0000-0002-5496-584X>

<sup>2</sup> University of Mosul, Iraq, [jwan.m@uomosul.edu.iq](mailto:jwan.m@uomosul.edu.iq), <https://orcid.org/0000-0001-5529-6345>

<sup>3</sup> University of Mosul, Iraq, [dr.saad.nursing@uomosul.edu.iq](mailto:dr.saad.nursing@uomosul.edu.iq), <https://orcid.org/0000-0002-8505-7393>



## **Introduction:**

Gestational diabetes mellitus (GDM), also called transient diabetes or glucose intolerance with first onset and recognition in pregnancy, and usually resolves not long after delivery (Kramer et al., 2019). International-Diabetes Federation (IDF) approximations, conferring toward the most current (2017); GDM impacts roughly 14 percent of pregnancy mothers globally, accounting for an estimated 18 million newborns each year (Saeedi et al., 2020 & Patterson et al., 2019). For more than 50 years, hyperglycemia which occurs throughout gestation and solve even after birth has already been identified; however constant global compromise is poor around threshold levels of hyperglycemic that importance for diagnosis of (GDM), and consequently management throughout pregnancy period. Presently, the common most medical problems during pregnancy is GDM. Also DM in mothers young and the incidence of undetected elevated blood glucose surge are increasing (McIntyre et al., 2019). On the other hand, pregnancy developments, local surge level and placental hormone; counting estrogen; lactogen of placental; leptin; cortisol; progesterone, in addition growth hormone of the placental together support the insulin resistance state (Lafta et al., 2021; Nadeau et al., 2020 & Barbou & Hernandez, 2018). GDM causes important short- and long-term health risks for the women, developing fetus, and children; this includes the high likelihood of subsequent maternal type 2 diabetes (T2DM), and possible adverse cardio-metabolic phenotypes in the children (Johns et al., 2018). Because of the lack of clinical signs and symptoms of GDM, screening tests are essential to identify women with GDM. One of the tests that is used in the diagnostic pathway is the 50-g glucose challenge test (Waters et al., 2020 & Gabbe et al., 2004). Several strategies of management GDM including: insulin and medical nutrition therapy, exercise and routine interferences; There is currently no treatment or appropriate preventative method. There is one cause for this, which is that the mechanisms of molecular causation (GDM) are unwell recognize (Al-Rubai et al., 2021 & Gabbe et al., 2004). One of factors that leading to increase morbidity & mortality in worldwide for mothers and baby is GDM. Therefore, GDM is has been a well-recognized medical prognosticator of diabetes mellitus risks in the future, through infected mothers demonstrating that more than 7-fold greater total prevalence of TYP2DM than their colleagues (Mohajan, 2016 & Bellamy et al., 2013). Therefore, the aims of the current study is concerned with assessing the knowledge level regarding Gestational Diabetes Mellitus amongst women's pregnant at Mosul city/Iraq.

## **Methodology**

### **1. Design, Sampling and Sitting of the Study:**

A descriptive, cross-sectional study design was achieve the objectives of the study on (60) pregnant women and target population is pregnant women joining antenatal care (ANC). The data was collected for the period from 10<sup>th</sup> of October 2021 to 1<sup>st</sup> of December 2021. A purposive sampling technique was adopted in the study. The study was conduct at two maternity teaching hospitals in Mosul city, namely, Al-Batool and AL Khansa teaching hospital in antenatal care unit (ANC). After explanation of the study rationality; in cooperation, oral and written

permissions existed gained from each women respondents, the women participants were completed the data of questionnaires at same day.

### **1.1 Study Sample: Inclusion Criteria**

1. Pregnant women.
2. Pregnant women who attended ANC.
3. Pregnant women who agreed to participate in the study

### **1.2 Exclusion Criteria of the Study Sample**

1. Non-pregnant women
2. Pregnant women who non attended ANC.
3. Pregnant women who disagreed to participate in the study

## **2. The Study Tool**

Prior to the research, expert's panel agreement on the building of the questionnaire. Some slight changes existed prepared after pilot study was conducted. Collection of Data: questionnaire based on face-to-face interview was used to gain data about characteristics of participants: socio demographical and knowledge on (60) eligible pregnant women. This instrument is consisting of two parts:

**A.** First Part: Socio- Demographic characteristics of the Study Sample. The first part was concerned with the determination of the demographical characteristics of the study sample which includes question regarding: age of women, educational level, residence, occupation, gestational age and previous GDM.

**B.** Second Part : Pregnant women's knowledge toward gestational diabetes mellitus and focused on : Risk factors, long-term consequence on baby, screening, and complication on mother.

## **3. Ethical approval**

Ethical approval was obtained from Ministry of Health, Nineveh. Formal permission of ANC at AL-Batool and AL-Khanasa teaching hospitals, and after explained the study purpose for the pregnant women and obtained informed agreement from every participant, the data was collected.

## **4. Statistical Analysis:**

Different statistical methods was used to analyze the data in the present study Statistical Package for the Social Science (SPSS, ver. 25) and all the statistical procedures were tested at p-value less than 0.05.

## Results

**Table (1): The Socio-Demographical Characteristics of Women Respondents in The study (No. = 60).**

Variables		F.	%.
Age	15-25 year	31	51.7
	26-35 year	18	30.0
	36-45 year	8	13.3
	≥ 46 year	3	5.0
Resident	Urban	45	75.0
	Rural	15	25.0
Level education	Illiterate	5	8.3
	Primary education	31	51.7
	Secondary education	13	21.7
	College education	11	18.3
Occupation	Student	11	18.3
	Employee	8	13.3
	Housewife	41	68.4
Gestational age (Trimester)	First trimester	18	30.0
	Second trimester	28	46.7
	Third trimester	14	23.3
Have you ever had gestational diabetes?	Yes	12	20.0
	No	48	80.0

Table (1) showed the socio demographical characteristics of the study sample. A majority (51.7%) of the sample was age group between (15-25) years, and following (30%) was age group between (26-35) years, according to residence (75%) of pregnant women were living in urban area. Regarding to the education of mothers, the high percentage (51.7%) of the sample were primary school education. As regard to occupation, (68.4%) were housewives. Forty-six (46%) of the sample was on second trimester of gestation, a highly percentage (80%) of pregnant women did not have gestational diabetes previously.

**Table (2): Knowledge of pregnant women regarding risk factors of GDM.**

No.	Risk Factors	F.	%
1.	Family history (T2DM)	25	41.8
2.	Mother age	11	18.3
3.	Previous GDM	9	15.0
4.	Obesity	3	5.0
5.	Polycystic ovary syndrome (PCOS)	2	3.3
6.	All of the above	10	16.6

Table (2): Indicates knowledge about risk factors that can cause GDM among participating pregnant women. A majority (25%) of the study sample stated that the pregnant women with family history of Type-2DM has affected with GDM, while (10%) of women participants knowledgeable with all risk factors. Women participants did not have a good overview of the impact of Polycystic ovary syndrome (PCOS) as a cause of GDM and only (3.3%) of women participants marked this as a risk factor.

**Table (3): Knowledge of pregnant women regarding to long-term consequences of GDM to the offspring who were born to mothers with GDM**

No.	GDM Long –term (complications) consequences in offspring	F.	%
1.	Obesity of Childhood /over-weight	9	15.0
2.	Intolerance of glucose	7	11.7
3.	Type 2 of DM	10	16.7
4.	*Other	4	6.6
5.	Don't know	30	50.0

\*other: Ophthalmic and Cardiovascular disease

Table (3): This table shows knowledge of the pregnant women regarding to long-term consequences of GDM in offspring. Fifty percent of participating pregnant don't recognize about GDM problems or consequences of long-term for infants born mothers with GDM. In contrast, most respondents (16.7%) were aware that type 2 of DM in adolescent is long –term consequences of GDM, followed by childhood obesity and glucose intolerance, 15% and 11.7%, respectively.

**Table (4): Knowledge of pregnant women regarding to how long after labor must the blood sugar test checked for mothers had (GDM).**

No	Timing ( how long)	F.	%
1.	After delivery(6-12 week)	14	23.3
2.	Within a year	5	8.3
3.	After year	3	5.0
4.	Don't know	38	63.4

Table (4): This table shows knowledge of the pregnant women regarding to how long after labor must the blood sugar test. More than half, (63.4%) of study sample did not know about period after delivery for blood sugar test. While (23.3%) of the participants answered that postpartum testing should be done between 6-12 weeks after childbirth; and the rest of women was not recognize regarding screening time after delivery.

**Table (5): Association between variables of demographic and overall knowledge of study sample.**

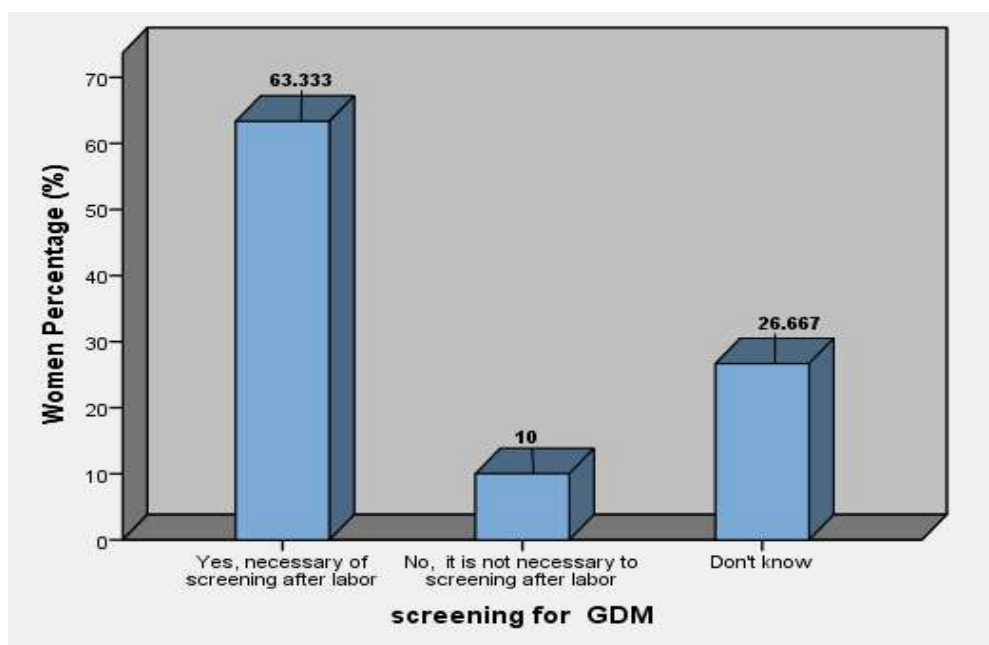
Variables	Overall Knowledge	
	X <sup>2</sup>	Sig. *P-value
Age	30.533	*H.S.
Resident	15.000	S.
Level education	25.067	S.
Occupation	33.300	H.S.
Gestational age (Trimester)	5.200	*N.S
Have you ever had gestational diabetes?	21.600	S.

P-value at < 0.005

HS : Highly significant

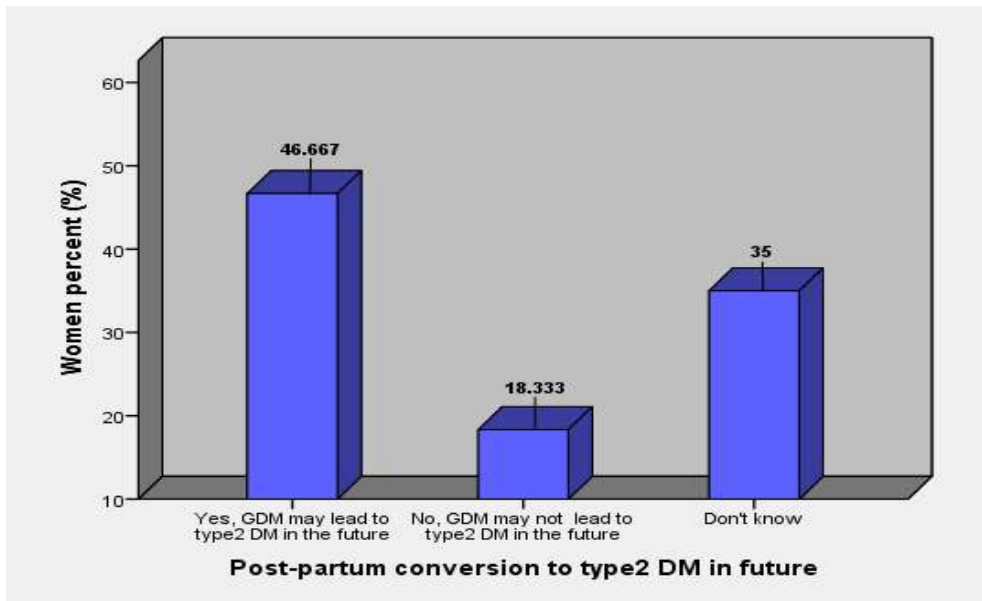
NS: no significant

Table (5): shows that there are a statistically significant between overall knowledge and socio-demographic at p-value < 0.05, while not significantly with gestational age (Trimester).



**Figure .1: Knowledge regarding Gestational Diabetes Mellitus GDM Screening**

The figure shows the vast majority of women participants (63.33%) felt that screening was necessary for GDM women to check their blood sugar after delivery, while (26.66%) were have a poor level of knowledge around they must undergo an investigation after birth (screening).



**Figure .2: Knowledge of women participants about post-partum conversion to type2 diabetes mellitus.**

The figure shows that less than half (46.667%) of the participating women stated, at future (GDM) might leading or converted into type 2 DM, while slightly of them had stated that GDM would not lead to type 2 DM (18.33%), or did not know (35%).

## Disussion

In order to diagnosis of GDM initial, prenatal mothers pregnancy must be taught around risk factors, screening or investigation processes & implications; in addition, reduce; study reported Women with GDM are more likely to acquire diabetes in the future than women with normal glucose tolerance throughout gestation (Carolan et al., 2010). This research is the first done in Mosul according our information for assess knowledge level regarding gestational diabetes amongst Mosul women, include: pregnant women who attending ANC. Considering the high frequency of pregnancy and GDM in Mosul city, one of the main study results was the poor knowledge associated with GDM amongst responding mothers, these study consistent with Alharthi et al., (2018) and Shriram et al., (2013) who reported the majority of participants had poor knowledge about gestational diabetes mellitus. This study inconsistent with study were done in semiurban by Kondamuri et al., (2021) who reported the majority of study sample which constituted fifty-one percentage were have a good level of knowledge. While, fourteen in percentage were fair level of knowledge concerning geatational-DM. Dhyan and his colleagues., (2018) demonstrated in research was done at Karnataka; indicated more than half of mothers participants that approximately fifty-seven percentage have middle aware level around gestational diabetes. But who has good knowledge, only few 21 in percent of the pregnant mothres participants. Besides, the results of this study are similar to the one conducted by Bhowmik et al., 2018 in Bangladeshi who found that (35.3%) of women were less than 30 years. Recently, gestational diabetes is also on the rise; the prevalence of gestational-DM is increase in the rural regions; while in the urban areas GDM can decreasing due to regular pregnant women

visiting antenatal care monthly (Bhavadharini et al., 2016). In our study, the high percentage (51.7%) of the sample were primary school education. This result consistent with Rashash (2002) who reported the high percentage of the sample were primary school graduated. The respondent's knowledge women of were not yet optimum, which might be associated with absence of the programs learning and education intermediates and promotions regarding GDM. According to risk factors of GDM; our current research found vast percentage (25%) of women participants aware about the family history type2 were an important risk factor of GDM during pregnancy. In addition, few (10%) of study sample had a good knowledge with all risk factors: obesity, mother age, polycystic ovary syndrome (PCOS) and previous GDM. This finding agreed with a study in South Tamil and Malaysia (Bhavadharini et al., 2016; Hussain et al., 2015). In particular, according to research, mothers seem to be more than 7 times more likely to get diabetes following Gestational diabetes mellitus, more than half of women having Gestational diabetes mellitus may develop symptoms in ten years, indicating GDM is one of assumptions of Type 2 diabetes. Type 2 diabetes can be avoided or prevented in women who have previous had GDM with lifestyle changes and/or medicinal therapy (Malcolm, 2012 ; Damm et al., 2016). Our Study findings revealed regarding long-term complications of GDM, half of study sample didn't recognize around consequences or complications of GDM for long-term on the newborn. Similarly the study were done in semiurban by Kondamuri et al., (2018) who stated in his study the knowledge of participants regarding long-term complication of GDM on fetus & newborn were realized merely in thirty to fifty in percentage of the respondents' mothers'. Also, this results consistent with Rashash, (2009) who reported majority (58%) of women don't know about long-term complication of GDM. In this study, more than half (63.4%) of women unaware about timing of test blood sugar checked after delivery. The finding for this current research existed comparable with finding of results that showed going on awareness around test blood sugar checked after delivery in Nepal by Gautam et al., (2014) and in Bangladesh by Mumu et al., (2014). We study results showed, important statistical-significant relationship were distinguished between knowledge regarding gestational-DM with age of mother, resident, level education, occupation and previous gestational diabetes. Analysis of our data revealed that there are a statistically significant correlation between overall knowledge on GDM and mother age, resident, level education, occupation and previous gestational diabetes at P-value(<0.05). This result were stable with a study by Dhyanani et al., (2014), nonetheless the authors stated a significant relationship between knowledge regarding GDM with just mothers' age and resident. On the hand, this results disagreement with Kondamuri et al., (2021) and Price et al., (2017) who stated in them study there are non-statistically significant correlation between overall knowledge on GDM and age, resident and occupation. The interesting in this study, all participant aware knowledge regarding screening of GDM and post-partum conversion of GDM into Type2 DM in the future. These findings were compared with other studies conducted in Saudi by Alharthi et al., (2018) and in Sharjah by Elmekresh et al., (2017) which showed that knowledge of level about screening of GDM and post-partum conversion of GDM into Type2 DM in the future were average knowledge of level. On the contrary, the research which done with Kaptein et al., (2015) indicated the many of mothers consider the screening of the GDM give the optimal indicator to adaptation for well lifestyle; so

vast percentage of participants stated an raised awareness in the future about risk of diabetes. Many believe that GDM consider the temporary disorder and just occur throughout pregnancy (Carolan et al., 2010). However, in the fact, the rate at which GDM developments to Type2 DM is arising. Previous researchers described the mothers has GDM may lead to or progress to TYP2-DM during 8 years after delivery (Bhavadharini et al., 2016). There might be various explanations for pregnant women's lack of awareness. A previous research in Chennai was done among a representative group of the community, and it was discovered that roughly 25% of the Chennai population was poorly informed about this problem known as diabetes (Deepa et al., 2005). As a consequence, healthcare provider must confirm the pregnant mothers receiving antenatal care (ANC) regulars stay advised on avoidance diabetes techniques for long-term. Although the current study's sample size is limited, the findings highlight to the necessity for widespread GDM education, not just for clinicians and para-medical, but also for the general population.

### **Conclusions**

Results of the current study concluded, A majority of women was age group between (15-25) years and 68.4% were housewives. There was statistically significant relationship between knowledge of pregnant women and socio-demographical characteristics: age, occupation, residence, education level and women with history of GDM at P-value < 0.05; and insignificant with gestational age (Trimester). Majority of the pregnant women had poor knowledge regarding gestational diabetes mellitus (GDM).

### **Recommendations**

The regular visit of pregnant women for antenatal care (ANC) during pregnancy; Which means there is an opportunity to educate women about GDM and how they can prevent it. Providing medical staff in prenatal care from specialized doctors and nurses to develop an educational program or a workshop on GDM. Also, Interventions has a vital role to education such as mass media promotions to educate the community as a whole.



## References

1. Alharthi, A. S., Althobaiti, K. A., & Alswat, K. A. (2018). Gestational Diabetes Mellitus Knowledge Assessment among Saudi Women. *Open access Macedonian journal of medical sciences*, 6(8), 1522–1526. <https://doi.org/10.3889/oamjms.2018.284>
2. Al-Rubai, S., Fouad, H. Q., & Muhsen, N. (2021). Metformin Versus Insulin in The Management of Gestational Diabetes Mellitus.
3. Barbour, L. A., & Hernandez, T. L. (2018). Maternal non-glycemic contributors to fetal growth in obesity and gestational diabetes: spotlight on lipids. *Current diabetes reports*, 18(6), 1-10.
4. Bellamy, L., Casas, J. P., Hingorani, A. D., & Williams, D. (2013). Type 2 diabetes mellitus after gestational diabetes: a systematic review and meta-analysis. *The Lancet*, 373(9677), 1773-1779.
5. Bhavadharini, B., Mahalakshmi, M. M., Anjana, R. M., Maheswari, K., Uma, R., Deepa, M., ... & Mohan, V. (2016). Prevalence of gestational diabetes mellitus in urban and rural Tamil Nadu using IADPSG and WHO 1999 criteria (WINGS 6). *Clinical diabetes and endocrinology*, 2(1), 1-11.
6. Bhowmik, B., Afsana, F., Ahmed, T., Siddiquee, T., Pathan, F., Mahtab, H., & Khan, A. K. A. (2018). Evaluation of knowledge regarding gestational diabetes mellitus: a Bangladeshi study. *Public Health*, 161, 67-74.
7. Carolan, M., Steele, C., & Margetts, H. (2010). Knowledge of gestational diabetes among a multi-ethnic cohort in Australia. *Midwifery*, 26(6), 579-588.
8. Damm, P., Houshmand-Oeregaard, A., Kelstrup, L., Lauenborg, J., Mathiesen, E. R., & Clausen, T. D. (2016). Gestational diabetes mellitus and long-term consequences for mother and offspring: a view from Denmark. *Diabetologia*, 59(7), 1396–1399. <https://doi.org/10.1007/s00125-016-3985-5>
9. Deepa, M., Deepa, R., Shanthirani, C. S., Manjula, D., Unwin, N. C., Kapur, A., & Mohan, V. (2005). Awareness and knowledge of diabetes in Chennai--the Chennai urban rural epidemiology study [CURES-9]. *The Journal of the Association of Physicians of India*, 53(4), 283-287.
10. Dhyani, V., Mahantashetti, N. S., Ganachari, M. S., Kambar, S., & Ghatnatti, V. (2018). Awareness of gestational diabetes mellitus among pregnant women attending a tertiary health center. *Indian Journal of Health Sciences and Biomedical Research (KLEU)*, 11(1), 51.
11. Elmekresh, Amr, Batool AbuHalimeh, Rawan Abukhater, Amina Bakro, and Samher Nahab. "Gestational diabetes awareness in women of childbearing age in Sharjah." *Global Journal of Obesity, Diabetes and Metabolic Syndrome* 4, no. 2 (2017): 051-053.
12. Gabbe, S. G., Gregory, R. P., Power, M. L., Williams, S. B., & Schulkin, J. (2004). Management of diabetes mellitus by obstetrician–gynecologists. *Obstetrics & Gynecology*, 103(6), 1229-1234
13. Gautam, A., Bhatta, D. N., & Aryal, U. R. (2015). Diabetes related health knowledge, attitude and practice among diabetic patients in Nepal. *BMC endocrine disorders*, 15(1), 1-8.
14. Hussain, Z., Yusoff, Z. M., & Sulaiman, S. A. S. (2015). Evaluation of knowledge regarding gestational diabetes mellitus and its association with glycaemic level: A Malaysian study. *Primary care diabetes*, 9(3), 184-190.
15. Johns, E. C., Denison, F. C., Norman, J. E., & Reynolds, R. M. (2018). Gestational diabetes mellitus: mechanisms, treatment, and complications. *Trends in Endocrinology & Metabolism*, 29(11), 743-754.
16. Kaptein, S., Evans, M., McTavish, S., Banerjee, A. T., Feig, D. S., Lowe, J., & Lipscombe, L. L. (2015). The subjective impact of a diagnosis of gestational diabetes among ethnically diverse pregnant women: a qualitative study. *Canadian Journal of Diabetes*, 39(2), 117-122.

17. Kondamuri, S. D., Samal, S., & Sen, M. (2021). Knowledge of gestational diabetes mellitus among pregnant women in a semiurban hospital-A cross-sectional study. *Clinical Epidemiology and Global Health*, *12*, 100854.
18. Kramer, C. K., Campbell, S., & Retnakaran, R. (2019). Gestational diabetes and the risk of cardiovascular disease in women: a systematic review and meta-analysis. *Diabetologia*, *62*(6), 905-914.
19. Lafta, I., Abdulhameed, W., & Nahla, A. B. (2021). Histochemical Study of Human Placental Tissues in Gestational Diabetic Mellitus. *Iraqi Journal of Embryos and Infertility Researches*, *10*(2), 29-38.
- Carolan, M., Steele, C., & Margetts, H. (2010). Knowledge of gestational diabetes among a multi-ethnic cohort in Australia. *Midwifery*, *26*(6), 579-588.
20. Malcolm J. (2012). Through the looking glass: gestational diabetes as a predictor of maternal and offspring long-term health. *Diabetes/metabolism research and reviews*, *28*(4), 307-311. <https://doi.org/10.1002/dmrr.2275>
21. McIntyre, H. D., Catalano, P., Zhang, C., Desoye, G., Mathiesen, E. R., & Damm, P. (2019). Gestational diabetes mellitus. *Nature reviews Disease primers*, *5*(1), 1-19.
22. Mohajan, H. (2016). Knowledge is an Essential Element at Present World.
23. Mumu, S. J., Saleh, F., Ara, F., Haque, M. R., & Ali, L. (2014). Awareness regarding risk factors of type 2 diabetes among individuals attending a tertiary-care hospital in Bangladesh: a cross-sectional study. *BMC research notes*, *7*(1), 1-9.
24. Nadeau, H. C., Maxted, M. E., Madhavan, D., Pierce, S. L., Feghali, M., & Scifres, C. (2020). Insulin Dosing, Glycemic Control, and Perinatal Outcomes in Pregnancies Complicated by Type-2 Diabetes. *American Journal of Perinatology*.
25. Patterson, C. C., Karuranga, S., Salpea, P., Saeedi, P., Dahlquist, G., Soltesz, G., & Ogle, G. D. (2019). Worldwide estimates of incidence, prevalence and mortality of type 1 diabetes in children and adolescents: Results from the International Diabetes Federation Diabetes Atlas. *Diabetes research and clinical practice*, *157*, 107842.
26. Price, L. A., Lock, L. J., Archer, L. E., & Ahmed, Z. (2017). Awareness of gestational diabetes and its risk factors among pregnant women in Samoa. *Hawaii Journal of Medicine & Public Health*, *76*(2), 48.
27. Rashash, D. S. (2009). Assessment Knowledge of Pregnant Women about Gestational Diabetes in Primary Health Care Centers at Al Nassiriya City/Iraq.
28. Saeedi, P., Salpea, P., Karuranga, S., Petersohn, I., Malanda, B., Gregg, E. W., ... & Williams, R. (2020). Mortality attributable to diabetes in 20-79 years old adults, 2019 estimates: Results from the International Diabetes Federation Diabetes Atlas. *Diabetes research and clinical practice*, *162*, 108086.
29. Shriram, V., Rani, M. A., Sathiyasekaran, B. W., & Mahadevan, S. (2013). Awareness of gestational diabetes mellitus among antenatal women in a primary health center in South India. *Indian journal of endocrinology and metabolism*, *17*(1), 146-148. <https://doi.org/10.4103/2230-8210.107861>
30. Waters, T. P., Kim, S. Y., Sharma, A. J., Schnellinger, P., Bobo, J. K., Woodruff, R. T., ... & Catalano, P. M. (2020). Longitudinal changes in glucose metabolism in women with gestational diabetes, from late pregnancy to the postpartum period. *Diabetologia*, *63*(2), 385-394.

The background of the cover is a grayscale photograph of several fish, likely Mastacembelus, packed together. Overlaid on the upper portion of the image is a histological section of tissue, stained with hematoxylin and eosin (H&E), showing cellular structures in shades of purple and pink. The text is centered over the histological section.

**SPONTANEOUS HISTOPATHOLOGICAL LESIONS OF THE INTESTINES, LIVER,  
PANCREAS AND HEART OF THE FRESHWATER FISH MASTACEMBELUS  
MASTACEMBELUS [BANKS & SOLANDER 1794]**

**FATIMAH Q.M. AL-HAYYALI**

**SPONTANEOUS HISTOPATHOLOGICAL LESIONS OF THE INTESTINES, LIVER, PANCREAS AND HEART OF THE FRESHWATER FISH MASTACEMBELUS MASTACEMBELUS (BANKS & SOLANDER 1794)**

**Fatimah Q.M. AL-HAYYALI<sup>1</sup>**

**Abstract:**

The purpose of this study was to report spontaneous histopathological lesions of the intestines, liver, pancreas and heart of *Mastacembelus mastacembelus* collected from Tigris river, Ninevha Province, Iraq. Parasitic infections of the intestinal tissues were common in these fishes and were in the form of parasitic nodules in the intestinal submucosa consisting of the parasites or their larval stages surrounded by fibrous tissue capsules. Focal or diffuse infiltrations of mononuclear cells (macrophages, lymphocytes and plasma cells) were seen involving most of the intestinal layers. Patchy degeneration and desquamation of the intestinal epithelium were observed in some of the infected fishes. The livers of these fishes showed dilatation of the sinusoids, focal hepatitis with the infiltration of inflammatory mononuclear cells, and portal fibrosis. Myocarditis occurred in these fishes and was characterized by the infiltration of mononuclear cells between the bundles of myocardial fibers. A similar infiltration of mononuclear cells was seen in the pancreatic struma. From results of this study it was concluded that naturally – occurring pathological lesions are common in fishes of the species *M. mastacembelus* and that further studies are needed to ascertain the nature of the etiological agents.

**Key words:** Histopathology, Lesions, Intestine, Liver, Pancreas, Heart, *Mastacembelus*, Fish.



<http://dx.doi.org/10.47832/MinarCongress5-24>



<sup>1</sup> University of Mosul, Iraq, [fatsbio25@uomosul.edu.iq](mailto:fatsbio25@uomosul.edu.iq), <https://orcid.org/org/000.0001-9384-279x>

## **Introduction:**

The class Actinopterygii, includes the Mastacembelidae (spiny eels) family, Order Synbranchioformes with 78 valid species that are primarily freshwaters species that are found in tropical and subtropical Africa, the Middle East and Southeast Asia (1). This family includes 78 valid species, nine of which are belong to the genus *Mastacembelus* which inhabit Asian inland waters. The majority of *Mastacembelus* species are valuable food fishes (2). *Mastacembelus mastacembelus* is a species of eels that lives in the Euphrates and Tigris River basin in the Middle East, including Turkey, Syria, Iraq and Iran, and it is known as Mesopotamian spiny eel because of its habitat (3, 4). In Iraq, the common names of the freshwater eels of the genus *Mastacembelus* are marmarij or mar masi (5). The prevalence of parasite illnesses was reported to be 89.06 percent in this type of fish gathered from Iraq's Greater Zab river (6). Parasites are known to be the chief causes of mass mortality in fish populations (7). The *Mastacembelus armatus* were found to be infected with the cestode parasite *Senga jadhavii* (8,9). In view of the facts that there is increased public demand for fishes of the species *Mastacembelus mastacembelus* as food and the fact that this type of fish may carry parasites of zoonotic importance, the purpose of this research was to look at the histology of parasite infections in *Mastacembelus* digestive tract. The current research is the first one on pathology of the digestive tract of this type of fish.

## **Materials and Methods:**

In order to conduct the histological investigation, pathological study, eighteen of the fishes that live in freshwater *Mastacembelus mastacembelus* were gathered from local Tigris river fishermen in Ninevha province, Iraq from March 2021 till the end of the year. These fishes were taken to the lab and dissected the intestines, liver, pancreas and heart were excised. Tissue specimens of suitable sizes were collected from these organs and fixed in 10% formalin for 48 hours. The sample was carefully cleaned with water after fixation and dehydrated in a graded series of alcohols (70, 90, 95 and 100) percent. At 56 degrees Celsius, the substance was cleaned in xylol and infiltrated in paraffin wax, and blocks were made. A rotary microtome was used to create cross sections with a thickness of 4-5 mm. Hematoxylin and eosin stain were used to stain the tissue slices (10). The samples were inspected under a light microscope (Olympus – Japan) and photographed with the same microscope using a Japanese digital camera (MDCE- 5A) with a of 100 ASH sensitivity coupled to a Dell portable computer.

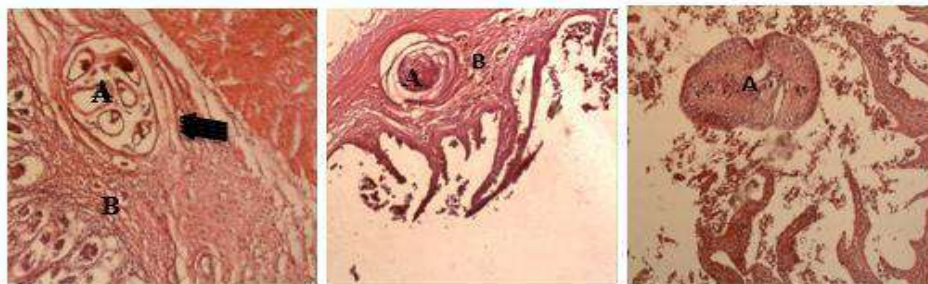
## **Results:**

*Mastacembelus* was photographed when brought to the lab (Fig.1), and tissues changes were examined after histological preparation. Parasitic nodules of variable sizes were seen in the intestinal submucosa causing thickening of this layer. A thin fibrous tissue capsule was noted around the nematode parasite (Fig.2) while thicker capsule was observed around the cestode parasite (Fig.3). In both cases the basic elements of the capsule were fibroblasts and collagen fibers. In some cases, free trematode parasites were seen free in the intestinal lumen (Fig.4). Degeneration, necrosis, and desquamation of epithelium of some of the intestinal villi (mucosa) and accumulation of these elements as tissue debris within the intestinal lumen were noted (Fig.5). Diffuse mononuclear cell infiltration was seen involving the whole thickness of the intestinal mucosa (Fig.6). An increase in the thickness of the intestinal submucosa was noted. The livers showed dilatation of the sinusoids and in few cases there was focal hepatitis as indicated by the focal infiltration of mononuclear cells (Fig.7). Portal fibrosis was observed in two cases (Fig.8). Myocarditis with the infiltration of mononuclear cells between bundles of

muscle fibers was seen in these two cases in the heart and Zinker necrosis in heart muscle (Fig.9). Pancreatitis was seen in some cases as indicated by the heavy infiltration of mononuclear cells in the pancreatic stroma congestion in necrotic pancreatic cells and thickness in blood vessels wall(Fig.10).



**Fig.(1).** *Mastacembelus mastacembelus* fish



**Fig 2**

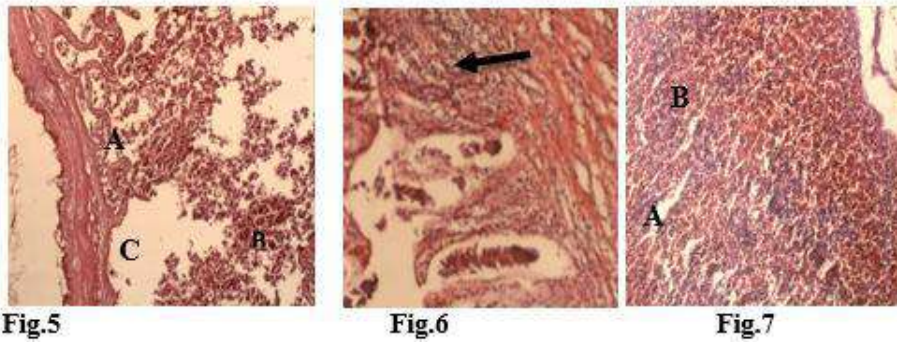
**Fig.(2).** Parasitic nodule (A) in the intestinal submucosa (B). Thin fibrous capsule surround multiple nematode parasites (arrow).H&S, 100X.

**Fig3**

**Fig.(3).** Parasitic nodule (A) in the intestinal submucosa .Thick multilayered fibrous capsule surrounds. (B).H&S, 100X.

**Fig4**

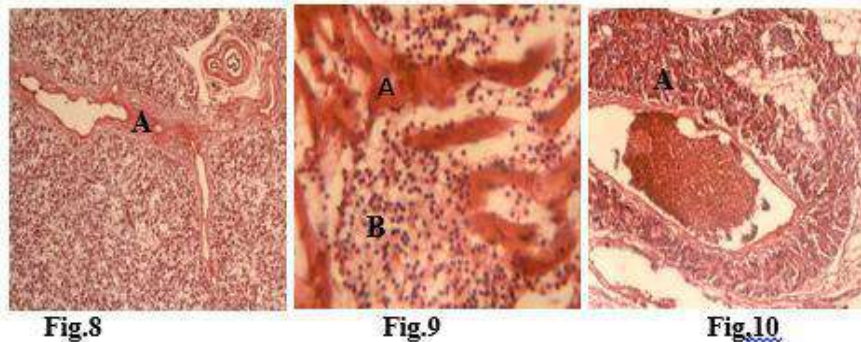
**Fig.(4).** Free trematode parasites in the intestinal lumen (A). H&S, 100X.



**Fig.(5).** Degeneration(A), necrosis(B) and desquamation (C) of epithelium in the intestinal villi (mucosa). H&S, 100X.

**Fig.(6).** Diffuse mononuclear cells infiltration causing thickness of the intestinal Mucosa (arrow).H&S, 100X.

**Fig.(7).** Dilatation of the sinusoids (A) in liver and focal infiltration of mononuclear cells (B) causing focal hepatitis. H&S, 100X.



**Fig.(8).** Portal fibrosis in the liver and thickness in bile duct wall(A). H&S, 100X.

**Fig.(9).** Myocarditis (A) with the infiltration of mononuclear cells (B) between bundles of muscle fibers in the heart. Zinker necrosis in muscle H&S, 100X.

**Fig.(10).** Heavy infiltration of mononuclear cells (A) in the pancreatic stoma H&S, 100X. causing pancreatitis, congestion in necrotic pancreatic cells and thickness in blood vessels wall.

## Discussion:

The freshwater fishes *Mastacembelus mastacembelus* are thought to be the most delicious fish in Ninevha province because of the tenderness of their muscles and the social notion that they have medical significance in the treatment of joint diseases. In spite of this fact, naturally – occurring lesions of various organ systems of this type of fishes have not been studied in Iraq. Therefore, this study could be considered among the very few studies dealing with spontaneous lesions of *M. mastacembelus*.

The intestinal lesions of *M. mastacembelus* described in this study are typical of parasitic infections and they are described for the first time in this species of fish. However, they are similar to those described in other species of fish such as *Mastacembelus armatus* collected from rivers in various districts of India (11,12) . Among the parasitic fauna, particularly of the intestines of the eel with spines *Mastacembelus mastacembelus* from the Iraqi Greater Zab river. (6) reported two species of digenetic trematodes (*Allocreadium transversal* and *Asymphylogora macrocetabulum*), Cestodes (*Polygonchobothrium magnum* and *Ligula intestinalis*),

and nematodes (*Agamospirura* sp. and *Procamallanus viviparus*). (13) has been proven that *Mastacembelus favus* are infected with five species of parasites :acanthocephalus, polymorphus, rhabdochona., senga fluke and cystacanth of acanthocephalan. Therefore, it could be assumed that the intestinal lesions found in the present study are due to some of these parasites or their larval stages.

In the present study, sub-acute to chronic hepatitis was a common lesion in *Mastacembelus mastacembelus*. Inflammatory mononuclear cell infiltrations and portal fibrosis were the characteristic features of these lesions.(14) reported the trematode parasite *Allocreadium khami* n. sp has been found in the liver of freshwater fish, *Mastacembelus mastacembelus*. Histopathological changes included cyst formations, hepatitis, disarray in the arrangement of hepatic cords, necrosis of hepatocytes and rupture of sinusoids. Focal hepatitis and fibrosis are known to occur in fish in response to various injurious agents (viral, bacterial, parasitic, fungal, toxic, or nutritional) (15).

Myocarditis was observed in some of the fish and it was similar to that reported in other species. Cardiomyopathies in fish could be due to viral, fungal or nutritional causes (15). As well as (16) revealed the presence of the Excysts metacercaria of *Centrocestus formosanus* in different organs of *Mastacembelus* fish.



## References

1. Ali, M.R.;Rahman,M.M.;Sarder,M.R.I. and Mollah,F.A.(2017).Histology study of the developing gonads of endangered freshwater spiny eel, *Mastacembelus armatus* during the reproductive cycle. J, Banglagesh Agril. Univ. 14(2):261-269. DOI:10.3329/jbau.v14i2.32702.
2. Pardeshi, P.R.(2017). Histopathological changes due to the infection of cestode parasite, *Cercumoncobothrium* sp. In fresh water fish, *Mastacembelus armatus* (Lecepede, 1800) . IJAPSA.O3(8): 2394-823X.DOI:10,22623.
3. Coad, B. W. (2006). Freshwater fishes of Iran. [http:// www.briancoad.com](http://www.briancoad.com)
4. Oymak, S. A ; Kirankaya, S.G. and Dogan, N. (2009). Growth and reproduction of Mesopotamian spiny eel (*Mastacembelus mastacembelus* Banks& Solander,1794) in Ataturk Dam Lake ( Sanliurfa), Turkey. J. Appl. Ichthyol.25(4):488-490.
5. Coad, B. W. (2007). Freshwater fishes of Iran.Scientific names checklist. A. Freshwater fishes. [www.briancoad.com](http://www.briancoad.com)
6. Bashe, S.K.R. and Abdullah, S.M.A. (2010). Parasitic fauna of spiny eel *Mastacembelus mastacembelus* from Greater Zab river in Iraq. Iran. J. Vet. Res. ,Shiraz University, 11(1): 18-27.
7. Vankara, A.P. and Vijayalakshmi, C. (2009). Histopathological changes of the esophagus of the freshwater eels, *Macrogathus aculeatus* (BI.) and *Mastacembelus pancalus* (Lac.) due to infection of metacercariae of *Clinostomum mastacembeli* Jaiswal , 1957. J. Parasit. Dis., 33(1-2) :65-69.
8. Fartade, AM. Fartade MM.(2015). New species of cestode parasite *Senga jadhavii* sp.Nov from freshwater fish *Mastacembelus armatus* from Godavari basin M.S.
9. (India), Journal of Entomology and Zoology Studies. 3(5): 249-253.
- 10.Nanware, SS, Bhure DD, Deshmukh VS. 2015. Incidence of infection of cestode genus *Senga* parasitic in freshwater fish *Mastacembelus armatus*, International Quarterly Journal of Biology & Life Sciences.; 21(1): 31-36.
- 11.Suvarna, S. K. ; Layuton, C. and Bancroft, J. D. (2013). Bancroft's theory and practice of histological techniques. 7<sup>th</sup> edition, Churchill Livingstone Press, New York – USA.
- 12.Malsawmtluangi C, Lalramliana(2016). Prevalence of helminth parasites infecting *Mastacembelus armatus* (Lacepède, 1800) from different rivers of Mizoram, northeast India. Mizo Academy of Sciences, 16(3): 144-150.
- 13.Gaikwad, R.B.; Bhagwan, H.K.; Sana, S.Z. and Inamdar, S.A.2021.Biochemical I studies on cestode parasites in *Mastacembelus armatus* in nasik district, M.S.(India). nt. J. S. Res. Sci. Technol. 4(11):384-385.
- 14.Phalee, A.N.P.(2018).Helminthic infection of tire track eels (*Mastacembelus Favus* Hora, (1923) in uthensongkram river the district, nakhon phanom province.Rajabhat J.

15. Sci.Humanit. Soc.Sci.19(1):81-88. Doi:org/0000-0002-4216-5941 Pardeshi, P.R.; Hiware , C.J. and Wangswad , C.(2012). Histopathology of the liver of *Mastacembelus armatus* (Lecepede, 1800) due to trematode parasite , *Allocreadium Khami* n.sp. J. Parasait. Dis., 36(1): 53-55.
16. Robertes, R.J. (2003). Fish pathology. 3<sup>rd</sup>. ed. W.B. Saunders, Edinburgh, UK
17. Al-Sa'adi, B. A. H.(2020).Spin eel fish *Mastacembelus mastacembelus* (Banks et
18. Solander in Russell, 1794) as a New Host to the Parasite *Centrocestus formosanus* Phase Excysts metacercaria for the First Time in Iraq. J Univ Babylon App Sci,28:1



**A NEW RECORDING OF IRAQI FLORAEPIIDIUMDIDYUM L. (BRASSICACEAE)**

**S.A.ALIWY  
L.G.A.AL-EZEREG**

## A NEW RECORDING OF IRAQI FLORALEPIDIUM DIDYMIUM L. (BRASSICACEAE)

S.A.ALIWY<sup>1</sup>

L.G.A.AL-EZERE<sup>2</sup>

### Abstract:

*Lepidium didymium* L. a new species of Iraqi flora, belonging to the Brassicaceae family, has been described, its specimen were collected from the gardens of Al-Jadriya campus at the University of Baghdad, as well as from the gardens of the Al-Aarass city in Baghdad. The species morphologically studied and the dimensions were taken detailed which was characterized by the presence of an abundance of hairs, leaf measurements and shape which was characterized by its Deeply lobed also included a describe of the reproductive parts such as the flower and the fruit which was distinguished by detailed two elongated adjacent lobe pollen grains, were of a tricolpate type, as well as determining the flowering period of the species, which started from the beginning of March and continued until the end of May. The sample was saved (BUH) in the College of Science, University of Baghdad, and the number was given 50386.

**Key words:** Brassicaceae, Iraq, *Lepidium Didymium*, New Record, Tricolpate.



<http://dx.doi.org/10.47832/MinarCongress5-25>



<sup>1</sup> University of Baghdad, Iraq, [anaamnoor@yahoo.com](mailto:anaamnoor@yahoo.com), <https://orcid.org/0000-0003-1435-3731>



<sup>2</sup> University of Baghdad, Iraq

## **Introduction:**

The Brassicaceae (Cruciferae) is one of the most important families having 338 genera, 3709 species distributed all over the world (Al-Shehbaz et al., 2006). Also the family called mustard family was recognized easily by its floral and fruiting characters. It is cosmopolitan but chiefly distributed in temperate and Mediterranean regions.

Genus *Lepidium* glabrous, papillose or with white simple hairs. Leaves simple or pinnately divided. Sepals not saccate at the base. Petals white, rarely yellow, rarely absent. Stamens 6, 4, or 2 filaments neither winged nor toothed; ovary with 2 ovules. Fruit a strongly compressed, angustiseptate, dehiscent silicle, winged or not. Seeds 2, mucilaginous on wetting (Townsend and Guest, 1980).

Genus *Lepidium* (Linnaeus, 1753: 643) belongs to the tribe Lepidieae of Brassicaceae family. There are approximately 250 species distributed across temperate and subtropical regions with a few species in the tropics (Al-Shehbaz, 2012). and one of the most taxonomic in abundance studied genera of Brassicaceae. An expository fact is that out of 265 hitherto accepted species have been described or firstly distinguished at relevant rank over the last decade (Al-Shehbaz 2010, 2012, 2015, 2016, 2017, De Lange et al. 2013, German 2014a, Sykes 2014, Dorofeyev 2019, Yıldırım 2019). *Lepidium didymum* (common name lesser swine-cress) is a herbaceous annual to biennial plant. South America is the site of the origination and geographic distribution of *L. didymum*. The plant has variable natural products which are biologically active, include flavonoid, coumarins, phlobatannins and terpenoids etc (Kashani et al., 2012) (Wajidullah et al. 2017). The species recorded in Turkey (Ibrahim Sırrı YÜZBAŞIOĞLU et al. 2013), and also recorded in Cook Island (Sykes, 2014). Many studies have been conducted about the family in Iraq, such as (Al-Ebrahimi, 2013; Al-dobaissi et al. 2020; Al-Masoudi, 2019; Al-Shehbaz, 2012; Dizayee, and Saleh. 2017; Al-Dobaissi and Al-Masoudi, 2021).

## **Material and Methods**

During field trips, which were conducted in late winter and early spring of 2021, and during a comprehensive survey of wild plant species distributed in the city of Baghdad / Iraq, the species belonging to the Brassicaceae family was collected and diagnosed and a number of samples were preserved in the herbarium of the University of Baghdad College of Science. It was studied morphologically and so saved samples in the Herbarium (BUH) which taken the number (50386), and took the dimensions of the different parts of the species, as well as pollen grains in the laboratories of the College of Science, Department of Biology, University of Baghdad.

## **Rustles and discussion**

An annual herb with soft green stems, 7-39 cm long, with dense simple hairs scattered along the stem. It is either erect or prostrate and stems the leaves are soft, lobed and alternately arranged, and the leaflets are opposite, the basal leaves in the shape of a Rosette, The average length of the leaf is 4-5 cm.

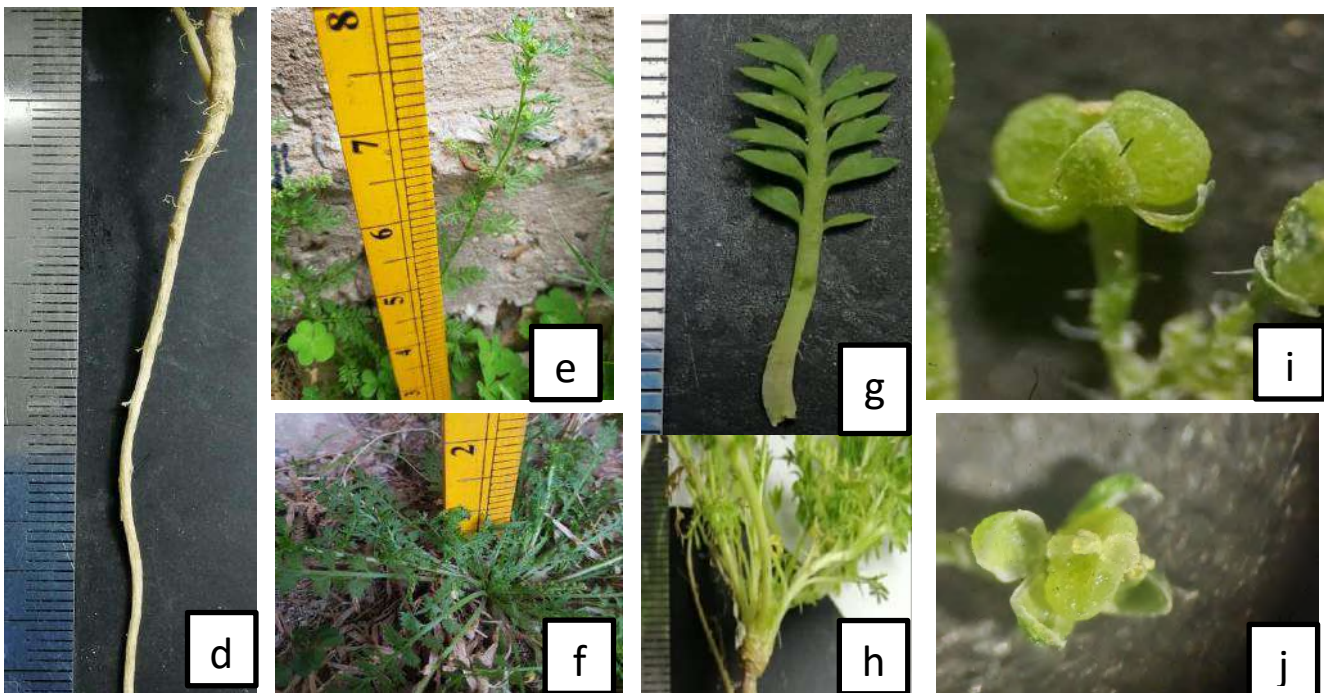
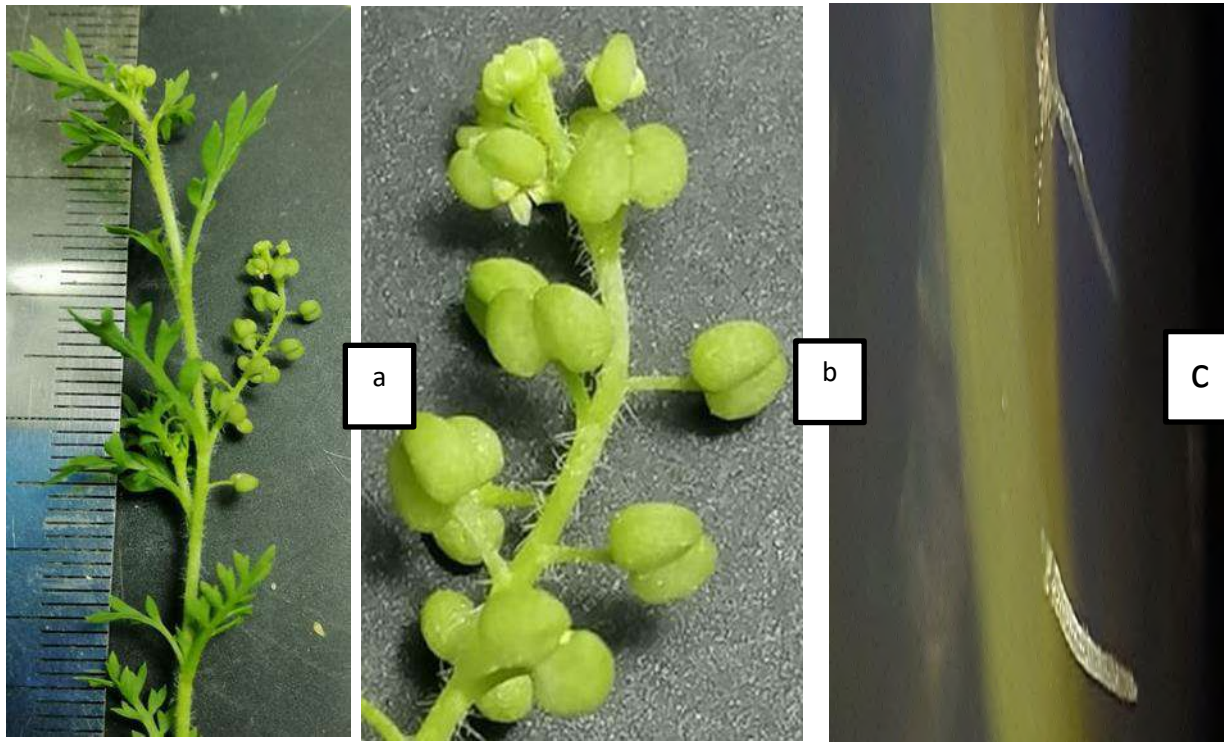
The inflorescence is raceme corymbs pedicels 1-2.5 mm. the flowers (25-30) which are small has four sepals green with membranous margins, petals absent, and this is rare cause the other species have four white to yellow petals. there are (2) stamens while most species of the genus have six stamens (tetradynmous), ovary with two ovules with yellow capitate sessile stigma and the style is lacked, fruits with (2) rounded lobed Townsend and Guest,1980) , and contain two seeds with drupelet type (Radford 1974), pollen grains are range from very small to small (18.2-20.8 micrometer) trilobed in polar view tricolpate sub spheroidal in shape with reticulate ornamentation (Erdtman,1971).

Flowering period: from late March to early May.

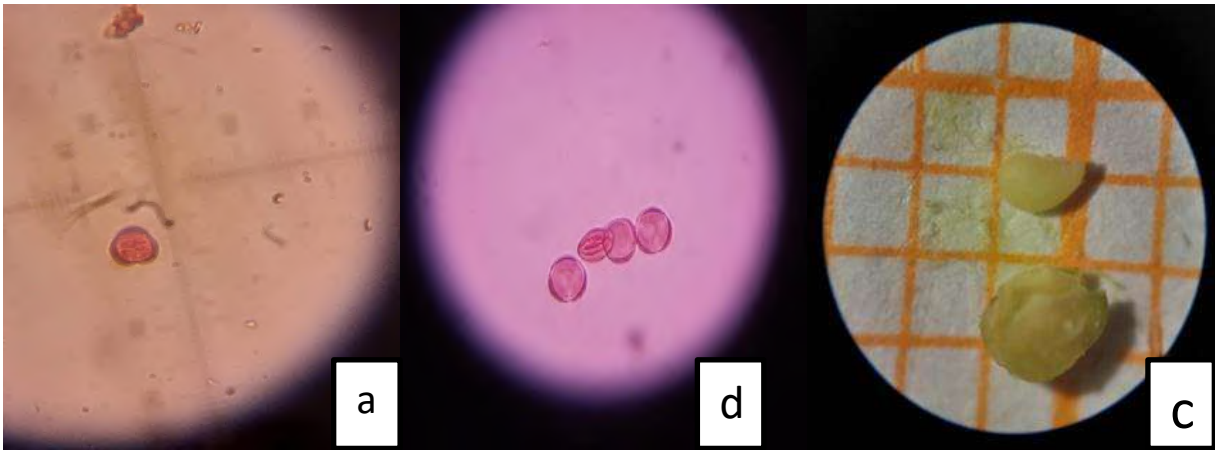
Synonym name: *Coronopus didymus*(L.) J. E. Smith kew gardens.

Common name: Bitter Cress, Lesser Swinecrss ,Wart cress.

Taxonomy: Syst.Nat. ed.12,2:433.1767.(Linnaeus,1767)



a-the species with small flowers and fruits as well as leaves; b-Fruit and small flowers with trichome on the stem ;c- hairs (d)- Root, tap root;; e-f-The base of the species that shows the branching of the leaves in Rosette form; G-Glabrous leaf with lobes appears with opposite leafletes; h- root ; i- flower; j-flower part with reproductive part



a-pollen grain polar view  
b-Pollen grain polar and equatorial view  
c-seed drupelet



## References

1. Al-Dobaissi ,I. A.M. and R.K.H. Al-Masoudi.(2021). Study of fruits morphological features for 33 species belong to Cruciferae family in Iraq. Iraqi Journal of Agricultural Sciences. 52(4):1039-1049.
2. Al-dobaissi, I.A.; R.K.H. Al-Masoudi and L.K. Al-Azerg. 2020. Palynological study of genus *Pteroccephalous* in Iraq. The Iraqi Journal of Agricultural Sciences. 51(2):565-573.
3. Al-Ebrahimi, S.H. 2013. A Comparative Taxonomic Study Of The Genus *Aethionema*( Brassicaceae) W. T. Aition in Iraq. Msc. Thesis. College of Science. Baghdad University. pp:170.
4. AL-Masoudi, R.K.H. 2019. Morphological, anatomical and geographical distribution studies of species *Horwoodiadicsoniae*(Turril) in Iraq. The Iraqi Journal of Agricultural Sciences. 50(6):1613-1620.
5. Al-shehbaz, Ī.H., M.A. Beilstein and E.A. Kellogg. 2006. Systematics and phylogeny of the Brassicaceae (Cruciferae): an overview. Pl. Syst. Evol., 259: 89-120 .
6. Al-Shehbaz, I.A. (2010) A synopsis of the South American *Lepidium*(Brassicaceae). Darwiniana 48 (2): 141–167.
7. Al-Shehbaz, I.A. (2012) A generic and tribal synopsis of the Brassicaceae (Cruciferae). Taxon 61: 931–954.
8. Al-Shehbaz, I.A. (2012) *Lepidium galapagoense* (Brassicaceae), a new species from Ecuador. Harvard Papers in Botany 17 (2): 231–233.
9. Al-Shehbaz, I.A. (2015) Brassicaceae. In: Hong, D.Y. (Ed.) Flora of Pan-Himalaya 30. Cambridge University Press, Cambridge; Science Press, Beijing, pp. 1–595.
10. Al-Shehbaz, I.A. (2016) *Lepidium seydelii*(Brassicaceae), a new species from Namibia. Harvard Papers in Botany 21 (2): 133–135.
11. Al-Shehbaz, I.A. (2017) Five new species of *Lepidium* (Brassicaceae): *L. pabotii* (Iran), *L. arequipa* (Peru), and *L. lapazianum*, *L. linearilobum*, and *L. stephanbeckii* (Bolivia). Novon 25 (4): 403–413.
12. Al-Shehbaz, I.A. 2012. A generic and tribal synopsis of the Brassicaceae (Cruciferae). Taxon. 61(5):931-954.
13. *Botanik Dergisi* 26 (1): 93–101.
14. De Lange, P., Heenan, P., Houlston, G., Rolfe, J. & Mitchell, A. (2013) New *Lepidium* (Brassicaceae) from New Zealand. *PhytoKeys* 24:1-147.
15. Dizayee, A.T.R and H.A. Saleh. 2017. Effect of different levels of nitrogen and potassium fertilizers application on nutrient balance and yield of Broccoli (*Brassica oleraceae*). The Iraqi journal of Agricultura Sciences. 48: (Special Issue): 101-112.
16. Dorofeyev, V.I. (2019) *Lepidium gobicum*(Cruciferae, Brassicaceae), a new species from Gobi Desert of Mongolia and China.
17. Erdtman, G. 1971. Pollen morphology and plant taxonomy. Angiosperms ( An Introduction palynology) 2ed. Hafner publishing. Co. New York. 553pp
18. German, D.A. (2014a) Taxonomic remarks on some Asian *Lepidiums*. 1. (Brassicaceae). *Phytotaxa* 186 (2): 97–105.
19. Kashani, H.H., E. S. Hoseini, H. Nikzad, M. H. Aarabi.(2012). Pharmacological properties of medicinal herbs by focus on secondary metabolites. Life Sci. J. 9(1): 509-520 .

20. Linnaeus, C. (1753) *Species plantarum*.Salvius, Stockholm, 1200 pp
21. Linnaeus, C. 1767. *Systema naturae per regna trianaturae, secundum classes, ordines, genera, species, cum characteribus, differentiis, synonymis, locis*. Editio duodecima, reformata. Tomus 1 (Regnum Animale), Pars 2: 533–1327.
22. Radford, A.E. ; W.C. Dikson ; J.R. Massey and C.R. Bell. 1974. *Vascular plant system*. Harper and Row. 891 pp
23. Sykes, W.R. (2014) A new species of *Lepidium* (Brassicaceae) in the Cook Islands. *Phytotaxa* 181 (3): 184–187
24. Townsend, C.C. and E. Guest (ed). 1985. *Flora of Iraq*. Vol. 4 part two. Ministry of agriculture and agrarian reform 827-892. .
25. *Turczaninowia* 22, 4: 37–41. [in Russian and English]
26. Wajidullah, N. Akhtar, S.S. Ali, S. Ahmed, S. Jan, Barkatullah, M.A. Khan and M.S. Khan. 2017. Phytochemical analysis of *Lepidium didymum*. *Pak. J. Weed Sci. Res.* 22(2): 155-164 .
27. Warwick, S.I., Francis, A. and Al-Shehbaz, I.A. (2006) Brassicaceae: Species Check-list. *Plant Systematics and Evolution*, 259, 249-258.
28. Yıldırım, Ş. (2019) Two new species of Brassicaceae, *Descurainia tugayana* and *Lepidium tuzgoelense*, from Konya, Turkey. *Ot Sistemik*
29. YÜZBAŞIOĞLU, İbrahim Sırrı, M. KESKİN. (2013). A new record for the flora of Turkey: *Lepidium didymum* L. (Brassicaceae). *Biological Diversity and Conservation*. 6/3 (2013) 46-48

**COMPARATIVE STUDY FOR VAGINAL INFECTIONS IN PREGNANCY  
AND NON PREGNANCY WOMEN IN NINEVEH GOVERNORATE**

**IBRAHIM TALAL DAWOOD  
HANAN SAMI NOURI  
NAJLAA ABDULLA FATHI**



## COMPARATIVE STUDY FOR VAGINAL INFECTIONS IN PREGNANCY AND NON PREGNANCY WOMEN IN NINEVEH GOVERNORATE

Ibrahim Talal DAWOOD<sup>1</sup>

Hanan Sami NOURI<sup>2</sup>

Najlaa Abdulla FATHI<sup>3</sup>

### Abstract:

Epidemiology study had achieved for vaginal infections disease for women in Ninawah governorate through see the files in some hospitals (Al-Khansaa, Al-Batool, Al-Salam) for (2019-2020-2021) years.

Bacterial Vaginosis (B.V.) is the most common causes for vaginal infection which Escherichia coli and Staphylococcus aureus appear highest proportion for it which attained (19.05%), (8.52%) sequently, the results showed that the highest proportion of this disease happened in age-level (36-41) years which attained (14.42%) while (60-65) years appeared less proportion which reached (10.43%), Also as noticed that high proportion of vaginal infections disease appeared in August (3.72%, 4.62%, 4.90%) sequently for (2019-2020-2021) years.

Results also show that pregnancy women more affected with bacterial vaginosis (B.V.) compared with non-pregnancy and barren women which attained (33.3%), high percentage of infection happened in women who live in country side and villages, the proportion attained (52.08%) followed by the cases of right side of Mosul city infection (7.85%) at least the left side infection (20.05%) through last three years.

Identifying the types of infections that affect females , The aim:

Attempting to shed light on the extent of the problem of vaginal infections in women by identifying the types of causes (bacteria, fungi, parasites) and determining their percentages, Comparative study for vaginal infections between pregnant, non pregnant & infertility women, Attempting to deduce the role of important factors such as age, physiological status (pregnancy, infertility) and residential area in the possibility of increasing the risk of exposure to the disease during the years, Determining the prevalence of vaginal infections among women during the three months of the three years 2019-2020-2021 in Nineveh 2021 -2019 Governorate.

**Key words:** Vaginal Swab, Pregnant Women, Epidemiological Study, Age.



<http://dx.doi.org/10.47832/MinarCongress5-26>

<sup>1</sup> University of Mosul, Iraq, [ibrahim.alsawaf@uomosul.edu.iq](mailto:ibrahim.alsawaf@uomosul.edu.iq)

<sup>2</sup> University of Mosul Iraq, [hanan.sami@uomosul.edu.iq](mailto:hanan.sami@uomosul.edu.iq), <https://orcid.org/0000-0002-0587-7990>

<sup>3</sup> University of Mosul, Iraq, [najasbio75@uomosul.edu.iq](mailto:najasbio75@uomosul.edu.iq)

## **Introduction:**

Vaginal infections: It is a pathological condition in females, where the natural balance of bacteria in the vagina is disturbed, where the overgrowth of certain bacteria is carried out compared to the rest of the bacteria that live naturally in the vagina, which leads to irritation in the vagina, this infection may sometimes accompany it Discharge, odor, pain, itching or burning (1).

Vaginitis is a common infection that affects all ages. It affects young girls and adult women. It is an inflammatory disease that includes the lower part of the vagina and the opening of the vulva. Vaginitis occurs for several reasons

1. Increased infections after surgeries such as hysterectomy and abortion
2. long-term use of antibiotics and exposure to chemotherapy
3. Pregnancy
4. Infertility
5. Diabetes.
6. Tension (mental state)
7. Lack of personal hygiene and wearing tight underwear made of nylon.
8. Complications that occur as a result of premature birth or miscarriage (2) .

## **Types of vaginal infections**

### **1- Bacterial infections**

Sixty-four percent of women develop vaginal bacterial infections at any time, making this the most common type and its causes include the proliferation of bacteria that live in the vagina, which disturbs the acidic environment, the transmission of *E. coli* that usually lives in the anus to the vaginal opening, and urinary tract infections. Frequent transmission of infection through the husband and the use of contraceptives, and its most common causes are *Mobiluncus sp.*, *E. coli*, *Gardnerella vaginalis*. Its symptoms include: itching, burning, vaginal secretion that has an unusual smell similar to the smell of fish with a yellow or green color (3).

### **2- Yeast (fungal) infections**

Studies indicate that (75%) of women get at least one yeast infection in their lifetime, and its causes include the proliferation of the fungus *Candida albicans*, which lives naturally in the vagina, long-term use of antibiotics or diabetes, obesity, pregnancy, and AIDS. Its symptoms include: severe itching, irritation in the vagina and vulva, white lumpy secretion (like a clot), and pain may occur during urination (4).

### **3- Parasitic infections**

It occurs as a result of the presence of *Trigomonas vaginalis*, as this type is not naturally present in the vagina and is transmitted during intercourse and its symptoms are: itching, burning, foamy secretion of green or gray color with an unusual smell, and pain may occur during urination (5) .

#### **4-Vaginal atrophy**

The vagina becomes atrophied, as atrophy and inflammation of the vaginal walls occurs due to low estrogen. Vaginal atrophy occurs most of the time after menopause, but it can occur during breastfeeding or at any time when the body's production of estrogen decreases. Studies indicate that more than half of women are in the menopausal stage. They suffer from vaginal atrophy (6).

#### **5- Vaginal dryness**

It is a general problem for women that affects them during and after menopause, noting that the lack of viscosity can occur at any age. Its symptoms include: itching, stinging around the vaginal opening, hormonal changes during the menstrual cycle as a woman grows, affecting the amount and breadth of the thin layer of moist mucus that covers the vaginal wall (7).

#### **7-Vaginitis diagnosis**

The diagnosis is made by going to the doctor to take a swab of vaginal secretions from the vaginal orifice and then microscopic examination or culture of the sample taken from the vagina so that the doctor can diagnose the source of the infection and treat it

##### **- for bacteria**

1-The puff test: A small amount of potassium hydroxide is added to a microscopic slide that contains vaginal secretions. A characteristic odor resembling the smell of fish rises, which is a positive result confirming the bacterial infection of the vagina.

2-A litmus paper is placed to check its acidity. Any pH greater than 4.5 is considered evidence of an infection with vaginal bacteria .

##### **- for fungi**

1-Using culture media to diagnose Candida in the middle . or blood agar and making a gram stain.

Germ tube test 2-

##### **- for parasites**

1-Microscopic examination and seeing Trichomonas vaginalis under a light microscope (8).

#### **-Treatment**

The usual course of treatment is to take the antibiotic Metronidazole

(500mg) twice daily, once every 12 hours for (7) days, or Glindamycin are effective treatment for vaginal infections (10,9).

#### **Research Methodology**

Numbers of cases of vaginal infections among women in Nineveh Governorate were obtained in some hospitals in the city of Mosul (Al-Khansa, Al-Batool, Al-Salam) by looking at the records of those hospitals for the years (2021-2019) and over the months of the three years, and all the causes were written down ( Bacterial, fungi, parasites), and the percentage of vaginal infections among women

was determined according to age, physiological status (pregnancy, infertility) and residential area as they are considered among the factors that have a role in increasing the possibility of infection with the disease. The implementation of the descriptive experimental design was determined and the data were analyzed in the form of percentages and geometric figures.

**Results and Discussion**

Vaginal infections are a public health problem in developing and developed countries, and the microorganisms causing them vary.

figer (1) shows the numbers and percentages of isolated microorganisms from vaginal infections for women in Nineveh Governorate for the years 2019 -2021, as the results showed the total number (1102) of the total vaginal swabs taken, which included (363) cervical swabs (CX) with a percentage of (32.9%) and (739) a smear for the top of the vagina (HVS) with a percentage of (67%), and both types of smears gave (43.28%) a negative result and (56.71%) a positive result, which included (502) bacterial isolates with a percentage of ( 45.5%) and (106) isolates of fungi with a percentage of (9.61%) and finally (17) isolates of parasites with a percentage of (1.54%). It is clear that bacteria is the most common cause of vaginal infections in women during the last three years .

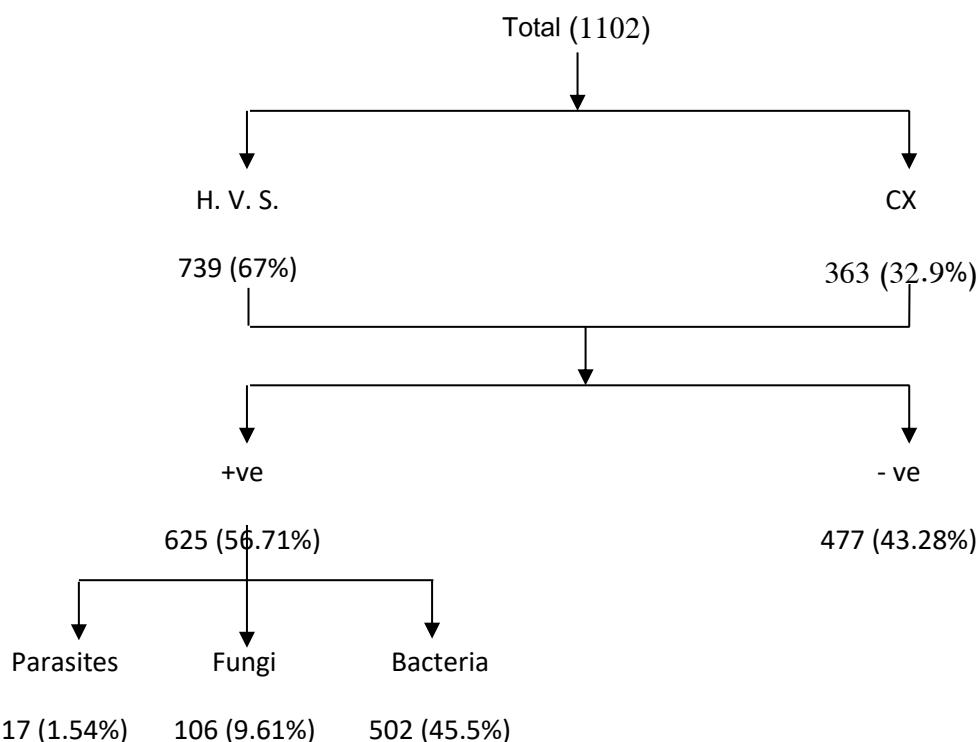


fig (1) numbers and percentages of microorganisms isolated from common vaginal infections for the years 2021-2019

Vaginal bacterial infection is one of the common diseases among women, and the microorganisms causing it vary, as the vagina is colonized by natural microorganisms, and when there is a defect, it becomes a pathogenic opportunist, in addition to the invasion of other pathogenic species, which leads to a bacterial infection (12,11 ).

Table (1) shows the numbers and percentages of the types of microorganisms that cause vaginal infections. The table shows that the highest percentage of microorganisms is with *Escherichia coli* bacteria (19.05%), followed by *Staphylococcus aureus* (8.52%), *Klebsiella pneumoniae* (7.98%), and *Staphylococcus epidermidis* (2.81%), followed by *Streptococcus sp.* (1.90%), while the lowest percentage was for *Pseudomonas sp.* (0.45%), as for the fungi, *Candida albicans* (5.08%) and *Candida sp.* (4.53%), and it ranked last as parasites causing vaginal inflammation with a percentage of (1.54%), and *Trichomonas vaginalis* appeared as the main cause of this type of infection.

Table (1) shows the numbers and percentages of the types of microorganisms that cause vaginal infections.

%	Isolates no.	microorganisms	Infectious disease
19.05	210	<i>Escherichia coli</i>	Bacteria
8.52	94	<i>Staphylococcus aureus</i>	
2.81	31	<i>Staphylococcus epidermidis</i>	
1.90	21	<i>Streptococcus sp.</i>	
1.45	16	<i>Proteus mirabilis</i>	
7.98	88	<i>Klebsiella pneumoniae</i>	
0.72	8	<i>Citrobacter sp.</i>	
1.63	18	<i>Enterobacter sp.</i>	
0.45	5	<i>Pseudomonas sp.</i>	
0.99	11	<i>Gardnerella vaginalis</i>	
5.08	56	<i>Candida albicans</i>	fungi
4.53	50	<i>Candida sp.</i>	
1.54	17	<i>Trichomonas vaginalis</i>	parasite

It is clear from Table (1) that The highest percentages infection with *E. coli* as a cause of bacterial causes of vaginitis reached (19.05%), and the reason may be due to its ability to adhere to the cell wall by cilia. Also, this bacteria *E. coli* naturally settles in the human intestine as part of the natural flora (Normal flora) and causes vaginitis to be transmitted From the rectum (anus) to the vagina as a result of the wrong movement during ghusl after defecation, as the ghusl must be from the front to the back and not the other way around from the vagina (13). As for *Staphylococcus aureus*, which reached (8.52%), it is considered one of the bacteria that is found as a natural flora on the skin, mucous membranes and the vagina in humans. It grows in aerobic and anaerobic conditions. It is considered one of the bacteria resistant to physical and chemical factors and has the ability to survive for 14 weeks in dry mucus. They have a wide range of acute and chronic disease infections, and they also have a great ability to cause opportunistic infections when appropriate conditions are available for them, such as a defect in immune defenses, infection with disease organisms such as viruses, or the presence of chronic diseases such as cancers, in addition to having many virulence factors. Bacteria of all kinds (10%) in the vagina of pre-menopausal women, and the percentage increases during menstruation (14).

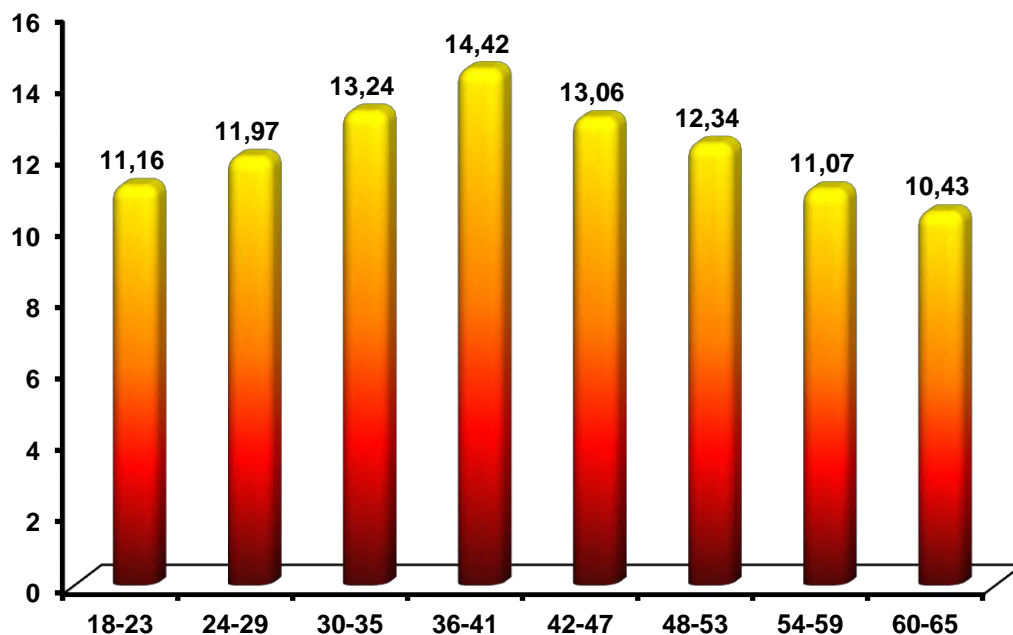
As for the fungi, *Candida albicans* is also present in the vagina. As a result of the change in the natural bacterial presence, including a reduction in the



proportion of *Lactobacillus* as a result of the pH imbalance, it may allow the most resistant bacteria to grow, multiply and secrete toxins, thus affecting the body's natural defenses and making the colonization of healthy bacteria more difficult. Stress (stress), antibiotic use, steroid hormone therapy, or diabetes (12) . As for the cause of the appearance of *Trichomonas vaginalis* in vaginal infections, at a lower rate than the rest of the causes, it is transmitted through or during intercourse, as it is not naturally present in the vagina .

The periodic differences in the acidic environment of the vagina and the periodic changes in the nature of the cervical mucus that are affected by the secreted sex hormones, in addition to the content of glycogen in the mucus, all of these factors combined affect the ability of microorganisms to bind to the epithelial cells lining the vagina, and then on the quality of the prevailing microorganisms (15).

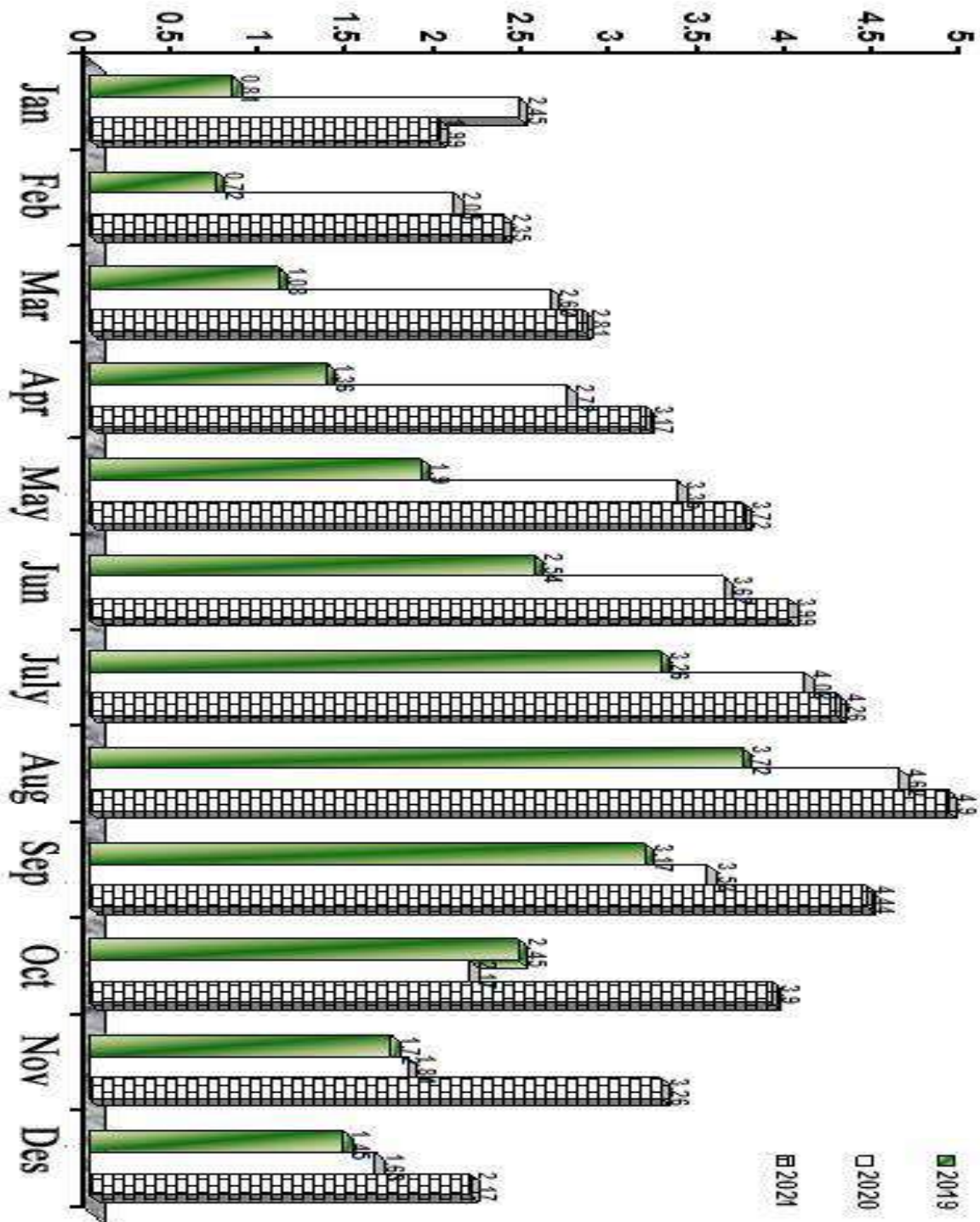
Figure (1) shows the percentages of vaginal infections among women according to different age groups. The results showed that the highest percentage of infection appeared in the age group (41-36) years, amounting to (14.42%), followed by the category (35-30) years, amounting to (13.24%). While the percentages began to decrease in the old ages (menopause) 45 years and over, and the reason may be due to the immune status of the mother, as it is believed that the host defense mechanisms develop with age and factors specific to the vagina such as pH (acidic middle) and the presence of microorganisms, and that the factors Physiological such as breastfeeding, frequent births and recurrent urinary tract infection cause vaginal infections. In addition, sexual activity is more in these age groups compared to large groups, which increases the incidence of infection (17,16), girls at puberty are exposed to *Streptococcus* bacteria sp and *Escherichia coli* is severely affected by bacteria transmitted from the anus due to non-compliance with healthy health conditions (13 ).



**Figure (1) shows the percentages of vaginal infections among women according to different age groups.**

As for the lowest incidence of infection, it appeared in the age group (65-60) years, which amounted to (10.43%), the reason may be due to the fact that before puberty and after menopause in women, atrophy occurs in the lining of the vagina, and the chance of infection increases, as out of every (10) women arrive Menopausal women (4) suffer from signs and symptoms of vaginal dryness due to low estrogen levels, menopause and sometimes due to cigarette smoking (2). Also, the removal of the ovaries may be one of the causes of vaginal infections because it causes immune disorders and causes irregular and insufficient bodily hormones, and frequent cases of vaginitis with age lead to stimulating the immune system to form antibodies to these different types of germs In addition, sexual activity is absent in this advanced age group, and vaginal infection increases in these groups due to the use of antibiotics for a long and repeated period, because antibiotics reduce the natural concentration of lactic acid bacilli, which increases the pH of the vagina, which promotes the proliferation of microorganisms In addition, there are many other factors such as weak immunity caused by poor nutrition, which leads to a decrease in the acidity of the vagina and a decrease in the percentage of lactobacilli bacteria, which hinders the growth of bacteria that cause inflammation at this age (18).

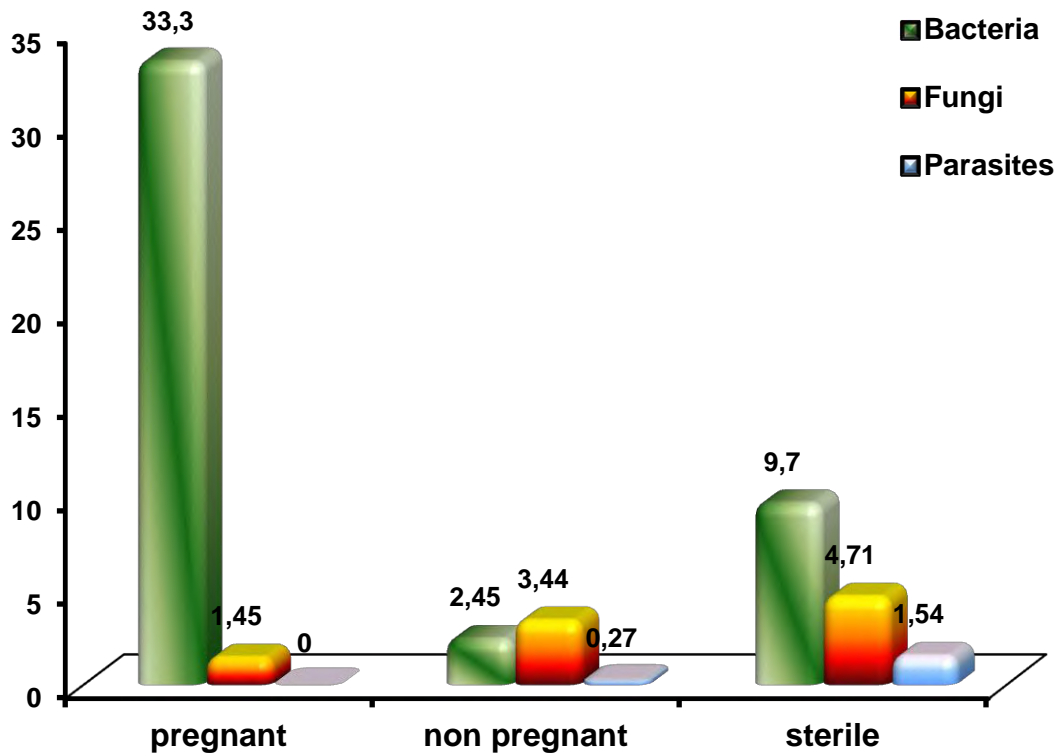
Figure (2) shows the percentages of vaginal infections among women during the months of the years 2019-2020-2021 , as the results showed that most vaginal infections appeared in August, reaching (3.72%), (4.62%), and (4.90%) for the years 2019 – 20 20 -2021 , respectively, and the lowest infection rate, the results showed a great discrepancy, as the lowest infection rate in 2019 was in February (0.72%), and in 2020 in December (1.63%), while in 2021 it appeared in January ( 1.99%), and the reason for the emergence of the highest rate of vaginal infections in August for the three years may be due to the fact that this month is one of the most high months of the year, which makes the affected area sweat a lot and becomes high humidity, which encourages the occurrence of itching and vaginal infections (1).



**Figure (2) shows the percentages of vaginal infections among women during the months of the years 2019-2020-2021.**

Figure (3) the percentages of isolated microorganisms among pregnant, non-pregnant and sterile women infected with vaginal. The infections, results showed that the highest bacterial infection rate appeared in pregnant women and amounted to (33.3%), followed by infection among sterile (9.70%) and then non-pregnant (2.45%). As for fungal infections, the highest infection was recorded in sterile women (4.71%), followed by infection among non-pregnant women (3.44%), then

pregnant women (1.45%), and finally parasitic infections showed the highest percentage in sterile women (1.54%).) No parasitic infection was recorded in pregnant women.

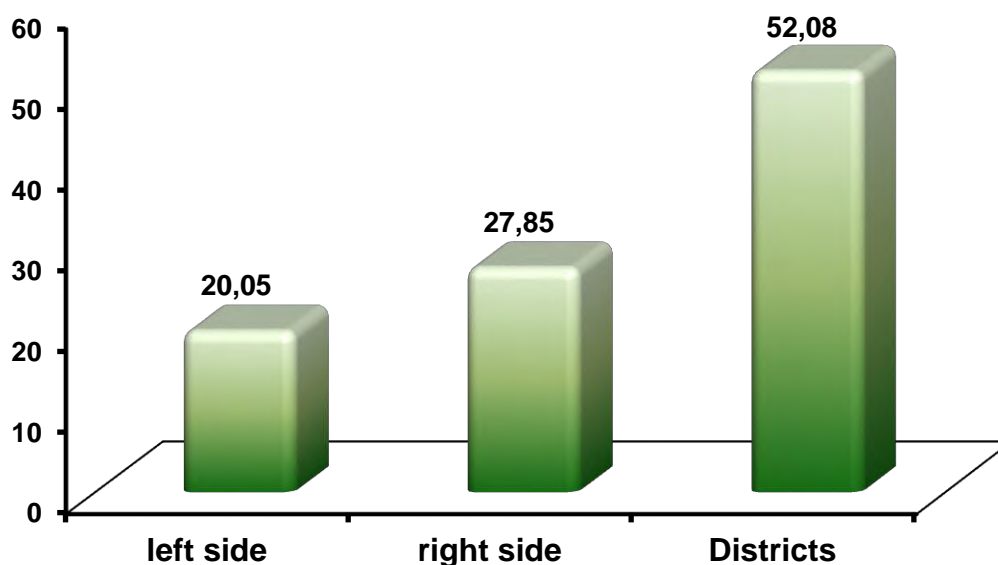


**Figure 3: Percentages of isolates of microorganisms among pregnant, non-pregnant and sterile women with vaginal infections.**

The reason is that bacteria form part of the normal flora of the vagina, as it is a common coexistence for women without causing any clinical symptoms, but its percentage increases during pregnancy, which confirms its opportunistic nature, and its numbers may increase in the event of a defect in the flora. The natural nature of the vagina, such as the absence of lactic acid bacilli, as in the case of infertility, and all of these depend on the physiological state of the pregnant, non-pregnant and sterile woman, and we mean by that (hormonal level and sexual activity) (19). Also, during pregnancy, the incidence of urinary tract infection increases due to the expansion of the ureter and bladder due to the action of the hormone progesterone, which increases its secretion during pregnancy and thus increases the rate of urine return from the ureter to the kidney. Which leads to inflammation in the urinary canal, and it has been noted that the rate of premature birth increases when germs appear in the last period of pregnancy, and that the rate of transmission to the newborn child is (1%) (21,20).

Figure (4) shows the percentages of the relationship between patients with vaginal infections and residential areas in the districts of Nineveh Governorate for the years 2021-2020-2019, as the results showed that the highest percentage of injuries appeared in the districts and sub-districts (52.08%), followed by the percentage of infection on the right side (27.85%). And the lowest percentage is on the left side (20.05%). The reason for the emergence of a difference in infection rates according to residential areas may be due to the low cultural and educational level

of women in the districts and sub-districts, which has an impact on increasing the infection rate because the remote areas lack health conditions such as water quality. And the lack of awareness of health issues related to this disease, and education has a great impact in avoiding infection, through the understanding of the review of the pathogen, how it is transmitted, its pathological effects and ways to treat it, and the number of reviews from districts and sub-districts is more than in the rest of the regions due to the deterioration of their economic and living conditions, which reduces the rate of They visit hospitals constantly and follow the instructions, so their hesitation is irregular, and due to the deteriorating living conditions in these areas, this affects the nutritional system, which in turn is reflected in the body's resistance to diseases. different and causes weak body immunity (1).



**figure (4): Percentages of the relationship between patients with vaginal infections and residential areas in the districts of Nineveh Governorate for the years 2019-2021**

## Conclusions

vaginal Infections and Bacterial vaginosis is the most common cause of is associated with many pathological conditions.

2-The bacteria isolated from vaginal samples mostly return to the normal flora of the vagina and intestinal tract.

3-The age group (41-36) years is the group most vulnerable to infection with vaginal infections, and the age group (65-60) years is the least affected.

4-There are factors that affect the incidence of vaginitis, such as seasonal changes, as the highest rate of infection appeared during the month of August for the last three years 2021-2020-2019.

5-The effect of physiological factors on the incidence of vaginal infections, as the infection appeared in pregnant women more compared to the sterile and non-pregnant women.

6-The economic and social level has a role in increasing the incidence of infection, as the highest infection rate appeared in the districts and sub-districts in Nineveh Governorate, then the right side patients came in second place, and finally the left side for the years 2021-2020-2019.

### **Recommendations**

1-Conducting periodic and continuous examinations for women of all ages to get rid of vaginal infections .

2-Maintaining cleanliness of clothing and body

3-Health awareness, which is the main factor in getting rid of many bacterial and parasitic diseases.

4-Avoid wearing underwear that contains (nylon), preferably cotton, in addition to avoiding tight clothing.

5-Wash the affected area well with water and medical soap three times a day, then dry the area well and keep it dry.

## References

1. Amsel, R.; Totten, P. A.; Chen, K. C.; Eschenbach, D. and Holmes, K. K. (2015). Non specific vaginitis. Diagnostic criteria and microbial & epidemiologic associations, *Am. J. Med.* 74(1):14-22.
2. Ness, R. B.; Hillier, S. L.; Kip, K. E.; Soper, D. E.; Stamm, G. A. and McGregor, J. A. et al., (2011). Bacterial vaginosis and risk of pelvic inflammatory disease. *Obstet. Gynecol surv.*, 60:99-100.
3. Ison, C. A. and Hay, P. E. (2019). Validation of a simplified grading of gram stained vaginal smears for use in genitourinary medicine clinics. *Sex. transm. Infect.*, 78(6): 413-415.
4. McDonald, H. M.; O'loughlin, J. A.; Vigneswaran, R.; Jolley, P.T.; Harvey, J. A. and Bof, A. et al., (2010). Impact of metronidazole therapy on preterm birth in women with bacterial vaginosis flora (*gardnerella vaginalis*):*Br. J. Obstet, Guneacol*, 104(12):1391-1397.
5. Okun, N.; Gronau, K.A. and Hannah, M.E. (2011). Antibiotics for bacterial vaginosis or trichomonas vaginalis in pregnancy: a systematric review. *Obstet. Gynecol*, 105:857-68.
6. Soper, D. E. (2019). Bacterial vaginosis and postoperative infections, *Am. J. Obstet. Gynecol.*, 169(2): 467-469.
7. McGregor, J. A.; Rfench, J. I.; Jones, W.; Milligan, K.; Mckinney P. T. and Patterson, E. et al., (2010). Bacterial vaginosis is associated with prematurity and vaginal fluid mucinase and Sialidase: results of a controlled trial of topical clindamycin cream. *Am. J. Obstet. Gynecol*, 170(4):1048-1059.
8. Nugent, R. P.; Krohn, M. A. and Hillier, S. L. (2018). Reliability of diagnosing bactrial vaginosis is improved by astandardized method of gram stain interpretation. *J. Clin. Microbiol.*, 29(2): 297-301.
9. Larsson, P. G. (2019). Treatment of bacterial vaginosis, *Int. J. Std. AIDs*, 3(4): 239-247.
10. Sobel, J.D. and Ferris, D. et al. (2019). "Suppressive antibacterial therapy with 0.75%, metromidazole vaginal get to prevent recurrent bacterial vaginosis." *American Journal of Obstetrics and Gynecology*, 194(5): 1283-1289.
11. Eschenbach, D.A.; Hillier, S.; Critchlow, C.; Stevens, C.; DeRouen, T. and Holmes, K.K.(2015). Diagnosis and clinical manifestations of bacterial vaginosis. *Am J Obstet Gynecol*, 158:819-28.
12. Hillier, S.L. (2018). Diagnostic microbiology of bacterial vaginosis. *Am. J. Obstet. Gynecol.*, 169:455-459.
13. Hay, P. E.; lamont, R. F.; Taylor, D. M.; Ison, D. J. and Pearson, J. (2018) Abnormal bacterial colonisation of the genital tract and subsequent preterm delivery and late miuscarriage. *Br. Med. J.*, 308(6924):295-298.
14. Sewankambo, N. (2018). "HIV -1 infection associated with abnormal vaginal flora morphology and bacterial vaginosis." *Lancet* 350(9083): 1 036-1036.
15. Soper, D.E.;Bump, R.C. and Hunt, W.G. (2010). Bacterial vaginosis and trichomonas vaginitis are risk factors for cuff cellulites after abdominal hysterectomy. *Am. J.Obstet Gynecol*, 163: 1016-23.
16. Keane, F. E.; Thomas, B. K.; Whitaker L. and Renton, A. (2019). An association between non-gonococcal urethritis and bacterial vaginosis and the implications for patients and their sexual partners. *Genitourin, Med.*, 73(5):373-377.

17. Yen, S.; Shafer, M. A.; Moncada, J.; Campbell, C. J.; Flinn, S. D. and Boyer, C. B. (2010). Bacterial vaginosis in sexually experienced and non-sexually experienced young women entering the military . *Obstet. Gynecol.*, 102(1):927-933.
18. McDonald, H.; Brocklehurst, P.; Parsons, J. and Vigneswaran, R. (2017). Antibiotics for treating bacterial vaginosis in olderlywomen. *Cochrane Database Syst. Rev.*, 5(2): 262.
19. Guise, J.M.; Mahon, S.M.; Aickin, M.; Helfand, M.; Peipert, J.F. and Westhoff, C. (2016). Screening for bacterial vaginosis in pregnancy. *Am. J. Prev. Med.*, 20(3 Suppl) :62-72.
20. Goldenberg, R.; Klebanoff, M.; Nugent, R.; Krohn, M.; Hillier, S. and Andrews, W. (2014). The Vaginal Infections and Prematurity Study Group. Bacterial colonization of the vagina during pregnancy in four ethnic groups. *Am J Obstet Gynecol*, 174:1618-21.
21. Varma, R. and Gupta, J. K. (2018). Antibiotic treatment of bacterial vaginosis in pregnancy: Multiple meta- analysis and dilemmas in interpretation. *Eur. J. Obstet Gynecol., Report. Biol.*, 124: 4-10.



**ANALYSIS OF HEAT FLOW IN DOUBLE-PIPE HEAT EXCHANGER WITH  
NANO-FLUID**

**MOHAMMED AHMED  
ABDULKADER AHMED ANNAZ  
MOHAMEED MHANA METEAB**



**ANALYSIS OF HEAT FLOW IN DOUBLE-PIPE HEAT EXCHANGER WITH NANO-FLUID**

**Mohammed AHMED<sup>1</sup>**  
**Abdulkader Ahmed ANNAZ<sup>2</sup>**  
**Mohameed Mhana METEAB<sup>3</sup>**

**Abstract:**

This communication contains a simplified model of a counter flow double-pipe type heat exchanger with known dimensions. The Mat lab code was used in the modelling of the fluid flow both with and without using Nano-particles. The heat transfers during the flow of the working fluid containing water as a base fluid and dispersed aluminum oxide particles with an approximate 20nm diameter size under turbulent flow conditions was studied based on Matlab software simulation. In parliamentary law, to obtain the results for using Nano-fluid on the studied model, a comparison was made with a model study on water only as a working fluid. Using the partial differential equation, which covered the system behavior under environmental conditions, the system was modeled, and the outlet temperature distribution, total heat transfer, and steady state time of the heat exchange was determined depending on the energy balance. The input parameters such as the inlet temperature and the speed of the working fluid were assumed as known parameters in the initial state conditions. The results obtained revealed an improvement in the model performance by using Nano-fluid as a working fluid. There was an approximate 26 % increase in the total heat transfer, about an 80% reduction in Exergy destroyed due to the reduction in the entropy generation, and near to 11% increase in the effectiveness of this model under the study. The modelling of this system and anticipated effects are extremely important in the preliminary stage of the heat exchange device and equivalent system design.

**Key words:** Heat Exchanger Design, Computational Analysis, Heat Transfer, Nano-Fluid.



<http://dx.doi.org/10.47832/MinarCongress5-27>



<sup>1</sup> Tikrit university, Iraq, [Mohammed.Ahmed72@tu.edu.iq](mailto:Mohammed.Ahmed72@tu.edu.iq)



<sup>2</sup> Tikrit University, Iraq, [abd.annaz@tu.edu.iq](mailto:abd.annaz@tu.edu.iq)



<sup>3</sup> Tikrit University, Iraq, [Muh.muhana@tu.edu.iq](mailto:Muh.muhana@tu.edu.iq)

## **Introduction:**

Conduction and convection are considered as the main mechanisms in energy transfer across solid surfaces in a heat exchange device such as a heat exchanger, which is widely used in different applications, for example; the automotive industries, refrigeration and air conditioning systems, power plants, heat recovery systems, food industries, and chemical processing.

In the simplest configuration of the heat exchanger, in the shell and tube shape, the fluid flows in the opposite direction or in the same direction depending on the design optimization. The dual-pipe configuration typically consists of two concentric tubes, with the inner pipe, and the fluid flow, separately, in the inner pipe and in the passage between the pipes.

Double-tube exchangers are usual in low-capacity applications, and are advantageous in flow distribution and disassembly for maintenance. Depending on both the first and second law of the thermodynamic, the simulation of the flow and energy transfer is of great importance for design engineers and manufacturers in order to compromise between the high effectiveness of the device and the optimum size and configuration for the specific application.

Kevin M. Lunsfordk [1] provides some technologies for increasing the shell-and-tube exchanger performance by studying the consequences of the excess pressure drop capability in the existing exchanges, the effect of the fouling factor on the heat exchange performance, and the utilizing of the augmented surfaces for high temperature transportation. These factors were analyzed and evaluated for specific cases regarding the estimation of their effect on the performance of a shell-and-tube heat exchanger.

Q.M. Thirumarimurugan et al [2] compared experimental findings such as overall heat transfer coefficients and exchanger effectiveness with a mathematical model prediction. They found that there was a good coincident between the predicted results and the experimental findings.

Paisarn Naphon [3] used the theoretical prediction and experimental outcome to analyze the heat transfer during the flow in the horizontal concentric tube type exchanger based on the second law analysis. The water base working fluid was used in both the hot and cold area. The results revealed that there was close agreement between the experimentally measured data and the predicted results.

H. Kotwal and D.S Patel [4] presented a review study in regard to the use of the CFD technique by analyzing the tube and shell heat exchanger. Due to the increase in computing power, the model found a good resolution for analyzing the multiphase flows in realistic and complex geometry.

V. Vasiny et al [5] was interested in the design of the tube and shell heat exchanger by modeling using the ANSYS 14.0. Thermal simulations were performed on the different face and edge assuming various thermal loads in a static steady state. Various refractory materials (aluminum, copper, steel, etc.) are appropriated to different parts of the thermal system under study to estimate the heat transfer performance. The results noticed that the preferable heat flux was achieved by using copper at all stages of the design.

Mohamed H. Shedid [6] used turbulence modeling to investigate the thermal behavior of Nano-fluid in an annular flow based on a numerical approach. The expected results were compared with several formulas for convection using Nano fluid flow, which appeared full assent with the Spalart-Allmaras model rather than the k-model.

The purpose of this investigation is twofold. First, the modelling of the system with specified geometry numerically to predict the temperature distribution, the steady

state time, and the amount of heat flux during the system operating under an imposed condition with and without using Nano-fluid. Second, we carried out a second law analysis on the system under the study to evaluate their characteristic performance regarding effectiveness, entropy generation, and Exergy loss. Hot water and cold water were both used as working fluids in the first stage, and hot water and cold Nano-fluid were used in the second stage.

## 2-Shell and Tube Heat Exchanger Analysis.

Convection and conduction mechanisms in a heat transfer are concerned in a heat exchanger. Convection takes place on each side of the working fluid, whereas the conduction allows the heat to transfer through the wall, which separates the two fluids. During this process, the temperature continually changes as it travels through its path in both the tubes, and the temperature of the separated wall located between the fluid varies along the length also [7].

The heat transfers from the hot tube to the cold side are evaluated using the equation below [8]:

$$q = UA \Delta T \quad (1)$$

q- Heat transfer rate.

A- Area across over the heat transfer.

U- Overall heat transfer coefficient and  $\Delta T$  is:

$$\Delta T = T_i - T_o \quad (2)$$

For the better approximation of the heat transfer occurring over the length scale of the model,  $\Delta T_{lm}$  (logarithmic mean temperature difference) was used.

$$\Delta T_{lm} = \frac{\Delta T_1 - \Delta T_2}{\ln(\Delta T_2/\Delta T_1)} \quad (3)$$

The temperature differences,  $\Delta T_1$  and  $\Delta T_2$ , in equation (3) are equal to the difference in the temperature between the two flows at the same side of HE.

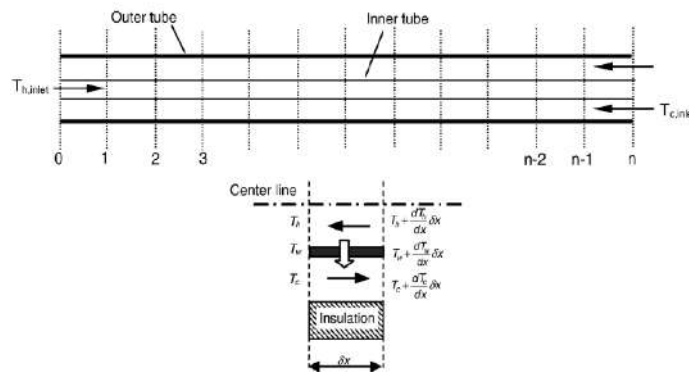
$$q = UA \Delta T_{lm} \quad (4)$$

The energy balance differential equation for the shell and tube side is considered as the best analysis of the heat exchanger as follows;

$$\frac{\partial T}{\partial t} = -v \frac{\partial T}{\partial x} - \frac{U2\pi(T_{in} - T_{out})}{row C_p r} \quad (5)$$

$$\frac{\partial T}{\partial t} = -v \frac{\partial T}{\partial x} - \frac{U2r_{in} \pi(T_{in} - T_{out})}{row C_p r} \quad (6)$$

Equation 5 in addition to Eq.6 in their partial differential form can be solved numerically by modeling the tube and shell depending on the control volume of each segment as illustrated in Figure 1.



**Fig.1- Schematic diagram of system simulation approach**

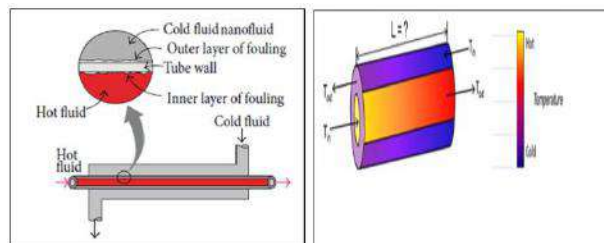
The result obtained was used to draw the temperature distribution profile along the total length of the model. The steady state time will be found by monitoring the graph until it reaches a steady state condition. After we find the numerical solution for the output temperature of the working fluid for both the tube and shell side, other parameters such as the entropy generation, the Exergy, and the effectiveness can be calculated depending on the first estimated results. The process will be repeated for two stages of the working fluid. In the first stage, both working fluids are taken as water, while in the second stage, the hot water is taken with the Nano-fluid as a cooling medium.

### 3- Modeling Assumption

To simplify the solution of the basic physical equations, which described the heat transfer characteristics depending on the conservation of energy, the following main assumptions are considered.

- Counter flow through the heat exchanger.
- Flows under a steady condition.
- Fluids flowing through both tubes are incompressible fluid.
- Convective heat transfer coefficient is equal for each side section.
- Thermal conductivity is constant for the material used.
- The heat capacity is not a function of the temperature.

The schematic diagram of the system model is shown in Figure 2.



**Figure 2. The schematic diagram of a shell and tube heat exchanger**

#### 4-The Operating Parameters of The Model

The operating parameters were set up as shown in Table 1. and the overall heat transfer coefficient, U, is 1700 W/m<sup>2</sup> K.

**Table 1.** Heat exchanger operating condition

Fluid Parameter	Inner tube (water)	Outer tube (Al <sub>2</sub> O <sub>3</sub> ) 6% volume fraction
T <sub>in</sub>	370 K	298 K
Roh ρ	1000 kg/m <sup>3</sup>	1099 kg/m <sup>3</sup>
C <sub>p</sub> (KJ/Kg.K)	4.184 kJ/kg K	4.174 KJ/Kg k
V(velocity)	0.01 m/sec	0.01 m/sec
D(diameter)	1 m	2 m
L (length)	4 m	4 m
K (W/m.K)	0.604	1.189
μ (kg/m.sec)	3.72*10 <sup>-4</sup>	4.278*10 <sup>-4</sup>

The heat transfers can be described by two equations Eq. (5) and (6). The initial condition and boundary conditions for each equation are taken as described in Table 2.

**Table 2.** The initial and boundary conditions.

For the inner tube the conditions are: Initial Condition : T(L=0 to L=4) = 370 K Boundary Conditions: T(x=0, t) = 370 K, T(x=4,t) ----- dT/dt=0
The outer tube. initial condition: T (x=0 to x=4) = 298 K Boundary Conditions: T(x=0,t) ----- dT /dt =0 , T(x=4,t) = 298 K

#### 5- The Second Law Analysis

In this configuration of the concentric tube, the heat transferred from the hot side (the inner tube) to the cold side (outer tube). The total entropy generation from the system can be obtained using the equation given below [3]:

$$S'_{gen} = S'_{gen,h} + S'_{gen,c} \tag{7}$$

$$S'_{gen} = (mC_p)_h \ln\left(\frac{T_{h,out}}{T_{h,in}}\right) + (mC_p)_c \ln\left(\frac{T_{c,out}}{T_{c,in}}\right) - (mR)_h \ln\left(\frac{P_{h,out}}{P_{h,in}}\right) - (mR)_c \ln\left(\frac{P_{c,out}}{P_{c,in}}\right) \tag{8}$$

Where the irreversibility of heat transfer is illustrated by the first two terms to the right of equation (8), while the last two terms in the same equation explain the irreversibility of fluid friction. Eq. (8) is reduced to the equation 9, since the irreversibility which come from fluid friction is not described in our model:

$$S'_{gen} = (mC_p)_h \ln\left(\frac{T_{h,out}}{T_{h,in}}\right) + (mC_p)_c \ln\left(\frac{T_{c,out}}{T_{c,in}}\right) \quad (9)$$

**Case A:**

The hot-side capacity rate,  $(mC_p)_h$ , is lower than the cold fluid,  $(mC_p)_c$ . The effectiveness,  $\epsilon$ , can be calculated from Eq.10 as follows:

$$\epsilon = \frac{(mC_p)_c(T_{c,out} - T_{c,in})}{(mC_p)_{min}(T_{h,in} - T_{c,in})} = \frac{(T_{h,in} - T_{h,out})}{(T_{h,in} - T_{c,in})} \quad (10)$$

Eq. (10) combined with Eq. (9), and rearranging them, we get:

$$S'_{gen} = C_{min} \ln\left[1 - \epsilon\left(1 - \frac{1}{T_R}\right)\right] + C_{max} \ln[1 + \epsilon C_r(T_R - 1)] \quad (11)$$

Where:

$C_{min}$  -minimum capacity rate,

$C_{max}$  - maximum capacity rate,

$T_R$  - is the temperature ratio,  $(T_h/T_c)$ , and  $C_r$  is the capacity rate ratio,  $(C_{min}/C_{max})$ , then the exergy loss,  $(I')$ , can be given by:

$$I' = T_0 S'_{gen} \quad (12)$$

where:  $T_0$  is the outer temperature.

**Case B:**

The capacity rate of the hot fluid,  $(mC_p)_h$ , is higher than that of the cold fluid,  $(mC_p)_c$ .

In this case, the effectiveness is calculated by applying the equation stated below:

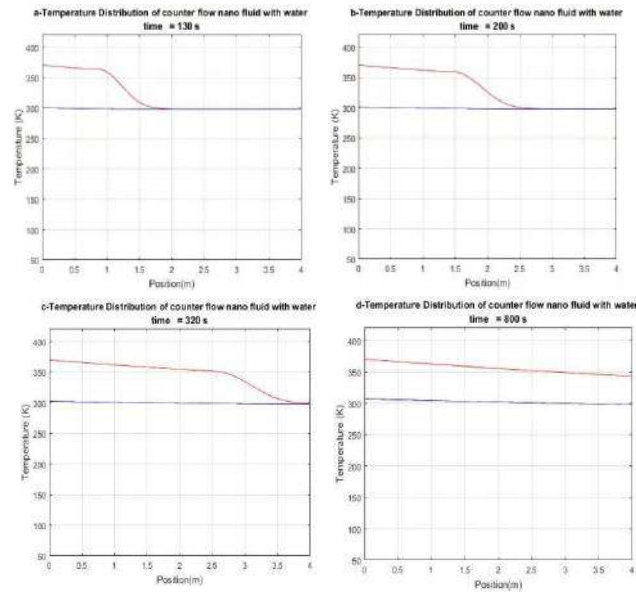
$$\epsilon = \frac{(T_{c,out} - T_{c,in})}{T_{h,in} - T_{c,in}} = \frac{(mC_p)_h(T_{h,in} - T_{h,out})}{(C_p)_{min}(T_{h,in} - T_{c,in})} \quad (13)$$

$$S'_{gen} = C_{min} \ln[1 + \epsilon(T_R - 1)] + C_{max} \ln\left[1 - \epsilon C_r\left(1 - \frac{1}{T_R}\right)\right] \quad (14)$$

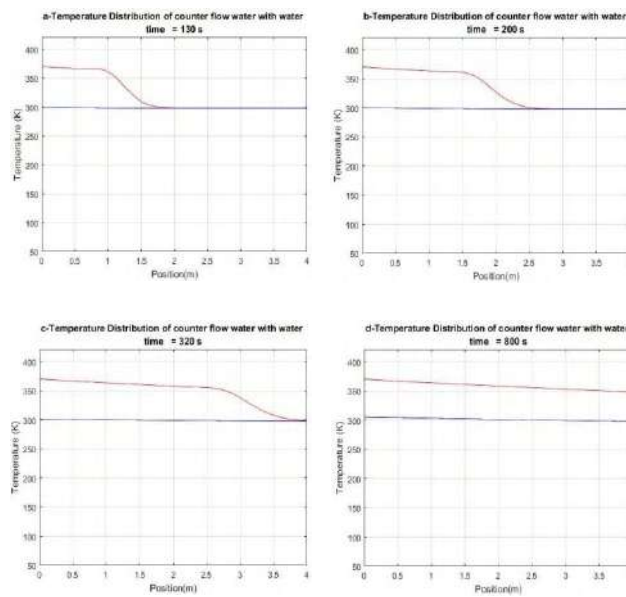
**6- Results**

The hot water was permitted to run through the internal pipe, and the cold Nano-fluid passes through the outer tube in order to perform an analysis of the model. The volume flow rate is assumed to be constant in both positions. Utilizing the Mat lab simulation, a solution was obtained for the tabular heat exchange system. The temperature distribution was found for both sides, and the total heat transfer was obtained numerically.

The results of total heat transfer which calculated by using log mean temperature difference were compared with the results which predicted from numerical approach for validation. The temperature profiles were plotted in Figures (4-5) for a different time stage both with and without using Nano-fluid. The model needed about 800 s to reach a steady state condition, which means that there will be no change in the temperature distribution with time.



**Figure 4.** a, b,c,d (in time 130 s & 200 s & 320 s& 800 s) represent the temperature Distribution of counter flow water with Nano-fluid



**Figure 5.** a,b,c,d (in time 130 s & 200 s & 320 s& 800 s) represent the temperature distribution of counter flow water with water



**Table 3.** The result of the numerical approach is as the following when we use only water in both tubes as a working fluid.

Inlet/Outlet Temperature for the inner tube is 370.00 K and 347.71 K
Inlet/Outlet Temperature for the outer tube is 298.00 K and 305.48 K
The total heat transfer by using the numerical solution is 732.28 kW
The total heat transfer by using the log mean temperature difference is 713.69 kW
The relative error is 0.03

**Table 4.** The result of this model was obtained as the following when we used Nano- fluid in the cold side.

Inlet/Outlet Temperature for the inner tube is 370.00 K and 339.88 K
Inlet/Outlet Temperature for the outer tube is 298.00 K and 308.21 K
The total heat transfer by using the numerical solution is 991.28 kW
The total heat transfer by using the log mean temperature difference is 964.92 kW
The relative error between the numerical solution and the log mean approach is 0.03 =3%

The results of applying the second law analysis is shown in Table 5.

**Table 5.** Second law analysis for the two cases.

Case A: using only water as working fluid .	
$\epsilon$ Effectiveness	= 32%
S' Entropy generation rate	= 2.34 kw/K
I' Exergy loss	= 697 Kw
Case B: using Nano- fluid as a coolant in the shell as a working fluid.	
$\epsilon$ Effectiveness	=43 %
S' Entropy generation rate	= 0.37 kw/K
I' Exergy loss	= 139.4 Kw

## 7- Conclusion

From the results shown in Tables 4 and 5, it is clear that there is an enhancement in the total heat transfer of approximately 26% by using the Nano fluid, keeping the relative error as the same in both cases. This behavior indicates the increase in the heat exchanger performance by using Nano-fluid. Furthermore, the second law analysis on the heat transfer of the double tube heat exchanger are presented as stated in Table 5, which reveals that there is near to 11% increase in effectiveness, and about an 84% decrease in the entropy generation rate, which leads to an approximate 80% reduction in the Exergy destroyed.

## References

1. K. M. Lunsford, "Increasing Heat Exchanger Performance," pp. 1–13, 2006.
2. A. Journal, A. Sciences, and S. Publications, "Performance Analysis of Shell and Tube Heat Exchanger Using Miscible System Department of Chemical Engineering, Coimbatore Institute of Technology, Coimbatore-641 014," vol. 5, no. 5, pp. 548–552, 2008.
3. P. Naphon, "Second law analysis on the heat transfer of the horizontal concentric tube heat exchanger ☆," vol. 33, pp. 1029–1041, 2006.
4. H. Kotwal and D. S. Patel, "CFD Analysis of Shell and Tube Heat Exchanger- A Review," *Int. J. Eng. Sci. Innov. Technol.*, vol. 2, no. 2, pp. 325–329, 2013.
5. V. Vasiny, P. Dubey, R. R. Verma, P. S. Verma, and A. K. Srivastava, "Steady State Thermal Analysis of Shell and Tube Type Heat Exchanger to Demonstrate the Heat Transfer Capabilities of Various Thermal Materials using Ansys," vol. 14, no. 4, 2014.
6. C. Paper, "Computational Heat Transfer for Nanofluids through an Annular Tube Computational Heat Transfer for Nanofluids through an," *Proc. Int. Conf. Heat Transf. Fluid Flow*, no. September.
7. R. Article, N. M. Jha, and N. M. Patel, "Heat exchanger using nano fluid," pp. 3–8.
8. R. Aghayari, H. Maddah, M. Zarei, M. Dehghani, S. Ghanbari, and K. Mahalle, "Heat Transfer of Nanofluid in a Double Pipe Heat Exchanger," vol. 2014, 2014.

**PROTECTING THE ENVIRONMENT FROM COVID-19 MEDICAL WASTE**

**MARIAM ADNAN IBRAHIM**



## PROTECTING THE ENVIRONMENT FROM COVID-19 MEDICAL WASTE

Mariam Adnan IBRAHIM <sup>1</sup>

### Abstract:

As economic and human development problems worsen, the majority of countries are relying on technological development to emerge from the crisis, whether it is the infectious disease crisis or the natural resource depletion crisis. Modern technology contributes to reducing the effects of both environmental pollution and the spread of HIV infection, Given the results of quarantine on the environment, it can be said that the importance of the latter is reflected in: Creating new vaccines and vaccines to eradicate the virus, Adopting environmentally friendly production mechanisms ,Adopt policies to reduce the depletion of natural resources, The trend towards the use of renewable energies to maintain the sustainability of the environment, Emphasizing the need to adopt a green economy and sustainable development.so the methods of disposing of medical waste differ from one country to another, In some places, waste is collected and sterilized, then sent to sanitary landfills or incinerated It is no secret to everyone that the amount of masks, gloves and other personal protection tools that were used during the pandemic period has exceeded twice their use before the pandemic. This in itself is a burden on an environment that already suffers from the problems of disposing of solid and liquid waste in a correct manner and in conformity with global health, After the transformation of medical waste into hazardous waste and the readiness of the competent teams to deal with the crisis, they were suffering from a weakness in the methods of disposing of this waste and with accurate preventive measures during the outbreak of the Covid-19 pandemic, We found it necessary to mention in this research the impact of the pollution resulting from those wastes that affected the countries of the whole world and how to find ways to increase the awareness of the individual in our Iraqi society, similar to advanced societies in dealing with the remnants of covid-19, Which has proven in some scientific sites with graphic documentation about the use of these wastes in their countries by some birds in building their nests and caused death to some of them after swallowing them and others by clashing in their claws and the difficulty of getting rid of them for weeks due to the incorrect disposal of solid waste in particular by the municipalities similar to the lack of support and experience.

**Key words:** Environmental Pollution, Medical Waste, Covid-19 Waste.



<http://dx.doi.org/10.47832/MinarCongress5-28>



<sup>1</sup> University of Tikrit, Iraq, [mariamadnan@tu.edu.iq](mailto:mariamadnan@tu.edu.iq), <https://orcid.org/0000-0003-1223-4261>

## **Introduction:**

The Covid-19 virus is a newly created virus, a new strain of coronavirus, and the danger of the virus is that it infects the human respiratory system, with no definitive treatment known yet, despite the availability of vaccines (G.W. Jones *et al.*,2020). Three hours exceeds a sufficient period for catching the virus, unless we follow proper prevention methods. This is considered an additional burden on the Iraqi environment, in which most members of his community suffer from a lack of awareness of waste disposal (Y. Fan,*et al.*,2019). In the increasing culture of vaccination, California-based Onsite West Technologies says that vaccinating the entire population of the United States, for example, requires quantities of needles if placed in a path that circles the globe, it would circle the planet 1.8 times. Experts have warned that medical waste disposal companies may face more than their capacity to absorb in front of the deluge of medical waste, and many environmental experts are calling for more sustainable solutions with the acceleration of vaccine distribution. Carlos Velo, president of the International Solid Waste Association, based in Rotterdam, says, “The emergence of an unexpected pandemic called a time bomb, which will have a horrific impact on human health, and revealed that the world lacks the necessary infrastructure to deal with any increase in waste and the acceptance that the waste of vaccination centers goes to inappropriate places it is the real disaster (OSHA,2020). Concerns about the fate of vaccine waste have also been raised in Europe, where European police (Europol) said in November that it was investigating some companies for mishandling Covid-19 waste. Studies have shown that garbage collectors in countries such as India collect syringes and needles from open landfills and resell them on the black market the environment(IETC, 2022).

### **1.1. Research problem**

Based on the above, the following problem can be raised:

- 1.1.1. How did corona pandemic pollutants contribute to environmental pollution?  
What is the importance of clean technology in protecting the environment?

### **1.2. Study divisions**

To answer the problem, we will try to divide the research into :

- \*What is the Corona Virus pandemic
- \*Corona pandemic and its implications for the environment and how to get rid of the materials and tools used to prevent and protect against viruses and get rid of the tools of the virus infected.
- \*Clean technology is a mechanism for protecting the environment.

## 2. The importance and objectives of the research:

- The importance of research in highlighting the environmental problems and environmental pollution caused by environmental pollutants, which necessitates the need to take care of them as the medium in which many organisms live.
- Highlight on the implications of the spread of COVID-19 to protect the environment based on the health pollutant prevention measures applied in most countries of the world.
- Emphasizing the need to adopt clean technology as a strategy to limit the spread of pollution to preserve natural resources.

## 3. Research methodology:

We relied on the analytical descriptive approach to identify the literature of the study, where we used the office and electronic survey of the various references related to the subject.

## 4. What is environmental pollution: Environmental pollution is defined as:

➤ Putting materials in places that are not suitable for them, or polluting the environment with human waste, as pollutants enter it in the form of waste and waste or by-products of industries (Zuhara S, 2018).

Throwing waste for disposal, which spoils the environment and its cleanliness, as a result of violating the components of the ecosystem, which paralyzes its effectiveness and loses the ability to self-dispose of pollutants by natural processes (National Institutes of Health U.S. Department of Health and Human Services, 2021)

➤ A physical, chemical or biological change that leads to a harmful effect on air and water, or what is harmful to humans and other living organisms.

➤ The human being to add substances or energy to the environment that have harmful effects, endanger health, or affect biological resources or ecosystems in a way that leads to a harmful effect on the legitimate uses of the environment (Safety Assessment of Nanomaterials to Eyes, 2019)

In general, environmental pollution is defined as a process that contributes to harming human life, its surroundings, or the rest of living organisms, through the introduction of foreign substances and pollutants that contribute to changing the properties of the ecosystem and destroying it.

## 5. Types environmental of pollution:

**5-1-Air pollution:** It is related to substances that harm the quality and composition of the atmosphere, and that lead to harm to humans, ecosystems and natural resources. Here it is related to:

**5-2-Water pollution:** It expresses the changes taking place in the nature, composition, quality and properties of water, making it unusable.

**5-3-Soil pollution:** It expresses the accumulation of some substances such as toxic compounds, salts, chemicals, radioactive materials, and all factors that cause soil diseases, which negatively affect the growth of plants, the health of animals, and

people. Among the factors that lead to soil pollution are the following:(Shehata, 2002)

## **6. what is the Food contamination:**

The term food contamination refers to the fact that food or water contains what makes it unfit for human or animal consumption,

whether harmful microorganisms, toxic chemicals or food contaminated with deadly radioactive substances, which may result from eating food infecting the consumer with diseases, The most famous of which is food poisoning. Food is an easy way to transfer pathogenic microbes, so it is necessary to prevent contamination of food and water with microbes to maintain public health in any human gathering, by following several preventive methods to protect food from contamination, such as not making food exposed to insects and dust, and washing vegetables and fruits well, taking into account Wash hands before and after eating any meal (Al-Hassan, 2016 ; Aouniyah,2021).

### **Food contamination results from the following sources:**

**Natural pollution:** resulting from food decomposition due to bacteria, fungi, long storage period, or natural radiation and other natural factors.

**Bacterial contamination:** It is one of the most famous and most common types and is caused by insects that come into contact with food.

**Unnatural pollution:** It results from irrational human behavior, most notably the chemical contamination of food.

## **7. Corona pandemic definition**

The World Health Organization announced that the Corona Covid 19 epidemic has reached the stage of a pandemic, as it appeared in China in December 2019 and spread to many countries of the world, if not to all countries of the world. The pandemic is defined as the global spread of a new disease that includes many countries, and the pandemic also means that the disease defies control and this explains its international spread and not confined to one country. (Al-Rub, 2020), it is also known as a disease that has economic, political and social repercussions on a global scale.

The spread of any epidemic can be classified into three stages:

The outbreak of the epidemic: It expresses the unusually small increase in the number of infections

- Epidemic: the spread of the virus in a larger geographical area, which may be in one country, or it may affect a group of countries

- Pandemic: the spread of disease to a large number of countries.(T. Singhal ,2020, 2020).

## **8. The negative side of Corona's repercussions on the environment:**

It is worth noting that measures to prevent the spread of the Corona virus have obligated many countries to take the necessary measures to prevent it, especially with regard to providing medical equipment and supplies.

Healthcare waste includes sharp and blunt tools, chemicals, pharmaceuticals

and radioactive materials, which can cause harm to humans and their surroundings if not handled properly (Balkhair A,2009).

## **9. medical waste (Health care waste)**

is of a special nature, as the possibility of infection with infectious diseases and wounds as a result of exposure to it is more than other types of waste, as the Improper handling of healthcare waste may cause health problems for the public and negative effects on the environment. Thus, management of healthcare waste is an important part of maintaining environmental health; And the fact that the most health waste that affected the environment of the countries of the world during this period was the waste of the Corona virus ( Imperial College COVID-19 Response Team ,2020).

### **Medical waste can be classified into**

**9-1-Infectious waste:** Infectious waste is suspected to contain pathogens (bacteria, viruses, parasites, or fungi) in a large enough quantity or concentration to cause disease.

#### **This category includes:**

- Cultures and vectors of infection from laboratories
- Waste from operations and autopsies of patients with infectious diseases (such as body tissues, materials or instruments after they come in contact with blood or other body fluids)
- Waste after coming into contact with patients receiving dialysis (eg dialysis equipment such as tubes, filters, towels, gloves, aprons, coats, and gowns)
- Infected animals from laboratories.

**9-2-Pathological waste:** Infectious material containing dead tissue may mask particularly dangerous infectious and/or infectious agents. This waste includes blood, body fluids, tissues, organs and body parts, human fetuses, and animal carcasses. There is a subcategory of pathological waste, which is surgical waste, and it consists of identifiable human or living and animal parts, healthy or otherwise.

**9-3-Sharps:** Tools sharp enough to cut or puncture the skin, such as knives, scalpels, other blades, pump sets, needles, hypodermic needles, saws, broken glass, nails, etc., which can transmit infection directly into the bloodstream. Sharps are generally treated as extremely hazardous medical waste regardless of whether they are contaminated or not (**Celitron Medical Technologies Kft,2020**).

The safe management of health waste is based on the following points:

- burn
- chemical cleansing
- Wet heat treatment (for steam sterilization)
- Microwave rays
- Disposal of waste in the land



#### **9-4-Installation processing**

Effective management of biomedical and healthcare waste requires appropriate identification, collection, separation, storage, transportation, treatment and disposal, as well as important related aspects including disinfection, personnel protection and training. The Meteorology and Environmental Protection Authority revealed five steps to dispose of medical waste related to the Corona virus, which includes disinfecting it at the beginning and carrying it in special containers, and then refrigerated cars, sterilizing and disposing of it through ovens or burial. The authority has confirmed that medical waste related to the Corona virus is classified within hazardous waste (K.Hamdan et al,2020).

#### **10. Clean technology as a mechanism for environmental protection:**

The quarantine measures applied in most countries of the world contributed to emphasizing the need for the environment for greater protection, based in its origin on correcting human behavior towards it. During the period of disruption of economic and human activity, the environment has known some kind of improvement, and therefore efforts must be continued in adopting new mechanisms and methods for exploiting and preserving nature's resources.

In light of the continuous spread of epidemics, it has become imperative for institutions and individuals to adopt new behaviors to preserve the environment, as it is the ocean that provides the necessary needs for living. In this context, clean technologies are considered one of the most important sustainable solutions for the planet (Clean technology from waste management; IONEL IOANA,2016)

#### **11. What is clean technology?**

Clean technology, or as it is called green technology, is defined as the continuous development of industrial processes, products and services with the aim of consuming natural resources, preventing pollution of air, water and soil at the source, and reducing waste at the source to reduce risks to humans and the environment (GREEN PAPER: On the management of bio-waste in the European Union, SEC,2008. 2936).

Green technology is also defined as industrial production methods that take into account the minimum possible pollution, as it depends on reducing the generation of waste from the source, so it seeks to find solutions to the waste of the industrial process through its treatment and disposal. Clean technology is concerned with achieving high efficiency of the production process, where the rational use of water resources (energy and raw materials) On the amount of need, with the adoption of the recovery of as much waste as possible.

In general, clean technology, we express the technology that encourages and stimulates the production of clean energy by environmentally friendly methods while trying to restore what has been damaged in the environment( G. Burke,2005).



## 12. Clean Technology Strategies:

Systematic technology depends in its applications on the following strategies: (G.Burke,2005).

❖ **Recycling:** It is related to the recycling of waste of glass, paper, plastic and metal origin to benefit from, and these materials are the most recyclable, where they are employed in line with the environment, and reduce the depletion of the earth's resources.

❖ **Environmental reform:** by eliminating all causes of pollution to the elements of the environment, such as water, air, and soil, and the processes vary between chemical, biological, and others. On those who deplete and exhaust the environment.

❖ **Renewable energy sources:** Countries and companies resort to converting and exploiting renewable resources to generate energy for societies, because the issue of being completely dependent on fossil fuels is forever impossible. Therefore, the most important renewable energy sources are water, sun, wind, and geothermal wells. **Alternative fuels:** Scientists are doing their best to produce alternative fuels as much as possible besides renewable energy sources in nature, and the most important of what is being exploited are hydrocarbons and fuel cells, and the secret behind the interest in clean coal is to reduce carbon dioxide emissions

❖ **Carbon and its negative effects on the environment.** It is considered a relentless pursuit to eliminate the presence of carbon dioxide emissions and reduce them as much as possible.

❖ **Sustainable development of the environment in construction:** Designers and architects resort to adopting some methods and steps to make the building completely green, and this depends on locating the building in the healthiest ways and methods to exploit natural conditions, including solar energy, and there is an important role for recycled materials, and the use of Environmentally friendly tools and delay from urban sprawl.

❖ **Green nanotechnology:** This technology is completely based on a group of materials that seek to transform manufacturing industries to become environmentally friendly, and in turn relies on the principles of chemistry and engineering in full to exploit them for the benefit of the environment and protect it from deterioration.

## 13. Types of clean technology

**There are many types of clean technologies:**

**13-1- Green Energy:** This is the most important trend with regard to green technology, which is witnessing a relentless pursuit to rely on the production of alternative fuels and the provision of other safe and renewable sources of energy.

**13-2-Green buildings:** Green buildings are among the things that require a great deal of study in order to be able to enter into force sufficiently, as scientists aim to rely on green materials when producing building materials and everything related to the establishment of buildings.

**13-3-Green chemistry:** Green chemistry is one of the most important areas in

which the field of green technology is concerned.

**13-4-Green nanotechnology:** There is no doubt that the field of nanotechnology has become imposing itself strongly on the scientific arena, given that it has an effective impact in all areas and aspects of life, whether agriculture, industry, health or others, and it depends mainly on the use of micro-particles in The size of the nano, which represents  $10^{-9}$  of a metre, and scientists are currently scrambling to apply the standards of green chemistry and green engineering in the nano field in order to also obtain safe and environmentally friendly nanoparticles that provide only benefits and do not result in any harm (A. B. Koltuniewicz, 2008).

**Clean Technology Objectives:** Countries and companies, through

their reliance on clean technology applications, seek to achieve the following:

- Developing production processes in a way that does not harm or deplete the earth's natural resources
- Finding alternative sources to generate the energy needed in the production processes as well as the daily life of the human being
- Reducing the use of fossil fuels that are harmful to the environment and its components
- Reducing pollution at the source.
- Conservation of raw materials and energy.
- Adopting environmentally friendly mechanisms and technology.
- Preserving natural resources for future generations and limiting their depletion.
- Achieving a shift towards sustainable development and a green economy.

#### **14. The relationship of clean technology to reducing the spread of epidemics:**

The recent spread of the Covid-19 virus contributed to emphasizing the need to increase support for the application of technology in all fields, especially in the field of health and the environment. industrial and machine learning,

**A- Mechanisms and ways to benefit from modern technology in the time of Corona: Modern technologies can be used in:** (WHO, 2022) :

**Prediction:** That is, scientists have confirmed that the growth of the world's population and the continued interaction with animals, has enhanced the spread of viruses of animal origin, and led to their easy transmission to humans. This is what was revealed with the Ebola virus in 2018 in West Africa. According to the US Centers for Disease Control, three out of every four new diseases in humans come from animals. Where this technology combines various data on previously known viruses, animal numbers, demographics, and cultural and social practices, to predict outbreaks.

**Detection:** When unknown viruses are transmitted to humans, time becomes a precious resource in order to take action and treat the infected effectively. In this context, a number of specialists have developed approaches using machine learning to extract data from social media to obtain indicators of disease symptoms, and through the use of Artificial intelligence results are achieved faster in disease detection.

**Response:** After a disease is detected and identified, timely decision-making is critical to limiting its spread and outbreak. AI can integrate

travel, population and disease data to predict where and how quickly a disease or virus will spread. It can also be used to improve and apply treatments and accelerate the development of New treatments. In the case of Corona, X-rays of people infected with the virus can be used in artificial intelligence as data so that doctors can make faster diagnoses. As for finding vaccines for such a virus, it is difficult, but artificial intelligence can be benefited from by examining data from similar viral diseases, and this is what has been done currently using malaria treatment for corona patients.

**Containment and recovery:** Once the spread of the disease is contained and ended, the governments and health and medical agencies involved make decisions about how to prevent or limit its spread in the future. In this step, machine learning can be used by testing and verifying health policies and initiatives. Artificial intelligence allows stakeholders to analyze data and make guesses based on the “what if” hypothesis that can help make data-driven decisions and increase the likelihood of their effectiveness.

**B-Techniques and applications of technology in the time of Corona:** Countries and bodies in charge of health implement a set of techniques and applications to monitor and control the development of the spread of the virus, which are :(WHO,2022).

- **BlueDot Prediction Algorithm:** Scientists have resorted to this AI-based technology to predict the spread of the virus, as the algorithm follows news reports, animal and plant disease networks, and official announcements to issue a prior warning to avoid areas of danger for the spread of the virus. Where the data of specialized companies is relied upon to follow the developments of unusual events, and indeed the algorithm correctly predicted the Corona virus, and that it would move from Wuhan to Bangkok, Seoul, Taipei and Tokyo in the days following its first appearance.

- **Social media:** In a new step taken by social media platforms and a number of the most used sites in the world, technology companies released applications to address the dissemination of misinformation during the Corona virus crisis, as Facebook, Google, Microsoft, Twitter, Wei, YouTube and LinkedIn

published A statement on March 17, 2020, says that these companies “are all working closely to enhance efforts to combat misinformation about the Corona virus, and their mission:

- Helping people to stay in touch during periods of self-quarantine.
- Fighting misinformation that may appear on its platforms.
- Jointly combating fraud and misinformation about the virus.
- Share important updates in coordination with government healthcare agencies around the world.

- **Telemedicine:** The epidemic will change the model of the place of providing health care, as the idea of telemedicine has been on the sidelines for years, as a low-cost and high-convenience system, but the necessity may increase the popularity of remote doctor visits in conjunction with the Corona pandemic and beyond, as staying At home and video chatting keeps you out of infection and away from waiting rooms and patients who need intensive care.

• **Digital monitoring:** It expresses the follow-up to a person infected with the Corona virus who drove and came into contact with his surroundings and his family, where everyone who had contact with the infected person is identified by relying on digital technology by following his path in the likely period of his infection.

• **Patient Path Application:** a technology launched by Christoph Fraser, an expert in infectious disease prevention methods at the University of Oxford, in March, where he developed an information program to find all people who were in contact with a patient. The program uses geolocation data and a huge amount of data What is included (applications) of the various communication and information tools, so that it is possible to identify each person who was in contact with the patient for a period exceeding a quarter of an hour and at a distance of less than two meters during the five days preceding the onset of symptoms of the disease (WHO,2022).

### 15. The importance of clean technology in the time of Corona to protect the environment from pollution

Despite the severe effects of the Corona virus on human life and the global economy, it contributed to emphasizing the necessity of adopting clean technology to protect the environment, especially after the positive results of quarantine on the environment (a decline in pollution rates in many countries.)

In the midst of the devastation, the pandemic has brought gains to sustainable industries, clean energy, and a world that allows for a cleaner living space for humans, animals and even plants.



Figure 1: The technology network for the service of the environment pollution (ESCWA, 2019).

This combination of modern technology contributes to achieving prospects for economic development and at the same time preserving the environment, which is known as the dimensions of sustainable development. It is divided in this way into four main groups:

Digital technology and innovations that allowed the production of new innovations such as artificial intelligence and robotics, the Internet and big data.

-Biological technology that allowed the development of agricultural and medical fields.

Advanced materials technology that has produced a new group of materials with amazing applications such as nano and biological materials.

-Energy and environmental technology, which seeks to achieve the goals of sustainable development.

Based on this, the most important technologies that help preserve the environment are Renewable energy (solar, wind, water, etc.)

-(Green buildings) the use of environmentally friendly materials in construction

-(Sustainable transport) means of transport relying on renewable energy sources to preserve the environment and reduce pollution

-(Water management): rainwater collection and reuse, sea water desalination, water power generation, and reuse of used water

-(Waste Management) Recycling production waste such as paper, plastic, glass and other recycling operations

(Sustainable Agriculture) Adapting technology in agriculture to meet the challenges of climate change.(UNEP ,2012).

## Conclusions

The impact of the Corona pandemic was very harsh on the environment, and we had to write an article about correct and modern options for proper disposal of these wastes, the most important of which was adopting environmentally friendly production mechanisms and moving towards renewable energies and modern technology to preserve the environment and its natural resources. The study showed alternatives to traditional treatment methods with low-cost and highly effective methods of treating polluted water.

## References

1. G.W. Jones, M.P. Monopoli, L. Campagnolo, A. Pietroiusti, L. Tran, B. F. adeel No small matter: a perspective on nanotechnology-enabled solutions to fight COVID-19 *Nanomedicine*, 15 (24) (2020), pp. 2411-2427
2. Y. Fan, K. Zhao, Z.-L. Shi, P. Zhou Bat coronaviruses in China *Viruses*, 11 (3) (2019), p. 210
3. (OSHA) Occupational Safety and Health Administration(2020).
4. International Environmental Technology Centre(IETC) (2020).
5. Zuhara S, Isaifan R. The impact of criteria air pollutants on soil and water: a review. (2018) 278–84. doi: 10.30799/jespr.133.18040205.
6. National Institutes of Health U.S. Department of Health and Human Services PO Box 12233 • Research Triangle Park, NC 27709 Phone: 919- 541-3345 • <https://niehs.nih.gov> May 2021.
7. Safety Assessment of Nanomaterials to Eyes: An Important but Neglected Issue Shuang Zhu, Linji Gong, Yijian Li, Haiwei Xu,\* Zhanjun Gu,\* and Yuliang Zhao *Adv. Sci.* 2019, 6, 1802289.
8. Shahata, hasan ahmad,2002. Environmental pollution - wrong behaviors and how to confront them, Cairo: Arab Book House, twelfth edition.
9. R.F.AL-Hasan,2012. Food Contamination,University of Babylon.
10. Aouniyah, bn zakora.2021.The Environment and the importance of Clean Technology in the Corona pandemic, Almuaskar university Algeria , *Journal of Advanced Economic Research* Volume 06 PISSN : 2572-0198 EISSN : 2676-1572.
11. T. Singhal ,2020.A review of coronavirus disease-2019 (COVID-19) *Indian J Pediatrics*, 1–6 (2020).
12. Balkhair A,2009. The struggle against pandemic influenza A (H1N1). *Sultan Qaboos Univ Med J* 2009 Dec;9(3):257-260.
13. Imperial College COVID-19 Response Team,2020. Impact of non- pharmaceutical interventions (NPIs) to reduce COVID-19 mortality andhealthcare demand. [cited 2020 April 10]. Available from: <https://www.imperial.ac.uk/media/imperial-college/medicine/sph/ide/gida-fellowships/Imperial-College-COVID19-NPImodelling-16-03-2020>.
14. Celitron Medical Technologies Kft,2020. Consulté le , sur. Infectious waste treatment.<https://celitron.com/sa/types-of-Biomedical-waste/definition>.
15. K. Hamdan; Alghamdi; Majid□Malek,2020. Saudi science teachers’ perceptions of the cultural factors in uencing elementary students’ sciencelearningAmani an3,corrected publication 2020
16. IONEL IOANA,2016.University “POLITEHNICA” of Timisoara .Bv. M. Viteazu, 1, 300222, Timisoara ,ROMANIA ,Ionel\_Monica@mec.upt.ro, [www.mec.upt.ro](http://www.mec.upt.ro).
17. GREEN PAPER, 2008. On the management of bio-waste in the European Union, SEC, 2936.
18. G. Burke, B. R. Singh, L. Theodore, Handbook of environmental management and technology, Wiley Interscience, A John Wiley & Sons, 2005.
19. A. B. Koltuniewicz and E. Drioli,2008. Membranes in Clean Technologies. Theory and Practice. WILEY-VCH Verlag GmbH & Co. KGaA, Weinheim ISBN: 978-3-527-32007-3
20. WHO,2022.facilities care health from waste sharp and infectious of treatment the for technologies of Overview (9-004361-4-92-978 ISBN)
21. UNEP (2012) for of Compendium of Technologies for TreatmentDestruction of health Waste care. <https://www.unenvironment.org/resources/report/compendium-technologies-treatmentdestruction-health-care-waste> accessed December (2016).



# **TWITTER DEMOGRAPHICS FOR IRAQI GOVERNORATES**

**AZZAH HAZEM ZAKI  
NOOR AHMED QARABASH**



## TWITTER DEMOGRAPHICS FOR IRAQI GOVERNORATES

Azzah Hazem ZAKI<sup>1</sup>  
Noor Ahmed QARABASH<sup>2</sup>

### Abstract:


Social media has in the last few years provided researchers with an invaluable source of information regarding human interactions. In a country like Iraq where social media platforms are rising in popularity as a tool for social change, understanding social media trends is critical. In this paper, we collected Twitter data examined how Iraqis use the Twitter platform across the ten largest cities in the country. Twitter is an emerging platform in the country that is growing rapidly. We attempted to establish a baseline for the demographic of Iraqi twitter users to serve as a guideline for future researchers aiming to use Twitter data for analysis.


By statistically analyzing languages used, time of activity, devices and applications used, and user trends, we were able to identify several patterns and connect them to socioeconomic observations about the demographics and life circumstances of Iraqis in the ten cities chosen.

**Key words:** Social Media, Twitter, Demographic Analysis, Statistical Analysis.

---

 <http://dx.doi.org/10.47832/MinarCongress5-29>

<sup>1</sup>  University of Information Technology and Communications, Iraq, [azza.hazem@uoitc.edu.iq](mailto:azza.hazem@uoitc.edu.iq), <https://orcid.org/0000-0001-6585-4531>

<sup>2</sup>  University of Information Technology and Communications, Iraq, [noor.ahmed@uoitc.edu.iq](mailto:noor.ahmed@uoitc.edu.iq), <https://orcid.org/0000-0003-2843-3708>

## Introduction:

Social media has become a research interest in the past few years for researchers hoping to observe group behaviors and patterns that reflect modern society. There have been countless avenues for this research in various fields. Studies have examined the reflection of social media activity on stock markets [1], the response strategies of global to disaster relief [2], and connecting between political affinity and twitter followers patterns [3]. When it comes to the middle east, most significant research has been conducted regarding terrorist (or Jihadist) groups activity on social media, the research in this area focused on methods of identifying user accounts that belong to these groups or support them [4] [5].

However, in recent years, more and more younger people in the middle east started engaging with social media to find a larger platform for exchanging ideas, most famously in the series of riots in several countries known as the Arab Spring, which caused noticeable growth in the use of social media in those countries[6]. Iraq, despite the ongoing political turmoil, and the prominence of technologically savvy generations, has been somewhat neglected in research, but there is now renewed interest for local and international researchers as the country went through its own social media fueled riots in late 2019 .

There have been some attempts to spotlight social media activity in the Middle East in general, the Arab social media report, a series that started in 2011, has documented the growth of social media in several Arab countries including Iraq using a combination of collecting user profiles via twitter API or surveys. In their second volume [7] they reported that Iraq had around 21,625 active twitter users in march 2011, posting around 342,000 tweets during that month. By March 2014 the number of active users reported grew to 184,000 posting 9,300,000 tweets[8]. In the last published report [9] Iraq was said to have seen a 97% increase in users, adding up to around 363,000 users by the end of March 2016, posting around 21,799,048 tweets per month. Table (1) summarizes the findings across the years.

Table (1) Twitter user growth in Iraq according to the Arab Social media report [7-9].

Date	Approximate Active users	Average Tweets per month
March 2011	21,625	342,000
March 2014	184,000	9,300,000
March 2016	363,000	21,799,048

Additionally, in a survey conducted in 2015, 22% of Iraqi participant reported having a twitter account [10], however, this does not reflect the level of activity of these individuals or if they use their accounts at all.

There have been extensive research efforts in the field of social media analysis and, the larger focus is usually on sentiment analysis, i.e using social media to measure the public's sentiment on an issue or people. Some studies have even focused on Iraq and attempted to outline Iraqi sentiment on several issues. [11] Analyzed Iraqi

sentiment on a famous athlete, that paper focused on the different machine learning algorithms and their accuracy rather than the characteristics of the user base.

This is a common issue that is noticeable in social media studies, only few papers have focused on the makeup of twitter users or attempted to analyse societal implications based on it. [12] researched the bias that could come with social media research, by analyzing user accounts around the area of England to determine age and gender, it was found that twitter users tend to be young and males outnumber females in twitter activity, the paper goes on to suggest that this bias can be overcome by calibration that factors in the differences between the general population and the sample. [13] also criticized research being done in this field for using broad sampling methods and not properly filtering the results which in turn mean they may not yield the most accurate results.

To reduce bias, [14] proposed linking twitter data with survey results, however that study notes such linking is hard to achieve as survey takers would have to agree to give their Twitter handles in surveys, but such a solution would ethically improve many study findings as it ensures that publicly available twitter data isn't used without a user's consent.

The previous research highlights the importance of establishing an understanding of an area being surveyed and understanding the underlying society represented before performing any deeper analysis. As political activism grows in the country, the lack of any additional information about Iraqi twitter users will complicate conducting any research and may invalidate drawing any conclusions based on Twitter data. This paper aims to identify demographic data of Twitter users in Iraq to provide groundwork for future studies; this paper is mainly concerned with how twitter activity differs across different Iraqi cities and the socioeconomic implications of these differences.

## **Methodology**

This research uses tweets collected from 10 of the most populated Iraqi cities. All tweets were collected using Twitter search API with the coordinates for these cities to acquire the tweeting traffic of users in 10 km radius of the center of each city [15]. Some of the smaller cities showed less activity and resulted in a lower number of tweets. Figure (1) shows the 10 cities used in this study and Table (2) shows a breakdown of the estimated population and the number of tweets collected of each city.



**Fig (1): The 10 Iraqi cities used in this study.**

Table (2) breakdown of the 10 cities, their population and twitter data collected.

City	Estimates population [16]	No. of tweets
Baghdad	8,340,711	30069
Basra	2985,073	3174
Mosul	3,828,197	256
Erbil	1,903,608	4285
Sulaymaniyah	2,219,194	417
Kirkuk	1,639,953	635
Najaf	1,510,338	1374
Karbala	1,250,806	1058
Misan	1,141,966	61
Al Diwaniyah	1,325,031	63
Total		41,392

For each city, the search query returned a number of tweets, the following information were recorded:

- No : A number assigned by programmer consisting of City name+ number
- created\_at : Date and time the tweet was posted formatted as MM/DD/YYYY hh:mm
- id : Tweet Id assigned by twitter
- is quote? : is the tweet a quote (or reply ) to another tweet (True/ false)
- retweets :number of retweets the tweet received
- likes: number of likes the tweet received

- language: languages of the tweet (could be und if unidentified)
- user name: The name of the user
- source: the device or application used to send the tweet.
- Geo-enabled : has the user enabled geo location (True/ false)
- Location : the location entered by the user in their profile
- User created at: the date the user created the profile formatted as MM/DD/YYYY hh:mm
- Followers: number of followers for the user
- Friends: number of friends for the user
- Favorites: number of tweets favored by the user
- Statuses: number of statuses posted by the user

Table (3) shows a statistical breakdown of the data collected for each city, the number of unique users, tweets and percentage of quote tweets (or re-tweets)

Table (3): Unique users, tweets and quote percentage in the collected dataset.

City	Unique users	No. of tweets	Percentage of Quote tweets
Baghdad	9,849	30,069	7.70%
Basra	974	3,174	3.43%
Mosul	95	256	7.03%
Erbil	1,606	4,285	3.78%
Sulaymaniyah	156	417	4.55%
Kirkuk	209	635	5.98%
Najaf	415	1,374	1.45%
Karbala	515	1,058	2.55%
Misan	17	61	13.11%
Al Diwanayah	21	63	17.19%
Total	13,857	41,392	5.47%

The data was analyzed using SPSS to find frequencies, averages, and correlation as well as to draw charts to demonstrate results when appropriate.

## Results and Analysis

The data collected was analyzed based on different variables to identify twitter demographic statistics in different cities.

### A. Languages used

The data was analyzed according to the languages used in every tweet; Table (4) shows a breakdown of the results across the 10 cities. The most commonly used languages are highlighted for each city. The first thing to stand out is the majority of tweets were in Arabic, which is expected since it is the formal language in Iraq, however, it's important to note that this pattern hold even in one none Arabic majority city in the Kurdistan region (Erbil). And contrary to what would be expected of Kurdish majority cities, the Kurdish language did not rate higher in any of them. Alternatively

we see that “other” languages prevailed in Sulaymaniyah and Kirkuk, this likely due to the mix of Arabic dialects, Kurdish and of Turkish used in Kirkuk and Sulaymaniyah being a hub for international activity. The city of Misan stands out as the only city where English is the most common language, which suggests that twitter usage in the city is driven by educated users and possibly activists trying to deliver a message to the international community, However considering Misan has the lowest number of tweets it’s hard to draw any conclusions based on the sample collected.

Furthermore, the category of “und” which is short for undefined, usually denotes the user posted only a picture or special characters such as emojis, generally considered a sign of younger users who prefer using images and emojis to express feelings.

Table (4): Percentages of languages used in every city.

City	Language				
	Arabic	English	Kurdish	others	Und
Baghdad	<b>75.20%</b>	9.90%	0.02%	8.04%	6.83%
Basra	<b>88.62%</b>	2.11%	0%	1.67%	7.63%
Mosul	<b>59.77%</b>	25.78%	0%	1.95%	12.89%
Erbil	<b>37.20%</b>	25.88%	10.71%	18.93%	7.28%
Sulaymaniyah	13.43%	16.07%	13.43%	<b>41.97%</b>	15.11%
Kirkuk	23.31%	5.67%	3.15%	<b>56.54%</b>	11.34%
Najaf	<b>69.36%</b>	5.68%	0%	0.87%	24.09%
Karbala	<b>90.08%</b>	0.28%	0%	2.17%	7.47%
Misan	21.31%	<b>49.18%</b>	0%	24.59%	4.92%
Al Diwaniyah	<b>93.65%</b>	0 %	0%	0%	6.35%

### **B. Twitter's Activity through the day**

We analyzed the time tweets were posted to map out activity patterns. For the majority of city activity peaked after 5 pm, were most citizen would be home after work in the public and private sectors. The activity goes down between 8-7 pm, we speculate this coincides with the time most Iraqis eat dinner and hang out with family. Twitter activity trended higher between dinner time and midnight, in some cities like Baghdad and Kirkuk, activity peaked during the evening time. In some of the smaller cities twitter activity almost died down after midnight and picked up gradually in the morning. These patterns suggest most Iraqis use Twitter in leisure times and not during the night or work hours. Figure (2) demonstrates the different usage patterns in the 10 cities.

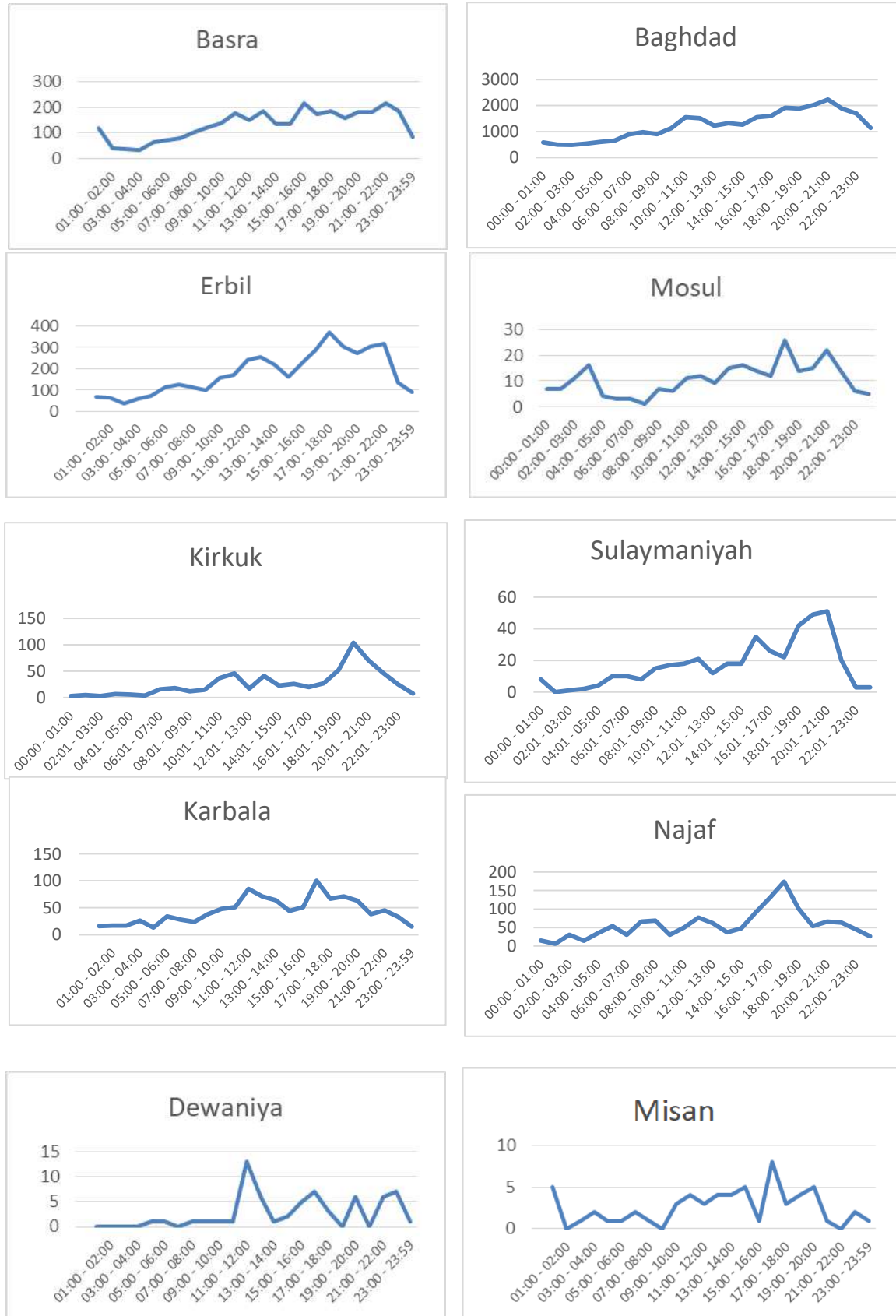


Fig (2): Twitter activity

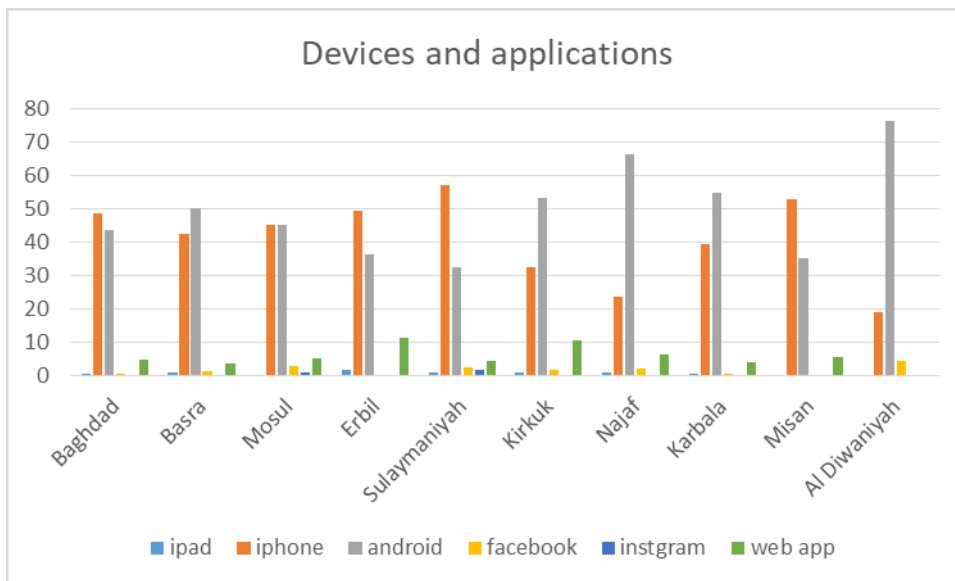


### C. Devices and applications used

Twitter API identifies the source of the tweet based on the device it originated from, as well as special cases in which a user would send tweets via sharing Facebook or Instagram posts. For our analysis these different sources were grouped and converted into percentage to account for the disparity of data collected from different cities. Figure (3) demonstrates the sources breakdown. From the percentages acquired we can see in general Android and iPhone devices were relatively equal in their usage. However in certain cities (Diwaniyah, Karbala, Najaf, Kirkuk) Android device outnumbered Apple devices, considering apple devices tend to be more expensive than Android devices, this breakdown likely reflects the economic status of these cities to be generally lower than others. Sulaymaniyah, Erbil and Misan on the other hand showed higher percentages of Apple devices being used, which suggest a higher income trend among twitter users of these cities.

It's worth noting that a small but noticeable minority of twitter users have used web apps to post tweets, which suggest that they used a computer device rather than a phone, however when compared to the usage of smart phones it's clear that most Iraqis depend on their phones for using twitter, and this suggest twitter users tend to be young as the youth is more comfortable around smart phones.

We can also note that very few users used other applications like Facebook and Instagram, likely because using the twitter app directly is more convenient.



**Fig (3): Devices and applications used to post tweets.**

### D. User trends.

To get a more detailed look at how users profile corresponds to their activity, we analyzed the average account age and the correlation between the years a user has been on the platform and the number of post, likes, followers and friends. When it came to average account age it ranged between 3.16 and 2.05 years, with Mosul and Baghdad being the highest while Najaf and Kirkuk had the lowest

average. This suggests that the platform is still new in Iraq in general but particularly so in smaller cities.

Furthermore, it appears there is little to no correlation between the account age and its popularity, exemplified in number of followers, friends, likes and posts. This could be due to a number of reasons, likely most Iraqis use twitter for business reasons so they don't receive a lot of interactions. Another reason could be the relative inactivity of some accounts that affected the overall results. Table (5) shows the different correlation breakdown.

Table (5): Correlation between variables and the average account age.

Cities	Average account age (in years)	Correlation			
		Followers	Friends	Favorites	Statuses
Baghdad	3.13	0.056671	0.051517	0.170699	0.229522
Basra	3.00	0.147707	0.093917	0.136606	0.166087
Mosul	3.16	0.264013	0.129111	0.185429	0.349959
Erbil	3.03	0.107735	0.059271	0.176496	0.199512
Sulaymaniyah	2.71	0.135889	0.173229	0.065102	0.184208
Kirkuk	2.05	0.129265	0.046693	0.02173	0.130252
Najaf	2.07	0.197183	0.123188	0.058466	0.20666
Karbala	2.84	0.087212	0.143269	0.115987	0.245619
Misan	2.72	0.619994	0.367517	0.046936	0.592052
Al Diwaniyah	3.05	0.250051	0.206849	-0.15277	0.266427

## Conclusions and Future Work

In this paper we examined certain aspects of tweets collected from different Iraqi cities to analyse them for demographic information. Our first observation is the low levels of twitter activity in Iraq and especially southern cities, this affirms earlier statistics about how Twitter is still relatively new in Iraq but it also highlights how any study involving twitter data from Iraq will have to account for the bias in data toward the larger cities, particularly Baghdad that represented over 70% of all Twitter data collected.

When it came to languages used, Arabic and English were the dominant languages even in majority Kurdish speaking cities. This is coupled with the patterns of activity throughout the day that peaked at late afternoon and early evening. From the two earlier observations we can conclude that Iraqis interact more with people outside Iraq, this coincides with the speculation that Iraqis started using twitter for activism and having a worldwide platform rather than chatting with friends. This means that studies looking for data on personal connection with family and friends might not be viable using twitter, this is corroborated by our final finding which showed that there is no correlation between the years a user spent on Twitter and their followers, "friends" and likes suggesting that the user base is somewhat stagnant because it's less personal and more focused on business and spreading news.

The assumption that twitters is more common among younger Iraqis can be confirmed through the majority of users reliance on smart phones for posting on twitter and the high usage of English as well as images in their posts. The difference between cities where Apple devices are more common than Android devices also shows economic disparity, however this wealth inequality only reflects

twitter users in these cities who are likely already somewhat affluent but can represent a larger trend for the population.

This study was limited in scope to focus only one few key parameters, however future studies should consider defining one more demographic which is gender and age. Assigning accurate gender and age values to twitter accounts is a complicated subject that has been explored by some studies but with focus on English profile names and descriptions as well as western profile picture conventions, such studies cannot be easily applied to Iraqi users, thus they require their own detailed research and could not be considered in this paper.

## References

1. E. Teti, M. Dallochio, and A. Aniasi, "The relationship between twitter and stock prices. Evidence from the US technology industry," *Technological Forecasting and Social Change*, vol. 149, p. 119747, 2019.
2. T. A. Gurman and N. Ellenberger, "Reaching the global community during disasters: findings from a content analysis of the organizational use of Twitter after the 2010 Haiti earthquake," *Journal of health communication*, vol. 20, pp. 687-696, 2015.
3. G. Stamatelatos, S. Gyftopoulos, G. Drosatos ,and P. S. Efraimidis, "Revealing the political affinity of online entities through their Twitter followers," *Information Processing & Management*, vol. 57, p. 102172, 2020.
4. J. Klausen, "Tweeting the Jihad: Social media networks of Western foreign fighters in Syria and Iraq," *Studies in Conflict & Terrorism*, vol. 38, pp. 1-22, 2015.
5. W. Magdy, K. Darwish, and I. Weber, "# FailedRevolutions: Using Twitter to study the antecedents of ISIS support," *arXiv preprint arXiv:1503.02401*, 2015.
6. F. Salem and R. Mourtada, "Social Media in the Arab World: Influencing Societal and Cultural Change?," United Arab Emirates 2012.
7. F. Salem and R. Mourtada, "Civil Movements: The Impact of Facebook and Twitter," Dubai School of Government United Arab Emirates 20.11
8. F. Salem, R. Mourtada, and S. Al-Shaer, "Citizen Engagement and Public Services in the Arab World: The Potential of Social Media," Dubai School of Government, United Arab Emirates2014.
9. F. Salem, "Social Media and the Internet of Things Towards Data-Driven Policymaking in the Arab World: Potential, Limits and Concerns," United Arab Emirates2017.
10. M. Ayish and N. Mellor, *Reporting in the MENA region: Cyber engagement and pan-Arab social media*: Rowman & Littlefield, 2015.
11. N. D. Zaki, N.Y. Hashim, Y. M. Mohialden, M. A. Mohammed, T. Sutikno, and A. H. Ali, "A real-time big data sentiment analysis for iraqi tweets using spark streaming," *Bulletin of Electrical Engineering and Informatics*, vol. 9, pp. 1411-1419, 2020.
12. D. Yildiz, J. Munson, A. Vitali, R. Tinati, and J. A. Holland, "Using Twitter data for demographic research," *Demographic Research*, vol. 37, pp. 1477-1514, 2017.
13. D. Parekh, A. Misansingam, L. Dawson, and D. Ruths, "Studying jihadists on social media: A critique of data collection methodologies," *Perspectives on Terrorism*, vol. 12, pp. 5-23, 2018.
14. T. Al Baghal, L. Sloan, C. Jessop, M. L. Williams, and P. Burnap, "Linking Twitter and survey data: The impact of survey mode and demographics on consent rates across three UK studies," *Social Science Computer Review*, vol. 38, pp. 517-532, 2020.
15. N. A. Qarabash and H. A. Qarabash, "Twitter Location-Based Data: Evaluating The Methods Of Data Collection Provided By Twitter Api," 2018.
16. CSO. (2019, 3/10/2021). *Demographic indicators* Available: <http://www.cosit.gov.iq/ar/2013-01-31-08-43-38>



**CURRENT CONTROLLED CHAOTIC SPIKING OF SEMICONDUCTOR LASER DIODE  
WITH OPTICAL FEEDBACK**

**YOUNIS TH. YOUNIS  
AHMED K. AHMED  
KAIS A. AL-NAIMEE**

## CURRENT CONTROLLED CHAOTIC SPIKING OF SEMICONDUCTOR LASER DIODE WITH OPTICAL FEEDBACK

**Younis Th. YOUNIS<sup>1</sup>**

**Ahmed K. AHMED<sup>2</sup>**

**Kais A. AL-NAIMEE<sup>3</sup>**

### **Abstract:**

The effects of bias currents on the carrier and photon dynamics of semiconductor laser diode SLD with optical feedback from fiber loop mirror have been verified by numerical solutions of Lang-Kobayashi differential equations. The numerical results showed existence a wide range of oscillation regimes (period one, period doubling, quasi-periodic and chaotic oscillations, then transition again to quasi-periodic oscillations) that is by increasing bias currents of the semiconductor laser diode. This were proved by the bifurcation diagram of maxima amplitudes of SLD output as a function of bias current (the control parameter) which showed diversity oscillation regimes in route to chaos.

**Key words:** Semiconductor Laser Diode, Chaos Control, Chaos Synchronization, Optical Feedback.



<http://dx.doi.org/10.47832/MinarCongress5-30>



<sup>1</sup> University of Mosul, Iraq, [younisthannon@uomosul.edu.iq](mailto:younisthannon@uomosul.edu.iq), <https://orcid.org/0000-0001-7037-4698>



<sup>2</sup> Al Nahrain University, Iraq, [ahmad.kamal@sc.nahrainuiv.edu.iq](mailto:ahmad.kamal@sc.nahrainuiv.edu.iq), <https://orcid.org/0000-0002-1524-4855>



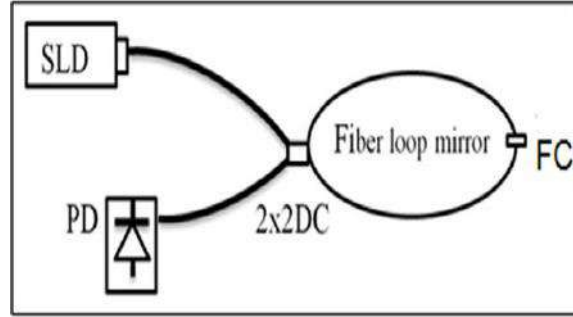
<sup>3</sup> University of Baghdad, Iraq, [kais.al-naimee@ino.it](mailto:kais.al-naimee@ino.it), <https://orcid.org/0000-0002-7682-4829>

### **Introduction:**

Chaos control is a broad topic in nonlinear dynamics [1-3], it involves changing the dynamical system behavior by means of control parameter, regardless the direction of the system state transition [4-6]. Specifically, semiconductor laser diodes (SLD) are of class B kind lasers (having two degree of freedoms, carrier and photon life times), hence they required extra degree of freedom to forcing them to unstable states transition [7-10]. Delayed optical feedbacks represent an opulent source of nonlinear dynamics, and a wide variety of dynamical instabilities can be obtained by such scheme of perturbation, such as steady state, multi-periodic oscillations, low frequency fluctuations (LFF) and chaotic oscillations [11-15]. Delayed optical feedback will impose infinity degrees of freedom upon SLD, and the dynamical state of the laser output will depends on the parameters of optical feedback (feedback strength  $\kappa$ , feedback delay  $\tau_f$  and feedback phase  $\phi_f$ ) [16-18]. Lang-Kobayashi model is an important tool for describing dynamics of SLD with optical feedback [19,28,29]. We have reported the experimental investigation of bias current rule in dynamics of SLD with optical feedback from fiber loop mirror [20]. In this research we will investigate by numerical simulation, the influences of bias current of SLD coupled with fiber loop mirror external cavity on the photon dynamics of the SLD output based on Lang-Kobayashi rate equations..

### **THEORY OF SLD WITH OPTICAL FEEDBACK**

Semiconductor laser diode (SLD) with external optical feedback EOF involves returning a portion of optical output back into SLD, as can be seen in Fig. (1). Optical feedback may be either beneficial or detrimental for optical fiber systems, optical readout with laser systems. SLD with external cavity OFB exhibit a large variety of dynamical instabilities, e.g. self-modulation at relaxation oscillation, low frequency fluctuations as well as nonlinearities in the light output versus injection current(L/I characteristics), these are depending on key parameters, comprising feedback strength, pump current, feedback delay, feedback type and laser non-linearity. The static and dynamical properties of single mode SLD with external cavity OFB described by Lang-Kobayashi model, which is a rate equation model representing the time evolution of the complex optical field and the carriers. They included the influence of the OFB by considering the interference of the laser field with its own coherent delayed field that had propagated once through the external cavity [9,19,21].



**Fig. (1) schematic diagram of SLD with optical feedback layout from fiber loop mirror, SLD: semiconductor laser diode, 2x2DC: four terminal directional coupler, FC: fiber connector, PD: photodetector**

The model can be written as equations for the excess number of carriers  $N(t)$ , and for slowly varying complex electrical field amplitude  $E(t)$  and with optical feedback field term  $E(t-\tau)$  given by set of delayed differential equations (DDE) [19,21,22,23]

$$\frac{dE(t)}{dt} = \frac{1+i\alpha}{2} \left[ G_N - \frac{1}{\tau_p} \right] E(t) + \kappa E(t - \tau_x) \exp(i\omega_0 \tau_x) \quad (1)$$

$$\frac{dN(t)}{dt} = \frac{1}{e} - \frac{N(t)}{\tau_c} - G_N |E(t)|^2 \quad (2)$$

$$G_N = \frac{G_0(N(t) - N_0)}{1 + \varepsilon |E(t)|^2} \quad (3)$$

where  $G_N$  is the optical gain,  $|E(t)|^2$  is the number of photons inside the laser cavity,  $\varepsilon$  is the gain saturation coefficient and considered because the laser biased above the threshold current. Feedback strength  $\kappa$  given by equation (4) [24, 25].

$$\kappa = f_{ex} / \tau_i = \frac{c}{2\eta l_D} f_{ex} \quad (4)$$

where  $\tau_i$  is intra-cavity round trip time,  $\eta_x$  is the refractive index of SLD active medium,  $c$  is free space light speed,  $l_D$  is SLD cavity length and  $f_{ex}$  is optical feedback parameter and is given by the equation (5)

$$f_{ex} = \frac{\text{reflected power}}{\text{emitted power}} = s(1 - R_2) \left( \frac{R_3}{R_2} \right)^{1/2} \quad (5)$$

where  $R_1, R_2$  are the front and rear facets reflectivity of laser respectively,  $s$  is mode mismatch coefficient. Prior making numerical solution of the system of differential equations (1, 2, and 3), we have to calculate the parameters of SLD at steady state operation to evaluate  $N(t)$ ,  $I_{th}$  and  $G_0$  from equations (1, 2, and 3), as shown in Table(1). The parameters of fiber loop mirrors cavity are shown in the Table (2), we have used fourth order Rung-Kutta solver to implement the numerical solution for SLD with external cavity differential equations (1, 2, and 3).



**INFLUENCES OF BIAS CURRENTS ON DYNAMICS OF SLD WITH OFB**

We have fixed OFB strength  $\kappa$  to  $6 \times 10^9 \text{s}^{-1}$  versus changing the bias current  $I$  each time with recording time series of electric field then evaluating its spectrum, phase attractor. Setting  $I$  on  $0.0148764 \text{A}$  we get Fig. (2-a) which shows time series trace of E-field that exhibit periodic regular oscillation and its FFT in Fig. (2-b) brings out the single frequency component, and its phase attractor trajectory in Fig. (2-c) which formed by sketching carrier number  $N(t)$  versus electric field  $E(t)$  of optical output of SLD, shows limit cycle loop (thick trace) whilst spiral loop is the initial buildup of the E wave. Increasing  $I$  to  $0.0149205 \text{A}$  we get: period doubling oscillation as can be seen in Fig. (3-a) where time series with two different amplitude heights and Fig. (3-b) shows its FFT exhibiting two frequency components spectrum, and Fig. (3-c) attractor showing two tangled trajectory loops.

Table (1) semiconductor laser parameters

Parameter	Specification	Value
$\alpha$	Line enhancement factor	6.5
$\tau_p$	Photon Life time	2ps
$\tau_c$	carrier lifetime	2ns
$G_0$	differential gain	$1.5 \times 10^4 \text{s}^{-1}$
$N_0$	Transparency carrier number	$1.5 \times 10^8$
R1=R2	Laser facets reflectivity	0.32
$\eta_i$	laser cavity refractive index	3.6
$\epsilon$	Nonlinear gain coefficient	$5 \times 10^{-7}$
$\lambda$	laser mode wavelength	1.55 $\mu\text{m}$
L	Laser cavity length	350 $\mu\text{m}$
$I_{th}$	solitary SLD threshold current	14.7mA

Table (2) parameters of fiber loop mirror external cavity

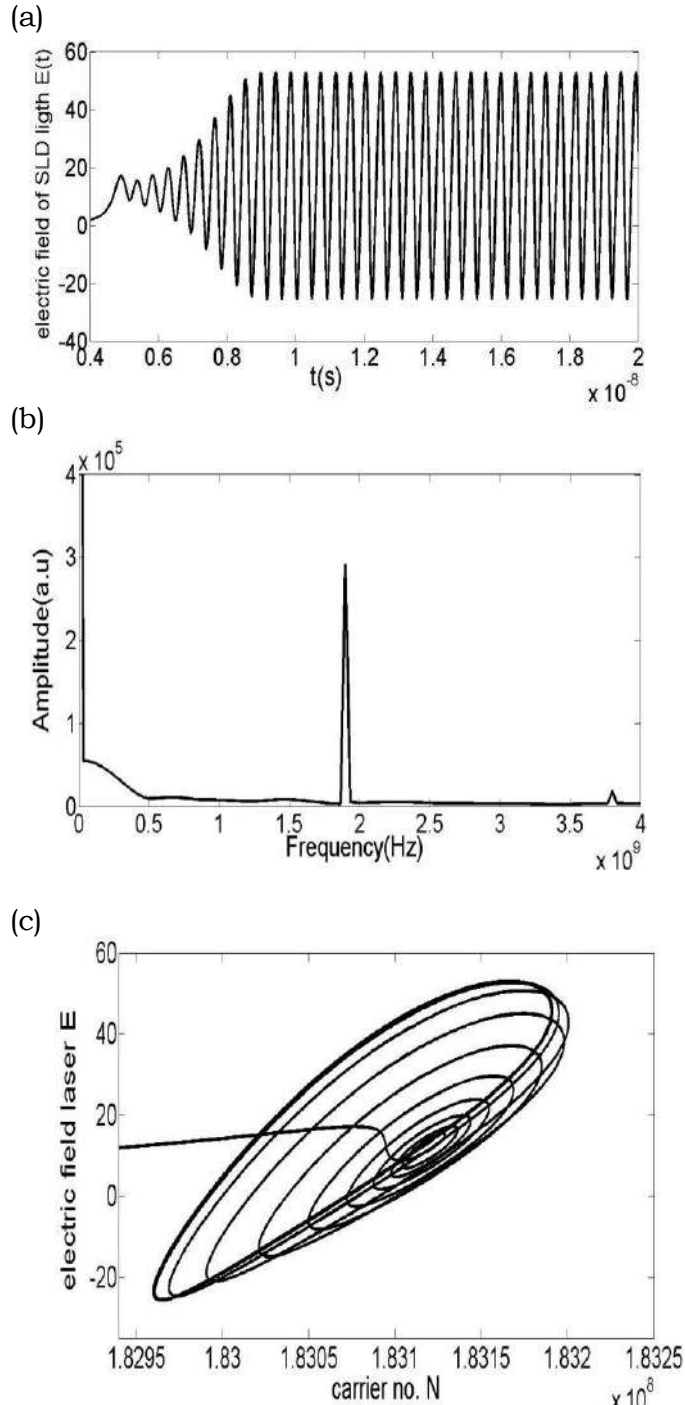
Parameter	Specification	Value
$L_x$	Fiber loop mirror cavity length	6.8m
$\eta_x$	External cavity refractive index	1.53
R3	External cavity reflector	0.031
$\tau_x$	External cavity delay time	70ns
s	Mode mismatch coefficient	0.2
$\kappa$	Optical feedback strength	$6.04 \times 10^9 \text{ s}^{-1}$

More increasing  $I$  to 0.0158466A the system converts to chaotic transition state, as appear in Fig. (4-a) where time series shows chaotic oscillation, Fig. (4-b) shows FFT of signal Fig, (4-a) broadband, and exponentially decaying spectrum, and Fig.(4-c) displays dense and complex overlapped trajectories indicating to coexistence of many attractors, (inter-cavity of laser and external cavity modes and anti-modes) [13, 22]. Additional increasing of  $I$  to 0.016464A pushes the system again toward quasi-periodic oscillation, as seen from time series in Fig.(5-a) and Fig.(5-b) shows its FFT diagram, where few frequency components appear, and Fig.(5-c) shows attractor with multiple tangled trajectory loops. The complete picture of the rule of current parameter  $I_b$  in dynamics of L-K model can be expressed by bifurcation diagram as in Fig. (6) where beginning of diagram, the values of  $I$ (0.0149-0.01505A) the system exhibiting period on oscillation.  $I$  from (0.01506-0.01554A) brings out multi-periodic oscillations. The range of  $I_b$  (0.01559-0.01644A) chaotic oscillations are predominant, then the dynamical regime returned back to quasi-periodic and periodic oscillations in the current range  $I$  (0.01649- 0.02A). The mechanism of bifurcation in route to chaos initiated from periodic, quasi-periodic and chaos then returning back to quasi-periodic and eventually to periodic oscillations that is by increasing bias current  $I_b$  as seen from Fig. (4), can be explained from point of view of SLD angular frequency  $\omega_0$  changes with respect to its bias current  $I$  [16,19,26,27]

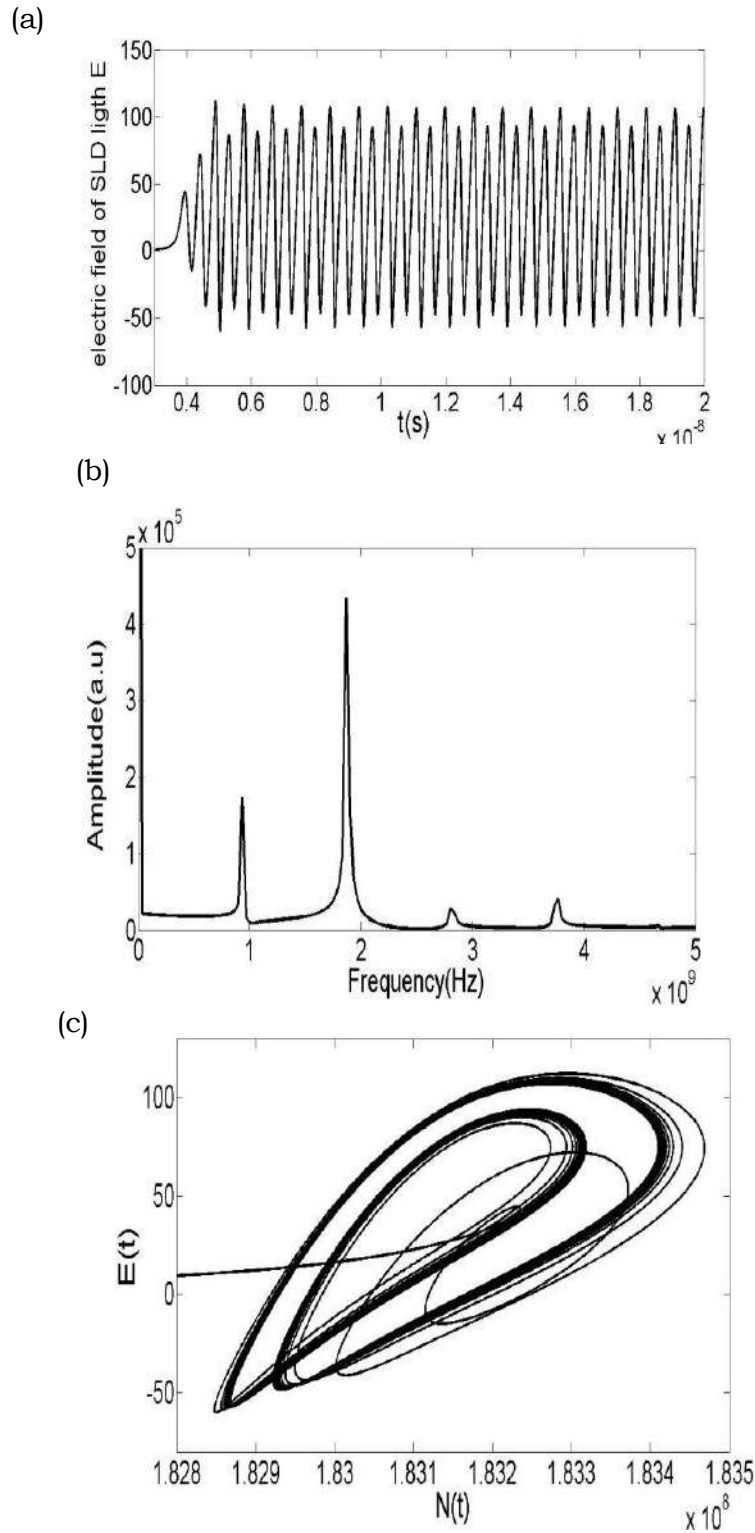
$$\omega_0 = \omega_c - \frac{\partial \omega_0}{\partial I} I \quad (6)$$

The *angular frequency* which denoted by  $\omega_c$  is determined *at certain bias current*  $I$ , and  $\frac{\partial \omega_0}{\partial I}$  is the *angular frequency conversion efficiency* (current tuning of SLD), where the current changes carrier concentration in active region, consequently refractive index, in turn will be changed causing shift in lasing wavelength (mode jump), namely wavelength tuning by the bias current, then the external cavity mode. ECM will be altered accordingly, i.e. ECM switches to

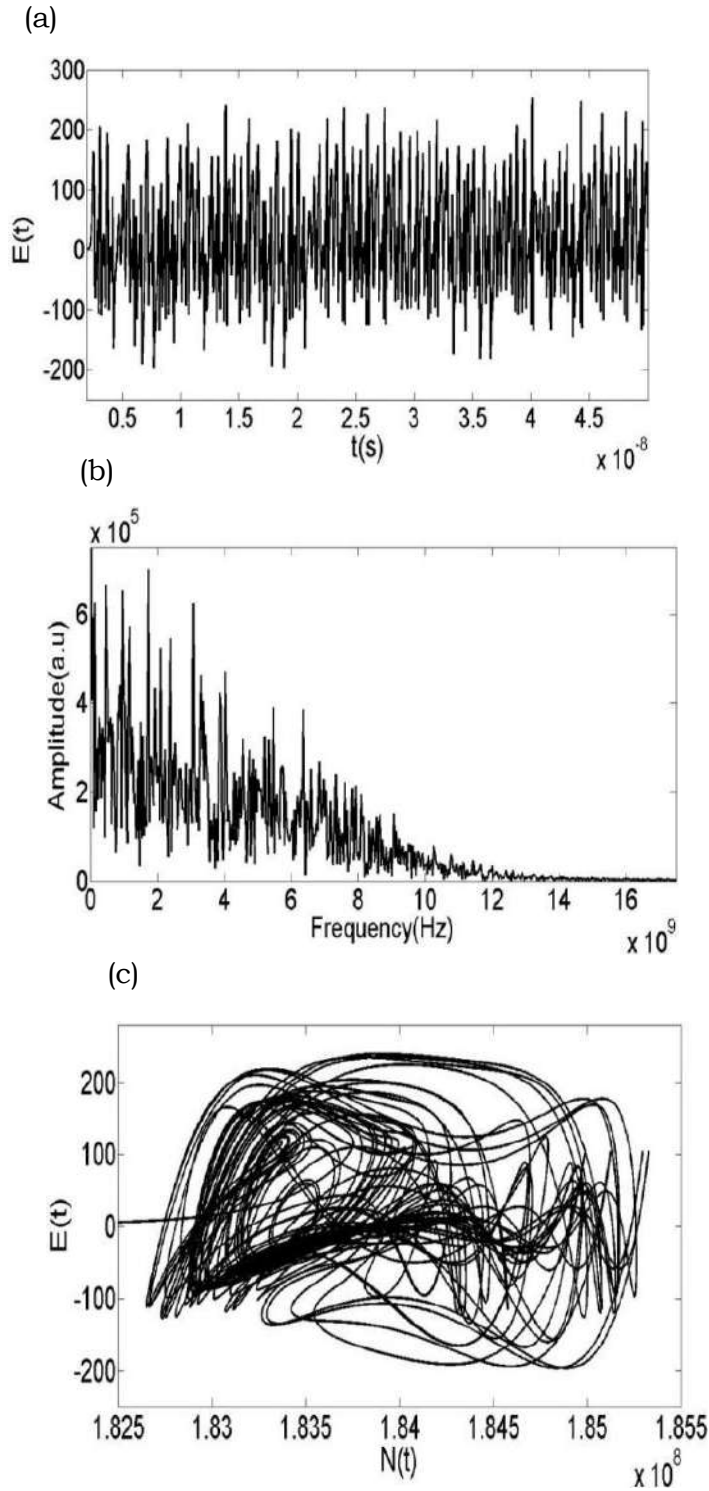
another oscillation mode at each value of the bias current [8,19]. Hence, at low current values the laser oscillates at period one, which is un-damped relaxation oscillation URO frequency, SLD become unstable with increasing the current, and it evolves into chaotic states then it is returned back to periodic states.



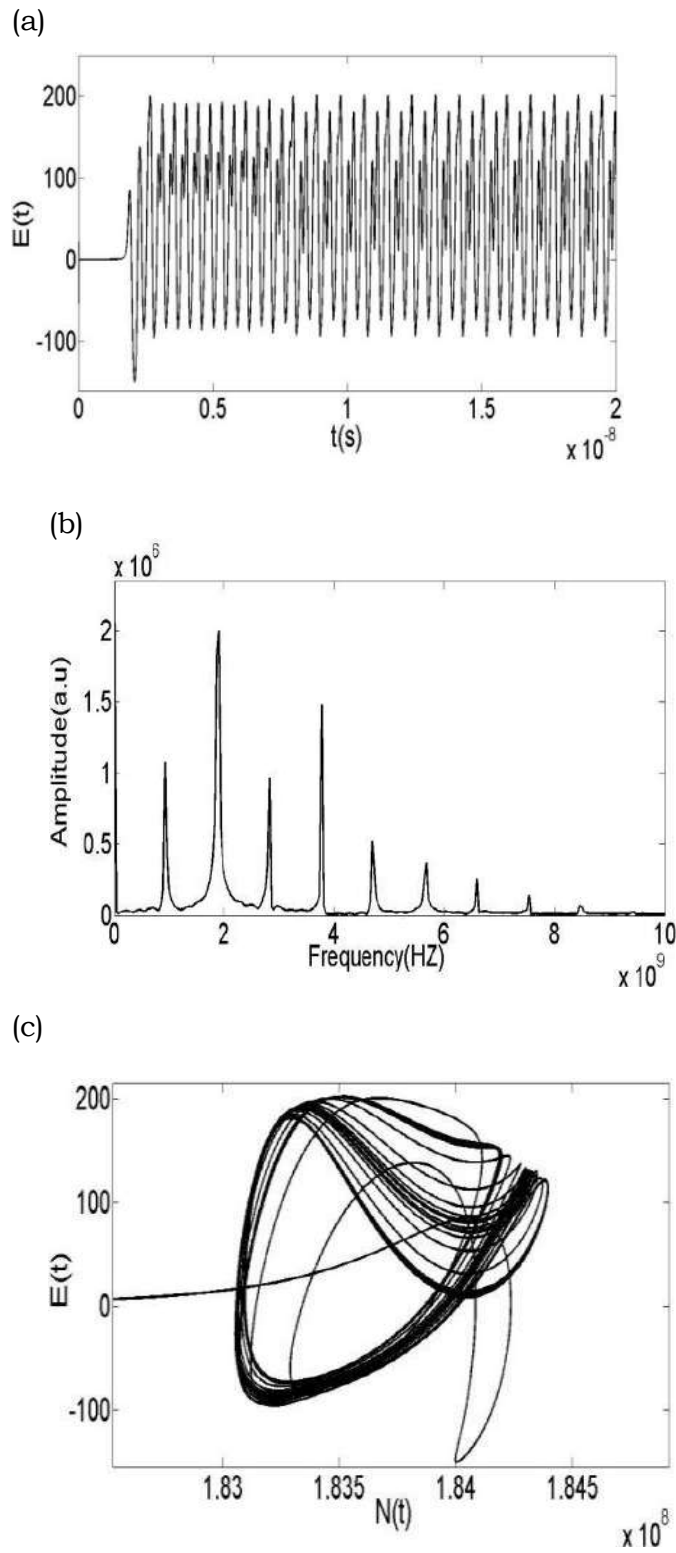
**Fig. (2) time series signal(a), FFT (b) and phase attractor(c) at bias current of the laser (I= 0.0148764A) period one state**



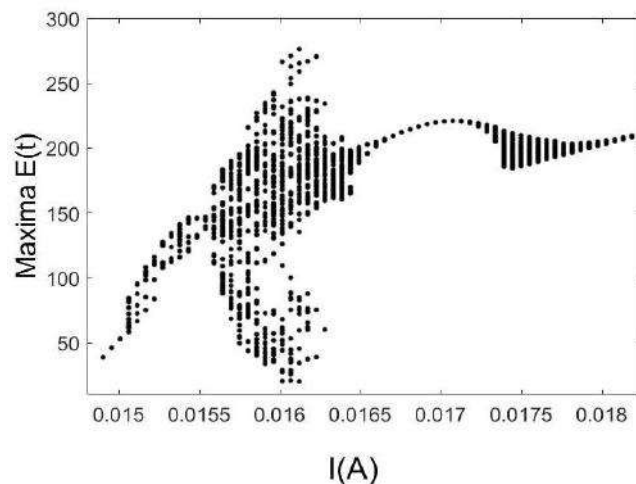
**Fig. (3) time series signal(a), FFT (b) and phase attractor(c) at bias current of the laser ( $I= 0.0149205A$ ) period doubling state**



**Fig. (4) time series signal(a), FFT (b) and phase attractor(c) at bias current (I=0.0158466A)**



**Fig. (5) time series signal(a), FFT (b) and phase attractor(c) at bias current of the laser ( $I= 0.016464A$ )**



**Figure (6) bifurcation diagram of electric-field of SLD optical output as a function of bias current parameter I**

## CONCLUSIONS

In this paper, we have presented simulation of semiconductor laser diode subjected to optical feedback from fiber loop mirror, by numerical solutions of the Lang-Kobayashi model for carrier number and electrical field of SLD optical output of with optical feedback. Numerical results appeared a wide regimes of spiking spanned from period one, multi-periodic, quasi-periodic, chaotic and again multi-periodic oscillations as a functions of bias currents of the laser diode at constant value of optical feedback strength. Time series of electric field of laser output, were analyzed by evaluating and plotting their frequency spectrums and phase attractor diagrams. Bifurcation diagram showed transitions of different oscillation regimes controlled by the bias current of the laser diode. FFT diagrams showed shifting toward high frequencies of the spiking oscillations by increasing bias currents of the laser diode.

**REFERENCES**

1. S. Lynch, A.L. Steele "Controlling chaos in nonlinear optical resonators", *Chaos, Solitons and Fractals* 11 (2000) pp 721-728
2. K. A. Al-Naimee, F. Marino, M. Ciszak, R. Meucci and F.T.Arecchi "Chaotic spiking and incomplete homoclinic scenarios in semiconductor lasers with optoelectronic feedback" , *New Journal of physics*, 073022 11, 2009
3. Grebogi, Celso, Ying-Cheng Lai" Controlling chaotic dynamical systems", Elsevier: *Systems & Control Letters* 31, 307-312, 1997
4. S. Boccaletti, C. Grebogi, Y.C. Lai, H. Mancini, D. Maza" *The Control of Chaos: theory and applications*", *Physics Reports*, 197, 329-103, Elsevier, Science direct, 2000
5. E., Ott, C. Grebogi, J. A. York" *Chaos control*", *Physical Rev. Lett.* Vol.64, No.11, 1990
6. Thomson, J.M. and H.B.Stewart "*Nonlinear Dynamics and Chaos*", John Wiley and sons, England, 2002.
7. Arecchi, F. Tito "*Instabilities and chaos in single mode homogeneous line laser*", Harison Ed.s, Springer Verlag, Berlin, 1987.
8. J. Ohtsubo " *Semiconductor lasers stability, instability and chaos*", Springer Verlag, XVIII, 2008
9. M. C. Soriano ,J. Garcia O., Claudio R. Mirasso and Ingo Fischer "*Complex Photonics :Dynamics and applications of delay-coupled semiconductor lasers*" *Reviews of Modern Physics* ,Vol.85,421-470(2013)
- 10.Arecchi, F.T. R.Meucci and W. Gadomski" *Laser Dynamics with Competing Instabilities*", *Phy. Rev.Lett.* Vol.58, No.21, 1987
- 11.Lenstra, D. and W. Van der Graaf" *Diode laser with optical feedback and injection: similarities and differences*", Invited paper, *IEEE Ex.*, 2011
- 12.Toomy, J. P., D. M. Kane, M. W. Lee, and K. A. Shore "*Nonlinear dynamics of semiconductor lasers with feedback and modulation*", 2 August 2010 / Vol. 18, No. 16 / *OPTICS EXPRESS* 16955
- 13.Davidchack, R. L., Y. C. Lai, A. Gavrielides and V. Kovanisb "Chaotic transitions and low-frequency fluctuations in semiconductor lasers with optical feedback", Elsevier, *Physica D* 145 (2000) 130–143
- 14.Rogister, F., P. Me'gret, and M. Blondel " *Saddle-node ghost-induced low-frequency fluctuations in an external-cavity laser diode*", *Physical Review*, **67**, 027202, 2003
- 15.Silvano D., and Ray-Hua Horng "*The Diagram of Feedback Regimes Revisited*", *IEEE J. of selected topics in Quantum Electronics*, Vol. 19, No. 4, 2013



16. Ohtsubo, J. " Feedback Induced instability and chaos in semiconductor Lasers and their Applications", Optical review, Vol.6, No.1, pp1-15, 1999
17. Heil, T., I. Fischer, and W. Elsässer " Dynamics of Semiconductor Lasers Subject to Delayed Optical Feedback: The Short Cavity Regime", Physical Review Letter, Vol.87, No.24, 10 Dec. 2001
18. Law, J.Y. and G. P. Agrawal " Effects of Optical Feedback on Static and Dynamic Characteristics of Vertical-Cavity Surface-Emitting Lasers", IEEE JOURNAL OF SELECTED TOPICS IN QUANTUM ELECTRONICS, VOL. 3, NO. 2, APRIL 1997
19. Lang, R. K. Kobayashi "External optical feedback effects on semiconductor injection laser properties" IEEE J. Quantum Electron, vol. QE-16, pp. 347–355, Mar. 1980.
20. Younis, Y. Th, Musa SK, Abdalah SF, Ahmed AK, Meucci R, Al Naimee KA. "The rule of bias current of semiconductor laser in chaos communications", Elsevier, Results in Physics. 2016;6: 243-251
21. Jones, R.J., P.S. Spencer, J. Lawrence and D.M. Kane "Influence of external cavity length on the coherence collapse regime in laser diodes subject to optical feedback" IEE Proc.-Optoelectron, Vol.148, No.1, 2000
22. Mork, Jesper, Bjarne Tromborg, and Peter L. Christiansen " Bistability and Low-Frequency Fluctuations in Semiconductor Lasers with Optical Feedback: A Theoretical Analysis", IEEE JOURNAL OF QUANTUM ELECTRONICS, VOL. 24, NO. 2, FEBRUARY 1988
23. S.Y. Xiang, Wei Pan, Bin Luo, Lian Shan Yan, Xi Hua Zou, Nianqiang Li, and H. Na Zhu "Wideband Unpredictability-Enhanced Chaotic Semiconductor Lasers With Dual-Chaotic Optical Injections" IEEE J. Of Quantum Electronics, Vol. 48, No.8, (2012)
24. Peterman, K., and N. Schunk "Laser diode characteristics with external optical feedback", Proc. European Conf. (1988).
25. Agrawal, Govind P. and N.K. Dutta "Semiconductor Lasers", 2nd Edition, Van Nostrand Reinhold, New York, 1993
26. Erneux, T., G. Hek, M. Yousefi, and D. Lenstra " The injection laser limit of lasers subject to optical feedback", Proceedings of SPIE-The International Society for Optical Engineering, 2004
27. Hek, G. and V. Rottschäfer "Semiconductor Laser with filtered optical Feedback bridge between conventional feedback and optical injection", ENOC-2005, Eindhoven, Netherlands, 7-12 August 2005

28. Xiang-H. Wang , Z. M. Wu , Z.F. Jiang and G.Q. Xia “Nonlinear Dynamics of Two-State Quantum Dot Lasers under Optical Feedback”, Photonics, MDPI, 2021
29. [Porte, X., D. Brunner, I. Fischer and M.C. Soriano ‘ Nonlinear Dynamics of a Single-Mode Semiconductor Laser with Long Delayed Optical Feedback: A Modern Experimental Characterization Approach”, Photonics, MDPI, 2022, 92

**COMPARE OF MEDIAN FILTER AND WIENER FILTER TO DETECT CONCEALED WEAPONS**

**MOUMENA SALAH YASSEN**



## COMPARE OF MEDIAN FILTER AND WIENER FILTER TO DETECT CONCEALED WEAPONS

Moumena Salah YASSEN<sup>1</sup>

### Abstract:

Many types of terror and terrorist attack aimed to finish our safety and friendly life. Therefore, detecting weapons has become a very important role in our life. Image processing and computer vision are one of the best field that targets to clarify different kinds of images, especially weapons images that can be a source of threat in many places such as metros stations, malls, airports, schools, and train stations. So that, there is a need to employ techniques for discovering different weapons, like guns, knives, and chemical explosives hidden in the clothing. In this paper, we will use different kinds of image filters Median and Wiener to detect images with different weapons. The experimental results ensure that wiener filter is best filter for eliminate noise from the concealed weapons images. Outcomes of this paper have been implemented on MATLAB.

**Key words:** Weapons, Image Processing, Computer Vision, Image Filters, Median Filter, Wiener Filter, Gaussian Noise.



<http://dx.doi.org/10.47832/MinarCongress5-31>



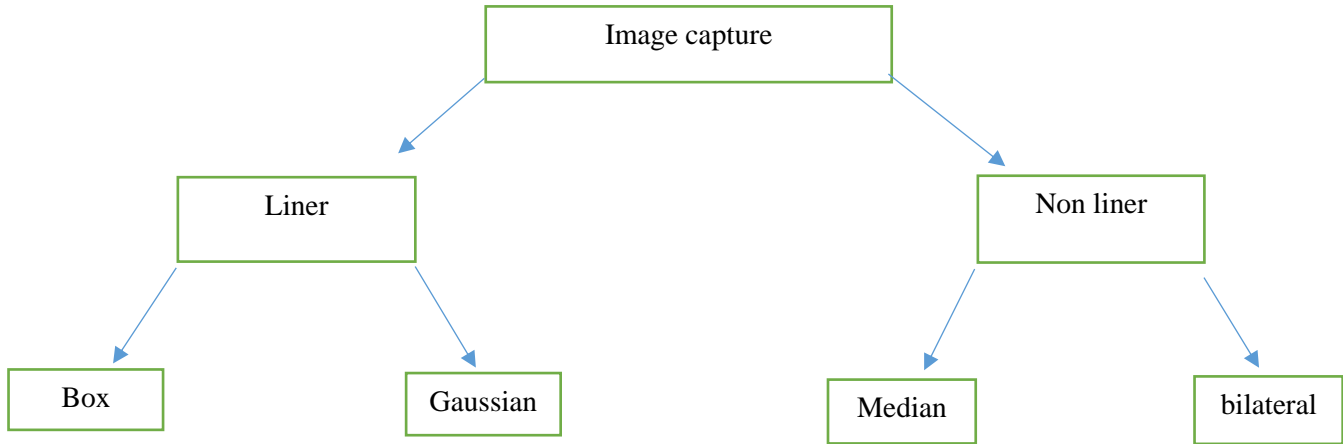
<sup>1</sup> University of Kirkuk, Iraq, [Moumena.salah@uokirkuk.edu.iq](mailto:Moumena.salah@uokirkuk.edu.iq)

## **Introduction:**

Image processing is the field that transform the image into digital form and apply different operations on it such as improving the image or extracting different useful information [1]. In our study, we will use image filters to detect weapons images like guns, knives, because the security must only be applied 24-hour, in many areas where human surveillance is not fine enough [2,3,4]. Image filtering is known as a method applied to detect the images in terms of size, shape, color, depth [1]. Also, the mechanism of filters is based on eliminate the noise from the image and detection its edges. In general, the filtering in image processing is divided by: linear and nonlinear; linear filter is done by applying convolution and Fourier multiplication in contrast, Nonlinear cannot be achieved by any of these [16]. Figure (1) is shown the diagram of filters.

The filters progress across the different places of the image passing of pixel by pixel for all the image. In our study, we used two types of filters to remove the noise: first Wiener filter its work based on computation a statistical estimate of un defined signal using a related signal as an input, then the filtering that known signal to present the estimate as an outcome. Second, Median filter is a non-linear digital filtering method, often used to minimize noise from an image or signal. Median filtering is very used in image processing and computer vision because it clarify edges while clean up the noise[16].

As previous works the researchers used different image processing methods to detect the weapons such as [7] the researcher apply a Phased Antenna Array to detect hidden weapon. [8] implemented Millimeter Wave Sensors to discover the hidden guns. [9] used AN AUTOMATIC HYBRID APPROACH TO DETECT CONCEALED WEAPONS USING DEEP LEARNING. [10] Image fusion is a technique apply of combining complementary information from many sensor images to produce a single image that presented a lot of description of the scene than single images. [11] ensured that image processing methods have been presented in combination with computer vision techniques as an effective technology for fast detection of hidden weapons through scanning. [12] presented imaging sensors that can be simply interfaced with modern user electronics to take images that can detect specific electromagnetic spectrum to produce uniform image outcome. All these methods contain filtering or interpolation and quantization algorithms.



**Figure (1)[1]**

**1. Median Filter:** calculates the median of all the pixels under the kernel window and the central pixel is changed with this median value. This filter is the best in eliminate salt-and-pepper noise [16]. (Koenderink 1984) defined this filter as the method used to change the value at every pixel of the image by the average of the values within slot around the point. Iterating this operation simplifies the image. Applying the mean as the averaging operator outcomes in a filtering equivalent to linear method. Moreover, median filtering is known by a simple equation and has implemented in many applications in image processing and computer vision. It should be used productive to seem the using averaging parameters than the mean. In addition, Median filter has been clarified by Guichard & Morel (1995)[14].

The gray- images has  $x_{(i,j)}^{(0)}, x_{(i,j)}^1, \dots, \dots, x_{(i,j)}^n$  Here, the first image  $x_{(i,j)}^{(0)}$  is noisy image (i,j)is the position of pixels in the image where  $1 \leq i \leq M, 1 \leq j \leq N$  , , N and M refer direction of pixels in vertical and horizontal direction and  $x_{(i,j)}^n$  is the image after nth iteration.

Suppose a window  $(2W+1) \times (2W+1)$  around  $x_{(i,j)}^{n-1}$

where  $-W \leq k \leq W, -W \leq l \leq W$  and  $W \geq 1$ .

2) Finding windows, median value  $m_{(n-1)}^{(i,j)}$ ,

$$m_{(n-1)}^{(i,j)} = \text{median value}(x_{(n-1)}^{(i+kj+1)}) \tag{1}$$

3) The absolute difference of  $x_{(i,j)}^{n-1}$  and  $m_{(n-1)}^{(i,j)}$

$$f_{(n)}^{(i,j)} = \begin{cases} f_{(n-1)}^{(i,j)} & \text{if } |x_{(i,j)}^{(n-1)} - m_{(n-1)}^{(i,j)}| < T \\ 1 & \text{otherwise} \end{cases} \tag{2}$$

4) If noise is detected in (i,j)th then the value of  $x_{(n)}(i,j)$  will be replaced as

$$x_{(i,j)}^{(n)} = \begin{cases} m_{(n-1)}^{(i,j)} & \text{if } f_{(n)}^{(i,j)} = 1 \\ f_{(n-1)}^{(i,j)} & \text{otherwise} \end{cases} \tag{3}$$

$$X(n-1)(i, j), \text{ if } f_{(n)}^{(i,j)} = 1 \tag{4}$$

All these steps needed to be repeated for p times. Where p can be 2,3,4. . . . and so on. Then the p th iteration, x (p) (i,j) and f (p) (i,j) are two images[1] .

**2. Wiener Filter:** is a filter applied to present an estimate of a desired random process by linear time. This filtering of an observed noisy process, assuming known stationary signal and noise, and additive noise. The Wiener filter decreases the mean to the minimum average square of the distance between the estimated filtered output and the desired signal [13,15].

$$F^{\wedge}(u, v) = \left[ \frac{H^*(u,v)}{|H(u,v)|^2 + K} \right] G(u, v) \quad 5$$

$F(u, v)$  = the estimate

$G(u, v)$  = damaged image

$H(u, v)$  = degradation function

$H^*(u, v)$  = complex conjugate of  $H(u, v)$

$K$  = constant

Eq. (5) Wiener Filter and it is implemented in the frequency way.

**3. Performance Parameter** The execution parameters are most critical criteria to determine the simulation results. Peak signal to noise ratio (PSNR) and mean square error (MSE) are known as parameters [16]. MSE is the mean square error between original image and clear image with M\*N size and R is largest value of pixel appear in an image.

$$MES = \frac{1}{N \cdot M} \sum_{i=0}^{N-1} \sum_{j=0}^{M-1} [x(i, j) - y(i, j)]^2$$

#### 4. Experimental Results:

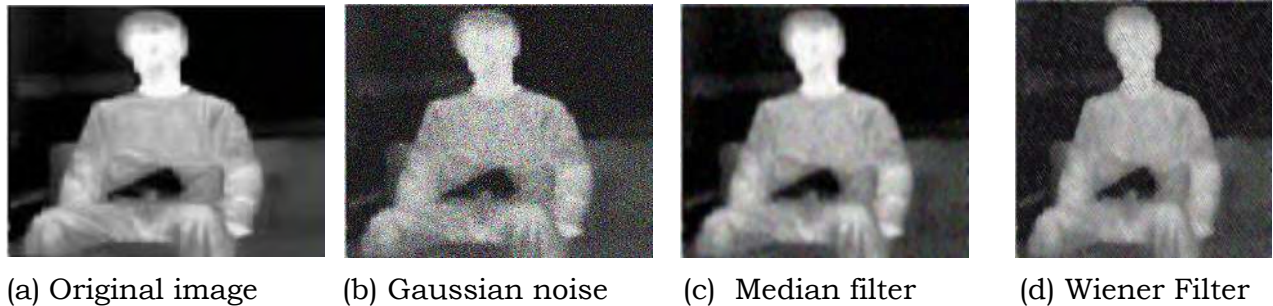
Median Filter and Wiener Filter implementation using MATLAB. Figure (2) shows some results of denoising images. The image in Fig(2)(b) is selected by “salt and pepper” noise. The image has Gaussian noise that has different intensity which has drawn from a Gaussian distribution and is a very suitable model for many types of sensor noise, like the noise due to camera reflections [16]. The median filter with a 4x4 kernel is used to filter the impulse noise. The enhanced image shown in Fig(2)(c), it has a clear quality improvement. However, the enhanced image also seems smoothed, thus, the high-frequency information is reduced.

For median filter a larger size kernel is appropriate for median filtering, as a result for to the larger group of pixels the median value deviates from the pixel value. We found Median filter cleaned up images and clarify it. As seen in Figure(2)(c) illustrates the effectiveness of Median Filter in restoring damaged images. Previously, the 4x4 and 5x5 kernel sizes were applied to denoise the images, but they might produce the similar effect. Then, the kernel size was increased up to 10x10 and the outcome presented the difference more clearly. The results ensure that Median Filter can reduce noise well.

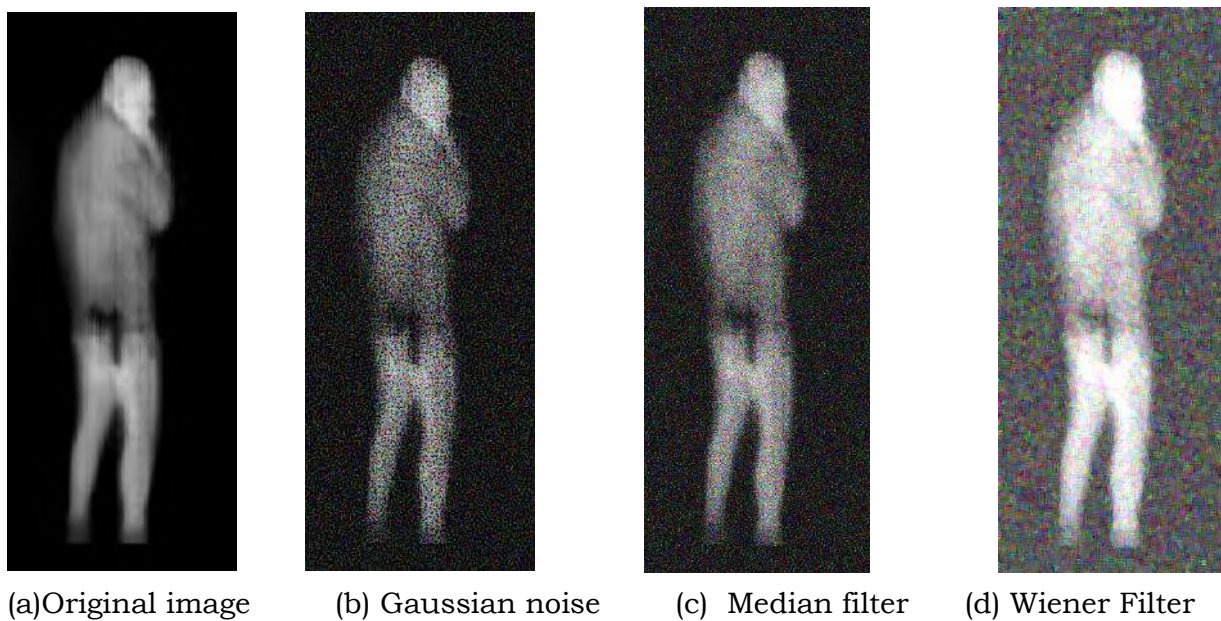
On the other hand, Wiener filter is known as a linear filter. It presents linear estimation of a wanted signal sequence from other related sequence [16]. Wiener filter present solution in providing signal estimation for stationary signals. Wiener filter is

good on statistical method. It also presented output image with a little noise as shown in Figure (2) (d)

We implemented Median Filter and Wiener Filter in many images, and the experimental results ensured that median filter can decrease noise and the result image clear than that of Wiener Filter. Wiener Filter produce a good output image with a little noising also not clear enough.



**Figure (2) (a) is the original image (b) is the Gaussian noise image (c) Median filter (d) Wiener filter**



**Figure (3) (a) is the original image (b) is the Gaussian noise image (c) Median filter (d) Wiener filter**



**Conclusion:**

Many digital image processing and computer vision applications need to remove the noise in order to improve the image and present more efficient output. To decrease noise, we implement two filters target at smoothing the image to decrease some form of noise. First, we applied median filtering, and we choose the kernel size, list the pixel values covered by the kernel, and determine the median filter. If the kernel passes by every number of pixels, the average of two median values is used. Also before applying median filtering should be zeros then it be padded around the row edge and the column edge. Second, Weiner filter was implemented to decrease the Gaussian noise from degraded image based on the estimating statistics for every neighbor per pixel. These two filters were efficient to improve the images of person has hidden gun, but we noticed that median filter is the best because it can minimize noise than that of Wiener Filter. Wiener Filter produce a good output for simultaneously de noising but still the result image has less clear.

## References

1. B Desai, U Kushwaha, S Jha “Image Filtering -Techniques, Algorithm and Applications” , Applied GIS SCIENCE JOURNAL, ISSN NO : 1869-9391, December 2020.
2. S Al-Shoukry, “AN AUTOMATIC HYBRID APPROACH TO DETECT CONCEALED WEAPONS USING DEEP LEARNING” ARPN Journal of Engineering and Applied Sciences, VOL. 12, NO. 16, AUGUST 2017.
3. H Moghaddasi, S Sajjadi and M Kamkarhaghighi “ Reasons in Support of Data Security and Data Security Management as Two Independent Concepts: A New Model “ The Open Medical Informatics Journal” 2016 .
4. P Pratihari, A Yadav, “ Detection Techniques for Human Safety from Concealed weapon and Harmful EDS “ International Review of Applied Engineering Research, ISSN 2248-9967 Volume 4, Number 1 (2014), pp. 71-7.
5. G Das, N Anwar , S Chowdhury , K Rahman “ Design and Fabrication of an Image Processing Based Autonomous Weapon” , International Journal of Engineering Research, Volume No.5, Issue No.12, 1 December 2016, pp : 931-935.
6. Bingi Yogi Gopinath, Vasa Suresh Krishna, G.Srilatha “Concealed Weapon Detection Using Image Processing” , IJECT Vol. 5, Issue Spl - 3, Jan - March 2014
7. S.W.Harmer, S.E.Cole, N.J. Bowring, N.D Rezgui, and D. Andrews, “On body concealed weapon detection using A Phased Antenna Array”, Progress In Electromyetics Research, Vol.124, 187-210, 2012.
8. S. Erukulla, “Design and Optimisation of Millimetrewave Sensors for Security Imaging, Master’s Thesis, Chalmers University of Technology, G”oteborg, February 2006.
9. Suhad Al-Shoukry “ AN AUTOMATIC HYBRID APPROACH TO DETECT CONCEALED WEAPONS USING DEEP LEARNING” ARPN Journal of Engineering and Applied Sciences, VOL. 12, NO. 16, AUGUST 2017
10. Ancuti CO, Ancuti C, De Vleeschouwer C, Bovik AC. 2017. Single-Scale Fusion: An Effective Approach to Merging Images. IEEE Transactions on Image Processing. 26(1): 65-78.
11. Brown KW, Sar DR, Gallivan JR, Phillips WM. 2014. Infrared concealed object detection enhanced with closed-loop control of illumination by. mmw energy. Google Patents.
12. Russ JC. 2016. The image processing handbook: CRC press.
13. Le-Anh Tran, “ Image Processing Course Project: Image Filtering with Wiener Filter and Median Filter” April 2019.
14. L. Griffin “ Mean, median and mode filtering of images” , The Royal Society, 2000.
15. H. Kareem, R Husain A. and Ali, Jaber, “ Noise Removed by Processing the Lightness and Chromatic Components Basic on YCbCr Color Space” Journal of Babylon University/Pure and Applied Sciences/ No.(9)/ Vol.(24): 2016 .
16. R. C. Gonzalez and R.E.Wood “digital image processing” 2002.

**STUDY SOME TYPE OF FISH AS INDICATORS OF POLLUTION IN  
AL - SANIYAH RIVER/ AL -DIWANIYAH/IRAQ**

**LUJAIN EBRAHEM HUSSAIN**



## STUDY SOME TYPE OF FISH AS INDICATORS OF POLLUTION IN AL- SANIYAH RIVER/ AL-DIWANIYAH/IRAQ

Lujain Ebrahim HUSSAIN <sup>1</sup>

### Abstract:

This study was conducted on Al- Saniyah River, Al-Diwaniyah/ in three locations. Some physical and chemical properties of the water were studied for this river , the temperature it was reached 17-26 ° C and the pH value was 7.87- 7.89, while the turbidity ranged from 19.45- 68 NTU. The electrical conductivity is 1515-1770 µs/cm, and the total dissolved salts are 896-1001 mg/L. While the value of dissolved oxygen was 8.5-9.2 mg/L, BOD5 was 4.3-4.8 mg/L, the total hardness was 584-677 mg/L, and the total baseline was 267-348 mg/L. The concentrations of some heavy metals were studied in the muscles of four types of fish found in AL- Saniya River, and they were Alburnus sp., Aspius sp., Barbus sp. and Cyprinus sp.

The heavy metals are lead Pb, cadmium, Cd, and zinc, Zn, where the values of lead ranged between 5.09-13.1 µg/g dry weight, while the values of cadmium reached 4.90-11.36 µg/g dry weight, and the values of zinc ranged between 69.94- 129.07 µg/g dry weight. The highest values were recorded in March and the lowest values were recorded in January during the study period.

**Key words:** Al- Saniyah River, Cadmium, Lead.



<http://dx.doi.org/10.47832/MinarCongress5-32>



<sup>1</sup> University of Al- Qadisiyah, Iraq, [lujain.ibrahim@qu.edu.iq](mailto:lujain.ibrahim@qu.edu.iq), <https://orcid.org/0000-0001-6185-5852>

## **Introduction:**

Water is one of the most important natural resources. It is an essential factor in human life and all his activities. It is one of the resources that is renewable during a specific period of time by the hydrological cycle. The last twenty years have been characterized by a significant deterioration in the Iraqi natural environment, starting with air pollution and ending with soil and water pollution ,where Iraq is going through a stage of great neglect related to water quality, as a result of the multiple sources of pollution in it and the lack of strategies to develop and strengthen the foundations to provide clean water.( Zhang,2011).

River pollution is one of the most dangerous types of water pollution, because it affects drinking water and water used in agriculture and irrigation. The pollution of rivers and lakes results from several sources, including the discharge of various chemical pollutants resulting from factories, sewage and agricultural wastes, which are loaded with many organic fertilizers and pesticides, and torrential waters loaded with organic and chemical dissolved substances. It cannot be quantified or controlled.( Werner ,2003). Fish is the basic food consumed by humans from the aquatic system. It is also a good indicator as life guides for the pollution of the aquatic environment with heavy metals, as it has the ability to accumulate these elements in higher concentrations than in water, and sediments due to its feeding on algae and small organisms in addition to the organic materials present in the environment aquatic(Rashed ,2001), Heavy metals can penetrate the metabolic cycle of fish and become toxic when they accumulate in various tissues and muscles, which leads to an imbalance in physiological functions and a reduction in their ability to grow and reproduce, thus it enters the food chain directly and these elements move from one organism to another to reach the top of the pyramid in the chain, and it is the human who feeds on materials containing toxic elements (Benzer,at.al.,2013).

The aim of the study is to know the physical and chemical properties of water in the study area and determination the concentration of heavy metals (lead pb, cadmium Cd, zinc Zn) in the muscles of four species of fish (Alburnus sp, Aspius sp., Barbus sp. and Cyprinus sp.) in the water of the study area.

## **Materials and methods**

**1- Description of the study area:** The Sunni River is one of the branches of Al-Diwaniyah River before entering the governorate center , The area is characterized by agricultural activity, and three sampling sites were chosen, at the beginning of the river and at the middle inside the city and after the city before entering Al-Diwaniyah Governorate.

**2- Physical and chemical properties of water:** Water samples were collected from 3 stations during three months (November, January and March).

The temperature was measured by thermometer (0-100), turbidity using (turbidity meter), pH by pH meter, electrical conductivity EC and total dissolved solid TDS by (EC&TDS meter), dissolved oxygen and the biological oxygen demand (BOD5) by (DO

meter). The total hardness was measured by titration with NaEDTA solution and Eriochromic black T as indicator and the total, while total alkalinity was measured by titration with HCL solution with methyl orange as indicator (APHA,2003)

Total Alkalinity (mg/ l) =  $A \times N \times 50000 / \text{ml of sample}$

3- **After collecting fish samples** (4 species) with 3 replicates for each type for the three studied months and transferring them to the laboratory, they were washed with distilled water, the fish were explained for the purpose of muscle separation, the method mentioned in (APHA,1999) for the digestion of fish samples for the purpose of measuring the ions of trace elements in them.

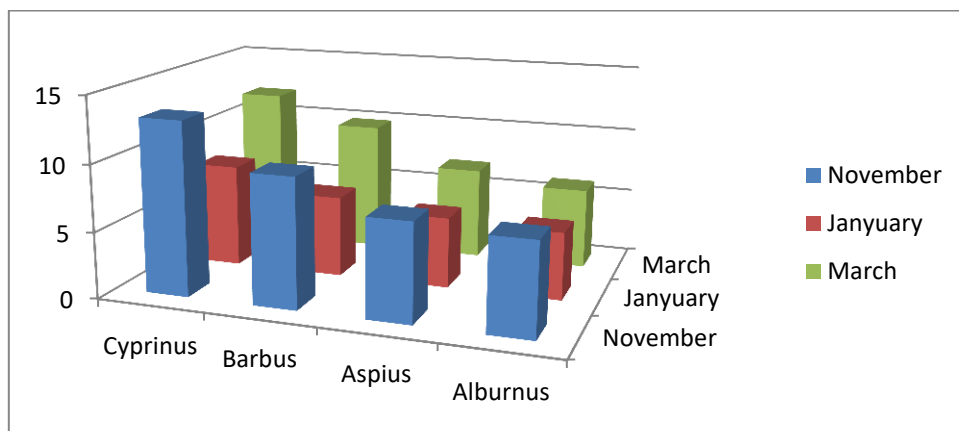
### Results and discussion:

**Table 1 physical & chemical properties of water in studied stations**

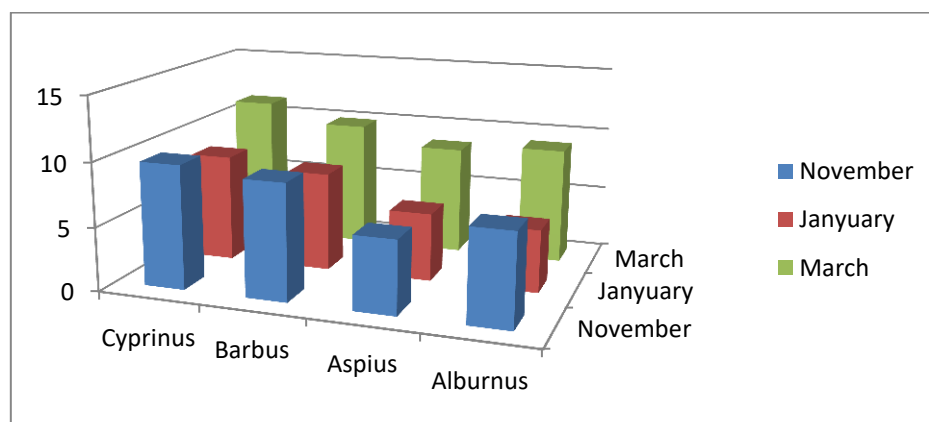
months of study				Properties
March	January	November		
24	18	25	S1	Temp.c°
22	17	25	S2	
23	17	26	S3	
7.98	7.88	7.88	S1	pH
7.97	7.87	7.89	S2	
7.98	7.87	7.89	S3	
67	55.12	20.12	S1	Turbidity NTU
68	55.23	19.45	S2	
65	54.16	19.5	S3	
1768	1515	1665	S1	EC $\mu\text{s/cm}$
1770	1518	1678	S2	
1766	1519	1650	S3	
1050	896	878	S1	TDS mg/l
1001	897	879	S2	
1020	896	977	S3	
9.2	9.1	8.7	S1	DO mg/l
9	9.0	8.6	S2	
9	9.1	8.5	S3	
4.8	4.4	4.8	S1	BOD5 mg/l
4.6	4.5	4.6	S2	
4.8	4.3	4.8	S3	
676	584	614	S1	Total hardness mg/l
677	588	618	S2	
675	585	612	S3	
346	267	301	S1	Total alkalinity mg/l
345	268	305	S2	
348	269	300	S3	

Table 1 shown the temperature the high value 26C° S3 in November and the lower value 17 C° in S2 and S3 January , This difference in temperature is due to the climatic conditions, which include the intensity of solar radiation reaching the surface of the water, the length of the day and the seasons.(Dallas, 2019).

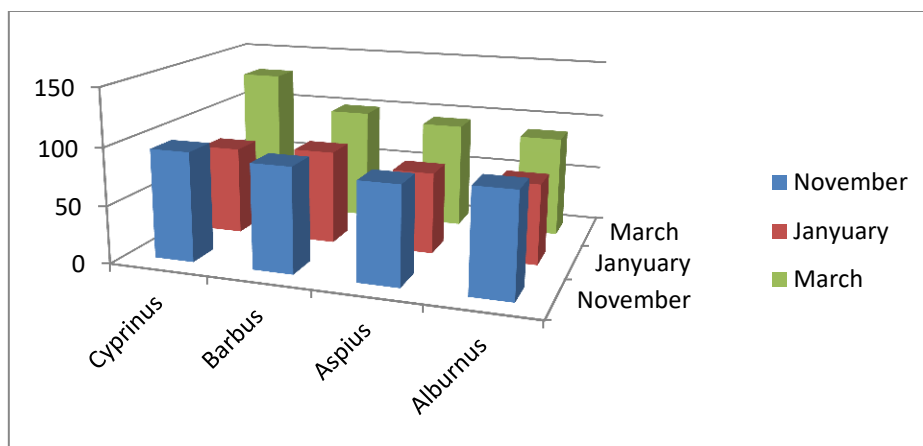
The range of pH in this study was (7.98- 7.87) in S1and S3 sequentially, It is within the permissible limits Iraqi and international (6.5 to 8.5).pH is one of the most important characteristics that affect the metabolism and physiology of aquatic organisms its affects the existing materials or elements and nutrients(USA EPA,2022).The range of turbidity was recorded (68-19.45)NTU in march and January in S2 Turbidity affects the transparency of the water body ,the cause of turbidity is due to the sewage dumped in the river without treatment and some waste.(MIPCA,2008).The EC.and TDS was recorded (1770- 1515) µs/cm , (1050-878) mg/l.



**Fig (1) concentration of Pb in the muscles of the studied fish**



**Fig (2) concentration of Cd in the muscles of the studied fish**



**Fig (3) concentration of Zn in the muscles of the studied fish**

In fig (1) shown the concentration of Pb in the muscles of the four types of studied fish The highest values were 13.1  $\mu\text{g/g}$  dry weight in November and the lowest values were 5.09  $\mu\text{g/g}$  dry weight., Lead is a toxic element that enters aquatic ecosystems through industrial and sewage waters and waste streams. High levels of lead cause changes in the brain and nerves of fish and other aquatic organisms, It causes an imbalance in the liver cells with a decrease in their ability to get rid of harmful substances (Timub and Afua ,2013) Fig (2) shown the concentrations of Cd in studied types of fish , the high value was 11.36  $\mu\text{g/g}$  dry weight in Cyprinus sp. while the less value was 5.33  $\mu\text{g/g}$  dry weight Cadmium activates antioxidant enzymes, which results in an increase in the oxidative effort in tissues and then damage them. Available reports indicate that gills, liver and kidneys are the most affected by cadmium in fish (Ahmed , 2020) .fig (3) shown the Zn concentrations in muscles of types of fish ,the high value 129.7 in march and the less value was 69.94 in January , Zinc has harmful effects on fish, including its effect on growth and breathing, physiology of the heart, imbalance and defects in gill tissue, which leads to lack of ventilation (Kori, 2008). It was noted that the highest percentages in all types of fish were in the species Cyprinus sp. The values were and this type is common in Iraqi aquatic environments and bears different environmental conditions and is fed by a mixed diet of mollusks, crustaceans and algae there for the elements was accumulate in this type. ( Ahmed et.al,2020: Al- Mohmood , et al.,2017). The lowest value in species Alburnus sp.in all elements It is a less prevalent species in the Iraqi environment. It is distinguished by its limited nutrition on aquatic insects and plankton. For this reason, the entry of heavy elements into the body of this type of fish is reduced.(Mohamed et.al,.2015) . The highest values were recorded in March, due to the increase in agricultural and household wastes to the river without treatment, as well as the low water level due to the lack of rain during this season. As for the lowest values, it was in January due to the lack of agricultural activities during this period, and thus the lack of heavy elements that move into the river waters. We conclude from



this study that there is pollution in fish samples from all studied elements, which indicates the pollution of the river with heavy metals.

**Reference:**

1. **Ahmed ,Arafat R. , Jihad M. Al-Zewar, Nadia Al-Mudaffar Fawzi and Adil A. Abulhasan** .(2020) . Culture of common carp (Cyprinus carpio L.) in Basrah Governorate, southern Iraq; Current status and suggestions for development . Eco. Env. & Cons. 26 (2); pp. (824-83) .
2. **Al-Mahmood, Saevan Saad; Dlyna Wrya Bakir and Soma Hillal Hussien** .(2017). Gross and histopathological study on common carp Cyprinus carpio L. diseases in rearing culturing ponds in Kirkuk Province – Iraq. The Iraqi Journal of Veterinary Medicine, 41(1):109-117.
3. **American Public Health Association (APHA)**1999. Standard Methods for the Examination for Water & Waste. 17PthP ed., American Public Health Association 1015 fifteen Street, N.W., Washington DC.
4. **APHA American Public Health Association**. (2003). Standard methods for examination of water and wastewater, 20th, Ed. Washington DC,USA.
5. **Benzer, S., Arslan, H., Uzel, N., Gül, A., and Yilmaz, M.** (2013). Concentrations of metals in water, sediment and tissues of Cyprinus carpio L., 1 758from Mogan Lake (Turkey). Iranian Journal of Fisheries Sciences, 12(1), 45-55.
6. **Hellen,Dallas** (2019) .The effect of water temperature on aquatic organisms, water research commission .University of Captown , Republic of South Africa.
7. **Kori- siakPere,O.,and Ubogu,E .O**(2008). Sublethal haematological effects of zinc on the freshwater fish, Heteroclarias SP.(Osteichthyes: clariidaey). African Journal of Biotechnology,7(12).
8. **Minnesota Pollution Control Agency** .(2008). Turbidity:Description Impact on water Quality ,Sources ,Measures – Ageneral over view.
9. **Mohamed ,Abdul-Razak M., Layla A. Aufy and Basim M. Jasim** ( 2015). Some Biological Aspects of the Bleak, Alburnus mossulensis in the Southern Reaches of Euphrates River, Iraq . Asian Journal of Applied Sciences .vol.3. (ISSN: 2321 – 0893).
10. **USA Environmental protection Agency** .(2022). PH effect .vol 12.
11. **Rashed, M. N.**,( 2001). Monitoring of environmental heavy metals in fish from Nasser lake. Environmental International, 27,( 27) .33-37.
12. **Tiimub, B. M., and Afua, M. A. D.** (2013). Determination of selected heavy metals and iron concentration in two common fish species in Densu River at Weija District in grater Accra region of Ghana. American International Journal of Biology, 1(1), 45-55.
13. **Werner, I., Clark, S. and Hinton, D.E.** (2003). Biomarker and understanding of aquatic organism responses to environmental stressors. California Agriculture, 57 (4): 110-115.
14. **-Zhang, H., Hu, D., Chen, J., Ye, X. N. Wang, S. X., Hao, J. M., Wang, L., Zhang, R. Y., and An, Z. S.** (2011): Particle size distribution and polycyclic aromatic hydrocarbons emissions from agricul-ture crop residue burning, Environ. Sci. Tech., 45, 5477–5482.





ISBN 978-605735535-5  
9 786057 355355